

DEEP-SEATED MAGMATISM, MAGMATIC SOURCES AND THE PROBLEM OF PLUMES

Proceedings of International Workshop

ГЛУБИННЫЙ МАГМАТИЗМ, МАГМАТИЧЕСКИЕ ИСТОЧНИКИ И ПРОБЛЕМА ПЛЮМОВ

Материалы международного совещания



VLADIVOSTOK
2002

*Russian Academy of Sciences
for Eastern Branch
Far Eastern Geological Institute*



Deep-seated magmatism, magmatic sources and the problem of plumes

**(Глубинный магматизм, магматические источники и
проблема плюмов)**

PROCEEDING
of II International Workshop
«Deep-seated magmatism, its
sources and plumes »

Edited by Dr. Yu. A. Martynov, N. V. Vladykin

VLADIVOSTOK

2002

Deep-seated magmatism, magmatic sources and the problem of plumes. Proceeding of International Workshop. Vladivostok: Dalnauka, 2002. 276 p. ISBN 5-8044-0253-6

The proceedings of the International Workshop held in Far East Geological Institute (Far Eastern Branch of the Russian Academy of Sciences, Vladivostok, September 2002) are devoted to complex processes of alkaline rocks formation. The issues of plumes origin, dynamics of its movement toward the surface, problems of ore formation and link between the sources of rare metal magmatism and plume-related processes in Central Asia and Baltic Shield regions as well as the petrology of lamproites from Eastern Priamurye and Antarctica were examined. Geochemical data on Ca-carbonatites, mantle xenoliths from the Siberian Craton, Primorye and Colorado Plateau, diamondiferous deep-seated rocks from the Achangelsk region and Canada have been described. On the basis of geochemical studies of Cenozoic basalts of the Russian Far East and Korea, the reconstruction of composition and evolution of mantle matter from the transition continent-ocean zone and geodynamic features of this zone development is suggested.

The book is intended for petrologists, geochemists, teachers of Higher Schools and students.

Executive Editor: Alexander Khanchuk

Editorial Council: Yu. A. Martynov, N. V. Vladykin

ISBN 5-8044-0253-6

Far Eastern Geological Institute, 2002 г.

Предисловие редактора

В последние годы в связи с интенсивным развитием гипотезы плюмовой тектоники в мире и России проявился повышенный интерес исследователей к изучению петрологии и геохимии внутриконтинентального магматизма повышенной щелочности. К ним относятся кимберлиты, породы щелочных комплексов, щелочные базальты. Щелочные породы- уникальные образования Земли. С ними связаны крупнейшие месторождения Nb,Ta, Zr,Y,TR, Cu, P и других рудных элементов, а также и уникальные месторождения самоцветов: чароита, Cr- диопсида, дианита. В лампроитах Австралии добываются алмазы. Сложности процессов их образования вызывали многолетние научные споры, которые не утихают и до сих пор. Развитие новых методов исследований постоянно углубляют знания об особенностях их вещественного состава, генезиса, что в свою очередь, позволяет расшифровать глубинную геодинамику Земли.

Решению этих проблем был посвящен международный семинар «Щелочной магматизм и проблемы мантийных источников», прошедший в 2001 году в Институте геохимии СО РАН г.Иркутск. Вместо традиционных малообъемных тезисов напечатаны заказные доклады до семинара на английском языке, а после семинара - на русском языке. Этот метод оправдал себя и в настоящее время эти книги пользуются большим спросом .

Второй семинар по этим проблемам проведен в этом году в ДВГИ ДВО РАН в г. Владивостоке в 2002 году. В заказных докладах данного сборника рассмотрены вопросы зарождения плюмов и динамика их движения к поверхности, проблемы образования рудных формаций, связи источников редкометального магматизма с плюмовыми процессами для Центральной Азии и Балтийского щита, рассмотрена петрология лампроитов Восточного Прианбарья и Антактиды. Приводятся данные геохимического изучения Са-карбонатитов, мантийных ксенолитов Сибирского кратона, Приморья и плата Колорадо, алмазоносных глубинных пород Архангельской провинции и нетрадиционных источников алиазов в щелочных минеттах Канады. На основании геохимического изучения кайнозойских базальтов российского Дальнего Востока и Кореи сделана попытка реконструировать состав и эволюцию мантийного вещества зоны перехода континент – океан, геодинамические особенности её развития.

Мы надеемся, что подобные встречи ученых по генетическим вопросам глубинного магматизма будут продолжены и такие семинары станут традиционными для Сибирского региона, как геохимические школы щелочного магматизма в Москве.

Председатель оргкомитета

Член-корреспондент РАН

А.И.Ханчук

CONTENTS

1. Letnikov F. A. Deep Fluid Systems of the Earth and Problems of Ore Formation	5
2. Kovalenko V, L. Yarmolyuk V. V., Vladykin N. V., Kozlovsky A. M. Problem of plumes and their bearing on sources of rare-metal magmatism in Central Asia	29
3. Arsamastsev A. A., Bea F., Anamastseva L. V, Montero P. Devonian plume magmatism in the NE Baltic shield: rare earth elements in rocks and minerals of ultrabasic alkaline series as indicators of magma evolution.	51
4. Kvgarko L.N. The Role of sulphide-carbonate-silicate and carbonate-silicate liquid immiscibility in the genesis of Ca-carbonatites	82
5. Vladykin N. V. and M.I. Lelyukh Lamproite rocks of the eastern Anabar region	95
6. Okamura S. and Martynov Yu. A. Cenozoic volcanism of Far East Russia: the relative importance of subcontinental lithosphere and asthenospheric mantle	113
7. Mikhalsky E. V. and Sheraton J.W. Antarctic lamproites: an overview	120
8. Kulikov V.S. and Kulikova V. V. High-magnesian volcanic rocks of the Precambrian in Russian Fennoscandia	137
9. Martynov Yu. A. and Lee Dong-Woo. Cenozoic Basaltic Volcanism of South Korea	154
10. Spetsius Z. V. Evidence for the resemblance of the subcontinental lithospheric mantle in the areas of kimberlite-lamproite magmatism: constraints on the evolution of the Siberian craton	173
11. Gornova M.A. and Solovjeva L.V. Application of rare element composition of garnet and clinopyroxene from peridotite xenoliths. (Udachnaya kimberlite pipe) for modelling of the primitive mantle melting.	190
12. Ashchepkov I. V., Vladykin N.V., Mitchell R H., Coopersmith H., Garanin V. C., Saprykin A. I., Khmelnikova O. S., Anoshin G. N. Geochemical features of the minerals from the heavy concentrate from KL-1 (Kelsey lake) kimberlite pipe, State Line, Colorado: petrologic reconstruction	203
13. Sablukov S. M., Sabtkova L.I., Verichev E. M., Essential types of mantle substrate in the Zimny Bereg region in connection with the formation of kimberlite hosting rounded and flat-faced diamonds	215
14. Shehukin V. S., Sablukov S. M., Sablukova L. I., Belousova E. A., Griffin W. L. Late Vendian acrial alkaline volcanism of rift type in the Zimny Bereg kimberlite area (<i>Arkhangelsk diamondiferous province</i>)	235
15. Askchvpkov I. V., Saprykin A. I., Gerasimov P. A. , Khmelnikova O. S., Cheremnykh L.V., Safonova I. Yu., Roskazov S. V., Kutolin V. A., Vladykin N. V. Petrochemistry of mantle xenoliths from Sovgavan Plateau, Far East Russia	246
16. Voinova I. P. and Prikhodko V. S. Meymechites in Central Sikhote Alin	257
17. Nivin V. A. and Ikorsky S. V. Some genetic features of the Lovozero rare-metal deposits (NW Russia) as it follows from noble gas (He, Ar) isotope abundances	265
18. Makagon V.M. and Zagorsky V. Ye. Deep magmas of rare-metal pegmatites in Precambrian riftogenic structures of the Siberian platform southern margin (Eastern Sayan Mts, Russia)	290
19. Goryachev N. A. and Khanchuk A.I. The origin of Late Cretaceous alkaline granitoids and basalts in the Upper Kolyma River area (the Slab Window tectonic model)	299

DEEP FLUID SYSTEMS OF THE EARTH AND PROBLEMS OF ORE FORMATION

F. A. Letnikov

Institute of the Earth's Crust, S D. R A S, Irkutsk,

Abstract—A fundamentally new model is proposed for the generation of heat and ultradeep fluids in the Earth's liquid core. Considering the rheological properties of the liquid core (viscosity from 10^3 - 10^5 to 10^7 - 10^9 poises), pressure and temperature gradients, and relative rotation velocities of liquid layers with different viscosities, heat is concluded to generate as a result of internal and external friction. That is, a mechanism for transformation of gravitational energy of the Sun into heat in the rotating liquid core of the Earth is proposed. Heat generation causes explosions and is accompanied by plumes developed in the steady-state regime and superplume outbursts in case loss of stability. The separated gas plumes possessing high potential energy ($P_{fl} > 1300$ kbar and $T > 4000^\circ\text{C}$) burn through the mantle reaching the upper lithospheric layers where they cause melting and formation of ore-magmatic systems. The ascending plumes and superplumes are inherently enriched in C and S, which results in the formation of carbonatite magmas and sulfide accumulations in the upper mantle. Thermal activation of asthenospheric layers at the base of continental plates results in concurrent processes related to plumes and fluid systems of the asthenosphere of various maturity and various ore and geochemical characteristics.

INTRODUCTION

Fluids play a crucial role in the processes of rock and ore formation. The Earth's lithosphere was formed through the global degassing of the planet. During this process, tremendous amounts of matter were removed from the interior into the upper lithospheric levels and beyond the lithosphere. Degassing of the outer mantle shell resulted in the three-layered structure of the continental lithosphere: granite-gneiss layer, depleted mantle, asthenosphere. The term "fluid" refers to a predominantly gaseous, water-gas, water, or vapor medium composed of fluid components in combination with rock-forming ore, and other components and residing or moving within lithospheric rocks. The fluids of deep-seated processes occurring at $T > 400^\circ\text{C}$ are represented by gas mixtures. Gas mixtures are compressible, and at great depths their density may be very high. Consequently, they are unique heat carriers that can accumulate a considerable amount of heat energy in a relatively small volume of compressed fluid. Thus, the study of fluid conditions of endogenous processes involves the study of heat sources of these processes and the genesis of heating-transporting fluid systems [26,27].

Recent geophysical data on the interior structure of the Earth demonstrate unambiguously that the major and largest fluid-bearing systems are the asthenosphere and the outer liquid core, which are clearly distinguished by geophysical methods. They generate the most intense fluid flows, providing the basis for all endogenous systems developing in the upper horizons of the

lithosphere. Recent achievements in geochemistry, petrology, and geophysics have cast doubt on the significance of radioactive decay in the formation of global heat flow. This is especially true with respect to the mechanism of heat pulsation in the Earth's history, accompanied by extensive endogenous processes [36,35,4]. The thesis on the importance of deep-derived fluids and the outer core of the Earth in the generation of the planetary heat field seems to be adequately substantiated.

THE EARTH'S OUTER CORE

The Earth's outer core extends from the depth of 2900 km to 5150 km, i.e., over 2250 km. It is a high-gradient system, whose physical parameters vary from top (the boundary with the mantle) to bottom (the boundary with the solid core) as follows: P , from 1350 to 3300 kbar; T , from 4000 to 5700°C; viscosity, from 10^3 - 10^5 to 10^7 - 10^{10} poises; and density, from 9.9 to 12.5 g/cm³. In addition, there is a

Avsyuk [4] emphasized that the solid shell and liquid core might have different rotational velocities. Similar relationships might be characteristic of the inner core-liquid core system. Since the inner core is suspended in the liquid core, its connection with the bulk Earth may be considered not rigid. Taking into account that the orbital motion of the Earth accelerates or decelerates, the cyclicity of its motion within the Earth-Moon system (365 d.), periodic rotation around the barycenter (27.5 d.), and longer periodic movements within this system (18.6, 8.85, and 6 y.) imply suggestion on the presence of perpetual external disturbances affecting the Earth and its interior zones. The Earth and its core

function in an oscillatory regime. The Earth, Sun, and Moon together make up a nonsteady-state oscillatory system with a transition from linear to nonlinear development of processes. Geomagnetic boundary layer in the lower mantle (D_2), which extends from 2870 to 2900 km, with physical characteristics that differ from those of the outer core: density of 5.5 g/cm³ and viscosity of 10^{20} poises [8]. This boundary zone shows a stepwise change in density and viscosity, which could have important consequences, as will be discussed below. Thus, the outer liquid core of the Earth is bounded by the mantle and the solid core (Fig. 1).

It is assumed that one of the heat sources in the Earth's core is radioactive decay or the latent variations suggest distortions of the steady-state regimes, while the nonlinear character of these variations suggests instability of the system as a

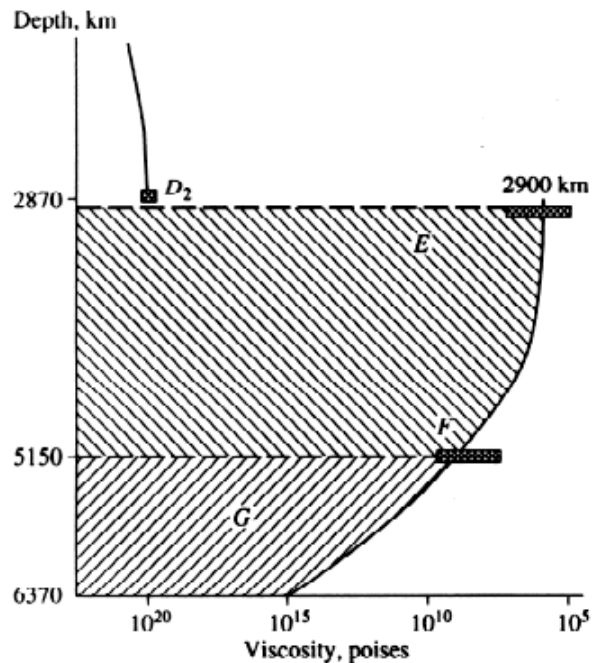


Fig. 1. Variations of viscosity in the Liquid (E) and solid core (G) and in the adjacent zone of the mantle (D_2)

whole [4].heat of solid core crystallization at the expense of the enclosing liquid. Since the core diurnally rotates together with the Earth, the difference in the rheological properties of the outercore and mantle on the one hand, and the solid core and liquid core on the other hand inevitably results in the drag of a quasi-flow on the boundaries of these media and frictional heating along the whole perimeter of these boundaries. Moreover, since the density, T , P , and viscosity of the outer liquid core change (the latter parameter, by 4-5 orders of magnitude) throughout the section, there is an inevitable stratification of the viscous matter of the outer core into zones with different densities and viscosities (Fig. I). This phenomenon results in the formation of the layers on mega-, macro- and micro-scales moving with different velocities relative to each other, in the rotating mass of the outer core. Eventually, a great number of melt bands with different viscosities appear in the section of the outer core. Friction of low-viscosity matter at the boundaries with the mantle and the inner core, as well as between the bands with different viscosities within the

outer core results in heat generation. Taking into account the tremendous volume of the outer core, the major contribution of heat generation there will be result from the interior friction between the layers of low viscous substrate moving relative to each other. Given the size of the outer liquid core and the distance of more than 2000 km between its upper and lower boundaries, it is evident that their velocities will be different. Because of this, a velocity gradient, $\Delta V/\Delta n$, forms within the section of the outer core, where Δn is the layer size. This gradient shows the change of absolute velocity value per per unit length in a direction perpendicular to the velocity vector, i.e., to liquid layers. According to the theory, the existence of a velocity gradient between adjacent liquid layers results in the appearance of interior frictional forces. According to Newton, the shear stress (τ) of interior friction forces is proportional to the velocity gradient, $\tau = \eta \Delta V / \Delta n$, where η is the coefficient of interior friction or viscosity of the medium. Thus, the greater the velocity contrast between separate layers and the larger the number of such layers, the higher is the value of friction and the scale of heat generation due to friction. The degree of friction between layers depends on dynamic viscosity, H , which is the quotient of the tangential force (F) necessary to maintain the velocity gradient between two parallel layers of flowing media equal to one and, thus, the contact area of these layers:

$$\eta = F / (dV/dL)\Delta S,$$

where F is the module of inner friction force between liquid layers, $\Delta V/dl$ is the module of the velocity gradient, and ΔS is the contact area of the liquid layers. Dynamic viscosity is measured in Pascals per second by second (Pa s). Kinematic viscosity $\{V\}$ is equal to the ratio of dynamic viscosity and density (p) of the matter: $V = \eta/p$, m^2/s or mm^2/s , where one square meter per one second is the kinematic viscosity of the medium with a dynamic viscosity of 1 Pa s and a density of 1 kg/m^3 [39].

Thus, the dynamic viscosity is primarily a function of the interior friction between the layers of flowing medium. The layers composing the outer liquid core might be continuous or discrete, but in either case the huge size of the liquid core results in a total contact area of tens of millions of square kilometers.

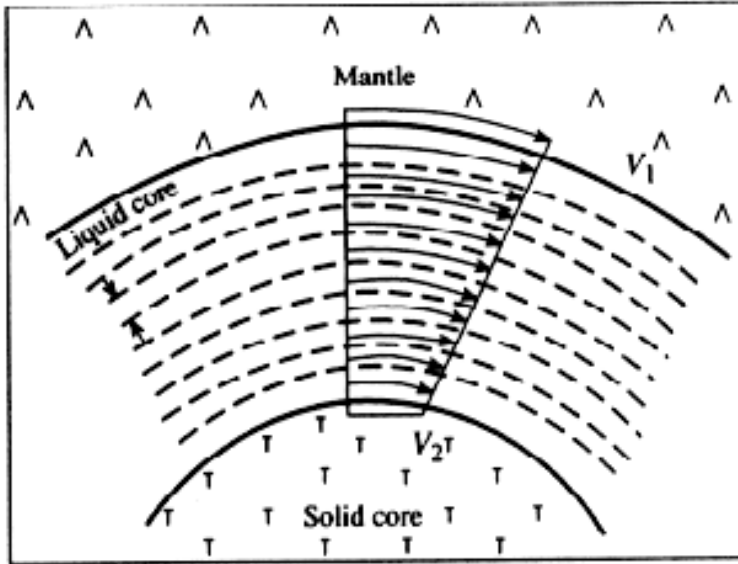


Fig. 2. A scheme of heat generation due to friction in the liquid core of the Earth (see text for explanation).

if the velocity of the solid mantle at the boundary with the liquid core is V_1 and that at the boundary with the solid core is V_2 , then $V_1 \gg V_2$. Velocity distribution in the intermediate layers of the liquid core decreases from the outer to the inner part of the liquid core. In other words, the velocity gradient $\Delta V / \Delta n$ shows the rate of change in absolute velocity value per a length unit in the direction perpendicular to the liquid layers and

correspondingly, to the velocity vector. In a general, this situation is illustrated by Fig. 2.

The question of the existence and number of layers in the liquid core remains unsolved. The following facts support the conjecture on the presence of layers with contrast rheological properties in the outer liquid core of the Earth.

I. The huge size of the outer core (~2250 km) suggests the obvious conclusion that, owing to daily rotation, liquid layers at the boundary with D_2 (2900-3000 km) move faster than the layers adjacent to the solid core (at a depth of ~5150 km). In other words, Such a situation is favorable for the appearance of individual layers in a heterogeneous medium, where T , P , density, and viscosity change within the section considered.

2. In a rotating liquid sphere, stratification of the medium will be inevitable when along a distance of 2250 km pressure increases from 1350 to 3300 kbar; T from 4000 to 5700°C; viscosity, from 10^3 - 10^5 to 10^7 - 10^{10} poises; and gravitational acceleration changes. Moreover, such stratification was experimentally obtained for rotating liquid media with constant physical parameters [40].

3. Since the dynamic viscosity is primarily a function of the internal friction between liquid layers, friction heating will depend on the dynamic viscosity. It is evident that the greater the number of layers with different viscosities in a given section, the higher the degree of heat generation by the melt mass. The released heat will dissipate along the vector T into the enclosing colder mantle (conduction

heat transfer), compensate heat loss, and prolong the conservation of the mobile medium in a liquid state.

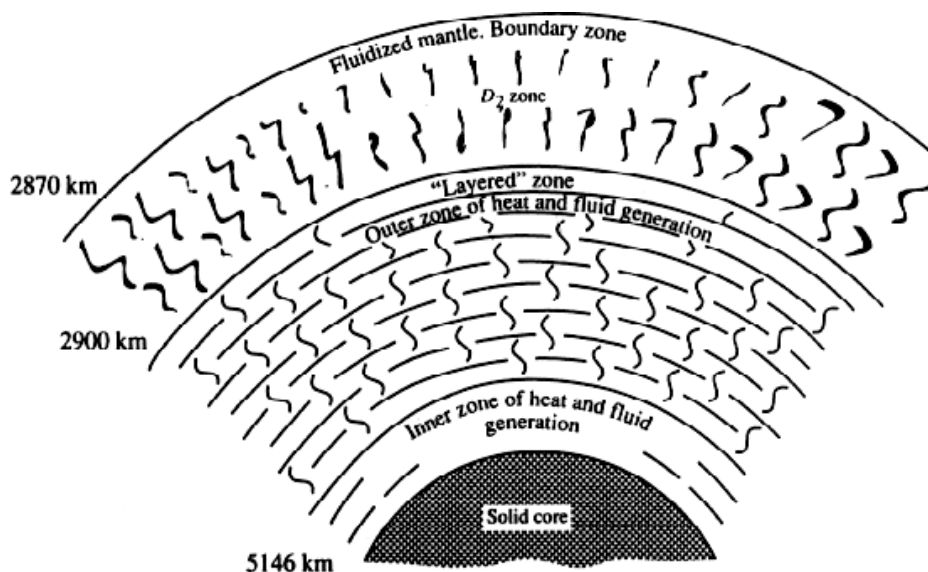


Fig. 3. A generalized model of heat generation in the liquid core of the Earth.

The proposed model and mechanism of heat generation in the outer core of the Earth illustrates realization of the mechanism of the Sun's gravitational energy transformation, forcing the Earth to rotate, into the friction heat energy in its outer liquid core (Fig. 3). In this context, it is evident that as long as the Earth possesses a sufficiently large outer liquid core that generates heat flow, the steady-state heat flux toward its surface will persist.

Composition of the liquid core is controversial in many respects. Independent of the chemical composition of the outer core, its low viscosity is explained to a large extent by anomalous fluidization of the matter. According to experimental data, at P and T approaching the conditions of the liquid core, Si solubility in molten Fe is no higher than 1%, even at unrealistically high oxygen fugacity ($\log f_{O_2}$ from 10^{-1} to 10^{-7}), although there is a tendency toward increasing Si solubility in liquid Fe at increasing P and T [13].

According to some estimates, the outer core consists of three major components: 86% Fe, 12% S, and 2% Ni. Even taking into account the extreme estimates of P and T in the liquid core, the analysis of the carbon phase diagram implies an important conclusion about the possible occurrence of liquid carbon in the liquid core, especially in its deeper part. Besides, H^{\wedge} and other reduced fluid components (CH_4 , CO), considerable amounts of sulfur and carbon may occur in the liquid core. This can have important geochemical consequences, because the problem of S and C sources in deep-derived fluids and rocks is not yet adequately understood.

Ringwood [34] suggested that during the Earth's shells and core formation, FeO was partially retained in mantle silicates, whereas C and H were removed

from the mantle with Fe descending into the core. According to this model, Si occurs in the core in a reduced form, and S content might be as high as 10-15%.

The Earth's outer core probably consists of Fe or Fe-Ni alloy, whose ability to dissolve gases and especially hydrogen is universal. This is equally true for the melts of these metals.

Taking into account the high density of the matter in the liquid core ($>9.9 \text{ g/cm}^3$), of particular importance is the problem of the dynamic compressibility of Fe and its compounds. Furthermore, according to the models of Bullen and Berg, in addition to major Fe, a certain amount of lighter elements must be present in the core [12]. The density of crystalline iron under the standard-state conditions is 7.9 g/cm^3 . Thus, it is necessary to account for the compressibility of solid and liquid iron under P - T conditions of the Earth's core, because otherwise it would be necessary to assume the occurrence of a number of heavy elements with densities $>8\text{-}9 \text{ g/cm}^3$, namely Au, Pt, Os, Ir, Pd, Ni, Ag, etc.

Unfortunately, despite multiple investigations carried out under static and dynamic conditions, there is uncertainty in comparison of the data obtained by different methods that results in incompatibility of these data. One of the major problems here is the subjective estimation of T at the boundary of the Earth's inner solid and the outer liquid cores at $P=330 \text{ GPa}$. The estimates vary from 4000 to 9000°C [12]. Thus, in spite of considerable research, the problem of the Earth's liquid core composition remains controversial, although Fe predominance is accepted by all researchers.

Proceeding from the hypothesis of hydrogen-dominant composition of fluids in the Earth's core and the reliable concept of metallic iron liquid and solid core, the most interesting question concerns the interaction of hydrogen with metals, primarily with Fe. Analysis of the published data revealed no experimental studies on hydrogen/metals interaction at P and T of the Earth's core. The data are limited to P no higher than 2000 MPa and T lower than 2000°C . Nevertheless, general tendencies were established on the interaction of hydrogen with the metals of various groups of the periodic table [3,5]. It should be noted that at increasing temperature, hydrogen dissociates into atoms, and the degree of dissociation is as high as 0.9469 at 1 atm and 5000°C . Thus, it can be suggested that hydrogen occurs in the core mainly in the atomic state and displays a high chemical activity. Interaction of hydrogen with metals under reduced conditions produces various hydrides. However, there is no reliable evidence on the processes of hydride formation under the conditions of liquid core ($P > 1300 \text{ kbar}$ and $T > 4000^\circ\text{C}$). Thus, one can only rely on the general data obtained at lower P and T , which are just preliminary. As far as the liquid and solid metallic core is concerned, of particular interest are the metallic hydrides, which represent solid solutions of hydrogen in Cr, Fe, Ni, Cu, Mo, Co, Mg, Al, Pt, Pd and other platinum-group elements (PGE). All these metals dissolve hydrogen, forming true solutions, with Pd showing the highest hydrogen solubility. The reaction of hydride formation is endothermic and accelerates with increasing T . The set of elements in the series of

metallic hydrides is remarkable. It includes, on the one hand, elements typical of sulfide deposits in mantle-related rocks: Ni, Cu, Cr, Fe, Mg, Co, Pt, Pd, and PGE; and, on the other hand, elements of copper-molybdenum porphyry deposits: Cu, Mo, and Al, which are related to the influence of mantle fluid systems in the continental crust.

As mentioned above, this group of metals shows an increase in hydrogen solubility with increasing T , when the changing hydrogen concentration in metals is proportional to the square root of H_2 partial pressure. In the gas-metal system, the formation of solid solution consumes one atom of gas per 1000 atoms of metal at the highest P and T , whereas the formation of a chemical compound at saturation produces stoichiometric compounds of MeH_2 , MeH , and Me_xH types [3].

The ability of hydrogen to react with the aforementioned metals suggests that hydrogen might occur in great amounts in the metallic core, either dissolved in metals as solid solutions, or forming chemical compounds of the hydride type [37,19].

Acknowledging reliability of the statement on the liquid state of the outer core composed mainly of Fe, and considering its behavior as a consistent system, we must operate within the concept of a high-temperature metallic liquid occurring under ultrahigh pressure. Unfortunately, there are no data on the structure and properties of such metallic liquids.

Proceeding from the described model of frictional heat generation along the boundaries and within the liquid core of the Earth, of utmost importance is the problem of the pulsed ejection of compressed high-temperature fluid accumulations from the liquid core known as plumes. In essence, these are heat explosions manifested on giant scales. First the theory of heat explosion was quantitatively formulated in 1928 by Semenov [35], and then it was developed in the works of other researchers [11, 28].

In the context of our model of heat generation in the liquid core of the Earth, the hydrodynamic problems of the theory of heat explosions considered by Merzhanov [29] become the most interesting. In fact, a heat explosion is such a rapid emission of heat in condensed or non-condensed media, when the mechanism of conductive heat transfer is unable to remove heat from its generation zone. This definition suggests that the heat explosion phenomenon is accompanied by a gas-phase release, which is a heat carrier.

Applied to a moving liquid in the outer core of the Earth, the hydrodynamic problem of heat explosion is reduced to the internal-friction-generated heat that cannot be opportunely removed into the overlying mantle, which results in a nonlinear increase in T . The increase in T under isobaric conditions results in the decrease in gas solubility in a melt, and the increasing tendency of its separation into an independent phase. Accumulation of gas and its separation in a melt mass stimulates instability of the system and ejection of the gas accumulated from the liquid core into the mantle. This is the mechanism of plume formation and outburst from the liquid core. For the moment, this generalized model does not account for

chemical reactions that accompany this process and can substantially increase the energy potential of the plume.

Such a model helps explain the mechanism of pulsed plume separation from the liquid core, whose character is believed to be either deterministic [9] or stochastic [23].

A number of authors distinguished the periodicity of endogenous processes in the crust and mantle. This work reflects the search for reliable criteria for discrimination of the mechanism of deep-seated “heat machine” action producing outbursts of heat energy from the Earth's interiors. The studies of terrestrial magnetic field inversions in the context of the changing interaction character of solid and liquid portions of the Earth's core [4] pursued the same goal. Conflict of opinions, when some researchers [38] relate the frequency of magnetic inversions with rearrangements in plate kinematics, whereas the others [20] argue against the relationship between magnetic inversions and mantle plume activity, caused us to abstract from these opinions and approach the processes in the core from the point of synergetics.

The liquid core of the Earth is an open, nonequilibrium, nonlinear, dynamic system [4,1]. According to our model, heat release due to internal friction in the liquid core is also nonlinear. Changes in the heat regime under isobaric conditions are accompanied by changes in entropy production in the system, which is expressed through the universal evolutionary criterion of an open system far from equilibrium, $\delta_x \sigma$ where σ is the local entropy production in the system [14]. The stability condition for a steady state far from equilibrium is $\delta_x \sigma > 0$. Figure 4 shows various situations of entropy (S_i) changes in an open system. The areas of steady states are distinguished (C_1 , C_2 and C_3), which are characterized by positive fluctuations of the local entropy production ($\delta_x \sigma > 0$). Such fluctuations disappear shortly after their generation owing to the principle of minimum entropy production. After fluctuation, the system relaxes to the initial steady state (arrows on Fig. 4, $\delta_x \sigma > 0$). In other words, this is the region of the formation and relaxation of fluctuations, and the steady state in general can be characterized as stable if entropy production is not a function of state [23].

It is known that a steady-state system continuously exchanges matter and energy with the environment and is characterized by the presence of constant gradients. The maintenance of a steady state requires a continuous input of free energy. In the framework of a given steady state, the rate of irreversible processes occurring in the system is quasi-constant and the work of the system is directed toward its conservation in the steady state.

Quite a different situation occurs with the appearance of negative fluctuations, when $\delta_x \sigma < 0$, which characterizes the instability of a steady state. In such case, the whole system loses stability over a certain time interval, and disturbances of the energy state and changes of gradients occur in the system. After some period of time, the

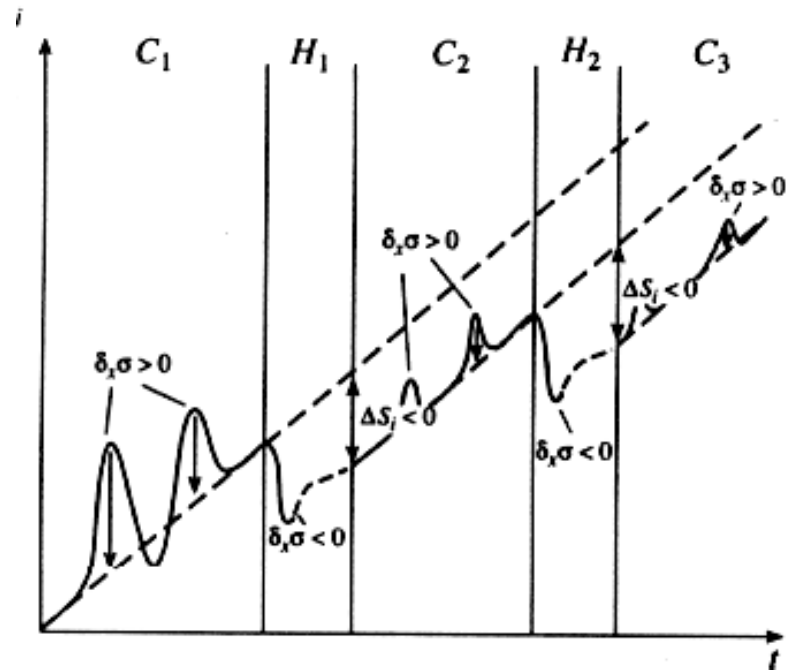


Fig. 4. Changes in entropy (S_i) and entropy production ($\delta_x \sigma$) in steady states (C_1, C_2, C_3) and at the loss of system stability (H_1 and H_2).

system passes into a new branch of development characterized by a new steady state, when entropy production in the system due to irreversible processes is equal to $\Delta S_i < 0$, which indicates an increase in system ordering and formation of new structures in it [14]. Returning to the liquid core of the Earth and proceeding from the described model of a nonlinear open system, we come to the definite conclusion that two fundamentally different types of states are possible in the Earth's core: steady-state and unstable. The energy potentials of magnetic field inversion and plume activity are incomparable [4,1] and are connected with quite different states of the core.

In our opinion, normal fluctuations in a steady-state regime of the liquid core correspond to separation of moderate-scale plumes. Such a process is possible at a certain periodicity for the given steady state. It should be clarified that the frequency of fluctuations and their energy potential will change in geologic time owing to changes in the energy potential of the core. The disturbance of the steady-state regime and transition of part of the core into an unstable state will be manifested in the formation of superplumes [41,8,39], which transport tremendous amounts of heat energy into the upper lithosphere.

Magnetic field inversions are probably not related to the process of plume formation and are caused by the repeated stochastic loss of stability of the Earth's solid core.

PLUMES

Disturbances of the steady-state regime of the outer core are accompanied by heat explosions with spontaneous extensive outbursts of gases and the formation of superplumes on this basis. In the context of self-organization theory [18], heat explosions at the liquid core-mantle boundary may be classified as regimes with exacerbation. The regime with exacerbation is heat transport in a medium with constant heat conductivity under the conditions, when at the boundary of a medium temperature or heat flux approaches the infinity in a finite time interval of exacerbation.

Considering the heat explosion phenomena in liquid core in terms of synergetics, it is evident that nonlinearity results in the new nonexponential laws of instability growth and the formation of new structures, which are represented by plumes. The nonexponential character of attenuation of any heat disturbances is a consequence of system transition into the domain of nonlinearity, when instability occurs and processes of self-organization and formation of new structures take place in open nonequilibrium dynamic systems. One of the elements of such structure-formation is fluid separation from the matrix, represented by silicate or metal-based melt in the liquid core.

Taking into account P-T parameters of the liquid core, it is evident that a gas-dominant phase is separated with plumes at $P > 1300$ kbar and $T > 4000^\circ\text{C}$. Interaction of such energy-rich fluid with the lower mantle will result in rock sublimation into the gas phase. It should be pointed out that in this case the process is nonequilibrium. This is a unidirectional irreversible process of “burning” of the mantle by an ascending gas jet.

Unfortunately, there is no experimental evidence on the solubility of elements in ultracompressed high-temperature gases in dynamic systems. A few studies, which used concentrated sources of energy (lasers, electron and ion beams, shock and electromagnetic waves, etc.), do not provide the necessary information for substantiated conclusions on the quantitative parameters of concentration in high-temperature compressed gases in the P and T range under consideration [6]. The problem of saturation of such super-fluid by rock components remains unsolved. It is certain that, on the one hand, the concentration of these components in gas will increase and its ability to dissolve (gas capacity) will decrease. On the other hand, the volume of gas mixture will increase at ascent and decompression, which will increase the capacity of the ascending plume to consume material of burned rocks [40]. Moreover, it is necessary to take into account that as long as the plume is connected with the parental liquid core via a conduit, a new portion of super-fluid will be supplied, which will increase its energy potential and promote its further movement into the upper mantle levels. According to our model, separation of a plume or a superplume from the liquid core may be accompanied by a series of heat explosions and the formation of a high-energy gas accumulation.

In such case, the gas flow will “burn” the mantle and simultaneously will be enriched in the elements of the solid mantle. The process of sublimation of the lower mantle matter will consume large quantities of heat energy, i.e., the process will be endothermic. At first sight this circumstance seems to play a negative role in the development of the plume, because high-energy consumption must result in its degradation and disappearance. Nevertheless, the process of chemical interaction of a reduced hydrogen-dominant fluid with oxygen-bearing matrix will be accompanied by exothermic reactions, which will compensate a significant portion of the heat loss. In other words, a hydrogen plume sublimates oxygen-dominant material (in mantle rocks, oxygen accounts for 60 to 80% of the volume of rock-forming minerals) and compensates for the loss of heat energy at the expense of exothermic reactions of hydrogen and oxygen. Realization of such a mechanism results in the transition of a primary hydrogen plume into a hydrogen-water one, whose gas phase contains volatile compounds of the aforementioned components, primarily, Si, Mg, Fe, S, and Ni, and to a lesser extent, Al, Ca, Na, Cr, Mn, Ti, etc. The input into the plume of sublimates from the lower mantle material “burned” by the gas jet during the ascent of such plume will result in the increase of its volume, and compensation of the heat energy loss. No less important is the decrease in viscosity of the heated environment of the plume if, of course, it is not limited by the processes of phase transition and formation of denser phases. Besides exothermic effect, the interaction mechanism of hydrogen and oxygen from the lower mantle

minerals will have a considerable petrologic significance, namely, enrichment of the plume head in H₂O. This factor plays a crucial role in the increase of P_{H_2O} in the frontal part of the plume, because at the transit from sublimation to melting of the matter the increase of P_{H_2O} is responsible for the decrease in solidus temperature of the melts generated therein.

Remember that the melting of rocks is accompanied by an increase in volume (+ ΔV). The dependency of melting temperature on the external pressure is specified by the Clausius-Clapeyron equation:

$$dT_f / dP = \frac{(V_L - V_S) T_f}{ML_f} ,$$

where T_f is the temperature of fusion; ML_f is the molar latent heat of fusion, i.e., the amount of heat consumed at the transition of one mole of solid matter into the liquid state; and V_L and V_S are the molar volumes of liquid and solid, respectively. Temperature and heat of melting are rather approximately connected by the relationship $ML_f = 2.2T_f$. Accordingly, the molar heat of sublimation is the amount of heat adsorbed at the transition of one mole of solid matter into the gaseous state. Sublimation requires much more energy than melting, because

sublimation heat (L_S) is equal to the sum of melting heat (L_f) and heat of evaporation at the same temperature v):

$$L_S = L_f + L_v.$$

The increase of fluid P and T will always result in an increased amount of sublimated matter. Besides, sublimation is greatly controlled by the plume's gas phase composition, being directly related to its enthalpy (H) and free energy (G_{TP}).

Melting of the mantle matter is also an endothermic process accompanied by heat energy consumption. This process, however, is unidirectional, and exothermic reactions of fluid component dissolution (H_2O , H_2 etc.) in a newly formed melt cannot compensate for the decrease of heat energy due to rock melting.

In other words, if the process of mantle matter gas sublimation is to some extent of compensational and energy-saving character, the process of melting is energy-consuming and is limited by P , T parameters of the fluid on one hand, and mantle matter composition, on the other hand. Letnikov [22] demonstrated that along with the normal volume melting of silicates, under certain conditions, contact and mechanical melting inclusive, the mechanisms of pre-melting are realized. In the rock in which these two processes occur, they bring up the same effect – the decrease of the rock's strength and viscosity. In other words, contact and mechanical melting phenomena could take place in the mantle matter during the mantle plume ascent. In any case, these processes result in the decrease of surrounding rocks' viscosity and the increase of the plume's velocity as it ascends throughout the lithosphere.

Thus, the plume's movement through the mantle is accompanied by two processes: sublimation of solid rocks, with partial compensation of heat energy of the plume by exothermic reactions between the reduced gas components and the oxygen of sublimated rocks, and complete or partial melting of the upper mantle matter proceeding with predominant consumption of heat energy. The melting zone in the plume head is a sort of peculiar heat trap, where, along with heat consumption due to rock melting, the fluid components are dissolved in the newly formed melt (Fig. 5).

The zone of melting of a formed in the plume head can attain substantial sizes, and itself plays the role of heat anomaly. Its durable existence is supported by the heat energy accumulated in the melt and inputs of heat and fluid from the lower plume.

Letnikov and Dorogokupets [26] pointed out that heat capacity of the gas composed of H_2 ,

He, N_2 , CH_4 , and CO and launched from the depth of 2900 km is several orders of magnitude higher than the enthalpy of peridotite melting under T - P conditions of the upper mantle. That is why, the heat energy of such gases is sufficient to melt the upper mantle rocks and to cause destruction of the upper

lithosphere horizons (Fig. 6). There is, however, a certain limitation. In accord with the Clausius-Clapeyron equation for melting:

$$dP / dT = \Delta H / T \Delta V,$$

where the decrease of total pressure ΔP and the increase in volume ΔV at melting are closely related. This fact is of special significance for silicate rocks, whose melting always results in a volume increase. Since melting occurs with an increase in volume, the process is possible only if the pressure of the melt is higher than the lithostatic load of overlying rocks.

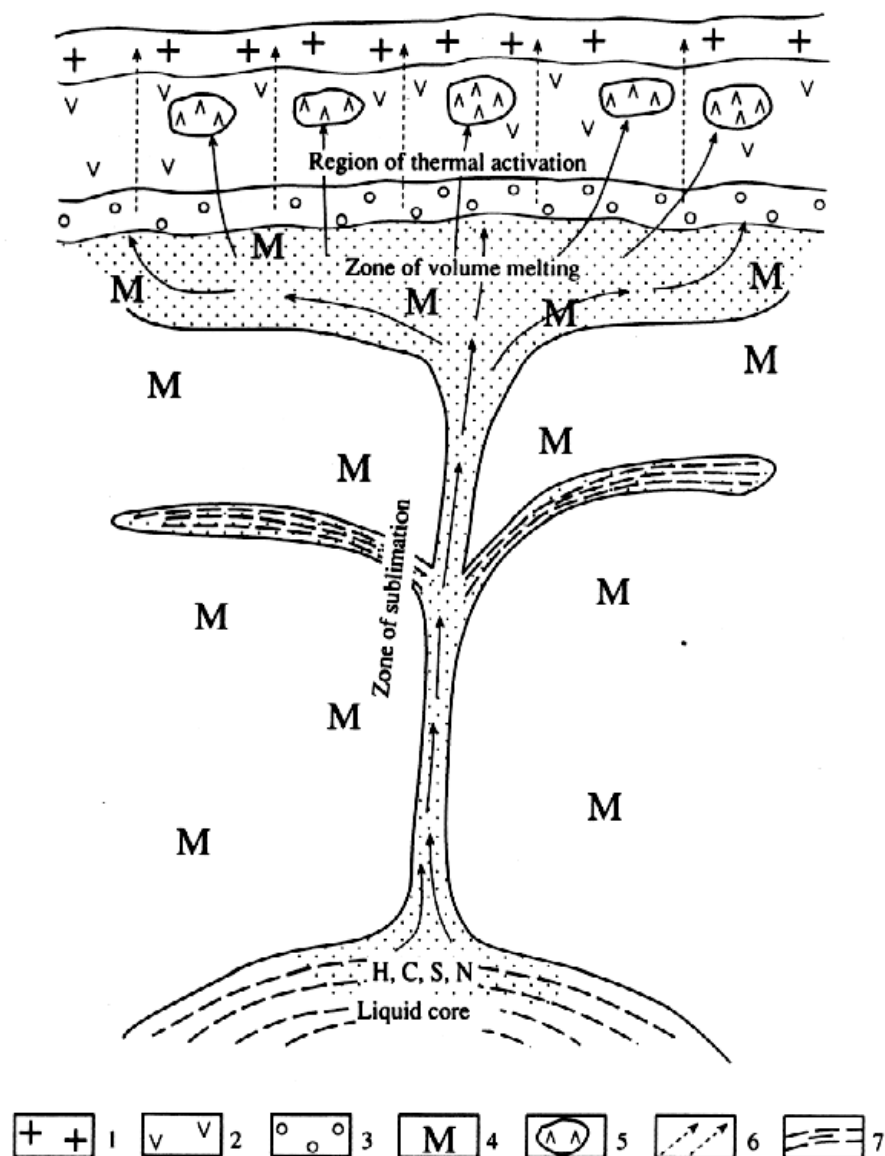


Fig. 5. A generalized model of a plume in the lithosphere. (1) Continental crust; (2) depleted mantle; (3) asthenosphere; (4) upper mantle beneath the asthenosphere; (5) melting zones in a subcrustal layer; (6) pathways of fluid ascent from the asthenosphere; (7) zones of possible contact and mechanical melting in the mantle.

Thus, specific critical levels must exist in the mantle section, where the processes of extensive melting of material are forbidden. This is mainly controlled by total pressure of the overlying rock column. Any processes in the mantle tending to decrease total pressure induce melting processes.

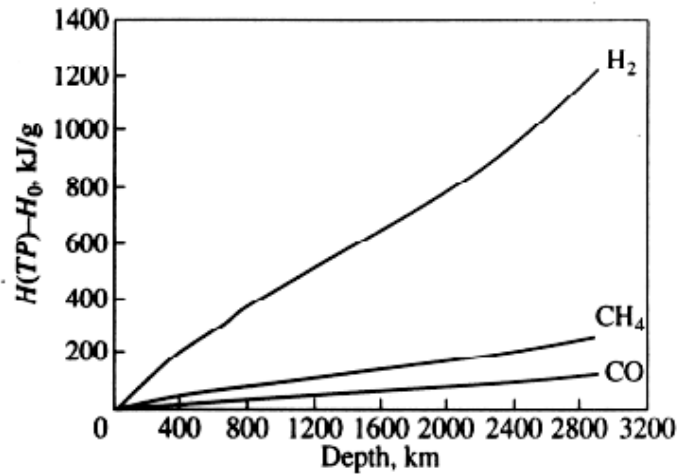


Fig. 6. Energy capacity of H₂ CO, and CH₄ released with a plume from the liquid core.

When this critical barrier is overcome, extensive mantle material melting takes place at $P_{fl} > P_{tot}$. Fluid composition of is of particular importance, especially if the fluid is dominated by H₂ and H₂O.

The widely recognized significance of sulfur in the formation Earth's liquid core, with sulfur concentration being over 10%, is indirectly confirmed by the analysis of igneous, in particular, extrusive processes in the Earth's crust. Indeed, the petrogenetic analysis of igneous systems with abundant sulfide minerals has repeatedly revealed the deficit of sulfur necessary for bonding of tremendous amounts of Fe, Cu, Ni, and other chalcophile elements in sulfides. This peculiar phenomenon, of the Norilsk-type deposits in particular, is still not explained. Even better, it is manifested in the areas of recent volcanism, where sulfur compounds, primarily hydrogen sulfide, are the major components of volcanic gases, especially at a postvolcanic stage, when prolonged and significant ejection of H₂S may continue for many decades after the termination of volcanic activity.

The controversy is that equilibrium solubility of S and its compounds in silicate melts is rather low and insufficient for extensive formation of sulfides on the basis of igneous melts. Completely different is the situation when a plume separated from the Earth's liquid core contains considerable amounts of S⁰ and H₂S. Even upon intense interaction of plume fluids with the mantle matter, H and C will react first, due to their higher chemical affinity to the oxygen of mantle minerals, while S and H₂S will accumulate in the residual fluid. That is why S and H₂S can reach the upper lithospheric levels with plume heads. In the shallow upper mantle or intermediate crustal chambers, these components can participate in country rock melting and react with chalcophile elements forming sulfide

accumulations. In other words, according to this scheme, large sulfur accumulations in form of sulfides or gas jets in volcanic areas can be

Ain apriori considered as relics of the former extensive plumes ascending from the liquid core of the Earth. This scheme explains the giant sulfur accumulations related to igneous and volcanic processes, where S and H₂S, occurring mainly as bubbles or larger concentrations, not only saturate but oversaturate the bulk of the melt. Judging by prolonged functioning of sulfur jets on the Earth's surface ("roaring fumaroles" of the Paramushir Island), it is reasonable to consider the fluid-magma systems connected with prolonged emission of sulfur and its compounds at depth to be the relic fluid systems previously separated from the liquid core together with plumes.

A number of publications describes the mechanism of plume movement into the upper lithosphere. Most of them are based on simplified physical models or the results of model experiments. Among the aspects these experiments studied was determination of the conditions of a deep-derived plume passing through 660-km mantle heterogeneity, when an abrupt change in viscosity occurred. It is manifested in plume configuration, which consists of a thickened head and an extended conduit. These experiments and analysis of geochemical data resulted in the conclusion about the bimodal character of volcanism on the Java Plateau in 122 and ~90 Ma, which was controlled by configuration of the plume that caused mantle melting [17].

Taking into account the tremendous size and great energy potential of the core, it is evident that even small fluctuations in the mass of the liquid core will be accompanied by significant emissions of heat energy, mainly in the form of plumes. Since the liquid core accounts for 31 % of the total mass of the Earth, even small deviations in the state of this dynamic system, which occurs in the diurnal motion around the Earth axis, will be accompanied by energy effects of such a magnitude that their action will affect the state of the Earth's crust and the upper mantle.

PROCESSES OF ROCK AND ORE FORMATION

The record of heat flow action in the Earth's crust is diverse. It includes a wide spectrum of rocks and ores. The heat impact on the lithosphere always causes transformation in the solid substrate: metamorphism, metasomatism, or melting, while the processes of ore generation correspond to a lower hierarchical level both in the scale of phenomena and energy consumption for their realization. Thus, it is reasonable to analyze the effect of superdeep fluid systems on the rocks of the crust and upper mantle from the viewpoint of petrogenesis, assuming that the ore-forming systems are derivatives of the deep-derived fluid systems partially transformed by interaction with the lithospheric matter. The recognition of the fluid flows nature is also complicated by the fact that since the processes of mass transfer from planetary interiors toward outer shells are driven by P and T

gradients, the planet as a whole is a nonlinear dissipative hypersystem, where multiple subsystems of mass transfer at lower hierarchical levels operate simultaneously. Within a single plate, several fluid megasystems of various natures may occur simultaneously, being different in energy potential, ore and geochemical characteristics, and physico-chemical parameters. Taking into account that derivation of igneous rocks in the crust and in the mantle needs different heat amounts, it is reasonable to assume that maturing time for such magmatic systems and the related ore-bearing fluid systems is also different.

Grachev [16] proposed the criteria for discrimination between mantle plumes and hot spots. In his opinion, the hot spots result from the within-plate tectonic and magmatic activity, whereas the mantle plumes are manifestations of the within-plate tectonic and magmatic activity related to core and lower mantle processes. Great scales of continental flood and plateau basalt occurrence typical of interaction processes between deep-derived plumes and the lithosphere are among such criteria. According to Anderson [2] and Grachev [16], hot spots are the derivatives of shallow upper mantle fluid systems, showing a different extent of endogenous activity and specific enrichment in trace elements. This, to some extent, suggests their connection with the fluids from asthenospheric layers.

Letnikov [23] demonstrated that asthenospheric layers underlying lithospheric blocks of various maturity have a fluid nature and are the products of irreversible process of the upper mantle degassing.

Figure 7 schematically shows the situation when the unidirectional removal of fluid and

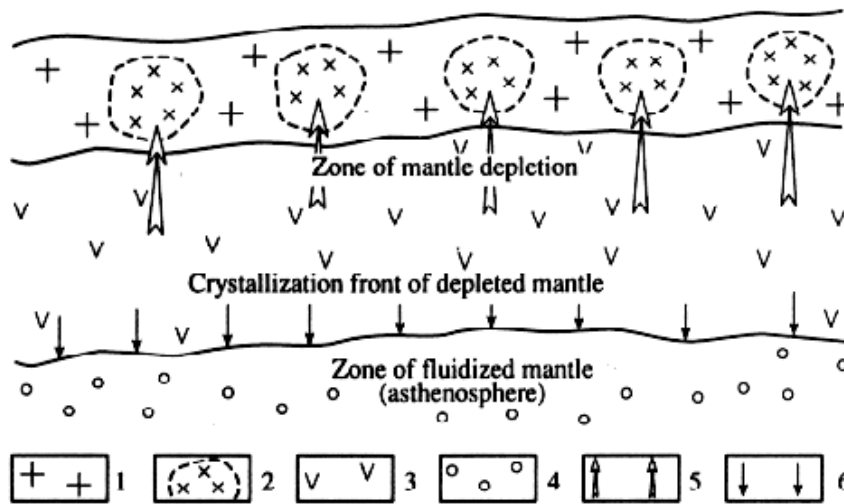


Fig. 7. A scheme of the simultaneous formation of triad granite-gneiss layer-depleted mantle-asthenosphere. (1) Earth's crust; (2) granite-gneiss domes; (3) depleted mantle; (4) asthenosphere; (5) pathways of granitizing fluids and incompatible elements; and (6) ways of squeezing of fluid and super-stoichiometric component by the crystallization front.

incompatible components from the mantle must cause its impoverishment in these components and crystallization of rocks. This results in squeezing of fluid and trace components at the crystallization front and formation of the asthenosphere. In

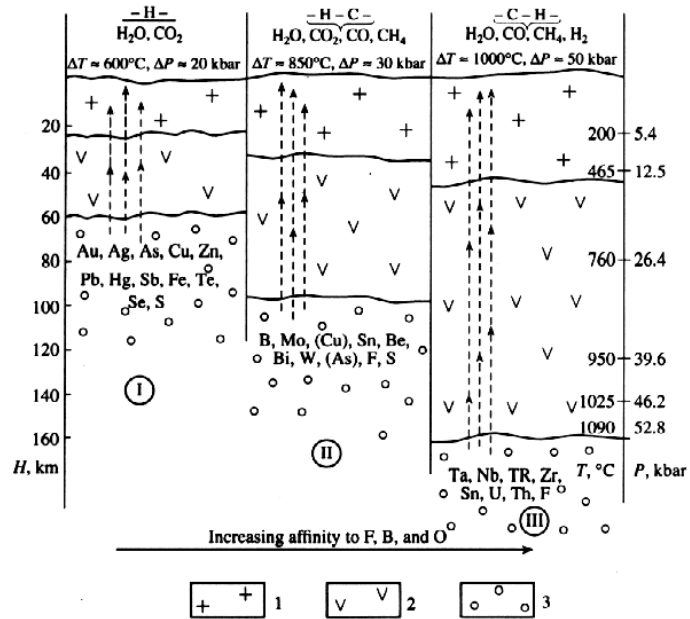


Fig. 8. Fluid and geochemical specialization of asthenospheric fluid systems under lithosphere of various maturity (increases from I to III). (1) Earth's crust; (2) depleted mantle; and (3) asthenosphere.

accord with the maturity of a particular lithosphere, each asthenospheric layer shows individual ore and geochemical characteristics (Fig. 8). In asthenospheric layers underlying continental plates began to form simultaneously with the plates, then with lithospheric thickness growth they moved downward and lost fluid components. This is specifically why the heat flow on depths of several tens of kilometers in contrast to 140-200 km on ancient (3-4 Ga) continents. Within some continents is much lower than that of the oceanic plates,

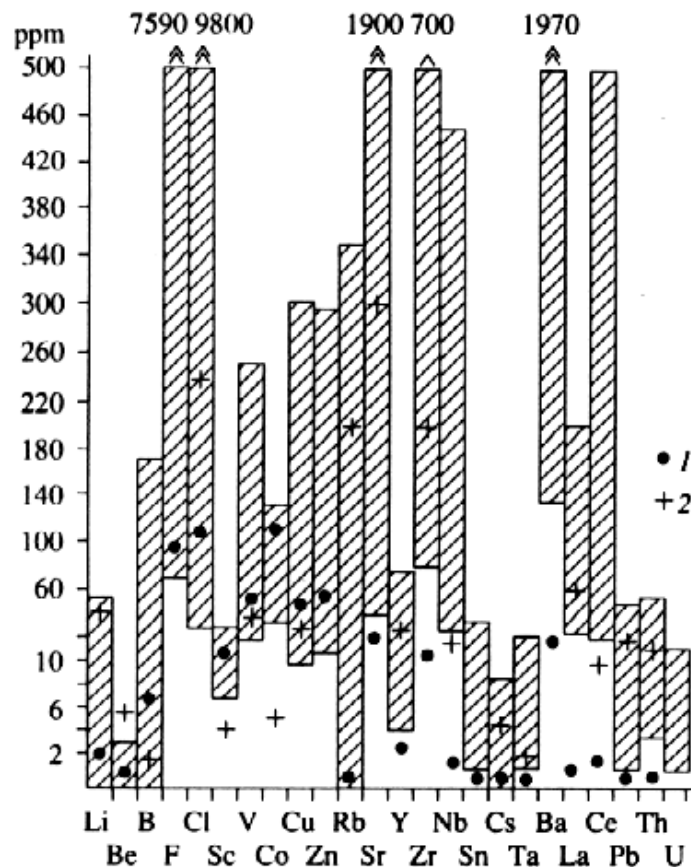


Fig. 9. Trends in the redistribution of ore components at the depletion of the upper mantle. (1) Ultrabasic rocks of the upper mantle and (2) granitoids. Shaded are ranges of distribution in kimberlites as a derivative of the asthenospheric layer.

where the asthenosphere occurs at Archean cratons, the asthenosphere is unusually thin or is even not observed at all. In the latter case, the absence of asthenospheric layer is caused by prolonged processes of its depletion in fluid components, which occurred repeatedly in the course of several billion years [22]. Figure 9 shows the general tendency in redistribution of trace and some fluid components in course of the concurrent processes of granite-gneiss crust, depleted mantle, and asthenospheric layer formation.

The heat affect of a deep superplume on the lithosphere is obscured by the involvement of all available fluid systems into the processes of melting in the crust and mantle. Only the unusually high contents of Mg, S, Cu, Ni, Co, Pt, and PGE in the mantle-derived or crustal melts can be indicative of their primary plume nature.

Correlation between high magnesium content and concentrations of the aforementioned elements suggests their transportation from the planetary interiors together with core-derived plumes.

Taking into account the high energy potential of ultra-deep fluids and their ability to extend laterally in the upper mantle and at the crust base, the inference on their interaction with fluid systems of asthenospheric layers and the relics of the former fluid systems buried in the mantle is quite obvious. All this together with differences in dynamics, fluid regime, and physico-chemical parameters of mantle melting, significantly complicates nature understanding of the fluid systems, whose activity resulted in the processes of mantle melting.

Deep seismic tomography of mantle revealed the zones corresponding to the onset of plume ascent toward the upper lithosphere and the traces of the former degraded plumes. The observed phenomena are responsible for the chaotic nonlinear character of plume-related seismic anomalies [30]. It is evident that throughout the section, from core-mantle boundary to crust base, the mechanisms of plume-derived gas interaction with mantle material may be different. At the initial stage when T and energy capacity of the plume are the highest, the mechanism of sublimation dominates, and the plume is shaped as narrow ascending channel or a slit-like cavity. This was proved by a model and numeric experiments [17,9]. Decreasing energy potential of gas in the plume results in a different mechanism of its ascent. Terminated sublimation results in penetration of high-temperature gas occurring under very high fluid pressure ($P_{ff} > P_{in}$) along the boundaries of mineral grains and the development of contact melting processes [21] with the formation of submolecular melt films, which are able to dissolve fluid components. At this stage, the area of fluid action increases and the basis is formed for volume melting and segregation of considerable melt masses. Extension of plumes at the crust base records the upper levels of significant plumes' influence on the mantle matter mainly through the mechanism of contact melting. That is why, the laterally extended and relatively narrow bands of low-velocity material in the mantle represent the relics of formerly active plumes and superplumes. In accord with the wave theory of stress distribution in pressurized continuous media [23], subhorizontal areas in the mantle distinguished by reduced seismic velocities

reflect the character of the extension-zone distribution in the lithosphere, where superdeep fluid systems are concentrated at the condition $P_{ff} > P_{tot}$ (Fig. 10).

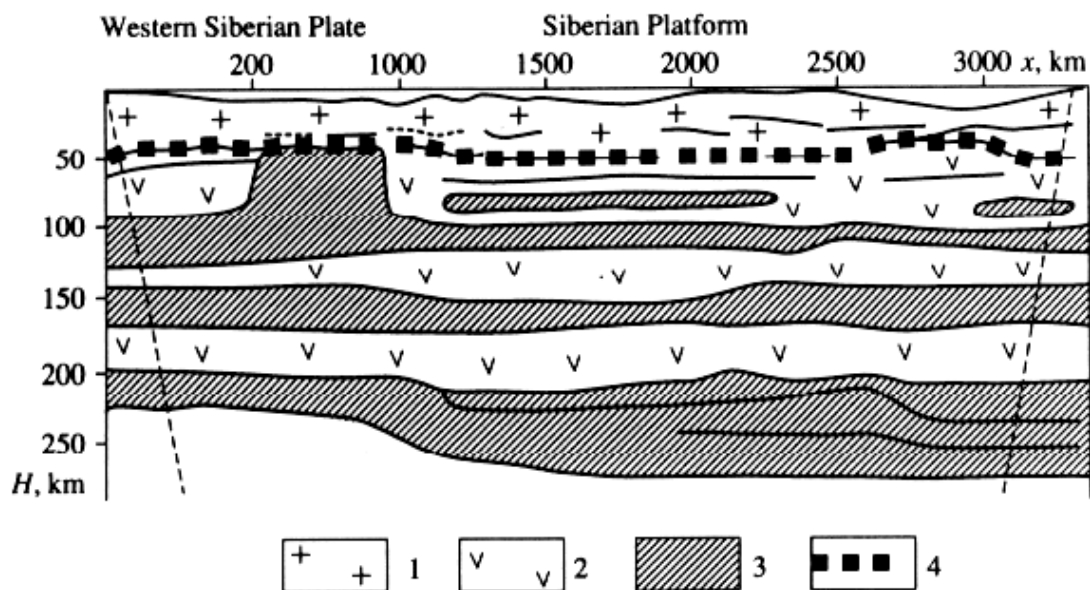


Fig. 10. Typical seismic velocity sections of the upper mantle [33]. (1) Earth's crust; (2) mantle; (3) low-velocity (presumably, fluidized) part of the mantle; and (4) Mohorovicic discontinuity.

In essence, the lateral and vertical mantle heterogeneity is the result of the influence of plumes that did not reach the Earth's surface for various reasons. To some extent, they could represent the relics of ancient plumes buried in the mantle, whose decomposition could proceed both in vertical and horizontal directions. In any case, configuration of plumes and their levels of interaction with the enclosing rocks are controlled by plume mass and energy potential. This is observed in deep tomography. In petrology, the indirect criterion for the energy inventory of plumes assessment is the ratio of Mg/Fe in the mantle-derived melts. Magnesium-rich basalts characterize higher T of melting and, consequently, energy-rich fluid systems.

A heat flow measured at the Earth's surface cannot adequately characterize the total heat flow from the Earth's interiors toward the surface in a particular geologic time. Any melting zone in the mantle or crust is a heat sink adsorbing heat energy carried by fluid. Thus, in the regime of active melting, the zone of melt formation will seal an ascending deep-derived fluid flow that serves as a heat carrier. Only after a sufficiently large magma chamber is formed, can it begin to play the role of heat anomaly generating the excess magmas and fluids. The degradation of the magma chamber causes the heat flow below it to decrease and shifts isotherms to greater depths.

A very different situation is characteristic of fluidization processes in the upper lithosphere or in the crust. In this case, the pathways of plumes are

controlled by tectonic forces breaking up the lithosphere. The existence of weakened tectonic zones promotes relatively rapid fluid ascent

to certain levels in the lithosphere, where they begin actively reacting with the environment. Compositions of fluid and the matrix, which this fluid reacts with control the resulting composition and association of rocks and ores formed during this process. In other words, the fluid systems of asthenospheric layers are relatively autonomous and show little interaction with the enclosing rocks along their way toward the upper lithospheric horizons. This conclusion is supported by high geochemical and ore specialization of asthenospheric fluid systems in the lithospheric blocks of various maturity, which provided a basis for generation of the deposits with strictly specialized characteristics.

The synchronous occurrence of mantle and crustal magmatism is established not only in various geody-namic settings but also in the ocean and in continents. This suggests that in the Earth's geologic history there existed giant superplumes whose heat energy resources were sufficient for voluminous melting of both mantle and crustal materials [7,8,39]. Recognition of a single primary source of energy brings about the conclusion on the diverse fluid system types in the mantle and crust involved into endogenous activity due to the energy supplied by the plumes from the Earth's outer core.

In the context of the problem under consideration, it is obvious that since an active fluid source lies at the base of endogenous rock- and ore-forming processes, the analysis of endogenous activity in the lithosphere is subdivided into two independent aspects.

1. Degassing of the Earth as a cosmic body, formation of the Earth's crust, lithosphere, and asthenosphere as elements of a single process of heat energy dissipation and conservation in the volume of rocks. This scheme distinctly differentiates the elements of regularly occurred magmatism, granitization, metamorphism, and mineralization processes depending on time of a particular geologic block development and depth of an asthenospheric layer occurrence. Letnikov [25] formulated the concept of fluid geochemical lithospheric facies, which control the formation of typical endogenous mineral deposits. Tectonic impulses of lithospheric block activation result in the ascent of asthenospheric fluid systems into the upper crustal levels, which form the basis for a variety of endogenous processes. That is why blocks with similar maturity levels are characterized by similar associations of rocks and mineral deposits.

2. Regular occurrence of endogenous processes in lithospheric blocks of various maturity is distorted by powerful energy impulses of thermal impact on the lithosphere, being, in the first place, characterized by dominated extensive generation of mantle and crustal melts. The areas of these large-scale phenomena manifestation involve lithospheric blocks of various maturity. Numerous observations unambiguously prove that the energy (in essence, fluid) source of all these processes is located deep in the mantle below the asthenosphere and correlates with the influence of deep-derived fluid plumes on the lithosphere.

Besides, a high-energy deep-derived plume may sometimes cause energetic activation of asthenospheric layers underlying the lithosphere. This conditions further occurrence of ore-magmatic systems inherent of the initial lithospheric block. In this scenario of ultra-deep fluid plume systems' influence on the lithosphere, the boundary areas between lithospheric blocks of different maturity show characteristics of both deep-derived plume and asthenospheric layers underlying lithospheric blocks. Plume tectonics that recently came into being is based on abundant geological evidence suggesting giant scales of basic magmatism and lesser scales of felsic magmatism both in the ocean and on continents at the thermal impact duration of several tens of millions years [7,9].

Among geological studies of superplumes, of particular importance is that of Yarmolyuk *et al.* [40], who traced the whole spectrum of the within-plate Phanerozoic magmatism over the vast Siberian platform and its folded framing. Basing on convincing arguments they concluded that in the Early Paleozoic to Cenozoic the within-plate magmatic regions of various age were related to the plumes whose activity was caused by decomposition and heat degradation of the North Asian superplume. Such large-scale generalization was made for the first time. Returning to the author's inferences on "hot" and "cold" plumes, it should be noted that extensive melting in the mantle and crust was accompanied by considerable consumption of heat energy. That is why, any melting zone is a heat trap adsorbing a considerable amount of heat energy. Extensive interaction of a plume with mantle or crustal rocks causes melting and will obviously result in heat degradation of the latter and formation of so-called "cold" plume areas.

The concept that discriminates between the crustal and mantle sources of ore material has formed as an enduring part of the theory of mineral deposits. During the recent decades new data were obtained on isotopic geochemistry of elements in ores and genetically related igneous rocks. Basing on these isotopic data some authors advocate a crustal-mantle origin for the sources of ore matter. They suggested that, owing to various processes, crustal material was transported into the mantle and then participated in the formation of ore-magmatic systems [31]. Due to convergence of isotopic characteristics [10] and diversity of not completely understood factors controlling isotope fractionation, such inferences cannot be considered reliable.

Proceeding from Rb-Sr, U-Th-Pb, Sm-Nd, and Re-Os isotopic characteristics, a number of authors pointed out the prevalence of a mantle component in the formation of deposits related to typical mantle magmatic systems: Khibiny, Lovozero, and Norilsk [31]. These isotopic systems are highly informative; they were tested on a great number of objects. The same authors, however, write that isotopic compositions of C, O, and S from the same series of rocks and ores show considerable variations. This allowed some researchers to argue about significant assimilation of crustal material by mantle magmas and crust-mantle interaction not only in the crust but also in the mantle [31]. Faure [11], however, pointed out that determination of isotopic composition of the mantle carbon was rather problematic.

The processes of isotope fractionation occur even at a very high temperature, and the influence of isotope heterogeneity of the mantle carbon and its possible fractionation result in significant variations in isotopic composition of carbon in carbonatites and diamonds. This is true even to a greater extent for the isotope geochemistry of sulfur and oxygen in complex heterogeneous ore-magmatic systems of the initial mantle origin. The influence of plume fluid systems derived from the Earth's core on ore-magma systems in the upper mantle just adds uncertainty to interpretation of S, C, and O isotopic data.

Having analyzed the available data we were to recognize three major sources of heat energy and ore matter of the Earth.

1. The Earth's outer liquid core, which is a generator of global heat flows and high-temperature plumes composed of reduced gases.

2. Relicts of plumes, which failed to attain the mantle-crust boundary and are distinguished by geophysical methods as laterally extended zones of reduced viscosity through the whole mantle section.

3. The least deep global heat source represented by the fluid systems of asthenospheric layers underlying continental and oceanic plates.

Our ideas asserting that the steady states of the core are changed by the periods of stability loss may correlate with the endogenous activity cycles of planetary character: Wilson supercycles, Bertrand-Shatsky cycles, Stille cycles, etc. [16]. Direct correlation, however, would be a rather rude approximation, as from the point of synergetics and cooperative occurrence of unidirectional processes, analyses of these phenomena should account the influence of cosmic factors [4] and discontinuous-continuous process of lithosphere formation. These processes are manifested in fluid activation of the lithosphere of different maturity at various stages of its formation [23,24]. Perhaps, the continuous linear unidirectional process of the Earth formation as a cosmic body, that follows the inherent and not completely understood regularities, is arbitrarily divided into the cycles involving the processes related to different factors and supplied by different energy sources. Understanding these regularities is an objective for future investigations.

The work was financially supported by the Russian Foundation for Basic Research, project no. 99-05-64169, and the Program of Support for Leading Scientific Schools, project no. 00-15-98573.

REFERENCES

1. Adushkin, V.V., An, V.A., and Ovehinnikov, V.M., Structural features of Earth's internal constitution // *Fiz. Zemli.*, 2000. N. 12. P. 3-26.
2. Anderson, D.L., Hot spots, basalts, and evolution of magma, *Solid Earth*, Drake, J. and Schmitt, L., Eds., New York: Science, 1981. Translated under the title *Sovremennye problemy geodinamiki*, Moscow: Mir 1984. P. 197-217.
3. Archakov, Yu.L., *Vodorodnaya korroziya stali (Hydrogenous Corrosion of Steel)*, Moscow: Metallurgiya, 1985.

4. Avsyuk, Yu.N., Prilivnye sily i prirodnye protsessy (Tide Powers and Natural Processes), Moscow: Ob"ed. Inst. Fiz. Zernii Ross. Akad. Nauk, 1996.
5. Baum, B.A., Metallicheskie dliidkosti (Metallic Liquids), Moscow: Nauka, 1978.
6. Bushman, A.V. and Fortov, V.E., Models for equations of the material state, Usp. Fiz. Nauk. 1983. V. 140, N. 2. P. 177-232.
7. Dalziel, J.W.D., Lamver, L.A., and Murphy, I.B., Plumes, Orogenesis, and supercontinental fragmentation //Earth Planet. Sci. Lett. 2000. V. 178 P. 1-11.
8. Dobretsov, N.L., Periodicity of geological processes and depth geodynamics //Geol. Geofiz. 1994. N 5. P. 5-19.
9. Dobretsov, N.L., Permian-Triassic magmatism and sedimentation in Eurasia as a representation of a superplume. //Dokl. Akad. Nauk. 1997. V. 354, N. 2. P. 220-223.
10. Dobretsov, N.L. and Kirdyashkin, A.G., Glubinnaya geodi-namika (Depth Geodynamics), Novosibirsk. 1994. Jinioz, R., Earth's core, V mire nauki (Scientific American, published in Russian). 1983. N 2. P. 16-27.
11. Faure, G., Principles of Isotope Geology, New York: Wiley, 1986. Translated under the title Osnovy izotopnoi geologii. Moscow: Mir, 1989.
12. Frank-Kamenetskii, D.A., Diffuziya i teploperedacha v khimicheskoi kinetike (Diffusion and heat transfer in chemical kinetics), Moscow: Akad. Nauk SSSR. 1947.
13. Funtikov, A.I., Phase diagram of iron //Fiz. Zemli. N II. P. 70-76.
14. Gessmann, O.K., Wood, B.J., Rubie, D.C., and Kilburn, M.R., Solubility of silicon in liquid metal at high pressure. //Earth Planet. Sci. Lett. 2001 V. 184. P. 367-376.
15. Glandsdorff, P. and Prigogine, I., Thermodynamic Theory of Structure, Stability, and Fluctuations, London: Wiley, 1971.
16. Grachev, A.F, Extended plumes and problems of geodynamics. //Fiz. Zemli, 2000, N 4. P. 3-37.
17. Khain, V.E.. Large-scale cyclicity in tectonic history of the Earth //Geotektonika N 6 P. 3-14.
18. Kumugaiu, J. and Kurita, K., On the late of mantle plumes at density inlurfoces //Earth Planet. Sci. Lett. 2001. V. 179. P. 63-71.
19. Kurdyumov, S.P., Kurkina, E.S., and Tel'kovskaya, O.V., Regimes with intensification in two-component media //Mat. Model, 1989, N 1. P. 34-50.
20. Larin, V.N.. Cipotezft iznachel'no gidridnoi Zemli /Hypothesis or the initially hidride Earth. Moscow: Nedra, 1975.
21. Larson. R.L. and Olson, H., Mantle plumes control magnetic iversal frequency, //Earth Planet. Sci. Lett. 1991. V. 107. P. 437-447.
22. Letnikov, F.A., Granitoidy glybovykh oblastei /Granitoids of block regions. Novosibirsk: Nauka. 1975.
23. Letnikov, F.A., Maturity of Lithospheric Blocks and problems of endogenic ore formation, Clubinnye usloviya elulogelwogo rudoobrawvaniya /Depth conditions of endogenic ore formation. Moscow: Nauka, 1986. P. 16-24.
24. Letnikov, F.A., Sinergetika geologicheskikh sistem /Synergy of geological systems. Novosibirsk: Nauka, 1992.
25. Letnikov. F.A., Fluid Facies of the continental lithosphere and problems of ore formation, Snumovskii sbom'ik-99 /Smirnov Symposium-99. Moscow: Moscow State Univ., 1999. P. 63-98.
26. Letnikov, F.A. and Dorogokupets, P.I., Sinergeticheskie aspect)' sostoyaniya vnutrennego yodra Zemli. Vnatrenee w(hr> Zentli (Synergistic aspects for the state of internal core of the Earth. internal core of the Earth), Moscow: Oh'ed. Inst. Fiz. Zemli, 2000.
27. Letnikov, F.A.. Dorogokupcls, P.I., and Lashkevich, V.V., Energy parameters of fluid systems in the continental and oceanic lithosphere. //Petrologiya. 1994. V. 2, N 6. P. 563-569.

28. Letnikov, F.A., Men'shagin, Yu.V., Lashkevich, V.V., and Dorogokupets, P.I., Comparative energy characteristic of fluid and silicate systems of the lithosphere //Petrologiya, 1997. V. 5, N 6. P. 666-670.
29. Merzhanov, A.G. and Dubovitskii, A.F., Present-day state of the heat explosion theory //Usp. Khim. 1966. V. 35, N 4. P. 656-690.
30. Pinin, V.E.. Wave character of plastic deformation in solid bodies, /v. V'ssh. Uchebn. Zaved., Fiz.. 1990. N 2. P. 4-19.
31. Pushcharovskii, Yu.M. and Pushcharovskii, D.Yu.. Geo-spheres of Earth's mantle //Geotektonika. 1999. N 1. P. 3-14.
32. Pushkarev, Yu.D., Gorokhovskii, B.M., Larin, A.M., et al., The role of interaction between crustal and mantle material //Regional'naya geologiya i metallogeniya. 2000. N 2. P. 73-80.
33. Puzyrev, N.N., Melody i ob"ekty seismicheskikh issledovaniy //Methods and objects of seismic studies, Novosibirsk: Sib. Old. Ross. Akad. Nauk Nauchno-Issled. Tsentr Ob"ed. Inst. //Geol. Geochem. Mineral. 1997.
34. Ringwood, A.E., Composition and Petrology of the Earth's Mantle /New York: McGraw-Hill, 1975. Translated under the title Sostav i petrologiya mantii Zemli, Moscow: Nedra. 1981.
35. Semenov, N.N., O nekotorykh problemakh khimicheskoi kinetiki i reaktsionnoi sposobnosti (On some problems of chemical kinetics and reaction capacity) Moscow: Akad. Nauk SSSR. 1947.
36. Smyslov.A.A., Moiseenko, U.I., and Chadovich, T.Z., Teplovoi redlim i radioaktivnost' Zemli (Thermal regime and radioactivity of the Earth), Leningrad: Nedra. 1979.
37. Verhoogen, J., Turner, F., and Weis. L., The Earth. An Introduction to Physical Geology, New York: Holf. Reinhart and Winston, 1970. Translated under the title Zemlya. Vvedenie v obshchuyegeologiyu, Moscow: Mir. 1974.
38. Vernadskii, V.I., History of minerals of the Earth's crust, librannye sochineniya (Selected Works). Moscow.: 1960. V. 4, N 2. P. 13-14.
39. Vogt, P.R., Changes in geomagnetic reversals frequency at times of tectonic change. //Earth and Planet. Sci. Lett. 1975. V. 25. P. 313-321.
40. Yarmolyuk, V.V, Kovalenko, V.I., and Kuz'min, M.I., North Asian superplume in the Phanerozoic, Geotektonika, 2000, N 5. P. 3-29.
41. Yavorskii, B.M. and Pinskii, A.A., Osnovyfiziki (Fundamentals of Physics), Moscow: Fizmatlit, vols. 1, 2. Zhuze, T.P., Szhatye gazy kak rastvoriteli (Compressed Gases As Solvents), Moscow: Nauka. 1974.
42. Zonenshain, L.P. and Kuz'min, M.I., Paleogeodinamika (Paleogeodynamics). Moscow: Nauka, 1993.

**PROBLEM OF PLUMES AND THEIR BEARING ON SOURCES
OF RARE-METAL MAGMATISM IN CENTRAL ASIA**

Kovalenko V.I. *, Yarmolyuk V.V. *, Vladykin N.V. **, Kozlovsky A.M. *

** Institute of Geology of Ore Deposits, Petrography, Mineralogy, and Geochemistry,
RAS; 35 Staromonetnyi per., Moscow, 109017 Russia, vic@igem.ru*

*** Institute of Geochemistry, SB of RAS, Irkutsk, vlad@igc.irk.ru*

The Central-Asian folded belt (CAFB) is characterized by abundant rare-metal alkaline and lithium-fluorine granites, pegmatites, nepheline syenites, and various carbonatites as well as by some rocks of salt systems (apatite-rich, fluorite-rich and others). These magmatic assemblages are related to within-plate magmatism represented by various alkaline rocks, including mafic and felsic varieties and spanning a broad age interval from the late Riphean to Cenozoic. The long-lived magmatic activity within CAFB derived from the specific character of geodynamic settings within the Siberian Continent and its folded surroundings during the Phanerozoic. In Riphean time, under the action of the superplume, a wide array of ultramafic complexes and the related carbonatites have evolved. Since the end of the Riphean period, after a breakup of the supercontinent has occurred, the Siberian area was displaced in another superplume-affected region, namely, the Asian superplume. The influence of the latter superplume existed over the whole range of Phanerozoic time. The formation of a succession of age - variable within-plate magmatic provinces in the Siberian region that conditioned a scope of rare metal metallogenic provinces for each time interval was favoured by the continent rotation occurred above the mantle plumes of the superplume.

Formation of rare metal mineralization in the study region was due to the deep differentiation of parent magmas. Isotopic data obtained indicate that the main among sources of rare metal melts are sources of crust, mantle, and crust-mantle nature. In different time intervals, the sources of within-plate magmas in CAFB included: depleted mantle (DM), moderately depleted mantle (PREMA and/or HIMU), enriched mantle (variable in enrichment degree: EM-I, EM-II), and various combinations of the above-listed mantle sources.

INRODACTION

Igneous rocks strongly enriched in Zr, Hf, Nb, Ta, Y, Li, Rb, Cs, Be, and rare earth elements (REE) (up to commercial contents) are termed herein as “rare-metal magmatic rocks”. Under ordinary conditions, the above-mentioned elements are either disseminated within rock-forming minerals or make up own accessory mineralization not affecting a standard rock composition. These elements are often concentrated in lithium-fluorine and alkaline granites, in granitic pegmatites, in carbonatites and some other rocks of salt systems (phosphate, carbonate, sulphate, fluoride and so on) as well as in various rare metal-bearing alkaline rocks (mariupolite, lujavrite, naujaite, leucite lamproite (wolgidite) and its pegmatites. Such the rocks are fairly often described in literature and we shall not dwell on its characterization. We will now highlight only one thing. The technologies of forthcoming centuries will be in many respects founded on rare elements usage.

The per capita consumption of rare elements may be considered even at present as a quality of technological progress.

The Central-Asian folded area framing the Siberian Platform on the south and recognized as the Central-Asian folded belt (CAFB) is marked by abundant rare-metal deposits. This territory is also characterized by a peculiar block-mosaic tectonics as well as by special magmatism that was spatially and temporally isolated from plate boundary magmatism called also off-geosyncline magmatism, activation magmatism et cetera. The purpose of the present paper was to investigate the causes of extensive distribution of rare-metal mineralization within this region, its sources and geodynamic conditions of their formation.

MAJOR AREALS AND STAGES OF WITHIN-PLATE RARE-METAL-TYPE MAGMATISM

Figure 1 shows the main within-plate magmatic occurrences in the Central Asia region, including the largest Phanerozoic granitoid batholiths (Angara-Vitim, Khangai and Khentei) as

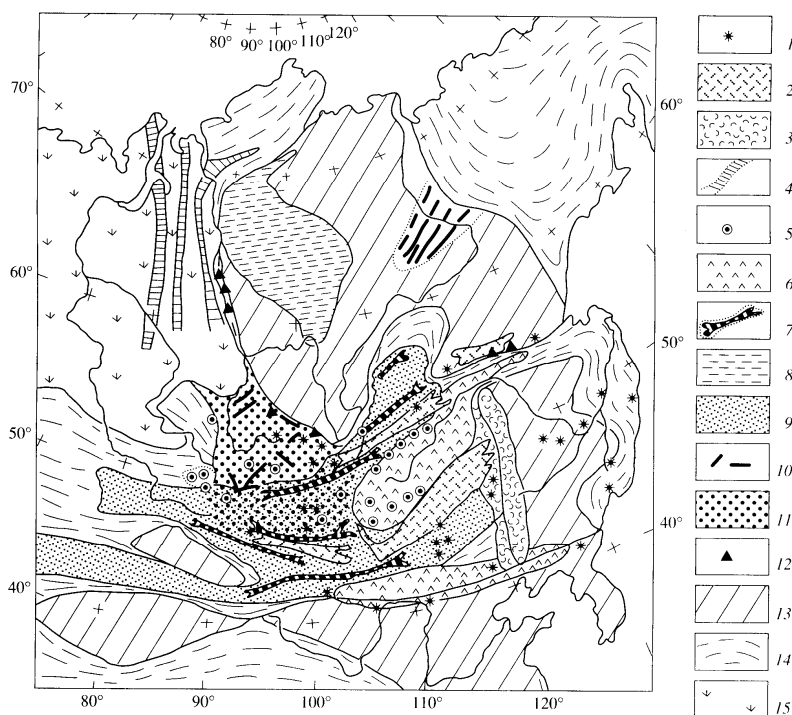


Fig. 1. Location scheme of the main continental igneous areals in the Siberian Craton and Central-Asian folded area framing Siberia in the south.

1 – 12 igneous complexes : 1- Cenozoic complexes from fields of hot spots; 2,3 – Late Mesozoic complexes: 2 – intracontinental rift zones and areas of hot spots fields, 3 – the marginal belt of Bolshoi Khingan; 4 – 6 – Early Mesozoic complexes ($T_2 - J_{1,2}$): 4 – rift system of western Siberia, 5 – within-plate volcanic and plutonic assemblages of autonomous type, 6 – collisional assemblages in the Mongol-Okhotsk and Yan-Shan belts; 7 – 9 – Late Paleozoic-to- Early Triassic complexes ($C_2 - T_1$): 7- rift zones from the Central-Asian rift system, 8 – the Siberian trap, 9- Late Paleozoic marginal belt; 10,11 – Middle Paleozoic complexes ($S - C_1$): 10 – rift zones, 11 – Devonian marginal belt; 12 Late Riphean Rhodinia disintegration zones; 13 – Pre- Riphean continents and microcontinents; 14 – folded belts; 15 – West-Siberian Plate.

well as the structures such as continental rifts controlling within-plate magmatism in Central Asia. Figure 2 gives the locations of major rare-metal deposits and occurrences in the study region. The total set of the rare-metal occurrences has been referred to as the Central Asian rare-metal province. This province is mostly located between the Siberian Craton to the north and Tarim and Korea-Chinese Cratons to the south and comprises Caledonian and Hercynian structures as well as Riphean formations of microplates such as the Tuvino- Mongolia microplate etc. [7, 20]. The rare-metal occurrences are controlled by within-plate tectonic structures (basically by grabens, troughs and depressions) found in all structure-formational zones of the Central-Asian folded belt. The same structures determine the entire within-plate magmatism in the region. The rare-metal-bearing magmatic rocks are derivatives of common within-plate magmatism represented by various alkaline rocks, including subsilicic rocks and granitoids (normal, lithium-fluorine, alkaline [4].

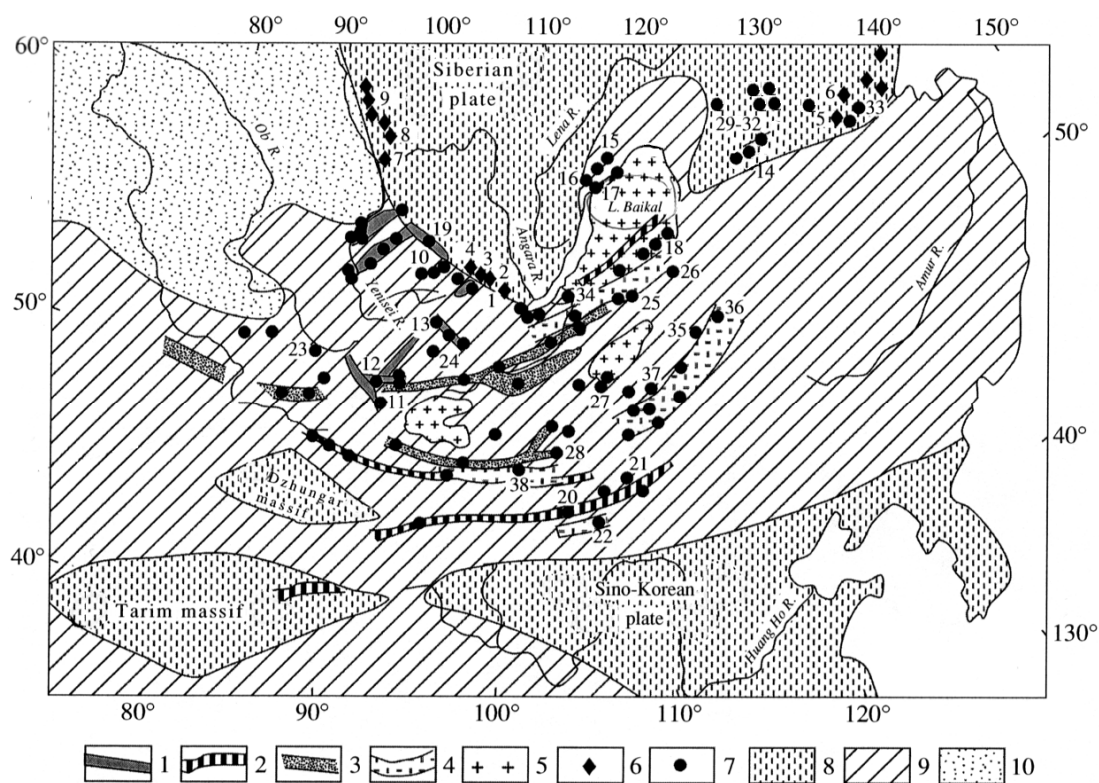


Fig. 2. Location map of of rare metal mineralization in the Central-Asian rare metal province.

1 – 5 – areas of within-plate igneous occurrences: 1 – of Early-to- Mid- Paleozoic age, 2 – of Late Carboniferous age, 3 – of Permian age, 4- of Mesozoic age, 5- batholiths, 6-7- rare metal deposits and occurrences: 6 – of Prephanerozoic age , 7 – of Phanerozoic age, 8 – cratons, 9- folded areas, 10 – young platform.

We will look at the basic regularities in the distribution of rare-metal-type igneous occurrences within CAFB region in relation to major time intervals (epochs) of the within-plate magmatism. Inception of magmatism under consideration is recorded **since Late Riphean time** (720-600 Ma). Magmatic formations of this age interval are represented by alkaline rocks distributed in Yenisey Kryazh (Ridge), East Sayany and Aldan areas as well as by dike belts in western Pribaikal region [1]. There is relation between these rocks and rare-metal carbonatites and some salt systems rocks. Till now, we are short of geologic and especially isotope studies for this time interval. Based on the data of many workers, a single supercontinent Rhodinia must have been in existence in the vicinity of the equator at that period of time. All previously formed continental blocks of the Earth were parts of Rhodinia arisen as a result of Grenville orogeny. Within the supercontinent Rhodinia, Siberia bordered on Laurentia along its southern side [12] and a breakup of the supercontinent into the two above-mentioned blocks occurred along the southern Siberia border (Fig. 3). The above stated within-plate igneous rocks and the known dike belts [14] recorded rifting-related Rhodinia disintegration. Since the interval of 750-600 Ma, nearly all continents displayed signatures of within-plate activity thereby recording the continued disintegration of Rhodinia into separate blocks. This proves that there was initiated a large superplume beneath the Rhodinia area. Japanese researchers proposed plume tectonics concept [10] identify the above mentioned superplume with the present-day South-Pacific superplume that is recorded by seismic tomography. Figure 4 gives a projection of this South-Pacific superplume at a moment of Rhodinia disintegration. The above noted the Riphean within-plate alkaline magmatism of south Siberia as well as numerous deposits and occurrences of rare-metal carbonatites located in the southern portion of Siberia Craton appear to reflect disintegration of Rhodinia and formation of Paleo-Asian Ocean on which place the Central-Asian folded belt (CAFB) was developed.

The further geodynamic history of within-plate magmatism which, according our large set of rock datings, proceeded with the periods of relative magmatic quiescences and activation throughout the Phanerozoic up to Holocene time. In history of within-plate magmatism, based on igneous recrudescences, the early to middle Paleozoic, late Paleozoic to early Mesozoic, late Mesozoic to early Cenozoic, and late Cenozoic epochs are recognized (Fig. 5). We consider the location and character of rare-metal-type magmatism as well as its relation to within-plate magmatic activity in CAFB for each specific epoch. In table 1, the main provinces and areas marked by within-plate activity as well as examples of rare-metal deposits and occurrences within CAFB for the each epoch are summarized.

Figure 6 reveals that there is relationship between the location of within-plate magmatic occurrences of **the Early to Middle Paleozoic epoch** and the position of extensional zones, i. e., grabens, depressions and adjoining to them areas. This epoch covers a time span of about

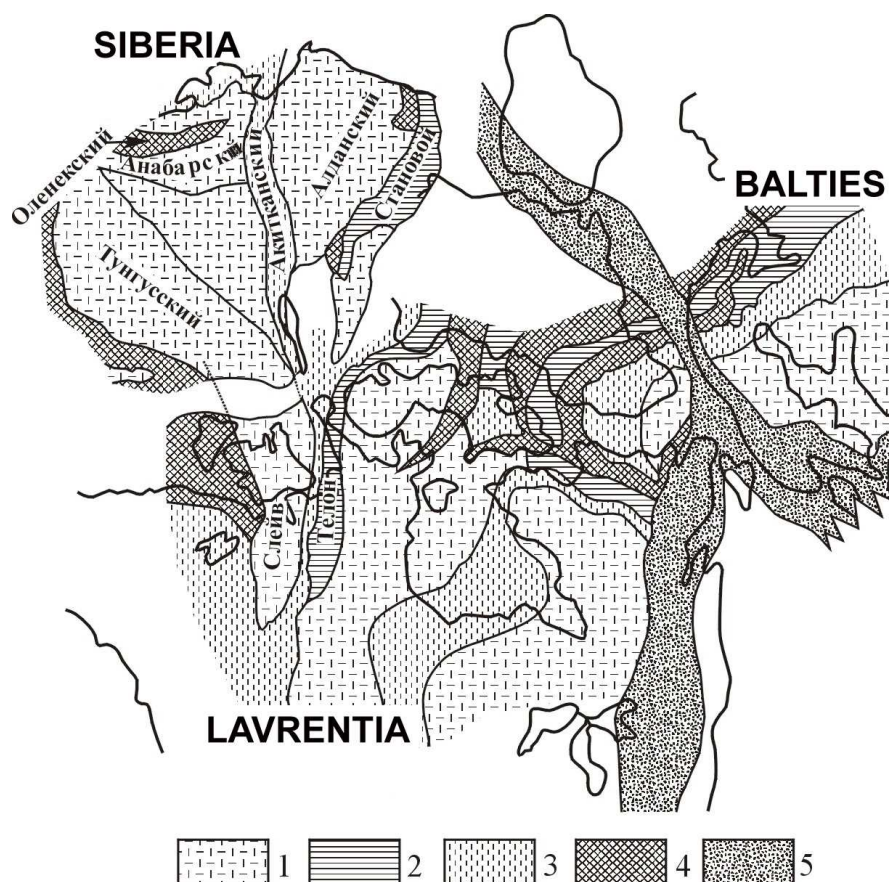


Fig. 3. Reconstruction of the Rhodinia supercontinent - after [12].

1 – 2 structures of Archean age: 1- cratons, 2 – reworked structures within the time interval of 2,000 –1,900 Ma; 3 - 4– structures of Proterozoic age: 3 – with juvenile crust (2,000 –1,900 Ma), 4 – structures of folded belts, 5 – folded belts arisen as a result of Grenville orogeny.

200 m.y. The earliest (older than 500 Ma) within-plate alkaline rocks of this period started to form in the area of Yenisey Kryazh, but the extensive burst of within-plate-type magmatism occurred during the interval between 500 and 360 Ma has embraced the vast territory within described CAF belt (500 x 700 km²), including the Minusinsk Depression, the area of East and West Sayany, the north-western part of Mongolia. In the Early to Middle Paleozoic, within Yenisey Kryazh region, the earliest rare-metal rocks [1] may be exemplified by the Srednevorogovskiy massif represented by alkaline granites rich in pyrochlore and euxenite with an age of 567-526 Ma and, probably, by the Kyisky massif composed of ultramafic alkaline rocks and related high-rare-earth carbonatites. Slightly younger rare-metal deposits [3, 2 and others) are found in north-eastern Tuva (the Aksug and Aryska alkaline granites dated between 460 and 450 Ma), in the East Sayany area (a number of rare-metal lithium-fluorine granites) and in Pribaikal region (the ultramafic alkaline rocks with associated carbonatites making up Saizhen massif. However, the most intense within-plate magmatism of the epoch under

consideration was characteristic of the time interval of 450-300 Ma. Among examples of magmatism and related mineralization of this age are: (1) within the Minusinsk Depression, the

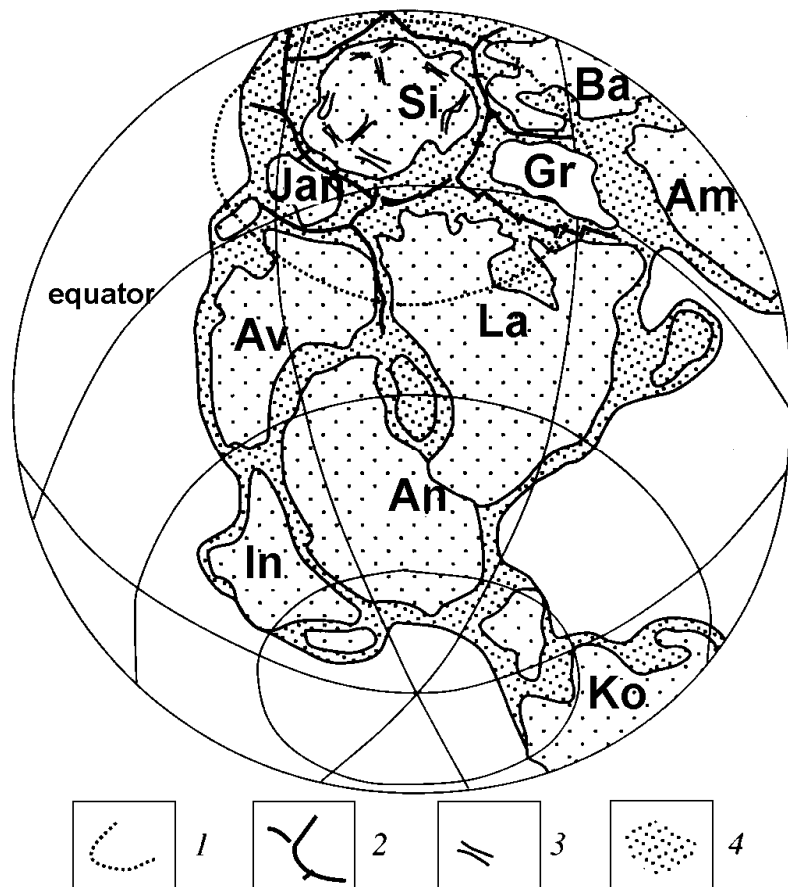


Fig. 4. Schematic reconstruction of the Late Riphean Rhodinia supercontinent for time of its disintegration (750 – 650 Ma) – after [10].

1 – projection of the presumptive Pacific hot superplume; 2 – split zones of supercontinent; 3 – continental rifts of the Siberian Platform; 4 – structures welding and fringing continental blocks, including shelf ones.

Av- Australia; Am – Amazon area; An – Antarctic Continent; Ba – the Baltic Sea region; Gr – Greenland; In – India; Ko – Kongo; La – Laurentia; Si – Siberia; Jar – Yangtze (Kiang).

Number of determinations for 20 Ma intervals

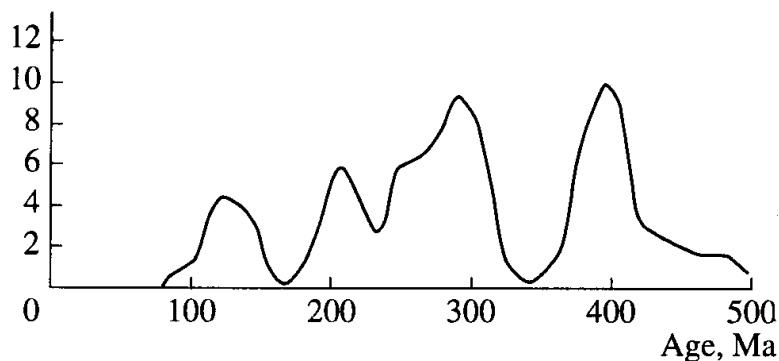


Fig. 5. Distribution of geochronologic datings on alkaline and Li-F granites, alkaline and nepheline syenites, and carbonatites in the Central-Asian rare metal province.

Provinces and major areas of within-plate magmatism and some rare metal deposits and occurrences within the Central-Asian folded belt

Epochs of igneous activity	Provinces and areals of within-plate igneous activity in the Central Asia region, major magmatism types, including rare-metal-bearing magmatism (numbers in parentheses indicate ages of magmatic rocks, Ma)	
Early to Middle Paleozoic	<p>Altai-Sayany province (O-D₂) - alkaline magmatism [490, 460, 450-410, 390, 375]: alkaline and Li-F granites Alkaline granites (REE, Zr, Nb): Aryskan[454], Khaldzan-Buregtey [375], Ulan-Tologoi Li-F granites: Khoroiisky, dikes related to Bugulminsky massif [404]</p> <p>Vilyui (S-C₁) –basaltic and alkaline magmatism. Carbonatites (REE, Nb, Ta): Tomtorskyy Group, massifs of Sette-Daban area</p>	
Late Paleozoic to early Mesozoic	<p>Barguzin-Vitim province (C₃-P₁) - alkaline magmatism [330–290] Synnyrsky rift zone [310, 290] Alkaline granites (REE, Zr, Nb): Synnyrsky [293], South-Sakunsky [288], Burpala massifs. Alkaline and Li-F granites (Nb, Ta, REE): Zashikhinsky Udino-Vitim rift zone Carbonatites: Saizhensky</p> <p>Siberian trap province (P₂²-T₁) Ultramafic complex with carbonatites (Nb, P): Gulinsky complex [253] Chadobetsky massif</p> <p>West Siberian rift province (T₂-J₁) - bimodal and trachybasaltic magmatism [235-218]</p> <p>Altai-Sayany province (T₂-J₁) – Alkaline granites (REE, Nb, Zr): Ulug-Tanzek [180] Plumasitic (Li): Alakhinsky, spodumene pegmatites located in Tuva</p> <p>Late Paleozoic rift system of Central Asia – bimodal, agpaitic and plumasitic (Li-F) magmatism Gobi-Tien-Shan rift zone (C₃-P₁) [310-285] Alkaline granites (REE, Zr, Nb): Khan-Bogdinsky [290] Li-F granites: Yugodzysky [283] Gobi-Altai rift zone (P) [275] Alkaline granites (REE, Zr, Nb): Tszarta-Khuduk North-Mongolian rift zone (P₂) [265-250] Early Mesozoic Mongolia-Transbaikalye rift system (T-J₁) – bimodal, agpaitic, plumasitic (Li-F) and alkali-carbonatite magmatism West-Transbaikalye rift zone (T₃-J₁) [230-190] Alkaline granites (Be): Ermakovsky [224], Orot, Aunik, Amandak North-Gobi rift zone [230-185] Li-F granites: Zhanchivlansky [190], Barun-Tsogt Areal-type magmatism occurrences: Carbonatites: Lugin-Golsky massif [250]</p>	
Late Mesozoic	<p>Central-Asian intracontinental province – alkaline-basaltoid-, alkaline, agpaitic, plumasitic (Li-F), and alkali-carbonatite magmatism [160-90]</p>	
to Cenozoic	<p>South-Khangai area Carbonatites (REE, P, Sr): Mushugai-Khuduk [150], Ulugei-Khid West-Transbaikalye area Carbonatites (REE, P, Sr): Khalyutinsky, Arshansky [120]</p>	<p>East-Mongolian area Li-F granites: Sokuisky, Etyka, Arybulak [140, 143] Aldan area Carbonatites: Murunsky [140] Alkali-ultramafic complexes (Pt, Au): Inagli [145], Konder</p>

Kiya-Shaltyr' foyait containing stock, the Petropavlovsk massif of alkaline rocks with the related carbonatites, the Dedov massif composed of higher-rare metal nepheline-syenite, (2) within East Tuva, the Chavach intrusion with rare metal-bearing nepheline-syenite, the Kharly, Bayankol, Chik intrusions and related carbonatites, the Terekhol intrusion with rare-metal-bearing mariupolites, the

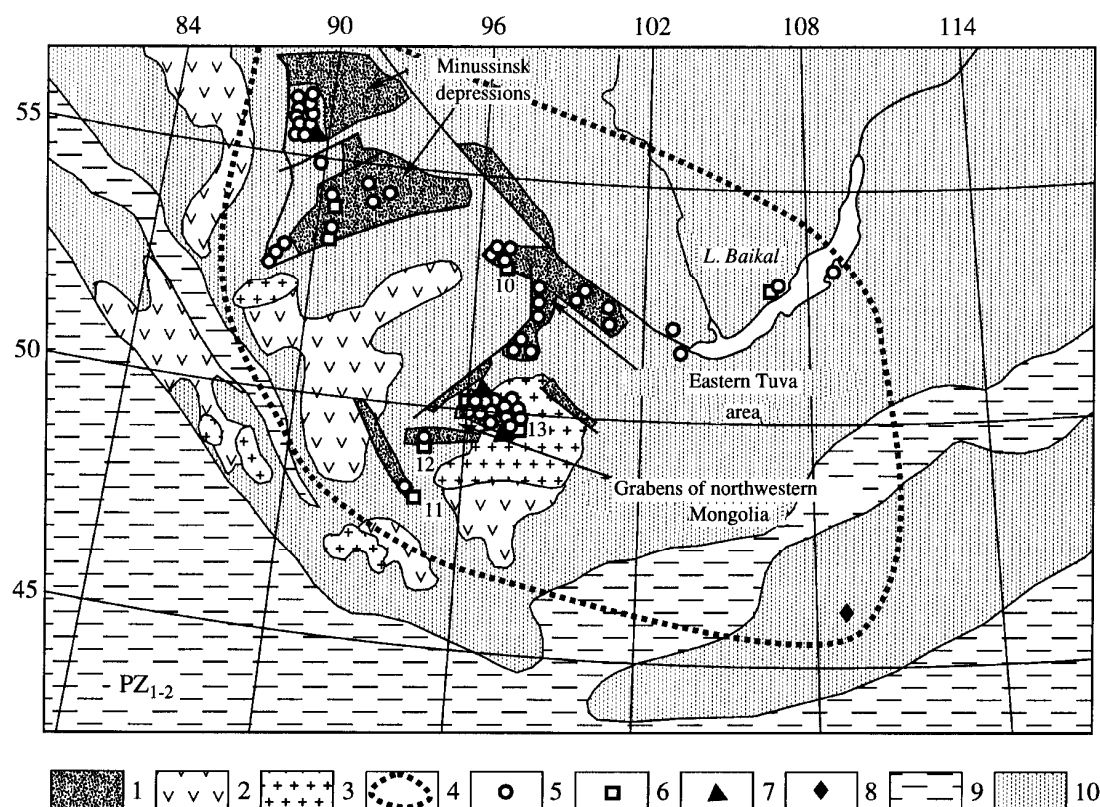


Fig. 6. Schematic representation of rare metal-type magmatism occurrences in system of the Early – Middle Paleozoic igneous assemblages of the Central-Asian folded belt.

1 – 3 - igneous assemblages: 1 – bimodal and alkaline assemblages of rift structures; 2 – calc-alkaline assemblages of marginal volcanic belts; 3 – batholith assemblages; 4 - outer circuit of within-plate activity area; 5 – alkaline granites; 6 – rare metal deposits; 7 – carbonatites; 8 - lithium-fluorine granites; 9 – oceanic basins; 10 – continental massifs.

Pichekhol' massif and related to it rare-metal nepheline pegmatites, (3) in North-West Mongolia, the peralkaline granitoid-related Khaldzan-Buregtey rare-metal deposit [5] and occurrences of similar mineralization in the area of the Khan-Khukhey Ridge, and (4) in the area of Central Mongolia, the Khukh-Del-Ula field of rare-metal lithium-fluorine pegmatites [16]. Much geochronologic data by V.A. Kononova, R.M. Yashina, E.D. Andreeva and others for above mentioned areas are summarized by L.N. Kogarko [1]. Using the paleomagnetic data, figure 8 presents a reconstruction of Siberia and some microcontinents with respect to the areas with within-plate igneous activity (i.e., with respect to mantle plumes projections). Since this time Siberia has been displaced toward the mid-latitudes. A lull in igneous within-plate activity occurred after Rhodinia disintegration was likely to be related to Siberia moving away the South-Pacific superplume. The intense magmatism resumed during Ordovician to Devonian times, most probably, took place when Siberia was coincident with new active within-plate source that is referred by us as the Asian hot field of mantle or the Asian superplume consisted of four individual plumes. Their activity resulted in the above-named consequences, including formation of multifarious enriched in rare elements igneous rocks.

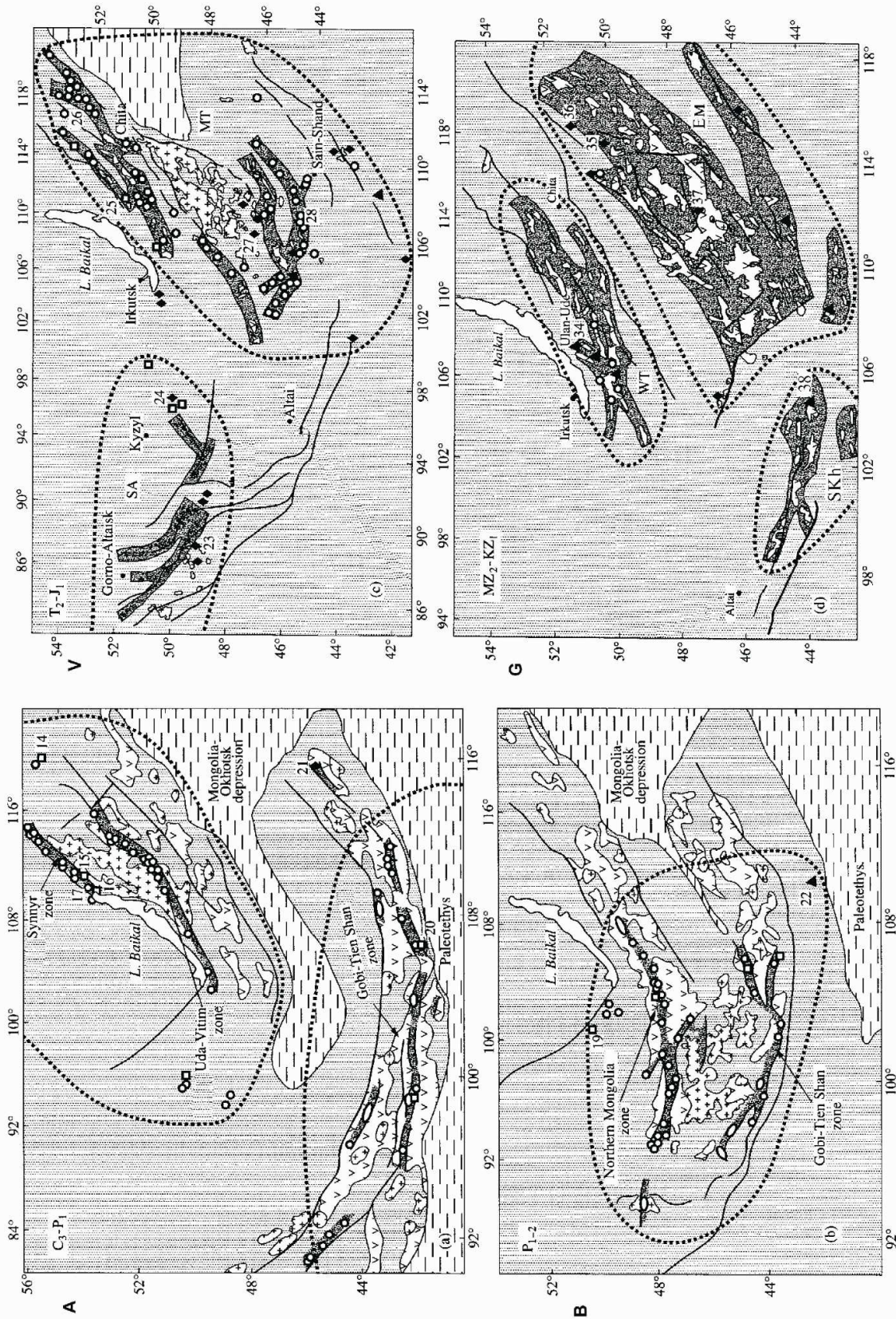


Fig. 7. Schematic representation of rare metal -type magmatism occurrences in system of the Late Carboniferous- Early Permian (a), Permian (b), Early Mesozoic, and Late Mesozoic -to- Early Cenozoic (d) igneous assemblages of the Central-Asian folded belt. See Fig. 6 for explanation of the symbols

Geodynamic setting in CAFB for the **Late Paleozoic to Early Mesozoic epoch** (330-185 Ma) is shown in figure 8. By this period, Siberian continent was enlarged through the South-Mongolia Hercynides being accreted to it and via its collision with Kazakhstan microcontinent. The major geologic event of the epoch under consideration was development of a vast Central Asian rift system. This system represented a sub-east–west striking belt composed of several subparallel rift zones (Fig. 8-a, b, c) filled with bimodal basalt-pantellerite-alkali-granite assemblages accompanied and followed by formation of large belts of dikes compositionally similar to above mentioned assemblages. This rift system created during the interval 280 –250 Ma was mainly recorded within the area of Mongolia and was found in the area adjacent to the Pribaikalye region as well. Among igneous rocks of the Central Asian rift system, rare metal-bearing rocks are in abundance. They include the Khan-Bogdin and Kharkhad massifs of rare metal alkalic granites with age of 280 Ma located in Southern Mongolia [15]; the Synnyr and Byrpalin massifs of high-potassium alkalic rocks (approx 290 Ma) and related to them rare metal and other type (K-Al, P) mineralization found in the northern part of Pribaikalye; the Sakun massif of rare metal-bearing rocks in the area of the Aldan Shield. Within East Tuva, the Late Paleozoic-Early Mesozoic epoch saw formation of rare metal nepheline syenite and its pegmatites related to the Dugdin massif with emplacement age of 290-280 Ma, the Korgeredabin massif (with a age of 304 Ma) as well as to the Ylanergin massif dated at 322 Ma. We believe that the enormous in size Angaro-Vitim batholith, estimated as old as 320-290 Ma and comprising some lithium-fluorine granite massifs shows within-plate signatures [19]. The Luginol massif and a number of smaller high-potassium alkaline intrusions and the related rare earth carbonatites (dated at 250 Ma) as well as the Yugodzyr massif made up of rare metal lithium-fluorine granites with an age of 280 Ma [6, 7] have been recorded at the southern periphery of the Late Paleozoic within-plate magmatic areal. During Late Paleozoic-Early Mesozoic epoch, the Late Paleozoic and Early Mesozoic areals characterized by zonal arrangement of igneous rocks were formed on the final stage of within-plate magmatic activity. The cores of these two areals are made up of the Khangai batholith (its age is 250 Ma) (Fig. 8-b) and of the Khentey or Kyrin (with an age of about 200 Ma) batholith (Fig. 8-c), respectively. Their northern and southern peripheries consist of diverse granites, including alkaline and lithium-fluorine varieties as well as volcanic rocks. The rare metal deposits and occurrences formed during the Early Mesozoic are the Dzarta-Khuduk occurrence of rare metal alkaline granites and pantellerites (dated at 200 Ma) in Central Mongolia; the Zhanchivlan, Abdar, Bagagazzryn massifs of rare metal lithium-fluorine granites [6, 7] as well as the Ermakovskoe [11, 9], Orotskoe and other rare metal deposits (of 220-210 Ma in age) in west Transbaikalye. The Early Mesozoic within-plate magmatic activity was also characteristic of the Altay areal in which the unique rare metal spodumene granites and ongonites of the Alakhinsky and Kulgutinsky deposits are found [2]. The Altay areal covers the Tuva region and northwestern Mongolia as

well (Fig. 8-c). In East Tuva, the dikes of rare metal nepheline syenites, the pegmatites related to the Kadyros and Kyshtag massifs (dated at 212 Ma), and the Ulugtanek rare metal deposit have been formed during this period. Separate rare metal occurrences of Early Mesozoic age are known in the Pribaikal region (the Akit occurrence of rare metal alkaline pegmatites and parisite-and xenotime-bearing fluorite-carbonate rocks, of 199 m. y. old).

As is shown in Figure 7, at the boundary of the Carboniferous and Permian, Siberia separated by oceanic basins from China and Central-Mongolia microcontinent continued to interact with the Asian hot field of mantle. Included in this hot field are the Barguzino-Vitim and Gobi-Tien-Shan plumes. Beginning in the Permian/Triassic boundary and continuing up to the early Jurassic, the Central-Asian Plume was in operation and, as a consequence, the Central-Asian rift system has been developed. The Late Permian was characterized by an activity of the Siberian plume which gave rise to the formation of vast trap province situated in the central and northern portions of Siberia. The early Mesozoic West-Siberian plume caused the

formation of the West-Siberian rift system and small Ob' paleo-ocean. On the whole, during Permian to early Mesozoic time, within-plate activity in CAFB was gradually reduced.

The Late Mesozoic to Early Cenozoic epoch of within-plate magmatic activity started at about 180-170 m. y. Ago and ended at the boundary of the earliest Miocene (about 25 Ma). The within-plate magmatic activity of this period was mainly centered in Transbaikalye, central and eastern Mongolia and at the northern periphery of the Aldan Shield [17] (Fig. 8-d).

In Transbaikalye and eastern Mongolia, during this epoch rare metal deposits and occurrences related to lithium-fluorine granites and ongonites (within the Transbaikal region, among them are the Orlovka, Ytyka, Ary-Bulak deposits dated as 140 Ma; within eastern Mongolia, among them are the Borun-Zogt, Yugodzyr, Ongon-Khaierkhan deposits dated as 150-120 Ma) have been formed. Within Central Mongolia and Western Transbaikalye, the alkaline complexes with REE, lead, and barium-strontium mineralization found in the related carbonatites, apatite-rich and fluorite-rich rocks have been formed. Among ore deposits located in Central Mongolia, the Mushugai-Khuduk, Khotogor, Ulugei dated at 140-130 Ma are worthy of notice (Kovalenko, Samoilov, 1983); as examples of mineralization found in Transbaikalye it may be considered the Khalyutin, Arshan and others occurrences dated at 130-120 Ma. Mineralization of similar type is observed in Tuva (the Kara-Sug occurrence). It is noteworthy that in the vicinity of Mushugai-Khuduk deposit volcanic rare metal lithium-fluorine ongonites are recorded. The presence of intrusions of nepheline syenites with associated rare metal mariupolites and pegmatites (the Borgoi massif, 125 Ma) is noticed in western Transbaikalye. The late Mesozoic rare metal occurrences are most commonly distributed at the northern periphery of the Aldan Shield. Noteworthy are the following unique rocks with rare metal mineralization (Vladykin, 1997):

the charoites and benstonitic carbonatites of Malomurun massif (145 Ma); the Inagli rare metal alkaline pegmatites (137-129 Ma); the Yllymakh vein-type eudialyte syenites (165-133 Ma) and others. Everywhere over the volcanic regions of discussed here epoch, volcanic complexes were dominated by alkaline and subalkaline flood basalts. Taking into account their volume, the bulk of within-plate magmatism of this epoch may be as much as the mid-Paleozoic within-plate magmatism capacity. So, within the above mentioned epochs, the two main maximums in activity of within-plate magmatism are evident. During the Late Cretaceous-to-Early Cenozoic the activity of within-plate magmatism in CAFB was gradually decreasing. As illustrated in Fig. 7, activity of the Central-Asian plume covering southern Siberia was extended to Mongolia and China as well. Everywhere over these areas the compositionally variable occurrences of within-plate magmatism and related rare metal-type magmatism are wide spread.

In Late Cenozoic epoch the within-plate activity continued with the eruption solely of basaltic rocks characterized by a higher alkalinity. No rare metal occurrences of this epoch have been found.

SOURCES OF WITHIN-PLATE MAGMATISM

Sources of within-plate compositionally varied magmatism are different. Most granitoid samples in our data set are assigned to the Caledonian isotope province of CAFB. So, the Caledonian continental crust can be considered as source of rare metal lithium-fluorine granites and ongonites. This can be shown in Fig. 9, where the isotope compositions of rare metal lithium-fluorine granites are situated in the field of isotope evolution of Caledonian continental crust [6, 7]. Individual massifs of rare metal lithium-fluorine granites were derived from older Precambrian continental crust and thus, they display more low values of ϵ_{Nd} (Fig. 9). In these cases, such massifs are located within Precambrian blocks. In CAFB, continental crust of different ages was formed due to the multiple-stage transformations of oceanic crust into continental one in the areas of converging plate boundaries. Besides, within-plate magmatism supplied additional material to continental crust. However, the main role of within-plate magmatism consisted in thermal influence on continental crust with its subsequent anatexis. Strong differentiation of such the anatexis-related melt, especially in the presence of mica and apatite in anatexis process, stimulated formation of rare metal lithium-fluorine granites and ongonites. Mantle plumes which controlled within-plate igneous activity were also responsible for processes developed at the area of plate boundaries.

The other types of rare metal-bearing igneous rocks are related to mantle sources [8]. These variant types will be considered on the examples of bimodal and alkaline within-plate magmatic assemblages of various age. Figure 10 shows the fields of isotope compositions of within-plate magmatic rocks, with contours of fields corresponding to each of the above mentioned epochs. In the same figure,

the fields of mantle and crustal sources are given. Among described sources, there are fields of enriched mantle EM-I, EM-II, relatively depleted mantle HIMU which in its properties and composition is close to the most common mantle PREMA, depleted mantle DM as well as fields of island arcs, of Central Asian

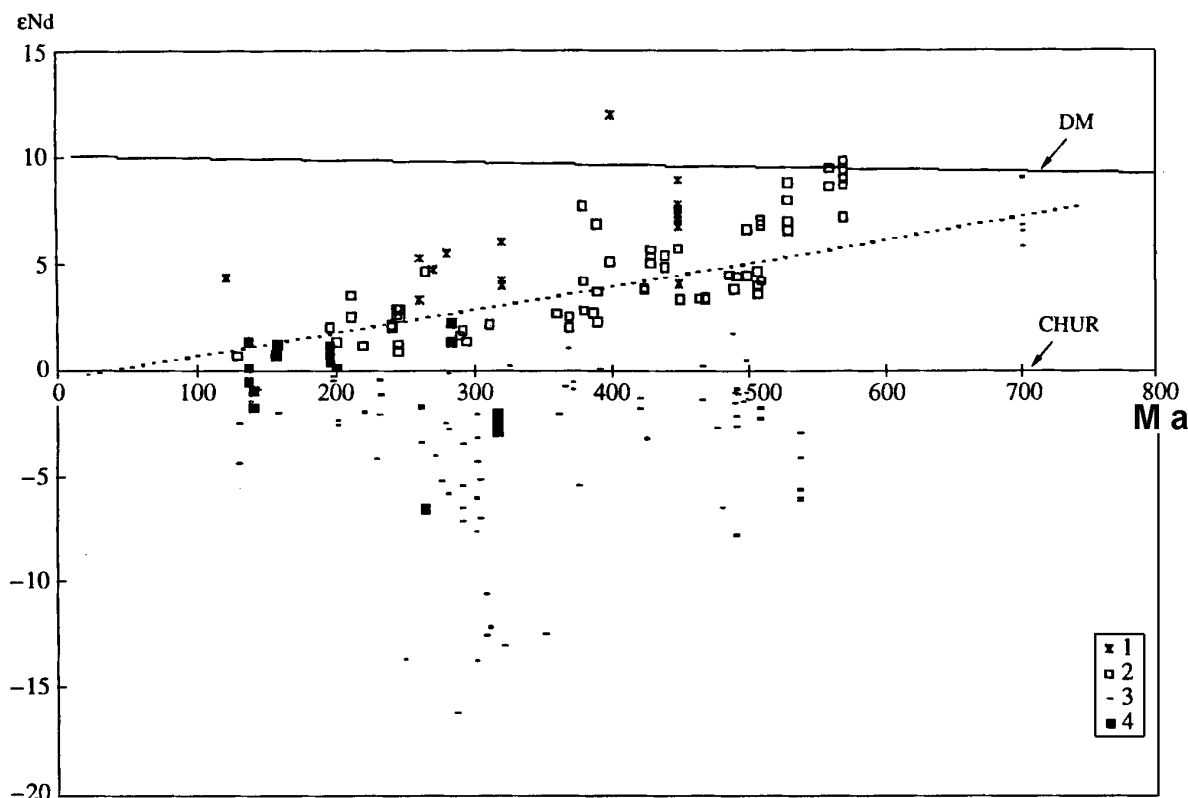


Fig. 9. Scheme showing dependence of ϵ_{Nd} of granites in the Central-Asian folded belt on its ages and location in provinces of isotope crustal sources (after [6]).

1 – normal granites from Hercynian province; 2 - normal granites from Caledonian province; 3 - normal granites from Precambrian province; 4 - lithium-fluorine granites.

DM- depleted mantle; CHUR-chondritic unexhausted reservoir. Dotted line –evolution line of average composition of the Caledonian continental crust.

ophiolites and continental crust components. The last-named component is represented in the figure by isotope compositions for granitoids from the largest in the study region batholiths (the Angaro-Vitim, Khangai, Khentei batholiths). In figure 10 and in the next ones, the fields of isotopic compositions for rocks from model regions for alkaline granitoids, such as Pantelleria Island in the Mediterranean region and Voznesenia Island in the Atlantic ocean, are plotted for comparison. The isotopic compositions for the studied within-plate magmatic rocks of Central Asia fall into the fields of isotopic compositions for the all above-listed sources lying in the area correlated with mantle. However, the data demonstrate that the within-plate rocks exhibit some compositional variation with respect to the fields reflecting their emplacement age. The isotopic compositions for the Early–to Mid-Paleozoic within-plate magmatic areal display the highest and

relatively constant values of ϵ_{Nd}^T (most often $> +5$) with rather broad variations of initial ratio Sr^{87}/Sr^{86} (I_0^{Sr}). On the whole, the compositions of this areal embrace the sources of DM, HIMU, island arcs, and young continental crust. Within the described areal, general variations in isotopic compositions of mafic and felsic (alkali-granitic) rocks are similar, suggesting the affinity of its magma sources. The

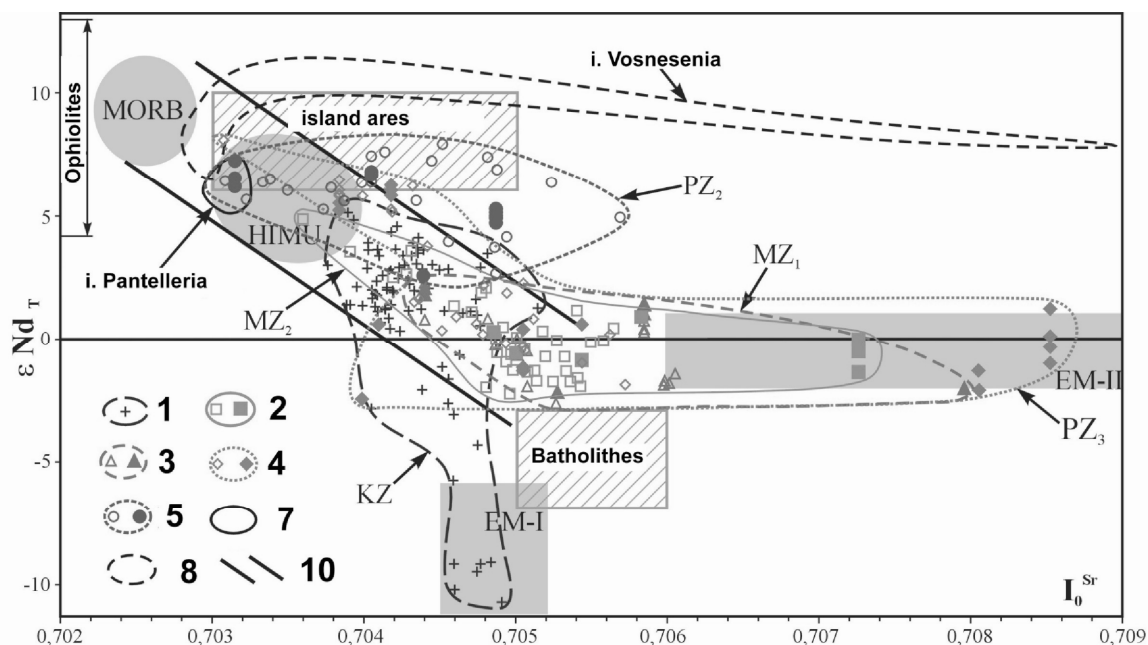


Fig. 10. The initial Sr and Nd isotope compositions for within-plate igneous rocks from Central Asia and for typical mantle and crustal sources.

For the region of Central Asia: 1 – Cenozoic igneous rocks; 2 - Late Mesozoic igneous rocks (here and in next figures – filled symbols = felsic rocks, open symbols – mafic rocks); 3 – Early Mesozoic igneous rocks; 4 - Late Paleozoic igneous rocks; 5 – Middle Paleozoic igneous rocks; 6 – ophiolite complexes (are shown in Fig. 12); 7,8 – for other areas characterized by occurrences of alkaline granites and their volcanic equivalents: 7 - Pantelleria Island in the Mediterranean region; 8 - Voznesenia Island in the Atlantic ocean; 9- arrow indicates the displacement of isotope compositions of continental crust and MORB on passing from the Paleozoic to the Mesozoic (see Fig. 12); 10 – field of mantle trend. Explanation are discussed in the text.

ϵ_{Nd}^T values show closeness of the Early–to Mid-Paleozoic magmatic areal to the isotopic compositions for rocks from Pantelleria and Voznesenia Islands. The isotopic compositions of felsic rocks from Voznesenia Island, moreover, are characterized by relatively broad variations in values of Sr^{87}/Sr^{86} ratio. The isotopic compositions of the Late Paleozoic within-plate magmatic areal partially fall into the fields of isotopic compositions for the Mid-Paleozoic rocks (the Gobi-Tien-Shan belt), but the greater part of them (the Gobi-Altay, North-Mongolian belts) is situated between fields of isotopic compositions of DM, HIMU, batholiths (or of Riphean continental crust) and EM-II. Isolated figurative points fall on the trend inclining to EM-I source. On the whole, similarly to Middle Paleozoic time, variations in values of ϵ_{Nd}^T for the Late Paleozoic mafic and felsic rocks are alike. In the field of EM-II, there are situated nepheline syenites strongly enriched in

radiogenic strontium and related to them rare earth element mineralization-bearing carbonatites of the Luginol massif (Gobi-Tien-Shan belt). In model regions, felsic rocks are rather more enriched in radiogenic strontium than the comagmatic mafic rocks [18].

For the Early Mesozoic within-plate magmatic areal, based on a small set of isotopic analyses, the magma sources for bimodal assemblages lie between the sources of DM (or HIMU) and of EM-II. Isotopic data on Nd and Sr isotopes for mafic and felsic rocks are similar (Fig. 10).

As to the Late Mesozoic within-plate magmatism areal, isotope compositions of rocks are also arranged between sources of DM (or HIMU), continental crust (batholiths) and of EM-II. Isotope compositions for felsic and mafic rocks are alike. The one exception is represented by the volcanic field in the area of the Gusinoe Lake, western Transbaikalye, where the compositions of felsic rocks located within the field of EM-II are shifted into the region of enriched in radiogenic strontium compositions (Fig. 10). The alkaline rocks and carbonatites from the Aldan Shield [17] reveal isotope compositions of EM-I field.

And finally, in the Cenozoic within-plate magmatic areal, where only mafic rocks were found, the majority of its isotope compositions is situated between fields of DM (or HIMU), EM-I, batholiths and EM-II field. Thus, the presented isotopic data suggest that the sources of felsic agpaitic magmas as well as of related mafics, fluctuating within the bounds of main mantle trend, range from depleted mantle DM or HIMU (the Mid-Paleozoic magmatic areal and Gobi-Tien-Shan belt of the Late Paleozoic magmatic areal) to enriched mantle EM-II (the Late Paleozoic, Early and Late Mesozoic) and EM-I or to mixture of depleted mantle and continental crust. The consanguinity of isotope signatures of mafic rocks and alkaline granites, pantellerites and other alkaline felsic rocks proves that all these rocks were derived from common sources and are genetically affined.

A considerable body of isotopic data concerning alkaline granitoids and their volcanic analogues from other world-wide occurrences also falls into the field of main mantle trend and isotope compositions of felsic and mafic rocks from those objects proved to be mostly similar. For rocks from Pantelleria Island, as an example, Sr and Nd isotopic compositions for mafic and felsic rocks (trachytes and pantellerites) are similar. As to the mafic-comendite-alkaligranitic association from Voznessenia Island, felsic and mafic rocks exhibit similar variation in ϵ_{Nd} values, but value of $^{87}\text{Sr}/^{86}\text{Sr}$ initial ratios for felsic rocks proved to be higher (up to ~ 0.709). This distinction is attributable to the effect of hydrothermally altered oceanic crust upon felsic rock composition. The similar pattern is also characteristic of rocks from the regions of main Ethiopia Rift and the Tuareg Shield (Algeria). Within the main Ethiopia Rift, felsic rocks (pantellerites and comendites) and mafics revealed a variation in $\epsilon_{\text{Nd}}^{\text{T}}$ values from +1.9 to +3.5, and from +1.3 to +3.7 (10), respectively. Within the Tuareg Shield, $\epsilon_{\text{Nd}}^{\text{T}}$ values vary from +6.6 to +6.7 for mafic rocks of Pan-African age and range from +4.8 to 7.7 for agpaitic alkaline granites. from +4.8 to 7.7.

Nd isotope composition is noticeably less influenced by various factors than Sr isotope composition. Initial Sr values are hard to determine with a necessary low error because of high Rb/Sr ratios frequently occurring in pantellerites and alkaline granites. In case of high Rb/Sr ratios the appreciable variations in I_0^{Sr} values are made possible due to even small variations in assessment of rocks age. If alkaline granitoids and its volcanic equivalent display

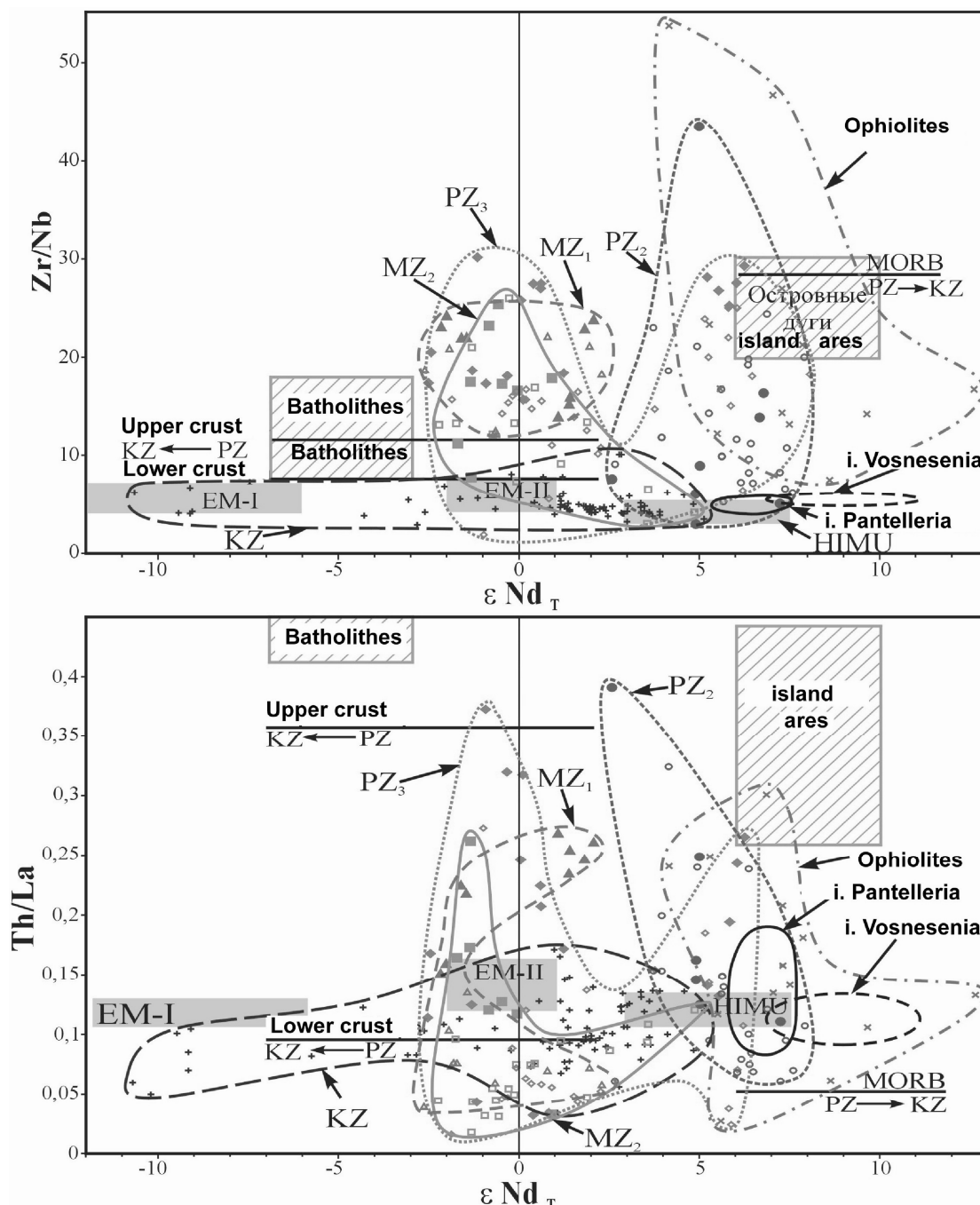


Fig. 11. Nd isotope compositions vs. the Zr/Nb (a), Th/La ratios for within-plate igneous rocks of Central Asia, Pantelleria Island, Voznesenia Island and typical mantle and crustal sources.

See Fig. 10 for explanation of the symbols.

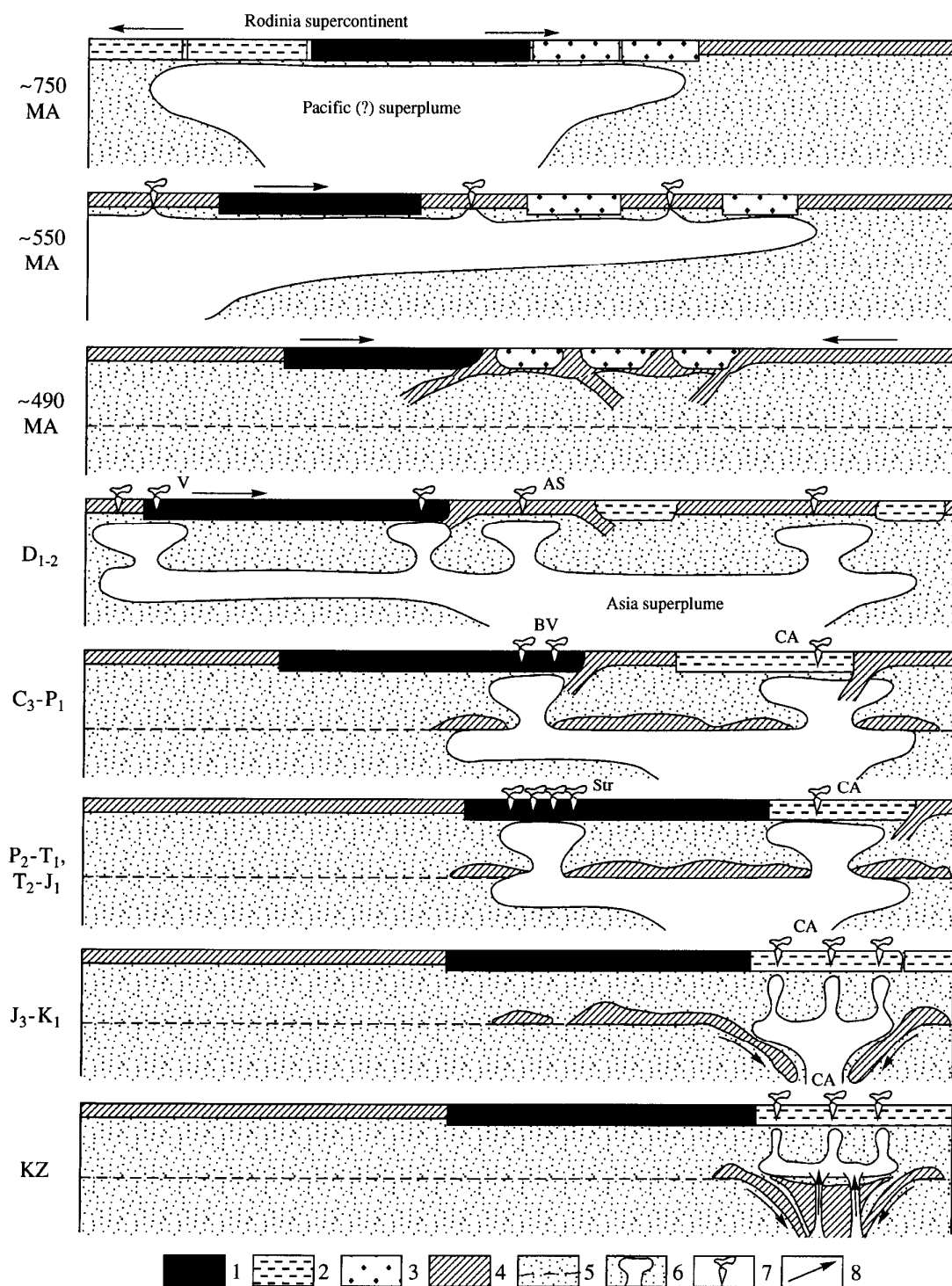


Fig. 12. Scheme illustrating model of mantle superplumes contribution to the formation of the Central-Asian folded belt.

Volcanic fields and provinces: - V – Viluyi; AS – Altai-Sayany; BV – Barguzin-Vitim; CA – Central-Asian; Str-Siberian trap;

1 – Siberian Continent; 2 – craton regions of Rhodinia; 3 – Riphean microcontinents of the Central-Asian folded belt; 4 – oceanic crust; 5 – mantle and boundaries of upper and lower mantle; 6 – “hot mantle of superplume”; areas of within-plate activity; 8 – trends of mantle flows motions.

low Sr concentrations, changes in Sr isotope composition may taking place even at small contamination of melt by material with higher Sr content (for instance, by sediments or marine water). If reliable isochrons or estimations of ages by the U-Pb zircon method are not available, all the above testifies to smaller reliability of I_0^{Sr} values assessment for alkaline granitoids in comparison with estimations of ϵ_{Nd}^T values

The magma sources can be estimated also from the correlations of trace elements, especially if their bulk crystal–melt partition coefficients are very small. For the present purpose the diagrams $\epsilon_{Nd}^T - Zr/Nb$ and $\epsilon_{Nd}^T - Th/La$ were used (Fig. 12). Zr/Nb ratio is poorly sensitive to degree of magma differentiation up to saturation of magmatic system by zirconium and niobium and a proportion of these elements may be kept practically constant in the genetically related igneous rocks assemblages under various geodynamic conditions. The geochemical character of Th/La ratio is essentially identical to those of Zr/Nb ratio. It is to be noted that the magma sources such as DM or island arc components and HIMU, merged practically on isotope diagram of Fig.11, can be recognized by values of Zr/Nb ratio. The sources EM and continental crust components that are almost indistinguishable from each other in Fig. 11 may be recognized from Th/La ratios. Figure 12 shows that the within-plate associations of mafic and alkaline felsic rocks of Early-to-Middle Paleozoic age were formed from mixed source consisting of DM or island arc components and HIMU with, in certain cases, participation of EM-II and continental crust components. The Late Paleozoic igneous rocks likely to be derived from mixing sources DM and HIMU, but the most probable its derivation was connected with mixture of (DM+HIMU) with EM-II (sometimes with EM-I) and continental crust. This provides an explanation for the extension of isotope compositions field in relation to ϵ_{Nd}^T as well as for the presence of branch (“apophysis”) of this field in direction of Th/La high ratios (Fig. 11).

Isotope compositions of within-plate igneous rocks of Early and Late Mesozoic age have been formed with a considerable participation of EM-II and continental crust. This is supported by elongated form of fields for the Early-to-Late Mesozoic rocks located between the regions of the above mentioned sources (Fig. 11). Judging by predominant position of isotope compositions of the Mesozoic felsic rocks in the field with high values of Th/La ratio, among the rocks in this field, the alkaline granitoids derived largely from material of continental crust may be present. At the same time in the field with values of Th/La ratios less than 0.2, there is assumed also a contribution of source (DM + HIMU) recorded by the extension of isotope compositions field in relation to ϵ_{Nd}^T values (Fig. 11). In addition to the diagram presented in Figure 10, Figure 11 reveals that isotope compositions of Cenozoic rocks indicate a presence of HIMU and EM-I or EM-II sources. However, as is seen from Figure 10, none figurative point of the Cenozoic areal fall into the field of EM-II source. Thus, the oblongness of fields

corresponding to isotope compositions of the Cenozoic mafic rocks in relation both to ϵ_{Nd}^T and to Th/La ratio values is due to assimilation by the mafics of small portion of continental crust.

So, the presentation of our data concludes that there existed **diverse magma sources for within-plate mafic rocks and related to them alkaline granites and other felsic alkaline rocks, including rare metal-bearing ones.**

All available isotopic geochemistry evidence for most of these rocks indicates that they were genetically related to mantle sources of mafic rocks, though for the Early Mesozoic igneous, the essential contribution of continental crust component to the source is quite possible (Fig. 12). The necessity now arises of isotope-geochemical systematization of alkaline granitoids and its volcanic equivalents in terms of their sources. Using for convenience the types of mafic rocks in terms of its sources, alkaline granitoids and the related volcanics can be classed into the following types: DM, HIMU, EM-I, EM-II and their mixtures as well as CC-type (continental crust). The last-named type of alkaline granitoids (CC-granites and CC-comendites) requires additional substantiation. Most of studied alkaline granitoids represent mixed types: according to major components of magma sources, the Early-to-Middle Paleozoic rocks belong to (DM + HIMU + KK)-type, the Late Paleozoic granitoids are classified as (HIMU + DM + EM-II + KK)-type, the Early- and Late Mesozoic rocks are assigned to (EM-II + KK)-type, the Cenozoic alkaline magmatites represent (HIMU + EM-I + KK?)-type. The published materials suggest that the rocks from Pantelleria Island belong to HIMU-type whereas bimodal assemblage from the Ethiopia Rift are of (HIMU + EM)-type. According to current isotopic geochemistry concepts, the component EM-I is located on border of a core of the earth and lower mantle and the EM-II component is centered on border of lower mantle and upper mantle.

Sources of within-plate igneous activity in the Central-Asian folded belt are related to mantle plumes. The latter can be attributed to enriched mantle. However, the mixtures of various mantle components in sources of within-plate magmatism of different ages suggest that within plume, the various constituents of these sources not only interacted with each other but these constituents interacted with depleted mantle of lithosphere as well.

The general model of a role mantle plumes in the structure of CAFB is represented in Figure 12. In the initial stage supercontinent Rhodiniya situated at the equator zone has broken up under the effect of the South-Pacific hot superplume. Within the block of future Siberia, the large rare-metal carbonatite deposits of Late Riphean age (the regions of Yenisey Ridge, East Sayany, northeastern Aldan) have been formed. Since the Early Paleozoic Siberia has been displacing to the north from the equator, toward the mid-latitudes, probably, due to breaking superplume "cap". The within-plate igneous activity rather decreased but it continued to produce magmatites, including rare metal-bearing ones. We also assume the second, more probable, variant in development of CAFB. We suppose that during the interval of Ordovician-to-Devonian Siberia in the course of its drift

has got in the area of the Asian hot field of mantle. The Early-Middle Paleozoic within-plate magmatism province with numerous rare metal deposits hosted within carbonatites, alkaline granites and others rocks was formed under the influence a series of plumes of this mantle plume system. In Late Paleozoic-to-Early Mesozoic time the within-plate igneous activity continued with probable reduction of the area of magmatic occurrences due to sinking cold sial material into superplume field. In the Late Mesozoic, "degradation" of the Asian plume continued culminating in the Early Cenozoic. However, spatially limited within-plate magmatism including its rare metal occurrences continued. From about that time within-plate activity became more intense and it continues up to the present days being related to deeper source EM-I.

This work was supported by the Russian Foundation for Basic Research (projects ¹ 99-65645,99-05-65647, 00-05-65288).

REFERENCES

1. Kogarko L.N., Kononova V.A., Orlova M.P., Woolley A.R. Alkaline rocks and carbonatite of the World: part 2, Former USSR. London-Glasgow-Weinheim-New-York-Tokio, Melbourne-Magras. Chapman and Hall. 1995. 226 p.
2. Kostisyn Yu. A., Vystavnoi S.A., Vladimirov A.G. Age and genesis of the spodumen-bearing granites of the SW Altai (Russia): an isotopic and geochemical study // Acta Universitatis Carolinae-Geologica. 1998. V. 42. P. 60-63.
3. Kovalenko V.I., Popolitov E.I. Petrology and geochemistry of rare elements in alkaline and granitic rocks of North-East Tuva. Moscow: Nauka Press. 1970. 258 p. (in Russian).
4. Kovalenko V.I. Petrology and geochemistry of rare metal granitoids. Novosibirsk: Nauka Press. 1977. 206 p. (in Russian).
5. Kovalenko V.I., Tsareva G.M., Goreglyad A.V., Yarmolyuk V.V., Troitsky V.A. The peralkaline granite-related Khaldzan-Buregtey rare metal (Zr, Nb, REE) deposit, Western Mongolia // Econ. Geol. 1995. V. 90. P.530-547.
6. Kovalenko V.I., Kostisyn Yu. A., Yarmolyuk V.V., Budnikov S.V., Kovach V.P., Kotov A.V., Salnikova E.B., Antipin B.S. Magma sources and isotopic (Sr, Nd) evolution of rare metal Li-F granitoids // Petrology. 1999. V. 7. No. 4. P. 401-429. (in Russian).
7. Kovalenko V.I., Yarmolyuk V.V., Budnikov S.V., Kotov A.V., Salnikova E.B. Crust-forming processes and crust and mantle structures in formation of the Central-Asian folded belt: Sm-Nd isotopic evidence // Geotectonics. 1999. No. 3. P. 21-41. (in Russian).
8. Kovalenko V.I., Yarmolyuk V.V., Kozlovsky A.M., Ivanov V.G. Magma sources of alkaline granitoids and the related rocks from within-plate igneous assemblages of Central Asia // Doklady RAN. 2001. V.377. No. 5. P. 672-676. (in Russian).
9. Lykhin D.A., Kostisyn Yu. A., Kovalenko V.I., Yarmolyuk V.V. Ore-producing magmatism of the Ermakov beryllium deposit in west Transbaikalye: age, magma sources and correlation with mineralization // Geologiya rudnykh mestorozhdenii (*Geology of ore deposits*). 2001. V. 43. No. 1. P. 54-72. (in Russian).
10. Maruyama S. Plume tectonics // Journ. Geol. Soc. Japan. 1994. V. 100.No. 1. P. 114-127.
11. Novikov M.I., Shpanov E.P., Kupriyanova I.I. Petrography of the Ermakov beryllium deposit, West Transbaikalye // Petrology. 1994. V. 2. No.1. P. 114-127. (in Russian).
12. Rainbird R.H., Stern R.A., Khudoley A.K., Kropachev A.P., Htaman I.M., Sukhorukov V.I. U-Pb geochronology of Riphtan sandstones and gabbro from southeast Siberia and its

- bearing on the Laurentia-Siberia connection // *Earth Planetary Sci. Lett.* 1998. V. 164. No. 3-4. P.409-420.
13. Samoilov V.S., Kovalenko V.I. Alkaline and carbonatite rock complexes of Mongolia. Moscow: Nauka Press. 1983. 200 p. (in Russian).
 14. Sklyarov E.V., Gladkochub D.P., Mazukabzov A.M. Dike swarms in south flank of the Siberian Craton – indicators of supercontinent Rhodinia disintegration // *Geotectonics*. 2000. No. 6. P. 59-75. (in Russian).
 15. Vladykin N.V., Kovalenko V.I., Dorfman M.D. Mineralogical and geochemical features of the Khan-Bogdo peralkaline granite massif. Moscow: Nauka Press. 1981. 136 p. (in Russian).
 16. Vladykin N.V., Kovalenko V.I., Dorfman M.D. Mineralogy, geochemistry and genesis of rare-metal topaz-lepidolite-albite pegmatites in the Mongolian People's Republic // *New data on minerals in USSR*. Moscow: Nauka Press. 1974. V. 23. P. 6-49. (in Russian).
 17. Vladykin N.V. Petrology and ore potential of K-alkali rock complexes in the Mongol-Okhotsk magmatism area. Abstr. of doctoral geol.-miner. Sci. Thesis. Irkutsk. 1997. 80 p. (in Russian).
 18. Weis D., Demaiffe D., Cauet S., Javoy M. Sr, Nd, O, and H isotopic ratios in Ascension Island lavas and plutonic inclusions; cogenetic origin // *Earth Planetary Sci. Lett.* 1987. V. 82. P.255-268.
 19. Yarmolyuk V. V. Kovalenko V.I., Kotov A.B., Salnikova E.B. Angaro-Vitim batholith: on problem of batholith-formation geodynamics in the Central-Asian folded belt // *Geotectonics*. 1997. No. 5. P. 18-32. (in Russian).
 20. Yarmolyuk V. V. Kovalenko V.I., Kuzmin M.I. North-Asian Superplume in Phanerozoic time: magmatism and deep geodynamics // *Geotectonics*. 2000. No. 5. P. 1-27. (in Russian).

DEVONIAN PLUME MAGMATISM IN THE NE BALTIC SHIELD: RARE EARTH ELEMENTS IN ROCKS AND MINERALS OF ULTRABASIC ALKALINE SERIES AS INDICATORS OF MAGMA EVOLUTION

A. A. Arzamastsev*, F. Bea, L. V. Arzamastseva*, and P. Montero****

* *Geological Institute, Kola Science Centre, Russian Academy of Sciences, 14 Fersmana St., Apatity, Murmansk Oblast, 184200 Russia, e-mail: arzamas@geoksc.apatity.ru*

** *University of Granada, Dept. of Mineralogy and Petrology, Fuentenueva s/n., 18002, Granada, Spain*

In order to elucidate evolutionary paths for the alkaline ultramafic series of the Kola province, we studied distribution of rare earth elements (REE) in rocks and constituent minerals of the rock sequence dunite, clinopyroxenite, melilitolite, melteigite, ijolite, nepheline syenite. Abundances of REE and other trace elements were measured in olivine, melilite, clinopyroxene, nepheline, apatite, perovskite, titanite, and magnetite. Distribution of most of trace elements in Kovdor-type rocks is shown to differ fundamentally from that in the Khibiny alkaline ultramafic suite and to have been controlled by perovskite crystallization. Primary olivine melanephelinitic melts of the Kovdor series are demonstrated to be characterized by early crystallization of perovskite, the most important REE mineral. Perovskite co-precipitating with olivine and clinopyroxene leads to a dramatic REE depletion of the residual melt, to produce REE-depleted derivatives, ijolites and nepheline syenites. By contrast, the genesis of the Khibiny alkaline ultramafic series was complicated by mixing of minor batches of phonolitic melt with the primary olivine melanephelinitic magma, which led to changes in the crystallization order of REE-bearing titanates and Ti-silicates and to enrichment of late melt batches in the most incompatible elements. As a result, Khibiny ijolites have the highest REE abundances, which are accommodated by high-REE apatite and titanite.

INTRODUCTION

In the northeastern Baltic Shield, the Paleozoic stage of tectonic and magmatic reactivation involved generation of alkaline plutonic complexes, which have been customarily divided into two rock suites: (i) alkaline ultramafic rocks associated with carbonatites (Kovdor, Vuoriyarvi, Afrikanda, Seblyavr, and other massifs) and (ii) agpaitic nepheline syenites, represented in the vast Khibiny and Lovozero plutons. Available isotope ages indicate that all the Paleozoic alkaline massifs of the Kola province were coeval, and their parental melts were derived from the same mantle sources [23, 26]. The hallmark of the region's alkaline rocks is their immense abundances of REE, Y, Sr, Zr, Hf, Nb, Ta, and Th. These are either concentrated in apatite, titanite, perovskite, and other accessories or, given their concentrations in melts were high enough, form their own discrete minerals, such as loparite, pyrochlore, and eudialyte, whose economic deposits provide the basis for the region's mining industry.

Geologic observations and experimental evidence suggest that alkaline ultramafic rocks forming parts of carbonatite complexes originated through crystal fractionation in nephelinitic melts, which resulted, at early stages, in olivine, clinopyroxene, and melilite cumulates and their complementary foidolites and nepheline syenites [3, 11, 19, 30, 40, 51]. Available data on behavior of incompatible elements during magma genesis suggest that with advancing magma crystallization, such elements as Sr, Zr, Hf, Nb, Ta, Th, and REE are likely to become enriched in terminal melt derivatives of the alkaline ultramafic series. This is indeed the case in alkaline ultramafics of the Khibiny massif, at whose lower horizons large fragments of such bodies are found surrounded by agpaitic syenites [4, 16]. However, in the majority of alkaline ultramafic plutons, terminal crystallization products (ijolites, nepheline syenites, and cancrinite syenites) are appreciably depleted in Nb, Ta, and rare earths.

This work is intended to study how the above trace elements behave in alkaline ultramafic suites and, in particular, to find out why rare earth elements follow different distribution patterns in ultramafic carbonatite intrusions and in the Khibiny massif. Our study draws on mineralogical and geochemical data on representative samples from the Kovdor, Vuoriyarvi, Cape Turiy, Salmagora, and Afrikanda massifs, the Lesnaya Varaka and Ozernaya Varaka intrusions, and the Khibiny complex. ICP-MS analyses were made on whole-rock samples and on separates of coexisting perovskite, apatite, titanite, clinopyroxene, melilite, olivine, nepheline, and magnetite. Data obtained enable us to identify those factors responsible for the diversity of REE distribution patterns in alkaline ultramafic suites and, in particular, to assess the role of high-REE accessory phases perovskite, apatite, and titanite.

2. GEOLOGIC STRUCTURE OF THE INTRUSIONS

In the northeastern Baltic Shield, intracratonic magmatism that spanned some 40 to 50 m.y. can be divided into three episodes. The initial episode, from 405 to 380 Ma, coinciding with the final phase of Caledonian orogeny, involved inception of the Khibiny, Lovozero, and Kontozero calderas in the foreland of the Caledonian front, accompanied by subalkaline volcanism and emplacement of ultramafite and Ne-syenite intrusions. The principal period of igneous activity, between 380 and 360 Ma, gave rise to the multiphase Khibiny and Lovozero plutons and to alkaline ultramafic intrusions associated with carbonatites [26, 27] (Fig. 1). The final episode resulted in dike swarms and diatremes made up of alkaline picrites, melanephelinites, melilitites, and kimberlites.

2.1. Alkaline ultramafic plutonic suites forming parts of carbonatite intrusions (Kovdor type)

Plutonic alkaline ultramafic suites are found forming parts of multiphase intrusions. Lithologic zonation of the intrusive bodies portrays the following order

of emplacement of rocks that constitute the series (i) dunite, (ii) pyroxenite, (iii) melilite-bearing rocks (turjaite, melilitolite, okaite), (iv) melteigite, (v) ijolite, (vi) nepheline/cancrinite syenite, and (vii) carbonatites and phoscorites. The complete set of lithologies is represented in the Kovdor, Cape Turiy, and Vuoriyarvi massifs, whereas in the rest of intrusions only particular groups of rock varieties are exposed at the present topographic surface. In most intrusions, olivine and clinopyroxene cumulates make up their cores, melilite rocks and foidolites

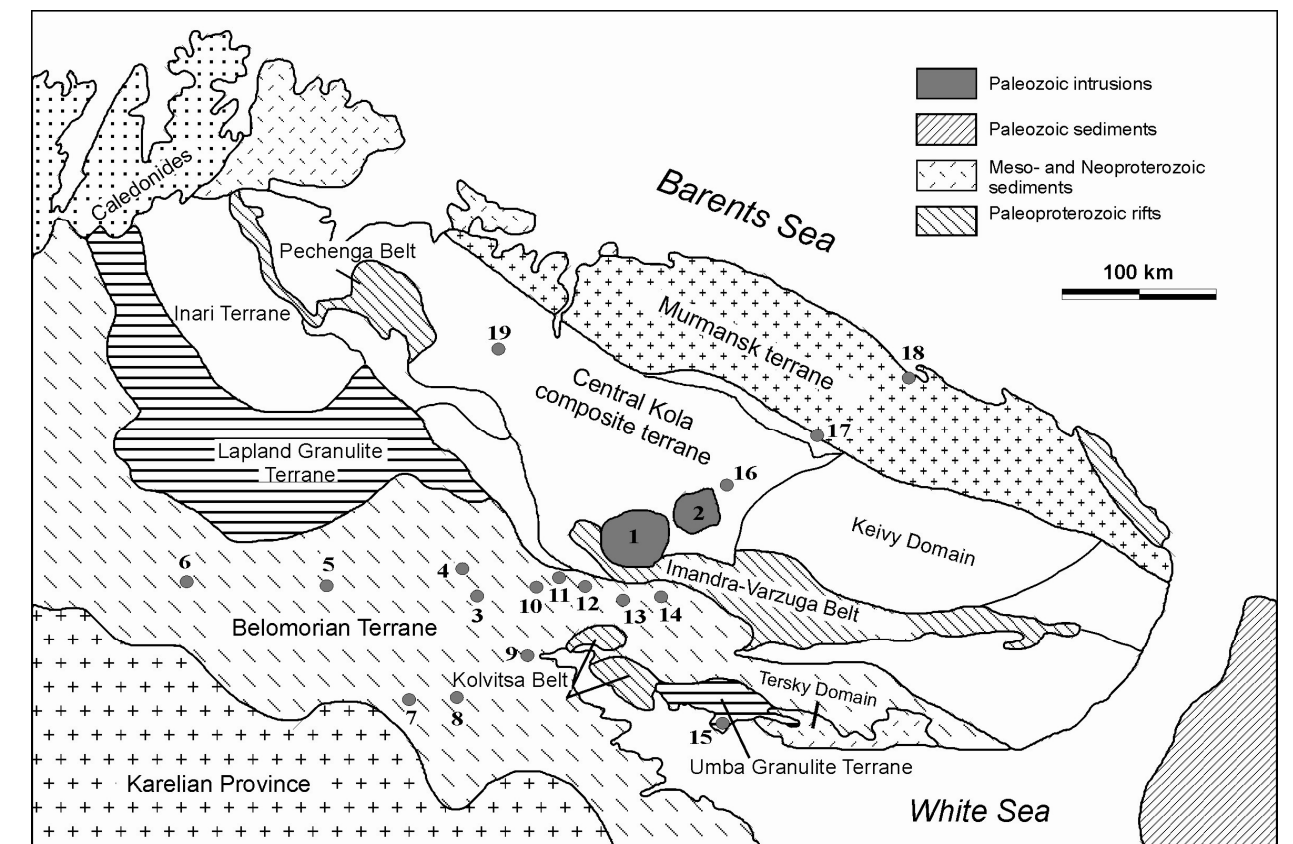


Fig. 1. Location scheme for Paleozoic igneous occurrences in northeastern Baltic Shield.

Intrusions: 1 – Khibiny, 2 – Lovozero, 3 – Niva, 4 – Mavraguba, 5 – Kovdor, 6 – Sokli, 7 – Sallanlatva, 8 – Vuoriyarvi, 9 – Kandaguba, 10 – Afrikanda, 11 – Ozernaya Varaka, 12 – Lesnaya Varaka, 13 – Salmagora, 14 – Ingozero, 15 – Cape Turiy, 16 – Kurga, 17 – Kontozero, 18 – Ivanovka, 19 – Seblyavr. Terrane location scheme, after [6]

occurring in peripheral zones (Fig. 2). Nepheline and cancrinite syenites either make up detached satellite bodies near the intrusions (e.g., the Maly Kovdor) or fill in veins in alkaline ultramafics (Ozernaya Varaka). Boss-like carbonatite bodies, surrounded by carbonatite stockworks, are usually located centrally in the intrusions, but occasionally they are displaced from geometric centers of the ring bodies of alkaline ultramafites. The order of emplacement, based on generalized field evidence from all the intrusions of the region, is consistent with that reported for alkaline ultramafic intrusions worldwide [22, 32, 39, 53]. Alkaline ultramafic intrusions occur in spatial association with bodies of olivine melteigite porphyry

and with dikes and diatremes of alkaline picrite, Ol-melanephelinite, nephelinite, and melilitite.

2.2. Alkaline ultramafic plutonic suites forming parts of agpaitic syenite complexes (Khibiny type)

According to geophysical data [4], volumetrically, alkaline ultramafic rocks make up at least 30% of the Khibiny pluton within the 12.5 km depth range accessible to gravity surveying. The pluton is thus shown to comprise the complete series of rocks typical of alkaline ultramafic massifs of the province: peridotites, pyroxenites, melilitolites, melteigites, ijolites, and carbonatites. The Khibiny complex displays at least three phases of emplacement of alkaline ultramafic melts with intervening stages of Ne-syenite magma injection (Fig. 3). The peridotites, pyroxenites, and melilitolites originated at the earliest formative phase of the massif, which preceded agpaitic syenite injections. The ring melteigite-ijolite intrusion took shape after the emplacement of nepheline syenites forming the margin of the Khibiny massif, but prior to the formation of the Ne-syenites found in its core. The Khibiny alkaline ultramafic series culminated in carbonatites, which cut through the Ne-syenite core of the massif and carry pyroxenite, ijolite, and melteigite xenoliths.

3. Analytical techniques and sample preparation

Sixty-nine representative samples, collected from drill cores and outcrops in the Khibiny, Kovdor, Afrikanda, Cape Turiy, Lesnaya Varaka, Ozernaya Varaka, Seblyavr, Salmagora, Sallanlatva, Vuoriyarvi, and Ivanovka intrusions, were selected for this study from a total of more than 500 samples.

Whole-rock major element analyses were carried out at the Geological Institute, Kola Science Center, Russian Academy of Sciences, using a routine technique of sample fusion with $2\text{Na}_2\text{CO}_3+1\text{Na}$ -tetraborate followed by dissolution in HCl. Si, Al, Mg, Ca, Fe, Ti, Ni, Co, Cr, and V were measured by atomic absorption on a Perkin Elmer 403 instrument with an accuracy (coefficient of variation, CV) better than 3% (G. Gulyuta, analyst). Na, K, Li, Rb, and Cs were measured by flame photometry (CV ~ 5%); P and S, by photolorimetry and polarography from the same solutions with an accuracy of ~ 5% and ~ 10%, respectively; and F and Cl, by the ion-selective electrodes method (CV ~ 15%).

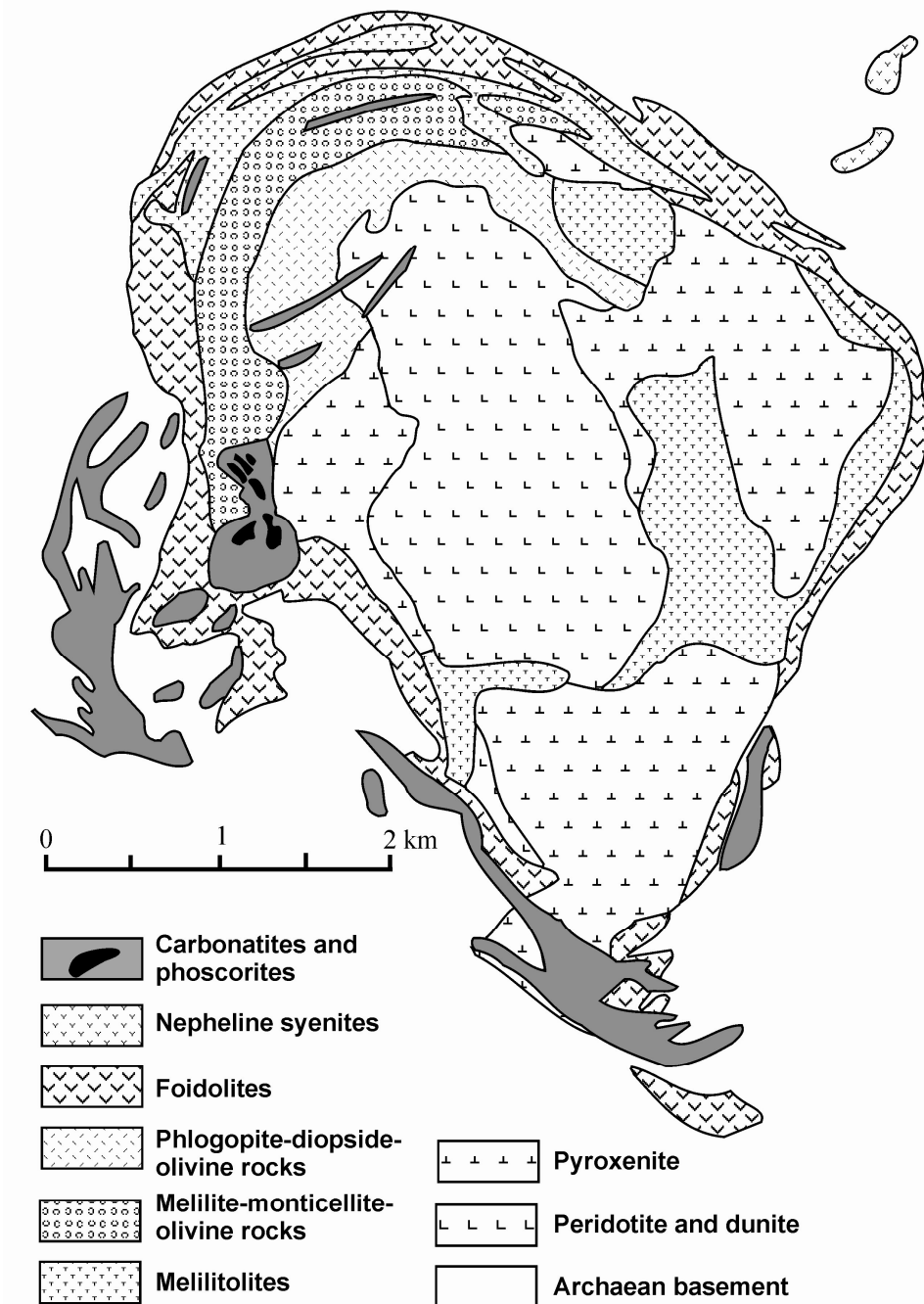


Fig. 2. Scheme showing geologic structure of the Kovdor massif, simplified after [47].

The $\text{Fe}^{2+}/\text{Fe}^{3+}$ ratio was measured by titration (CV ~ 10%). H_2O and CO_2 were analyzed by the gravimetric method (CV ~ 10%). Trace elements were analyzed by ICP-MS at the University of Granada. Sample charges of 0.1 g were allowed to stand for 30 min in an $\text{HNO}_3 + \text{HF}$ mixture in Teflon-lined containers at $T = 180^\circ\text{C}$ and ~200 p.s.i., evaporated until dry, and dissolved in 100 ml of 4% HNO_3 . Each specimen was analyzed three times on an ELAN-5000 PE SCIEX instrument using a rhenium within-lab standard. Accuracies were ± 2 rel.% and ± 5 rel.% or better for concentrations of 50 and 5

ppm, respectively. Major elements in minerals were measured at the Geological Institute, Kola Science Center, on a Cameca MS-46 ion microprobe using natural and synthetic standards. Acceleration voltage was 30 kV for Sr and Zr and 20 kV for the rest of the elements; sample current was 20–40 nA, and ion beam diameter, 1.5–3 μm.

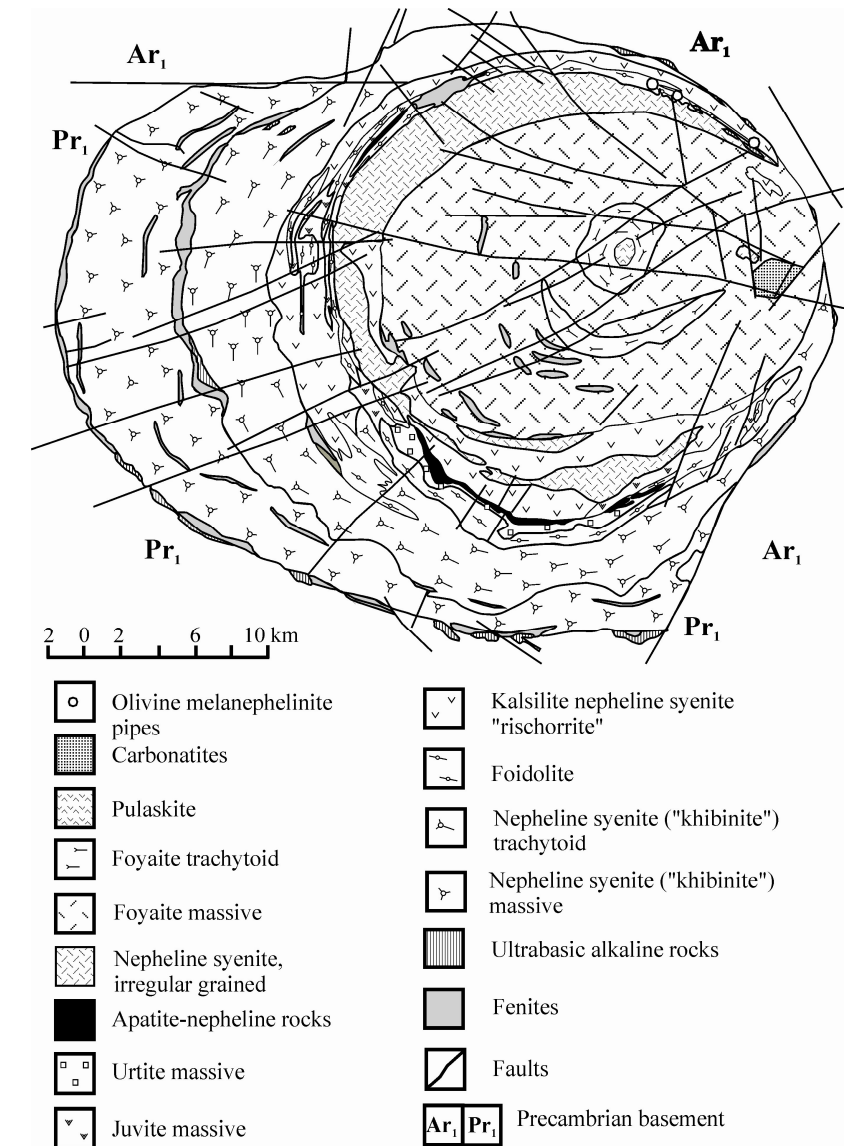


Fig. 3. Geological map of the Khibiny massif. Generalized from the map of MGRE "Sevzapgeologiya".

Mineral grains separated for trace-element analysis were inspected under an optical microscope in order to reject foreign inclusions. A number of samples were inspected under a scanning electron microscope. Minerals were separated on a magnetic separator and in heavy liquids. Finally, 8–10 mg charges were cleaned by repeated hand-picking to 99.9 vol % purity. Trace element abundances in sample charges were measured by ICP-MS as described above.

4. Petrography of the rocks and distribution of REE-bearing mineral phases

Ultramafic rocks. Kovdor-type dunites, Ol-clinopyroxenites, and pyroxenites are adcumulates and mesocumulates with olivine and clinopyroxene as cumulus phases and ore minerals, phlogopite, spinel, and nepheline, as intercumulus. The only primary high-REE minerals are perovskite and apatite. In the dunites, perovskite occurs sporadically as an intercumulus phase forming small rounded grains. In the pyroxenites, perovskite is present as an early cumulus phase accounting for as much as 40 vol % in Vuoriyarvi rocks, 19–31 vol % in Afrikanda, and 11–16 vol % in the Salmagora massif [25, 30]. In ultramafic rocks, apatite is less common, dunites containing no more than 0.2% and pyroxenites usually bearing up to 3% apatite by volume. The only exception is Vuoriyarvi and Afrikanda pyroxenites, in which apatite accounts for as much as 8% of rock volume [30]. Besides perovskite and apatite, the pyroxenites contain sporadic titanite that forms secondary segregations partially replacing perovskite and magnetite.

Ultramafic rocks encountered in the Khibiny and Lovozero massifs are represented by peridotites and, chiefly, by pyroxenites, which are texturally and compositionally similar to ultramafics of the Kovdor suite. Pyroxene with characteristic cumulus features is in places partially replaced by richterite and/or phlogopite. REE-bearing accessories are represented by apatite and titanite (up to 6 and 2 vol %, respectively). An important distinction is that perovskite is a rare accessory in all ultramafic rocks from the Khibiny.

Melilite-bearing rocks, dominantly uncomphagrites and turjaites, form independent intrusion phases in the Kovdor and other alkaline ultramafic massifs. In the Khibiny and Lovozero, melilite rocks are encountered as xenoliths. Melilite together with phlogopite compose large oikocrysts with clinopyroxene and nepheline inclusions. REE-bearing phases, represented by perovskite, apatite, and, less frequently, titanite, occur sporadically. Interstitial segregations of magnetite are not infrequently rimmed by secondary perovskite, indicative of a Ti-bearing phase having been exsolved from primary titanomagnetite [38].

Foidolites occur widely in both the Kovdor and Khibiny alkaline ultramafic suites. The rocks are ortho- and mesocumulates with nepheline segregations varying in habit from anhedral to euhedral in less and more leucocratic rocks, respectively. Clinopyroxene makes up zoned segregations whose compositions are different in the Kovdor and Khibiny suites. In foidolites of the Kovdor and other alkaline ultramafic massifs, pyroxene is represented by diopside, which makes up grain cores, while grain rims are composed of aegirine-augite. Pyroxenes in Khibiny ijolite-melteigites are more alkaline than in the Kovdor suite and, unlike the latter, are composed of aegirine-augite rimmed by aegirine. Accordingly, late amphiboles developed after clinopyroxene have different

compositions, mostly pargasitic in Kovdor foidolites and corresponding to richterite or magnesiocataphorite in the Khibiny suite.

Distribution patterns of REE-bearing accessories are different in Kovdor and Khibiny foidolites. In Kovdor, Vuoriyarvi, and Cape Turiy, melteigites and ijolites, the early-generation perovskite, just as apatite and titanite, is a typical accessory phase. Not infrequently, the perovskite is observed to be replaced by titanite. The mean titanite abundance in ijolites is < 1 vol %. Apatite abundances in foidolites attain a critical maximum of 1.2 wt % in the most melanocratic lithologies [5].

Unlike the Kovdor suite, Khibiny foidolites contain apatite and titanite not only as late magmatic accessories, but also as widespread primary REE minerals. Both apatite and titanite are most abundant in melanocratic foidolite varieties, where they account for 4 and 5 vol % on average, respectively. A distinctive feature of Khibiny foidolites is that they lack primary perovskite.

Nepheline and cancrinite syenites in Kovdor-type massifs show evidence of early crystallization of light-colored phases, nepheline and K–Na-feldspar. Just as in foidolites, pyroxene is represented by zoned grains of diopside rimmed by aegirine-augite. REE-bearing accessories are titanite and apatite.

Arzamastsev et al. [4] showed that neither Khibiny nor Lovozero agpaitic Ne-syenites are cogenetic with rocks of the alkaline ultramafic series. This is evidenced, in particular, by the fact that the REE-bearing mineral assemblage in agpaitic syenites differs fundamentally from that in the alkaline ultramafic rocks. Lovozero lujavrites have as much as 90 vol % eudialyte and 12 vol % loparite, while in Khibiny Ne-syenites the most widespread primary magmatic phases are eudialyte and apatite. Distribution, composition, and origin of these economically important minerals were studied by Kogarko [20, 24] and Kravchenko et al. [28] and are beyond the scope of this work.

5. Results

5.1. Rock chemistry

5.1.1. Major elements

Bulk-rock analyses of representative of Kovdor- and Khibiny-type alkaline ultramafic suites are listed in Table 1. Compositional variation trends for both suites, plotted on the totality of major-element analyses amassed to date (Fig. 4), show the ultramafic portion to be controlled by precipitation of olivine and clinopyroxene, whereas the foidolite trend is controlled by fractionation of clinopyroxene and nepheline. The decrease in Mg# through this rock sequence from 0.90 in dunites to 0.56 in Ne-syenites of the Kovdor suite is correlative with variations of Ni, Cr, Co, V, and Sc.

The following distinctions exist between the Kovdor and Khibiny suites in terms of major-element abundances. Khibiny foidolites are relatively lower in MgO and higher in SiO₂ and alkalis (Fig. 4). Thus, weighted mean abundances of these oxides in Khibiny foidolites are 43.62 wt % SiO₂, 9.40 wt % Na₂O, 3.59 wt

% K₂O, and in Kovdor-type foidolite intrusions, 41.64 wt % SiO₂, 8.10 wt % Na₂O, 2.73 wt % K₂O. The high contents of silica and alkalis are manifested in modal-mineral compositions of Khibiny foidolites, such that K–Na-feldspar is a characteristic accessory mineral in ijolites, where it accounts for as much as 10 vol %. Among other distinctions between Kovdor and Khibiny rocks, one should note the higher F content of Khibiny rocks and the differences in TiO₂ and P₂O₅ distributions. Thus, in Kovdor suite the highest TiO₂ abundances are detected in pyroxenites, which have 8–15 wt % MgO on average, whereas in Khibiny suite, TiO₂ is highest in the most evolved rocks, ijolites and melteigites, which have 3–7 wt % MgO.

5.1.2. Rare earth elements (REE)

Chondrite-normalized plots for REE from both rock suites, listed in Table 2, are shown in Fig. 5. Along with data for specific samples, all the plots display the REE pattern for the weighted mean composition of alkaline ultramafic rocks of the Kola province [3].

All the Kovdor-type alkaline ultramafic rocks lack Eu anomaly and show depletion in the light REE relative to the heavy REE (Fig. 5). The lowest total REE contents and (La/Yb)_N ratios (11.7–17.4) were detected in olivine cumulates from the Kovdor, Lesnaya Varaka, and Salmagora massifs. By contrast, pyroxenites from the majority of massifs, which contain perovskite and, to a lesser extent, apatite, are sharply REE-enriched relative to the mean composition of alkaline ultramafic rocks. These rocks have steeper REE patterns with (La/Yb)_N = 52–226. More evolved derivatives (melilitolites, foidolites, and Ne/cancrinite syenites) have lower REE contents compared to the mean alkaline ultramafic rock composition for the province, at 5 × 10 to 3 × 10² times the chondritic level. Therefore, with advancing differentiation of the Kovdor suite, late-stage ijolite and Ne-syenite derivatives become progressively depleted in REE.

Khibiny alkaline ultramafic rocks have a REE distribution pattern, which is sharply dissimilar to the Kovdor suite (Fig. 5). By and large, REE abundances of perovskite-free peridotites and pyroxenites are close to the estimated mean values for the alkaline ultramafic series. Due to low (La/Yb)_N ratios, ranging 31.4–53.4, the light REE contents are 0.5–0.7 times the mean values for the alkaline ultramafic series, whereas the medium and heavy REE contents are 2 times higher than the mean values. Just as in pyroxenites, REE abundances in Khibiny melilite rocks are within the range of mean values established for the alkaline ultramafic rocks. On the other hand, the latest derivatives in the suite, ijolites and melteigites, are markedly REE-enriched relative to the mean composition of alkaline ultramafic rocks of the province. In particular, melteigites from the Khibiny layered complex, which have up to 8 vol % titanite and 5 vol % apatite, show 2 × 10³ times the chondritic REE concentrations. To sum up, the Khibiny alkaline ultramafic suite is characterized by a progressive REE enrichment of its late derivatives.

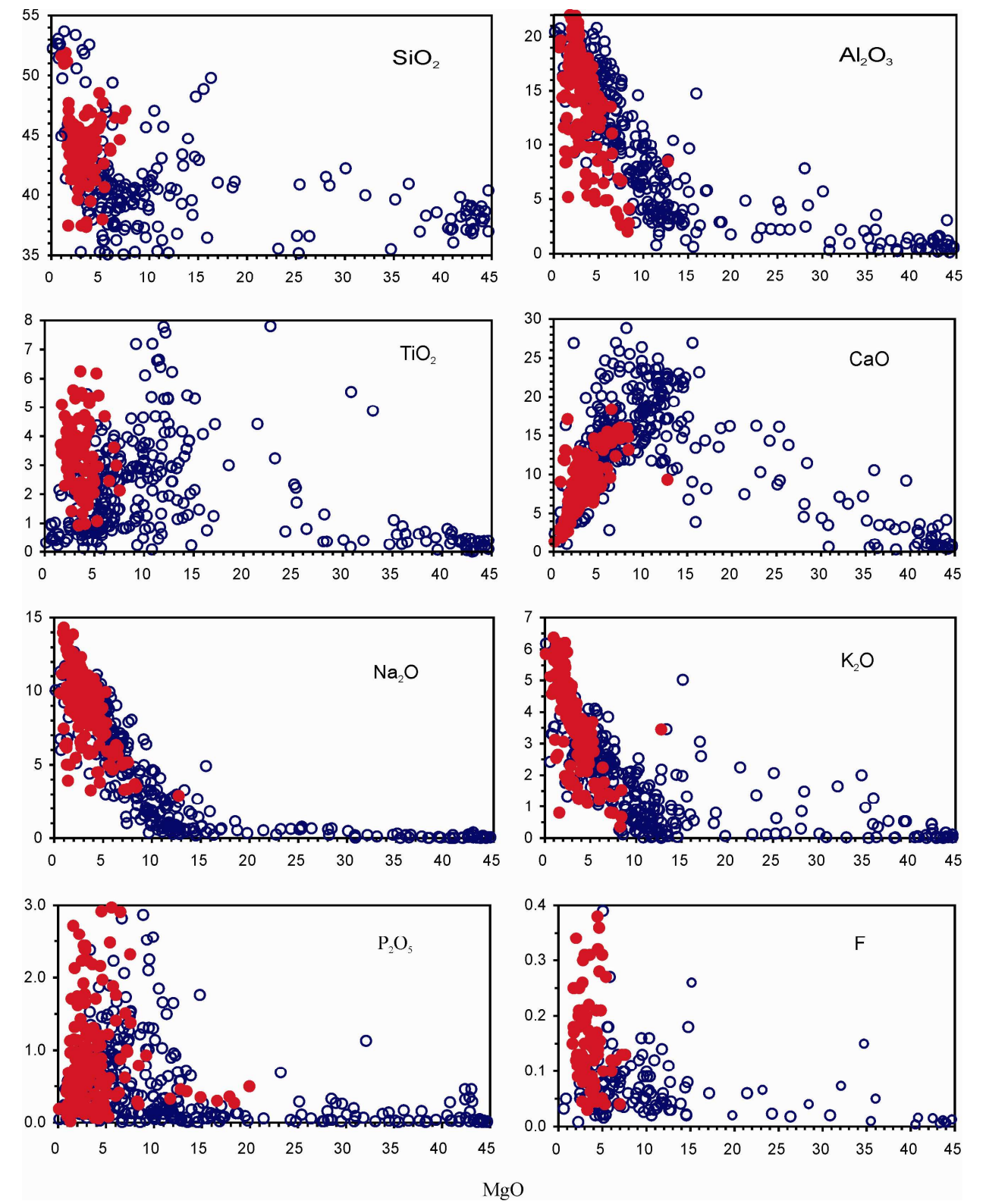


Fig. 4. Major oxides (wt %) vs. MgO in alkaline ultramafic rocks of the Kovdor (empty circles) and Khibiny (solid circles) type.

Table 2.
Rare earth elements analyses (ppm) of the rocks from the Kola ultrabasic alkaline and carbonatite intrusions.

Rock	DUN	PRX	PRX	MELT	MLG	MLG	IJL	SFN	PRD	PRX	MEL	MLG	MLG	IJL	AVER*
Massif	LSV	AFR	VUO	KVD	KVD	OZV	KVD	KVD							
Sample	Z-6	AFR-5	282/ 224	227/ 43	5/740	8-OV	27/ 65	MK-10	1010/ 1052	A-1036	1010/ 1059	455/ 345	1010/ 1186	455/ 402	
La	0.95	354	1046	28.5	8.25	169	18.5	52.1	85.6	102	251	222	380	69.4	131
Ce	1.66	551	2800	52.9	18.5	315	36.2	88.7	176	223	465	441	747	150	249
Pr	0.17	53.0	256	5.71	2.32	34.1	4.19	8.40	20.3	26.4	49.2	50.8	88.9	16.6	27.4
Nd	0.55	189	888	19.9	8.14	116	16.1	27.3	79.9	105	173	190	323	62.2	96.9
Sm	0.11	31.1	125	2.69	1.58	15.1	2.92	3.99	13.7	18.0	23.3	30.4	49.5	10.4	14.4
Eu	0.02	9.23	33.1	0.52	0.36	3.60	0.97	0.78	3.92	5.08	6.18	8.97	14.3	3.04	3.60
Gd	0.08	24.8	86.9	1.62	1.02	11.1	2.52	2.84	10.8	13.2	13.8	22.8	33.1	7.63	10.2
Tb	0.02	3.18	10.1	0.16	0.14	1.28	0.37	0.39	1.39	1.65	1.66	3.08	4.37	1.05	1.26
Dy	0.09	16.0	32.1	0.71	0.77	5.26	2.07	2.16	6.42	7.57	7.85	14.6	21.0	5.26	6.02
Ho	0.02	2.74	4.52	0.13	0.14	0.82	0.40	0.44	1.04	1.22	1.18	2.46	3.42	0.93	1.05
Er	0.05	5.92	7.55	0.28	0.40	1.87	0.99	1.26	2.45	2.63	2.67	5.61	7.83	2.37	2.42
Tm	0.01	0.67	0.75	0.04	0.07	0.25	0.15	0.19	0.28	0.31	0.29	0.66	0.86	0.32	0.32
Yb	0.06	3.50	3.65	0.25	0.42	1.50	0.93	1.22	1.54	1.82	1.66	4.06	4.80	2.20	1.83
Lu	0.01	0.49	0.41	0.04	0.08	0.25	0.14	0.18	0.21	0.27	0.22	0.59	0.60	0.34	0.26
(La/Yb) _N	11.7	71.1	193	81.9	13.9	76.2	14.0	30.0	39.1	39.3	106.8	38.5	55.7	22.2	48.4

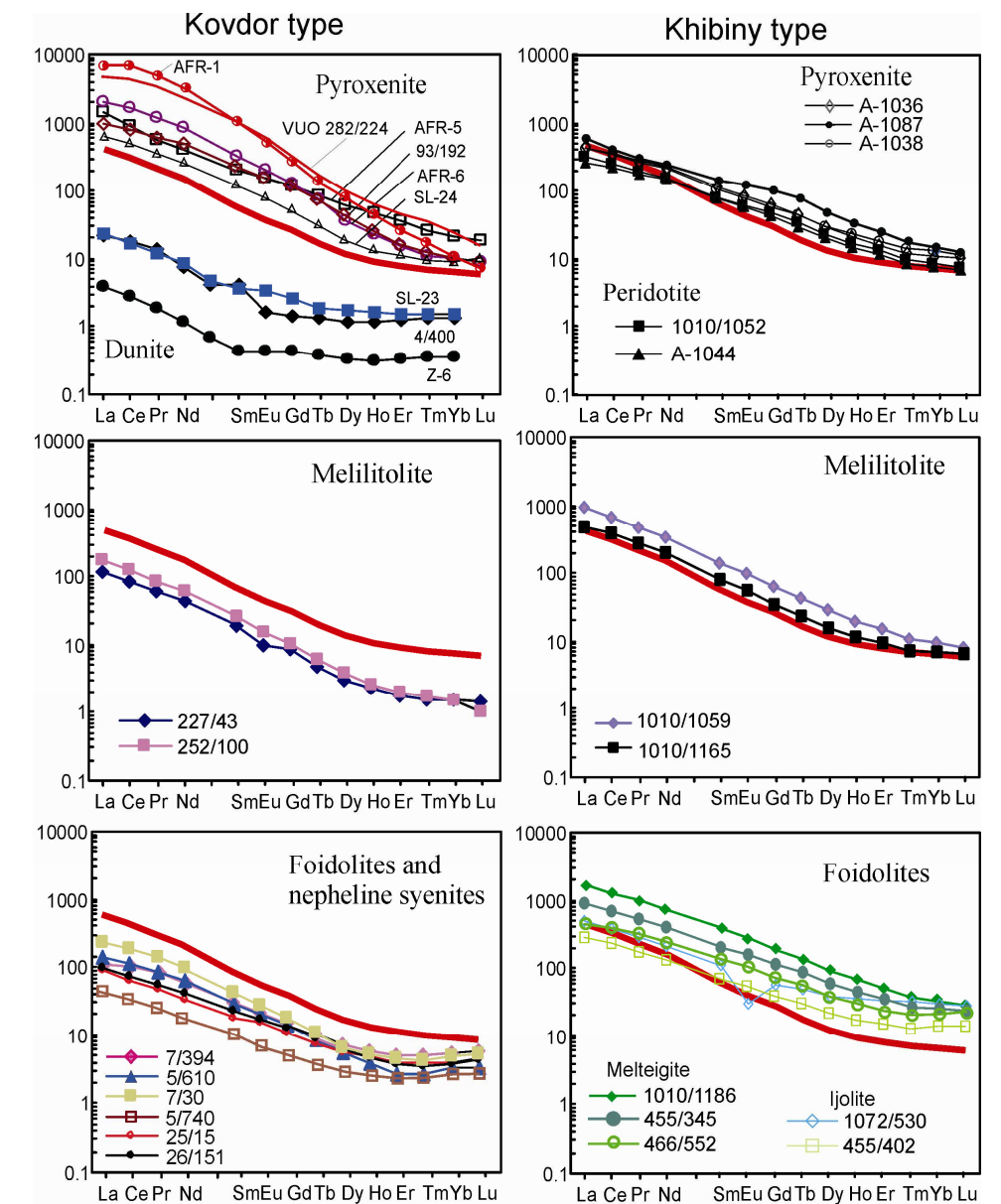


Fig. 5. Chondrite-normalized REE patterns for alkaline ultramafic rocks of the Kovdor and Khibiny types. In all the plots, heavy line shows REE pattern for the weighted mean composition of the alkaline ultramafic series. Normalizing values, after [1].

5.2. REE distribution in minerals

5.2.1. REE-bearing phases

Perovskite. Two generations of perovskite have been reported from alkaline ultramafic rocks of the province. Generation I perovskites originate from the early igneous stage of alkaline ultramafite crystallization, as evidenced by the fact that melilitolites and foidolites, makes up rims around perovskite I and around magnetite. According to [35, 46], the early-generation perovskites are compositionally close to the ideal formula CaTiO_3 , whereas late perovskite segregations follow a loparite trend associated with enrichment in Na, LREE, Nb,

and Th. Established are appreciable compositional distinctions between the early and late generations of the perovskites extracted for analysis. Generation I perovskites (Table 3) have the lowest REE, Nb, Ta, Y, U, Th, and Sr abundances, which have been detected in Vuoriyarvi pyroxenites. On the other hand, in Generation II perovskites, as represented by samples from Kovdor melilitolites and Ozernaya Varaka ijolites, the listed elements have 2 to 10 times the concentrations of the early magmatic perovskites. Overall, all the perovskites are sharply LREE enriched ($(La/Yb)_N = 207\text{--}518$) (Fig. 6). Compared to perovskites from other carbonatite assemblages worldwide, the varieties under study are closely similar to those from the Oldoinyo Lengai foidolites [12] and kimberlites [37] in terms of REE contents, but the latter have higher $(La/Yb)_N$ ratios.

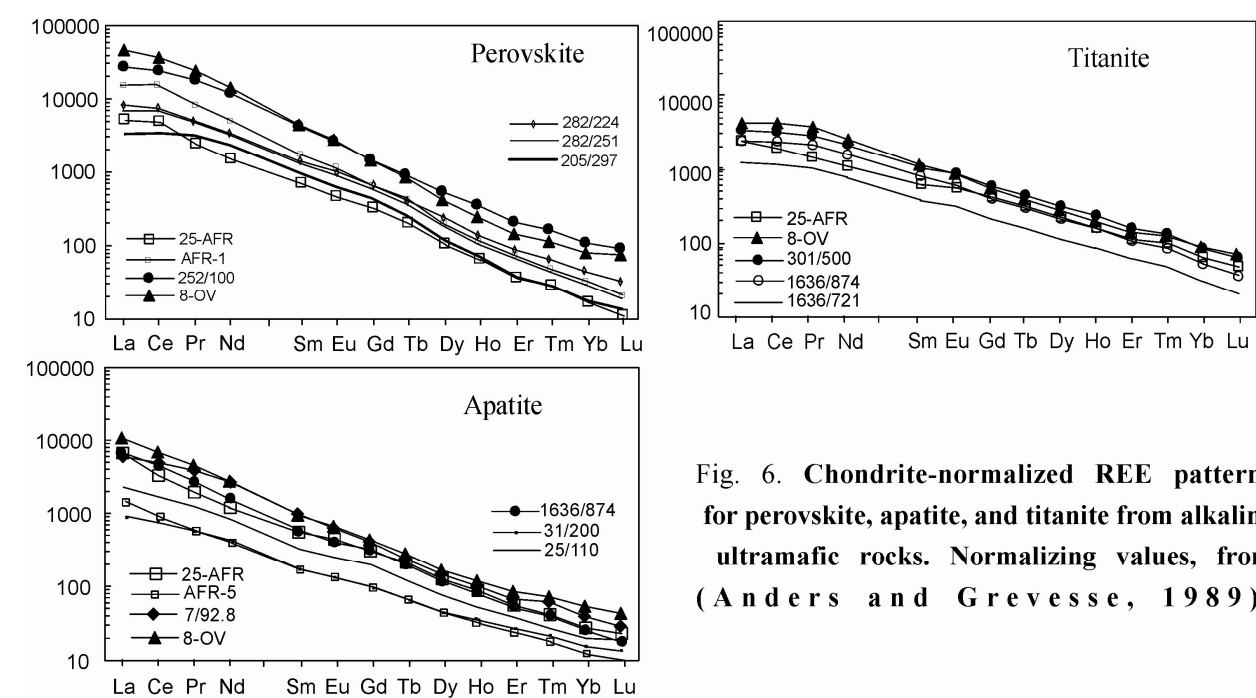


Fig. 6. Chondrite-normalized REE patterns for perovskite, apatite, and titanite from alkaline ultramafic rocks. Normalizing values, from (Anders and Grevesse, 1989).

Apatite. Besides Ca, P, and F, apatites from all the rocks under study have appreciable abundances of Sr, Y, and REE (Table 3), the late apatite generation having highest values. Apatites from pyroxenites and foidolites of the Kovdor, Afrikanda, Sallanlatva, and Khibiny plutons have very narrow ranges of both total REE contents and $(La/Yb)_N$, 57–278. Chondrite-normalized REE spectra (Fig. 6) for apatites are nearly parallel and broadly correlative to the REE abundances of host rocks. The earlier report on Eu anomaly [29] has not been confirmed by any single measurement. Comparison with other provinces in terms of REE contents and patterns shows that apatite compositions under study resemble those from carbonatites of the Alno, Sokli, and Fen massifs [17].

Titanite. We have analyzed late titanites, which replace perovskite in Afrikanda pyroxenites, and groundmass titanites from Ozernaya Varaka and Khibiny ijolites. Comparison shows that Khibiny varieties are appreciably enriched

Table 3.

Trace element composition (ppm) of perovskite and apatite in the rocks of the Kola ultrabasic alkaline series.

Mineral	Perovskite I				Perovskite II			Apatite						
	PRX	PRD	AFR	PRX	MELT	IJL	OZV	AFR	PRX	KVD	OZV	IJL		KHI
Rock	AFR	AFR	AFR	VUO								SLN	SLN	
Sample	25-AFR	AFR-1	205/297	282/224	282/251	252/100	8-OV	25-AFR	AFR-5	7/92.8	8-OV	31/200	25/110	1636/874
La	1246	3510	880	1962	1629	6587	10700	1573	320	1417	2625	221	515	1798
Ce	3081	9255	2301	4582	4274	14822	22177	2023	499	3068	4423	438	984	2740
Pr	216	803	277	486	460	1645	2210	175	49.1	350	425	49.9	108	239
Nd	683	2570	1039	1716	1621	5644	6719	554	169	1247	1315	184	379	755
Sm	98.1	277	137	236	211	672	677	84.6	25.6	158	151	26.5	51.9	85.5
Eu	25.2	66.9	35.0	63.6	54.6	162	159	25.8	7.86	38.3	40.2	7.74	14.3	23.2
Gd	64.1	178.2	91.7	164	142	328	299	63.9	24.3	89.6	95.9	23.7	42.9	71.4
Tb	7.36	18.8	9.55	18.0	15.4	35.9	31.1	7.93	2.91	9.30	10.8	2.81	4.89	8.22
Dy	25.5	53.2	28.8	66.9	46.2	140	111	32.9	12.0	39.8	45.4	12.0	19.8	32.7
Ho	3.63	6.52	3.92	8.24	6.17	21.1	14.3	5.17	2.02	6.18	7.23	2.19	3.38	5.00
Er	5.91	10.5	6.11	13.7	10.0	36.2	24.0	9.53	4.18	12.0	15.3	4.78	7.12	9.66
Tm	0.64	0.99	0.61	1.33	0.90	3.89	2.60	0.97	0.47	1.49	1.76	0.60	0.81	0.99
Yb	2.80	4.89	2.73	6.38	4.40	19.83	13.92	4.83	1.81	7.16	9.80	2.61	3.80	4.35
Lu	0.28	0.52	0.31	0.69	0.45	2.49	1.88	0.60	0.24	0.78	1.17	0.35	0.46	0.44
(La/Yb) _N	300.3	483.3	217.3	207.3	249.6	223.8	517.9	219.3	119.1	133.4	180.5	57.0	91.4	278.5

in Sr, whereas Ozernaya Varaka and Afrikanda titanites have elevated concentrations of Zr, Hf, U, and Th (Table 4). All the varieties have narrow ranges of REE contents and relatively low $(La/Yb)_N$ ratios (40–53), which results in gently sloping, straight chondrite-normalized patterns (Fig. 6).

Table 4.

Trace element composition (ppm) of titanite and magnetite in the rocks of the Kola ultrabasic alkaline series.

Mineral	Titanite					Magnetite		
Rock	PRX	IJL				DUN		MELT
Massif	AFR	OZV	KHI			KVD	LSV	KVD
Sample	25-AFR	8-OV	301/500	1636/874	1636/721	4/400	Z-6	252/100
La	693	1260	961	678	382	8.12	1.22	24.0
Ce	1416	3323	2463	1813	989	12.8	2.25	53.7
Pr	154	407	309	228	123	1.43	0.23	5.69
Nd	556	1423	1148	840	442	4.28	0.57	20.3
Sm	109	209	194	137	70.0	0.60	0.15	2.87
Eu	36.3	59.6	58.7	41.4	20.7	0.01	n.d.	0.84
Gd	98.0	135	143	109	54.7	0.35	0.05	1.93
Tb	13.2	16.9	18.9	14.3	7.29	0.06	0.01	0.27
Dy	62.5	78.6	90.3	63.1	32.2	0.34	n.d.	1.09
Ho	10.2	12.8	14.8	10.3	5.33	0.05	n.d.	0.18
Er	20.9	25.7	29.7	20.3	11.1	0.09	n.d.	0.39
Tm	2.40	3.11	3.36	2.25	1.24	0.01	n.d.	0.04
Yb	11.6	16.0	15.4	9.80	5.11	0.03	n.d.	0.18
Lu	1.26	1.87	1.66	0.86	0.49	0.00	n.d.	0.02
$(La/Yb)_N$	40.1	53.2	42.1	46.6	50.4	173.0	-	95.8

5.2.2. Rock-forming minerals

Olivine. To analyze trace element contents, we selected the purest olivine grains of Fo_{82-91} composition from Kovdor and Lesnaya Varaka dunites. This, however, did not ensure the absence of magnetite microinclusions, which are distributed evenly within olivine crystals.

Scanning electron microscopy detects extremely thin perovskite rims around primary chromite inclusions in olivine. On the one hand, positive correlation of Nb and Ta with REE in olivine (Table 5) implies the presence of perovskite microinclusions. On the other hand, all the olivine specimens analyzed show negative Eu anomaly, also observable in magnetite that coexists with olivine (Fig. 7). The highest Eu oxidation degree ($Eu/Eu^* < 0.08$) was established in Lesnaya Varaka dunites, which contain significant amounts of magnetite. Based on

Table 5.

Trace element composition (ppm) of rock-forming minerals of the Kola ultrabasic alkaline series.

Mineral	Olivine			Pyroxene				Melilite		Nepheline		
Rock	DUN			PRX	MELT	IJL	MLG		MELT		IJL	
Massif	KVD		LSV	AFR	KVD		OZV	KHI	KVD		KVD	KHI
Sample	4/400	4/898	Z-6	25- AFR	252/100	7/30	8- OV	301/500	227/43	252/100	7/30	455/402
La	19.9	17.3	2.29	16.1	14.8	9.17	23.3	36.6	39.2	38.3	22.40	4.81
Ce	33.0	29.8	3.85	29.1	32.4	22.6	52.5	84.9	70.2	66.2	40.3	9.42
Pr	3.34	3.21	0.42	3.09	3.87	3.19	6.04	10.0	7.48	7.01	3.68	1.00
Nd	11.5	9.44	1.31	11.1	15.4	12.1	22.4	38.0	25.2	25.2	12.6	3.35
Sm	1.87	1.20	0.07	1.85	2.73	1.94	3.46	6.45	3.48	3.40	1.72	0.64
Eu	0.33	0.19	0.002	0.53	0.68	0.35	0.94	1.95	0.67	0.78	0.30	0.03
Gd	1.19	0.73	0.10	1.76	1.82	1.39	2.51	4.88	1.82	1.81	1.04	0.57
Tb	0.18	0.08	0.02	0.25	0.23	0.14	0.34	0.66	0.19	0.20	0.12	0.07
Dy	0.98	0.31	0.06	1.15	1.15	0.74	1.81	3.67	0.95	0.93	0.45	0.34
Ho	0.19	0.02	0.01	0.16	0.19	0.14	0.30	0.71	0.15	0.13	0.05	0.05
Er	0.48	0.02	n.d.	0.38	0.46	0.36	0.83	1.99	0.24	0.25	0.08	0.10
Tm	0.07	0.001	n.d.	0.06	0.07	0.07	0.13	0.36	0.03	0.03	0.01	0.01
Yb	0.51	n.d.	n.d.	0.58	0.52	0.95	1.00	3.39	0.16	0.13	0.03	0.07
Lu	0.09	n.d.	n.d.	0.10	0.09	0.19	0.18	0.66	0.02	0.02	0.00	0.01
(La/Yb) _N	27.7	-	-	19.7	20.2	6.8	16.4	7.6	177.8	202.8	463.3	47.7

this evidence, we assume that a considerable fraction of REE contained in olivine grains is concentrated not in this mineral proper, but in perovskite and magnetite microinclusions.

Clinopyroxene. In early cumulates of the alkaline ultramafic series, clinopyroxene is represented by diopside $Di_{80}Hd_{15}Ac_5$, with foidolites and nepheline syenites containing zoned segregations that range in composition from augite $Di_{55}Hd_{40}Ac_5$ to aegirine-augite $Di_{50}Hd_{30}Ac_{20}$ [2,30]. A study of zoned pyroxene grains using the laser ablation technique (Arzamastsev et al., in press) shows that zone-to-zone variations of major elements within crystals are not accompanied by any marked variations in the contents of trace elements, in particular, REE. This is further supported by analyses of pyroxene separates from pyroxenites, melilitolites, and ijolites from carbonatite massifs of the province, which reveal a narrow range of REE variations in all the groups of rocks (Table 5). The higher REE contents are observed in rock varieties from Khibiny ijolites, although all the rocks have the same REE distribution pattern. Plots shown in Fig. 8 demonstrate all the clinopyroxenes to be enriched in Yb and Lu relative to Dy, Ho, and Er. *Melilite.* Microprobe measurements on melilitites from rocks of the Kovdor massif yield the following composition (mol %): Mg-akermanite, 49–70; Fe-akermanite, 5–11; Na-melilite, 36–40. As compared with previously published data on melilite compositions in the rocks of the province

[7], the analyzed melilites have higher Mg/Fe ratios, a feature typical of Ne-free alkaline ultramafites [46, 34]. Overall, the melilite is high in Sr due to the isomorphous replacement $\text{Sr}^{2+} \rightarrow \text{Ca}^{2+}$. Unlike Khibiny melilites, Kovdor ones display no appreciable enrichment in Sr (Table 5). As compared with the scanty reported REE measurements on melilites from various provinces [42, 36], Kovdor specimens have somewhat lowered total REE contents and straight patterns with relatively high $(\text{La}/\text{Yb})_{\text{N}}$ ratios of 178–203 (Fig. 7).

Nepheline. Nepheline compositions in rocks of the Kovdor-type alkaline ultramafic intrusions range from $\text{Ne}_{77.8-82.5}\text{Ks}_{9.6-18.9}\text{Qz}_{1.4-3.2}$ to $\text{Ne}_{78.6-81.6}\text{Ks}_{15.2-20.1}\text{Qz}_{1.4-3.2}$ in foidolites and Ne-syenites, respectively. Nephelines from Khibiny foidolites are higher in the kalsilite end-member and silica ($\text{Ne}_{68.4-72.8}\text{Ks}_{21.5-26.1}\text{Qz}_{4.8-7.4}$). Because of high Fe_2O_3 contents in the matrix of nepheline, all the nepheline grains are replete with aegirine microlites representing exsolution products. REE contents in all the nepheline varieties range from low to very low (Table 5). Chondrite-normalized REE patterns are straight (Fig. 7), nephelines from Khibiny ijolites having negative Eu anomaly ($\text{Eu}/\text{Eu}^* = 0.13$), evidently due to the presence of magnetite microinclusions, rather than aegirine ones only. On the other hand, in nephelines from Kovdor ijolites, which are least abundant in aegirine microlites, Eu anomaly is expressed poorly ($\text{Eu}/\text{Eu}^* = 0.69$).

5.2.3. REE distribution in coexisting mineral phases

Data on REE distribution in principal REE-bearing phases—perovskite, apatite, and titanite (Tables 3, 4) — enable us to calculate partition coefficients for these phases. Comparison of coefficients obtained for the coexisting pairs perovskite/apatite ($D_{\text{Prv}/\text{Ap}}$), perovskite/titanite ($D_{\text{Prv}/\text{Tit}}$), and apatite/titanite ($D_{\text{Ap}/\text{Tit}}$) (Table 6) shows that in early pyroxene–perovskite cumulates, REE partition preferentially into the perovskite. Overall, during magmatic crystallization, REE enter the above minerals in the following order: perovskite > apatite > titanite. According to our calculations, the early-generation perovskite (sample AFR-5) extracts medium- and heavy REE most strongly ($D_{\text{Prv}/\text{Ap}}$ for Tb–Lu > 3), whereas in perovskite II–apatite pairs (sample 8-OV) the bulk of the heavy REE partition into the apatite. The results obtained are consistent with microprobe measurements on minerals from Ugandan clinopyroxenites and kamafugite lavas [33] and from the plutonic Oldoinyo Lengai alkaline ultramafic rocks [11, 12], which reveal a relative constancy of REE distribution in the perovskite–apatite pair ($D_{\text{Prv}/\text{Ap}}$: La 9, Ce 16, Nd 9.5).

5.2.4. Estimating REE distribution between minerals and rocks

In view of the fact that alkaline ultramafic rocks under study are differentiates, and their chemistries do not necessarily correspond to compositions of those melts that precipitated the mineral phases contained in these rocks, estimates of mineral/melt partition coefficients (D_{mineral}) may be very tentative.

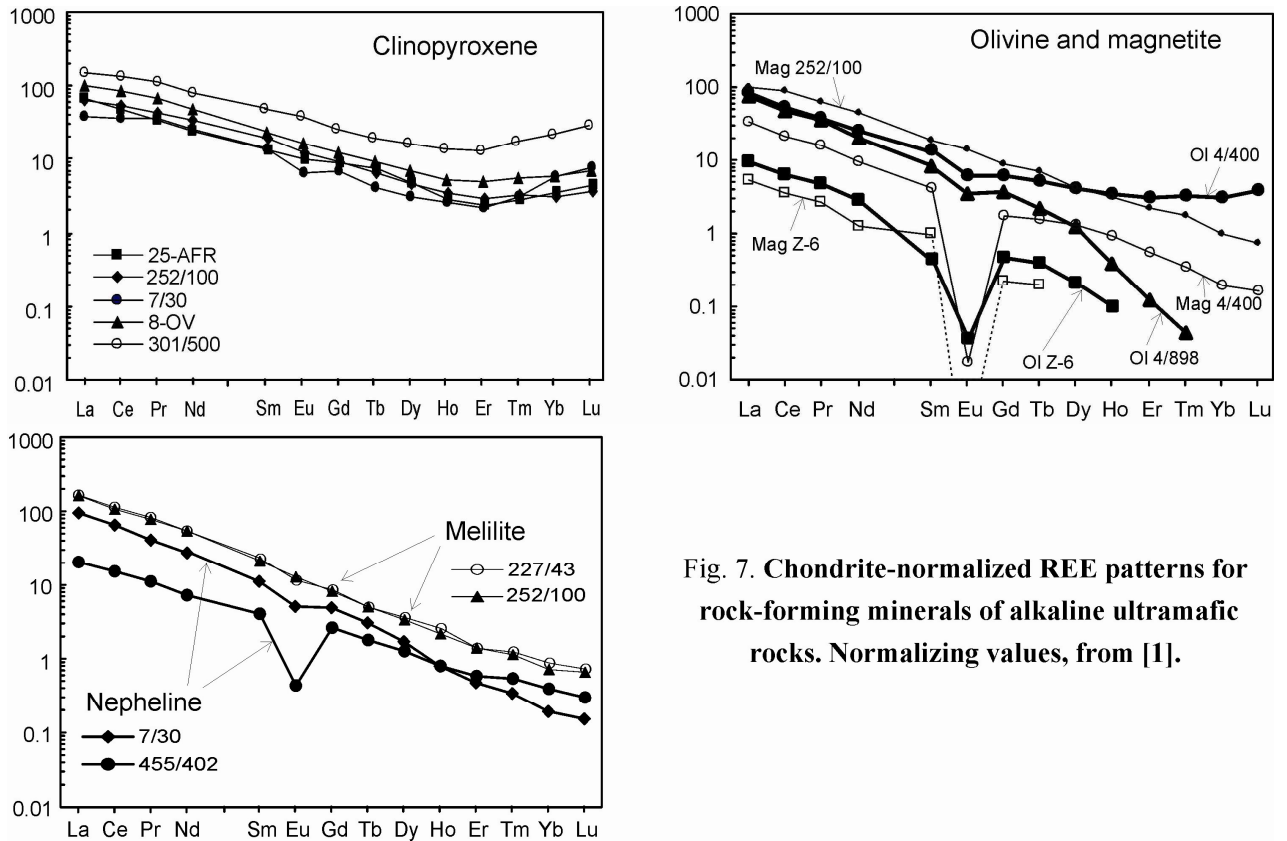


Fig. 7. Chondrite-normalized REE patterns for rock-forming minerals of alkaline ultramafic rocks. Normalizing values, from [1].

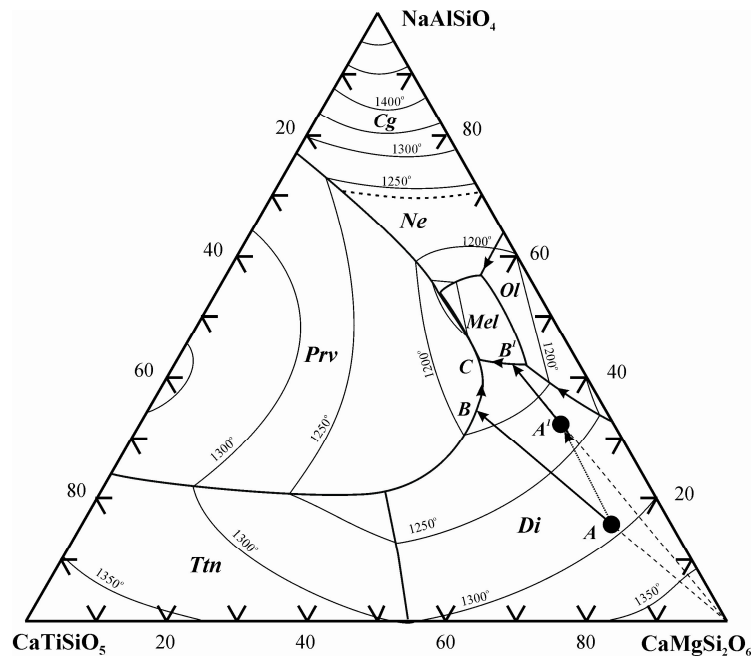


Fig. 8. Melting diagram for the system nepheline–diopside–titanite, after [48].

Di – diopside, *Prv* – perovskite, *Ttn* – titanite, *Mel* – melilite, *Cg* – carnegieite, *Ne* – nepheline, *Ol* – olivine, *L1* + *L2* – immiscibility region. Point *A* signifies the weighted mean composition for the Kovdor-type primary alkaline ultramafic magma. Point *A*¹ represents the hypothetical primary magma of the Khibiny-type alkaline ultramafic series, whose composition has been changed by mixing with phonolitic melt.

Table 6.

Inter-phase REE partition coefficients for perovskite, apatite and titanite.

	$D_{\text{per/ap}}$	$D_{\text{per/ap}}$	$D_{\text{per/ap}}$	$D_{\text{per/tit}}$	$D_{\text{per/tit}}$	$D_{\text{ap/tit}}$	$D_{\text{ap/tit}}$	$D_{\text{ap/tit}}$
Rock	PRD	PRX	MLG	PRX	IJL	PRX	MLG	IJL
Sample	AFR-5	25-AFR	8-OV	25-AFR	8-OV	25-AFR	8-OV	1636/874
La	1.43	0.79	4.08	1.80	8.49	2.27	2.08	2.65
Ce	1.79	1.52	5.01	2.18	6.67	1.43	1.33	1.51
Pr	1.86	1.23	5.20	1.40	5.42	1.14	1.04	1.05
Nd	1.89	1.23	5.11	1.23	4.72	1.00	0.92	0.90
Sm	2.30	1.16	4.49	0.90	3.24	0.78	0.72	0.63
Eu	2.73	0.98	3.94	0.69	2.66	0.71	0.67	0.56
Gd	2.61	1.00	3.12	0.65	2.21	0.65	0.71	0.66
Tb	3.32	0.93	2.87	0.56	1.84	0.60	0.64	0.57
Dy	4.38	0.77	2.43	0.41	1.41	0.53	0.58	0.52
Ho	4.99	0.70	1.97	0.35	1.11	0.51	0.57	0.49
Er	5.67	0.62	1.57	0.28	0.93	0.46	0.59	0.48
Tm	6.58	0.66	1.48	0.27	0.84	0.40	0.57	0.44
Yb	8.77	0.58	1.42	0.24	0.87	0.42	0.61	0.44
Lu	7.69	0.46	1.61	0.22	1.01	0.48	0.63	0.51

$D_{\text{Prv/Ap}}$ values similar to those obtained by us for the late perovskite II–apatite pairs were established for Kaiserstuhl calcite carbonatites [17], $D_{\text{Prv/Ap}}$ in these rocks decreasing from 6.8–4.9 for the LREE to 3.0–1.5 for the MREE through to 0.5 for Yb.

Hence, when calculating D_{REE} for early phases from pyroxene and olivine cumulates, REE contents were correlated not with their host rocks, but with the mean composition for alkaline ultramafic rocks (Table 1), which best approximates the composition of the melt parental to the series. Coefficients thus obtained are listed in Table 7 and are compared to published experimental values. In the plot showing $D_{\text{Prv/melt}}$ for the entire REE spectrum, partition coefficients for Kola perovskites, while plotting somewhat lower, stay nonetheless with the same trend as does $D_{\text{Prv/melt}}$ in melilite–olivine basalts, as determined by Onuma et al. [42].

In calculations of D_{REE} for minerals from the more evolved members of the alkaline ultramafic series (ijolites), we assumed their constituent phases (clinopyroxene, melilite, apatite, and titanite) to have been in equilibrium with the host rocks. The obtained $D_{\text{Cpx/rock}}$ and $D_{\text{Ap/rock}}$ values, listed in Table 8, are broadly compared to those for minerals in alkaline volcanites from other regions [9, 15, 18, 31, 42]. On the other hand, partition coefficients for titanites from Khibiny and Ozernaya Varaka ijolites are lower than those for phonolite-hosted titanites [54].

Table 7.

Mineral - bulk rock REE partition coefficients for pyroxene and olivine cumulates of the ultrabasic alkaline series.

Rock	Perovskite					Apatite	
	PRX	PRD	PRX	PRX	PRX	PRX	PRX
Sample	25-AFR	AFR-1	282/224	205/297.5	282/251	25-AFR	AFR-5
La	9.5	26.7	14.9	6.7	12.4	12.0	2.4
Ce	12.4	37.1	18.4	9.2	17.1	8.1	2.0
Pr	7.9	29.3	17.7	10.1	16.8	6.4	1.8
Nd	7.0	26.5	17.7	10.7	16.7	5.7	1.7
Sm	6.8	19.3	16.4	9.5	14.7	5.9	1.8
Eu	7.0	18.6	17.6	9.7	15.1	7.2	2.2
Gd	6.3	17.4	16.0	9.0	13.9	6.2	2.4
Tb	5.8	14.9	14.3	7.6	12.2	6.3	2.3
Dy	4.2	8.8	11.1	4.8	7.7	5.5	2.0
Ho	3.5	6.2	7.9	3.7	5.9	4.9	1.9
Er	2.4	4.3	5.7	2.5	4.1	3.9	1.7
Tm	2.0	3.1	4.2	1.9	2.8	3.1	1.5
Yb	1.5	2.7	3.5	1.5	2.4	2.6	1.0
Lu	1.1	2.0	2.7	1.2	1.7	2.3	0.9

Note. $D_{Prv/Rock}$ and $D_{Ap/Rock}$ is a ratio between mineral phase and weighted average composition of the ultrabasic alkaline series (Table 2, analysis AVER*).

6. DISCUSSION

Petrologic evidence, supported by experimental data [41, 52, 13, 32, 43, 44, 49], indicate that the main process responsible for the genesis of alkaline ultramafic suites of various provinces worldwide was fractional crystallization of primary olivine melanephelinitic magma. Coherence of the rock formation sequence from early olivine- and clinopyroxene cumulates to melilitolite, foidolite, and Nesyenite, is corroborated by geologic and petrographic observations. Estimates of magma compositions for the Kola alkaline province [3] allow the inference that alkaline ultramafics of the Kovdor and Khibiny types originated from the same primary magma. This is further supported by isotope studies, indicative of a single mantle source for Khibiny and ovdor alkaline rocks [26]. Variation trends in major-element plots for both suites reflect sequential precipitation of olivine, clinopyroxene, and melilite. Foidolites are produced through a reaction that involves resorption of melilite and formation of diopside and nepheline:

$$3\text{CaMgSi}_2\text{O}_6 + 2\text{NaAlSiO}_4 = \text{Mg}_2\text{SiO}_4 + \text{Ca}_2\text{MgSi}_2\text{O}_7 + \text{NaCaAlSi}_2\text{O}_7 + \text{NaAlSi}_3\text{O}_8$$

diopside
nepheline
olivine
melilite (solid solution)

liquid

Published data concerning distribution of trace elements in the above principal mineral phases of the alkaline ultramafic series are indicative of REE, Sr,

Table 8.
Mineral – bulk rock REE partition coefficients for melilitolites and ijolites of the ultrabasic alkaline series.

Massif Rock Sample	Apatite				Titanite				Pyroxene				Melilite			
	SLN IJL	SLN IJL	KVD IJL	OZV MLG	KHI IJL	KHI IJL	OZV MLG	OZV MLG	KHI IJL	KHI IJL	KVD IJL	KVD IJL	MELT IJL	MELT IJL	KVD MELT	KVD MELT
	25/110	31/200	7/30	8-OV	1636/721	1636/721	8-OV	8-OV	301/ 500	1636/ 721	8-OV	7/30	252/ 100	301/ 500	252/ 100	227/43
La	4.56	5.72	25.57	15.54	8.81	8.81	7.46	7.46	8.83	1.87	0.14	0.17	0.35	0.34	0.90	1.37
Ce	4.55	5.27	25.96	14.04	8.26	8.26	10.55	10.55	10.70	2.98	0.17	0.19	0.43	0.37	0.87	1.33
Pr	4.55	5.06	26.64	12.45	7.90	7.90	11.94	11.94	12.32	4.06	0.18	0.24	0.48	0.40	0.87	1.31
Nd	4.39	4.81	27.11	11.34	7.86	7.86	12.27	12.27	12.85	4.60	0.19	0.26	0.56	0.43	0.92	1.26
Sm	4.08	3.99	26.51	9.97	7.13	7.13	13.83	13.83	13.64	5.82	0.23	0.33	0.73	0.45	0.91	1.29
Eu	3.94	3.86	26.39	11.18	7.16	7.16	16.56	16.56	14.83	6.39	0.26	0.24	0.82	0.49	0.93	1.28
Gd	3.94	3.94	25.81	8.64	7.62	7.62	12.21	12.21	12.70	5.84	0.23	0.40	0.88	0.43	0.88	1.12
Tb	3.52	3.24	25.27	8.47	6.85	6.85	13.22	13.22	12.80	6.08	0.26	0.38	1.06	0.45	0.91	1.15
Dy	3.28	2.48	26.89	8.64	6.69	6.69	14.94	14.94	13.82	6.59	0.34	0.50	1.27	0.56	1.03	1.34
Ho	3.04	2.61	23.32	8.82	5.82	5.82	15.61	15.61	12.96	6.20	0.36	0.53	1.39	0.63	0.97	1.21
Er	2.84	2.35	16.89	8.18	4.91	4.91	13.77	13.77	12.20	5.64	0.44	0.51	1.44	0.82	0.80	0.88
Tm	2.50	2.03	14.50	7.04	3.44	3.44	12.43	12.43	11.68	4.32	0.51	0.67	1.67	1.23	0.65	0.76
Yb	2.22	1.47	9.97	6.53	2.23	2.23	10.64	10.64	10.07	2.62	0.66	1.32	2.22	2.22	0.57	0.63
Lu	2.02	1.18	6.29	4.67	1.28	1.28	7.47	7.47	9.61	1.44	0.72	1.56	3.38	3.80	0.69	0.53

Y, Zr, Hf, Nb, and Ta enrichment of final derivatives. Indeed, taking into account that partition coefficients for these elements in the first phases to crystallize, olivine and diopside, and considerably lower than 1, incompatible elements should be concentrated in late ijolite and Ne-syenite melts. Such distribution is exemplified by Khibiny-type alkaline ultramafics, in which, as follows from the plot in Fig. 5, late ijolites are abnormally high in REE, Sr, and Y. On the other hand, as appears from the diagram in Fig. 5, within the Kovdor-type alkaline ultramafic series, late ijolites and nepheline syenites of the Maly Kovdor, Vuoriyarvi, and Ozernaya Varaka massifs are more strongly depleted in REE than early differentiates. A similar pattern is found in alkaline ultramafic suites of the Maimecha–Kotui province in Siberia [14], the Gardiner complex in East Greenland [38], and Tanzanian plutonic alkaline suites [11].

Let us consider the main factors responsible for the differences in REE enrichment patterns between Kovdor- and Khibiny-type alkaline ultramafic rocks, which should include (i) conditions, under which the primary alkaline ultramafic magma precipitates the principal REE phases (perovskite, apatite, and titanite), and (ii) changes in the composition of the primary magma and, accordingly, in the crystallization order of principal and accessory mineral phases as a result of mixing with batches of phonolitic melt supplied from an independent source.

According to experimental data [21,48] and to studies on melt inclusions [20, 49], perovskite and apatite crystallized at early stages. This is evidenced by the fact that euhedral perovskite and apatite crystals contain inclusions that were homogenized at temperatures of $>970^{\circ}\text{C}$ and $1000\text{--}700^{\circ}\text{C}$, respectively [38, 24]. Hence, crystallization paths of the alkaline ultramafic series must be considered with due account of REE-bearing phases, in the context of the six-component systems $\text{SiO}_2\text{--TiO}_2\text{--Al}_2\text{O}_3\text{--CaO--MgO--Na}_2\text{O}$ and $\text{SiO}_2\text{--P}_2\text{O}_5\text{--Al}_2\text{O}_3\text{--CaO--MgO--Na}_2\text{O}$.

In the pseudo-ternary nepheline–diopside–titanite melting diagram (Fig. 8), perovskite and the five remaining phases correspond to the mineral assemblage constituting rocks of the alkaline ultramafic series. According to (Veksler and Tepteleev, 1990), perovskite forms a large crystallization field contiguous to the fields of all the phases except olivine. The primary alkaline ultramafic melt of composition *A*, which contains 2–3 wt % TiO_2 , plots in the diopside crystallization field, so that resultant melts evolve toward the cotectic lines Di–Prv (points *B* and *C*) to produce olivine and pyroxene–perovskite cumulates and melilitolites. One factor controlling perovskite stability in melts is silica activity, described by the reactions $\text{CaTiO}_3 + \text{SiO}_2 = \text{CaTiSiO}_5$ and $2\text{CaTiO}_3 + \text{NaAlSi}_3\text{O}_8 = \text{NaAlSiO}_4 + 2\text{CaTiSiO}_5$ [8, 48]. Hence, even small amounts of a more silicic material, when added to silica-undersaturated olivine melanephelinitic melt (the melt evolution course $A^I\text{--}B^I\text{--}C^I$), prevent early crystallization of perovskite. As a result, Ti-silicates will crystallize not in initial melt derivatives in the form of perovskite, but in more evolved products (ijolites and nepheline syenites) in the form of titanite.

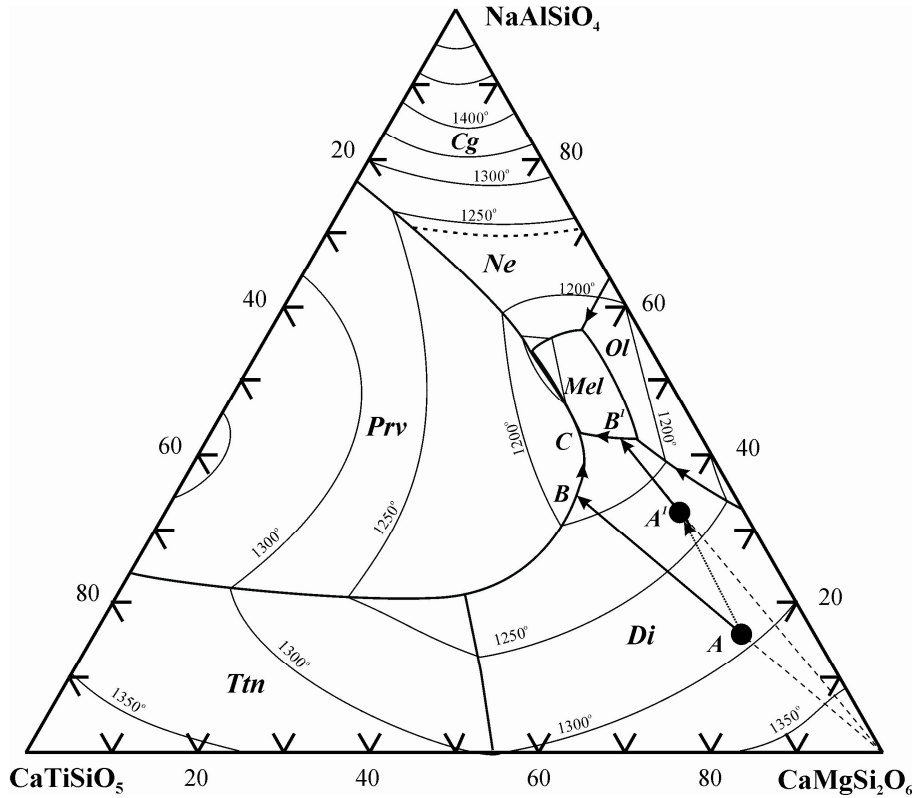


Fig. 9. Melting diagram for the system nepheline–diopside–apatite, after [21].

Di – diopside, *Ap* – apatite, *Pho* – Ca-phosphate, *Mel* – melilite, *Cg* – carnegieite, *Ne* – nepheline, *Ol* – olivine, *L1* + *L2* – immiscibility region. Point *A* signifies the weighted mean composition for the Kovdor-type primary alkaline ultramafic magma, and point *A*¹, the hypothetical composition for the primary magma of the Khibiny-type alkaline ultramafic.

The behavior of apatite during evolution of the alkaline ultramafic series can be approximated by the section $\text{NaAlSiO}_4\text{--CaMgSi}_2\text{O}_6\text{--Ca}_5(\text{PO}_4)_3\text{F}$ (Fig. 9), as discussed by Kogarko (1990), where the primary olivine melanephelinitic melt falls in the diopside crystallization field. Since the P_2O_5 content of the initial melt is 1.26 wt % (Table 1), apatite is unlikely to precipitate at early stages of rock crystallization. The series fact that P_2O_5 distribution in all the members of the series points to the existence of a maximum of 2.8 wt % in melanocratic members of the foidolite trend [5] suggests that apatite appears on the liquidus during crystallization of nepheline–pyroxene assemblages. Based on the above experimental models for crystallization of REE-bearing titanium minerals and phosphates, the following evolution paths for alkaline ultramafic suites of the Kola province can be considered.

6.1. Evolution of the Kovdor-type alkaline ultramafic series

According to the first scenario, which is apparently materialized in the Kovdor-type rock sequence, the olivine melanephelinitic melt *A* of Fig. 8, after having precipitated olivine, will evolve toward the diopside–perovskite cotectic,

where perovskite–clinopyroxene cumulates are formed. Early crystallization of a phase that has $D_{\text{REE}} \gg 1$ will result in a dramatic depletion of residual melt, which will sequentially produce the series of REE-depleted derivatives (ijolites and nepheline syenites). The dominant role in early extraction of REE from melt was thus played by perovskite, although apatite may also have played a subordinate role at this stage, because it could, in principle, have reached the liquidus as well (Fig. 10). With respect to the Kovdor-type alkaline ultramafic series, evidence for the model just proposed is as follows:

(1) The Afrikanda, Vuoriyarvi, Salmagora, and Cape Turiy massifs contain clinopyroxene–perovskite cumulates composed of primary magmatic perovskite. In some intrusions (Kovdor, Afrikanda, Ozernaya Varaka, Vuoriyarvi), local clinopyroxenite zones with up to 3% primary magmatic apatite have been found.

(2) The latest derivatives of the Kovdor series are sharply depleted in REE, Nb, Ta, and Sr relative to both the mean parental magma composition and to earlier cumulates.

quential precipitation of olivine, clinopyroxene, and melilite. Foidolites are produced through a reaction that involves resorption of melilite and formation of diopside and nepheline:

(3) Primary REE-bearing accessories in late differentiates of the Kovdor series are relatively low in REE and Sr due to the melts being depleted in these elements. Thus, apatites from Ozernaya Varaka cancrinite syenites have as little as 0.67–0.71 LREE₂O₃ and 0.60–0.68 wt % SrO, and those from Maly Kovdor nepheline syenites, as little as 0.33–1.31 LREE₂O₃ and 0.59–1.07 wt % SrO [5].

Data on REE distribution in alkaline intrusions of various provinces indicate that early fractionation of REE-bearing phases is a characteristic feature of alkaline ultramafic suites. Thus, the Oldoinyo Lengai plutonic suite has been reported to comprise clinopyroxenite (jacupirangite) cumulates with up to 28% perovskite [11]. The character of REE distribution in the Oldoinyo Lengai rocks corresponds exactly to that in the Kovdor series: REE are enriched in early cumulates and sharply depleted in terminal members of the series (ijolites and eucolite-bearing Ne-

syenites). Another example is provided by the Maimecha–Kotui province, where the Kugda, Guli, and Odikhincha massifs are reported to contain olivine and clinopyroxene cumulates rich in primary magmatic perovskite [14]. The Nizhnesayansky carbonatite massif (southern Siberia) has also been reported to incorporate a rock suite encompassing the full spectrum of alkaline ultramafites, including clinopyroxene cumulates with as much as 15% perovskite [10].

6.2. Evolution of the Khibiny-type alkaline-ultramafic series

The set of rock varieties that make up fragments of the alkaline ultramafic suite in the Khibiny massif, the order of their formation, and overall major-element characteristics were formerly believed to suggest similar courses of REE evolution

and distribution for the Khibiny and Kovdor suites. However, according to geologic observations and geochemical data for the Khibiny alkaline ultramafic suite, generation of early olivine and clinopyroxene cumulates was not accompanied by massive precipitation of perovskite. This is the reason why REE

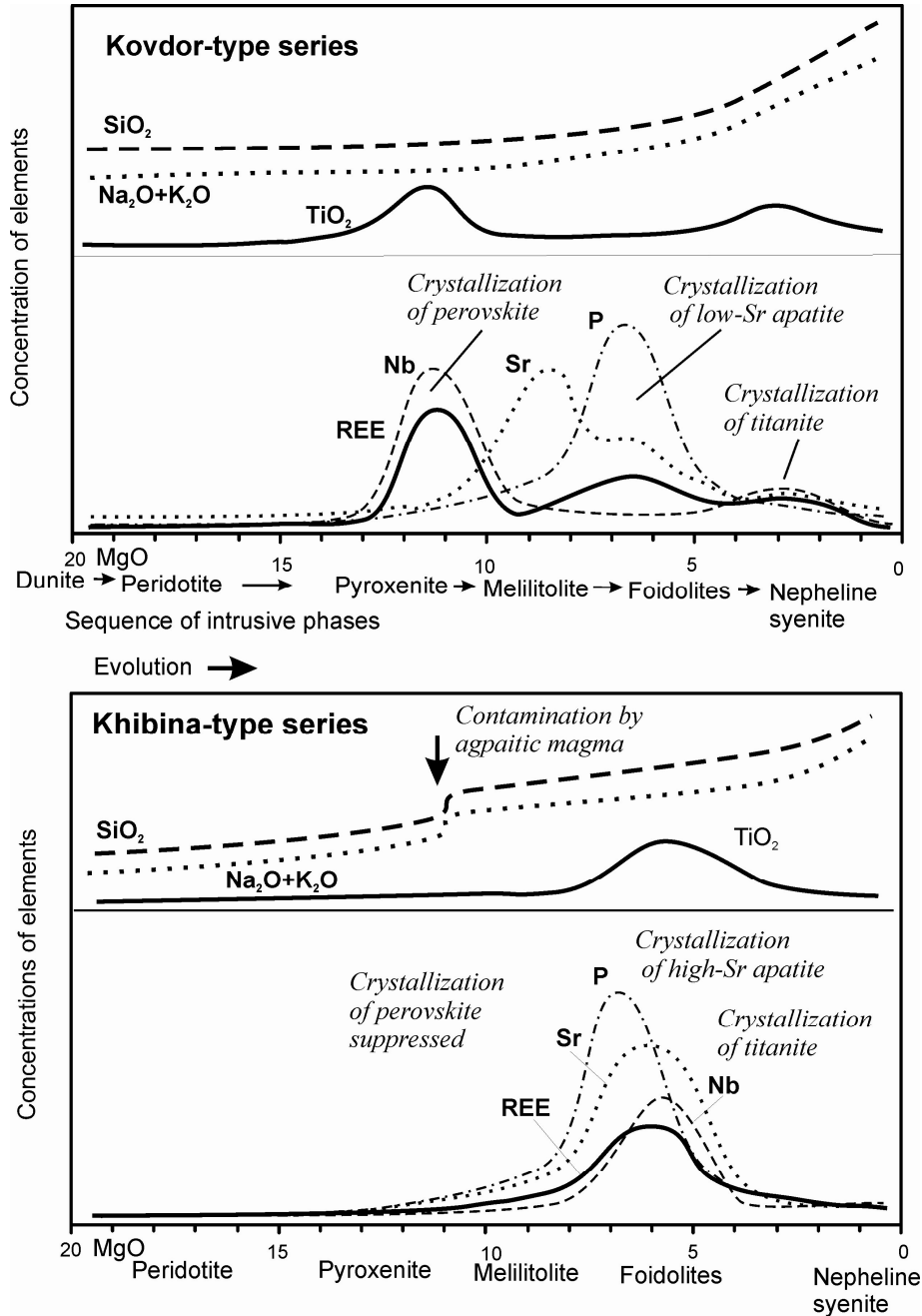


Fig. 10. A scheme showing distribution of selected major, trace, and REE in the ultrabasic alkaline series of the Kovdor type and Khibina.

remained in residual melt until final stages of crystallization, and REE enrichment did not occur until late ijolite derivatives started to form. Two factors preventing early crystallization of perovskite can be considered, both of them being apparently related to a drastic increase in silica activity in the melt. Firstly,

the change in SiO_2 activity may result from interaction of the primary olivine melanephelinitic magma with surrounding Precambrian basement rocks. This, however, is at variance with Sr and Nd isotope data, which suggest that crustal material was not involved in alkaline magmagenesis in the Kola province [26]. Secondly, the change in SiO_2 activity may have been caused by mixing of the olivine melanephelinitic magma with a more silicic melt. A likely candidate for such a melt might be the phonolitic magma that gave rise to the Khibiny agpaite plutonic suite. This suite, according to isotope geochemical and petrologic data [4, 27], evolved independently, and its origin is related to a mantle source other than that of alkaline ultramafic melts. The main feature of agpaite melts is their relatively higher SiO_2 (52–56 wt %), alkali ($\text{Na}_2\text{O} + \text{K}_2\text{O} > 16$ wt %), and F contents. However, REE contents in agpaite syenites, according to our data [4], are only a little higher than in alkaline ultramafites. Hence, addition to the primary silica-undersaturated melanephelinitic magma of even minor batches of phonolitic melt would increase silica and alkali contents of the magma while changing its REE content only slightly. Indeed, in comparison to Vuoriyarvi, Ozernaya Varaka, Sallanlatva, and Kovdor ijolites, their Khibiny counterparts are much higher in SiO_2 , Na_2O , and K_2O (Tables 1, 2), and feldspar-bearing varieties are widespread among them. In the nepheline–diopside–titanite melting diagram (Fig. 8), the change in the composition of crystallizing melt will be expressed in that the initial liquid of composition A shifts away from the perovskite cotectic surface A^1 to produce perovskite-free olivine–diopside, diopside–melilite, and diopside–nepheline rocks (option A^1 – B^1 – C^1). Accordingly, REE will be enriched progressively in these differentiates, and extraction of REE from melt will not occur until the melt has reached the apatite and/or titanite liquidus surface at the final stages of alkaline ultramafic petrogenesis. Therefore, evolution of the alkaline ultramafic series in the Khibiny massif was disturbed by mixing of minor portions of phonolitic melt with the primary olivine melanephelinitic magma, which led to a change in crystallization order of REE-bearing titanates and Ti-silicates and enrichment of late batches of melt in the majority of incompatible elements (Fig. 10).

6. Conclusions

Our study of REE distribution in rocks and minerals of Paleozoic alkaline ultramafic rocks of the Kola province affords the following conclusions:

(1) REE patterns in rocks of the Kovdor, Afrikanda, Vuoriyarvi, and Salmagora massifs indicate a systematic depletion from earlier to later (ijolite and nepheline syenite) melt derivatives. Analysis of rock suites to be found in alkaline intrusions of other provinces (Maimecha–Kotui province of southern Siberia and East African province) shows that the above trend has a general character, inherent in many alkaline ultramafic suites.

(2) REE distribution in Kovdor-type alkaline ultramafic suites is controlled by crystallization of perovskite and, to a lesser extent, apatite. Primary olivine melanephelinitic melts of this series experienced crystallization of perovskite, the main REE-bearing mineral. Perovskite coprecipitating with the first phases to crystallize from melt, olivine and clinopyroxene, leads to a dramatic REE depletion of the residual melt and to formation of REE-depleted derivatives, ijolite and nepheline syenite.

(3) Petrogenesis of the alkaline ultramafic suite of the Khibiny massif was upset by mixing of minor batches of phonolitic melt with the primary olivine melanephelinitic magma, with an ensuing change in the crystallization order of REE-bearing titanates and Ti-silicates and enrichment of late batches of melt in the majority of incompatible elements. As a result, Khibiny ijolites, which are late and the most evolved derivatives of the alkaline ultramafic magma, have the highest REE concentrations, accommodated by high-REE apatite and titanite.

Acknowledgments. This work would have been impossible without the painstaking and crucial procedure of mineral separation, which was performed by Lyuda Koval, and microprobe analyses of accessory mineral grains, carried out by Yakov Pakhomovsky. The study was supported by the Russian Foundation for Basic Research (project no. 00-05-64229).

References

1. Anders, E., and N. Grevesse, Abundances of the elements: meteoritic and solar // *Geochim. Cosmochim. Acta*. 1989. V. 53. P. 197-214.
2. Arzamastsev, A., and L. Arzamastseva, Evolution of foidolite suites in alkaline massifs of the Kola province: Mineralogic and geochemical evidence (in Russian) // *Petrologiya*. 1993. V. 1, N 5. P. 524-535.
3. Arzamastsev, A., F. Bea, V. Glaznev, L. Arzamastseva, and P. Montero, Kola alkaline province in the Paleozoic: evaluation of primary mantle magma composition and magma generation conditions // *Russian Journal of Earth Sciences*. 2001. V.3, N 1. P. 3-24.
4. Arzamastsev, A., L. Arzamastseva, V. Glaznev, and A. Raevsky, Deep structure and composition of lower horizons of the Khibiny and Lovozero complexes, Kola Peninsula, Russia: A petrologic/geophysical model (in Russian) // *Petrologiya*. 1998. V. 6, N 5. P. 478-496.
5. Arzamastseva, L., and A. Arzamastsev, Evolution of the Paleozoic nephelinite series of the Kola province: Evidence from P and Sr distribution // *Geochemistry International*. 1996. V. 34. P. 360-369.
6. Balagansky, V., V. Glaznev, and L. Osipenko, Early Proterozoic evolution of the northeastern Baltic Shield: A terrane analysis (in Russian) // *Geotektonika*. 1998. V. 2. P. 16-28.
7. Bell, K., L. A. Dunworth, A. G. Bulakh, and V. V. Ivanikov, Alkaline rocks of the Turij Peninsula, Russia, including type locality turjaite and turjite: a review // *Canadian Mineralogist*. 1996. P. 34. P.265-280.
8. Carmichael, J. S. A., J. Nicholls, and A. L. Smith, Silica activity in igneous rocks // *American Mineralogist* 1970. V. 55. P. 242-264.
9. Caroff, M., R. C. Maury, J. Leterrier, J. L. Joron, J. Cotton, and G. Guille, Trace element behavior in the alkali basalt – comenditic trachyte series from Mururoa Atoll, French Polynesia // *Lithos*. 1993. V. 30. P. 1-22.

10. Chernysheva, E., G. Nechelyustov, T. Kvitko, and B. Veis, Perovskite compositions in alkaline rocks of the Nizhnesayansky carbonatite complex (in Russian) // *Geokhimiya*. 1991. V. 8. P. 102-108.
11. Dawson, J. B., J. V. Smith, and I. M. Steele, Petrology and mineral chemistry of plutonic igneous xenoliths from the carbonatite volcano, Oldoinyo Lengai, Tanzania // *Jour. Petrol.* 1995. V. 36, N 3. P. 797-826.
12. Dawson, J. B., J. V. Smith, and I. M. Steele, Trace element distribution between coexisting perovskite, apatite and titanite from Oldoinyo Lengai, Tanzania // *Chem. Geol.* 1994. V. 117, N 1-4. P. 285-290.
13. Edgar, M. J., The genesis of alkaline magmas with emphasis on their source regions: inferences from experimental studies, in *Alkaline Igneous Rocks*, edited by J. G. Fitton and B. G. J. Upton // *Geol. Soc. Spec. Publ.* 1987. V. 30. P. 29-52.
14. Egorov, L., *Iiolit-karbonatitovyi plutonizm (Ijolite–Carbonatite Plutonism)*. Leningrad: Nedra, 1991. 260 pp.
15. Foley, S. F., S. E. Jackson, B. J. Fryer, J. D. Greenough, and G. A. Jenner, Trace element partition coefficients for clinopyroxene and phlogopite in an alkaline lamprophyre from Newfoundland by LAM-ICP-MS // *Geochim. Cosmochim. Acta*. 1996. V. 60, N 4, P. 629-638.
16. Galakhov, A., *Petrologiya Khibinskogo shchelochnogo massiva (Petrology of the Khibiny Alkaline Massif)*. Leningrad: Nauka, 1975. 256 pp.
17. Hornig-Kjarsgaard, I., Rare earth elements in sovitic carbonatites and their mineral phases // *Jour. Petrol.* 1998. V. 39, N 11-12. P. 2105-2121.
18. Irving, A. J., and R. C. Price, Geochemistry and evolution of lherzolite-bearing phonolitic lavas from Nigeria, Australia, East Germany and New Zealand // *Geochim. Cosmochim. Acta*. 1981. V. 45, N 8. P. 1309-1320.
19. Ivanikov, V. V., A. S. Rukhlov, and K. Bell, Magmatic evolution of the melilitite–carbonatite–nephelinite dyke series of the Turiy Peninsula (Kandalaksha Bay, White Sea, Russia) // *Jour. Petrol.* 1998. V. 39, N 11-12 P. 2043-2059.
20. Kogarko, L. N., D. A. Plant, C. M. Henderson, and B. A. Kjarsgaard, Na-rich carbonate inclusions in perovskite and calzirtite from the Guli intrusive Ca-carbonatite, Polar Siberia // *Contrib. Mineral. Petrol.* 1991. V. 109, N 1. P. 124-129.
21. Kogarko, L. N., Ore-forming potential of alkaline magmas // *Lithos*. 1990. V. 26, N 1-2. P. 167-175.
22. Kogarko, L. N., V. A. Kononova, M. P. Orlova, and A. Woolley, *Alkaline Rocks and Carbonatites of the World. Part 2. Former USSR*. Chapman and Hall, London, 1995. 226 pp.
23. Kogarko, L. N., Issues of the genesis of giant deposits of apatite and rare metals in the Kola Peninsula, Russia (in Russian) // *Geol. Rudn. Mestorozhd.* 1999. V. 41, N 5 P. 387-403.
24. Kogarko, L. N., *Problemy genezisa agpaitovykh magm (Issues of Agpaitic Magmagenesis)*, Nauka, Moscow, 1977. 294 pp.
25. Korobeinikov, A. N., F. P. Mitrofanov, S. Gehor, K. Laajoki, V. P. Pavlov, and V. P. Mamontov, Geology and Copper Sulfide Mineralization of the Salmagorskii Ring Igneous Complex, Kola Peninsula, NW Russia // *J. Petrol.* 1998. V. 39, N 11-12 P. 2033-2041.
26. Kramm, U., and L. N. Kogarko, Nd and Sr isotope signatures of the Khibina and Lovozero agpaitic centres, Kola Alkaline Province, Russia // *Lithos*. 1994. V. 32. P. 225-242.
27. Kramm, U., L. N. Kogarko, V. A. Kononova, and H. Vartiainen, The Kola Alkaline Province of the CIS and Finland: Precise Rb-Sr ages define 380-360 age range for all magmatism // *Lithos*. 1993. V. 30. P. 33-44.
28. Kravchenko, S., A. Belyakov, P. Babushkin, and V. Kalyuzhny, Sodic nepheline syenites of the Khibiny massif: Likely derivatives of a high-Ca alkaline ultramafic magma (in Russian) // *Geokhimiya*. 1992. V. 5. P. 685-697.

29. Kravchenko, S., D. Mineev, and E. Kamenev, REE and Sr in rocks and minerals of the ijolite-urtite complex of the Khibiny massif (in Russian) //Geokhimiya. 1979. V. 7. P. 1035-1045.
30. Kukharenko, A., M. Orlova, A. Bulakh, E. Bagdasarov, O. Rimskaya-Korsakova, E. Nefedov, G. Ilyinsky, A. Sergeev, and N. Abakumova, Kaledonskii kompleks ul'traosnovnykh, shchelochnykh porod i karbonatitov Kol'skogo poluostrova i Severnoi Karelii (The Caledonian Assemblage of Ultramafic and Alkaline Rocks and Carbonatites of the Kola Peninsula and Northern Karelia). Moscow: Nedra, 1965. 772 pp.
31. Larsen, L. M., Distribution of REE and other trace elements between phenocrysts and peralkaline undersaturated magmas, exemplified by rocks from the Gardar igneous province, South Greenland //Lithos. 1979. V. 12. P. 303-315.
32. Le Bas, M. J., Nephelinites and carbonatites, in Alkaline Igneous Rocks /Ed. J. G. Fitton and B. G. J. Upton, Geological Society Special Publication. 1987. N 30. P.53-83.
33. Lloyd, F. E., A. D. Edgar, and K. V. Ragnarsdottir, LREE distribution in perovskite, apatite and titanite from South West Ugandan xenoliths and kamafugite lavas //Miner. Petrol. 1996. V. 57, N 3-4. P. 205-228.
34. Mitchell, R. H. , The Melilitite clan, in Undersaturated Alkaline Rocks: Mineralogy, Petrogenesis and Economic Potential /Ed. R. H. Mitchell, Mineral. Assoc. Canada, Short Course 1996. V. 24. P. 123–152.
35. Mitchell, R. H. , Perovskites: a revised classification scheme for an important rare earth element host in alkaline rocks, in Rare Earth Minerals: Chemistry, Origin and Ore Deposits /Ed. A. P. Jones, F. Wall, and C. T. Williams Mineral, Soc. (UK) 1996. Ser. 6. P. 41-76.+ Chapman and Hall, London.
36. Mitchell, R. H., The classification of melilite clan, in Alkaline Magmatism and the Problems of Mantle Sources, Irkutsk, 2001. P. 117-150.
37. Mitchell. R. H., and, S. J. B. Reed, Ion microprobe determination of rare earth elements in perovskite from kimberlites and alnoites //Mineral. Mag. 1988. V. 52. P.331-339.
38. Nielsen, T. F. D., I. P. Solovova, and I. V. Veksler, Parental melts of melilitolite and origin of alkaline carbonatite: evidence from crystallized melt inclusions, Gardiner complex //Contrib. Mineral. Petrol. 1997. V. 126. P. 331-344.
39. Nielsen, T. F. D., Tertiary alkaline magmatism in East Greenland: a review, in Alkaline Igneous Rocks /Ed. J. G. Fitton and B. G. J. Upton, Geol. Society Special Publication. 1987. V. 30. P. 489-515.
40. Nielsen, T. F. D., Alkaline dike swarms of the Gardiner complex and the genesis of alkaline ultramafic complexes (in Russian) //Geokhimiya. 1993. V. 8. P. 1112-1132.
41. Onuma, K., and M. Yamamoto, Crystallization in the silica-undersaturated portion of the system diopside–nepheline–akermanite–silica and its bearing on the formation of melilitites and nephelinites //J. Fac. Sci. Hokkaido University. 1993. V. 4, N 17. 347-355.
42. Onuma, N., S. Ninomiya, and H. Nagasawa, Mineral groundmass partition coefficients for nepheline, melilite, clinopyroxene and perovskite in melilite nepheline basalt, Nyiragongo, Zaire //Geochem. J. 1981. V. 15, N 4 221-228.
43. Pan, V., and J. Longhi, Low pressure liquidus relations in the system Mg_2SiO_4 – Ca_2SiO_4 – $NaAlSiO_4$ – SiO_2 //Amer. J. Sci. 1989. V. 289, N 1, P.1-16.
44. Pan, V., and, J. Longhi, The system Mg_2SiO_4 – Ca_2SiO_4 – $CaAl_2O_4$ – $NaAlSiO_4$ – SiO_2 . One atmosphere liquidus equilibria of analogs of alkaline mafic lavas //Contrib. Mineral. Petrol. 1990. V. 105, N 5. P. 569-584.
45. Rass, I., Parageneticheskii analiz zonal'nykh mineralov (The Paragenetic Analysis of Zoned Minerals). Moscow: Nauka, 1986. 144 pp.

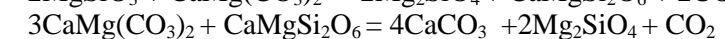
46. Shakhmurdyan, A., and R. H. Mitchell, Evolution of perovskite chemical compositions in alkaline ultramafic rocks during metasomatic processes (in Russian)// *Zap. Vses. Mineral. o-va.* 1998. V. 1. P. 57-69.
47. Ternovoi, V., *Karbonatitovye massivy i ikh poleznye iskopaemye* (Carbonatitic Massifs and Their Economic Mineralization). Leningrad State University. Leningrad, 1977. 168 pp.
48. Veksler, I. V., and M. P. Teptev, Conditions for crystallization and concentration of perovskite-type minerals in alkaline magmas // *Lithos.* 1990. V. 26, N 1-2. P. 177-189.
49. Veksler, I. V., T. F. D. Nielsen, and S. V. Sokolov, Mineralogy of crystallized melt inclusions from Gardiner and Kovdor ultramafic alkaline complexes: Implications for carbonatite genesis // *Jour. Petrol.* 1998. V. 39, N 11-12. P. 2015-2031.
50. Veksler, I. V., Y. M. Fedorchuk, and T. F. D. Nielsen, Phase equilibria in the silica-undersaturated part of the $KAlSiO_4$ - Mg_2SiO_4 - Ca_2SiO_4 - SiO_2 -F system at 1 atm and the larnite-normative trend of melt evolution // *Contrib. Mineral. Petrol.* 1998. V. 131, N 4. P. 347-363.
51. Verhulst, A., E. Balaganskaya, Y. Kirnarsky, and D. Demaiffe, Petrological and geochemical trace elements and Sr-Nd isotopes characteristics of the Paleozoic Kovdor ultramafic, alkaline and carbonatite intrusion, Kola Peninsula, NW Russia // *Lithos.* 2000. V. 51, N 1-2. P. 1-25.
52. Wilkinson, J. F. G., and A. J. Stolz, Low-pressure fractionation of strongly undersaturated alkaline ultrabasic magma: the olivine-melilite-nepheline at Moiliili, Oahu, Hawaii // *Contrib. Mineral. Petrol.* 1983. V. 38. P. 363-374.
53. Woolley, A. R., *Alkaline Rocks and Carbonatites of the World. Part 1. North and South America.* British Museum (Natural History), London. 1987. 216 pp.
54. Worner, G., J.-M. Beusen, N. Duchateau, R. Gijbels, and H.-U. Schminke, Trace element abundances and mineral/melt distribution coefficients in phonolites from the Laacher Sea Volcano (Germany) // *Contrib. Mineral. Petrol.* 1983. V. 84, N 2-3. P. 152-173.

THE ROLE OF SULPHIDE-CARBONATE-SILICATE AND CARBONATE-SILICATE LIQUID IMMISCIBILITY IN THE GENESIS OF CA-CARBONATITES

L.N.KOGARKO

Vernadsky Institute of Geochemistry, Moscow

During the investigation of a harzburgite nodule from the Montana Clara Volcano (Canary island archipelago) evidence of a primary carbonate melt was discovered. This carbonate is enriched in calcium and it occurs together with glass containing sulphide globules. In addition to primary olivine and orthopyroxene there are pockets of fine-grained minerals belonging to the metasomatic second generation (more magnesium olivine, sodium-bearing clinopyroxene, less aluminous spinels). The metasomatic assemblage was formed by reaction of sodium-bearing dolomitic melt with the harzburgite according to the reactions:



The calciocarbonatite and sulphide phase almost invariably form globules in silicate glass indicating the existence of three immiscible liquids under certain upper mantle conditions resulting from melting of the metasomatized mantle material during the uprising and adiabatic decompression. Our experiments reveal carbonate-silicate-sulphide immiscibility. Therefore, the investigated mineral assemblage, including carbonate and glass, can be considered as a micro model of the generation of the Ca-rich carbonatitic magmas during the processes of the partial melting of carbonatized metasomatized oceanic mantle. The development of carbonatite magmatism on the Canary Islands (Lanzarote) and the Cape Verde Islands is likely to be related to the partial melting of carbonatized mantle in the South Atlantic, which took place over a vast territory.

Another example of carbonate-silicate immiscibility under crustal conditions is represented by phonolites (Polar Siberia, Maimecha-Kotui) containing carbonate globules. We investigated some dykes of carbonatitic massif Dolbykha which comprise olivine and melilite nephelinites, nosean, calcite and cancrinite phonolites, calcite trachytes and calcite carbonatites. Some ultra alkaline phonolitic dykes contain carbonate-bearing globules. Globules consist of polycrystalline calcite aggregate and contain albite, mica, apatite, Sr-lueshite, zircon, ancylite, ilmenite and strontianite. There are phenocrysts of albite, mica and ilmenite in phonolites. There are also albite, mica, calcite and nepheline present in the groundmass. The analysis of these materials in light of experimental data on the liquid immiscibility in carbonate-silicate systems suggests that the separation of carbonatite melts from phonolitic ones took place due to the immiscibility while in the liquid state. We propose that originally carbonate melts contained significantly higher alkali concentrations which were subsequently lost in the fluid phase due to incongruent dissolution of calcium-sodium carbonates in aqueous fluid at low temperatures. Our discovery of nyerereite in carbonatite of Polar Siberia confirms this assumption.

Thus one of the very important mechanisms of the genesis of Ca-rich carbonatite melts was the formation of liquid immiscibility which may take place in mantle or crustal conditions.

INTRODUCTION

At present three groups of carbonatite origin models are generally discussed:

1 - carbonatites may be formed during the partial melting of carbonated mantle; 2 - carbonatites emerge due to the liquid immiscibility in carbonate-silicate magmatic systems; 3 - carbonatites appear at the terminal stage of prolonged fractional crystallization. Recently detailed studies of the geochemistry of mantle nodules and primary mantle carbonates permit the conclusion that carbonatite magmas may be generated in the mantle [1,25,18]. Experimental data [33,34,8] support the possibility of the generation of carbonatites in the processes of partial melting of carbonated mantle substrate. Mineralogical and geochemical investigations of some carbonatitic complexes [3,17] are also in agreement with these ideas.

The experimental investigations conveyed by many authors suggest that liquid immiscibility plays the leading role in the genesis of carbonatites [11,12,14]. Experimental data demonstrated the presence of the extensive fields of two immiscible liquids in the system $\text{SiO}_2+\text{Al}_2\text{O}_3+\text{TiO}_2-\text{MgO}+\text{FeO}-\text{CaO}-\text{Na}_2\text{O}+\text{K}_2\text{O}-\text{CO}_2$. The immiscibility gap expands with increasing pressure and alkalis content and, according to Woh-er and Wyllie (1996), with the decrease in magnesium concentration. From these data the conclusion was drawn that residual magmas enriched in alkalis during differentiation may intersect the boundary of the silicate-carbonate liquid immiscibility gap under crustal conditions. Recently, however, Woh-er and Wyllie (1994, 1995) discussed a number of limitations on the hypothesis of the genesis of carbonatites by liquid immiscibility and they maintained that, beyond any doubts, there is no single process responsible for the formation of all carbonatites. According to their opinion, fractional crystallization of carbonate-bearing alkaline magmas might be a very important process of carbonatites origin. Similar ideas were proposed by Twyman and Gittins (1987).

Because the problem of the genesis of carbonatites continues to remain unsolved, field evidence, particularly geological and mineralogical observations on the interrelationships between carbonate and silicate material in magmatic rocks has become very important.

In this paper we investigate the metasomatic interaction between sodium- and Ca-rich carbonate liquid with mantle material from Montana Clara Island (Canary archipelago) resulted in the wehrlitization and carbonatization of primary harzburgite. The partial melting of this material leads to the formation of silicate-carbonate-sulphide liquid immiscibility and the generation of Ca-rich carbonatitic melts. We have investigated the immiscibility in the system Ca-rich carbonate-Fe, Ni sulphide-silicate melt of phonolitic composition containing F. The immiscibility has been observed in the investigated system as exhibited in the complete separation of carbonate and silicate liquids whereas sulphide melt was present in the form of globules in both liquids. Therefore the investigated mantle material can be considered as a micro model of the generation of the Ca-rich carbonatites which form during the processes of the partial melting of wehrlitized and carbonatized mantle.

Moreover we studied carbonate-silicate liquid immiscibility phenomena in a phonolitic dyke from Maimecha - Kotui province (Polar Siberia) containing carbonate globules. The interrelationships between silicate and carbonate materials in this phonolite and the compositions of minerals testify to the immiscibility phenomena in these rocks. Recently Peterson (1989), Kjarsgaard and Peterson (1991) reported the possibility of the generation of alkali-poor carbonatites of Shombole Volcano (East Africa) as a result of silicate-carbonate immiscibility. This study was based on the petrographic and experimental observations of nephelinites, containing carbonate globules. In this paper we summarize data on petrography, mineral compositions of carbonate-bearing phonolites from Polar Siberia and proffer the suggestion that carbonate globules in this phonolite represent quench droplets of carbonate immiscible melt which separated in intermediate magmatic chambers during the differentiation of alkaline magma. The liquid immiscibility is strongly controlled by the CO₂ pressure (depth of magma chamber).

PARTIAL MELTING OF CARBONATED PERIDOTITE AND CARBONATE-SILICATE- SULPHIDE LIQUID IMMISCIBILITY IN THE UPPER MANTLE

We investigated unique harzburgite nodule (Mc-1) from the Montana Clara Island (Canary archipelago) where we, for the first time, discovered evidence of primary carbonates

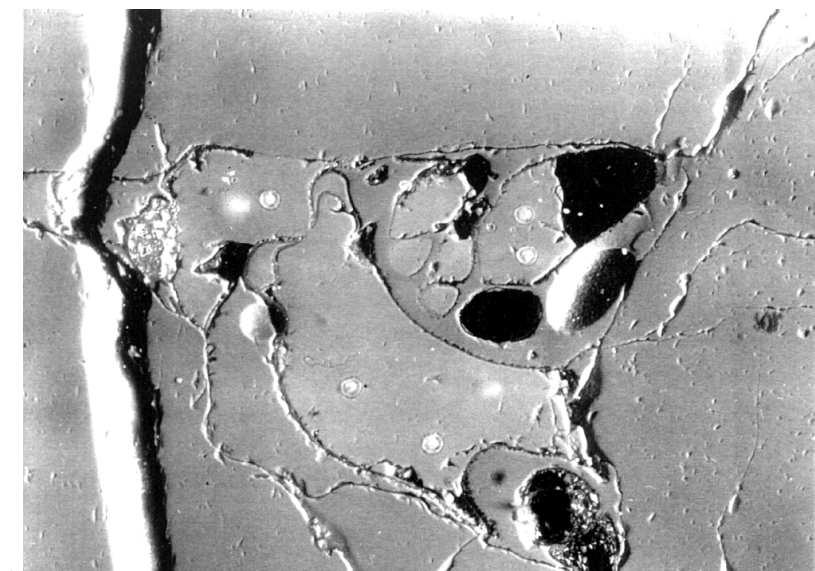


Fig.1 Back-scattered electron images of carbonate-silicate segregations in Montana Clara nodule MC-1: Interstitial patch between first generation olivine crystals (abbreviations: *C* carbonate, *pc*-‘plucked-out’ carbonate, *G*-silicate glass, *S*-sulphide global, *as*-altered sulphide bleb, *Ol* -olivine.

Table 1

Compositions of nodules and minerals and carbonates from nodule MC-1

sample	SiO ₂	TiO ₂	Al ₂ O ₃	FeO	MnO	Cr ₂ O ₃	NiO	MgO	CaO	Na ₂ O	K ₂ O	P ₂ O ₅	S	Sum	Mg
nodule MC-1	44.5	0.03	0.88	7.7	0.13	0.30	n.a.	45.6	0.75	0.11	0.04	0.05	n.a.	100.1	0.91
nodule MC-12	44.1	0.05	1.4	7.9	0.15	0.57	n.a.	44.4	0.73	0.10	0.09	0.05	n.a.	99.5	0.91
minerals															
Olivine (I) ^{*1,***}	41.6	-	-	8.6	-	-	0.31	50.1	0.07	-	-	-	-	100.7	0.91
Orthopyroxene ^{**}	57.4	-	1.0	5.2	0.11	0.50	0.11	34.6	0.21	-	-	-	-	99.1	0.92
Olivine(II) ⁺	39.3	-	-	7.3	0.14	-	0.37	51.1	0.20	-	-	-	-	98.4	0.93
CPX(II) ^{***}	54.3	-	3.0	2.6	0.12	0.97	-	17.9	19.8	1.1	-	-	-	99.8	0.93
CPX(II) ^{***}	53.5	0.05	2.6	2.3	0.10	0.34	0.11	18.3	21.5	0.19	-	-	-	98.9	0.94
Spinel(I) ^{**}	-	0.03	30.3	15.4	-	39.5	0.10	15.4	-	-	-	-	-	100.7	0.67
Spinel(II) ^{**}	-	-	25.7	13.9	-	44.7	0.10	15.0	-	-	-	-	-	99.4	0.66
Spinel(II) ^{**}	-	0.10	19.3	11.4	-	53.8	-	-	-	-	-	-	-	100.3	0.71
Glass ⁺	63.8	0.7	16.0	2.0	-	0.06	-	2.5	3.8	6.4	3.8	-	-	99.0	0.69
Carbonate ⁺	4.1	-	1.2	0.59	0.09	0.14	-	6.8	54.3	0.20	0.13	1.9	0.24	69.7	0.95
Carbonate ⁺	1.1	-	0.27	0.28	-	0.18	-	3.1	50.8	0.31	-	-	-	56.0	0.93
Carbonate ⁺	-	-	-	0.10	-	-	-	3.1	47.0	0.13	-	0.15	0.14	50.6	0.98
CPX(host lava) ^{***}	49.5	1.6	5.7	5.8	-	0.57	-	14.3	22.8	0.67	-	-	-	100.9	0.82

*1 First (I) and second (II) generation; n.a.-not analysed;- -not detected Nodule analysed by XRF at Institute of Geochemistry, Moscow; minerals by electron microprobe at Manchester University (** ED, Cameca Camebax;

+ ED, Jeol SEM) and Moscow (** WD, Cameca) with beam Current 15 nA and spot size 2 μm except for glass and carbonate where beam was 10 μm.

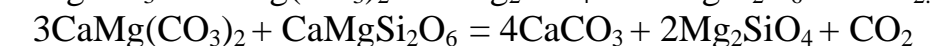
The investigated xenolith which is 8 cm x 6 cm consists of olivine (86%) first and second generation, orthopyroxene (11%), spinel (<1%), clinopyroxene (2,1%), carbonate (<1%) and glass (3%). First generation minerals (olivine, orthopyroxene, spinel) are cut by fine-grained aggregates consisting of clinopyroxene, glass, and carbonate (1 Fig. 1)

Carbonate in the investigated nodules forms typically small 10-30 μm segregations of oval, rounded and wormiclar shape, which are found only in association with (krishtonite?). glass, second generation olivine and spinel or with clinopyroxene. Carbonate is enriched in calcium and has low concentrations of magnesium and iron (Table. 1). Tiny crystals of fluorite were found in carbonate. Apatite is possibly also present. There is a mineral phase of rounded shape in one of carbonate segregations whose size is smaller than 1 micron (the size of an electron beam) which contains chromium, cerium and lanthanum, Ce being prevailing over La. From these semiquantitative analysis one may assume that this phase represents the mixture of very fine crystals of carbonates of cerium, lanthanum and chromite or it represents a mineral belonging to the spinel group with the formula $AM_{12}O_{19}$, where A is Ce-La and M is Cr

Glass forms wormiclar interstitial veinlets and embayments between crystals. The color of the glass is slightly brownish and sometimes unquestionably brown. Very often the glass is associated in veinlets with rather small crystals of

clinopyroxene, second generation olivine, spinel and carbonates. Glass composition plots into trachyte (syenite) field with a rather high albitic index (0.8-0.9). Very small (10 µm) globules of originally sulphide rich material are present in the silicate glass, usually very close to glass-carbonate boundaries. Microprobe analyses indicate that these globules are compositionally and mineralogically complex, with 1µm thick oxide rims and cores containing mixed sulphides and fine-grained oxide phases of Fe, Ni and Cu, including Fe-bearing bunsenite (NiO), trevorite (ideally NiFe₂O₄), and magnetite. Pyroxene with up to 7.6 wt% NiO has also been found. Similar oxide-sulphide mixed phases have been reported from an ophiolite complex [28]. This phase assemblage, by analogy with sulphides in other upper mantle nodules [21], could have initially formed as immiscible Fe-, Ni-, Cu-rich monosulphide melt globules, which subsequently exsolved into pentlandite, pyrrhotite, and chalcopyrite, and ultimately were altered by low temperature oxidizing fluids.

In one thin section of the investigated xenolith we found segregation of carbonate in association with glass of rather large size (250 x 150 microns) situated at the boundary between two olivine crystals (Fig.1). Carbonate is immersed into glass and forms with it a distinct meniscus. Smaller segregations of carbonate form rounded or oval blebs surrounded by glass and there are oval-shaped holes which obviously represent carbonate crushed out during polishing. This is a high-calcium carbonate with a low magnesium concentration; the carbonate of this composition is similar to calcite carbonatite-sovites. Textural features of the investigated nodule and chemical composition of its minerals testify to a metasomatic interaction of harzburgite in the mantle of Montana Clara Island with primary dolomitic melt. The latter was probably transported from the lower zones of a carbonatized mantle during its partial melting. As a result of this interaction and the following reactions:



the assemblage of secondary minerals olivine plus pyroxene, plus spinel appeared which means that partial wehrlitization of starting harzburgite took place. During this process depleted harzburgite was considerably enriched in light rare earths (Table 1) The primary carbonate melt of the mantle material of Montana Clara Island was to a large extent enriched in sodium because clinopyroxene in the investigated nodule contains up to 1.1% Na₂O which, according to our calculations based on experimental data of Dalton and Wood, (1993), corresponds to 5% Na₂CO₃. Therefore a metasomatic assemblage of secondary minerals was in equilibrium with a sodium-containing dolomitic composition. However, the investigated carbonate from the nodule contains

low sodium concentrations (0.1-0.3%). It is probable that sodium was dissolved by the late low temperature fluids whose evidence is manifested in oxidation and decomposition of sulphides. From the experimental data [7] one may conclude that

nyerereite, which is the main sodium compound in natrocarbonatites, is dissolved incongruently under the conditions of low temperature hydrothermal process. Sodium carbonate enters solution during nyerereite interaction with hydrothermal fluid while the solubility of calcium carbonate is lower by an order of magnitude. During the reaction of primary carbonate melt with harzburgite the Ca/Mg and Mg/Fe ratios in the metasomatising liquid change. According to experimental data [6] with decreasing pressures Ca-Mg partitioning between melt and clinopyroxene shifts to a more Ca rich liquid; the Ca/Ca+Mg+Fe+Na ratio in the carbonate melt reaches up to 0.92. The magnesium to iron ratio also increases. The presence of calcium-rich carbonates confined to wehrlite veinlets of the investigated nodule which are characterised by very high Ca/Ca+Mg+Fe+Na (0.84-0.91) and Mg/Mg+Fe-(0.95) ratios result from reactions taking place at pressures below 20 kb.

Using two pyroxene thermometers [5] we estimated the lower temperature limit of the metasomatic reaction between carbonate melt and harzburgite because, in this case, orthopyroxene is an unstable phase in this process. The estimated temperatures fall into the range 1150-1075° C. Oxygen fugacity was estimated from olivine-spinel-orthopyroxene geobarometry [32] and yielded a range of 0.76- to 0.06 log units below the QFM (quartz-fayalite-magnetite) buffer.

Our investigations revealed a very complicated geological history of the mantle material of Montana Clara Island. The extremely depleted character of the investigated xenolith (Table 1) points to processes of substantial melting - more than 25% - during which the initial substrate lost so-called basaltic elements: CaO, Al₂O₃, TiO₂, Na₂O and others. All the sulphur should have been lost during this process due to the low melting temperatures of mantle sulphides. Later this depleted mantle material was penetrated by metasomatising carbonate melt with the prevailing dolomite component and containing sodium and possibly potassium, sulfur, light rare earths, strontium and phosphorus. During the metasomatic reactions partial wehrlitisation along the veinlets and fissures of the initial harzburgite took place. Later, during the very rapid ascend of mantle material (otherwise primary carbonate would not survive) wehrlitic mineral assemblage which contained carbonate melted during decompression. The character of interrelationships between carbonate, sulphide globules and glass (Fig.1) testifies to the processes of immiscibility between carbonate, silicate and sulphide melts.

The immiscibility between silicate and sulphide melts has been known for many years. Many authors also reported immiscibility between silicate and carbonate liquids in a wide range of temperatures and pressures (Koster van Groos, Wyllie, 1966 and many others). However, the immiscibility in carbonate-silicate-sulphide systems has so far not been revealed. Using a piston-cylinder apparatus, we have investigated the immiscibility in the system Ca-rich carbonate- Fe, Ni sulphide-silicate melt of phonolitic composition containing F. Experiments were made at 1250°C and 4-15 kbar. The double Pt capsule method was employed in order to control oxygen fugacity. Immiscibility has been observed in the

investigated system as exhibited in the complete separation of carbonate and silicate liquids, whereas sulphide melt was present in the form of small globules in both liquids (Fig.2). Sulphur solubility in silicate melt varies from 0.15% to 0.35% and in carbonate liquid it ranges from 0.02% to 3.7% depending on alkali content. These results permit us to suggest that the immiscibility of carbonate, sulphide and silicate melts took place during the partial melting of upper mantle material. The glass in the investigated nodule is enriched in alkalis and silica probably due to the incongruent melting of jadeite-bearing clinopyroxene during the reduction of pressure.

Therefore the investigated unique mineral assemblage including carbonate and glass can be considered as a micro model of the generation of the carbonatitic magmas during the processes of the partial melting of wehrlitized and carbonatized mantle. The development of carbonatite magmatism on the Canary Islands and Cape Verde Islands is likely to be related to the partial melting of carbonatized mantle in the South Atlantic, which took place over a vast territory.

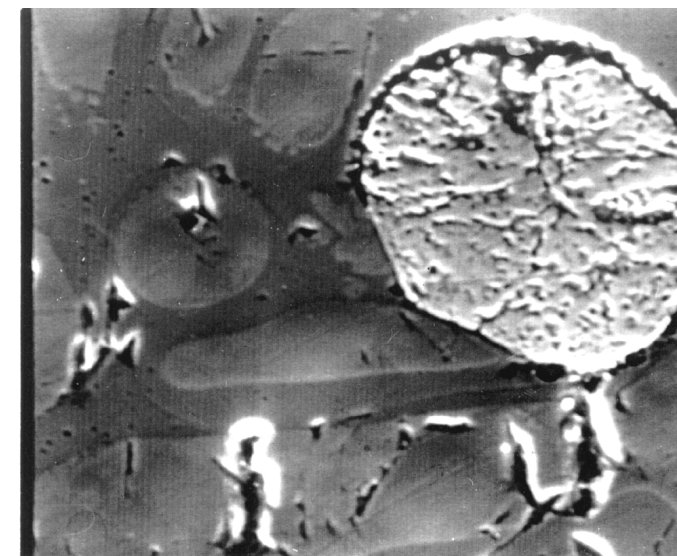


Fig.2 Back-scattered electron image of the run product, T-1220⁰ C, P-8kb. Sulphide-silicate-carbonate immiscibility, S-sulphide liquid, C-carbonate liquid, Gl-glass, silicate liquid. Magnification $\times 30.000$

In summary, the investigated mineral assemblage of carbonate + glass + sulphides + clinopyroxene + orthopyroxene + spinel is the outcome of the process of metasomatic interaction of depleted mantle with carbonate melt and subsequent partial melting forming carbonate liquids similar to carbonatites. It may be concluded that high-calcium carbonate melts may be formed during partial melting of wehrlitic mantle. It may be noted in this respect that earlier [27] we have found

xenoliths of carbonated wehrlite with calcium-rich carbonate containing 3.52% MgO on San-Vincente Island (Cape Verde Islands) where carbonatite volcanism is wide spread.

THE ROLE OF CO₂ IN DIFFERENTIATION OF ULTRAMAFIC ALKALINE SERIES. LIQUID IMMISCIBILITY IN CARBONATE BEARING PHONOLITIC DYKES (POLAR SIBERIA)

One of the largest of its kind in the world, the Maimeicha-Kotui province of ultramafic alkaline rocks, is situated in the North of the Siberian platform in Polar

Siberia and extends over an area 220 x 350 km between Maimecha and Kotui rivers [9,18]. There are 37 ultramafic alkaline and carbonatitic massifs of complicated structure. This province is particularly noteworthy not only for the abundance of carbonatites but for the association of many of them with ultramafic rocks. The representative rocks types include dunite, pyroxenite, ijolite, melteigite, jacupirangite, phoscorite, a range of melilite-bearing rocks and numerous and varied carbonatites. There are hundreds of dykes, including radial dykes which surround the ultramafic-alkaline massifs (for instance Bor-juryakh, Romanicha, Odichincha, Dolbykha, Kugda).

We investigated a series of radial dykes of Dolbykha massif which comprise alnoite, olivine-nephelinites, nephelinites, melilite nephelinites, cancrinite, nosean and calcite phonolites, calcite trachytes, calcite carbonatites and monchiquites.

Some dyke phonolites contain carbonate-bearing globules of rounded and oval shapes ranging in size from 1-2 mm to 17-20 mm. One globule-bearing phonolite (N 873) was chosen for detailed investigation. Phonolite consists of phenocrysts (~10%) represented by albite, mica, and ilmenite, globules (~20%) and groundmass (~70%). Globules consist of polycrystalline calcite aggregate and contain albite, mica, apatite, cancrinite, Sr-lueshite, zircon, ancylite, ilmenite, strontianite (Fig.3, 4). Occasionally the reaction relations between mica and albite are observed. Albite grains form rims around mica. Carbonate-bearing globules are characterized by sharp contact with ground mass, and they are seemingly flowed around by the crystals of groundmass (mainly albite). Groundmass is fine-grained and it includes albite and mica with subordinate K-feldspar and nepheline. Among accessory minerals, apatite, ilmenite, ancylite, and Sr-lueshite were observed. Representative microprobe analyses of mineral phases are given in Table 2. The substantial substitution of Ca by Sr in apatite and calcite was observed. A similar feature was described by Kjarsgaard and Peterson (1991) in globular nephelinite from Shombole.

The consideration of this material in the light of experimental data on the liquid immiscibility in carbonate-silicate systems suggests that the separation of carbonatite melts from phonolitic ones took place due to their immiscibility while in liquid state.

Petrographic data support this hypothesis because crystals of ground mass (albite and mica) obviously flowed around carbonate globules. It may be noted that there is great similarity in the composition of minerals in groundmass and in globules, which demonstrates the existence of equilibrium in this carbonate-bearing phonolitic system (Table 2). As has been already noted, the increasing alkalinity of carbonate-bearing magmatic systems favours the appearance of immiscible liquids. It should be pointed out that the boundary of liquid immiscibility field in the system $\text{Na}_2\text{O} + \text{K}_2\text{O} - \text{Al}_2\text{O}_3 + \text{SiO}_2 - \text{CaO} - \text{CO}_2$ corresponds to an alpaicity index $\text{Na}_2\text{O} + \text{K}_2\text{O} / \text{Al}_2\text{O}_3$ close to 1. (see Fig 15-1,[4]). This implies that in alpaitic melts liquid immiscibility is more likely to occur. The investigated phonolite belongs to peralkaline type (agp. ind. = 1.1), and therefore formation of

immiscible liquids is more probable. The crystallisation of mica phenocryst enriched in Al also results in an increase in the peralkalinity of residual melt.

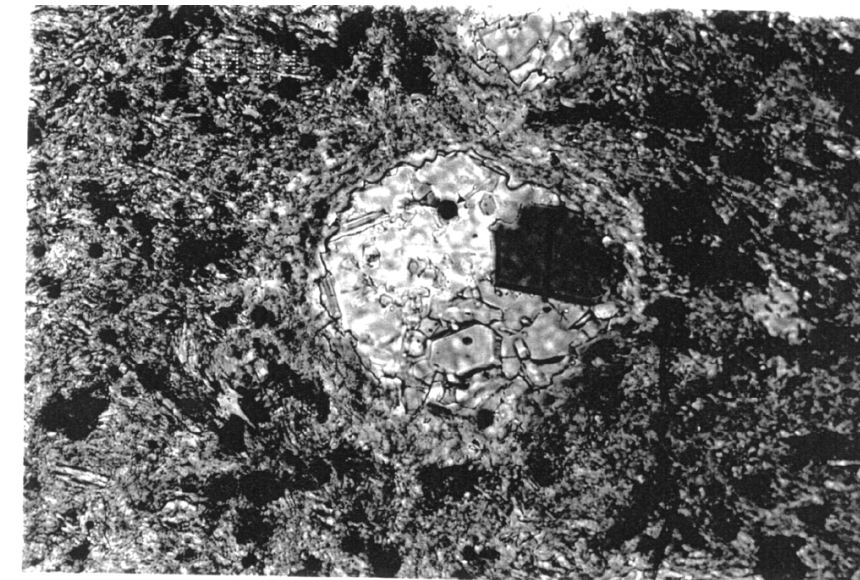


Fig.2 Carbonate globule in phonolite N 873 crossed nicols magnification $\times 250$

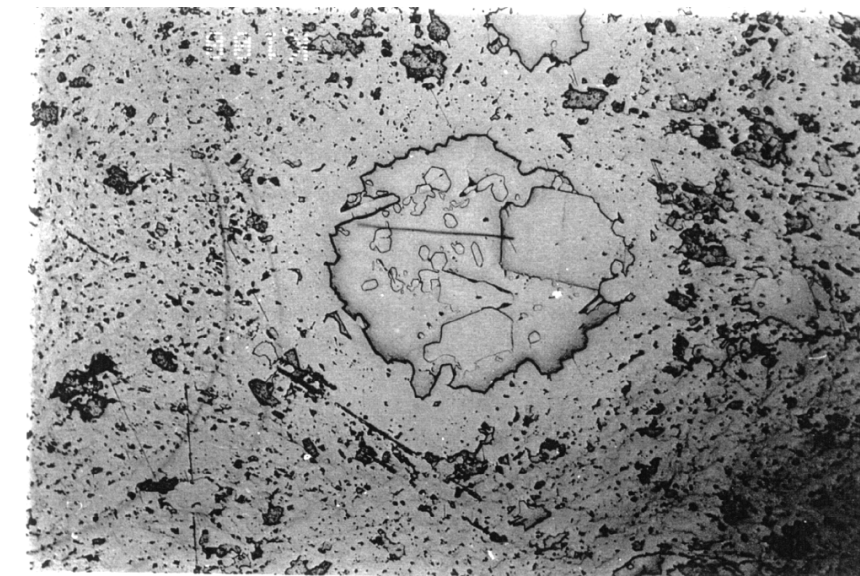


Fig.3 The same carbonate globule in phonolite N 873, reflected light mc - mica, Anc - ancyllite, Ab - albite, cc-calcite, Ap-apatite

The presence of Sr lueshite in globules of investigated phonolite also supports the oversaturated in respect alkalis character of carbonate melt because lueshite can crystallize only from peralkaline compositions according our experimental data on $\text{Na}_2\text{O}+\text{K}_2\text{O}-\text{SiO}_2+\text{Al}_2\text{O}_3-\text{CaO}-\text{CO}_2$ system in which the direction of the tie-line corresponds the more alkaline composition of equilibrium carbonate immiscible liquids.

Table 2
Compositions of phonolite, minerals from globules and groundmass.

Elem. wt. %	Phonolite	Albite			Mica			Calcite		Ilmenite		Strychite	Analcite	Apatite	Strontite
		Phen.	G. m.	Globe	Phen.	G. m.	Globe	G. m.	Globe	Phen.	Globe				
SiO ₂	47.02	67.98	68.08	68.89	37.09	37.23	36.65	0.41	0.23	0.63					
TiO ₂	0.6				3.12	2.36	2.26	0.13		52.28	53.79	3.45	0.1		0.3
Al ₂ O ₃	16.31	19.65	19.33	19.52	13.27	11.77	12.85	0.23	0.1	0.35					
FeO	5.01	0.19	0.10		20.17	21.50	22.18	3.14	2.42	45.43	45.14	1.29			
MnO	0.16		0.09					1.01	1.26	1.15	1.39	0.26			
MgO	2.71				13.28	11.86	12.61	0.83	0.73	0.17				0.22	
CaO	8.43	0.39		0.18	0.09	0.26	0.02	52.87	54.96	0.19		12.09	2.83	52.9	8.18
Na ₂ O	6.88	10.52	11.22	11.73	1.17	0.60	0.63	0.17	0.22	0.28	0.28	7.85			
K ₂ O	4.17	1.01	0.2	0.09	8.59	9.36	9.69	0.23							
P ₂ O ₅	1.33													40.84	
CO ₂	6.95														
F														3.87	
Total	100.09	99.75	99.02	100.4	96.79	95.07	94.81	60.36	61.05	100.4	100.6	93.87	75.79	98.06	68.62
SrO								1.16	0.91			5.03	27.23	1.19	58.56
BaO								0.19	0.2			0.08	0.28		1.85
Nb ₂ O ₅												63.39			
La ₂ O ₃												0.17	17.04		
CeO ₂												0.24	22.47		
Nd ₂ O ₃													5.40		

Globe-Compositions of minerals from globules.

G.m.- Compositions of minerals from ground mass Phen.- Compositions of phenocrysts.

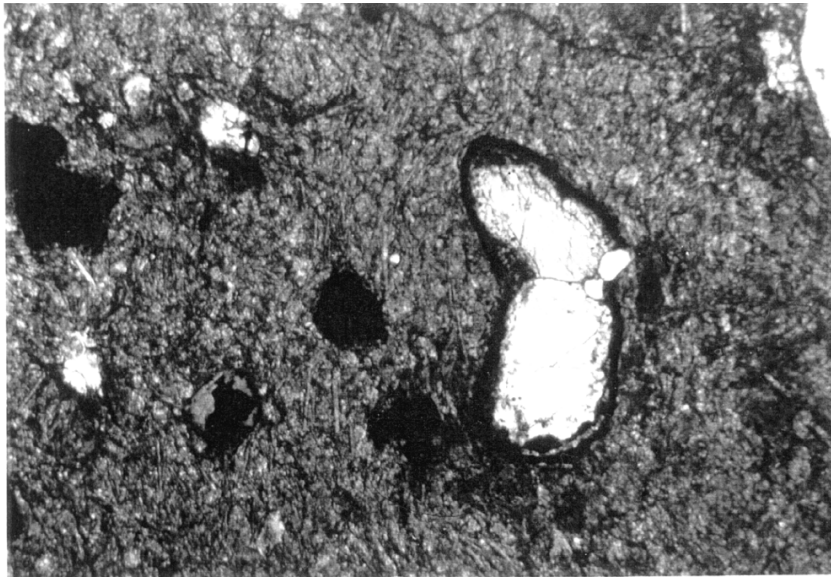


Fig. Phenocrysts of calcite in phonolite N 2003, mg 100 crossed nicols magnification $\times 250$.

The alkalis were subsequently lost into fluid phase due to incongruent [15] dissolution of calcium-sodium carbonate in aqueous fluid at lower temperatures [7]. Our discovery of nyererite as solid microinclusions in perovskite in the Guli carbonatite of Polar Siberia [16] confirms this assumption. From recent experimental data of Woh-ler and Wyllie (1995) we can conclude that under higher pressure (2.5 GPa) liquid immiscibility does exist even in mafic melts, while under lower pressure (1 GPa) in the same system immiscibility phenomena are absent mostly due to degassing. Calcite, melilite and wollastonite may crystallize as liquidus phases if the melt becomes very Ca-rich. In one phonolitic dyke (N 2003) of Dolbykha complex there is liquidus calcite as the phenocrysts without signs of any immiscibility phenomenon (Fig.5).

The regime of CO_2 in alkaline systems controls differentiation of residual phonolitic magmas. Under high carbon dioxide pressure the separation of an immiscibility carbonate liquid occurs. At lower P_{CO_2} values liquid immiscibility is not observed and calcite may crystallize either as phenocryst or in groundmass. At still lower pressure carbonates are not formed due to the loss of carbon dioxide and mineral assemblages, including either melilite or wollastonite, occur. Some melilite-bearing rocks of Polar Siberia are a result of this process.

Thus one of the important mechanisms of the genesis of carbonatite melts in Polar Siberia were phenomena of liquid immiscibility in strongly differentiated phonolitic magmas. The generation of the carbonatites is probably controlled by the depth (and P_{CO_2}) of the intermediate magma chamber where differentiation took place, and probably by the alkalinity of melts and the speed at which the magma ascended to the surface.

CONCLUSION

The above examples demonstrate an important role of liquid immiscibility in the genesis of Ca-rich carbonatite magmas. The formation of immiscible liquids during processes proceeding in the upper mantle results in the generation of phonolite and carbonatite liquids.

Among the continental carbonatite formations there are Ca-rich carbonatites exclusively occurring with syenites Okorusu, Namibia [23], Siilinjarvi, Finland [24], Stjernoy, Norway [26], and Vishnevye Gory, Russia [18]. It is possible to suggest that the origin involves liquid immiscibility in these cases. It should be pointed out that the Phalabora Complex, South Africa, which contains a satellite plug of alkali syenite, alkali quartz syenite and alkali granite in association with calciocarbonatite [10], is also characterized by the presence of Cu-Fe sulphide deposits. This leads us to speculate that calciocarbonatite-silicate-sulphide immiscibility similar to that observed in the Montana Clara nodule might have played some role in the genesis of this complex.

Under the conditions of earth's crust the carbonate-silicate liquid immiscibility arises at the late stages during the prolonged differentiation of ultrabasic-alkaline magma. The principal factors controlling the generation of carbonatites during formation of immiscible liquids are the CO₂ partial pressure and alkalinity of magmatic systems.

Acknowledgments

This work was done with financial support of RFBR N 96-05-64151 and INTAS 95-IN-RU-953

REFERENCES

1. Amundsen, Evidence for liquid immiscibility in the upper mantle //Nature. 1987. V. 327. P. 692-696.
2. Baker, P.J. Wyllie, Liquid immiscibility in a nephelinite-carbonate system at 25 kbar and implications for carbonatite origi //Nature. 1990.V. 346. P. 168-170.
3. D.K. Bailey, Carbonate melt from the mantle in the volcanoes of south-east Zambia. //Nature. 1989. 338. P. 415-418.
4. Bell, K. (ed.), Carbonatites: Genesis and Evolution. Unwin Hyman, London, 1989. 618p.
5. Brey, T. Kohler, Geothermometry in four-phase lherzolites. II. New thermobarometers and practical assessment of existing thermobarometries. //Geochim Cosmochim Acta. 1990. V. 31. P. 1353 –1378.
6. Dalton, B.J. Wood, The compositions of primary carbonate melts and their evolution through wallrock reactions in the mantle. //Earth Planet Sci Lett. 1993. V. 119. P. 511-525.
7. Dernov-Pegarev S.D., Malinin, Calcite solubility in high temperature aqueous solutions of alkaline carbonatites and problems of carbonatite formation. //Geochemie. 1976. V.5. P. 643-657.
8. Eggler, D.H Carbonatites, primary melts, and mantle dynamics /Ed. Bell, K. Carbonatites Genesis and Evolution. Unwin Hyman, London, 1989. P. 561-579.
9. Egorov., Ijolite carbonatite plutonism (case history of the Maimecha-Kotuy complexes of northern Siberia) Leningrad: Nedra, 1991. P. 260 pp.
10. Eriksson, Phalaborwa: a saga of magmatism, metasomatism, and miscibility: /Ed. Bell, K. Carbonatites genesis and evolution. Unwin Hyman, London, 1989. P. 221-249.
11. Freestone, & D.L. Hamilton, The role of liquid immiscibility in the genesis of carbonatites //Contributions to Mineralogy and Petrology. 1980. V.73. P. 105-117.

12. D.L Hamilton., P. Bedson, J., Esson, The behaviour of trace elements in the evolution of carbonatites, /Ed. K. Bell, Carbonatites: Genesis and Evolution. Unwin Hyman, 1989. P. 405-427.
13. Henderson I., Pacheco A.H., //Contribution to Mineralogy and Petrology. 1995. V. 121. P. 267-275.
14. Kjarsgaard and T. D. Peterson, Nephelinite-carbonatite liquid immiscibility at Shombole Volcano, East Africa //Mineralogy and Petrology. 1991.V. 43. P. 293-314.
15. Kogarko, A.A. Tugarinov, L.D. Krigman., Phase equilibria in the nepheline-luestite system //Doklady Akademii Nauk. 1982. V. 263. P. 985-987.
16. Kogarko, D.A. Plant, C.M.B. Henderson, and Kjarsgaard B.A., Na rich carbonate inclusion in perovskite and calzirtite from the Guli intrusive Ca-carbonatite, Polar Siberia //Contributions to Mineralogy and Petrology. 1991.V. 109. P. 124-129.
17. Kogarko, L.N., Geochemical characteristics of oceanic carbonatites from the Cape Verde Islands. //S.Afr.Geol. 1993. V.96. P. 119-125.
18. Kogarko, L.N., V.A. Kononova., M.P. Orlova., and A.R. Woolley, Alkaline Rocks and Carbonatites of the World.//Part 2: 1995. Former Soviet Union
19. Koster van Groos, and P. J. Wyllie, Liquid immiscibility in the system $\text{Na}_2\text{O}-\text{Al}_2\text{O}_3-\text{SiO}_2-\text{CO}_2$ //Amer. Journal Sci. 1966. V. 264. P. 234-255.
20. Koster van Groos and P. J. Wyllie, Liquid immiscibility in the join $\text{NaAlSi}_3\text{O}_8-\text{Na}_2\text{CO}_3-\text{H}_2\text{O}$ ($\text{NaAlSi}_3\text{O}_8-\text{Na}_2\text{CO}_3-\text{H}_2\text{O}$) and its bearing on the genesis of carbonatites //Amer. Journal Sci. 1968. V. 266. P. 932-967.
21. Lorand, J. P., F. Conquere, Contribution a l'etude des sulfures dans les enclaves de lherzolite a spinelle des basaltes alcalins (Massive Central et Languedoc, France) //Bull Mineral. 1983. V. 106. P. 585-605.
22. Peterson Peralkaline nephelinites I. Comparative petrology of Shombole and Oldoinyo. //Contribution to Mineralogy and Petrology. 1989. V.101. P. 458-478.
23. Prins, The geochemical evolution of the alkaline and carbonatite complexes of the Damaraland Igneous Province //S.W. Africa Ann Univ Stellenbosch Ser Al Geol. 1981. V. 3. P. 145-278.
24. K Puustinen, The carbonatite of Siilinjarvi in the Precambrian of eastern Finland: a preliminary report. //Lithos. 1969. V.3. P. 89-92.
25. Pyle & S.E. Haggerty silicate-carbonate liquid immiscibility in upper-mantle eclogites: implications for natrosilicic and carbonatitic conjugate melts //Geochimica et Cosmochimica Acta. 1994. V. 58. P. 2997-3011.
26. Robins, Syenite-carbonatite relationships in the Seiland Gabbro Province, Finnmark, northern Norway //Nor Geol Unders. 1971. V. 272. P. 43-58.
27. Ryabchikov ID, Brey G, Kogarko LN, Bulatov VK. Partial melting of carbonated peridotite at 50 kb. //Geokhimiya. 1989. V. 1. P. 3-9.
28. M Tredoux de M.J. Wit, RJ Hart, RA Armstrong, N.N.M. Linsay, J.P.F. Sellschop, Platinum group elements in a 3.5 Ga nickel-iron occurrence: possible evidence of deep mantle origin. //J Geophys Res. 1989. V. 94B. P. 795-813.
29. Twyman and J Gittins, in J.G. Fitton and B.G.J. Upton, eds., Alkaline igneous rocks. /Oxford and London, Blackwell Scientific, Geological Society Special Publication 1987. N 30. P. 85-94.
30. L Woh-er and P.J. Wyllie. Experimental data bearing on liquid immiscibility, crystal fractionation, and the origin of calciocarbonatites and natrocarbonatites //International Geological Review. 1994. V. 36. P. 797-819.
31. L.Woh-er and Peter J.Wyllie. Liquid immiscibility and calciocarbonatite magmas //Submitted to Journal of Petrology. 1995.
32. Wood, L.T. Bryndzya, Johnsen KE. Mantle oxidation state and its relationship to tectonic environment and fluid speciation //Science. 1990. V. P. 248:337-345.
33. Wyllie, Origin of carbonatites: evidence from phase equilibrium studies. In K. Bell, Carbonatites: Genesis and Evolution: London, Unwin Hyman, London. 1989. P. 500-540.
34. Wyllie, M.B., Baker, and B.S. White, Experiment boundaries for the origin and evolution of carbonatites. //Lithos. 1990. V. 26. P. 3-19.

LAMPROITE ROCKS OF THE EASTERN ANABAR REGION

Vladykin N.V¹, Lelyukh M.I.²

¹ *Vinogradov Institute of Geochemistry SB RAS, Irkutsk, E-mail: vlad@igc.irk.ru*

² *JSC «ALROSA», Mirny.*

The diatremes of the Eastern Anabar Region, briefly called Preanabaria, and the Tomtor massif contain rocks referred to the lamproite family in terms of chemical and mineral composition [13]. Olivine, leucite and sanidine varieties of lamproites have been distinguished in the study area. All rocks of diatremes undergo intense carbonatization. Besides, complete pseudomorphoses of carbonate are formed after olivine and leucite crystals, thus making their diagnostics fairly complicated. The technique of recovering primary chemical composition of rocks via removing carbonate by hydrochloric acid was proposed. Kimberlites are transformed into lamproites, with the amount of mica increased to 80%. In petrochemical and geochemical parameters lamproites of Preanabaria are close to lamproites of the other regions. As regards the ratio of isotopes, Sr and Nd picrites of Eastern Preanabaria and carbonatites of the Tomtor occur in the transitional area of enriched mantle between EM - 1 and EM - 2. The diamond-bearing lamproite tuffs of the Tomtor massif are assumed to be the source of the Ebelyakh placer.

Introduction

Lamproites represent exotic deep-seated rocks arising profound scientific and practical interest [4,6,7,11] and hosting a large diamond field-Argyle [2]. In Eastern Preanabaria (Fig.1) two zones were found to contain lamproite group rocks: 1- East Anabar and 2- Tomtor [13,16].

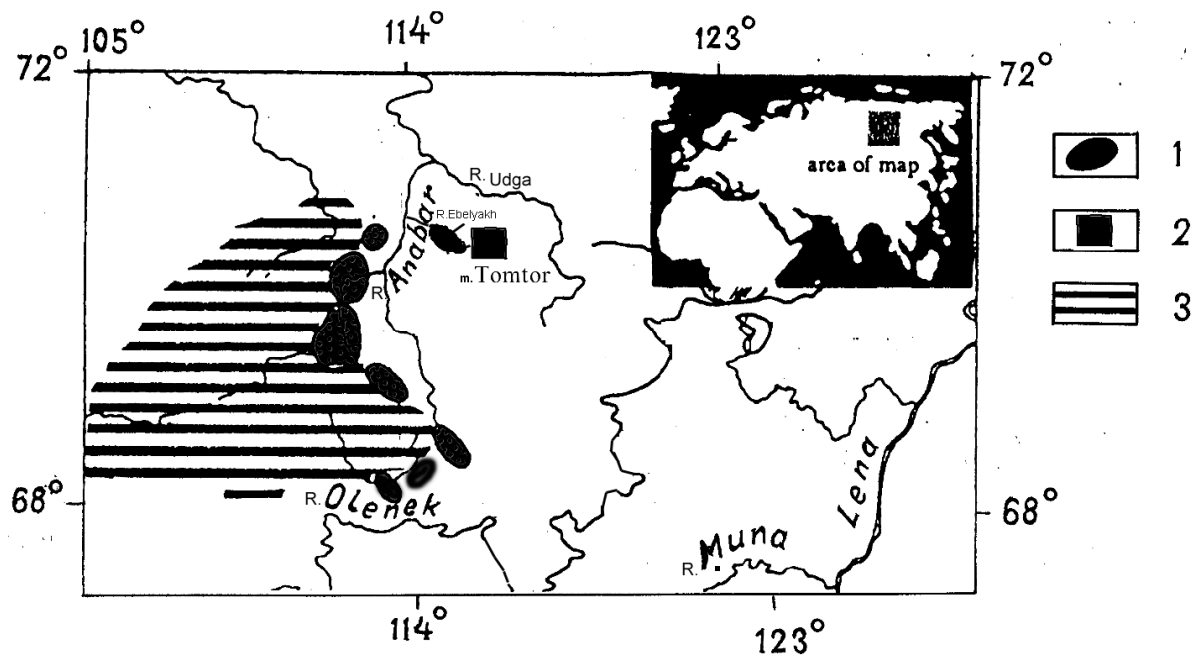


Fig.1. Geographic settlement of Preanabarska lamproite province: 1- Anomalies of Eastern Preanabaria, 2- Tomtor massif , 3- Anabar Shield.

The first zone covers the entire contact between the Anabar shield and Siberian platform.

It consists of picrite-(kimberlite)-aleneite-lamproite association of rocks with abundant carbonatites. The Tomtor massif occurring within the Udzhinsky uplift is located 200 km to the east of the former zone [8,3]. This is where the picrite-lamproite-syenite-carbonatite association of rocks is predominant [15]. The carbonatites of the massif enclose a large deposit of rare elements. Besides, the Ebelyakh diamond-bearing placer, its original sources not known, was discovered on the Preanabaria area. One region is located to the east of the Ebelyakh diamond-bearing placer, the other one to the west. Thus, lamproites of these regions will be looked upon separately considering different rock assemblages.

TECTONIC SETTING AND ISOTOPE SOURCES OF LAMPROITE MAGMATISM

In the summary study on kimberlites D.B.Dauson [1] reported on the spatial location of large diamond-bearing kimberlite occurrences of the central parts of platforms and on the minor amount of diamond-bearing kimberlite rocks of the peripheral part of platforms where kimberlite magmatism is combined with alkaline magmatism. This pattern is valid for the Siberian platform as well. The examination of tectonic setting of lamproite occurrences [12] revealed two different areas of geodynamic settings typical of lamproite magmatism fall

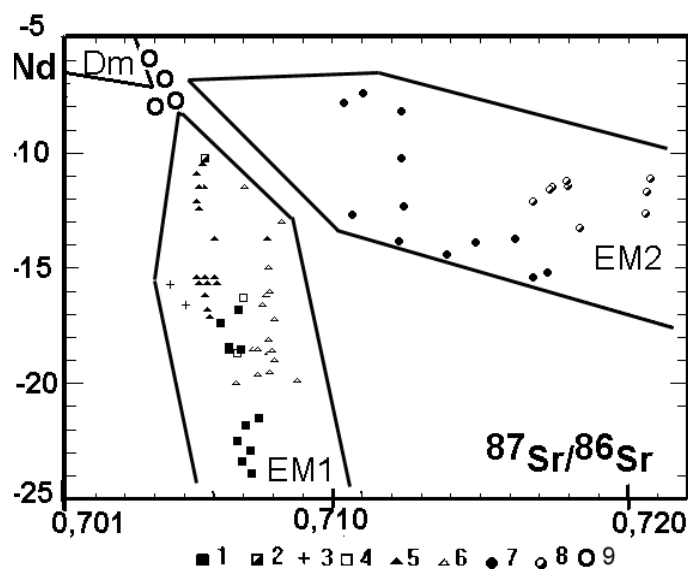


Fig.2. $^{87}\text{Sr}/^{86}\text{Sr}$ isotope ratio and Nd epsilon in the lamproites worldwide. Aldan: 1- Murun, 2- Yakokut, 3- Bilibinsky, 4- Khani; the USA [6]: 5- Leucite Hills, 6- Montana; 7- Australia [2], 8- Spain [6]; 9- Tomtor and- East Preanabaria. 1-4 and 9 represent the authors' data [12,14].

occurrences. 1. The areas of complete folding in the platform surroundings: Spanish, Italian, SW Australian (Ellendale zone), the Uralian province.

2. The platform margins and areas of shield juncture: Argyle, Aldan, North American, also some sites of the Chinese, Paraguay and Indian provinces of lamproites. In the second geodynamic setting the lamproite magmatism is spatially and genetically related to the occurrences of deep-seated K-alkaline magmatism, like in the Aldan and North-American (Leucite Hills) provinces. We studied in detail the lamproite magmatism of these two provinces [7,11,14]. These studies [12] pointed out that lamproites of the Aldan and North American province, identical in geochemical parameters and isotope ratios (Pb, Sr, Nd), into the same area in the plot [5,12] representing the deepest enriched source EM-1 (Fig. 2). The lamproite occurrences of these provinces are located in the young rift zones between the northern part of the Aldan shield and Siberian platform, as well as the southern part of the Canadian shield and North-American platform. In spite of the difference in age (Aldan lamproites of Jurassic-Cretaceous and American lamproites of Tertiary and Quaternary) they are similar in many parameters [12]. Geodynamic settings of lamproite magmatism of type 1 (area of complete folding attached to platforms) in the ratio of isotopes Sr and Nd have enriched isotope source EM-2 [12]. Lamproites of Argyle and Greenland province [6] have Sr and Nd isotope ratios, which fall into the area of EM-1 and EM-2 junction.

LAMPROITE ROCKS OF THE EASTERN ANABAR REGION

If kimberlites occur in the Central part of the Siberian platform the lamproite occurrences must be located in its peripheral part. In the southern termination of the Siberian platform (Aldan shield) lamproites are widespread and are studied in detail [11]. Earlier in the northern termination of the Siberian platform (Preanabaria) one occurrence of the feldspar type of lamproites has been described [10].

The Anabar diamond-bearing province is located in the eastern and southeastern part of the Anabar shield and extends as an arc-like zone 50 km wide and 300 km long. The province contains kimberlite and kimberlite-like rocks (picrites, alnoites and meimechites). In the rivers of the province over 300 diamond placers, their original sources not known, have been found. The detailed observation of the core from the wells drilled in the magnetic anomalies of the Anabar province led to discovery of rocks of the lamproite series [13].

Lamproite rocks produce diatreme explosion pipes, stocks, sills, dykes and cut metamorphic and sedimentary rocks of Precambrian and Cambrian. They occur in association with kimberlite and alkaline rocks of the province which have Lower Mesozoic and Mesozoic age. The rocks of the lamproite group occur in different fields of the East Anabar province, e.g. Luchikansky, Birigindinsky, Djukensky and Ary-Mastakhsky. They have been currently surveyed in the Djukensky field. The lamproite rocks of the Djukensky field are tectonically and structurally

different from those of the Tomtor massif. In these parameters they are close to picrites and alnoites, with which they produce continuous series. In the East Anabar region olivine and sanidine lamproites are found in some places. The olivine lamproites of the Djukensky field are the greenish-gray rocks of the porphyry appearance, massive, with fine-grained, rarely glassy mass. The phenocrysts consist of rounded separations of the early olivine, its content reaching 10%, that of mica 20-30% or over. The aphyre bulk mass consists of fine mica, altered olivine, rarely pyroxene and amphibole, as well as apatite, carbonate and in places garnet. Spinelides – titanium magnetite, chromite, perovskite, and sulfides are abundant. Genetically, these lamproites are less differentiated. In addition to the secondary carbonate they contain magmatic carbonate not detached from the silicate magma so far.

The dyke in anomaly 97/63 represents specific variety of lamproite. This is fine-grained rock of light brownish color, which seems to consist of mica only. In fact it consists of small phenocrysts of olivine (20%), which are surrounded by the aggregate of grown small grains of light green amphibole and brown tetraferriphlogopite and ore mineral.

CHEMICAL COMPOSITION AND PETROCHEMICAL FEATURES OF EASTERN PREANABARIA LAMPROITES

Table 1 yields chemical composition of lamproites. Due to intense processes of lamproite carbonatization and olivine serpentinization, the chemical composition of rocks does not correspond to their primary composition. The abundance of many elements are underestimated because of high concentrations of the carbonate and aqueous components. The chemical experiment was conducted to reduce primary composition via dissolution of carbonate and analysis of insoluble residue. This technique will be considered in detail when reporting on the Tomtor lamproites. Processed samples represent olivine lamproites. The contents of K₂O in the study rocks are reduced incompletely because of dissolution of broken mica. The Djukensky lamproites are characterized by high contents of Ti, Ba, Sr, Cr and Ni. The correlation plots for petrogenic elements of the Anabar lamproites, picrites, kimberlites and Aldan lamproites are represented in Figure 3. All lamproites show similar trends of the element content variations. The lamproites of Aldan have lower Ti content. The compositions of rocks of picrite-kimberlite series of Preanabaria occupy compact area in the angular part of the diagram. This is what markedly distinguishes them from the lamproite series rocks of the same region (Fig.3). Such a regularity is observed on the diagram of pair correlation of MgO and K₂O with c Al₂O₃. Lamproite rocks produce extended trend of compositions, the rocks of the kimberlite-picrite group make up a compact field of a small size (Fig. 3). Such behaviour of petrogenic elements is explained by higher differentiation of the rocks of lamproite group against picrite-kimberlite one. On the plot picrites display clear correlation between MgO and CaO, and

absence of correlation of these elements for lamproites. This pattern is explained by greater contribution of carbonates to formation of kimberlites. In lamproites, CaO is involved into composition of 2 minerals – carbonate and pyroxene. In the East Anabar region lamproites do not form genetically isolated group of rocks,

Table 1
Chemical composition of lamproites from anomalies of Eastern Preanabaria (weight. %).

boil	38/89		90/63		17/63	17/63	17/63	36/63	36/63	36/63	36/89	41/63	41/63	97/63	109/63
depth	63		36,4		37	38	39	50	51	52	26	102	110	27	40,5
	a	b	a	b											
SiO ₂	25,65	41,62	24,63	42,34	33,02	32,89	32,84	30,49	27,55	30,70	28,83	30,29	31,59	32,42	34,63
TiO ₂	1,98	3,35	3,26	6,08	4,76	4,41	4,92	3,66	3,15	3,98	0,50	4,89	3,84	4,74	5,50
Al ₂ O ₃	3,67	4,87	3,20	5,42	3,63	3,72	4,07	4,58	4,27	5,14	6,54	3,98	5,23	2,88	4,02
Fe ₂ O ₃	7,09	9,65	8,51	12,15	7,22	6,60	8,20	8,15	6,22	8,23	4,21	9,27	9,27	10,37	8,26
FeO	3,78	4,85	2,78	4,49	7,09	6,74	5,39	3,68	3,86	4,94	0,99	3,32	3,5	3,68	6,73
MnO	0,21	0,21	0,25	0,23	0,22	0,19	0,23	0,21	0,17	0,20	0,15	0,16	0,19	0,20	0,22
MgO	21,18	23,73	22,02	16,53	26,89	26,50	26,99	22,08	20,49	22,71	22,21	28,13	27,00	24,01	23,41
CaO	16,15	1,47	15,33	2,49	5,13	5,27	4,11	10,69	16,22	9,84	16,65	5,33	4,84	7,13	4,13
BaO	0,22	0,30	0,26	0,41	0,20	0,23	0,29	0,21	0,20	0,24	0,19	0,23	0,47	0,23	0,23
SrO	0,17	0,02	0,16	0,02	0,12	0,09	0,14	0,09	0,14	0,08	0,09	0,08	0,05	0,05	0,05
K ₂ O	1,92	2,45	1,81	2,94	2,15	3,00	1,57	3,45	3,11	4,06	3,53	3,38	4,41	6,03	2,51
Na ₂ O	0,13	0,11	0,07	0,07	0,10	0,10	0,12	0,02	0,10	0,10	-	0,10	0,10	0,25	0,10
P ₂ O ₅	1,28	0,06	1,23	0,02	0,70	0,73	0,84	0,77	1,66	0,72	1,06	0,46	0,38	0,17	0,32
CO ₂	11,88	0,03	9,81	0,03	0,45	1,65	0,93	4,92	6,99	0,31	9,55	1,38	2,05	3,20	0,82
H ₂ O	4,62	6,93	6,60	6,32	8,15	7,76	9,07	6,64	5,75	8,52	5,00	9,15	6,77	4,36	8,96
F	0,32	0,33	0,25	0,25	0,25	0,30	0,29	0,41	0,24	0,38	0,37	0,22	0,34	0,36	0,33
S	-	-	-	-	0,09	0,12	-	-	0,20	0,10	0,05	0,02	0,04	0,11	0,07
Sum	100,12	99,84	100,06	99,68	100,06	100,17	99,88	99,88	100,22	100,09	99,76	100,30	99,93	100,04	100,15

Note: a – initial rock; b – rock after HCl treatment. Data of quantitative XRF, analysed by Finkelshtein A. Concentrations of CO₂, F, S were defined by chemical method, analyst Matveeva L.N., Institute of Geochemistry SB RAS, 1999.

they have gradual transitions with kimberlite-picrite rocks. We have a series of samples with a gradual increase of mica in the bulk mass (80%). It appears that the boundary between alkaline kimberlites and lamproites is reasonable to conduct with K₂O= 3-4 % in fresh unaltered rocks.

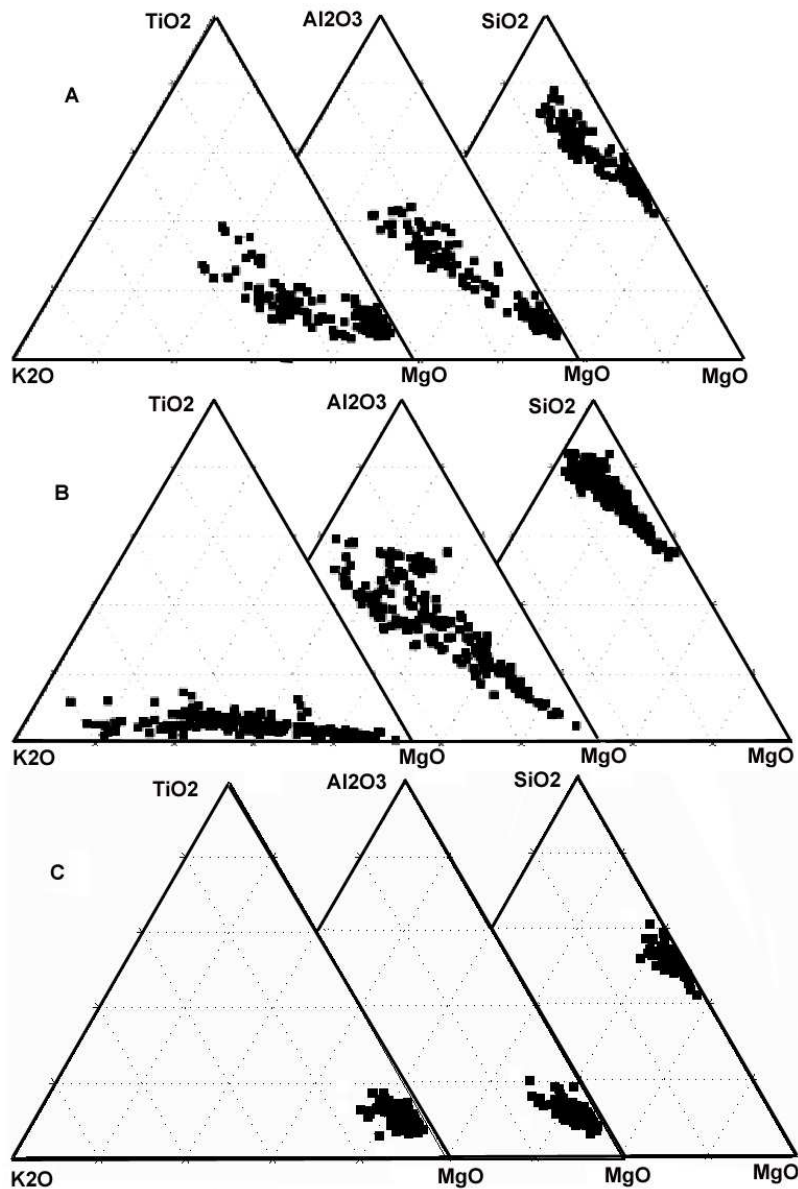


Fig 3. Plots of triple correlation of petrogenic elements in lamproites of Eastern Preanabaria (a), Aldan lamproites (b), picrite-kimberlites of East Preanabaria (c).

GEOCHEMICAL FEATURES OF LAMPROITES OF THE EASTERN ANABAR REGION

The rare elements of lamproites are given in Table 2 . The Ba, Sr, Cr and Ni contents in the study rocks lie within the typical levels of their concentrations characteristic for lamproites. Large variations of rare element concentrations in lamproites are due to a wide spectrum of their compositions. The variations of ratios Ba to Sr and Cr to Ni indicate the contribution of magmatic differentiation

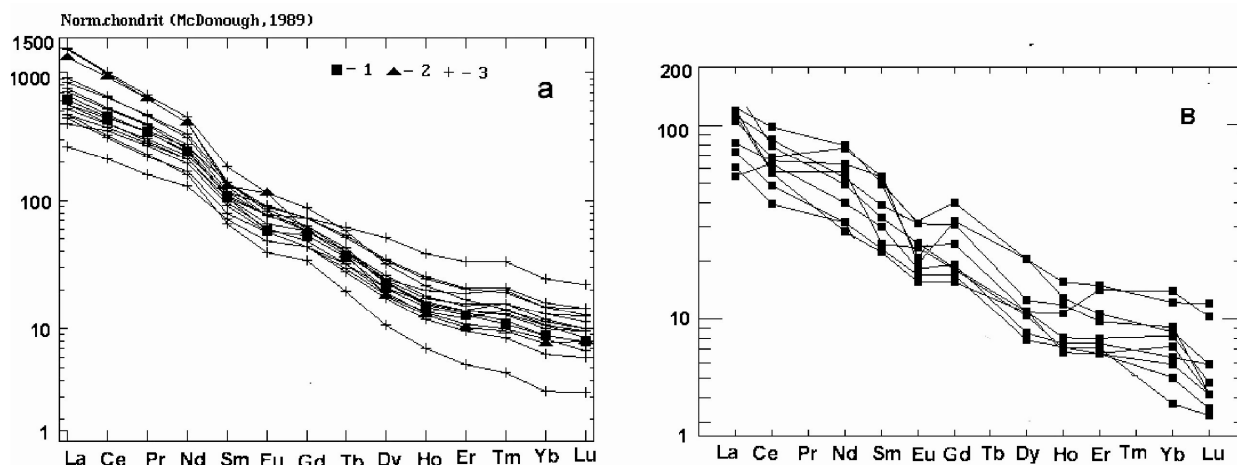


Fig. 4. Rare-earth element spectra in lamproites of Aldan (b), Preanabaria (a), and Australia (a): 1- Argail, 2- Ellendail-11 - olivine lamproites, 3- crosses – Preanabaria.

Contents (ppm) of rare elements of lamproites from anomalies of Eastern Preanabaria.

boil	38/89	90/63	17/63		17/63	17/63	36/63	36/63	36/63	36/89	41/63		41/63	97/63	109/63
depth (m)	63	36,4	37		38	39	50	51	52	26	102		110	27	40,5
	a	b	a	b											
Ba	1964	2679	2321	3661	1820	2080	2589	1875	1790	2170	1720	2050	4240	2030	2040
Sr	144	169	136	169	996	750	118	762	1210	703	730	659	464	398	385
Cr	530	1000	510	900	650	1000	740	790	900	800	81	750	340	910	710
Ni	1100	1300	710	1000	1200	1400	1800	1100	1100	1200	160	1000	660	1400	1100
Co	60	80	51	70	71	85	84	65	60	70	45	84	45	60	85
V	250	300	180	250	250	300	170	230	250	220	370	120	170	170	180
Sc	14	28	13	25	18	30	12	15	15	16	21	5,2	24	11	26
Zr	280	320	230	280	221	290	220	250	242	277	91	93	209	259	143
Sn	3,1	3,5	4,1	4,5	4,1	5	3,6	3,4	3,2	3	1,4	2,4	3,9	2,6	3,5
Pb	17	10	25	17	11	7	11	2,2	8,0	6	9,8	1,7	6,6	20	5,6
Zn	87	95	100	110	120	140	130	82	100	90	72	67	150	100	110
Cu	63	70	94	100	120	150	130	120	100	110	20	59	410	23	91
Mo	0,6	1	1,5	2	0,7	1	1,1	0,8	1	1	0,06	1,7	1,6	0,4	0,4
B	36	30	15	11	34	28	63	18	15	8	6,7	48	64	43	56
Ag	0,1	0,2	0,2	0,3	0,09	0,2	0,12	0,11	0,10	0,10	0,03	1,5	1,6	0,05	0,06
Be	3,4	3,8	2,2	2,5	4	4,4	3,7	2,8	2,5	2,0	1,5	0,5	0,7	15	1,35

Note: a – initial rock; b – rock after HCl treatment Lamproite samples were analysed by: Ba, Sr- XRF, analyst Finkelshtein A.L., the rest elements by quantitative emission spectral method, analysts Kuznetsova A.I., Vorobieva S.S. and Chernysheva O. M.

processes. The charts of TR spectra in lamproites Preanabaria and Australia are similar (Fig. 4).The concentrations of other rare elements occur within variations

of their concentrations in lamproites. The levels of concentrations of rare elements in the study rocks confirm that they were correctly attributed to the family of lamproites. This province is a good polygon for classification of lamproites with transitions between picrites and lamproites, kimberlites and lamproites, like nowhere else in the world.

LAMPROITES OF THE TOMTOR MASSIF

West off the Ebelyakh placer, a great Tomtor massif of K-alkaline rocks, lamproites, and carbonatites lies. It will be considered in detail. In 1980's a large deposit of Nb-TR carbonatites was discovered in the massif. The survey of this deposit mainly touched upon the ore sequence, while silicate rocks were given minor attention. These were basically ijolite-syenite rocks, which were studied, the rest were attributed to the foidite-tinguaite series, though Porshnev reported in [8] that in every well the upper horizons are composed of decomposed K-effusives of picrite type.

In the massif numerous occurrences and diatremes of K-ultrabasic rocks were found [8]. The major contribution to the investigation of diamond-bearing capacity belongs to Grigory Porshnev, who found a diamond in a diatreme. Available rock samples were classified as picrites and kimberlites. Some rocks of diatreme breccias [9] were referred to lamproites, however abundant melilite was later found in these rocks, so they cannot be referred to lamproites. Diatremes with the rocks of the picrite-alsoite series were described in the southern termination of the Tomtor massif.

Detailed studies of the Tomtor massif led to the discovery of the lamproite series rocks [13,16] and thus magmatism of the Tomtor massif was interpreted differently [15].

ROCKS OF THE LAMPROITE SERIES OF THE TOMTOR MASSIF

The picrite-lamproite-carbonatite series of rocks of the Tomtor massif is referred to the volcanic stage of development of the Tomtor volcano-pluton. These rocks were found in core of the upper sections in many wells drilled in the massif. These are essentially disintegrated rocks of greenish color, bearing voluminous disintegrated mica. The rocks look very much as picrites [8], however their primary composition is hard to be regained. Fairly thick strata (to 50 m) are flatly-lying sills or sloped dykes composed of olivine lamproites. In the two wells (0865 and 0855) leucite lamproites were found.

Olivine lamproites look as fine-grained rocks of gray color, composed of porphyry separations of odd olivine crystals which are covered with more fine-grained micaceous-pyroxene mass. The crystals of mica phenocrysts produce flow textures, very typical of rocks of the lamproite series [5]. After crystallization of lamproites the fluid-enriched carbonatite magma intruded and they underwent intense carbonatization. Olivine is

totally replaced with carbonate of different composition. Pyroxene is often disintegrated after carbonatization.

Leucite lamproites consist of leucite phenocrysts of cut and rounded habits which are covered by micaceous-pyroxene aggregate. The mica separations are often confined to leucite crystal faces. The separations of leucite, the same as olivine, are totally replaced by carbonates. The process of lamproite carbonatization is widespread in the Uralian and Indian lamproites.

CHEMICAL COMPOSITION OF THE TOMTOR LAMPROITES

A difficult determination of the true composition of lamproites in the Tomtor is due to overlapped process of carbonatization. To distinguish the primary composition of lamproites carbonate was dissolved in 30 samples.

Technique of dissolution: 30 grams of lamproite was dissolved during 5 minutes in 300 ml of cold HCl (1:1). Solution was poured off, filtered, and analysed. Insoluble residue was carefully washed with water, dried and analysed. Chemical compositions of rocks of lamproite group prior to (a) and after (b) acid treatment are given in Table 3.

Primary compositions of carbonatized rocks show low amounts of SiO₂ and high CaO and CO₂, therefore they were attributed to the rocks of picrite-kimberlite group. After removing carbonate the contents of SiO₂, MgO, K₂O, and TiO₂ increased and they corresponded to compositions of lamproites. In some rock varieties, the carbonate constituents were represented by the minerals of dolomite-ankerite composition. Their removal did not bring to marked increase of MgO and iron, however their concentrations remained within the compositions of lamproite series rocks. The treatment with acid did not bring to dissolution of silicate minerals, otherwise a sharp oxidation of FeO would have taken place. In some samples, disintegrated pyroxene was removed, thus leading to decrease in CaO contents in rocks. Apatite was also dissolved, so the phosphorus concentrations were not heightened. It is hardly probable that after carbonate was removed the rocks were totally recovered. However, this was sufficient for a true diagnostics of rocks of the lamproite series.

To prove that after acid treatment the rocks of the other series did not acquire lamproite composition, Table 3 yields compositions of treated pyroxenite (analyses 29-30) and melilite-bearing rocks (analyses 27-28). After the acid treatment their chemical compositions differ from those of lamproites. Selective dissolution of carbonate and a sharp increase in some petrogenic elements are evident on the plot of paired correlations of some petrogenic elements (Fig. 5). Dissolution does not distort trends of differentiation of elements and in a general trend lamproites of the Tomtor massif are not different from lamproites of the Aldan shield and classical lamproites worldwide.. As seen from

Table 3
Chemical composition of lamproites from Tomtor massif (weight. %).

Boil	0865		0873		1625		1625		1625		1625		2417		2425		2446	
	50-115		50		95		150		188		48-55		140-150		68			
Depth (m)	a	b	a	b	a	b	a	b	a	b	a	b	a	b	a	b	a	b
Nb ₂ O ₅	1	2	3	4	5	6	7	8	9	10	11	12	13	14	15	16		
SiO ₂	24,31	42,34	25,53	43,05	32,02	42,19	35,34	45,98	34,58	41,60	31,83	41,98	28,74	47,04	29,02	47,75		
TiO ₂	2,29	4,29	3,08	5,30	3,83	5,44	3,52	5,03	4,36	5,22	3,35	4,40	3,34	5,54	3,12	5,39		
Al ₂ O ₃	6,54	9,72	6,02	9,43	7,62	7,74	10,54	11,08	8,72	9,15	6,94	8,44	7,31	10,30	6,59	10,57		
Fe ₂ O ₃	5,22	9,28	5,45	6,84	7,04	7,95	3,71	3,63	3,68	2,68	5,68	5,85	4,44	7,42	4,73	6,84		
FeO	3,68	4,04	5,12	5,66	5,84	4,94	7,27	8,53	9,25	9,79	6,91	6,74	5,66	5,30	6,20	5,30		
MnO	0,26	0,19	0,28	0,14	0,19	0,12	0,24	0,27	0,42	0,37	0,43	0,30	0,24	0,05	0,24	0,03		
MgO	9,48	12,89	11,29	13,21	12,59	13,25	6,63	8,37	13,82	14,08	13,80	15,35	10,48	9,76	9,75	8,74		
CaO	21,76	2,50	17,57	1,29	11,34	2,36	12,87	1,73	7,76	1,36	12,06	4,53	14,19	0,33	13,69	0,30		
BaO	0,31	0,45	0,17	0,25	0,15	0,12	0,63	0,70	0,36	0,41	0,30	0,33	0,13	0,17	0,11	0,14		
SrO	0,58	0,49	0,41	0,37	0,11	0,11	0,50	0,52	0,53	0,49	0,24	0,26	0,32	0,33	0,20	0,20		
ZrO ₂	0,04	0,07	0,05	0,07	0,05	0,08	0,06	0,07	0,05	0,05	0,03	0,04	0,04	0,06	0,03	0,05		
K ₂ O	3,78	6,34	4,67	7,28	4,44	5,83	4,19	6,18	7,94	7,93	4,96	6,10	5,40	8,14	5,51	8,74		
Na ₂ O	1,57	2,15	1,55	2,08	2,40	2,52	3,44	3,60	0,57	0,63	1,31	1,61	1,60	2,63	1,80	2,91		
P ₂ O ₅	2,72	2,76	1,73	1,73	0,73	0,75	1,00	1,04	1,96	1,95	0,56	0,52	0,51	0,42	0,61	0,66		
CO ₂	13,58	-	16,92	-	9,35	-	8,26	-	4,64	-	9,41	-	15,94	-	17,20	-		
F	0,43	0,52	0,68	0,88	0,35	0,36	0,25	0,51	1,05	1,26	0,70	0,84	0,49	0,69	0,63	0,97		
S	0,11	0,38	0,12	0,07	0,02	0,04	0,08	0,24	0,03	0,02	0,02	0,01	0,18	0,44	0,01	0,02		
H ₂ O	2,67	1,29	0,50	1,80	1,36	5,50	0,96	2,21	0,20	2,62	1,09	2,31	0,50	0,97	0,20	0,76		
Sum	99,33	99,70	99,74	99,45	99,43	99,30	99,49	99,69	99,92	99,61	99,52	99,61	99,51	99,59	99,64	99,37		

Table 3
Chemical composition of lamproites from Tomtor massif (weight. %).

Boil	0865		0873		1625		1625		1625		2417		2425		2446	
	50-115		50		95		150		188	48-55		140-150		68		
Depth (m)	a	b	a	b	a	b	a	b	a	b	a	b	a	b	a	b
№№	1	2	3	4	5	6	7	8	9	10	11	12	13	14	15	16
SiO ₂	24,31	42,34	25,53	43,05	32,02	42,19	35,34	45,98	34,58	41,60	31,83	41,98	28,74	47,04	29,02	47,75
TiO ₂	2,29	4,29	3,08	5,30	3,83	5,44	3,52	5,03	4,36	5,22	3,35	4,40	3,34	5,54	3,12	5,39
Al ₂ O ₃	6,54	9,72	6,02	9,43	7,62	7,74	10,54	11,08	8,72	9,15	6,94	8,44	7,31	10,30	6,59	10,57
Fe ₂ O ₃	5,22	9,28	5,45	6,84	7,04	7,95	3,71	3,63	3,68	2,68	5,68	5,85	4,44	7,42	4,73	6,84
FeO	3,68	4,04	5,12	5,66	5,84	4,94	7,27	8,53	9,25	9,79	6,91	6,74	5,66	5,30	6,20	5,30
MnO	0,26	0,19	0,28	0,14	0,19	0,12	0,24	0,27	0,42	0,37	0,43	0,30	0,24	0,05	0,24	0,03
MgO	9,48	12,89	11,29	13,21	12,59	13,25	6,63	8,37	13,82	14,08	13,80	15,35	10,48	9,76	9,75	8,74
CaO	21,76	2,50	17,57	1,29	11,34	2,36	12,87	1,73	7,76	1,36	12,06	4,53	14,19	0,33	13,69	0,30
BaO	0,31	0,45	0,17	0,25	0,15	0,12	0,63	0,70	0,36	0,41	0,30	0,33	0,13	0,17	0,11	0,14
SrO	0,58	0,49	0,41	0,37	0,11	0,11	0,50	0,52	0,53	0,49	0,24	0,26	0,32	0,33	0,20	0,20
ZrO ₂	0,04	0,07	0,05	0,07	0,05	0,08	0,06	0,07	0,05	0,05	0,03	0,04	0,04	0,06	0,03	0,05
K ₂ O	3,78	6,34	4,67	7,28	4,44	5,83	4,19	6,18	7,94	7,93	4,96	6,10	5,40	8,14	5,51	8,74
Na ₂ O	1,57	2,15	1,55	2,08	2,40	2,52	3,44	3,60	0,57	0,63	1,31	1,61	1,60	2,63	1,80	2,91
P ₂ O ₅	2,72	2,76	1,73	1,73	0,73	0,75	1,00	1,04	1,96	1,95	0,56	0,52	0,51	0,42	0,61	0,66
CO ₂	13,58	-	16,92	-	9,35	-	8,26	-	4,64	-	9,41	-	15,94	-	17,20	-
F	0,43	0,52	0,68	0,88	0,35	0,36	0,25	0,51	1,05	1,26	0,70	0,84	0,49	0,69	0,63	0,97
S	0,11	0,38	0,12	0,07	0,02	0,04	0,08	0,24	0,03	0,02	0,02	0,01	0,18	0,44	0,01	0,02
H ₂ O	2,67	1,29	0,50	1,80	1,36	5,50	0,96	2,21	0,20	2,62	1,09	2,31	0,50	0,97	0,20	0,76
Sum	99,33	99,70	99,74	99,45	99,43	99,30	99,49	99,69	99,92	99,61	99,52	99,61	99,51	99,59	99,64	99,37

Table 3 continued

boil depth (m)	3225		3233		7265		117		117		118		14/81		48/8		2447	
	a	b	a	b	a	b	a	b	a	b	a	b	a	b	a	b	a	b
N ₂ N ₀	17	18	19	20	21	22	23	24	25	26	27	28	29	30	31	32	33	34
SiO ₂	23,80	41,13	20,62	36,14	32,06	43,06	26,42	38,78	29,23	40,11	30,28	40,93	26,33	42,07	23,83	40,41	25,96	36,41
TiO ₂	2,84	4,95	1,88	3,37	2,61	3,54	1,64	2,48	3,74	5,17	3,37	4,67	2,63	4,28	2,60	4,17	2,75	4,22
Al ₂ O ₃	5,66	9,40	6,06	10,47	6,69	8,38	4,65	6,69	8,52	10,51	7,03	8,90	4,30	7,25	4,83	7,41	6,91	8,66
Fe ₂ O ₃	4,66	6,19	5,60	10,70	7,03	8,60	6,67	6,69	7,61	9,52	7,06	10,36	5,78	9,53	5,31	8,19	8,73	11,36
FeO	5,12	7,45	3,32	3,86	5,03	3,68	4,04	4,13	6,02	5,84	4,76	5,39	4,76	3,32	5,30	5,30	3,32	4,04
MnO	0,36	0,14	0,70	0,53	0,56	0,12	0,24	0,12	0,33	0,25	0,27	0,29	0,25	0,15	0,21	0,12	0,33	0,37
MgO	10,64	15,02	10,35	17,34	16,65	17,10	19,04	19,22	11,94	15,35	11,91	15,70	20,58	20,14	15,36	13,56	10,55	13,64
CaO	20,40	0,29	24,55	2,51	8,23	0,89	12,41	4,04	12,83	1,23	14,84	2,48	11,32	0,66	13,42	3,19	21,58	9,65
BaO	0,22	0,14	0,40	0,61	0,11	0,12	0,11	0,16	0,03	0,41	0,31	0,37	0,27	0,30	0,13	0,18	0,40	0,54
SrO	0,90	0,60	0,80	0,76	0,09	0,09	0,14	0,17	0,27	0,25	0,42	0,02	0,10	0,02	0,12	0,15	0,43	0,39
ZrO ₂	0,45	0,54	0,06	0,09	0,40	0,54	0,02	0,03	0,04	0,05	0,06	0,07	0,33	н.обн.	0,04	0,06	0,05	0,07
K ₂ O	5,07	8,25	4,56	7,81	4,33	5,26	4,04	5,63	5,01	6,14	4,86	5,81	4,32	5,71	3,87	5,88	3,37	3,54
Na ₂ O	1,08	1,53	0,20	0,20	2,27	3,02	1,99	2,73	1,12	1,21	2,19	2,60	0,61	0,83	1,67	2,62	0,81	0,87
P ₂ O ₅	1,22	1,23	2,68	2,85	1,06	1,07	0,23	0,27	0,49	0,45	0,94	0,04	0,58	0,02	0,19	0,19	1,93	1,91
CO ₂	16,60	н.обн.	16,58	-	9,75	н.обн.	17,37	-	9,92	-	9,94	-	13,00	0,29	20,91	-	10,25	-
F	1,24	0,96	0,36	0,26	0,81	0,79	0,67	1,15	0,51	0,48	0,60	0,83	0,85	1,00	0,85	1,09	0,24	0,12
S	0,29	0,63	0,09	0,13	0,04	0,08	0,44	0,44	0,07	0,08	0,04	0,04	0,80	н.обн.	0,28	0,16	0,11	0,17
H ₂ O	0,20	1,00	0,59	1,85	2,50	4,00	0,36	6,66	1,66	2,39	0,54	0,89	3,60	4,92	0,56	6,81	1,78	3,63
Sum	100,22	99,05	99,40	99,48	99,88	100,01	100,48	99,39	99,34	99,44	99,42	99,39	100,06	100,07	99,58	99,49	99,50	99,59

Table 3 continued

boil	6189	50	59	59	101	118	0841	0865	0865	1625	2441	3125	14/81	14/81	4060
depth (m)	65-75	50	90	137	24		38	114	128	81	66,5	121	10	30	17,4
	a	b													
№№	35	36	40	41	42	43	44	37	45	46	47	48	49	50	51
SiO ₂	30,12	36,50	32,47	32,28	36,89	31,38	23,22	30,86	27,97	34,99	30,65	23,9	23,06	35,04	29,71
TiO ₂	2,57	3,80	2,65	2,80	3,61	2,38	2,09	7,04	2,76	3,24	3,43	1,63	2,25	2,50	5,85
Al ₂ O ₃	10,23	9,02	5,77	5,78	3,07	6,66	5,27	7,53	7,41	7,84	7,02	6,48	7,42	9,89	9,53
Fe ₂ O ₃	7,36	10,58	9,46	7,68	5,47	7,39	6,38	6,39	5,72	4,62	6,45	4,14	4,12	5,35	10,12
FeO	4,76	6,20	3,14	4,94	7,27	3,14	3,32	8,35	5,84	7,63	5,21	4,58	4,76	4,94	6,11
MnO	0,47	0,60	0,21	0,19	0,13	0,19	0,26	0,23	0,27	0,23	0,21	0,41	0,50	0,17	0,21
MgO	7,89	11,21	17,96	19,45	16,17	15,00	15,30	8,65	11,76	14,74	10,02	15,74	13,06	14,01	17,92
CaO	18,97	11,59	14,71	13,88	11,19	18,05	15,39	11,12	13,55	11,21	12,96	16,00	20,93	10,75	5,07
BaO	1,11	1,16	0,12	0,32	0,14	0,23	0,14	0,22	0,16	0,10	0,02	0,27	0,15	0,20	0,25
SrO	0,43	0,43	0,09	0,13	0,06	0,16	0,17	0,13	0,12	0,10	0,19	0,21	0,12	0,14	0,04
ZrO ₂	0,06	0,08	0,33	0,38	0,27	0,32	н.о.б.н.	0,08	0,55	0,54	н.о.б.н.	0,41	0,69	0,68	н.о.б.н.
K ₂ O	2,17	3,42	3,22	2,84	2,14	3,17	4,00	4,80	5,82	5,58	5,67	5,07	3,07	5,87	5,77
Na ₂ O	2,64	0,75	0,33	0,10	0,30	0,65	1,51	2,73	0,38	0,99	2,02	0,99	0,10	1,98	0,32
P ₂ O ₅	2,18	0,60	0,49	0,83	0,54	1,15	0,97	1,30	1,13	0,96	0,82	0,26	1,28	1,45	0,85
CO ₂	7,01	-	4,48	7,44	8,33	7,73	20,17	7,75	10,25	5,53	14,33	17,77	9,68	6,10	2,96
F	0,21	0,18	0,24	0,23	0,28	0,35	0,26	0,46	0,60	0,49	0,62	0,57	0,26	0,46	0,35
S	0,16	0,24	0,04	0,13	1,87	0,19	н.о.б.н.	0,31	0,02	0,27	н.о.б.н.	0,04	0,03	0,15	н.о.б.н.
H ₂ O	1,08	3,04	4,68	6,14	2,92	2,39	1,18	1,53	5,91	1,77	0,83	2,15	9,13	0,67	4,42
Sum	99,42	99,40	100,28	100,18	100,41	100,39	99,52	99,48	99,97	100,62	100,19	100,38	100,50	100,15	99,33

Note: a – initial rock; b – rock after HCl treatment. 27-28 Bt – pyroxenite, 29- 30 melilitite-bearing rock, the rest lamproites. Data of quantitative XRF, analysed by Finkelshtein A. Concentrations of CO₂, F, S were defined by chemical method, analyst Matveeva L.N., Institute of Geochemistry SB RAS, 1999.

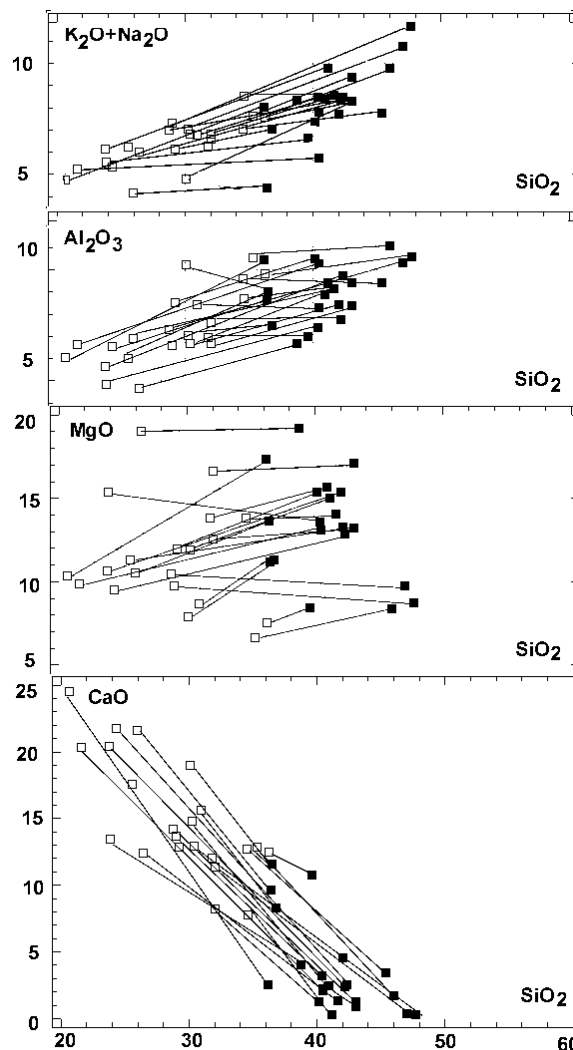


Fig. 5. Paired correlations of petrogenic elements in lamproites of the Tomtor massif. Captions: empty squares – original rocks, black – after HCl treatment.

diagram of triple correlations of the main petrogenic elements the trends of compositions of the Anabar and Aldan lamproites are close (Fig. 3), although TiO₂ contents in the Tomtor lamproites are considerably higher than those of Aldan and are comparable with Australian ones..

In mineral composition the lamproites of the Tomtor massif are found to contain olivine and leucite varieties. After the process of carbonatization takes place, only some crystal forms are left from olivine and leucite. In the less altered olivine lamproites, olivine is commonly replaced with serpentine. The olivine lamproites consist of phenocrysts of olivine and trachytoid micaceous-pyroxene mass covering early phenocrysts. In places the bulk rock contains 80% of mica. Secondary minerals are apatite, perovskite and ore mineral. In places garnet concentrations are high, which is not typical of lamproites. Garnet is inferred to be formed by the process of lamproite carbonatization, particularly when pyroxene is replaced.

Leucite varieties occur in the core of only two wells. They differ from olivine lamproites in very viscous mechanical properties. The leucite lamproites -treated samples the contents of these elements are raised, those of Sr increase not so markedly as such of Ba, which is associated with dissolution of strontium contained in carbonate. The Pb contents, available in carbonate, fall drastically. Some samples display lowered Cr and Ni contents. This is probably due to removal of these elements from broken pyroxenes. The Tomtor lamproites have high scandium and yttrium, which is common for other rocks as well, thus indicating their affinity. In addition, like with Australian lamproites, the Zr and REE concentrations are fairly high (Table 5). As follows from diagram in Fig. 4, the TR spectra of the Preanabaria lamproites, normalized after chondrite, ideally coincide with the spectra of diamond-bearing olivine lamproites of Australia, both in sloping of spectra and ratio of TR elements, which is pretty rare in the lamproite group of rocks. In contrast to the Aldan lamproites, the TR spectral lines are more sloped. Absence of Eu fractionation indicates minor degree of differentiation in the period from melt origination to its crystallization, which is a positive

Table 4

Contents of rare elements (ppm) of lamproites from Tomtor massif.

boil	2417		2446		2447		48/8		0865	0873	1625			2425	3225
Depth (m)	48-55		68		20-30		164		50-115	50	95	150	188	140-150	210-260
№№	1	2	3	4	5	6	7	8	9	10	11	12	13	14	15
Ba	2710	2960	960	1220	3540	4820	1140	1590	4000	2190	1111	6290	3650	1470	1210
Sr	2063	2194	1720	1710	3658	3285	1049	1254	4129	3096	912	4393	4126	2756	5056
Zr	235	274	244	396	357	487	300	470	483	541	581	544	404	427	403
Cr	800	840	530	800	260	350	800	1500	830	940	580	270	410	740	620
Ni	570	800	530	920	90	130	700	800	500	780	560	140	220	500	500
Co	41	62	42	56	24	35	47	78	90	61	58	39	37	44	31
V	250	300	360	440	230	310	290	610	550	440	420	280	240	400	370
Sc	22	25	22	40	30	33	30	17	21	46	23	25	5,1	43	40
Sn	3,2	3,4	3,3	4,8	3,3	4,6	2,4	3,7	6,3	5,5	5,6	5	3,3	4,7	6,8
Pb	53	5,2	15	10	22	6,7	15	15	2,4	16	6,5	4,4	1,5	4,2	7,4
Zn	230	210	100	110	140	170	96	140	180	150	160	140	270	83	160
Cu	66	84	49	78	52	97	87	170	150	110	54	100	37	84	60
Mo	11	15	9,7	25	2,1	3,2	0,8	1,6	33	32	1	21	3,2	32	15
B	2,5	3,2	2	3,1	8	11	5,8	12	17	3,4	10	12	2,1	2,7	4,4
Ag	0,06	0,07	0,06	0,06	0,11	0,14	0,07	0,09	0,25	0,09	0,09	0,07	0,04	0,05	0,06
Be	6,3	14	15	18	4,3	5,7	24	56	30	45	14	8	12	35	15

are distinguished by lattice-like structure of the mica crystal location. The bulk of leucite lamproites contain separations of K-feldspar. In spite of heightened contents of sodium in some samples, plagioclase is not discovered.

RARE ELEMENTS IN LAMPROITES OF THE TOMTOR MASSIF

Tables 4 and 5 provide concentrations of rare and spectra of rare-earth elements in carbonatized and acid-treated rocks. The lamproites of the Tomtor massif show heightened amounts of Ba, Sr, Cr, and Ni, which is common for lamproites, and distinguishes them from the rocks of other series. In the acid

Table 5

Contents of REE and Y(ppm) of lamproites from Tomtor massif

boil	59	71	101	0841	0865	1625	2441	3125	7932	14/81	14/81	av-1/3	av-1/4
depth (m)	137	100	24	38	114	86	66,5	121	38	117	20		
La	105	135	215	160	113	125	63	360	150	200	170	145	315
Ce	190	270	400	290	230	245	130	600	270	390	320	280	570
Pr	21	34	44	33	27	29	15	60	24	45	37	33	60
Nd	79	125	145	113	100	106	61	190	105	155	120	115	190
Sm	12	21	20	16	16	18	11	21	19	21	17	16	20
Eu	3,3	5,2	4,4	3,8	4,5	5,3	2,8	4,8	5	5	4,5	3,4	6,7
Gd	9	15	13	12	12	15	9	12	12	13	15	11	12
Tb	1,03	2	1,5	1,4	1,5	1,9	1,2	1,5	1,6	1,6	2,3	1,35	1,4
Dy	4,4	8,9	6,3	6,1	6,6	8,7	5,3	5,8	7,10	6	13	5,3	4,6
Ho	0,67	1,46	1,14	0,99	1,03	1,4	0,93	0,93	0,95	0,89	2,2	0,84	0,73
Er	1,6	3,5	3,1	2,6	2,5	3,4	2,3	2,3	2,5	2,3	5,5	2,1	1,7
Tm	0,22	0,54	0,52	0,41	0,41	0,5	0,34	0,41	0,31	0,33	0,87	0,28	0,25
Yb	1,07	2,7	2,5	2	2,2	2,5	1,8	2,2	2,1	1,7	4,2	1,5	1,3
Lu	0,15	0,36	0,36	0,25	0,28	0,32	0,24	0,31	0,32	0,24	0,55	0,2	0,2
Y	19	44	33	30	31	42	29	31	23	27	74	25	21

Note: the last two analyses represent lamproites of Australia: 1/3 – olivine massive lamproites, Argyle; 1/4- olivine lamproites of Ellendale-11.

Data obtained from ICP MS, analysts Smirnova E.V. , Mitrofanova A.Yu..

PROBLEMS OF DIAMOND-BEARING CAPACITY

It was inferred that the study rocks are referred to the lamproite series rocks, and in some parameters are close to lamproites of Australia. In addition to sills and dyke bodies, they compose destroyed lava flows and breccias of diatremes which encompass the tuff varieties. Considering duration and complexity of origination of magmatism of the Tomtor massif and its volcano-plutonic character, the plentiful ore-bearing massifs of carbonatite tuffs and breccias and the volume of lamproite formations, it is assumed that explosion of a significant amount of lamroite tuffs was also the case. Generally the tuff “clouds” are scattered to different sides from acting volcanoes at a distance of 200 km. The focus of the Tomtor volcano was of

the area about 200 km². So it is supposed that the Ebelyakh diamond placer, 50 km away from the Tomtor massif, could have formed in washing out in place of lamproite tuffs of Tomtor. They are broken and do not contain minerals of high pressures of kimberlite association which is representative of the Ebelyakh placer. Porshnev has found a diamond in a picrite diatreme of Tomtor. Besides, diamonds of the Ebelyakh placer are “dirty” and often contain plentiful small inclusions which is explained by their tuff origin.

The first data on xenoliths in rocks of the kimberlite-lamproite association, obtained by Ashepkov I.V., suggest their dunite and dunite-harzburgite composition. The following parameters of the mantle were derived from the diagrams of the xenolith mineral compositions: $t^{\circ}C = 1000 - 1200^{\circ}$, $P = 50-68$ kb, depth about 200 km. With these parameters in mind, the potential diamond-bearing capacity of picrite-lamproite-carbonatite association of Preanabaria rocks may be assumed. The major problem of diamond-bearing capacity of these rocks is preservation of diamonds in their transportation to the surface and rock crystallization. In this geological situation the most promising should be tuff varieties of rocks. With the Sr/Nd isotope ratio (Fig. 2) picrites of Eastern Preanabaria and carbonatites of the Tomtor fall in the transitional area of the enriched mantle between EM - 1 and EM - 2.

CONCLUSIONS

1. In eastern Preanabaria and the Tomtor massif, K-alkaline basaltoids are referred to the group of lamproites. Olivine, leucite, and sanidine varieties have been found.
2. The rocks of diatremes and geophysical anomalies of Eastern Preanabaria produce kimberlite-picrite-lamproite-carbonatite association. All these rocks are genetically associated with and have the same mantle source. With increasing mica amount (to 80%) in the bulk mass of rock kimberlites are gradually transformed into lamproites.
3. The lamproite rocks, like all rocks of diatremes, undergo intense carbonatization with complete pseudomorphoses of carbonate after olivine and leucite crystals, thus making their diagnostics difficult. When carbonate is dissolved the primary chemical composition of lamproite is regained.
4. As regards the petrochemical parameters, lamproites of Preanabaria are close to lamproites of Australia and other lamproites.
5. The lamproites of the Tomtor massif, against those in diatremes, are more voluminous and produce sills, lava, and tuff flows. They are more differentiated and crystallized. Considering a large volume of alkaline and lamproite magmas of the Tomtor massif, the intensity of volcanic processes in the massif and proximity of the Ebelyakh river issue, it appears that the Ebelyakh placer was formed by the wash-out of lamproite tuffs of the Tomtor massif.

6. The data on geochemistry of isotopes and P-T parameters of mantle xenoliths from the rocks of the kimberlite-lamproite association indicate the deep-seated origin of their primary magma.

REFERENCES

1. Dawson J.B. Kimberlites and Their Xenoliths. Springer Verlag, New York, 1980, 300p.
2. Jagues A.L., Lewis J.D., Smith C.B. The kimberlites and lamproites of Western Australia Geol. Surv. W. Australia. Bull. 1986. Vol. 132. P. 268.
3. Egorov L.S., Surina N.P., Porshnev G.I. Udzhinsky ore-magmatic complex of ultrabasic alkaline rocks and carbonatites// Ore-magmatic complexes of the NW Siberian platform and Taimyr. Leningrad: Nedra, 1985, p. 138-154.
4. Lamproites. M., Nauka, 1991, p.300.
5. Mitchell R.H., Smith C.B., Vladykin N.V. Isotopic composition of Sr and Nd in potassic rocks of the Little Murun complex, Aldan Shield, Siberia. // Lithos, 1994, 32, p.243-248.
6. Mitchell R.H., Bergman S.C. Petrology of lamproites.// New York, Plenum Publishing Corporation, 1991, 447p.
7. Panina L.I., Vladykin N.V. Lamproitic rocks of the Murun massif and their genesis. // Geology and geophysics, 1994, v.35, N12, pp.100-113
8. Porshnev G.I., Stepanov L.L. Geological structure and phosphate potential in the Tomtor massif// Alkaline magmatism and apatite potential in the north of Siberia. Leningrad, NIIGA, 1980, p. 84-100.
9. Shikhorina K.M. Highly-potassic rocks of the Chimaro-Udzhinsky region (NE Siberian platform)// Izvestia AN SSSR, Ser. Geol., 1991, № 3, p. 58-64.
10. Vishnevsky S.A., Dolgov Yu.A., Sobolev N.V. Lamproites of the Talakhtakh diatremes in the eastern slope of the Anabar shield// Geology and Geophysics, 1986, № 8, p. 17-27.
11. Vladykin N.V. Geochemistry and genesis of lamproites of the Aldan shield // Russian Geology and Geophysics, v.38, N. 1, 1997, pp.128-141.
12. Vladykin N.V. Petrology and ore-bearing capacity of K-alkaline rocks of the Mongol-Okhotsk magmatic area. Thesis, 1997, Иркутск, p.1-80.
13. Vladykin N.V., Lelyukh M.I., Tolstov A.V. Lamproites of the Anabar region, the northern rimming of the Siberian platform // 7 Kimberlite Conference, Cape-Town, 1998, p. 946-948.
14. Vladykin N.V. The Malyi Murun Volcano-Plutonic Complex: An Example of Differentiated Mantle Magmas of Lamproitic Tupe.// Geochemistry International, Vol. 38, Suppl. 1, 2000, pp. S73-S83.
15. Vladykin N.V. K-alkaline rocks and lamproites of the Tomtor massif. Proc. Conf. "Alkaline magmatism", 2001, Москва, p.17-19.
16. Vladykin N.V., Lelyukh M.I., Torbeeva T.S., Tolstov A.V., Serov V.P. Lamproites of the Tomtor massif. Vestnik ISU, 2002, # 4, Irkutsk, p.3-30

CENOZOIC VOLCANISM OF FAR EAST RUSSIA: THE RELATIVE IMPORTANCE OF SUBCONTINENTAL LITHOSPHERE AND ASTHENOSPHERIC MANTLE

S. OKAMURA¹ AND Y. A. MARTYNOV²

¹*Sapporo Campus, Hokkaido Education University, Sapporo 002-8502, Japan,
okamura@sap.hokkyodai.ac.jp*

²*Far East Geological Institute, Vladivostok 690022, Russia*

Abstract Far East region of Russia comprising Sikhote-Alin and Sakhalin (SAS) underwent lithospheric extension during late Tertiary events related to the Japan Sea formation. Within the SAS volcanism, the Eocene-Oligocene (EO, 55-24 Ma) lavas are characterized by both large ion lithophile element and rare earth element enrichments with respect to depleted Early Miocene (EM, 23-15 Ma) tholeiites, which also shows a depletion in high-field strength element (HFSE). The EO basalts and EM basalts show significant positive correlations of ⁸⁷Sr/⁸⁶Sr with La/Yb. This suggests that the sites of magma generation beneath SAS region have moved from the subduction-related enriched lithosphere down into the MORB-type asthenosphere as Japan Sea spreading progressed. The Late Miocene to Pliocene (LMP) samples are alkali basalts and subalkali basalts, including the most recent post-Japan Sea opening (14-5Ma) samples from the SAS region. The LMP lavas encompass wide ranges in trace element abundances that vary between two distinct end-member types. The relatively minor LMP alkali basalts are found at the late stage of the lava sequences, and they have high Nb/La and Sr-Nd-Pb isotope compositions that fall within the field for the OIB consistent with melting of asthenospheric mantle at depth. By contrast, low alkali quartz and olivine tholeiites from the other extreme have concentrations of the HFSE that are much lower than elements of similar incompatibility. The relative depletions in HFSE are not a feature of crustal contamination processes, but rather of their mantle source regions.

INTRODUCTION

Far East Russia consisting of Sikhote-Alin and Sakhalin (SAS) (Fig. 1) was affected by subduction since the Mesozoic, and by extension to produce the Japan Sea during the Cenozoic. Basaltic rocks in the region may bear imprints of both processes. Until recently, little was known about the chemistry of the Cenozoic volcanic rocks from SAS region, although chemical and isotopic studies of Sikhote-Alin have suggested that there was a change from subduction-related to intraplate magmatism as the Japan Sea opening progressed [3, 6, 11]. However, the genetic relationship between such subduction-related magmatism and intraplate magmatism remains unsolved. Petrological study of these rocks can be used to constrain the nature of the source region and the timing of the magmatic events that are responsible for the evolution of this continental margin. In this paper we present geochemical analyses on suites of samples from Sikhote-Alin and Sakhalin, and discuss the implications of all of our data for the origin of Cenozoic magmatism along the northeast Eurasian margin and its relation to those of northeast China.

GEOLOGY

The Cenozoic volcanism of the SAS region is composed of the distinct stages: (1) active continental-margin volcanism in the Eocene-Oligocene (EO, 55-24 Ma) along the northeastern edge of Eurasia, concurrent with continental-rift basalts associated with northeast-trending grabens in northeast China; (2) Early Miocene (EM, 23-15 Ma) volcanism surrounding the opening Japan Sea in Sikhote-Alin, Sakhalin, and the frontal Japanese island arc, yielding subduction-zone volcanism; (3) Late Miocene to Pliocene (LMP, 14-5 Ma) volcanism in SAS, yielding plateau basalts filling interfluves. The base of the plateau basalt sequence is unconformable on the Early Miocene to Eocene Formations.

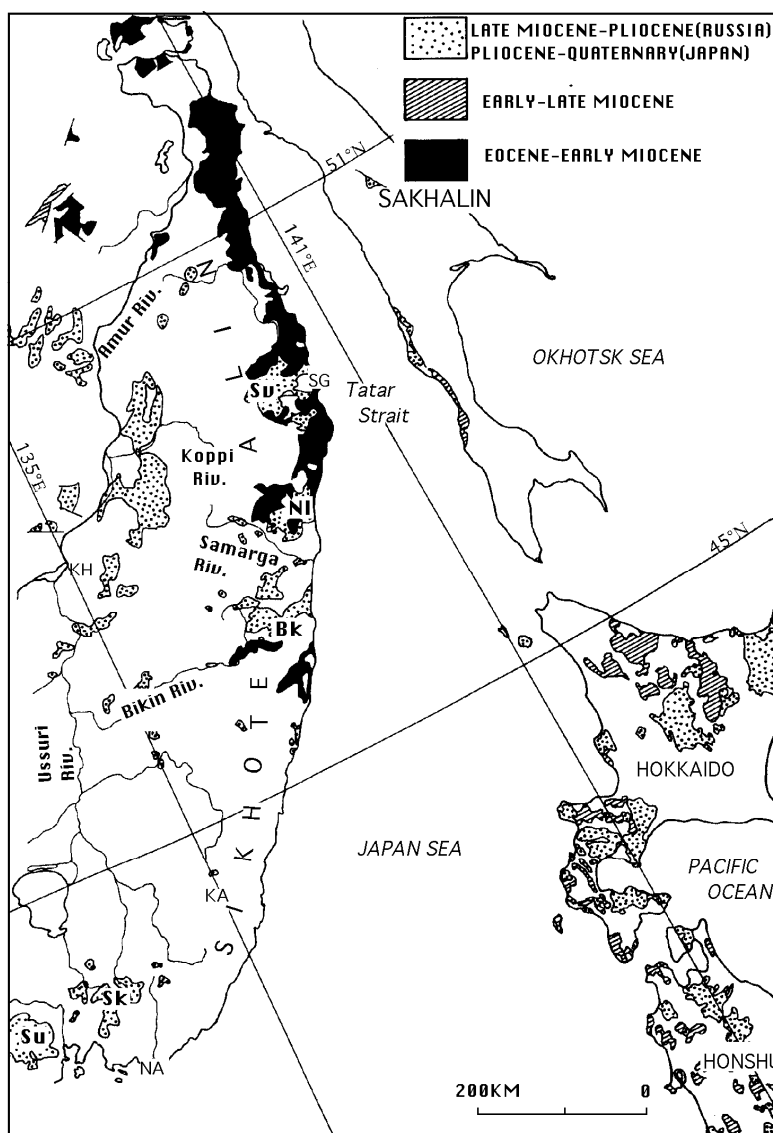


Fig. 1. Generalized map of the Sikhote-Alin and Sakhalin region. Abbreviations are: BK, Bikin Plateau; NI, Nelma Plateau; SK, Shukotovo Plateau; SU, Shufan Plateau; SV, Sovgavan Plateau. SG: Sovgavan, KH: Khabarovsk, KA: Kavalerovo, NA: Nakhodka.

PETROLOGY AND GEOCHEMISTRY

Cenozoic volcanism within SAS includes alkali olivine basalts, olivine basalts, and basaltic andesites lavas. CIPW normative variation ranges from tholeiite (qz- and ol-normative) to alkali basalt (ne- up to 5%) and basanite (ne-normative >5%). For simplicity, basanite is included with alkali basalt. The EM lavas cluster ol- to qz-normative tholeiites, whereas EO and LMP lavas exhibit a more uniform distribution across the range of ne- to qz-normative compositions. More than 70% of the LMP basalts are qz- and ol-normative with the remainder mildly to moderately ne-normative. The LMP alkali basalts contain ultramafic xenoliths and crustal xenocrysts.

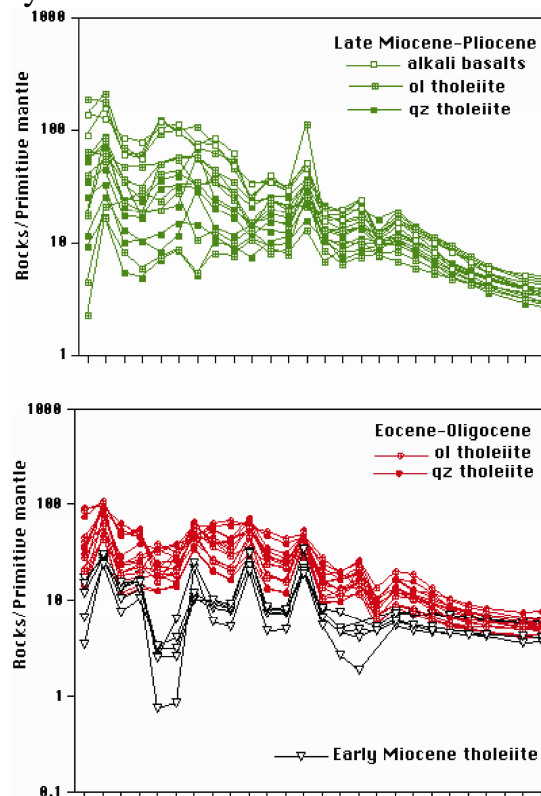


Fig.2. Primitive-mantle-normalized incompatible element diagrams for selected samples from the SAS region. Primitive-mantle values are from Hofmann (1988).

Within the SAS volcanism, a distinct subset of the EM tholeiites is identified by their generally lower trace element concentrations. The greatest depletions occur at Nb on mantle-normalized diagrams (Fig. 2), such as that commonly observed in island-arc volcanics. The EO lavas are characterized by both large ion lithophile element (LILE) and rare earth element (REE) enrichments with respect to depleted EM tholeiites, which also shows a depletion in high-field strength element (HFSE) even though Nb shows a mild negative anomaly compared to adjacent elements.

The LMP lavas from all the plateaus encompass wide ranges in trace element abundances and patterns that vary between two distinct end-member types. At one extreme, alkali basalts and high alkali olivine tholeiites have fairly smooth mantle-normalized patterns that are convex upwards, and they generally have maxima at either Ba or Nb (Fig. 2). These patterns are nearly indistinguishable from ocean island basalts (OIB) [10], suggesting that high alkali basalts have an asthenospheric source and have not been significantly contaminated by lithospheric mantle or crustal material. By contrast, low alkali quartz and olivine tholeiites from the other extreme have concentrations of the HFSE, particularly Nb, that are much lower than elements of similar incompatibility. Samples in this group display an irregular mantle-normalized pattern that typically peaks at Ba. The greatest relative depletions occur at Nb on mantle-normalized diagrams, such as that commonly observed in island-arc volcanics [4]. Their most striking geochemical feature is the relatively low abundance of the HFSE with respect to the LILE and the light rare earth element (LREE). Small troughs at Th, U, and Nb are common and most of the mantle-normalized diagrams also display a step between elements considered to be more or less incompatible than Ti. The incompatible element patterns of the LMP basalts are recognized as a common features in some late Cenozoic basalts from the U.S. Basin and Range province [7, 1].

DISCUSSION

CRUSTAL ASSIMILATION VERSUS ENRICHED LITHOSPHERE

The SAS basalts lack significant correlation between $^{87}\text{Sr}/^{86}\text{Sr}$ and Rb/Sr (Fig. 3). The decoupled systematics is thus unlikely to reflect wall rock reaction, but probably attributable to effects of differential partial melting prior to and during magma formation. Some EO basalts exhibit a trend of increasing $^{87}\text{Sr}/^{86}\text{Sr}$ with increasing Rb/Sr ratios, particularly among the quartz tholeiites. Such trends are consistent with a role for crustal contamination in these rocks. Based on incompatible-element abundances, it is evident that the petrogenesis of the LMP tholeiites was unlike that of oceanic island tholeiites. There are two principal scenarios that can explain the isotopic and trace element variations exhibited by the LMP basalts. They may represent (1) mixing between asthenospheric melts (e.g., alkali basalt lavas) and metasomatized/enriched ancient lithosphere, or (2) mixing between asthenospheric melts and continental crust. Ormerod et al. [7] argued that the low Nb contents of the U.S. Basin and Range lavas (10-20 ppm) could not be generated by any crustal contamination scheme involving an OIB-type (asthenospheric) parental magma (~50 ppm) since something of the order of 150-400 % crustal material would have to be assimilated. To reduce the concentration of Nb in the LMP OIB-type magma from a range of 40-70 ppm to the 4-20 ppm range characteristics of the LMP quartz tholeiitic basalts, therefore, would require the addition of large amounts of crustal material, assuming the latter were entirely

devoid of Nb. Thus the relative depletions in HFSEs are not a feature of crustal contamination processes, but rather of their mantle source regions.

Moreover, The additional of modern pelagic sediment can not explain all the variation in the data. A component with very low $^{143}\text{Nd}/^{144}\text{Nd}$ and low La/Nb is also required. Such a component could only evolve in a low Sm/Nd (i.e., light rare earth element enriched) environment over long periods and ancient. The chemical and isotopic characteristics of the SAS volcanic rocks can not, therefore, be entirely due to the effects of relatively recent subduction on the lithosphere. Subduction-related

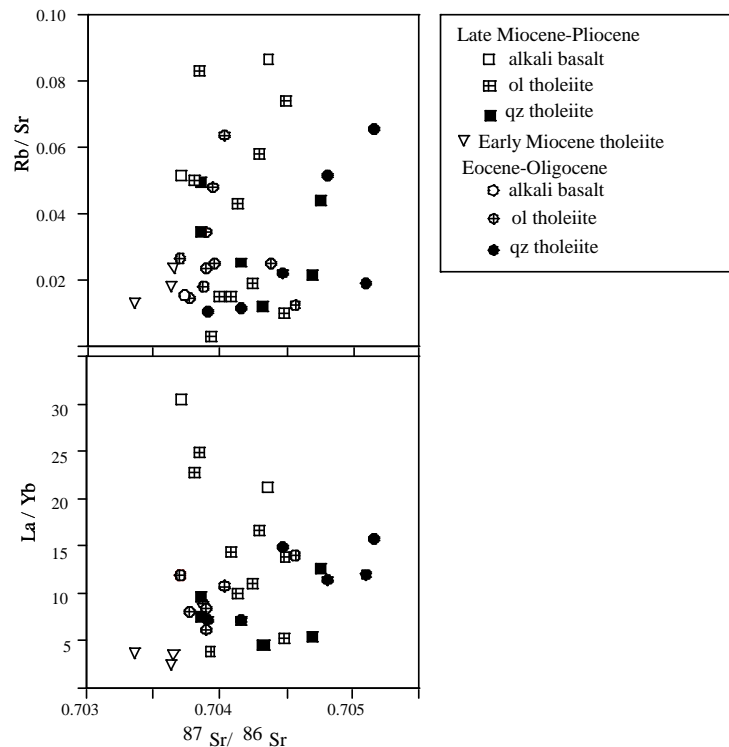


Fig.3. $^{87}\text{Sr}/^{86}\text{Sr}$ versus Rb/Sr and La/Yb for SAS volcanic rocks

enrichment of the lithosphere at the time of crustal accretion is one possibility supported by isotopic data. The isotopic and trace element data presented here are best interpreted as reflected variable contributions from a lithospheric mantle source which has a low $^{143}\text{Nd}/^{144}\text{Nd}$ that low Sm/Nd and U/Pb ratios can coexist over long periods of time within the subcontinental mantle lithosphere [2], but Rb/Sr ratios may be more

IDENTIFICATION OF SOURCE COMPONENTS

Comparison of the average compositions of the EO basalts with the LMP basalts indicates that they are generally higher concentrations of Ba, Rb and Zr. These differences can be further explored by considering the covariation of Nb and Zr contents, as an indication of mantle source compositions. Figure 4 suggests that the SAS basalts form two major trends with different Zr/Nb ratios. The LMP

basalts show overlapping to lower values of Zr/Nb (~4) relative to the Hannuoba and the Mudanjiang basalts from northeastern China next to Sikhote-Alin. Significantly higher Ba/Nb and Rb/Nb ratios in the EO basalts are characteristics that long have been associated with subduction-related rocks. These similarities suggest that subduction processes have played a role in the petrogenesis of the EO basalts. The chemical signature inherited from the lithosphere is very clear. It implies that the lithospheric mantle is enriched in Ba, and sometimes in Sr, and depleted in Nb. Fluids driven off a subducting slab may inherit their elemental characteristics from pelagic sediment and could therefore be very similar to those inferred to have affected the lithospheric mantle beneath the SAS region. These fluids will infiltrate and variable so must be metasomatize the overlying mantle wedge which will eventually become accreted to the subcontinental mantle, just as island arc material eventually becomes accreted to the continental crust [8]. The EO basalts and EM basalts show significant positive correlations of $^{87}\text{Sr}/^{86}\text{Sr}$ with La/Yb (Fig. 3). They indicate mixing with an incompatible-element-depleted component with a trace element signature similar to MORB (low La/Yb, $^{87}\text{Sr}/^{86}\text{Sr}$ and high $^{143}\text{Nd}/^{144}\text{Nd}$). This suggests that the sites of magma generation beneath SAS region have moved from the subduction-related enriched lithosphere down into the MORB-type ..asthenosphere as Japan Sea spreading progressed.

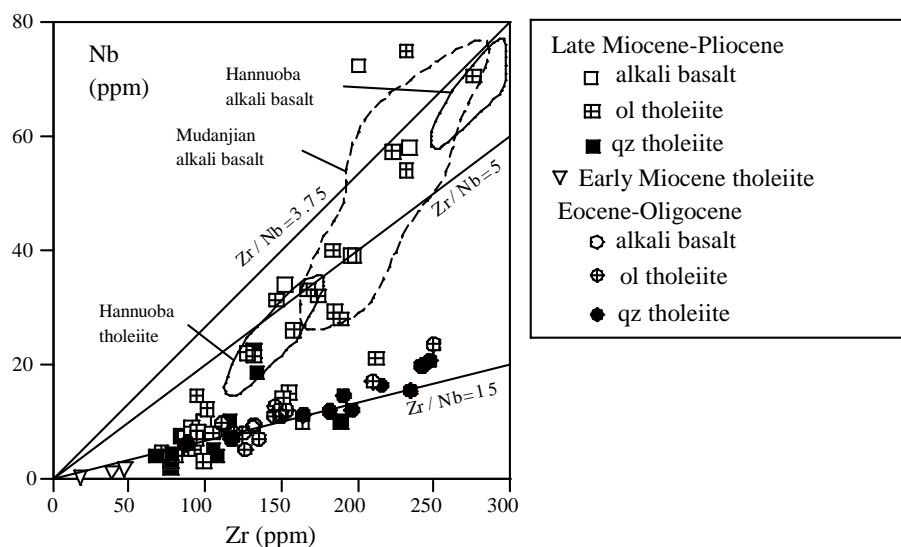


Fig. 4. Nb versus Zr for SAS volcanic rocks as well as Mudanjiang and Hannuoba basalts [Zhi et al., 1990].

The decoupling of trace element and isotopic ratios among the SAS lavas, and their decoupling from patterns observed in plume-related OIB, suggests that local enrichment processes operating over varying time scales played a role in their origin. The relatively minor LMP alkali basalts are found at the late stage of the lava sequences in the LMP lavas, and they have high Nb/La and Sr-Nd-Pb isotope compositions that fall within the field for the OIB basalts [6]. The normalized trace-element abundances of the LMP alkali basalts are more similar to Hawaiian

alkali basalts. OIB is the product of melting of several components within the mantle [13]. However, OIB undoubtedly represents magma generated within the asthenosphere, with or without additions from lower mantle plumes. The trace element and isotope characteristics of the uncontaminated LMP alkali basalts are similar to those of the Hannuoba alkali basalts consistent with melting of asthenospheric mantle at depth [9], and we can be confident that deviations from OIB composition must represent input from additional sources. The LMP tholeiitic magmas are characterized by low $^{206}\text{Pb}/^{204}\text{Pb}$ coupled with high $^{207}\text{Pb}/^{204}\text{Pb}$ and $^{208}\text{Pb}/^{204}\text{Pb}$, typical features of the oceanic DUPAL isotopic province [6]. Similar Pb isotope characteristics, and broadly similar Sr and Nd isotope compositions, are seen in the nearby contemporaneous East Asian basalts, such as Hannuoba [9]. Thus, by inference, it appears that the low $^{206}\text{Pb}/^{204}\text{Pb}$ characteristic of the LMP magmas is a mantle feature.

REFERENCES

1. Bradshaw T.K., Hawkesworth C. J. & Gallagher K. Basaltic volcanism in the southern Basin and Range: No role for a mantle plume //Earth and Planetary Science Letters. 1993. V. 116. P. 45-62.
2. Dudas F. O., Carlson R. W. & Eggler D. H. Regional middle Proterozoic enrichment of the subcontinental mantle source of igneous rocks from central Montana //Geology. 1987. V. 15 P. 22-25.
3. Esin V. Ponomarchuk V. A. Shipitsin Y. G. & Palesskii S. V. Petrogenesis of the Sovgavan tholeiite-alkaline basalt plateau in the eastern Sikhote-Alin //Russian Geology and Geophysics. 1995. V. 36. P. 60-68.
4. Gill J. B. Orogenic Andesites and Plate Tectonics. Springer, Berlin. 1981. P. 385.
5. Hofmann A. W. Chemical differentiation of the Earth: the relationship between mantle, continental crust, and oceanic crust //Earth and Planetary Science Letters. 1988. V. 90. P. 297-314.
6. Okamura S., Arculus R. J., Martynov Y. A., Kagami H., Yoshida T. & Kawano Y. Multiple magma sources involved in marginal-sea formation: Pb, Sr, and Nd isotopic evidence from the Japan Sea region //Geology. 1998a. V. 26. P. 619-622.
7. Ormerod D. S., Hawkesworth C. J., Rogers N. W., Leeman W. P. & Menzies M. A. Tectonic and magmatic transitions in the Western Great Basin, USA //Nature 1988. V. 333. P. 349-353.
8. Othman D. B., White W. M. & Patchett J. The geochemistry of marine sediments, island arc magma genesis, and crust-mantle recycling //Earth and Planetary Science Letters. 1989. V. 94. P. 1-21.
9. Song Y., Frey F. A. & Zhi X. Isotopic characteristics of Hannuoba basalts, eastern China: Implications for their petrogenesis and the composition of subcontinental mantle //Chemical Geology. 1990. V. 85 P. 35-52.
10. Sun S. S. & McDonough W. F. Chemical and isotopic systematics of oceanic basalts: Implications for mantle composition and processes. // Magmatism in the ocean basins /Eds. Saunders A. D. & Norry M. J., Geological Society Special Publication. London. 1989. V. 42. P. 313-345.
11. Tatsumi Y., Sato K. & Sano T. Transition from arc to intraplate magmatism associated with backarc rifting: evolution of the Sikhote Alin volcanism //Geophysical Research Letters 2000. V. 27. P. 1587-1590.
12. Zhi X., Song Y., Frey F. A., Feng J. & Zhai M. Geochemistry of Hannuoba basalts, eastern China: Constraints on the origin of continental alkali and tholeiitic basalt //Chemical Geology. 1990. V. 88. P.1-33.
13. Zindler A. & Hart S. R. Chemical geodynamics //Annual Review of Earth and Planetary Sciences. 1986. V. 14. P. 493-571.

ANTARCTIC LAMPROITES: AN OVERVIEW

E.V. Mikhalsky¹ and J.W. Sheraton²

¹ *VNIIOkeangeologia, Angliisky Avenue, 1, St Petersburg 190121, Russia*

² *Stoneacre, Bream Road, St Briavels, Glos. GL15 6TL, UK*

This paper presents a summary of both previously published and unpublished mineralogical (including mineral compositions) and geochemical data on lamproitic rocks from three regions of East Antarctica. Ordovician (480–460 Ma) lamproite dykes crop out in Enderby Land and the Prince Charles Mountains, and Gausberg (Wilhelm II coast) is a Pleistocene subglacial olivine leucite volcano. Most rocks are phlogopite-rich, and contain sanidine or leucite, or late-stage minerals developed after these minerals. Available isotopic ratios (Sr, Nd, Pb) indicate derivation from highly enriched mantle source(s). In general, the Antarctic lamproites bear some features typical of Western Australian or Spanish lamproites. Apart from the Gausberg lavas, they are located in areas which underwent some late Neoproterozoic to early Palaeozoic tectonic reactivation of early Precambrian cratons, which is believed to reflect a distal respond to the waning stages of (presumably intraplate) orogeny in adjacent regions.

INTRODUCTION

Lamproites constitute a volumetrically minor, but petrologically important, magmatic suite in all East Gondwana continents, and are mostly believed to have been emplaced in intracratonic tectonic environments. The antarctic lamproites are even more scarce, but nevertheless formed the one of the first Antarctic rocks (at Gausberg) discovered in 1902 by the German Antarctic Expedition led by E. von Drygalski. A number of papers have been published on Antarctic lamproites, presently known from, the three areas (Enderby Land, the Prince Charles Mountains, and Gausberg, Fig. 1), providing geological, petrographic, geochemical, and isotopic data on these unusual rocks. However, most of these publication are not easily available for Russian readers. The main goal of this report is to present a compilation of the available data on the Antarctic lamproites, and to summarise the petrogenetic and tectonic constraints.

GEOLOGICAL FEATURES AND MINERAL COMPOSITION

ENDERBY LAND

Lamproite dykes are known from a few localities in Enderby Land, namely the Priestley Peak, Tonagh Island, and Hydrographer Islands, all within 70 km. Lamproite forms dykes and thin veins intruding granulite-facies metamorphic rocks of the Archaean Napier Complex. Dykes at Priestley Peak also cut unmetamorphosed Mesoproterozoic mafic dykes, whereas those on the Hydrographer Islands cut late shear zones and presumably Cambrian pegmatite bodies.

The *Priestley Peak* dykes consist primarily potassic magnesio-arfvedsonite (8–37%), phlogopite (5–47%), ferrian K-feldspar (microcline, 26–48%), apatite (4–10%), quartz (up to 5%), titanite (up to 4%) and minor rutile (intergrown with small amounts of opaque minerals), zircon, and barite [21]. The rocks are markedly heterogeneous, mainly because of variations in the proportions of phlogopite and amphibole in rather irregular, discontinuous layers, although there are also considerable variations in the abundances of K-feldspar, quartz, and titanium minerals.

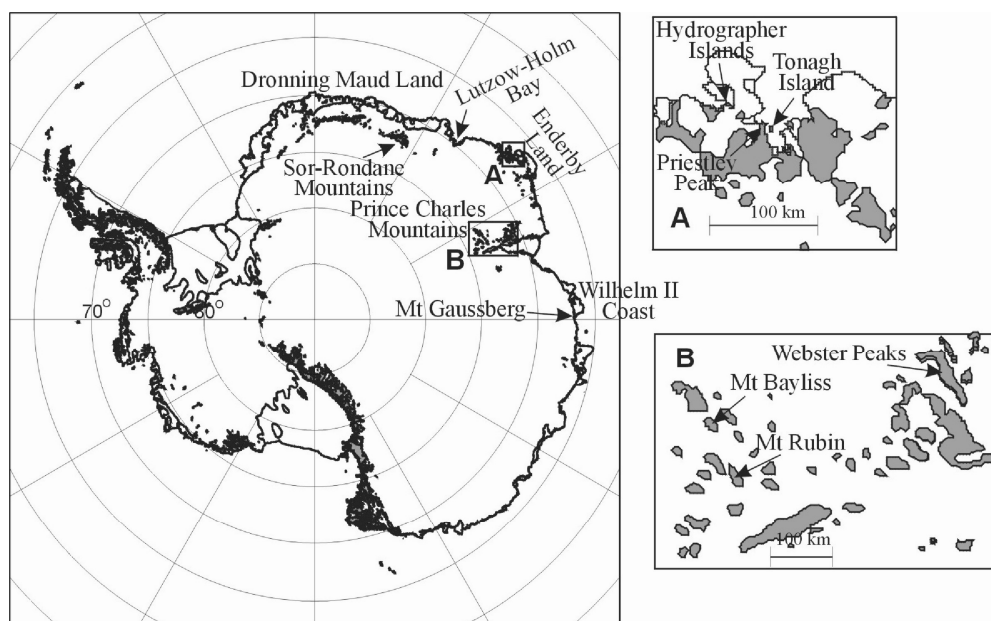


Fig. 1. Locality map.

Contacts between zones of different composition (up to a few decimetres across) are fairly sharp, with abrupt changes in grain size, suggesting intrusion of a heterogeneous magma and possibly multiple intrusions [21]. Slightly pleochroic K-arfvedsonite and orange-brown phlogopite are the major mafic minerals. Rounded aggregates of secondary, fibrous pale green K-arfvedsonite, up to 1 cm across and mantled by phlogopite, may represent altered pyroxene phenocrysts or xenocrysts, although they are of similar composition to the well-crystallised amphibole throughout the rock. Barite occurs as grains up to 1 mm across, commonly in association with quartz in late felsic segregations. Opaque minerals include pyrrhotite and chalcopyrite. Chilled dyke margins contain phenocrysts of phlogopite and apatite.

A Rb–Sr isochron (phlogopite, K-feldspar, K-arfvedsonite, apatite, and whole-rock) for a Priestley Peak dyke defined an age of 482 ± 3 Ma, with the initial ratio of 0.70852 ± 0.00007 [2].

Dykes on the *Hydrographer Islands* contain richterite, aegirine-augite, and barite [19].

Lamproite at the *Tonagh Island* [11] forms north–south-trending, thin

Table 1

Chemical compositions of rock-forming minerals

Mineral	Bt (n=9)	Bt (n=3)	K-rcht (n=14)	K-rcht (n=16)	K-fsp (n=12)	K-fsp (n=20)	Phl	Phl	Phl	Phl	Phl
Sample #	TM9901 13-01a	TM9901 13-01F	TM9901 13-01a	TM9901 13-01F	TM9901 13-01a	TM990113 -01F	7728 3949b	7728 3951a	7328 1545	7328 1545	35647-3
Locality	Tonagh Island	Priestley Peak	Priestley Peak	Mount Bayliss	Mount Bayliss	Mount Rubin					
SiO ₂	43,02	44,34	55,53	55,08	64,55	63,84					40,48
TiO ₂	2,80	3,70	0,33	0,38							9,56
Al ₂ O ₃	8,77	5,51	0,24	0,08	16,09	15,60					9,14
Cr ₂ O ₃	0,22	0,54	0,16	0,01							0,17
Fe ₂ O ₃					2,54	3,22					
FeO	14,58	16,28	12,18	12,56							11,81
MnO	0,16	0,09	0,29	0,24							0,19
MgO	16,09	15,35	15,73	15,29							17,81
CaO			4,25	3,12	0,04	0,02					
Na ₂ O	0,65	0,62	5,08	5,47	0,80	0,46					
K ₂ O	10,31	10,18	3,97	5,04	16,43	16,46					10,58
NiO											
Total	96,60	96,64	97,76	97,27	100,45	99,60					99,87
O	22	22	23	23	8	8	22	22	22	22	22
Si	6,324	6,569	8,069	8,097	3,004	3,004	6,654	6,4	5,576	6,125	5,767
Ti	0,309	0,412	0,036	0,042			1,308	0,214	0,961	0,634	1,024
Al	1,519	0,967	0,041	0,015	0,882	0,865	1,19	1,698	2,002	1,294	1,535
Cr	0,0025	0,063	0,018	0,002							
Fe ³⁺					0,089	0,114					
Fe ²⁺	1,792	2,017	1,48	1,544			1,518	1,616	0,837	2,859	1,407
Mn	0,02	0,012	0,036	0,03			0,016	0,024			0,023
Mg	3,525	3,391	3,408	3,35			3,76	3,98	3,992	2,713	3,783
Ca			0,662	0,491	0,002	0,001	0,028	0,006			
Na	0,184	0,178	0,736	0,946	0,975	0,988					
K	1,933	1,925	1,43	1,56	0,072	0,042	2,024	2,004	1,788	1,94	1,923
Ni											
Total	15,631	15,534	15,916	16,077	5,024	5,014					

subvertical veins ranging from a few centimetres to one meter in thickness and up to several meters in length. The lamproite is holocrystalline and ranges from medium to dark green. Some specimens contain spangles of biotite up to 2 cm across, and others have centimeter-scale layering defined by variations in grain size and mineral proportion. Feldspar megacrysts and autoliths, up to 3 cm across, are locally present.. The lamproite consists mainly of microcline, K-richterite, biotite and apatite. Trace amounts of quartz are present in most samples. Rounded titanite and small rutile grains are relatively abundant, and carbonate, zircon, and monazite are additional accessories. Microcline grains typically show characteristic cross twinning, as well as fine zoning and anomalous interference colours (probably due to the relatively high Fe₂O₃ contents). Subhedral biotite, K-richterite, and apatite grains are surrounded by small microcline grains. Some

Table 1 finished

Mineral	Phl	Am (core)	Am (rim)	K-fsp (n=20)	Ol	Cpx	Lc	Bt
Sample #	35647-3	35647-3	35647-3	35647-3	n= 12	n= 10	n= 11	n= 4
Locality	Mount Rubin	Mount Rubin	Mount Rubin	Mount Rubin	Gaussberg	Gaussberg	Gaussberg	Gaussberg
SiO ₂	41,41	55,29	51,50	63,84	40,30	53,60	55,00	40,60
TiO ₂	9,13	1,04	1,74	0,04		0,97	0,21	9,00
Al ₂ O ₃	7,03		0,03	18,43		0,44	21,40	6,90
Cr ₂ O ₃	0,09	0,11	0,21		0,03	0,82		
Fe ₂ O ₃						0,69	0,96	
FeO	12,26	19,93	27,55	0,44	10,50	2,60		11,90
MnO	0,10	0,86	0,65	0,22	0,19	0,10		0,05
MgO	18,92	11,24	5,85	0,55	48,20	17,20	0,28	17,60
CaO		0,64	2,91		0,33	22,80		
Na ₂ O		5,27	4,64			0,51	0,10	0,41
K ₂ O	10,75	5,50	5,06	17,40			21,80	9,30
NiO					0,38	0,08		0,04
Total	99,69	99,88	99,84	99,92	99,30	99,81	*99,85	**96,80
O	22	23	23	8	4	6	6	22
Si	5,895	8,407	7,908		0,995	1,961	2,016	5,958
Ti	0,953	0,119	0,202			0,027	0,006	0,993
Al	1,179	0,013	0,006			0,019	0,925	1,193
Cr	0,01		0,026		0,001	0,024		
Fe ³⁺	0,117		0,134			0,019	0,026	
Fe ²⁺	1,342	2,077	3,424		0,217	0,078		1,496
Mn	0,012	0,11	0,085		0,004	0,003		0,006
Mg	4,015	2,548	1,347		1,773	0,938	0,015	3,85
Ca		0,104	0,482		0,009	0,894		
Na		1,554	1,389			0,036	0,007	0,117
K	1,952	1,067	0,997				1,019	1,741
Ni					0,008	0,002		0,005
Total					3,007	4,001	4,015	15,417

Bt - biotite, *Phl* - phlogopite, *K-fsp* - alkali feldspar, *Am* - amphibole, *K-richt* - potassian richterite, *Ol* - olivine, *Cpx* - clinopyroxene, *Lc* - leucite.

* Includes 0.09% BaO; ** Includes 1,0% BaO

biotite crystals are mantled by K-richterite coronas. K-richterite and microcline become finer-grained toward the dyke margins, whereas biotite and apatite do not. Autoliths consist largely of the same minerals, but are coarser grained. Barite is present in one such autolith. Mineral compositions are listed in Table 1. The rock-forming minerals generally have very low Al₂O₃, which reflects the peralkaline composition of the bulk rock (see below). The amphibole is largely potassic richterite, but some analyses correspond to potassic magnesio-arfvedsonite. Microcline has high Fe (calculated as Fe₂O₃). Biotite is characteristic high in TiO₂ (2.5–3.7%), although K-amphibole contains much

less TiO₂ than the typical lamproite amphiboles [9]. Miyamoto et al. [11] suggested that amphiboles were depleted in Ti during cooling, the Ti being

incorporated in rutile and titanite. Rb-Sr internal isochrons (biotite, K-richterite, non-magnetic fraction, and whole-rock) defined ages of 466 ± 4 and 476 ± 6 Ma, with initial ratios of 0.070949 ± 0.00010 and 0.70966 ± 0.00010 , respectively [11].

SOUTHERN PRINCE CHARLES MOUNTAINS

A 5 meter-thick dyke at *Mount Bayliss*, and a moraine specimen collected nearby are described in detail by Sheraton & England [21]. The massive medium-grained dyke rock comprises K-feldspar (52%), amphibole (39%), phlogopite + biotite (3%), and apatite (3%). Opaque phases, anatase (probably replacing ilmenite), zircon, and calcite are minor constituents. K-feldspar (microcline with near-maximum obliquity) forms untwinned grains up to 2 mm across. Amphibole includes both K-richterite and K-arfvedsonite. Zoned

K-richterite forms subhedral crystals 1–2 mm long, and K-arfvedsonite occurs mostly as rims and overgrowths on K-richterite. Dark reddish-brown mica grains are up to 1 mm long, and are locally intergrown with amphibole. The moraine specimen is petrographically similar, but much finer grained. It contains more phlogopite (13%) and less amphibole (K-arfvedsonite, 17%); anatase, ilmenite, and zircon are minor constituents. The

groundmass is largely K-feldspar (microcline), with about 4% of calcite. Rounded to subhexagonal aggregates of turbid K-feldspar, up to 0.4 mm across, appear to pseudomorph leucite, although they do not consist of pseudoleucite. Relatively larger (up to 6 mm) leucocratic ocelli, which contain quartz, K-feldspar, calcite, zircon, anatase, and minor K-arfvedsonite, probably represent the droplets of an immiscible liquid.

Mineral compositions are listed in Table 1. Marked zoning in amphibole reveals a trend of O and Fe-enrichment. Early crystallized K-richterite is relatively magnesian ($mg = \text{atomic Mg}/(\text{Mg}+\text{Fe}) = 0.74$), and poor in Fe^{3+} (calculated). K-arfvedsonite rims on K-richterite have lower mg (less than 0.52) and appear to be richer in Fe^{3+} and Na. These rims may have been produced by the reaction between the early formed amphibole and the late, more oxygen-rich fluid phase. All amphiboles are poor in Al and exceptionally rich in K. Micas ranges from Ti-rich phlogopite to late-crystallized Al-poor biotite.

K-richterite has given Silurian K–Ar ages of 413 and 414 ± 10 Ma, and K-arfvedsonite 430 ± 12 Ma [21], but these ages probably reflect cooling stages rather than emplacement.

A 3 to 4 meter-thick, east–west-trending lamproite dyke crops out at *Mount Rubin*. It is a massive fine-grained dark greenish-grey rock, with abundant small rounded grains of K-feldspar and a few large (0.3–1.0 cm) felsic ocelli. The rock consists of K-feldspar (40 %), alkali amphibole (25–30%), phlogopite (20–25%), and opaque minerals (up to 5%). Accessory apatite, zircon, and titanite make up about 2–3 volume percent. Phenocrysts comprise olivine and alkali amphibole. Secondary minerals (sericite, chlorite, and carbonate) constitute up to 5 percent of

the rock.

K-feldspar occurs as rounded, pseudo-hexagonal, or more rarely elongated, grains, 0.1–0.8 mm across. It is characterized by an inhomogeneous, sieve-like texture, and was probably formed by replacement of leucite at the late-magmatic stage. Opaque mineral inclusions are abundant within some inner zones. The unit cell parameters of the feldspar indicate sanidine [8]. The sanidine has very low $^{87}\text{Sr}/^{86}\text{Sr}$ (0.702) and Rb/Sr (0.002), which are presumably the features of the mantle source. It is partly replaced by microcline, which was probably formed at the subsolidus stage. Small flakes and aggregates, 0.1–0.3 mm across, of randomly oriented high-Ti phlogopite (TiO_2 9–10%, *mg* 73–75) partly fills interstices between the sanidine grains. The phlogopite is compositionally similar to that in the West Kimberley volgidites [10]. Fibrous aggregates of brownish-green (with a bluish tinge) amphibole make up the remainder of the groundmass. The amphibole comprises low-Ti potassic varieties of ferrichterite and magnesian arfvedsonite, similar to lamproitic amphiboles [10], but being different in much lower TiO_2 (1–2%) and higher total FeO (20–27%) and Na_2O (4.6–5.7%). The grains are zoned, with cores enriched in MgO (*mg* 52–55) and Na_2O , and rims enriched in FeO (*mg* 28–39) and TiO_2 and depleted in Na_2O .

The ocelli are made up of coarse-grained aggregates of carbonate, opaque minerals, barite, chlorite, nepheline, alkali feldspar, and plagioclase in various proportions. Their outer zones, up to 0.5 mm thick, are distinguished by a brown colour that is due to the development of fine-grained unidentified minerals. The ocelli are generally rounded, with complex reticulated outlines. Small angular fragments of the same composition were also found, which might suggest that the ocelli represent reworked country rock fragments. The low initial $^{87}\text{Sr}/^{86}\text{Sr}$ ratio of plagioclase recovered from these ocelli (0.7048) however, does not support this suggestion.

The compositions of minerals from the Mount Rubin lamproite indicate crystallization from an evolved melt at low pressure and temperature [10], but the petrographic features suggest that crystallization did not occur entirely after magma emplacement. Strong zoning of amphibole is consistent with a high degree of melt fractionation.

Bulk-rock and mineral individual (microcline and phlogopite) compositions define the Rb–Sr isochron age of 461 ± 23 Ma ($\text{Sr}_i = 0.716$) [8]. This date may reflect igneous crystallization or autometamorphic (deuteric) alteration, which was accompanied by the formation of the microcline, but, either way, probably approximates the emplacement age.

A compositionally similar dyke crops out at the northern *Webster Peaks* in the Northern Prince Charles Mountains [12].

WILHELM II COAST

Lamproites (olivine leucitites of Sheraton & Cundari [20]) of late Cainozoic age form the extinct volcano of *Gaussberg* on the coast of the Antarctic ice sheet. Gaussberg is a fairly regular volcanic cone about 370 m high, with out a crater. It consists largely of pillow lavas, although much of the mountain is covered by lava fragments and talus. Pillows are mostly 0.5–2 m across. They have a well-defined black glassy crust about 3–5 cm thick, and the surface commonly has a ropey texture. However, a submarine origin for the pillow-like structures at Gaussberg was questioned by Tingey et al. [23], who likened them to pahoehoe structures. They argued for a subglacial eruption, perhaps in a series of pulses to account for a number of terraces distinguished on the mountain [24], although these could also be erosional features due to changes in the regional ice levels.

Much of the lava is vesicular, the vesicles in the pillow core being generally larger than those near the margins. Most vesicles are lined with black glass which also occurs in irregular veinlets about 1 mm thick. Thin layers of palagonite tuff are locally present. Fused crustal xenoliths, up to 15 cm across and mostly of quartzo-feldspathic gneiss and rapakivi granite, are fairly common. Mantle xenoliths are much less common and comprise spinel lherzolite. The Gaussberg lava is dark, massive, and almost aphyric with microphenocrysts of leucite, olivine, and phlogopite. It is composed essentially of olivine, clinopyroxene, and leucite up to 1 mm across in a yellow-brown glassy matrix, generally full of quench crystal growth. The latter is largely confined to the inner parts of the pillow and consists of very fine-grained (0.01–0.1 mm) leucite, diopside, reddish-brown mica, and small amounts of reddish-brown amphibole. Ilmenite and chromite occur in the groundmass of some samples. One specimen contains a small (2.5x1 cm) ultramafic nodule composed of olivine, orthopyroxene, clinopyroxene, and spinel. Modal compositions include olivine (7–10%), clinopyroxene (6–10%), leucite (22–29%), and glass (53–67%). Mineral compositions are listed in Table 1. Leucite crystals are generally twinned indicating a slow rate of cooling. The compositional range is small and very close to the ideal leucite stoichiometry. No significant differences in chemistry were found between the leucite crystals occurring in the lava and those in the cognate inclusions. Significant Ba (up to 0.3 wt. % BaO) is present. Olivine compositions are in the range $Fe_{0.86-0.90}$, with high NiO (0.3–0.6%) and CaO (0.2–1.0%). Clinopyroxene is diopside, low Al_2O_3 (0.3–0.7%) and high Cr_2O_3 (up to 1.1%) and NiO (up to 0.16%), reflecting the Mg-rich nature of the lava (mg 0.69–0.71). Mica and amphibole occur as late-crystallizing phases. The mica is titaniferous phlogopite, containing very high BaO (1.0%).

K-Ar dating gave the average age of 56000 ± 5000 years [23], which is believed to reflect the time of eruption.

CHEMICAL COMPOSITION

Major and trace element compositions of the Antarctic lamproites are listed in Table 2. These rocks have distinctive chemical features, e.g., Niggli mg, Niggli k, molar K_2O/Na_2O , and molar K_2O/Al_2O_3 , all fitting the criteria cited by Mitchell &

Table 2

	1	2	3	4	5	6	7	8	9	10	11
Sample #	1202	1205	1206	1301	1302	1510	1605a	1605b	TM9901 13-01a	TM9901 13-01b	TM9901 13-01c
Locality	Tonagh Island										
SiO ₂	53,64	51,09	54,43	54,66	52,79	53,15	47,66	47,74	57,53	57,36	55,83
TiO ₂	2,18	2,74	2,14	2,34	2,60	2,50	4,95	4,93	1,87	1,93	2,34
Al ₂ O ₃	8,29	8,41	9,26	8,19	7,66	8,88	8,41	8,52	9,05	9,15	10,15
Fe ₂ O ₃	3,42	2,83	3,18	3,42	3,63	3,24	3,14	3,16	*6.12	*5.86	*5.09
FeO	2,69	2,79	2,08	2,69	3,02	2,60	1,77	1,79			
MnO	0,12	0,09	0,09	0,10	0,12	0,12	0,07	0,07	0,12	0,12	0,10
MgO	6,05	7,22	5,64	5,26	6,10	5,31	8,12	8,09	5,21	5,23	5,59
CaO	6,22	6,83	5,75	5,41	5,86	5,85	5,30	5,15	5,19	5,36	4,76
Na ₂ O	1,95	1,45	1,81	1,66	1,93	1,34	1,03	1,08	1,70	1,71	1,62
K ₂ O	9,47	9,52	10,30	9,56	9,33	9,40	10,45	10,46	10,43	10,49	11,66
P ₂ O ₅	2,90	4,21	3,08	2,66	2,83	2,68	3,30	3,29	2,87	2,99	2,84
CO ₂	0,37	0,11	0,26	1,55	1,44	2,21	0,89	0,74			
H ₂ O ⁻	0,13	0,17	0,19	0,24	0,23	0,31	0,23	0,22			
H ₂ O ⁺	0,33	0,44	0,32	0,43	0,47	0,62	0,68	0,67			
Rest											
Total	97,76	97,90	98,53	98,17	98,01	98,21	96,00	95,91	100,09	100,20	99,96
Trace elements, ppm											
Li	105,5	187	54,1	26,4	35	61,8	24,3	23,1			
Be	11,9	12,4	6,6	15,2	18,5	11,4	9,4	10			
B	30	30	24	20	30	<20	28	26			
F	11900	12900	10600	9000	10500	7700	14400	13300			
Cl	264	220	215	117	200	225	319	314			
S	136	160	168	264	520	1260	3790	3560			
Sc	26	24	26	24	24	24	16	16			
V	116	114	68	92	126	76	98	94			
Cr	188	232	158	160	224	138	416	428	126	111	139
Ni	166,4	199,8	144,9	146,2	193,8	120,4	339,3	345,2			
Cu	39,6	115,7	49	92,1	92,2	78,1	69	67,3			
Zn	130,9	108,4	89	107,5	137	84,3	89,1	87,8			
Ga	4,5	14,8	15,6	16	11,3	16,8	16,8	15,4			
Ge	0,4	0,9	1,8	1,1	1,9	<.60	<.60	0,5			
As	4,5	2	4,2	1,4	2	1	<.90	<1			
Se	<.40	<.30	<.30	<.40	0,5	<.40	0,6	<.40			
Br	1,7	1,4	3,1	1,1	1,9	1,7	0,8	1,8			
Rb	282,5	320,1	297,7	263,5	252,5	280,4	478,7	458,6	321	313	353
Sr	2374	3306	2423	2506	2547	2976	2505	2469	2331	2399	2788
Y	77,7	42,1	75	39,9	34,3	44,4	18,9	18	156	158	82
Zr	1690	1310	1570	1710	1860	2130	2400	2380			1175
Nb	91,9	89	91,7	112,2	151,1	97,2	198,5	209,1	127	112	25
Mo	0,8	0,9	2,1	1,5	0,7	1,9	4	2,4			
Ag	0,3	0,3	0,2	<.10	<.20	<.20	<.30	<.30			
Cd	<.10	<.10	<.20	<.10	<.20	<.20	0,6	0,6			

Table 2 continued

	1	2	3	4	5	6	7	8	9	10	11
Sn	5,8	4,4	3,4	5,5	5	8,7	10,6	10,5			
Sb	<.10	<.10	<.20	<.10	<.20	<.20	2,6	2,5			
Te	<.30	<.30	<.30	<.30	<.30	<.30	10,6	9,8			
Cs	<.60	<.60	<.70	<.70	<.80	<.90	15,6	13,5			
Ba	931	815	1191	1737	2901	3376	13359	12992			
La	274	298	510	272	242	286	272	282			
Ce	828,1	774,8	1146	625,2	538,9	701,2	599,5	624			
Pr	124,2	101,1	152	76,8	67,6	101,5	138,3	135,4			
Nd	380	325	405	245	225	300	195	195			
Hf	49,2	34	42,4	41,3	50,9	53,6	59,6	61,9			
Ta	4,5	6,1	5,2	5,3	<5	7	9,1	11,9			
Tl	1,3	2,3	2,3	1,5	2	2,5	1,8	2,7			
Pb	400	48	76	92	200	90	66	78			
Bi	2,9	1,5	1,4	2	2,1	2,3	2,7	2			
Th	13	13	33	52	26	145	28	69			
U	10	13	37	17	14	16	8	8			

Table 2 continued

	12	13	14	15	16	17	18	19	20	21
Sample #	TM9901 13-01d	TM9901 13-01f	447	450	479	7728 3949c	7728 3949d	7728 3950	7728 3951a	7328 1545
Locality	Tonagh Island	Tonagh Island	Hydrog- rapher Islands	Hydrog- rapher Islands	Hydrog- rapher Islands	Priestley Peak	Priestley Peak	Priestley Peak	Priestley Peak	Mount Bayliss
SiO ₂	57,40	54,44	48,58	59,07	68,31	52,6	49,6	50,4	52	52,90
TiO ₂	2,36	2,40	1,31	1,07	0,930	3,4	3,27	3,52	2,85	4,45
Al ₂ O ₃	9,21	8,21	12,23	9,55	10,24	8,67	9,1	8,95	8,74	8,92
Fe ₂ O ₃	*5.61	*6.40	*9.75	*8.29	*7.10	2,03	2,45	1,97	3,19	2,64
FeO						4,12	4,06	4,63	3,39	5,30
MnO	0,12	0,11	0,190	0,090	0,090	0,09	0,08	0,1	0,11	0,11
MgO	5,36	6,19	9,06	2,81	1,20	7,43	8,77	8,55	7,29	5,95
CaO	5,09	5,48	9,06	3,59	1,79	4,97	5,32	5,47	4,54	4,00
Na ₂ O	1,44	1,93	1,78	0,72	0,28	0,73	0,89	0,85	1,9	2,05
K ₂ O	10,80	10,18	4,42	9,62	8,34	8,32	9,83	8,49	8,34	9,35
P ₂ O ₅	2,82	3,12	1,40	1,81	0,684	3,05	3,28	3,32	2,76	1,75
CO ₂			0,21	0,21	0,10	0,16	0,02	0,02	0,06	0,25
H ₂ O ⁻			0,41	0,20	0,29	0,05	0,06	0,02	0,04	
H ₂ O ⁺			1,30	0,52	0,44	0,77	0,84	0,86	0,88	0,89
Rest										0,99
Total	100,20	98,47	99,67	97,54	99,77	100,56	100,82	100,67	100,09	99,55
Trace elements, ppm										
Li			11,4	32,4	16,8					
Be			1,4	12,9	11,5					
B			<20	<20	<20					
F			840	4900	1280					2800
Cl			487,7	433,2	166,2					
S			0,063	0,198	0,045					360
V			161	72	40	168	143	152	170	94
Cr	125	207	360	56	10	274	348	362	249	215
Ni			164	35	7	243	298	300	220	131
Cu			28	45	9	7	80	27	94	43
Zn			112	133	120	82	86	85	78	140
Ga			16	17	17	13	15	15	12	20
Ge			1,7	<0,8	<0,9					
As			<0,5	<1,9	<0,6					
Se			0,4	0,4	<0,5					

Table 2 continued

b	363	266	153	213	176	252	314	284	186	210
Sr	2643	2642	470	1528	518	2910	2950	2950	2350	1779
Y	111	58	36	88	93	32	36	39	29	32
Zr		1388	493	1099	1578	1770	1420	1780	1690	1582
Nb	82	150	54	16	27	59	43	63	49	145
Mo			0,5	<1.4	<1.3					
Ag			0,2	<0.3	<0.2					
Cd			0,3	0,7	0,5					
Sn			3,1	7,2	4,8					
Sb			0,2	5,3	2,0					
Te			<0.3	9,3	2,8					
Cs			<0.8	6	<1.1					
Ba			3085	11130	4863	15100	9700	10100	13600	412
La			128	332	317	172	138	173	153	162
Ce			270	750	630	294	268	335	273	276
Pr			9	102	56					
Nd			80	260	180					
Hf			14	35	43					
Ta			5	<3.6	9					
Tl			0,9	2,1	2,2					
Pb			24	433	41	24	58	28	83	28
Bi			1,0	1,8	2,0					
Th			19	59	145	7	48	21	10	14
U			2	9	38	7	6	10	8	2,0

Table 2 continued

	22	23	24	25	26	27	28	29	30	31	32
Sample #	R11370	35647-3	NM11	7728 4870A	7728 4870B	7728 4872	7728 4875	7728 4883	7728 4887	7728 4888	7728 4889
Locality	Mount Bayliss	Mount Rubin	Webster Peaks	Gauss- berg							
SiO ₂	50,30	50,40	51,87	50,80	50,20	50,70	50,50	50,10	51,60	51,60	51,00
TiO ₂	5,43	5,38	2,51	3,43	3,36	3,34	3,28	3,34	3,47	3,50	3,50
Al ₂ O ₃	8,90	7,35	12,16	9,95	9,79	9,95	10,04	9,92	10,00	10,05	9,98
Fe ₂ O ₃	2,72	*4,44	4,2	2,47	2,40	2,32	2,77	3,12	2,33	2,12	2,48
FeO	6,00		3,2	3,76	3,85	3,84	3,39	3,14	3,84	4,00	3,83
MnO	0,11	0,09	0,12	0,09	0,09	0,09	0,09	0,09	0,08	0,08	0,09
MgO	5,56	7,57	7,14	8,09	7,92	8,34	8,19	8,21	7,53	7,50	7,81
CaO	5,06	5,41	5,01	4,78	4,72	4,76	4,84	4,91	4,48	4,50	4,81
Na ₂ O	1,75	1,86	0,92	1,78	1,64	1,70	1,53	1,17	2,19	1,85	1,55
K ₂ O	8,90	8,44	9,99	11,49	11,54	11,54	11,30	10,97	11,50	11,87	11,68
P ₂ O ₅	1,85	1,36	0,68	1,46	1,46	1,44	1,46	1,46	1,49	1,48	1,50
CO ₂	1,45		0,44	0,09	0,07	0,03	0,02	<0.01	0,13	0,02	0,04
H ₂ O ⁻		3,81	1,41	0,07	0,07	0,06	0,03	0,04	0,05	0,03	0,04
H ₂ O ⁺	1,06		0,16	1,24	1,03	1,09	1,13	2,72	0,84	0,65	1,14
Rest	1,05	0,53									
Total	100,14	96,65	99,81	99,50	98,14	99,20	98,57	99,19	99,53	99,25	99,45
Trace elements, ppm											
F	3300			3100	3200	3400	3400	3000	2800	3500	3400
Cl				600	530	870	300	275	720	770	700
S	400			680	480	400	480	320	440	440	400
Sc											
V	133	97	119	112	108	110	108	107	107	104	107
Cr	180	339	234	308	333	311	324	338	303	272	315
Ni	128	153	153	223	231	234	243	234	231	249	226
Cu	34		30	29	31	27	28	26	32	29	28

Table 2 continued

Zn	116		81	77	93	83	73	72	89	74	75
Ga	22		22	18	17	18	18	18	18	17	17
Ge											
As				4	3	3	3	2	3	3	3
Se											
Br											
Rb	149	142	303	309	305	311	311	313	315	316	307
Sr	1259	972	571	1870	1890	1830	1860	1940	1740	1760	1840
Y	37	36	16	19	19	18	18	18	19	19	18
Zr	1242	1185	515	903	915	901	890	893	957	972	943
Nb	102	138	101	88	89	88	87	88	87	90	93
Mo											
Ag											
Cd											
Sn				2	4	2	2	1	<1	2	2
Sb											
Te											
Cs											
Ba	1320	1043	4706	5550	5440	5620	5850	5970	5640	5480	5380
La	156			214	207	211	213	215	212	206	204
Ce	270			348	334	339	341	338	335	331	321
Pr											
Nd											
Hf											
Ta											
Tl											
Pb	19	52	9	36	37	36	35	36	37	38	35
Bi											
Th	19	41	17	29	29	28	28	30	29	28	29
U	2,0		1	3	3	2	2	3	3	2	3

Bergman [9]. Noteworthy are some significant deviations from the average composition given by Rock [17], e.g., greater enrichment of some rocks (especially those from Tonagh Island) in K_2O , Na_2O , P_2O_5 , F, Cl, Sr, Zr, LREE, Y, Pb, and U. Many samples are lower in TiO_2 , MgO, Cr, and Ni.

The Mounts Bayliss and Rubin rocks belong to the rare ultrapotassic mafic rock suite which includes the leucite lamproites of the West Kimberley area of Western Australia [16] and the volcanic rocks of the Leucite Hills, Wyoming [3]. Such extreme compositions are though reflect small degrees of melting of highly enriched (metasomatised), phlogopite-bearing mantle source regions, with much of the LILE and probably some of the LREE having ultimately been derived by dehydration and/or partial melting of subducted sediments [14, 18].

A highly enriched mantle source for the Mount Rubin dyke is evidenced by its very low ϵ_{Nd} (T= 460 Ma) of -15 [8]. Model T_{DM} ages for two samples are 1270 and 1330 Ma ($\epsilon_{Nd}(460) = -7.6$ and -8.7 , respectively), which may be interpreted as the time of mantle enrichment processes corresponding to the major crust

Table 2 continued				
	33	34	35	36*
Sample #	7728 4893A	7728 4893B	7728 4894	77284876 (glass)
Locality	Gauss- berg	Gauss- berg	Gauss- berg	Gauss- berg
SiO ₂	51,20	51,50	51,00	53,6
TiO ₂	3,44	3,54	3,42	6,2
Al ₂ O ₃	9,42	9,49	9,89	6,9
Fe ₂ O ₃	2,54	2,31	2,15	
FeO	3,86	4,12	3,94	9,5
MnO	0,09	0,09	0,08	0,11
MgO	8,19	7,95	7,76	5,4
CaO	4,35	4,38	4,37	3,3
Na ₂ O	1,53	1,65	1,53	2,6
K ₂ O	11,73	12,16	11,89	10,4
P ₂ O ₅	1,48	1,53	1,50	
CO ₂	0,03	0,02	0,05	
H ₂ O ⁻	0,06	0,07	0,08	
H ₂ O ⁺	1,17	0,92	0,96	
Rest				
Total	99,09	99,73	98,62	**98.96
Li				
Be				
B				
F	3100	3400	3600	
Cl	570	630	580	
S	360	320	400	
Sc				
Table 2 finished				
V	100	101	107	
Cr	287	284	288	
Ni	240	223	228	
Cu	31	31	30	
Zn	80	78	75	
Ga	18	18	17	
Ge				
Table 2 continued				
As	4	5	3	
Se				
Br				

formation event in this area. The high Zr contents of dykes from both Southern Prince Charles Mountains occurrences are comparable to the typical lamproites [10], but some other incompatible elements (Ba, Sr, and Sm) are relatively low, so that Rb/Sr and Rb/Ba are high. These dykes also have low K/Ti and only small negative Nb and P anomalies. Some of these features are similar to the Western Australian lamproites [1], but the much lower Ba and Rb are more typical of lamproites from Southeastern Spain [15]. The negative Sr and Ba anomalies, as well as relatively low Ni and Cr of the Antarctic dykes are consistent with the mineralogical evidence of extensive melt evolution during ascent through the crust. In view of diversity and complexity of the processes probably involved in petrogenesis of lamproites, including small degrees of melting with a variety of major and accessory residual phases, fluid activity, source metasomatism, etc., it is not surprising that there should be such

Rb	336	330	313	
Sr	1710	1720	1720	
Y	18	19	18	
Zr	1350	1360	955	
Nb	96	97	87	
Mo				
Ag				
Cd				
Sn	2	7	2	
Sb				
Te				
Cs				
Ba	5450	5340	5320	
La	211	211	204	
Ce	343	343	334	
Pr				
Nd				
Hf				
Ta				
Tl				
Pb	42	66	37	
Bi				
Th	33	35	28	
U	3	4	3	
Data sources: 1-13, Miyamoto et al. (2000); 14-16, unpublished data by M.Sandiford & E.Grew; 17-22, Sheraton & * - by microprobibg; ** - includes 0,89 BaO and 0,06 NiO. England 1980; 23, Mikhalsky et al. (1994); 24, Munksgaard et al. (1992); 25-35, unpublished data by J.Sheraton; 36, Sheraton & Cundari (1980). Data obtained mostly by XRF in different laboratories; Fe ³⁺ by wet chemistry (when determined); * total Fe as Fe2O3; Li, Be by ICP-MS, B by ICP-AES, F by ion-sensitive electrode (Miyamoto et al., 2000).				

a range of trace-element abundances. Perhaps more surprising are the geochemical similarities. The *Webster Peaks* dyke differs in being silica undersaturated (Ol, Lc, and Ne-normative), and having higher Ba and Rb, and lower Ti, Na, P, Sr, and Zr than the Mounts Bayliss and Rubin dykes[12].

The *Gaussberg* lamproites, like the other Antarctic examples, are noteworthy for their very high Ti, K, P, F, Rb, Sr, Zr, Nb, Ba, La, Ce, Pb, Th, and U. Al, Ca, and Na are relatively low, and *mg* values are high (0.69-0.71). Cr and Ni contents are moderately high, similar to the values in primitive, little-fractionated basaltic rocks. Compared with other Antarctic lamproites, the Gaussberg rocks (which are much younger) are relatively enriched in K, but depleted in P, CO₂, Sr, Yr, Nb, and, to lesser extents, Pb and U, but not Th. Gaussberg lamproites

show the pronounced enrichment in Rb–Sr and Sm–Nd isotopic systems: $\epsilon_{Nd}(0) = -13$ to -15 , $Sr_i = 0.7092-0.7109$ [4]. T_{DM} the model ages of 1280–1220 Ma are thought reflect the minimum age of the mantle source enrichment processes, whereas Williams et al. [25] calculated enrichment ages of 1.4–1.8 Ga employing Pb isotopic assumptions. Crustal xenoliths yield T_{DM} model ages of 2.4–2.5 Ga.

The Gausberg lamproites show distinctive lead isotopic characteristics ($^{206}\text{Pb}/^{204}\text{Pb}= 17.5895$, $^{207}\text{Pb}/^{204}\text{Pb}= 15.662$, $^{208}\text{Pb}/^{204}\text{Pb}= 38.440$) similar to those of the Western Australian lamproites [13]. These authors concluded that the lamproites from both areas were derived from an extremely ancient mantle source region which had high U/Pb early in its history, followed by a more recent lowering of U/Pb, relative to the array shown by ocean island basalts and MORB.

Comparisons between the Antarctic lamproites from the areas described above show that there are significant systematic differences in rock composition. Thus, Tonagh Island rocks are characterised by mostly higher in Ca, Cu, Pb, and U; Hydrographer Islands rocks by higher in Si, Al, and Fe, but lower in P, Ni, Rb, and Sr; and Priestley Peak rocks are higher in V and Cr, and lower in La and Ce; the Prince Charles Mountains rocks tend to be high in Ti, and low in Sr, La, and Ce.

A number of hypotheses have been proposed to account for the very unusual chemistry of potassium-rich mafic rocks. Probably the most favoured are those involving low degrees of partial melting of the K-enriched (phlogopite-bearing) mantle source, some authors suggesting that K was derived from the subducted oceanic crust. In any case, it seems necessary to postulate the mantle source enriched in K and other lithophile elements to account for the observed lamproite compositions. The presence of phlogopite can explain the extreme enrichment of some elements (K, Ba, Rb), but the high concentrations of others can only be accounted for if the phases such as apatite (P, F, Sr, Th, U, and LREE) and perovskite, ilmenite, or rutile (Ti, Nb, Ta) are also present in the mantle source. The melt composition is generally regarded as being dependent on fluid composition and partial pressure. The carbonate-bearing Antarctic lamproites (except Gausberg) were probably derived under the elevated CO_2 pressures. Most of the observed geochemical differences between the various Antarctic lamproite groups may be due to mineralogical differences between the source regions, together with varying fluid composition and depths of melt segregation and crystallization.

None of the Antarctic lamproites seems to have experienced significant crustal contamination, although fractional crystallization is likely to have modified most of rock compositions to some extent, only the Gausberg rocks representing near-primary magmas.

In general, lamproites have been recognized in both intracratonal (either old stable cratons or recently stabilized ones) and relatively mobile (young fold-belt terranes) tectonic environments, in some cases possibly involving subduction processes. It is noteworthy that the western part of the Enderby Land has experienced some Late-Neoproterozoic to Early Palaeozoic thermal activation, as evidenced by pegmatite intrusion and resetting of isotopic systems, and much more pronounced tectonothermal activity (ductile deformations, high-grade metamorphism, and granite emplacement) of this age is well documented in the neighbouring terranes to the west (Lutzow-Holm Bay, Sor-Rondane Mountains, central Dronning Maud Land [7, 22, and references therein]. These areas are

intruded by Early Palaeozoic high-K dykes of lamprophyric, rather than lamproitic, affinities [5, 6]. This fact may provide some indirect evidence for the Enderby Land lamproites being related to Pan-African activity in the Mozambique Belt and its continuation in the Antarctica. Lamproites in the Prince Charles Mountains cannot be so readily related to orogenic processes, although their compositions are generally similar to those in Enderby Land. However, in recent years evidence has emerged confirming Pan-African tectonic activity in the Prince Charles Mountains, especially in its eastern portion. Thus, it is possible that only the Gaussberg lamproite was generated in a truly stable within-plate tectonic environment, in spite of the puzzling fact that it is located right at the edge of the East Antarctic shield, on a possible continuation of the Kerguelen line.

Acknowledgements. The authors thank E. Grew and M. Sandiford for providing unpublished geochemical data on the Hydrographer Islands rocks, and lamproite polished thin sections for further research.

REFERENCES

1. **Bergman, S.C.**, Lamproites and other potassium-rich igneous rocks: a review of their occurrences, mineralogy and geochemistry. In: Fitton, J.G. & Upton, B.G.J. (editors), *Alkaline igneous rocks*. //Geological Society of London Special Publication. 1987. V. 30. P. 103–190.
2. **Black, L.P. & James, P.R.**, Geological history of the Napier Complex of Enderby Land. In: Oliver, R.L., James, P.R. & Jago, J.B. (editors), *Antarctic earth science*. Australian Academy of Science, Canberra, 1983. P. 11–15.
3. **Carmichael, I.S.E.**, The mineralogy and petrology of the volcanic rocks from the Leucite Hills, Wyoming //Contributions to Mineralogy and Petrology. 1967. V. 15. P. 24–66.
4. **Collerson, K.D., & McCulloch, M.T.**, Nd and Sr isotope geochemistry of leucite-bearing lavas from Gaussberg, East Antarctica. In: Oliver, R.L., James, P.R. & Jago, J.B. (editors), *Antarctic earth science*. Australian Academy of Science, Canberra. 1983. P. 676–680.
5. **Hoch, M. & Tobschall, H.J.**, Minettes from Schirmacher Oasis, East Antarctica-indicators of an enriched mantle source //Antarctic Science. 1998. V. 10. P. 476–486.
6. **Ikeda, Y., Shiraishi, K. & Kagami, H.**, Geochemical characteristics of mafic dike rocks from the Sor-Rondane Mountains, East Antarctica. Proc. NIPR Symp. Antarct. Geosci. 1995. V. 8. P. 49–64.
7. **Jacobs, J., Fanning, C.M., Henjes-Kunst, F., Olesch, M. & Paech, H.J.**, Continuation of the Mozambique Belt into East Antarctica: Grenville-age metamorphism and polyphase Pan-African high-grade events in the central Dronning Maud Land //Journal of Geology. 1998. V. 106 P. 385–406.

8. **Mikhalsky, E.V., Laiba, A.A., Beliatsky, B.V., Sosedko, T.A. & Andronikov, A.V.**, Lamproites from the Rubin Massif, Prince Charles Mountains, East Antarctica // *Petrologiya*. 1994. V. 2. P. 258–264.
9. **Mitchell, R.H. & Bergman, S.C.**, **Petrology** of lamproites. New York, Plenum Press. 1991. 447 pp.
10. **Mitchell, R.H.**, A review of the mineralogy of lamproites // *Transactions of the Geological Society of South Africa*. 1985. V. 88. P. 411–437.
11. **Miyamoto, T., Grew, E.S., Sheraton, J.W. et al.**, Lamproite dykes in the Napier Complex at Tonagh Island, Enderby Land, East Antarctica // *Polar Geoscience*. 2000. V. 13. P. 41–59.
12. **Munksgaard, N.C., Thost, D.E. & Hensen, B.J.**, Geochemistry of Proterozoic granulites from the northern Prince Charles Mountains, East Antarctica // *Antarctic Science*. 1992. V. 4. P. 59–69.
13. **Nelson, D.R., McCulloch, M.T. & Sun, S-S.** The origins of ultrapotassic rocks as inferred from Sr, Nd and Pb isotopes // *Geochimica et Cosmochimica Acta*. 1986. V. 50. P. 231–245.
14. **Nelson, D.R. & McCulloch, M.T.**, Enriched mantle components and mantle recycling of sediments. In: Ross, J. (editor), *Kimberlites and related rocks, Volume 1: Their composition, occurrence, origin and emplacement* // *Geological Society of Australia Special Publication*. 1989. V. 14. P. 560–570.
15. **Nixon, P.H., Thirlwall, M.F., Buckley, F. & Davies, C.J.**, Spanish and Western Australian lamproites: aspects of whole rock geochemistry. In: Kornprobst, J. (editor), *Kimberlites and related rocks* // Elsevier, Amsterdam. 1984. P. 285–296.
16. **Pridier, R.T.**, The leucite lamproites of the Fitzroy Basin, Western Australia. *Journal of the Geological Society of Australia* 1960. V. 6. P. 71–118.
17. **Rock, N.M.S.**, *Lamprophyres* /Glasgow, Blackie and Son. 1991. 285 pp.
18. **Rogers, N.W., Hawkesworth, C.J., Matthey, D.P. & Harmon, R.S.**, Sediment subduction and the source of potassium in orogenic leucitites // *Geology*. 1987. V. 15. P. 451–453.
19. **Sandiford M. & Wilson C.J.L.**, The geology of the Fyfe Hills–Khmara Bay region, Enderby Land. In: Oliver, R.L., James, P.R. & Jago, J.B. (editors), *Antarctic earth science*. // Australian Academy of Science, Canberra. 1983. P. 16–19.
20. **Sheraton, J.W. & Cundari, A.**, Leucitites from Gaussberg, Antarctica // *Contributions to Mineralogy and Petrology* 1980. V. 71 P. 417–427.
21. **Sheraton, J.W. & England, R.N.**, Highly potassic mafic dykes from Antarctica // *Journal of the Geological Society of Australia*. 1980. V. 27. P. 129–135.
22. **Shiraishi, K., Ellis, D.J., Hiroi, Y. et al.**, Cambrian orogenic belt in East Antarctica and Sri Lanka: implications for Gondwana assembly // *Journal of Geology*. 1994. V. 102 P. 47–65.
23. **Tingey, R.J., McDougall, I. & Gleadow, J.W.**, The age and mode of

formation of Gaussberg, Antarctica //Journal of the Geological Society of Australia 1983. V. 30. P. 241–246.

24. **Vyalov, O.S. & Sobolev, V.S.**, Gaussberg, Antarctica //International Geology Review, 1959. V. 1, N 7. P. 30–40.

25. **Williams, R.W., Collerson, K.D., Gill, J.B. & Deniel C.**, High Th/U ratios in subcontinental lithospheric mantle: mass spectrometric measurements of Th isotopes in Gaussberg lamproite //Earth and Planetary Science Letters. 1992. V. 111. P. 257–268.

HIGH-MAGNESIAN VOLCANIC ROCKS OF THE PRECAMBRIAN IN RUSSIAN FENNOSCANDIA

V.S.Kulikov, V.V.Kulikova

Karelian Research Centre of RAS, Petrozavodsk, Russia

A broad range of high-magnesian volcanic rocks of different age (Palaeoarchean, Mesoarchean, Paleoproterozoic, Mesoproterozoic) and belonging to different series (boninite, komatiite, tholeiite-picrite, meimechite, kamafugite) was recorded from the eastern part of the Fennoscandian shield (Russian Fennoscandia). These rocks and their intrusive comagmatic rocks are linked to deposits and ore occurrences of copper, nickel, chromites, PGE, diamonds and other minerals. Recent data on the geochemistry and geochronology of high-magnesian magmatic rocks [21, 34, 36, 37] enable their correlation and identification of their connection to certain geological events of the regional and global scale. Analysis of the chemical compositions of Precambrian magmatic greenstone belts and rift zones from the Fennoscandia showed that three elements such as Al, Ti and Mg are interrelated, permanent antagonism between the first two elements being characteristic.

INTRODUCTION

Geology of the South-East Fennoscandian Shield is based on a broad spectrum of Precambrian magmatic rocks ranging in age from the Early Archean to the Phanerozoic.

Some relics of the oldest strata were dated by isotope methods on the southeastern margin of Fennoscandia. Its eastern part is rich in magmatic rocks of the Upper Archean greenstone belts overlain by the Early Proterozoic volcanic-sedimentary complexes that form various structures from rifts to gently dipping trough-like depressions and evolved through the Mesozoic. The western and southwestern parts of Fennoscandia consist of Svecokarelian and Riphean complexes. Phanerozoic magmatic rocks are known in the Scandinavian and Kola peninsulas. Cenozoic ore nodes have been dated in Onega structure. It is advisable to discuss the composition of SE Fennoscandian magmatic rocks, their origin and evolutionary characteristics using a new geochronological scale based on galactic years (Table 1) and to combine the national stratigraphic scale accepted for the Precambrian in Russia, Finland, Sweden, and Norway with the chronometric scales accepted for the Archean and the Proterozoic by the International Sub-Commission on Precambrian Stratigraphy [11]. In the scale proposed by the authors, numerous geological events described and published in different countries and dated by various isotope methods are taken into consideration. Their scale has no substantial discrepancies with the main boundaries used in the International Scale. The quasi-uniform motion of the solar system in the galaxy plane with a period of revolution of ca. 215 million years is postulated [27]. The scale is based on the cyclic repetition of planetary-scale diastrophism in accordance with the laws of synergetica that reflect the dependence of a system of rank on cosmic effects. It

comprises "a multi-level hierarchical system of pulsation cycles differing in rank and duration" [16]. Each galactic year falls into four periods: summer (apogalactic - 85 Ma) rich in disastrous events accruing everywhere (meteorite bombardments, planetary-scale structure-forming processes, and indicator mantle magmatism); autumn (50 Ma) with indications of relaxed tectonomagmatic processes (various facies of metamorphism, granite and ore formation, etc.); winter (perigalactic -30 Ma); and spring (50 Ma) with an abundance of sediments of various facies (from pelites and dolomites to conglomerates), large-scale **gladatons** and active magmatism. Each year one or another form of carbon such as black shale, shungite, oil or kimberlites is manifested. Two pregeological and twenty-two geological galactic cycles (years) are distinguished. The authors propose the term "galacton" for a combination of geological structures, magmatites, sedimentary complexes, etc., formed in the galactic year. According to the model of heterogeneous Earth accretion, the first two galactic years are characterized by the consecutive fractionation of protoplanetary matter at the meteorite level from coaly to ferruginous [2, 3, 14, 15,](See Table 1). Since Earth formation time, galactons have been reflecting the complex differentiation history of this matter, which condensed and accumulated in the same order to form protogeospheres: the nucleus = iron meteorites; the lower mantle == iron and iron-stone meteorites; the upper mantle = chondrites and coaly chondrites. The evolution of magmatic parent melts formed in the geospheres has a certain pattern and can easily be traced by studying Precambrian magmatites of the Fennoscandian Shield that occurs in the complexes of different Archean and Proterozoic galactons.

Principles of designing a galactic scale of geological time:

1) Geological time is divided into equal intervals 215 Ma long, which correspond to an average sidereal galactic year (GY). The initial GY ages in the basis of aeons and eras must be in the maximum possible agreement with the accepted geochronological boundaries of the latter.

2) The names of the GY are derived from Greek (chiefly ancient Greek) words the meanings of which reflect the global events considered characteristic for the time in question.

Benefits of the new scale in relation to the ICSP scale: Geological time in the new scale is divided into intervals on the scientifically - founded (astronomical) basis. In the ICSP scale the division was made empirically and lacked geochronological data. The new scale is divided into more fractions in its pre-Proterozoic part. It is relevant to the present stage in the development of Precambrian geology and geochronology and ensures reliable correlation of global geological events at the galactic year (superperiod) level. The new scale is common for the whole geological time and eliminates the existing contradictions between Precambrian and Phanerozoic scales. The new scale offers great promise in the study of the Precambrian (cycles, trends and abnormalities in the Earth's evolution, etc.) regarding a different approach to the division of geological time.

THE MAIN CHARACTERISTICS OF THE GEOLOGICAL STRUCTURE OF SW FENNOSCANDIA

Paleoarchean (> 3.15 Ga) time (in Karelia - Saamian, Chudian, Skoltian)
supracrustal

complexes, described from different shield all over the world, are preserved solely as relics in younger granitoids. The Volotsk suite recognized in the Vodlozero gneiss complex is proposed as the Early Archean stratotype of the Fennoscandian Shield. This is due to the geological structure, detailed stratification, composition, and isotopic age of its amphibolite constituents which is more than 3.2 Ga.

Their reconstruction is possible in some areas unaffected by late deformation and anatexis such as Lake Volotskoye in the Archangelsk district where the Volotsk suite is recognized [9]. The ca. 4-km - thick suite composed mainly of amphibolites after basic to ultrabasic volcanics occurs largely in the northeastern part of the Vodlozero block. Structurally, it forms the Cherevsky greenstone belt, which is discordant with the Mesoarchean (Lopian) Sumozero-Kenozero greenstone belt [7]. The isotopic age of the amphibolites determined by the Sm-Nd method is 3391±76 Ma [18]. It probably indicates a certain metamorphic episode. The isotopic age of the tonalites, which cut the amphibolites is estimated to be 3.2-3.5 Ga mainly from zircons using the U-Pb method [13]. The stratigraphic subdivision of the Volotsk suite is based on the composition and texture as these **teaters** most conservative characteristics of rocks during regional metamorphism. The suite is divided into thin amphibolite units after tholeiitic basalts (1-2 flows) and komatiitic basalt flows. The komatiites, seen as 0,1 – 1,5 m - thick flows with a distinct top zone, form four units occurring in the lower part of the sequence. Although the units are apparently graded in a uniform manner, the komatiitic basalts pass clearly into tholeiitic basalts, and the amount of total iron as well as titanium increases. 40% of the rock volume gradually increase in size toward the lower part of the augen zone. Less often there are flows in which the largest augen are observed in the central part of the zone, their size decreasing toward the top and bottom. Finally, the augen may be approximately of the same size throughout the thickness. Downsection, the augen zone gives way to a massive zone with uniform texture. The contact between these zones is always sharp and usually is traced by the fusiform segregations of augen material. In some flows, the massive zone may be absent. (60-80%) and serpentine (10-15%); hornblende, chlorite, and magnetite are present in small amounts. The augen structure of the underlying zone is caused by the presence of fusiform and lenticular blebs of antigorite, 0.2-0.8 x 1-4 cm in size, oriented subparallel to the contact of individual 'bodies and the

Table 1.

GEOLOGICAL TIME SCALES

(A - after the International Subcommission on Precambrian Stratigraphy [19]

B - V. S. Kulikov and V.V. Kulikova [11]

A			B				
EON	ERA	PERIOD	EON	ERA	GALAYEAR (SUPERPERIOD)	Comments to the names of galayears (translated from Greek)	
PHANEROZOIC	Cenozoic 65	Quaternary	PHANEROZOIC	Cenozoic	NOETIAN	** ² NOETIAN - intelligence, understanding (noetis): planetary rifting was accompanied by the emergence of primates, the ionosphere and the information sphere	
		Tertiary			NT		
	Mesozoic 245	144 Cretaceous Jurassic Triassic Permian		Mesozoic	140 ¹ PHYTONIAN	**PHYTONIAN - plant (phyton): "plant revolution"	
Paleozoic	360 Carboniferous Devonian Silurian Ordovician Cambrian	PHANEROZOIC	Paleozoic	355 PHOSPHATIAN	PT	**PHOSPHATIAN - phosphates: accumulation of phosphoric formations, "skeletal revolution"	
					PP	*CRYOGENIAN-ice (cryos) and origin (genesis): evolution of global glaciation	
PROTEROZOIC	Neo-proterozoic 1000	650 CRYOGENIAN	Neo-proterozoic 1000	CRYOGENIAN	formation of extension zones and rift genesis		
		850 TONIAN		CG 785	*STENIAN-narrow (stenos): formation of narrow, intensely deformed and metamorphosed zones		
	Meso-Proterozoic 1600	1200 STENIAN	PROTEROZOIC	Meso-proterozoic 1645	TONIAN	*ECTASIAN-distribution (ectaxis): widening of platform cover	
					1400 ECTASIAN	SN 1215	*CALLYMIAN - cover (callymma): accumulation of platform cover
					CALLYMMIAN	ECTASIAN	*STATHERIAN - stable (statheros): stabilization of cratons (<i>vepsian</i>)
	Paleoproterozoic	1800 STHATERIAN	PROTEROZOIC	Paleo-proterozoic 2505	ET 1430	*OROSIRIAN - mountain range (orosira): orogenic processes (<i>ludikovian-kalevian</i>)	
					1600 CALLYMIAN	CL	*RHYACIAN-lava flow (rhyax): intrusion of layered massifs (<i>jatulian</i>)
					2050 OROSIRIAN	STHATERIAN	*SIDERIAN - iron (sideros): accumulation of iron formations (<i>sumian-sariolian</i>)
					2300 RHYACIAN	ST 1860	
	Paleoproterozoic	2500	PROTEROZOIC	Paleo-proterozoic 2505	OR 2075		
2290 RHYACIAN					RC		
					SIDERIAN	SD	

¹ Figures (Ma) indicate the geochronological borders.

² *- The Name after the International Subcommission on Precambrian Stratigraphy [19];

** - The Name after V. S. Kulikov and V.V. Kulikova [11].

Continue of Table 1.

2500	Neoarchean		2505	Neo- archean 2720	CRATONIAN CT	**CRATONIAN-hard, rigid (crathos): completion of Archean sialic crust formation (<i>emian</i>)
	Meso- archean			Meso- archean 3150	CHABOUSIAN CB	** CHABOUSIAN-waterbody, basin (chabousa): first big Witwatersrand-type platform basins (<i>vesian</i>)
	3200				CHLOROPETRIAN CP	**CHLOROPETRIAN – green (chloros) and rock, stone (petra): global greenstone belts (<i>lopian</i>)
	Paleoar- chean			Paleo- archean 3795	GNEISSIAN GS	** GNEISSIAN – gneiss (gneissose): formation of gneissic textured rocks, including some “grey gneisses”(skoltian)
3600		MAGNESIAN MN	** MAGNESIAN-magnesia: first komatiites and other Mg-rich magmatic rocks (<i>chudian</i>)			
		LITHOSIAN LT	**LITHOSIAN-rock (lithos): oldest Isua type supracrustal rocks			
ARCHEAN	Eoarchean		PRISKOAN	BOMBARDIAN BB	**BOMBARDIAN-bombardment (bombardismos): bombardment of Imbriantype planets	
				REGOLITHIAN RG	**REGOLITHIAN-regolith: fotation of regolithic shell on Earthtype planets	
				SELENIAN SL	** SELENIAN-Moon (Selena): Moon crust formation	
				ACCRETIAN AC	** ACCRETIAN-chaotic accretos): solar system planets began to form	
				METEORITIAN MT	** METEORITIAN-meteorite (meteorolithos): minor bodies of solar system were presumably formed	
			ILLIAN IL	** ILLIAN-matter, substance (illi): protoplanets, meteorites CI-II		
			5085			

cummingtonite schistosity within the sequence. These blebs constitute 10 to 40% of the zone volume and are embedded in a granoblastic aggregate of cummingtonite and hornblende. The massive lower zone of the flows is relatively

uniform and consists of a granoblastic aggregate of cummingtonite and antigorite (serpophite?). The content of the latter increases from 40-50 to 70-80% toward the lower part of the massive zone of the flows and then is reduced again to 30-40% at the very base. The textures apparently were produced as a result of at least three stages of metamorphic transformations. In the first stage, the igneous structures of the augen and massive zones, probably, corresponding to the **spinifex** and cumulate zones of classic differentiated komatiite flows, were pseudomorphously replaced by serpentine. In most regions where Late Archean komatiite lavas are developed, alteration went no farther than this stage. In the second stage, one of prograde metamorphism, probably under high-temperature amphibolite-facies conditions, the primary textures were deformed and the pseudomorphs of serpentine were recrystallized, forming lenticular granoblastic blebs of olivine embedded in a matrix of fine grains of cummingtonite and hornblende. In the final stage of retrograde transformation, the lenticular blebs of granoblastic olivine were again serpentinized and blue-green hornblende and chlorite were developed at the expense of cummingtonite and high-temperature hornblende. Relics of pseudomorphously replaced granoblastic olivine are preserved very clearly in the massive zone and less clearly in the zone with augen structure. Komatiitic and tholeiitic metabasalts, which constitute most of the section of the supracrustal sequence, form flows with massive or pillow structure. As a rule, the pillowed upper part of the flows is highly schistose, deformed, and abundantly injected with silicic material. The lower massive part of the flows is much better preserved. In petrographic respects, the metabasalts are a fairly uniform group of rocks; their mineralogical composition apparently reflects a limited range of composition of their igneous protoliths, and in part is related to superposed processes. They consist of a granoblastic aggregate of blue-green hornblende, developed after early brown hornblende, and plagioclase, more or less saussuritized and albitized. Quartz, an opaque mineral, epidote, sphene, and apatite are found as accessories. The superposed processes are manifested in chloritization, biotitization, actinolitization, and epidotization.

In Meso- Neoproterozoic (Lopian) (3.15 - 2.505 Ga)(in Karelia – Lopian, Vesian, Emian) time, high-magnesian magmatism of predominantly komatiite and lesser tholeiite series is related to the protorift development stage of greenstone belts [5, 25]. Best preserved are Kamennoozero and Toksha (Sumozero-Kenozero greenstone belt) [7,10], Koikary in Vedlozero-Segozero greenstone belts [23], Kostomuksha [1 et al.]. The reconstructed thickness of komatiite-tholeiite assemblages varies from 1.6 km in Kostomuksha to 4-5 km in Kamennoozero. At that time magmatism was mainly remarkable for the occurrence of spinifex-structured komatiitic basalts, most common at the 3150-2935 Ma super period, and the low metamorphic grade of basic to ultrabasic rocks [5]. Intrusive comagmatic rocks are usually represented either by ultramafic sills and stocks (e.g., the Kamennoozero) within the belts. Some contain Cu-Ni ore deposits (e. G. Vozhma). The emergence of sodium granites-trondjemites (2935-2720 Ma) and potassium

granites (2720-2505 Ma - neoarchaeon) in acid magmatism is also noteworthy. Another important event of that in water bodies reduction conditions changed to oxidation conditions [1].

The Sumozero-Kenozero greenstone belt in the SE Fennoscandian Shield is ~400 km long and up to 50 km wide and includes two main units with a total thickness of ~5 km [7]. The lower unit consists of oceanic plateau-type submarine mafic-ultramafic lavas [10]. Lopian rocks form relics of local greenstone structures which are included in the Sumozero-Kenozero and Yuzhno-Vygozero greenstone belts [25]. Best preserved are the Kamenozero and Toksha structures, which are dominated by meta-effusives and meta-sediments of the Vozhma series having a total thickness of 5-6 km.

This sequence includes numerous flows of komatiites and komatiitic basalts. Lopian komatiites with well-preserved spinifex textures have been found in the region of the Kumbuksa river [10]. Layered lava flows with well-developed cumulate, spinifex and flow-top breccia zones are exposed in this region. Greenschist-facies metamorphism has resulted in complete replacement of the magmatic minerals; however, the texture is well preserved and readily enables the primary mineralogy to be reconstructed. The lower zone, which is several metres thick, is composed of a serpentinized peridotite with relics of cumulative texture. The gradual upward transition to the spinifex zone is marked by the appearance of blade-like olivine aggregates up to 1.3 mm in length alongside the euhedral and pointed crystals of clearly cumulative olivine. The cores of these olivine blades were often filled with glass, which is now represented by fine aggregates of talc and tremolite. The spinifex-textured zone could be subdivided into four layers, each about 25 cm thick. The first and third layers (from base to top) have a lenticular appearance. These lenses, which are up to 50 cm long and 12-15 cm thick contained blades of olivine oriented approximately normal to the layering. Inside the blades magnetite crystals occur along fractures. These lenses are bordered by olivine blades up to 50 cm in length. The second layer contains extremely large (up to 1 m long) feather-like blades of olivine with a thickness of not more than 1.5 mm. Usually these blades form bundles situated subparallel to the layer boundaries. Dendritic crystals of magnetite and chromite sometimes form lattices on the olivine faces. The uppermost layer in the spinifex-textured zone contains angular fragments 1.5-25 cm in size. These fragments consist of euhedral or less commonly elongated olivine crystals surrounded by a completely altered glassy groundmass. The material between the fragments consists of spinifex-textured komatiite, with packets of olivine crystals 1 -3 cm in length and 0.5-1 mm in width. Magnetite crystals form chains within the olivine plates. Between the plates, small (1 XO.1 mm) needles of clinopyroxene replaced by actinolite occur at an acute angle to the olivine crystals. The top of the flows consists of breccias with rounded clasts 1-12 cm in size, only slightly displaced with respect to each other. Within the clasts rounded grains of olivine up to 1 mm in size are observed. This

breccia zone is about 10-25 cm thick. In addition to the layered flows with a well-developed spinifex texture, others with only a vague zoning are also present.

These Lopian rocks are intruded by ultra-mafics, gabbros and the later plagiogranites, which are accompanied by rhyolite and rhyodacite veins as well as small granitoid intrusives, the zircon ages of which are about 2.8 Ga [25]. The upper unit is made up of island arc-type volcanic BADR (basalt-andesite-dacite-rhyolite)-series rocks and **adakite**-series subvolcanic rhyolites. Both units are separated from the 3.2 Ga TTG-gneisses of the Vodla Block microcontinent by major thrust zones [9, 34]. U-Pb zircon age of 2875 ± 2 Ma for the upper unit BADR-series felsic volcanic rocks, and Pb-Pb and Sm-Nd ages of 2892 ± 130 and 2916 ± 117 Ma for the lower unit komatiites and basalts are in good agreement and correspond to the time of emplacement of both sequences. Komatiites of the lower unit were derived from a liquid containing ~30% MgO that erupted at a temperature of ~1570°C. The komatiite liquid began to melt at depths of 300-400 km in a mantle plume. The plume was some 250°C hotter than the ambient mantle and had the thermal potential to produce oceanic crust with an average thickness of ~35 km, which was at least in part unsubductable. The lower unit mafic-ultramafic lavas have high $\epsilon_{\text{Nd}}(\text{T})$ of $+2.7 \pm 0.3$, relatively unradiogenic Pb isotope compositions ($\mu_1 = 8.73 \pm 0.20$) are depleted in highly incompatible elements and show Nb-maxima ($\text{Nb}/\text{Nb}^* = 1.2 \pm 0.2$, $\text{Nb}/\text{U} = 43 \pm 6$) [37]. These parameters are similar to those found in a number of early Precambrian uncontaminated greenstones and in recent Pacific oceanic flood basalts. They are regarded as plume source characteristics.

The Sumozero-Kenozero greenstone belt reveals the coexistence of fragments of unsubductable oceanic crust represented by the lower unit mafic-ultramafic volcanic sequences, and the products of subduction-related magmatism of the upper unit. This observation is reconciled within a single model implying that overthickened plume-generated oceanic crust was first intruded and overlain by mafic and intermediate-felsic melts coming from both subducting slab and overlying mantle wedge and, later on, accreted to and obducted onto the microcontinent of the Vodla Block.

In Proterozoic time (2.505 - 1.65 Ga), Fennoscandia was a part of the Laurasian craton, and the evolution of magmatism reflected their common evolutionary trends. The Paleoproterozoic is represented by the following galactons (on regional stratigraphic scale) - 4 superperiods: Sumian-Sariolian - 2.5 - 2.29 Ga; Jatulian - 2.29 - 2.075 Ga; Ludicovian-Kalevian - 2.075 - 1.85 Ga, and Vepsian - 1.85 - 1.65 Ga.

In the Sumian-Sariolian (2505-2290 Ma) time high-magnesian magmatism was apparent at the protorift evolutionary stage of the FennoSarmat protoplatform. Volcanics of the komatiite series have been mainly reported from the Pechenga-Varsuga, Lapland, and East Karelian (Vetreny) protorifts. The most abundant lavas in the region are the komatiitic basalts, which are exposed over 5000 km², the total

thickness in some places exceeding 6 km. They probably built up a single rift zone extending for more than 1000 km. Unlike those described above these rocks are quite fresh in places and contain abundant relics of magmatic minerals. Lava, tuff, and vent facies are distinguished [20].

The layered peridotite-gabbro-norite terrains, which contain Cr, Ni, Cu, V and PGE, and widespread in the Kemi – Koilismaa - Kukasozero, Burakovsko-Monastyrskaya, Koitelainen, and Pechenga – Moncha - Varsuga, Kiy should, probably, be viewed as intrusive facies of high-magnesian magmas. The above magmatic units are thought to be either the boninite or komatiite series. Small-scale magmatism was apparent (Lehta structure). The Vetreny belt in the SE Fennoscandian Shield is a large volcano-sedimentary basin containing a 4 to 8 km thick sequence of basaltic to komatiitic lavas, which were erupted ~ 2.45 Gy ago in a continental rift setting during the interaction of a mantle plume and the Archean continental crust of the Karelian granite greenstone terrane.

In the central Vetreny Belt, an extensive 110 m deep Victoria's lava lake is exposed consisting of remarkably fresh differentiated komatiitic basalt. During eruption, the liquid had a temperature of 1380-1400°C and contained ~15% MgO. The lava was ponded in a large topographic depression soon after eruption. The differentiation of the lava lake was controlled by settling of transported olivine and chromite phenocrysts and caused the prominent internal layering. The last portions of the trapped liquid crystallized at temperatures of 1250-1070°C. A Sm-Nd isochrone of 2410 ± 34 Ma for whole rock samples, olivine, augite and pigeonite separates from the lava lake provides a reliable estimate for the time of formation of the uppermost sequences in the Vetreny Belt. Re-Os isotope data for olivine cumulate samples and chromite separates from the Victoria lava lake and the Golets flow 3 define isochrones with ages of 2387 ± 57 and 2432 ± 34 Ma, respectively. This age is in good agreement with the Sm-Nd and Pb-Pb isochrone ages of 2449 ± 35 and 2424 ± 178 Ma for the volcanic rocks from the same stratigraphic level in the northwestern Vetreny Belt [36]. Modeling of Nd-isotopes and major and trace elements shows that the komatiitic basalts at Lion Hills may have had a komatiite parent depleted in highly incompatible elements.

It can be shown that this initial liquid was contaminated with 7-9% of Archean upper crustal material from the adjacent Vodla and Belomorian Blocks en route to the surface, thus acquiring the observed geochemical and isotope signatures including relative enrichment in Zr, Ba, and LREE, negative Nb- and Ti-anomalies, and $\epsilon_{Nd}(T)$ of -1.

The Kalja flow described below is taken as an example of the lower Karelian komatiites, which have not all been studied in detail. This flow, which is named after its exposure located near the Kalja river in the Archangelsk district, is up to 100 m thick and has been chosen for its resemblance to the layered komatiitic flows of Canada in particular the "Fred Flow". As with the previous group, the primary rock textures have survived the metamorphism, which has destroyed all

the primary minerals with the exception of a few clinopyroxene relics in the komatiitic basalts. The following list shows from top to base the subdivisions of the flow, indicating where possible the relationships between the metamorphic rock and its igneous precursor: brecciated komatiitic basalt (5.0m); komatiitic basalt with spinifex texture relics (50.0 m); metabasalt (10.0m); mafic metabasalt (6.0m); metabasalt (6.0m); carbonate-chlorite-tremolite rock (3.5m); chlorite-tremolite rock, komatiite (7.0m); komatiite with porphyritic texture (8.0m); chlorite-tremolite rock, komatiite (0.5m)

The lava facies is composed of about 95% by volume of the Vetreny Poyas suite and includes numerous non-layered and sparsely layered flows. The non-layered flows Shapochka are composed of komatiitic basalts with massive or pillow structures 1.5-80 m thick. The layered flows usually consist of the following units (from top to base): 1) breccias and pumices - 0.1-1.5 m; 2) komatiitic basalts with olivine and clinopyroxene spinifex - 5-65 m; 3) basalts, olivine absent - 3-40 m; 4) cumulative layer - 0 – 15 m; 5) komatiitic basalt - 0.1-0.2 m.

Several varieties of komatiitic basalts and basalts are distinguished which differ in their mineral and textural features with gradual transitions between them. Basalts are divided into plagioclase-free and plagioclase-bearing varieties. The major mineral in the rocks of the first group is clinopyroxene (up to 40 vol.%) often displaying chemical zoning with a high-magnesia pigeonite as the core. The remaining part of the rock consists of the devitrified glassy groundmass with accessory Fe-chromite and sometimes sulphides. Minor amounts of olivine (0-5%) are occasionally present. The rocks have massive, banded, variolitic and rarely amygdaloidal structures. Spinifex-like textures are in this case formed by clinopyroxene crystals. The plagioclase-containing basalts do not significantly differ from typical basalts in their mineral composition and textures. Major minerals are clinopyroxene and plagioclase (51-65 mole % An), rarely olivine. Fe-chromite, pyrrhotite, pyrite and chalcopyrite are found as accessories. The rocks are characterized by their massive structure and porphyritic, tholeiitic or pyroxene spinifex textures. Komatiitic basalts consist of olivine (10-25 vol.%), acicular clinopyroxene (0-20 vol.%), and glassy groundmass (up to 80 vol.%). Fe-chromite is the most common accessory. These rocks have massive, pillow or amygdaloidal structures and olivine spinifex textures. Olivine phenocrysts are often characterized by chemical zoning from Fo_{95} in the core to Fo_{72} in the rims.

New isotope and trace element data are presented for komatiitic basalts and a related peridotite Vinela Dike from the large Vetreny Belt in the southeastern Fennoscandian Shield [36]. The MgO contents of the erupted and intruded magmas are inferred to increase from 13 to 17% towards the center of the belt, which implies the respective increase in liquidus temperatures from 1370 to 1440°C. The elevated liquidus temperatures suggest that the source of the komatiite magmas had a substantially higher potential temperature (1630°C) than the ambient mantle (1480°C) and are regarded as evidence for the existence of a mantle plume underlying the region at ~2.45 Ga. Magmas parental to the lavas and the Vinela

Dike were shown to have komatiite composition and were derived from a long-term LREE-depleted mantle source with $\epsilon\text{Nd(T)}$ of ca. +2.6. The obtained Sm-Nd internal isochrone ages of 2449 ± 35 and 2410 ± 34 Ma for the lavas, 2430 ± 174 Ma for the Vinela Dike, and a whole-rock Pb-Pb age of 2424 ± 178 Ma for the lavas together with a U-Pb zircon age of 2437 ± 3 Ma are identical to the reported U-Pb zircon and baddeleyite ages for numerous mafic-ultramafic layered intrusions in central and northern Karelia. From their chemical and isotope similarities, it is likely that these rocks had allied parental magmas. These magmas may have been emplaced in a continental rift setting during the interaction of a mantle plume and continental crust. Impinging of a plume head beneath the continental lithosphere resulted in its thinning, stretching, and rifting, but failed to open a new ocean. This extensive magmatic event was responsible for a substantial contribution of early Proterozoic juvenile material to the Archean continental crust in the Fennoscandian Shield.

In Jatulian (2290-2075 Ma) time, a platform regime with terrigenous sedimentation and plateau basalt volcanism at its initial stage existed over the entire territory [22].

In Ludicovian (2075-1940 Ma) time high-magnesian magmatism manifested itself at the protoplate developmental stage of the protoplateau during the rift-forming epoch in the Lapland, Pechenga-Varzuga, Onegozersko-Rybinsk, and Outokumpu-Kainuu protorift structures. Intrusive comagmatic rocks are represented by numerous mafic and ultramafic, occasionally nickel-bearing bodies, associated with the picrite series. The Ludicovian rocks constitute the lower Zaonega suite and the upper Suissaarian suite. The Zaonega suite has a thickness of up to 1800 m and is composed of submarine volcanic, volcanoclastic and sedimentary including clay-carbonate rocks, dolomites, shungite-bearing basalt tuffs and tuffites with “black smokers” massive, pillow and variolitic basalts. The Suissaarian suite is up to 500 m thick (5 members) and is made up of volcanic rocks accumulated at shallow-water depths (basalt tuffs and tuff-conglomerates, hyaloclastites, pillow and variolitic basalts, picrites and picrobasalts). The rocks were metamorphosed under the prehnite-pumpellyite to greenschist facies conditions.

The parental magmas of the Suissaarian lavas contained ~10% MgO and were derived from melts generated in the garnet stability field at depths 80-100 km. Sm-Nd mineral and Pb-Pb whole-rock isochrone ages of 1975 ± 24 and 1980 ± 57 Ma for the upper part of the plateau and a SHRIMP U-Pb zircon age of 1976 ± 9 Ma for its lower part imply the formation of the entire sequence within a short time span [37]. These ages coincide with those of picrites in the Pechenga-Imandra belt (the Kola Peninsula) and komatiites and basalts in the Karasjok-Kittilä belt (Norway and Finnmark). Average liquidus temperature of the Karasjok komatiite magmas is $1520\pm 20^{\circ}\text{C}$ [32]. This implies that the ascending mantle material, which was the source of the Karasjok komatiites, was about 250°C hotter than the surrounding

mantle. The Karasjok komatiites share the same Al- and HREE-depletion characteristics with the Suisaarian picrobasalts and Pechenga picrites suggesting that their parental magma formation also occurred in the garnet stability field. The calculated depth of the komatiite melting initiation was 240 ± 40 km [31]. We believe that the Karasjok komatiites were formed in a hot plume tail, whereas the Onega plateau and Pechenga-Imandra Belt basalts are probably the products of melting in a cooler plume head [28]. The Ludikovian plume head might have had a diameter of ~ 2000 km, comparable to the head size of the largest extant plumes such as the Iceland plume [29].

On the other hand, modern analysis of its geological structure has demonstrated: 1) “encircling” of the Onega plateau some 150 km in diameter by carbonaceous rocks – dolomites; 2) wide distribution of shungites owing to the reducing environments of unclear nature, in close association with basic rocks, predominantly dolerite sills; 3) development in its south-western part of a narrow zone of the so-called “Solomenskaya breccia” first described by F. Levinsong-Lessing [5]; 4) lamproite-like rock bodies in the centre of the plateau [26]; 5) repeatedly rejuvenated Se-U-V ore deposit throughout the ring structure area. These facts can be interpreted as the formation of the *Onega astroblem* in the Suisaarian period that had considerable effect on further evolution of the whole region. If the search for stress-minerals and other indicator elements in the “Solomenskaya breccia”, as well as new dating and specifying of the formation sequence of the “reduced carbon (shungites) – carbonaceous carbon (dolomite)” are successful, then it may notably change our ideas of both the genesis of the Onega plateau and the mechanism of the Ludikovian plume initiation.

In Kalevian (1940-1860 Ma) time mafic-ultramafic magmatism was most apparent as the intrusions in the Svecofennian province of the Fennoscandia and was more limited in the Kola – Lapland - Karelian province. The polyphase alkaline-ultramafic rocks with Fe, Ti, P and other occurrences and deposits (Gremyakh-Vyrmes, Yeletozero-Tikshezzero) are restricted to a NNE-striking line, which shifts the above suture and probably indicates a transform fault.

In Vepsian (1860-1645 Ma) time mafic magmatism was apparent as gabbro-dolerite sills and islandite (?) and others in the South Onega trough.

In the Riphean (1645-650 Ma) time alkaline magmatism of alkaline series is apparent as thin lamproite and kimberlite veins in the (Girvas-?), Zaonezhie, Kostomuksha, Vetreny Poyas, and Ladoga zones.

PETROCHEMICAL SERIES OF MAGMATIC ROCKS

The chemical compositions of Precambrian magmatic rocks from the Fennoscandian Shield and other regions were analyzed. These magmatic rocks suffered mineral alterations over a broad range of metamorphic facies from greenschist to granulite. Therefore, their primary composition is preserved and represented by the chemical composition of the rock. There are various factors that

characterize magmatic complexes and are responsible for the evolution of magmatism. However, the behavior of the most inert elements such as Al, Ti, Mg, REE, etc. is one of the main factors. Three important petrogenic elements such as Al, Ti, and Mg, characterized by the consistent antagonism of the first two elements, were found to be interrelated.

The shortcomings of modern classifications of highly magnesian volcanites [4, 17, 12] do not allow adequate division of the examined formations in Northwest Russia. The authors suggest new binary classification diagrams: $\lg(\text{Al}_2\text{O}_3:\text{TiO}_2) - \lg \text{MgO}$ [12] and $\text{Al}_2\text{O}_3/\text{TiO}_2 - \text{MgO}$. The latter one is suitable for the rocks with the MgO content $> 9\%$. The boundaries of the rock kinds within the series in the basic-ultrabasic composition area with respect to MgO content (recalculated for anhydrous basis) obtained by statistical treatment of the representative body of the data (several thousand tests) are 9, 14 and 24% [5, 6]. $\text{Al}_2\text{O}_3:\text{TiO}_2$ ratio is relatively stable and shows some signs of the modulus, which has a certain value for rocks of different petrographic series in the MgO content range of 9-45%, olivine control being predominant, (allivalitic - >70 ; boninitic - 70-30; komatiitic - 30-20 and 15-10; picritic - 10-6, and 6-4 (subalkaline); alkaline-ultrabasic (meimechitic, kimberlitic) - 4-1.8; lamproitic - 1.8 - 0.8). The term "aluminum-titanium modulus" (ATM), which can be used as an indicator at both rock and mineral levels, is proposed for $\text{Al}_2\text{O}_3:\text{TiO}_2$ ratio. The above series are well-defined in both the ternary diagram $\text{Al}_2\text{O}_3-10x \text{TiO}_2 - \text{MgO}$ [6] and the binary diagram ATM-MgO. A diagram, $\lg \text{ATM} - \lg \text{MgO}$ (recalculated for anhydrous basis) [12], is proposed to analyze and subdivide the entire spectrum of magmatic rocks from acid to ultrabasic rocks, where the elements have nonlinear distribution. It can be used to study the dynamics of changes in the composition of igneous complexes in individual structures on the basis of available information and to forecast the differentiation of new, kenningitic and ferroalkali series. As the melts evolve, all the elements, including the most inert ones, are subjected to the multi-factor effect of the system. Therefore, the most objective characteristics are revealed in logarithmic nonlinear space (in coordinates) $\lg(\text{Al}_2\text{O}_3:\text{TiO}_2) - \lg \text{MgO}$ (mass. %, dry precipitate). Logarithmic scale increases the scope of the graphic representation of the series spectrum: an anorthositic (kenningitic) series is distinguished at $\text{ATM} > 100$ and a ferroalkaline series is distinguished at $\text{ATM} < 1$. ATM, established in the magma, persists in the rock series derived from it. If the MgO content ranges from 5 to 9% with the module varying from 3 to 25, a range, which marks a boundary for all the above magmatic series, is established. In that range, olivine control gives way to other mineral phases (pigeonite, augite and plagioclase). The ATM for rocks with $\text{MgO} < 9\%$ is inversely proportional to magnesia and clearly reflects calc-alkaline and other magma clans (Bowen tendency).

The following relation is revealed at 45-9% MgO on the basis of experimental data. The boninitic series is characterized by the following association: olivine, olivine - orthopyroxene, olivine - orthopyroxene - plagioclase (analysis of deep-

seated inclusions showed that spinel is an indicator mineral in kimberlites); komatiitic series for Al-depleted (chondritic) varieties: olivine, olivine - spinel, olivine - orthopyroxene - clinopyroxene (garnet is an indicator mineral); picritic series: olivine, pigeonite - augite - plagioclase (magnetite is an indicator mineral); alkaline - ultrabasic series: two olivines, two olivine - spinel, two olivines - orthopyroxene - spinel, two olivines - clinopyroxene - orthopyroxene - spinel, olivine - melilite, olivine - spinel - melilite (with magnetite as an indicator mineral); ferroalkaline series: olivine - spinel, olivine - spinel - plagioclase (with ilmenite and armalcolite as indicator minerals). High - and moderate - Mg magmatic rocks are separated by a combination of the composition trends for the Skaergaard and other layered intrusions as well as basic dike complexes reflecting iron accumulation and a decline in ATM value from the anorthositic to ferroalkaline series (Fenner tendency). The overlapping trend range is subdivided on the basis of indicator minerals into the following zones (in terms of decrease in MgO): spinel, pigeonite, and plagioclase zones in series; augite and plagioclase zones in the tholeiite-picritic series; pigeonite, pigeonite-augite, and plagioclase-pigeonite zones in the ferroalkaline series, where the latter is the composition zone of magnetite, or into two zones on the basis of the presence of armalcolite. The minerals that have the same (pyroxenes, chrome-spinelids, etc.) in corresponding series have their specific alumotitanium modulus combined with the series (melt) modulus. When experimental data on rock melting under various conditions and the results of the homogenization of gas-liquid inclusions in intermediate and acid rocks are plotted on the diagrams $Al_2O_3-10x TiO_2-MgO$ and $lgATM-lg MgO$, they can successfully be used for the petrological study of magmatic rocks. ATM reveals the graded structure of any igneous body. It is a universal phenomenon. The model is controlled by PT-conditions and the presence of fluids, and MgO content directly affects the melting temperature of the melt. Based on experimental data and information on deep xenoliths from the kimberlite pipes on the $lgATM-lgMgO$ diagram, the consecutive succession of rock complexes in the lithosphere and asthenosphere and the dependence of their composition on substrate composition can be modeled.

The high-magnesian rocks ($Mg > 9\%$) of the Fennoscandian Shield were subdivided in terms of ATM into four petrochemical series with specific mineralization and ore deposits.

1. A boninitic series: $ATM > 30$; magmatic rocks found in some Paleoproterozoic layered intrusions in North Karelia, on the Kola Peninsula, and in Finland; deposits of Ni, Cu, Cr, PGE.

2. A komatiitic series: $ATM - 30-10$; some volcanics and plutonics and plutonic rocks occurring in the Archean greenstone belts of Fennoscandia and the Paleoproterozoic rift of Vetreny Poyas in East Karelia, Lapland in North Finland, and Imandra-Varsuga on the Kola Peninsula; Ni deposits, Au mineralization. There is in the komatiitic series of the Vetreny Poyas at the average rock ATM: 17-19 in clinopyroxene, 10-20 in chrome, and 18-28 in spinel.

3. A picritic series: ATM - 10-4 (3.5); volcanic and plutonic rocks of the Suissaarian (Karelia) and Pechenga (Kola Peninsula) complexes; deposits of Cu, Ni, Ti. ATM of Onega structure picrobasalt is 5-7, that of pyroxene is 3-5, and that of chrome-spinel is 5-8.

4. A kimberlitic and lamproitic series: - ATM<3.5; a Riphean diamondiferous lamproite dike complex, (West Karelia, Zaonegye).

CONCLUSION

The magmatic series distinguished in Fennoscandia characterize the Precambrian evolution of the Earth most completely (See Table 1) and the Phanerozoic time to a limited extent. The use of the properties of the most inert components Al, Ti and Mg as well as their relationships for the study of the composition of magmatic fluids has made it possible:

1) to find the position of any Fennoscandian magmatic rock in the global community of magmatic rocks and to determine corresponding petrochemical series;

2) to elucidate the formation pattern of magmatic complexes over a long segment in the Earth's history with regards for the well-known trends in the formation of deep-seated intrusive units (Fenner tendency) and crustal units under oxidation conditions (Bowen tendency);

3) to assess rapidly the approximate PT-conditions of the liquidus-solidus range of magmatic rock.

REFERENCES

1. Campbell I.H., Griffiths R.W., Hill R. Melting in Archean mantle plume: heads it is basalts, tails it is komatiites //Nature. 1989 V. 339. P. 697-699.
2. Gill R.C.O., Holm P.M., Nielsen T.F.D. Was a short-lived Baffin Bay plume active prior to initiation of present Icelandic plume? Clues from the high-Mg picrites in West Greenland. //Lithos. 1995. 34 P. 27-40.
3. Gorkovets V.Ya. and Rayevskaya M.B. Geologija i metallogeniya rayona Kostomukshskogo mestorozhdenija, Petrozavodsk, 1981. 149 p. (in Russian)
4. Khain V.E. and Bozhko N.A. Istoricheskaja geotektonika, docembriy. Moscow, .1988. 382 p. (in Russian)
5. Khain V.E. and Seslavinskiy K.B. Global'nye ritmy v fanerozoyskoy endogennoy aktivnosti Zemli. Stratigrafija. Geologicheskaja korreljacija, 1994. V. 2. P. 40-63. (in Russian)
6. Klassifikacija magmaticeskich porod i slovar terminov .Moscow. 1997 248p. (in Russian)
7. Komatiity i vysokomagnezial'nye vulkanity rannego dokembrija Baltijskogo shchita, Leningrad, 1988. 185 p. (in Russian)
8. Kulikov V.S. O raschlenenii vysokomagnezial'nyh vulkanitov dokembrija Karelii po dannym petrohimii i hromshpinelidam. /In Mineralogija dokembrija Karelii. Petrozavodsk, 1988. P. 141-146 (in Russian).

9. Kulikov V.S. and Kulikova V.V. K vydeleniyu Sumozersko-Kenozerskogo zelenokamennogo pojasa archeja na vostochnoy okraine Baltijskogo shchita. *Geologija rannego dokembrija Karelii*. Petrozavodsk, 1979. P. 70-76. (in Russian)
10. Kulikov V.S., Simon A.K., Kulikova V.V., Samsonov A.V., Kajrjak A.I., Ganin V.A., Sudin A.I. Evolution of Archaean magmatism in the Vodla Block, Karelian granite-greenstone terrane. /In: *Precambrian geology and geochronology of the East European platform*. Leningrad. 1990 P. 92-100 (in Russian)
11. Kulikova V.V. Volockaja svita - stratotip nijnego arheja Baltijskogo schita. Petrozavodsk, 1993. 255 p. (in Russian)
12. Kulikova V.V. and Kulikov V.S. Novye dannye ob archeyskikh peridotitovykh komatiitach Vostochnoy Karelii //DAN SSSR, 1981 V. 259, N 3. P. 693-697. (in Russian)
13. Kulikova V.V. and Kulikov V.S. Universalnaja galakticheskaja chronometricheskaja shkala. Petrozavodsk. 1997. 93 p. (in Russian)
14. Kulikova V.V., Kulikov V.S., Efremova S.V., Bichkov A.Y., Bichkova Y.V. Petrochemical series of magmatic rocks (status analysis, systematization challenges, preferred moduli chemical element, new trends) Petrozavodsk. 2001. 115 p. (in Russian).
15. Kulikova, V.V., Kulikov, V.S., and Puchtel, I.S.) Archaean greenstone belt from the South-Eastern part of the Baltic Shield. /Extended Abstracts for the Soviet-Finnish Symposium, Kostomuksha. 1991. P. 40-43.
16. Levchenkov O.A., Lobach-Zhuchenko S.B., Sergeev S.A. and Robonen V.I. Sovremennoe sostojanie geohronologicheskoy shkaly rannego dokembrija Karelii. In *Geologija i geohronologija dokembrija Vostochno-Evropeyskoy platfbrmy*. Leningrad. 1990, P. 72-80. (in Russian).
17. Marakushev A.A. Petrogenesis i rudoobrazovanie. Moscow. 1979. 262 p. (in Russian).
18. Marakushev A.A. and Bezmen N.I. Evoljucija meteoritnogo veschestva, planet i magmaticeskikh seriji. Moscow. 1983 184 p. (in Russian).
19. Milanovskiy E.E. Pul'sacii Zemli. //Geotektonika 1995. V.5. P. 3-24. (in Russian)
20. Nisbet E.G., Cheadle M.J., Arndt N.T., and Bickle M.J. Constraining the poential temperature of the Archaean mantle: A review of evidence from komatiites //Lithos. 1993 30, P. 291-307.
21. Petrograficheskiy kodex 1995. SPb, 128 p. (in Russian)
22. Puchtel I.S., Juravlev D.Z., Kulikova V.V. et al. Komatiity Vodlozerskogo bloka (Baltiyskiy schit) //Doklady Akademii Nauk SSSR. 1991a V. 317 P. 197-202. (in Russian)
23. Puchtel, I.S., Zhuravlev, D.Z., Kulikov, V.S., and Kulikova, V.V. Petrography and Sm-Nd age of a differentiated sheet of komatiitic basalt in the Vetreny belt, Baltic Shield. //Geochemistry International. 1991b, V. 28. P. 14-23.
24. Puchtel, I.S., Zhuravlev, D.Z., and Kulikova, V.V. Petrology and Sm-Nd and Pb-Pb isotope systematics of the early Archean high-magnesian metavolcanics of the Vodla Block, Baltic Shield //International Geology Review, 1993. V. 35. P. 825-839.
25. Puchtel, I.S., Hofmann, A.W., Mezger, K., Shchipansky, A.A., Kulikov, V.S., and Kulikova, V.V. Petrology of a 2.41 Ga remarkably fresh komatiitic basalt lava lake in Lion Hills, Central Vetreny Belt, Baltic Shield //Contrib. Mineral. Petrol. 1996. V. 124 P. 273-290.
26. Puchtel, I.S., Haase, K.M., Hofmann, A.W., Chauvel, C., Kulikov, V.S., Garbe-Schönberg, C.-D., and Nemchin, A.A. Petrology and geochemistry of crustally contaminated komatiitic basalts from the Vetreny Belt, southeastern Baltic Shield: Evidence for an early Proterozoic mantle plume beneath rifted Archean continental lithosphere //Geochim. Cosmochim. Acta. 1997 V. 61 P. 1205-1222.
27. Puchtel, I.S., Arndt, N.T., Hofmann, A.W., Haase, K.M., A. Kröner, Kulikov, V.S., Kulikova, V.V., Garbe-Schönberg, C.-D., and Nemchin, A.A. Petrology of mafic lavas

within the Onega plateau, central Karelia: Evidence for the 2.0 Ga plume-related continental crustal growth in the Baltic Shield //Contrib. Mineral. Petrol. 1998. V. 130 P. 134-153.

28. Puchtel, I.S., Brüggmann, G.E., and Hofmann, A.W. Precise Re-Os mineral isochron and Pb-Nd-Os isotope systematics of a mafic-ultramafic sill in the 2.0 Ga Onega plateau (Baltic Shield) //Earth Planet. Sci. Lett. 1999a. V. 170. P. 447-461.

29. Puchtel, I.S., Hofmann, A.W., Amelin, Y.V., Garbe-Schönberg, C.-D., Samsonov, A.V., and Shchipansky, A.A. Combined mantle plume-island arc model for the formation of the 2.9 Ga Sumozero-Kenozero greenstone belt, SE Baltic Shield: Isotope and trace element constraints //Geochim. Cosmochim. Acta. 1999b. V. 63. P. 3579-3595.

30. Puchtel, I.S., Brüggmann, G.E., Hofmann, A.W., Kulikov, V.S., and Kulikova, V.V. Os-isotope systematics of komatiitic basalts from the Vetreny belt, Baltic Shield: Evidence for a chondritic source of the 2.45 Ga plume //Contrib. Mineral. Petrol. 2001 V. 140. P. 588-599.

31. Semichatov M.A. Noveyshie shkaly obschego raschleneniya dokembrija: analiz. //Stratigrafija. Geologicheskaja korrelyacija. 1993. V.1: 4. P. 6-20. (in Russian)

32. Slyusarev V.D., Kulikov V.S. Geochimicheskaja evolyucia basit-ultrabazitovogo magmatizma proterozoja. Leningrad. 1973. 104 p. (in Russian)

33. Smolkin V.F. Komatiitovy i pikritovy magmatizm rannego dokembrija Baltijskogo schita. Sankt-Petersburg, 1992. 272 p. (in Russian)

34. Svetov A.P. Platformeimy bazal'tovy vulkanizm karelid Karelii. Leningrad, Nauka. 1979. 208 p. (in Russian)

35. Svetov S.A. Komatiit-toleitovyje asociacii Vedlozersko-Segozerskogo zelenokamennogo poyasa Centralnoj Karelii. Petrozavodsk. 1997. 172 p. (in Russian)

36. Usckov V.V. Kimozerskoe projavlenie almazonosnyh kimberlitov v Onezhskoy strukture. In: Geologija i polesnye iskopaemyh Karelii. Petrozavodsk. 2001. P. 94-98. (in Russian)

37. Vrevsky A.B. Arheyskiy suprakrustal'nyj pojas Polmos-Poros: Petrologija, etapy razvitija. Tests dis. kand.geol.-mineral.nauk., Leningrad. 1983 (in Russian)

38. Vulkanizm arheyskih zelenokamennyh pojasov Karelii Leningrad. 1981 152 p. (in Russian)

39. Yasamanov N.A. Opyt postroeniya shkaly geologicheskogo vremeni //Doklady Rossijskoi Akademii Nauk, 1993 V. 328. P. 487-489. (in Russian).

LATE CRETACEOUS - CENOZOIC BASALTIC VOLCANISM OF SOUTH KOREA

Yu.A Martynov¹ and Dong-Woo Lee.²

¹*Kongju National University, Department of Geoenvironmental Sciences, Kongju 314-701, Korea; Email: cdpil@knu.kongju.ac.kr*

²*Far East Geological Institute of Far East Branch, Russian Academy of Sciences 159, pr. Stoletiya Vladivostoka, Vladivostok, 690022, Russia; Email: martynov@fegi.ru*

Based on available geological and geochemical information on the Late Cretaceous to Cenozoic magmatism of the Korean Peninsula, a regular change in geochemical signatures of the basaltic magmas from the typical subduction-related (in Late Cretaceous time) to the typical within-plate ones (in Quaternary time) is shown. The data obtained suggest that there existed two main basaltoid magma sources pertaining to subduction and to within-plate processes. According to geochemical and isotopic evidence, the within plate source was located in the heterogeneous subcontinental lithosphere and determined the composition of basalts of various age. The proportion of the subduction component in magma generation abruptly reduced at the boundary of the Cenozoic. This combined with change in character of volcanism from essentially felsic to essentially mafic as well as a migration of the volcanic activity toward the east and northeast of the peninsula afford ground for suggestion that in the Early Paleogene the style of tectonic environment in this area became different, subduction was completed and rifting was starting to develop. Allowing for the previously published literature on the East Sikhote-Alin volcanic belt, our data are suggestive of a necessary correction for all current concepts on the tectonic evolution of the Eurasian continental margin in the Cenozoic, timing and mechanism of the Japan Sea opening.

INTRODUCTION

The detailed geological and petrological studies of the East Sikhote-Alin volcanic belt carried out during the last decades [18, 11, 12, et al.] suggest that the present views on the geodynamic evolution of the eastern Eurasia margin in Cenozoic time, including timing of the subduction cessation and opening of the Japan Sea as well as the cause and magma sources of the basaltic volcanism should be corrected. To understand these problems, the data on geology and geochemistry of volcanogenic sequences of the Korean Peninsula whose geological setting in the Late Mesozoic and Cenozoic was in many respects similar to those in the East Sikhote-Alin region are of great importance. Beginning in the 1980s, the careful geological investigations of both the northern [6, 1-4] and southern [13-17, 24 - 35] parts of the Korean Peninsula have been carrying out. However, the results obtained were primarily published in the local scientific papers and are little known to a foreign reader.

The purpose of the present paper is to examine crucially and summarise the published geological and geochemical information on Late Cretaceous to Cenozoic magmatism of the Korean Peninsula, with attempt to solve some controversial points regarding petrogenesis and geodynamic regime. The main attention is focused on the basaltic volcanism, as the most informative field of geology in solving problems of magmatic sources and geodynamics.

GEOLOGICAL CHARACTERISTICS OF MESOZOIC TO CENOZOIC VOLCANOGENIC SEQUENCES OF THE KOREAN PENINSULA

Since the Middle Jurassic (180 - 155 Ma), after the collision of the Sino-Korean, Sobaeksan-Hida, and Honshu continental blocks, the Korean Peninsula was a stable craton that has not been subjected to pronounced rotational or spatial displacements [20, 12, 17, et al.]. Most of the peninsula belongs to the Sino-Korean platform, only the northeastern and northwestern its parts are incorporated into the Sikhote-Alin and Catasiatic fold belts, respectively [5]. Volcanic activity within the peninsula is traced from the Late Jurassic (about 135 Ma), when, with the beginning of subduction of the oceanic Kula plate beneath Eurasian continent, the Late Jurassic -Early Cretaceous volcanic belt of North Korea was developed [4]. In Early Cretaceous time, the oblique subduction resulted in breaking of the volcanic structure, a displacement of its separate fragments and formation of a series of syn-strike-slip basins, including the Gyongsang basin [17].

In Late Cretaceous time, with the beginning of subduction of the Pacific oceanic plate, the South Korea - Japanese volcanic belt formed in the southern part of the Korean Peninsula. This belt is considered as a segment in the chain of continent-marginal volcanic belts extending along the east margin of Eurasia. The occurrences of the Late Cretaceous effusives are known in the southeastern portion of the peninsula. Its K-Ar age ranges from 79 to 57 Ma, the youngest volcanites occurring in the southmost part of the basin [5]. The lower part of the volcanic section is composed of basaltic lava and agglomeratic tuff that are underlain and overlain by tuffogenic argillite [10]. More upper sequence consists of basalts and andesibasalts that are overlain by chemically mafic volcanogenic conglomerates and agglomeratic tuffs. The uppermost part of this section is made up of andesitic, and toward the top, of dacitic and rhyolitic volcanic rocks. The total thickness of the Late Cretaceous volcanogenic sequence is 2,000 meters [24], with the thickness of the felsic constituent between 1,000 and 1,500 meters.

The formation of volcanic rocks in a regular succession from mafic to felsic effusives and the predominance of the latter over mafic volcanites are among the typical peculiarities of the Late Cretaceous volcanism. While, in individual cases, for instance, within the Chugaryong rift valley (the central part of the Korean Peninsula), green tuffs, tuff breccia, andesites, tholeiitic and alkaline basalts dominate [15].

Eocene volcanic rocks are of limited occurrence (Fig. 1). They are mainly found within the Kilchu-Myongchon rift graben in the northeast of the peninsula [1] as well as in the Pohang basin in the southeast [5]. In the Kilchu-Myongchon rift graben, the bottom of the Late Paleogene section is represented by the relatively thin (up to 150 m thick) bed of coal-bearing terrigenous deposits containing Late Eocene -Oligocene flora [1]. The higher level of the section is made up of volcanogenic sequence of about 1000 m thick which is conformable on the underlying bed. Effusive facies are composed of massive lava flows in the lower part of the volcanogenic sequence and of amygdaloidal, with a minor amount of pyroclastics, in its upper part. Basalts prevail, but toward the top, plagiophyric andesibasalts are found also.

Within the Pohang basin, the Middle Eocene stage of volcanism (46-44 Ma) includes basaltic lava flows and north-east trending dykes of mafic composition [24].

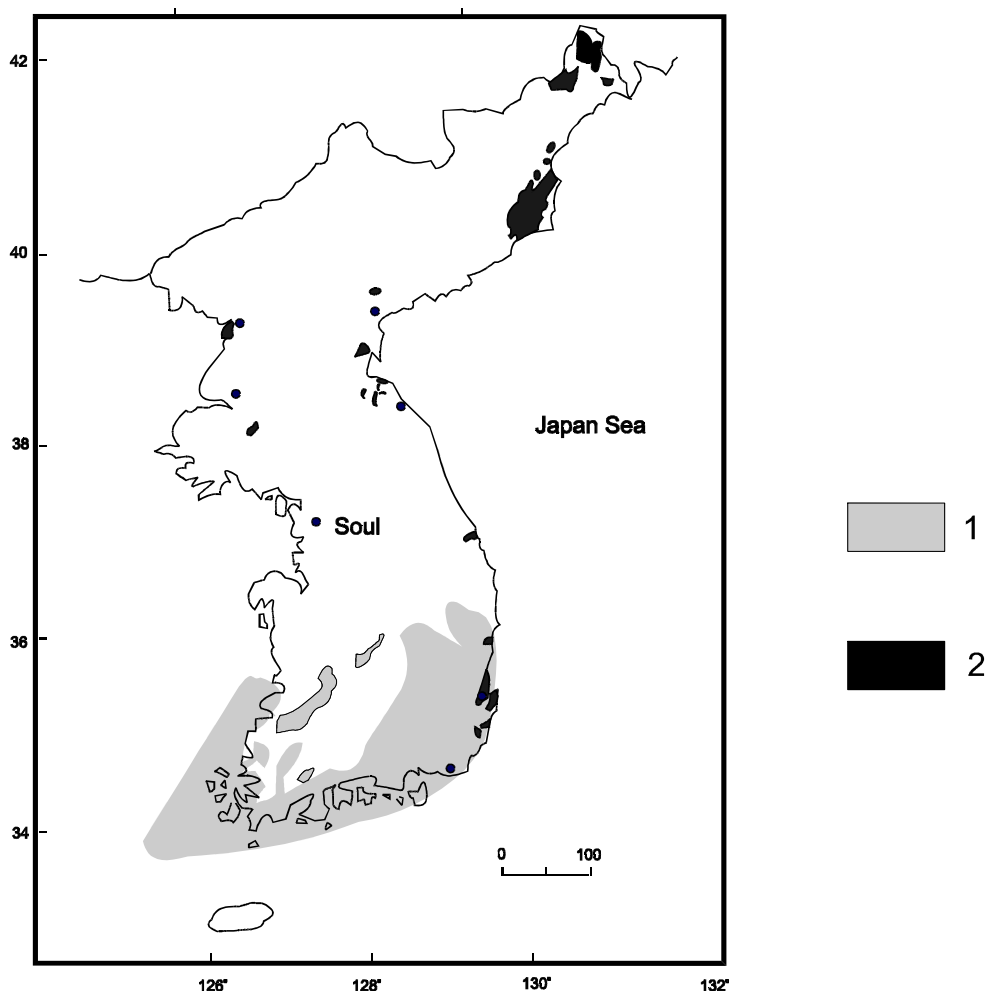


Fig. 1. Location scheme of (1) Late Cretaceous and (2) Paleogene-to-Miocene volcanic rocks in Korea. After [5], with the small supplements.

Up to the Early Miocene, a lull in volcanic activity occurred in the area. The Early Miocene effusives are mainly found in the Kilchu-Myongchon rift graben, at some places of North Korea (the Pectusan, Voisan, Anjuice, Charien areas) as well

as in the southern part of the Korean Peninsula (the Pohang, Zhangji and other basins) [1, 28].

In the central part of the Pectusan area the fragments of the Miocene section (12-20 Ma), 40-50 m in thickness, are represented by the alternating basaltic lava flows and agglomeratic mafic tuffs [1]. The middle part of the section (30-40 m) is largely composed of bedded terrigenous-tuffaceous deposits with less common basaltic flows. The Miocene section is completed by mafic lavas (20-30 m thick) represented by its amygdaloidal, fine-porphyrific to subaphyric varieties with the dominant plagioclase phenocrysts.

In the southeast part of the peninsula, the Miocene volcanic rocks are found in the Pohang basin [24, 26]. They are composed of extrusive andesites and dacitic flows that are dated at 23 to 21 Ma and are characterized by intercalation with terrestrial clastic rocks [26]. The overlying deposits consist of marine and terrestrial sediments alternating with sparse mafic and felsic lava flows. The K-Ar age of basalts is in the range of 21 - 18 Ma. This section is completed with marine sedimentary rocks which are overlain by basalts with absolute age of 13.6 - 15.2 Ma and cut by felsic dykes [28].

The character of these basalts section is somewhat different from place to place owing to changing voluminous proportions in tuff and lava facies.

The final stage of the volcanism on the Korean Peninsula began in the Pliocene [6, 1, 5]. The volcanic activity continued over the whole Quaternary period. Its recent occurrences were recorded in the vicinity of the Pectusan mount and the Cheju Island. Relatively small volcanic fields made up by young basalts are met throughout the peninsula. The study of young basalts areas indicates that there occurred eruptions of central type, but, within the Chugaryong rift valley as well as in the Kilchu-Myongchon rift graben, the signs of fissure type eruption are present [5]. The special feature of the Quaternary basalts is a predominance of lava facies over pyroclastics, essential variations in its compositions which are mainly alkaline. Discrete sections differ structurally and in thickness. In the north-east of the peninsula, the Pliocene - Quaternary volcanic complex is represented by bimodal assemblage consisted of basalt, andesibasalt, trachyte, trachyrhyolite with some variations in the voluminous proportions of felsic and mafic volcanics in the different structures [1]. To illustrate, within the Pectusan area, the predominant rocks are basalts which make up lava plateau, whereas, within the Kilchu-Myongchon rift graben, the bulk of the Quaternary section is composed of alkaline persilicic rocks which are overlain, and locally, underlain by basalt flows.

In the south part of the peninsula, the Quaternary effisives were examined in detail within the Chugaryong Rift Valley and on the Cheju Island. In the former case, volcanites of a K-Ar age of 0.27 Ma form a narrow and extended (up to 95 km) lava plateau that is considered as the result of filling with the lava material of the ancient the Khantan River valley [30]. An average thickness of the section made up only of basalt ranges from 10 to 40 m. Their thickness increases slightly

with approaching a volcanic activity centre. In the Cheju area, the section of the Quaternary effusives (0.9 - 0.035 Ma) is characterized by lava facies predominance over pyroclastic material.

THE BRIEF CHARACTERISATION OF PETROLOGICAL FEATURES

According to main petrochemical (low titanium dioxide contents and high contents of alumina) and geochemical (enrichment in large-ion lithophile elements (LILE) and depletion in high field strength elements (HFSE) characteristics, the Late Cretaceous volcanogenic formations of the Korean Peninsula belong to high-potassium calc-alkaline series [7, 13, 33, et al.]. The characteristic feature of rocks under discussion is weak negative Eu anomaly. Basalts located in lower parts of the section have high Sr concentration and low content of magnesium. The values of Sr^{87} / Sr^{86} ratios range from 0.7054 to 0.7062 [35]. The significant ranges in $\delta^{18}O$ values (from 3.1 to 7.6 ‰) in andesites are interpreted to be the result of meteoric water effect on oxygen isotope composition [13].

Basalts of Eocene age are relatively depleted in TiO_2 (0.7 - 1.3 wt. %) and enriched in Al_2O_3 (17 - 21wt. %). Hence, they may be classified as orogenic series. Total alkalis make possible to consider these basalts as transitional varieties between alkaline and calc-alkaline series, whereas high K_2O content (2.5-3.5 %) and K_2O / Na_2O ratios in range of 0.8-1.1 suggest that they are shoshonite [1]. High ratios between light rare earth elements and heavy rare earth elements (LREE/HREE), higher LILE contents, together with a high-charged cations deficiency ($Ba/Nb=270 - 280$; $La/Nb=6.7 - 7.0$), provide evidence in support of the last-named proposition. The pronounced Nb anomaly is typical of the multicomponent diagram normalised to MOR basalt [1].

From TiO_2 contents (1.2 - 1.7 %), the Early Miocene basalts of the Pectusan area hold an intermediate position between the orogenic and within plate series [1]. Basalts and andesibasalts are characterized by a high alkalinity in which Na dominates in content ($K_2O / Na_2O = 0.4 - 0.8$). In comparison with the Paleogene basaltoids, LILE enrichment and the higher contents ($Ba/Nb=37 - 47$; $La/Nb=2.1 - 2.7$) of high fusible elements (HFSE) are the characteristic features of the Early Miocene basalts. The absolute REE contents and LREE/HREE ratios are relatively high ($La_N / Sm_N = 2.3 - 3.3$). In the Pohang basin located in the southeast part of the Korean Peninsula, the Early Miocene basalts are represented by toleites among which the olivine, olivine-augite, and olivine-titanaugite varieties have been identified [26]. According total alkalinity, these basalts are classified as high alkaline toleitic series. Although the contents of TiO_2 and P_2O_5 are higher than those in island-arc-related tholeiites, they show the similarity with the latter in enrichment in LILE and depletion in HFSE. The negative Eu anomaly suggests that the plagioclase fractionation took place. $^{87}Sr / ^{86}Sr$ and $^{143}Nd / ^{144}Nd$ ratios range from 0.70385 to 0.70463 and from 0.512843 to 0.512845, respectively [26]. The

Late Neogene to Quaternary basalts known in the northeast part of the Korean Peninsula are represented by the titanium dioxide-rich varieties. They involve toleitic and alkaline lavas characterised by some differences in contents of incompatible elements and in LREE/HREE ratios. The toleitic basalts exhibit relatively high HFSE contents, whereas the alkaline and subalkaline varieties display a small Nb deficiency [1].

According to geochemical signatures, the volcanites developed in the south of the peninsula are belonging to toleitic and alkaline series, the first-named prevailing [34]. The alkaline lavas range compositionally from alkaline basalt, hawaiite, mugearite to trachyte and again to mugearite in the upper parts of the section [20, 16]. The toleitic and alkaline basalts are geochemically close to within-plate lavas [32].

GEOCHEMICAL INDICATORS OF MAGMATIC SOURCES OF BASALTIC MAGMAS

Petrogenesis problems of the Late Cretaceous to Cenozoic volcanic formations of Korea were described in detail by A. Pouclet with the co-authors [24]. Analysis of the radioisotopes distribution enables these authors to conclude that there existed three main magmatic sources: (1) depleted magma source (DMM) and two enriched ones - (2) EM I and (3) EM II. The origin of the Late Cretaceous to Miocene high alumina basalts and of the Pliocene to Quaternary within-plate lavas are considered as the result of mixing of DMM and EM II isotopic components and DMM and EM I isotopic components, respectively. DMM source is related to asthenospheric mantle and EM I and EM II sources are associated with various levels of heterogeneous subcontinental lithosphere reworked by subduction processes predated the Late Cretaceous subduction.

This investigation technique is widely used in geochemical researches to solve the problem of petrogenesis. But it is not quite workable approach, as the long-lived radioisotopes do not register or poorly register the relatively young subduction processes. In French scientists' model [24], for example, there is no place for Late Cretaceous subduction, though it, undoubtedly, played the important role in magmagenesis and formation of the structural pattern on the Korean Peninsula, at least, during Late Cretaceous time. This paper concerns the problem of magmatic sources of basaltoid magmas from the viewpoint of trace element abundance in volcanic rocks of Korea.

Numerous geological and geochemical data on the Late Cretaceous volcanogenic formations of the southern part of the Korean Peninsula are indicative of its relation to subduction process. Regarding basaltic effusives, among the geochemical signatures are its higher alumina contents, low FeO (table 1, Fig. 2), TiO₂, Nb contents, low Ti/V and Ni/Co ratios (Fig. 3). It is important to point out that though the formation of the basalts occurred within the continental crust, they are compositionally similar to high alumina basalts of recent mature island arcs.

Table

Major (wt %) and trace (ppm) element analysis of representative Cenozoic basaltic samples from Korea and East Sikhote-Alin

#	K-2	K-1	YB25	62	155/1B	37/2	K-3	19	307/7	K-4a	K-4b
Age (Ma)	73.1	100	65	54.81	31.45	-	45.3	21.1	-	19.5	18.5
	1	2	3	4	5	6	7	8	9	10	11
SiO ₂	50.01	50.66	54.68	53.75	50.13	50.38	53.29	49.65	53.46	50.06	49.38
TiO ₂	1.03	0.98	1.03	1.33	1.37	1.12	1.13	0.86	1.37	1.43	1.66
Al ₂ O ₃	16.72	16	17.15	17.83	17.74	17.28	15.72	18.61	18.20	18.94	14.91
Fe ₂ O ₃	1.2	0.93	8.62	-	3.36	1.57	0.97	-	1.1	1.13	1.45
FeO	7.98	6.21	0	7.34*	5.89	8.00	6.44	9.39*	5.60	7.54	9.66
MnO	0.15	0.12	0.16	0.14	0.17	0.17	0.14	0.19	0.13	0.15	0.18
MgO	6.5	7.03	3.84	3.72	5.65	4.67	6.44	5.9	4.59	4	4.75
CaO	4.94	6.57	8.41	8.05	9.2	7.44	5.35	11.29	6.4	9.54	9.13
Na ₂ O	4.11	3.91	3.52	3.86	3.69	3.20	3.89	2.52	4.12	3.47	3.13
K ₂ O	2.21	3.04	1.14	1.83	1.25	3.51	2.32	0.82	2.34	0.87	1.07
P ₂ O ₅	0.18	0.47	0.21	0.48	-	0.44	0.36	0.17	0.52	0.31	0.34
LOI	3.55	3.34	-	-	0.36	0.84	3.79	-	1.1	1.71	3.16
Cr	239	163	53.2	63	75	-	-	59	-	76	77
Ni	51	26	18.2	55	70	-	70	26	102	53	52
Co	42	45	-	28	39	-	-	33	-	62	77
V	174	177	309	145	158	-	-	279	-	256	319
Rb	53	75	38	48.9	35	155	82.9	16	45	18	22
Ba	825	597	337	573	-	850	677	203	-	228	265
Sr	1092	737	515	769	597	612	938	594	630	529	394
Nb	8	7	3.9	15.4	15	3	11.7	2	20	7	7.5
Hf	-	-	3.3	-	-	-	-	-	-	-	-
Zr	145	169	65	235	118	154	218	54	232	137	142
Y	25	23	23.7	26.4	30	-	27	27	36	29	35
Th	5.5	6	4.2	-	-	-	5.7	-	-	1.7	2
U	0.6	0.8	1	-	-	-	-	-	-	0.5	0.6
La	21.9	31.3	15.9	-	17.4	20	31.2	-	54	12.2	13.5
Ce	52.7	65.6	36.7	-	40	52	67.3	17.5	124	30.9	36.4
Nd	28.3	28.8	19.7	-	-	29	38.4	11.4	57	18.4	20.1
Sm	6.3	6	4.4	-	-	5.4	6.7	3	11	4.7	5.5
Eu	1.7	1.7	1.41	-	1	1.2	1.9	-	2.5	1.6	1.8
Gd	6.4	4.4	4.66	-	-	4.7	6.8	-	7.5	4.3	5
Dy	5.6	3.5	4.63	-	-	-	5.1	-	-	4.3	5
Er	2.1	2	2.54	-	-	1.4	2	-	3.6	2.4	2.7
Yb	2	2	2.29	-	2.7	-	2	-	2.6	2.5	2.9
Lu	0.3	0.3	0.33	-	0.41	-	0.3	-	-	0.3	0.4
⁸⁷ Sr/ ⁸⁶ Sr	0.71172	0.70948	0.70510	-	0.70389	-	0.70455	0.70336	-	0.70430	0.70436
¹⁴³ Nd/ ¹⁴⁴ Nd	0.51216	0.51270	-	-	0.51284	-	0.51272	0.51291	-	0.05128	-

Table: continued

3	1120	68	221	48	CB-10	25-4	KW-17	K-62b*
Age (Ma)	6.43	6.84	-	-	0.27	-	-	-
	12	13	14	15	16	17	18	19
SiO ₂	51.8	49.88	46.09	50.09	48.67	49.75	52.18	51.88
TiO ₂	1.77	2.12	1.31	2.34	1.92	3.11	1.77	2.05
Al ₂ O ₃	17.2	17.68	16.8	16.05	15.68	16.4	14.62	13.92
Fe ₂ O ₃	2.14	7.2	1.55	1.77	-	13.08**	-	1.49
FeO	8.02	3.51	7.89	9.05	11.46*	-	12.04*	9.92
MnO	0.15	0.14	0.15	0.16	0.16	0.14	0.15	0.15
MgO	7.8	3.22	7.38	4.96	8.73	4.07	8.52	6.12
CaO	6.52	6.39	11.22	8.69	8.14	7.45	7.03	8.16
Na ₂ O	2.87	4.15	3.21	3.63	2.65	3.85	2.58	3.25
K ₂ O	1.3	2.23	0.15	1.67	1.71	1.49	0.35	1.02
P ₂ O ₅	0.47	0.74	0.16	0.58	0.54	0.65	0.18	0.36
LOI	0.07	2.47	3.66	-	0.01	0.53	0.07	0.3
Cr	123	47	-	-	227	9	219	199
Ni	95	-	176	85	177	20	211	160
Co	45	-	-	-	80	-	-	66
V	140	-	-	-	-	-	-	188
Rb	27	94	5	27	20	26	8	28
Ba	355	953	122	-	282	484	161	243
Sr	558	1409	249	572	558	578	311	324
Nb	-	-	6	11	31	39	28.67	39.3
Hf	2.77	5.1	-	-	3.74	5.48	2.23	0
Zr	102	-	99	119	173	238	37	167
Y	-	-	25	17	27	29	23	25
Th	-	-	-	-	3.01	4.73	1.84	3.1
U	-	-	-	-	-	0.98	0.35	0.9
La	14.2	38.9	5	24	22.7	39.14	11.75	18.7
Ce	28.5	62.9	14	55	46.59	68.45	25	42.5
Nd	17.9	27.5	-	29	22.74	40.01	14.76	25.2
Sm	5.28	5.8	3.5	5.8	5.35	9.28	4.13	6.5
Eu	1.84	2.32	1	2.5	1.74	3.04	1.4	2.2
Gd	5.3	4.3	-	5	5.91	9.36	4.8	6.5
Dy	-	-	-	-	-	7.27	4.27	4.6
Er	-	-	-	1.2	0.75	3.28	2.06	1.8
Yb	2.01	1.7	-	-	2.27	2.76	1.64	1.6
Lu	-	-	-	-	0.25	0.36	0.19	0.2
⁸⁷ Sr/ ⁸⁶ Sr	0.70385	0.70380	-	-	-	-	-	0.704583
¹⁴³ Nd/ ¹⁴⁴ Nd	0.51282	0.51273	-	-	-	-	-	-

* - the total Fe as a FeO; ** - the total Fe as a Fe₂O₃.

1-3 – Late Cretaceous basalts of the southern part from the Korean peninsula [24, 16]; 4-7 – Paleogene basalts: 4 - East Sikhote-Alin (unpublished data of Martynov Yu.A.); 5 – Earst Sikhote-Alin, the northern part [3]; 6 – the northern part of the Korean peninsula [6]; 7 – the southern part of the Korean peninsula [24]; 8-11 – Early Miocene basalts: 8 – Earst Sikhote-Alin, the central part (unpublished data of Martynov Yu.A); 9 – the northern part of the Korean peninsula [6]; 10, 11 - the southern part of the Korean peninsula [24]; 12-19 – Quaternary basalts: 12 – Earst Sikhote-Alin, Samarga river [3]; 13 – Earst Sikhote-Alin, Sovgavan plato [3]; 14, 15 – the northern part of the Korean peninsula [6]; 16- the southern part of the Korean peninsula [30]. 17 –19 – Cheiju island [18, 34, 24].

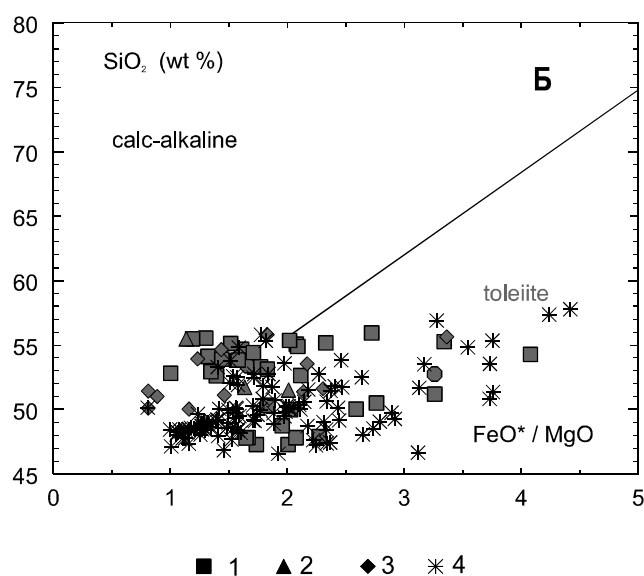
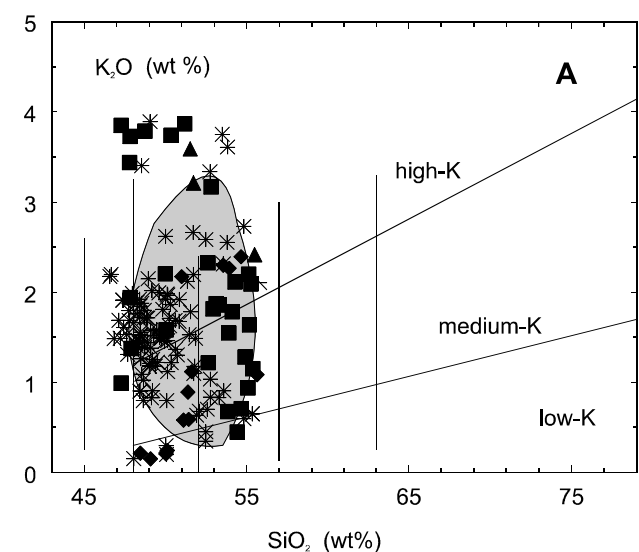


Fig. 2. Discriminant diagrams $K_2O - SiO_2$ and $SiO_2 - FeO^*/FeO$ for volcanites of the the Korean Peninsula.

1 - Late Cretaceous; 2 - Paleogene; 3 - Early Miocene; 4 - Quaternary.

Filled field - compositions of Paleogene-Early Miocene high-alumina basalts in the Sikhote-Alin region, after [19]. Data used in diagram are taken from: [1, 7, 13, 14, 16, 21, 24, 26, 28, 30, 32, 34].

Change in volcanism style from predominantly felsic to essentially mafic one and the displacement of the volcanic activity toward the north-east and east (Fig.1) were associated with a regular change in geochemical signatures of basalts. The first who have paid attention to this fact were A.V. Fedorchuk and N.I. Filatova [1]. The Paleogene alumina-rich basalts differ from the Late Cretaceous basalts by lower radiogenic strontium content (Fig. 4). The Early Miocene basaltic lavas display also higher contents of Nb, Ti and a number of other trace

elements. In such situation, most of data for these basaltic rocks plot between the field for the Late Cretaceous subduction-related and for Quaternary within-plate lavas in the discrimination diagrams (Fig.2, 3). Besides, the Late Miocene lavas display a specific EM I isotopic signature which is typical of within-plate basaltic series of China, Korea and the East Sikhote-Alin region. The Quaternary alkaline and toleitic volcanics of the Korean Peninsula correspond to typical volcanites of within plate geochemical series [32] characterised by significant variations in total alkalis content, higher FeO contents (Fig. 2), high HFSE abundances, and high Ni/Co, Ti/V (Fig. 3) La/Th, La/Ba ratios. The Korean Peninsula volcanics are peculiar by marked enrichment in LILE and their specific EM I isotopic signature. The same geochemical features are typical of within-plate basaltic series in active continental margins, in particular, within the East Sikhote-Alin volcanic

belt [19], thus indicating an involvement of subcontinental lithosphere metasomatized during anterior subduction process in melting.

The regular change in geochemical signatures of the Korean Peninsula basaltic rocks from typical of subduction-related basalts to typical of within plate ones during Cenozoic period suggests that two main magmatic sources – subduction-related and of within-plate nature - were involved in the generation of these rocks. The within-plate source was of decisive importance for composition of basaltic magmas as of various ages. This assertion has been substantiated by the resemblance of elemental patterns and the similarity of normalized concentrations of incompatible elements in the multicomponent diagrams (Fig. 5) as well as by close isotope

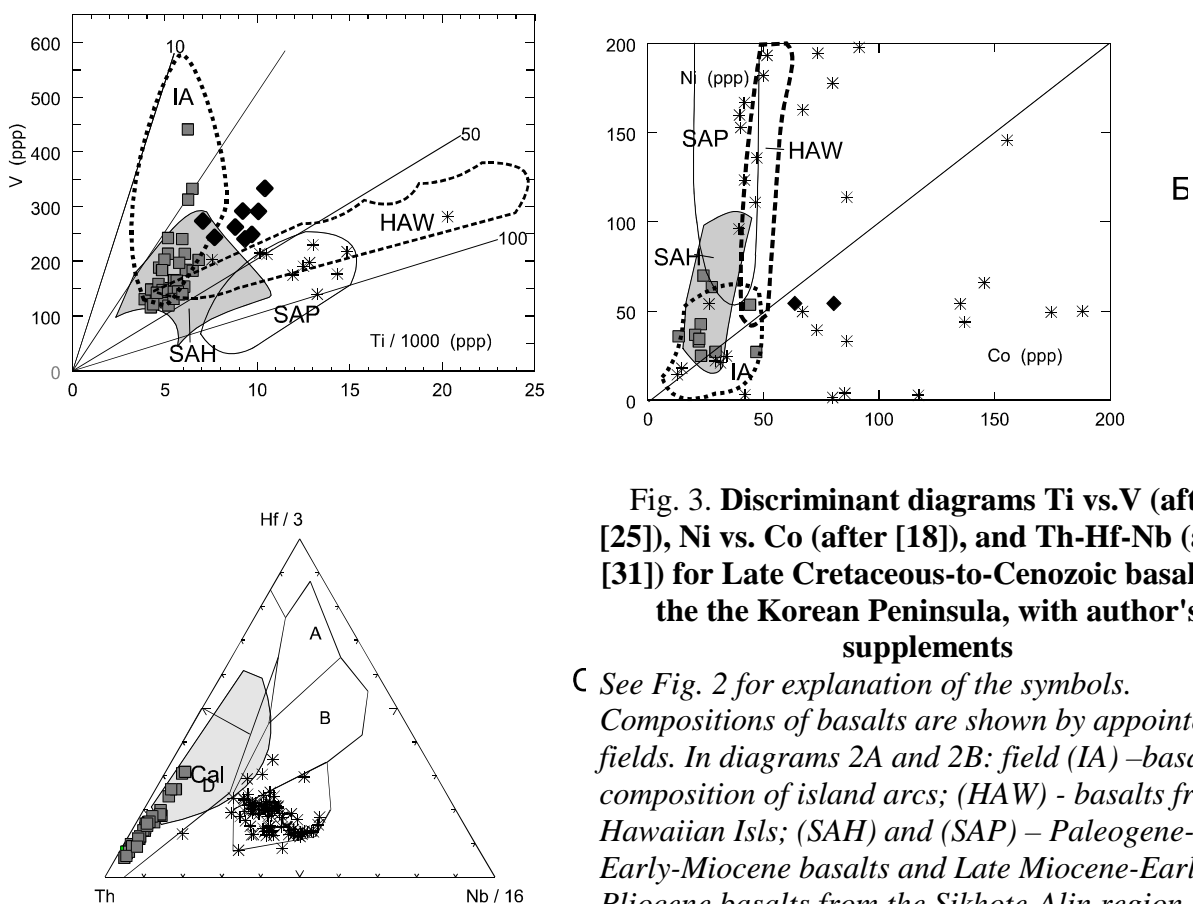


Fig. 3. Discriminant diagrams Ti vs.V (after [25]), Ni vs. Co (after [18]), and Th-Hf-Nb (after [31]) for Late Cretaceous-to-Cenozoic basalts of the the Korean Peninsula, with author's supplements

C See Fig. 2 for explanation of the symbols. Compositions of basalts are shown by appointed fields. In diagrams 2A and 2B: field (IA) –basalts composition of island arcs; (HAW) - basalts from Hawaiian Isls; (SAH) and (SAP) – Paleogene-Early-Miocene basalts and Late Miocene-Early Pliocene basalts from the Sikhote-Alin region, respectively. In diagram 2C: (A) – basalts from midocean ridges; (B) - basalts from midocean ridges and within-plate environments; (C) - - basalts from within-plate environments; (D) – basalts from island arcs and active continental margins.

Data used in diagram are taken from: [19, 1, 7, 13, 16, 21, 24, 30, 32, 34].

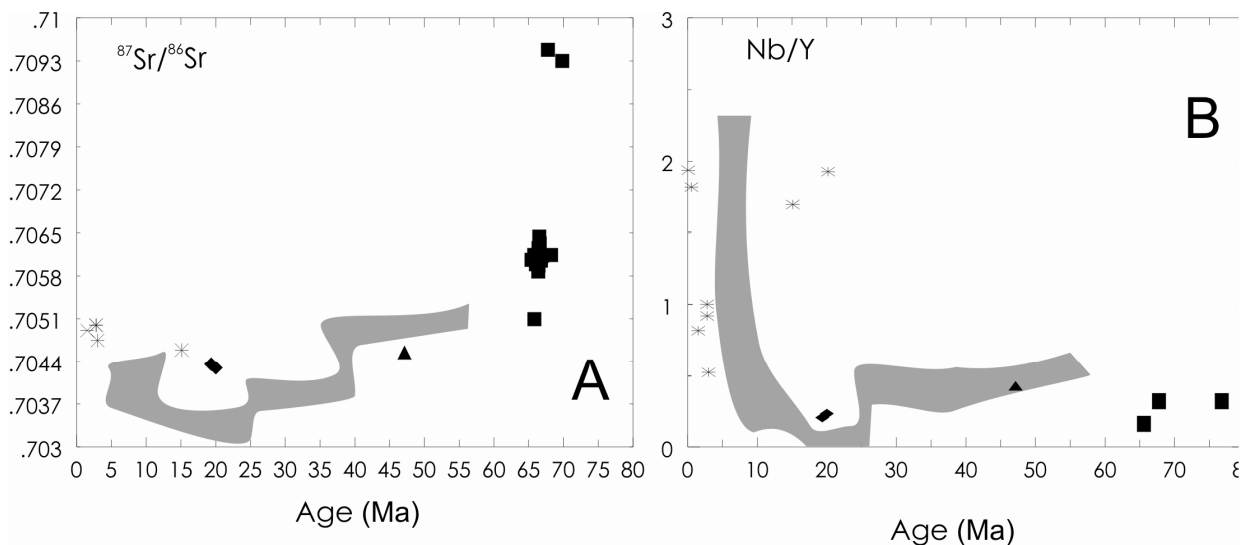


Fig. 4. Variations in isotopic (A) and geochemical (B) characteristics of the Korean Peninsula basalts relative to timing of its eruption.

See Fig. 2 for explanation of the symbols.

Filled field represents the range of compositions for Cenozoic high-alumina and within-plate basalts from the East Sikhote-Alin region, after [3]. Data used in diagram are taken from: [24, 35].

composition for rocks of all types, except Late Cretaceous rocks (Fig. 4). High radiogenic strontium content and the relationships between very highly incompatible (VHI), highly incompatible (HI), and moderately incompatible (MI) elements in the normalized diagrams (“VHI \gg HI \geq MI” is typical of Late Cretaceous lavas and “VHI $>$ HI $>$ MI” is typical of Cenozoic lavas) suggest that the above mentioned source was more enriched in radiogenic isotopes and in incompatible elements than enriched mantle in midocean ridges (FMM) [23]. These data, together with specific EM I isotopic signature and relatively high concentration of LILE in the Quaternary within-plate lavas, indicate that the within-plate source was located within subcontinental lithosphere.

The relatively low normalized concentrations of Nb and Zr in the Late Cretaceous subduction-related basalts (Fig. 5) are indicative of comparatively high degree of subcontinental mantle melting. When coupled with information on the peculiarities in distribution of a number of trace elements and radioisotopes this will allow us to assume the fluid nature of the subduction component. Figure 6 shows the correlation between trace element concentration ratios and bulk partition coefficients for basalts of various ages. For lack of fractionation among such elements in simple magmatic systems, it is evident that their proportions should be constant in the rocks formed under melting of a single source material. The Korean basalts of various age display about the same ratios of incompatible elements (La/Ce, Sm/Zr, Hf/Zr, Yb/Y) which were immobile in the presence of aqueous fluid. This is considered as supplementary verification of the proposal that there existed common magmatic source for all rock types. Compared to the younger

lavas, the Late Cretaceous subduction-related volcanics are characterized by relatively low values of TiO_2/Eu , $\text{Nb}/\text{K}_2\text{O}$ ratios.

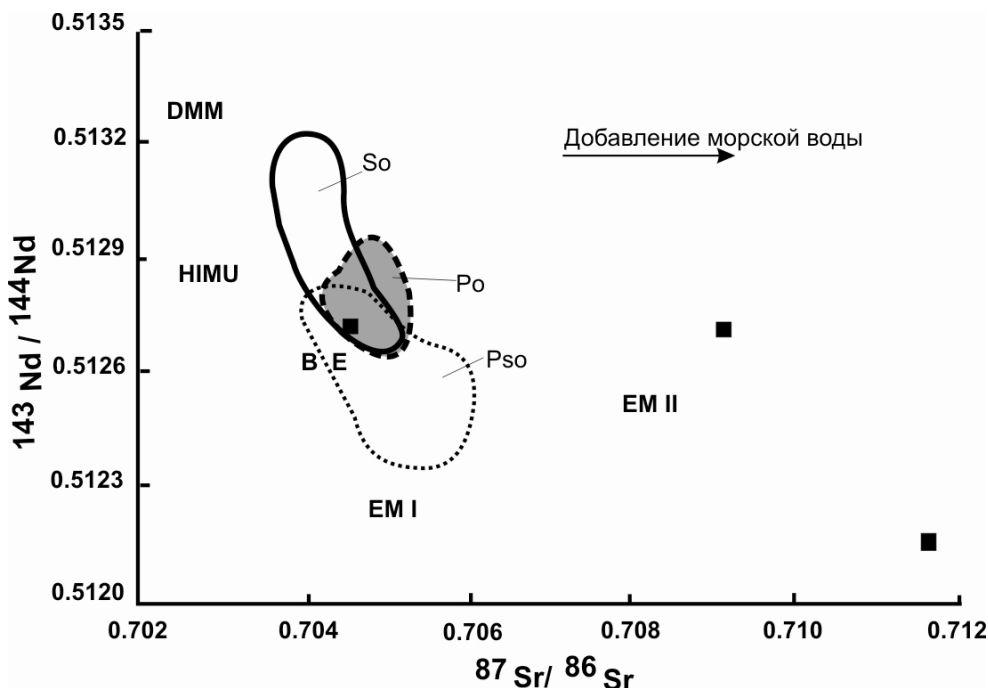


Fig. 5. Correlation of Sr and Nd isotopes in Late Cretaceous basalts of Korea (filled squares).

Fields represent the range of isotope compositions for basalts of different age in the Sea-of-Japan region: Po = Paleogene basalts, predated to opening of the Japan Sea; So = Miocene basalts, synchronous with opening of the Japan Sea; Pso = Late Miocene-to-Quaternary basalts postdated opening of the Japan Sea. After [24], simplified version.

Having the similar bulk partition coefficients in “dry” systems, niobium and potassium behave variously in the presence of aqueous fluid. Potassium and other large-ion lithophile elements are readily extracted by fluid phase, whereas niobium remains relatively immobile under these conditions [22, 23]. The determining factor in Ti behaviour is redox potential that, in its turn, depends upon amounts of water in the system. Expanding of crystallization field for water-containing minerals (primarily for amphibole) as well as for titanomagnetite produce a buffer effect on Ti content. As a consequence, a melt formed during melting of water-saturated and metasomatized mantle should be enriched in potassium and large-ion lithophile elements and depleted in Ti. Anomalous values of radiogenic strontium in the Late Cretaceous subduction-related volcanics which do not correlate to either immobile incompatible elements ratios (Fig. 4) or to ratios of Nd isotope (Fig. 7) are indicative of the fluid nature of the subduction component. It is believed in connection with this that sharp decrease in $^{87}\text{Sr}/^{86}\text{Sr}$ ratios in basalts at the boundary of Cenozoic time is testimony to a contraction of the proportion of the subduction component in basaltic magmogenesis.

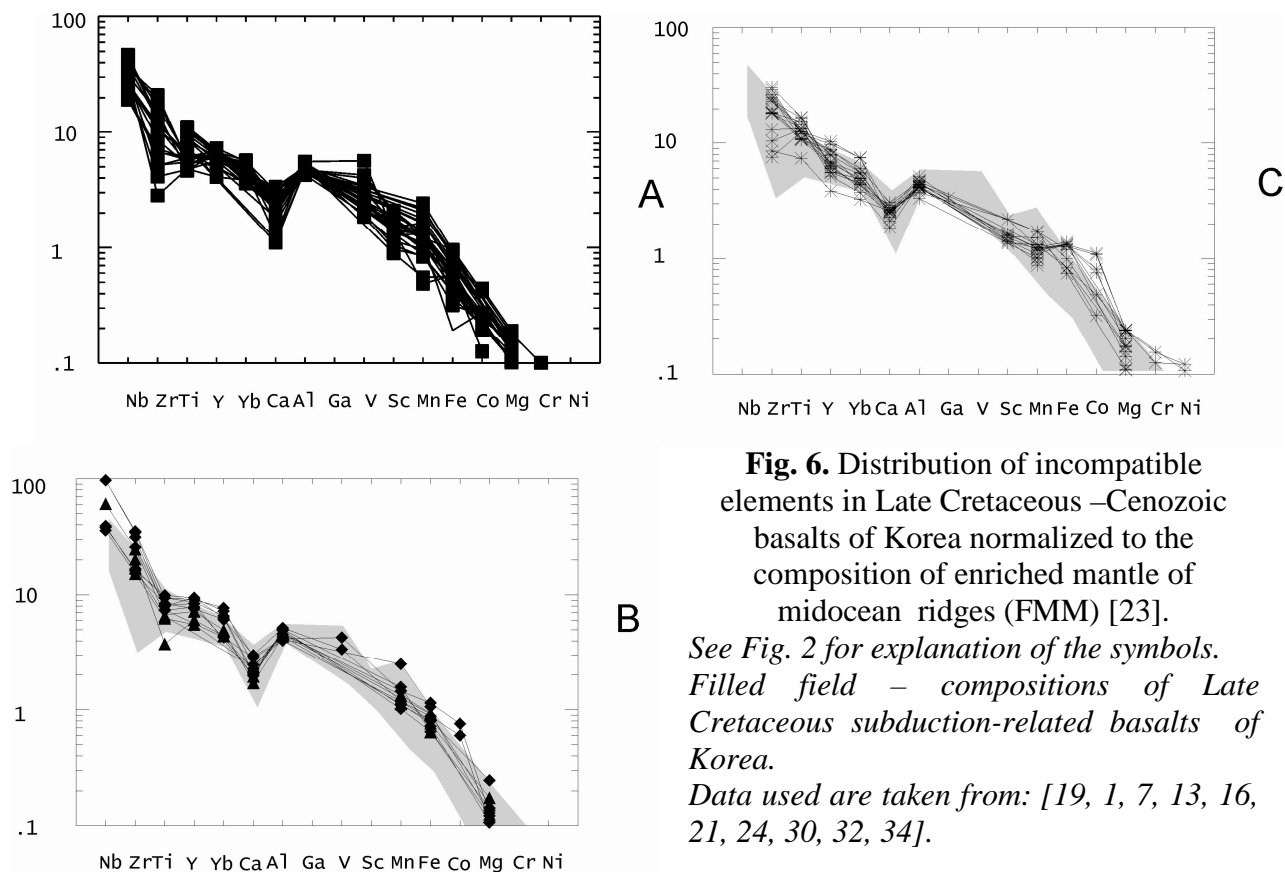


Fig. 6. Distribution of incompatible elements in Late Cretaceous –Cenozoic basalts of Korea normalized to the composition of enriched mantle of midocean ridges (FMM) [23].

See Fig. 2 for explanation of the symbols. Filled field – compositions of Late Cretaceous subduction-related basalts of Korea. Data used are taken from: [19, 1, 7, 13, 16, 21, 24, 30, 32, 34].

GEODYNAMIC ASPECTS OF THE CENOZOIC BASALTIC VOLCANISM AT THE EURASIAN CONTINENTAL MARGIN

The most important result of tectonic resetting of the Eurasian margin in Cenozoic time was the Japan Sea opening and the formation of modern Japanese island arc system. At the present time most investigators look upon this event as being Middle and Late Miocene in age (20-12 Ma) and as associated with back-arc spreading, receding of subduction zone toward a trench as well as with intrusion of depleted asthenosphere diapir into the extension zone. The large-scale extensional stage that had occurred in the Late Cenozoic (10 - 3 Ma) was followed by the formation of basaltic plateaus widespread at many places of China, Korea and southwest Japan.

The geological, geophysical, and petrological data pertaining to Japan Islands and in some respects to the Japan Sea support the idea of opening of marginal basin in the Miocene [8,29, 27, et al.] but do not fit well to the peculiarities of geological evolution of continental part of eastern Eurasia. Indeed, the structural rearrangement started since the Paleogene (but not in the Miocene) in the areas of east and northeast China. In the Eocene, recorded here are the activation of ancient faults and development of new northeast to southwest -trending strike-slip fault systems followed by the formation of syn-strike-slip sedimentary basins and by intense within plate-type basaltic volcanism.

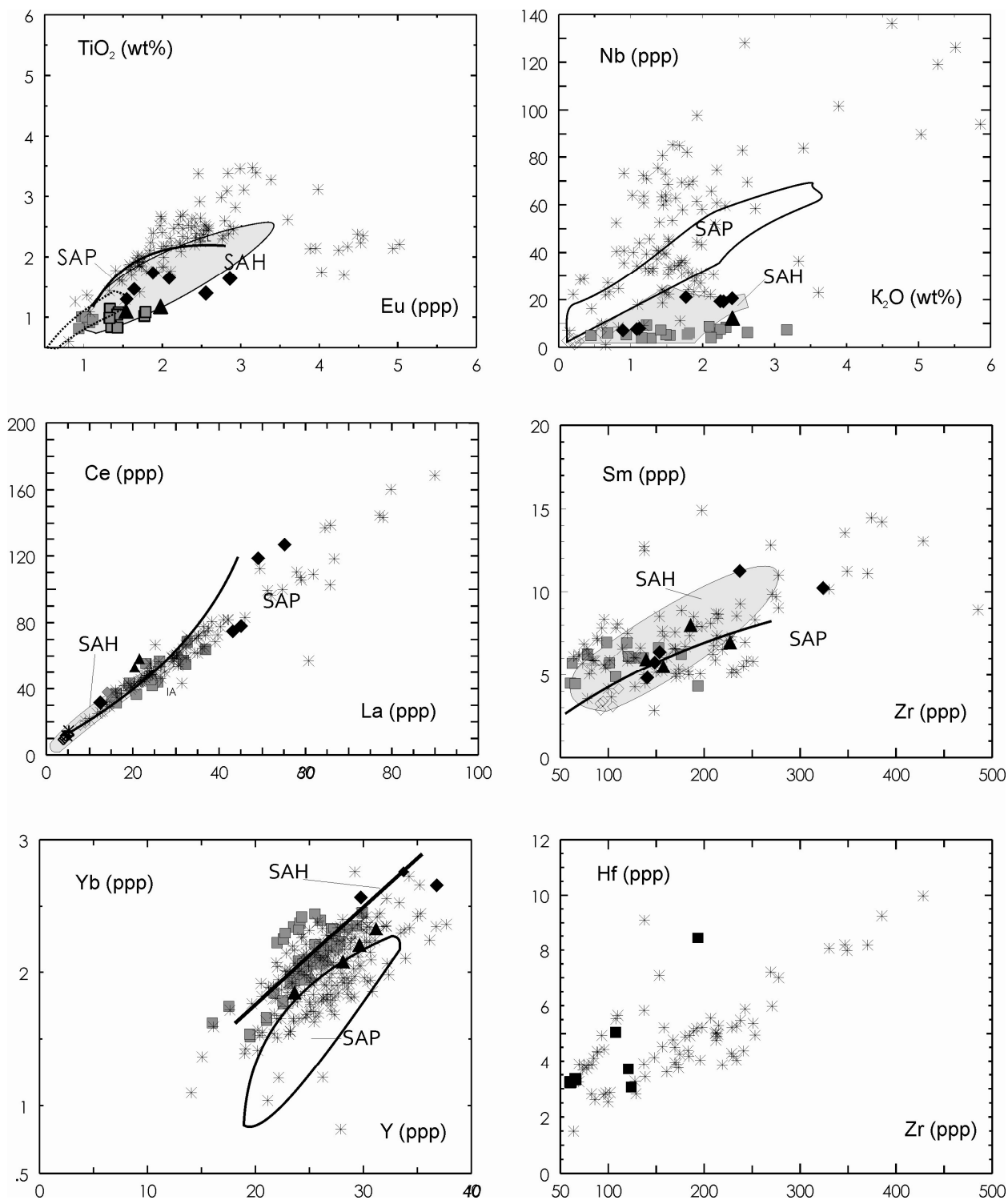


Fig. 7. Correlation of incompatible elements with similar bulk distribution coefficients in the Korean basalts of various ages.

Fields (SAH) and (SAP) = high-alumina and withinplate basalts in the Sikhote-Alin region, respectively.

See Fig. 2 for explanation of the symbols.

The tectonic activation is interpreted to be the result of collision of the Indian continental plate and of the variations in trend of the Pacific oceanic plate convergence [9, 10].

The Paleogene tectonic event is also recorded within the Eurasian continental margin - namely, on the Korean Peninsula and in the East Sikhote-Alin region. Here, the change in tectonic regime became apparent in changing the volcanic rocks composition and in an initiation of long run, practically over the entire period of the Cenozoic, basaltic volcanic activity. Compositionally, the basaltic rocks of these areas are different from those of the interior parts of China. Within the continent-marginal structures, up to the Late Miocene, eruption of high alumina calc-alkaline basalts considered by the majority of geologists as subduction-related occurred. However, on some geological and geochemical evidence, these rocks are distinguished from arc-related rocks. Petrological characteristic features of the Cenozoic high-alumina basalts from the East Sikhote-Alin region were discussed in an earlier paper [19]. On the Korean Peninsula, these features are usually very much more pronounced. Admitting a model of the Japan Sea opening in Miocene time, A. Pouclet et al. [24] recognize two major stages in the volcanic activity on the Korean Peninsula, namely subduction-related and rift-related ones. The subduction-related volcanics include the Late Cretaceous to Paleogene effusives, whereas the Miocene to Quaternary volcanites are considered as rifting-related. Among the rifting-related effusives, in its turn, the Miocene calc-alkaline basalts which were synchronous to opening of the Japan Sea and the Pliocene- Quaternary tholeiitic and alkaline lavas formed upon completion of the main extensional stage are distinguished. This classification should not be regarded as wholly satisfactory one because it does not provide an explanation for a sudden change in volcanism character at the boundary of the Cenozoic. Besides, the assignment of the Paleogene and Miocene alumina-rich basalts to the distinct tectono-magmatic stages of the Korean Peninsula development is inconsistent with their localization features and the isotopic data. As a matter of fact, in spite of some distinctive geochemical characteristics, the Paleogene and Miocene mafic effusives form the common volcanic fields that do not frequently coincide with the areas of occurrences of the Late Cretaceous subduction-related volcanites (Fig. 1). The Cenozoic Al_2O_3 -rich basalts make up actually its own volcanic zones extending along the Japan Sea coast from the Pohang basin in the south to the Khasan volcanic field (the Primorye territory) in the north. Due to the subduction-related volcanics, in view of the peculiarities of magmagenesis, are always located parallel to zone of convergence of the oceanic and continental plates (a trench), the presence of the Paleogene to Miocene basalts along the Japan Sea coast seem contrary to their subduction nature, whilst again, this fact points to the postulated important contribution of the tectonic processes associated with the marginal basin opening to their formation.

The post-subduction character of the Paleogene Al_2O_3 -rich basalts in Korea is supported by isotopic- studies. From the $^{87}Sr/^{86}Sr$ ratios range, the basalts under consideration are similar to the Miocene and Quaternary effusives and are markedly different from the Late Cretaceous subduction-related basalts.

Thus, geological and geochemical data obtained during the study of the Cenozoic basalts on the Korean Peninsula and in the East Sikhote-Alin area complement each other nicely and indicate that the Cenozoic tectonic evolution of the continental margin structures in east Eurasia was in many ways similar to the evolution of the interior parts of China. The timing of subduction cessation should be attributed to at least Eocene period, but not to Miocene one. At later time the prevailing process in the formation of structural pattern of this region was rifting.

The analysis of the isotopic data obtained for volcanic rocks of Korea, the East Sikhote-Alin area, and Japan allows us to distinguish the main stages of structural evolution within the marginal part of Eurasia. Among the features peculiar to the geological structures adjacent to the Japan Sea, noteworthy are so-called “isotopic jumps” “representing the great sudden changes in isotope composition of volcanites over the short lengths of time. These “isotopic jumps” inferred to mark changing magma generation conditions.

Such the earliest “isotopic jump”, with the sharp decreasing in $^{87}\text{Sr}/^{86}\text{Sr}$ ratios from ≈ 0.7093 to ≈ 0.7050 , is recorded in basalts of the Korean Peninsula at the boundary of Late Cretaceous-Paleogene time (4). This “jump”, as mentioned earlier, has evolved from an abrupt reduction of a subduction component contribution to basaltic magma genesis. The cessation of active subduction of the oceanic plate beneath the Asia continent would be dated at this period of time.

The isotopic characteristics for the Paleogene Al_2O_3 -rich basalts from the Korean Peninsula and the region of East Sikhote-Alin are similar to those for the Late Cenozoic within-plate lavas. This provides reason to assume that these rocks were generated by subcontinental lithosphere melting without the essential contribution of the depleted asthenospheric mantle. Hence, the initial stage of transition from the subduction-type interaction of continental and oceanic plates to the interaction of a transform nature was not accompanied by the essential extensional process in continental lithosphere and formation of slab windows.

An increase in the isotopic depletion of alumina-rich basalts in the East Sikhote-Alin region in a time interval of 40 - 35 Ma (the decline in $^{87}\text{Sr}/^{86}\text{Sr}$ ratios from 0.705 to 0.7037) coincides in time with intense magmatism resuming [3], thereby suggesting that subcontinental lithosphere was intruded by the hot and depleted asthenospheric matter. The timing of initiation of the Japan Sea opening is presumably of the same period of time.

The Miocene “isotopic jump” found in back-arc basalts of Japan (20 - 15 Ma) and in the basalts of the East Sikhote-Alin region (about 25 Ma) implies a decrease in $^{87}\text{Sr}/^{86}\text{Sr}$ ratios from ≈ 0.7037 to ≈ 0.703 , i.e., to the value that is typical of MOR basalts. This is testimony to the prevailing contribution of depleted asthenosphere in basalt genesis. The asthenospheric matter inferred to be intruded into subcontinental lithosphere during the most substantial final period of the marginal basin of Japan Sea opening.

CONCLUSIONS

The geological and geochemical data on the Late Cretaceous to Cenozoic basaltic volcanism of the Korean Peninsula and the earlier reported data on the East Sikhote-Alin volcanic belt suggest that some corrections must be made for the present geodynamic models concerning evolution of the continental margin of East Asia in Cenozoic time. Rifting-related processes (but not subduction-related ones) play a key role in the formation of volcanic structures and opening of the Japan Sea. Changing isotopic characteristics typical of the Late Cretaceous - Cenozoic basalts of Japan, Korea, and the East Sikhote-Alin region served the ground for identifying three main stages of tectonic evolution of the eastern margin of Eurasia: (1) the Early Paleogene stage which is related to subduction termination; (2) the Eocene -Oligocene stage which involved the beginning of destruction of subducted slab and the intrusion of the depleted asthenosphere matter into subcontinental lithosphere thereby initiating opening of the marginal basin; and (3) the Miocene stage in which the final phase of the Japan Sea marginal basin formation is recorded.

This research was supported by the Russian Foundation for Basic Research (grant №98-05-65337).

REFERENCES

1. Fedorchuk A.V., Filatova N.I. Cenozoic magmatism of North Korea and geodynamic environment of its formation // *Petrology*. 1993. V.1, No. 6. P. 645-656. (in Russian).
2. Filatova N.I., Chang L.X., Park S.O. Correlation of the Late Mesozoic formations of Korea and environment of its accumulation // *Stratigrafiya. Geologicheskaya korrelyatsiya*. 1999. V. 7, No. 4. P. 87-99. (in Russian).
3. Filatova N.I., Chang K.Ch. Late Mesozoic lateral rows of sedimentation environments in the Korea-Japan Region // *Doklady RAN*. 1999. V. 369, No. 1. P. 100-104. (in Russian).
4. Filatova N.I. Development of the Northern Korean volcanic belt. In: *Proceedings of the 15th International Symposium of Kyungpook National University*. 1995. P. 75-91.
5. *Geology of Korea*. Pyongyang. 1993. 663 p.
6. *Geology of Korea*. Seoul: Keohak-Sa Publishing Co. 1987.
7. Hwang S. K., Kim S. W. Petrology of Cretaceous volcanic rocks in the Milyang-Yangsan area, Korea: petrotectonic setting // *Jour. Geol.Soc.Korea*. 1994. V. 30. P. 229-241.
8. Isezaki N. A magnetic anomaly map of the Japan Sea // *J. Geomagn. Geoelectr.* 1986. V. 38. P. 403-410.
9. Jolivet L. America-Eurasia plate boundary in eastern Asia and the opening of marginal basins. // *Earth and Planetary Science Letters*. 1987. V. 81. P. 282-288.
10. Jolivet L., Huchon P., Brun J.P., Chamot-Rooke N., Le Pichon X., Thomas J.C. Arc deformation and marginal basin opening, Japan Sea as a case study. // *Journal of Geophysical Research*. 1991. V. 96. P. 4367-4384.
11. Khanchuk A.I. Tectonics and magmatism of the Californian type paleotransform continental margins in the Russian Far East In: *The general problems of tectonics. Tectonics of Russia. Proceedings of the XXXIII Tectonic Symposium*. Moscow: GEOS Press. P. 544-547. (in Russian).
12. Khanchuk A.I., Golozoubov V.V., Martynov Yu.A., Simanenko V.P. The Early Cretaceous and Paleogene transform continental margins (the Californian type) of the Russian

Far East In: Tectonics of Asia (Yu. A. Karyakin ed.). Moskow: GEOS Press. 1997. P. 240-243. (in Russian).

13. Kim K. H., Lee J. S. Petrochemical studies of the Cretaceous volcanic rocks from the Kyeongsang sedimentary basin // Jour. Geol.Soc.Korea. 1993. V. 29. P.84-96.

14. Kim C.S., Yun S.H., Cheong C.S. Volcanic stratigraphy and petrology of the Cretaceous volcanic rocks in the Mt. Sinbul-Youngchui area, Korea // Jour. Geol. Soc. Korea. 1998. V. 34. P. 137-153.

15. Lee D.S., Ryu K.J., Kim G.H. Geotectonic interpretation of Choogaryong rift valley, Korea // Jour. Geol. Soc. Korea. 1983. V. 19. P. 19-38.

16. Lee M.W., Won C.K., Lee D.Y., Park G.H., Kim M.S.. Stratigraphy and petrology of volcanic rocks in southern Cheju island, Korea // Jour. Geol.Soc.Korea. 1994. V. 30. P. 521-541.

17. Lee D.W. Strike-slip fault tectonics and basin formation during the Cretaceous in the Korean Peninsula // The Island Arc. 1999. V. 8. P.218-231.

18. Martynov Yu.A. Origin of island-arc-related basaltic series from data on Ni/Co ratios // Doclady AN SSSR.1983. V. 273, No. 5. P. 1230-1232. (in Russian).

19. Martynov Yu. A. Geochemistry of basalts from active continental margins and mature island arcs exemplified by northwest Pacific. Vladivostok: Dalnauka Press. 1999. 215 p. (in Russian).

20. Otofujii Y., Matsuda T., Nohda S. Opening mode of the Japan Sea inferred from the paleomagnetism of the Japan arc // Nature. 1985. V. 317. P. 603-604.

21. Park J.B., Kwon S.T. Geochemical evolution of the Cheju volcanic island (II): trace element chemistry for stratigraphically-controlled lavas from the Northern Part of Cheju island // Jour. Geol. Soc. Korea. 1996. V.32. P. 223-249.

22. Pearce J.A. Role of the sub-continental lithosphere on magma genesis at active continental margins. In: Continental basalts and mantle xenoliths. Nantwich: Siva Press. 1983. P.230-249.

23. Pearce J.A., Parkinson I. J. Trace element model for mantle melting: application to volcanic arc petrogenesis // Magmatic Processes and Plate Tectonics. Geol. Soc. Special Public. 1993. No. 76. P. 373 - 403.

24. Pouclet A., Lee J., Vidal P., Cousens B., Bellon H. Cretaceous to Cenozoic volcanism in South Korea and in the Sea of Japan: magmatic constrains on the opening of the back-arc basin // Volcanism associated with extension at consuming plate margin. Geol. Soc. Spec. Publ. 1995. No. 81. P. 169-191.

25. Shervais I.W. Ti-V plots and the petrogenesis of modern and ophiolitic lavas // Earth. Planet. Sci. Lett. 1982. V. 59, No. 1. P. 101-118.

26. Shimazu M., Yoon S., Tateishi M Tectonics and volcanism in the Sado-Pohang belt from 20 to 14 Ma and opening of the Yamato basin of the Japan Sea // Tectonophysics. 1990. V. 181. P. 321-330.

27. Shuto K., Kagami H., Yamamoto K. Temporal variation of Sr isotopic compositions of the Cretaceous to Tertiary volcanic rocks from Okushiri island, Northeast Japan Sea // Journ. Min. Pet. Econ. Geol. 1992. V. 87. P. 165-173.

28. Song S., Lee H. K., Yun H. Petrogenesis of Tertiary volcanic rocks from the southeastern part of Korea In: Tectonic evolution of Eastern Asian Continent / Ed. Lee, Y.I. and Kim J.H. Geol. Soc.Korea 50th Anniv. Int. I Symp. 1997. P. 219-224.

29. Tatsumoto M., Nakamura Y. DUPAL anomaly in the Sea of Japan: Pb, Nd, and Sr isotopic variations at the eastern Eurasian continental margin // Geochim. et Cosmochim. Acta. 1991. V.55. P. 3697-3708.

30. Wee S.M. Geochemical characteristics of the Quaternary Jungok basalt in Choogaryong rift valley, mid-Korean peninsula // Eron.Environ.Geol. 1996. V. 29. P. 171-182.

31. Won C.K., Kim Y.K., Lee M.W. The study on the geochemistry of Choogaryong alkali basalt // *Jour. Geol. Soc. Korea*. 1990. V. 26. P. 70-81.
32. Wood D.A. The application of Th-Hf-Ta diagram to problem of tectonomagmatic classification and to establish the nature of crustal contamination of basaltic lavas of the British Tertiary volcanic province // *Earth. And Planet. Sci. Lett.* 1980. V. 50. P. 11-30.
33. Won C. K., Lee M. W., Lee J. M. A study of the Cretaceous volcanic activity of the Bupseongpo area // *Jour. Geol.Soc.Korea*. 1991. V. 27. P. 416-433.
34. Won C.K., Lee M.W., Yun S.H., Ko B.K. Geochemical characteristics of the volcanic rocks in Pyoseon Area, southeast Cheju, Korea // *Jour. Geol. Soc. Korea*. 1998. V. 34. P. 172-191.
35. Yun S.H. Strontium isotope composition and petrochemistry of the Cretaceous Chaeyaksan volcanics, northern Yucheon volcanic field, South Korea // *Jour. Geol. Soc. Korea*. 1998. V. 34. P. 161-171.

**EVIDENCE FOR THE RESEMBLANCE OF THE
SUBCONTINENTAL LITHOSPHERIC MANTLE IN THE AREAS OF
KIMBERLITE-LAMPROITE MAGMATISM: CONSTRAINTS ON THE
EVOLUTION OF THE SIBERIAN CRATON**

Z. V. Spetsius

Institute of Diamond Industry, Mirny, Yakutia, 678170, Russia, Spetsius@yna.alrosa-mir.ru

Petrologic data indicate that kimberlite and lamproite magmas are originated at a great depth of subcontinental lithosphere mantle (SCLM). An ancient origin for the SCLM of the Siberian and other cratons is supported by Re-Os and Sm-Nd model ages of eclogite and peridotite xenoliths from kimberlite pipes, obtained by different authors.

This paper tries to combine our and other published data on the composition and evolution of the lithosphere mantle beneath the Siberian craton and to compare it with that of other cratons. Main results have been obtained from studies of mafic and ultramafic xenoliths from kimberlites. We used original data on distribution of different types of xenoliths and inclusions in diamonds in main industrial kimberlite pipes of the Yakutian kimberlite province. Some original trace element and isotopic data in minerals from eclogite and peridotite xenoliths and Re-Os determination of olivine megacrysts from kimberlites have been used to estimate the age of formation and time of depletion events in the Siberian lithosphere mantle and to compare it with the results for the South African and Canadian cratons.

The role and importance of mantle metasomatism, partial melting and coupled deformation in the evolution of the SCLM, origin of vertical and lateral heterogeneity beneath kimberlite province and subsequently under Siberian craton are of particular interest.

The SCLM of different cratons showing the kimberlite-lamproite magmatism was formed in the Archaean and is similar to other petrographic types of mantle xenoliths and coupled crustal rocks. The evolution of the SCLM of different cratons as well of different regions inside kimberlite province could be different both from the viewpoint of tectonics and abundance of mantle metasomatism, partial melting and deformation.

INTRODUCTION

Due to intensive field works industrial pipes have been discovered and started to be exploited not only in the Siberian and South African platforms but in different places around the world. Industrial kimberlite pipes and lamproite deposits with diamonds have been discovered in China, Australia, Canada and other regions. A brief review of tectonic-geographic setting of kimberlites and lamproites indicate that they mainly occur on stable sites of platforms [e.g., 5, 15]. Great amount of petrologic data show that kimberlite and lamproite magmas are originated at a greater depth of subcontinental lithosphere mantle (SCLM). Hence, from this point of view, deep seated xenoliths, megacrysts and diamonds are representatives of SCLM, which are trapped by kimberlite and lamproite pipes.

Thus, we can infer that xenoliths, megacrysts and diamonds contain important and real information about composition, geochemistry and other peculiarities of the SCLM. Comparison of these xenoliths from different regions and provinces allow the estimation of the similarity and difference of the upper mantle from different

platforms, as well of the SCLM of different cratons. As such a detailed analysis could be done only using abundant data we have to compare only the data on the composition of SCLM of Siberian craton as well as some results on the inclusions in diamonds.

Intensive investigations of Re and Os distribution in mantle xenoliths from kimberlites, as well in xenocrysts and diamonds from South Africa, Canada and Siberia [e.g., 10, 18, 23] took place within the last two decades. From Re/Os determinations the modal age of diamonds varies from 2.8-3.5 Ga while the age of mantle eclogite and peridotite xenoliths varies from 1.0 to 3.5 Ga. The above data help to understand the formation and differentiation of lithosphere mantle and coupled crust as well as subsequent evolution of the SCLM.

SAMPLES

More than 3000 samples of mafic and ultramafic mantle xenoliths from kimberlite pipes situated in different parts of the Yakutian kimberlite province were studied. A modal analyses have been performed for the major part of xenoliths. Rock composition was determined. Major-element analyses were performed for the rock-forming and minor minerals. Trace element composition was obtained for some minerals. All samples were classified into different varieties of eclogites and ultramafites according their petrographic and chemical features. A phase composition and element content of ore and sulfide minerals were investigated in many samples. All xenoliths were examined by petrographic, chemical and partly isotope methods to identify modal metasomatic minerals or other evidences of mantle metasomatism. These samples include different varieties of eclogites and ultramafic xenoliths from depleted dunites and harzburgites through coarse grained and sheared Gt-peridotites to ortho- and clino-pyroxenites.

DIAMONDS

Radiometric ages of silicate and sulfide inclusions show that diamonds are xenocrysts in kimberlite magmas and they could provide a valuable information not only concerning the conditions of their formation but also about the environment of mantle rocks giving rise to diamonds [e.g., 4, 18, 19].

Speaking about the morphology of diamonds it should be pointed that main varieties of different forms are available in kimberlite pipes around the world. Spectrum of morphology varies from pipe to pipe. A lateral heterogeneity in distribution of different morphological groups from the south to the north of province is found for populations of diamonds from the Yakutian kimberlites. It is explained by a complementary behavior showing a lateral petrographic mantle heterogeneity and partly the intensity of resorption and solution of diamonds in kimberlite magmas and in the process of mantle metasomatism [28]. Such a difference in the distribution of some diamonds by morphology is found for kimberlites of South Africa. For example, cubic crystals are abundant in the Mbuji-

Mayi pipe. In addition Ky-eclogites [8], which are the parent rocks for such diamonds should be present.

Inclusions in diamonds worldwide include two populations of eclogitic and peridotitic paragenesis. The distribution of syngenetic inclusions in main well investigated kimberlite pipes of Yakutia is shown in Table 1, the data are taken from the papers by Sobolev N.V and Bulanova G.P. [3, 4, 24].

Table 1.

Paragenises of inclusions in diamonds from the Yakutian kimberlites

Pipe	Eclogitic	Peridotitic
Mir	Gt, Cpx, Cs, Po	Ol, Chr, Gt, Cpx, Opx, Mag, Mss
Udachnaya	Gt, Cpx, Cs, Po	Ol, Chr, Gt, Cpx, Mss, Phl, Pn, Wu, Tae
23d Party Congres.	Gt, Cpx, Ru, Po	Ol, Mss, Wu, Fe
Yubileinaya	Gt, Po	Chr, Gt, Ol, Mss
Zarnitsa	Gt, Cpx, Po	Ol, Chr, Gt, Mss

Abbreviations: Mag-magnesite, Wu-vustite, Tae-tenite, Fe-native iron, Po-pyrrhotite, Pn-pentlandite, Mss-monosulfide solid solution.

The well-known data by M. Henry and others [14] and references for inclusions in diamonds from kimberlites of South Africa are similar both by the presence of the same eclogitic and peridotitic paragenises and by the composition of included minerals. There is still a discussion about abundance of sulfide inclusions in diamonds and their significance for the diamond formation. However, it is another topic and we only stress that sulfides are widespread in crystals from all kimberlite and lamproite pipes [e.g., 2, 29]. Within the last 10 years substantial discoveries resulted from successful investigations of inclusions in diamonds. New minerals such as the majorite component in garnets and phases of ferropericlaase and MgSi-perovskite have been described. These rare minerals are found in diamonds from Brazil, South Africa and Canada [11]. These data suggest the possibility of the formation of such inclusions as well hosting diamonds in the deep mantle probably lower mantle. The data also suggest thicker SCLM and roots under these areas of kimberlite magmatism. In spite of the fact that inclusions in diamonds from Yakutia are well studied such deep-seated inclusions haven't been found for Yakutian kimberlites. It confirms slightly different history and evolution of the SCLM of the Siberian craton. Probably continental roots under South Africa and other cratons containing inclusions at a great depth of the upper mantle or lower mantle are sicker than roots beneath the Siberian craton. Such an idea was demonstrated by W.Griffin using results on the distribution of garnets and other macrocrysts in kimberlites of different cratons [9].

The age of diamonds is studied from inclusions using Sm-Nd method for garnets or Re-Os for sulfides. A set of Ar/Ar data are also available. However, we will not discuss these results because of their high variation and most likely inadequacy of all estimations. The most precise dating of zircons is made only for one sample because of rare and unique finding of such inclusions. To compare

ages of diamonds from different deposits we used results and compilation data of G.Pearson [15, 18, 19, 23]. As Table 2 demonstrates the age of diamond formation varies from 2.0 to 3.3 Ga. These estimations and variations are similar for diamonds from the Siberian and South African platforms and suggest similar time of diamond formation in different areas as well as probable multistage formation of diamonds in mantle rocks as was demonstrated [e.g., 29].

Table 2.

Radiogenic isotope systems, localities, inclusions minerals ages for diamond dating studies

Isotope system	Locality	Minerals and paragenesis	Approach	Age (Ma)
Sm-Nd	Kimberley, SA	Gnts (P-HZ)	Model age (comp)	3300±100
Sm-Nd	Finsch, SA	Gnts (P-HZ)	Model age (comp)	3200±100
Sm-Nd	Finsch, SA	Gnts+Cpx (E)	Isochrone (comp)	1580±50
Sm-Nd	Finsch, SA	Gnts (E)	Model age(single di)	1657±77
Sm-Nd	Finsch, SA	Gnts (E)	Model age(single di)	1443±166
Sm-Nd	Finsch, SA	Gnts (E)	Model age(single di)	1824±66
Sm-Nd	Finsch, SA	Gnts (E)	Model age(single di)	2183±182
Sm-Nd	Finsch, SA	Gnts (E)	Model age(single di)	2408±181
Sm-Nd	Finsch, SA	Gnts (W)	Model age(single di)	2111±120
Sm-Nd	Orapa, B	Gnts+Cpx (E)	Isochrone (comp)	990±50
Sm-Nd	Argyle,Aus	Gnts+Cpx (E)	Isochrone (comp)	1580±60
Sm-Nd	Premier,SA	Gnts+Cpx (E)	Isochrone (comp)	1150±60
Sm-Nd	Premier,SA	Gnts+Cpx(P-LZ)	Isochrone (comp)	1930±40
Sm-Nd	Udachnaya,Ru	Gnts (P-HZ)	Isochrone (comp)	2010±60
Sm-Nd	Jwaneng, B	Gnts+Cpx (E)	Isochrone (comp)	1540±20
U-Pb	Mbuji Mayi,Zaire	Zircon	²⁰⁶ Pb/ ²³⁸ U single crystal	628±12
Pb-Pb	Finsch, SA	Sulfides(?)	Pb-Pb model age(comp)	>2000
Pb-Pb	Kimberley, SA	Sulfides(?)	Pb-Pb model age(comp)	>2000
Pb-Pb	Premier,SA	Sulfides(?)	Pb-Pb model age(comp)	~1200
Re-Os	Koffiefontein, SA	Sulfides(P)	Isochrone(single di)	68±30
Re-Os	Koffiefontein, SA	Sulfides(E)	Isochrone(single di-s)	1048±120
Re-Os	Udachnaya, Ru	Sulfides(P)	Model age(single crystal)	3100 - 3500±300
Re-Os	Udachnaya, Ru	Sulfides(P)	Model age(single crystal)	3502±100
Re-Os	Wellington, Aus	Sulfides(P)	Model age(single crystal)	3609±300

COMPOSITION OF THE SCLM OF THE SIBERIAN CRATON

Investigations of deep-seated xenoliths from different kimberlite pipes of Yakutia show that the subcontinental lithosphere mantle (SCLM) of the Siberian craton is differentiated both vertically and laterally [e.g., 9, 33]. The vertical heterogeneity is exhibited in a widespread spectrum of different types of mafic and ultramafic xenoliths in all kimberlite pipes of the province (Table 3). First of all, the vertical heterogeneity of the SCLM is the result of differentiation and formation of the primary mantle substance during the Archean [e.g., 10]. As show by these data, the SCLM of Siberian platform was formed and stabilized between

3.4-2.9 Ga. The mantle was added? Through the subduction after the main differentiation. A probable subduction of the oceanic crust in the central Daldynsky terrane of kimberlite province is confirmed by Ky- and Cs-eclogites in the Udachnaya, Sytykanskaya and other pipes (Table 3). It is also verified by Sm-Nd and Rb-Sr isotope data for the eclogite xenoliths from the Udachnaya and Mir pipes [26, 27].

Table 3.

Distribution of mantle xenoliths from kimberlite pipes of Yakutia

Type of xenoliths	Mir	Internazional	Sytykanskaya	Yubiley-naya	Udachnaya	Zarnitsa	Botuobinskaya
Eclogite-like rocks	-	-	+	+	+	+	+
Phlogopitites	-	-	+	+	+	-	-
Ilm-peridotites	+	-	+	+	+	-	-
Pyroxenites	+	-	+	-	+	+	-
Sp-peridotites	+	+	+	+	+	+	+
Gt-pyroxenites with Phl	+	+	+	+	+	-	-
Gt-Ilm-peridotites	+	-	+	-	+	-	+
Gt-Sp-lherzolites	+	+	+	+	+	+	+
Gt-lherzolites	+	+	+	+	+	+	-
Gt- coarse-grained lherzolites	+	+	+	+	+	-	+
Gt-lherzolites porphyric	+	-	+	+	+	-	+
Gt-pyroxenites porphyric	+	+	-	-	-	-	-
Gt-Ilm-peridotites	+	-	+	-	+	-	-
Grosopydites?, Ky-eclogites	-	-	+	-	+	+	-
Cr-pyrope dunites, Harzburgites, lherzolites	+	+	+	+	+	+	-
Gt-wehrlites	+	-	+	-	+	+	-
Sheared Gt-lherzolites	+	-	+	+	+	-	+
Cs-eclogites, eclogites	+	+	+	+	+	+	+
DI-dif.dunites, harzburgites	-	-	-	-	+	-	-
DI-dif. Ilm-Gt-lherzolites	-	-	-	-	+	-	-
DI-dif.pyroxenites	+	-	-	-	+	-	-
Diamondiferous eclogites	+	-	+	-	+	-	-

The horizontal heterogeneity of the mantle results from the presence of highly aluminous rock suite in the central area of kimberlite province. These rocks and particularly the Ky- and Cs-eclogites, alkremites and couplet with them lower crustal rocks such as eclogite-like rocks with kyanite are present in the Udachnaya and other kimberlite pipes from the central area (Table 3) However, they are not available on the south and north.

Rock chemistry and trace element data indicate that mafic and ultramafic xenoliths from the pipes located in the central part of the Yakutian province are divided into three distinguished groups: peridotites, pyroxenites and eclogites

[28]. This pattern changes for other areas and such xenoliths are rather less distinguished between each other and divided groups are overlapped.

COMPOSITION OF THE SCLM IN DIFFERENT AREAS OF KIMBERLITE MAGMATISM

Comparison and analysis of petrographic features and composition of mantle xenoliths from kimberlites of Yakutia and South Africa show a significant compositional resemblance and in some cases a real identity in terms of the set of main types of mantle mafic and ultramafic rocks that are present as xenoliths in kimberlites.

Almost a complete spectrum of mantle xenoliths is presented in a detailed monograph on Siberian kimberlites [1]. Such spectrum was earlier obtained for the South African kimberlites [6 and references therein]. The list of data was extended by adding diamondiferous eclogites and peridotites. Rare and unusual mantle xenoliths such as grosspydites, alkremites and samples with coesite were later discovered in Siberian and South African kimberlites [e.g., 5, 33 and references therein]. The petrographic spectrum of mantle rocks in the SCLM of different areas of kimberlitic magmatism is similar.

Moreover, similar petrographic types of the rocks from different cratons are found not only for the mantle level but also for the lower crust and for the intermediate lower crust-upper mantle zone. Eclogite-like rocks are abundant among xenoliths in kimberlites of Yakutia. They consist of the clinopyroxene, garnet and plagioclase. Rare samples from this zone include eclogite-like rocks with the kyanite. Such rocks were described in the Udachnaya and Zarnitsa pipes [1, 33] and are found also in kimberlite Mbudji-Maji pipe, South Africa [8]. The chemistry and mineralogy of these rocks in both provinces are the same.

Xenocrysts and megacryst assemblages in kimberlites of South Africa show the association $Ol+Opx+Cpx+Ilm+Phl+Zr$ that is found in many pipes of South Africa. Only the kimberlite Mir pipe contains a complete set of these mineral phases. Zircon is absent or scarce in pipes of Daldyn-Alakitsky region. Orthopyroxene megacrysts are also rare. The last fact could be partly explained by an unstable behavior of this mineral in hydrothermal processes and its intensive replacement by secondary minerals.

GEOCHEMISTRY AND EVOLUTION OF REPRESENTATIVES OF THE SCLM OF SIBERIAN CRATON

Geochemical features of substance in the SCLM of kimberlite-lamproite areas are discussed and compared using the data on content and distribution of trace elements in mafic and ultramafic xenoliths as well as the data for megacryst assemblage. The results of proton probe and partly ICPMS data on the content and distribution of the trace elements in eclogite xenoliths from the Udachnaya pipe and such pipes of South Africa as Monastery and others are very similar [31]. The

main difference is high enrichment of eclogites from the Udachnaya pipe by Sr and Ga and depletion of garnets and clinopyroxenes by Y and Zr. But eclogitic clinopyroxene of Udachnaya pipe are more LREE-depleted and less radiogenic than those from South Africa and garnet enriched in LREE [13, 26, 34]. Such a difference could result from more intensive metasomatic processes. ICPMS data for the eclogites from the Udachnaya pipe permitted the division into three groups in terms of trace element distribution [34]. Similar data were taken for the eclogites of Roberts Victor and Mbuji-Mayi [8, 22]. It should be emphasized that eclogites of the Udachnaya and Roberts Victor are very similar both in terms of rock petrographic, chemical and geochemical features of rocks.

The data on the distribution of trace element in different types of ultramafites mainly from the Yakutian kimberlites are scarce. However, we tried to discuss the features of ultramafite geochemistry on the base of data obtained from Re-Os systematics of sulfides from the olivine macrocrysts of the Udachnaya pipe. Macrocryst grains with sulfide inclusions were selected from coarse (5-8 mm) heavy-mineral concentrate. Before studying the absence of annealing and cracks were checked in sulfide inclusions. Grains were mounted individually in epoxy and polished to reveal sulfide inclusions ranging in diameter from 20 to ≈ 300 microns. All inclusions were polished just a little from the top to open enough for study of their composition by microprobe. After that we obtained a detailed Re/Os isotope composition of sulfides. In case two or more sulfide inclusions are present in one given grain they were repolished for the next analysis. If after Re/Os determinations some material of sulfides was left, they were studied for trace element content of PGE-group using methods from [20].

All these determinations were obtained using Merchantek LUV266 laser microprobe with a modified ablation cell, attached to the Nu Plasma multi-collector ICPMS at GEMOC. All ablations were carried out using He as the carrier gas. Most analyses were done at 4 Hz repetition rate and energies of ca 2 mJ/pulse; typical pit diameters were 50-80 microns. The analytical procedures for in situ Re-Os isotope analysis are described in detail [10, 20]. The selected analyses are given partly in Table 4 and variations of modal ages are illustrated on figure 1. More detailed results and full data are presented in paper [10].

Sulfides in olivine macrocrysts from the Udachnaya pipe mainly involve finely interfingered Ni-poor and Ni-rich monosulfide solid solution (MSS) with addition of pentlandite and chalcopyrite phases in some cases. 5 groups of sulfides are detected according to trace element data of PGE-content and Pe-Os distribution [10]. Only 2/3 from all investigated sulfide inclusions give a reliable modal age. The modal age of about 60 sulfide inclusions varies from 2.4 to 3.5 Ga [10]. The main peaks are found between 2.9 and 3.2. Ga. Multiple sulfide inclusions have been found and analysed in 10 olivines. In most cases combinations of different sulfides within a single olivine cannot yield Re-Os isochrones with meaningful ages and initial ratios. It suggests that these inclusions represent trapping of different sulfides generations in one olivine grain [10].

Table 4.

Re-Os Analyses of sulfide inclusions in olivines from the Udachnaya pipe

Sample	$^{187}\text{Re}/^{188}\text{Os}$	$\pm 2\text{se}$	Ppm Os	ppm Pt	Os/Pt	T(RD)	T(MA)	$\pm 2\text{sd}$
Ud-Ol-1	0.00638	0.00015	650	115	5.7	3.096	3.144	0.030
Ud-Ol-2	0.02390	0.00092	150	10	15.0	2.921	3.101	0.025
Ud-Ol-3	0.00076	0.00010	550	110	5.0	3.218	3.224	0.076
Ud-Ol-4	0.00553	0.00012	240	15	16.0	2.991	3.031	0.135
Ud-Ol-5	0.13828	0.00168	15	15	1.0	1.031	1.564	0.280
Ud-Ol-6	0.01092	0.00096	400	145	2.8	2.819	2.895	0.211
Ud-Ol-7	0.03333	0.00054	30	5	6.0	2.685	2.921	0.311
Ud-Ol-9	0.01845	0.00034	60	30	2.0	2.552	2.672	0.036
Ud-Ol-9-2	0.00452	0.00003	67	0.3	256.0	3.038	3.071	0.020
Ud-Ol-13	1.08125	0.02600	5	5	1.0		8.500	
Ud-Ol-14	0.00282	0.00004	151	5	28.4	3.114	3.136	0.019
Ud-Ol-16	0.04319	0.00380	50	70	0.7	0.935	1.047	0.117
Ud-Ol-17	0.05339	0.00074	350	220	1.6	2.473	2.843	0.198
Ud-Ol-18	0.58921	0.02200	15	95	0.2		11.600	
Ud-Ol-19	0.03440	0.00200	56	6	9.0	2.968	3.238	0.092
Ud-Ol-20	0.00738	0.00026	2600	325	8.0	3.123	3.180	0.163
Ud-Ol-21	0.04057	0.00260	3	0.3	10.0	2.122	2.356	1.250
Ud-Ol-22	0.09657	0.00064	85	15	5.7	1.818	2.382	0.083
Ud-Ol-23	0.05163	0.00018	111	7	14.9	2.639	3.018	0.016
Ud-Ol-24	0.05973	0.00300	530	140	3.8	2.230	2.611	0.069
Ud-Ol-26	0.02150	0.00164	10	0.5	20.0	2.276	2.402	0.289
Ud-Ol-27	0.01415	0.00048	330	20	16.5	2.839	2.940	0.030
Ud-Ol-28	0.07975	0.00140	135	150	0.9	1.627	2.023	0.362
Ud-Ol-29	0.21020	0.02400	5	1.5	3.3	neg	neg	
Ud-Ol-30	0.00160	0.00007	2750	2000	1.4	1.960	1.968	0.177
Ud-Ol-31	0.03121	0.00030	2800	575	4.9	2.480	2.684	0.046
Ud-Ol-32	0.24655	0.00860	10	35	0.3	neg	neg	
Ud-Ol-32-2	0.05757	0.00144	81	58	1.4	2.208	2.570	0.044
Ud-Ol-33	0.00251	0.00020	130	5	26.0	3.191	3.210	0.457
Ud-Ol-34	0.22172	0.01320	40	5	8.0	neg	neg	
Ud-Ol-35	0.10994	0.00152	150	40	3.8	1.760	2.410	0.047
Ud-Ol-36	0.01583	0.00028	2100	365	5.8	3.321	3.453	0.171
Ud-Ol-35-2	0.19798	0.00640	100	110	0.9	neg	neg	
Ud-Ol-36-2	0.00809	0.00007	600	5	120.0	2.860	2.917	0.014
36-2 dup	0.00757	0.00082	212	7	28.6	2.954	3.009	0.038
Ud-Ol-37-2	0.03481	0.00050	450	105	4.3	2.672	2.919	0.081

The majority of Re-Os determinations belong to the dating of sulfides in mantle xenoliths and diamonds from kimberlites. The characteristics for isotope distribution of Re and Os isotopes in mantle xenoliths are obtained for the whole rock samples and provide ages from 2.8 to 3.2 Ga for mafic and ultramafic xenoliths from Yakutian kimberlites [15, 17]. Re-Os isotope ratio of sulfide

inclusions in diamonds gives the model ages for Siberian kimberlites varying from 2.8 to 3.5 Ga [19 and references therein]. As shown by results of in-situ Re-Os

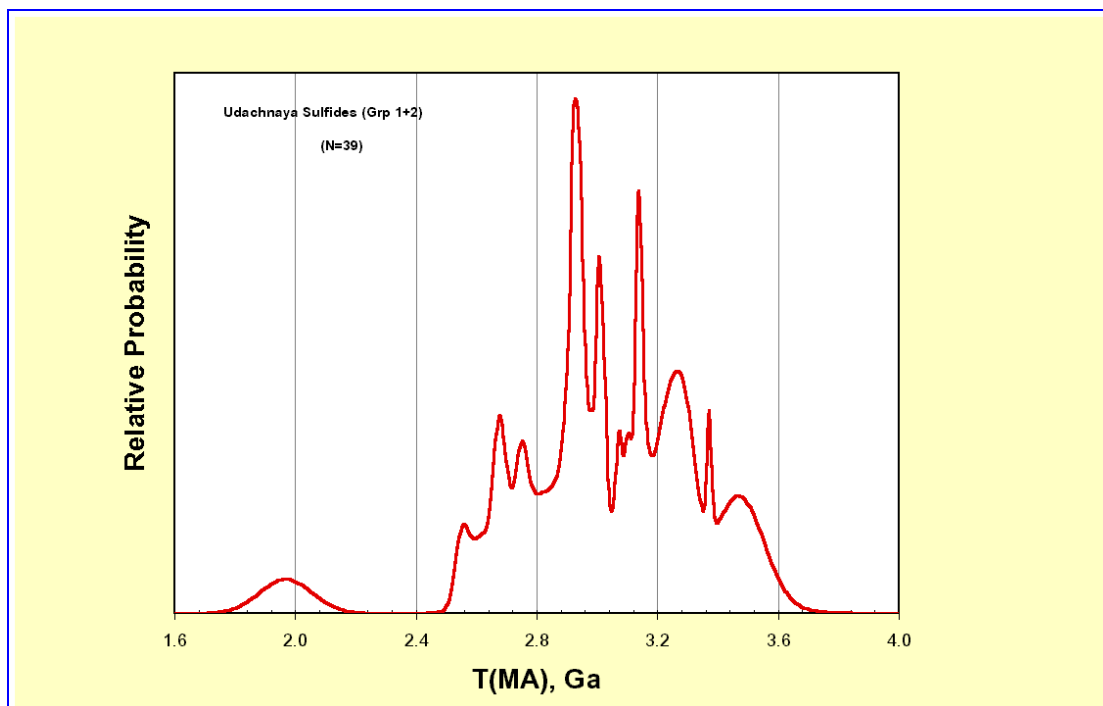


Fig..1. Cumulative probability plots of sulfide modal age data

analysis of sulfide inclusions in olivines from the Udachnaya kimberlite pipe their model age varies from 2.4-3.5 Ga with the two peaks at 2.9 and 3.2 Ga. It most likely shows main events in the lithosphere mantle under Siberian platform [10]. It should be noted that similar ages were obtained from investigation of Re-Os in sulfide inclusions from olivines of Canadian kimberlites with T_{MA} ranging from 2.6 to 3.3 Ga [20].

Using the above data we can suggest that much of the SCLM beneath the Udachnaya pipe as well beneath Siberian craton formed between 3.4 and 2.9 Ga ago by one or more major melting events. The results of Re-Os isotope study of sulfide inclusions in the mantle megacrysts from the Yakutian kimberlites show that the SCLM beneath the Siberian craton was stabilized predominantly between 3.0 and 2.8 Ga ago. The major peak of T_{MA} values of sulfides in olivines around 2.9 Ga coincides with the time of the cratonization and the termination of the SCLM formation as well with the eclogite formation and remelting [10, 17, 21, 23]. Several sulfide inclusions in olivines with low Re/Os and T_{MA} 2.4-2.6 Ga may represent new additions to the lithosphere and are connected with the late tectonic events and disturbing of Re-Os systematics. These results clearly demonstrate a complicated history of the Siberian SCLM. Younger Proterozoic Re depletion ages are interpreted to be predominantly the result of open system behavior during the late igneous activity and probable metasomatism [10]. Such a possible scenario of a complicated history of Re-Os systematics confirms the long living lithosphere

mantle under the Siberian craton. This scenario is consistent with the limited data on crustal formation in the Daldyn and other terranes [21].

PARTIAL MELTING OF MAFIC XENOLITHS

World-wide, most eclogite xenoliths from kimberlites display evidences of partial melting processes [e.g., 5, 29, 33, 35]. This is particularly well observed in eclogites from Udachnaya, Mir, and other Yakutian kimberlites. The crystallization products of these incomplete reactions, typically represented as a “spongy” texture around primary omphacite, include secondary clinopyroxene (with lesser Na₂O), spinel, feldspar, and glass. In intergranular partial-melt veins, orthopyroxene, plagioclase, amphibole, and phlogopite are also present. With such melting of kyanite eclogites, corundum and mullite are encountered. Primary garnet may be partially melted giving rise to orthopyroxene, spinel, olivine, and glass, forming portions of typical kelyphitic rims on garnet [33].

The chemistry of the systems involved indicate that the melting was not isochemical, but brought about by the introduction of metasomatic fluids rich in alkalis, mainly K, and probably volatiles. There are indications from secondary assemblages that similar but different reactions occurred, as a function of the chemistry of the primary minerals and that of the metasomatic fluids.

Detailed petrographic investigations of xenoliths from pipes in the Daldyn-Alakit and Malo-Botuobia regions, Yakutia demonstrate that the partial melting occurred in the majority of xenoliths, especially in eclogites, as well as garnet

Table 5.

Modal Compositions of Eclogites from the Udachnaya pipe and Partial-Melt Products

Sample	Total Eclogite Modes				Modal Compositions of Partial-Melt Products							
	Gt	Cpx	Ky	Prt/ml. product	Cpx	Plag.	Sp	Glass	Opx	Q+K-Fldsp	Cor+ Mull	Amph+ Phlog
U-2045	59.5	26.7	-	13.8	83.8	1.8	12.8	1.6	-	-	-	-
U-2110	67.6	8.7	-	22.8	-	19.7	25.3	-	54.2	-	-	-
U-720	37.3	44.6	-	18.1	54.6	20.5	9.5	-	2.8	-	-	10.4
U-26	32.8	49.4	0.9	16.9	66.9	21.9	11.2	+	-	-	-	-
U-9	46.7	42.7	1.1	9.5	42.4	30.7	9.4	17.5	-	-	-	-
U-1	28	30.9	8.4	32.7	43	+	8.4	13.1	-	12.2	12.9	2.5
U-947	25.5	47.8	4.8	21.9	31.6	+	1.3	43.2	-	23.3	+	0.9
U-820	34.6	30.1	1.3	34	35.9	+	5.1	12.8	-	25.6	15.4	5.2
U-228	17.9	22.6	3.5	56	9.5	-	9.1	10.4	+	1.7	3.5	65.8

websterites and pyroxenites. Such evidence is the case in both eclogites and kyanite eclogites, including diamondiferous varieties. Partially devitrified glass

and other products of melting are evident between garnet and clinopyroxene + mineral present as a single grain.

grains, sometimes in the form of veinlets that transect these minerals. The degree of partial melting varies between xenoliths, as well as the modal abundances of the melt products, as shown in Table 5.

The modal abundances of the partial-melt products are highly variable (see Table 5). The intergranular melt typically consists of newly formed clinopyroxene, plagioclase, and spinel, and more rarely, orthopyroxene and amphibole, with possible phlogopite and/or amphibole. The accessory minerals include calcite and sulfides. K-feldspar, with minor quartz, is present among the products in kyanite eclogites. Glass is typically available, and secondary corundum and mullite occur around kyanite. Primary omphacite is replaced by a mixture of glass, plagioclase, clinopyroxene, and often by veinlets of glass. The primary garnets and clinopyroxenes of these eclogites are well known; therefore, we will characterize mainly the minerals formed by crystallization of melts. Selected representative, major-element analyses of the products of the partial-melt assemblage are given in Table 6.

Table 6.

Representative compositions of mineral assemblage of partial-melt products in eclogite xenoliths from the Udachnaya pipe

Selected microprobe analyses of primary omphacites of eclogite xenoliths

	1	2	3	4	5	6	7	8	9
	U-26	U-720	U-9	U-388	U-947	U-2290	Ud-45	Ud-161	Ud-200
SiO₂	55.56	56.45	55.3	57.08	56.21	56.46	56.24	56.56	56.36
TiO₂	0.21	0.29	0.23	0.17	0.3	0.22	0.35	0.47	0.46
Al₂O₃	17.4	12.31	14.83	13.24	16.52	16.88	11.12	10.66	9.21
Cr₂O₃	0.04	0.05	0.05	<0.03	0.06	0.05	<0.03	<0.03	<0.03
FeO	2.52	2.15	2.82	1.83	1.98	1.77	4.72	4.78	4.86
MnO	<0.03	0.02	<0.03	<0.03	-	0.01	<0.03	<0.03	<0.03
MgO	5.63	8.56	7.05	8.35	5.8	6.56	8.5	9.16	10.54
CaO	10.06	12.14	13.12	13.24	10.06	9.98	11.55	12.26	12.56
Na₂O	7.72	6.95	4.02	6.51	8.88	8.04	6.73	6.56	5.88
K₂O	0.03	0.15	0.07	-	0.22	0.03	-	-	-
Total	99.20	99.07	97.52	100.48	100.03	100.00	99.27	100.51	99.93

1-2 – biminerall? eclogites, 3, 5-6 – Ky–eclogites, 4, 7-9 – diamondiferous eclogites

Microprobe analyses of secondary clinopyroxenes of partial-melt products (Table 6, continued)

	1	2	3	4	5	6	7	8	9
	U-26	U-9	U-720	U-388	U-947	U-2290	Ud-45	Ud-161	Ud-200
SiO₂	55.89	44.59	54.2	53.33	54.58	55.97	53.21	52.78	54.6
TiO₂	0.19	0.67	0.38	0.15	0.49	0.26	0.36	0.54	0.46
Al₂O₃	16.71	13.13	4.4	6.15	5.02	14.14	2.21	4.02	2.47
Cr₂O₃	0.03	0.05	0.06	0.16	<0.03	0.03	<0.03	<0.03	<0.03
FeO	2.71	10.49	3.15	2.56	6.81	2.65	6.72	6.29	6.48
MnO	<0.03	<0.03	0.02	<0.03	<0.03	0.02	<0.03	<0.03	<0.03
MgO	6.02	7.02	15.33	14.54	13.6	7.52	15.3	15.24	16.78
CaO	10.64	21.05	20.09	20.69	16.43	12.14	19.78	18.55	17.9
Na₂O	4.37	1.16	1.5	0.86	2.78	4.74	1.22	1.37	1.57
K₂O	0.1	0.03	0.09	-	-	0.1	-	-	-
Total	96.69	98.22	99.22	98.47	99.77	97.57	98.86	98.85	100.32

Secondary spinels of partial-melt products (Table 6, continued)

	1	2	3	4	5	6	7	8	9
	U-26 Core	U-26 rim	U-9	U-947	Ud-114 Core	Ud-114 rim	Ud-161	Ud-162 core	Ud-162 rim
SiO₂	0.17	0.15	-	0.25	n.d.	n.d.	n.d.	n.d.	n.d.
TiO₂	0.16	0.21	<0.03	0.14	<0.03	<0.03	0.35	0.3	0.17
Al₂O₃	55.55	57.81	63.43	60.09	62.45	61.49	60.74	62.46	63.17
Cr₂O₃	0.18	0.09	<0.03	0.09	0.21	0.16	<0.03	0.73	0.23
FeO	36.07	27.94	17.12	23.25	21.56	23.57	20.08	15.39	16.95
MnO	0.18	0.12	<0.03	0.17	<0.03	0.21	0.16	<0.03	0.21
MgO	8.03	12.26	17.49	14.87	15.97	14.49	16.64	20.43	19.33
CaO	0.08	0.06	-	0.07	n.d.	n.d.	n.d.	n.d.	n.d.
Na₂O	<0.03	<0.03	n.d.	n.d.	n.d.	n.d.	n.d.	n.d.	n.d.
K₂O	<0.03	0.01	n.d.	n.d.	n.d.	n.d.	n.d.	n.d.	n.d.
Total	100.49	98.68	98.13	99.93	100.25	99.95	98.00	99.34	100.06

Clinopyroxene is the most abundant melt product, usually forming xenomorphic grains about 0.01-0.4 mm long, sometimes appearing “sieve-like” due to spinel inclusions. Secondary clinopyroxenes (Table 6) are always lower in Na₂O (to < 3 wt%) and Al₂O₃ (to < 1 wt%) and contain scarce Jadeite component. Relative to the primary clinopyroxenes, they contain usually more MgO [12 to 16 wt% versus 8-11 wt%] and have variable Mg# from 70 to 87. CaO-contents are

similar to those in the primary omphacites. Pyroxene is sometimes enriched in TiO₂-content (up to 1.2 wt%).

In some eclogites, secondary pyroxene includes prismatic elongated crystals up to 0.2 mm long and with green-yellow pleochroism. This phase typically shows high-Na₂O content (≈10 wt%), but low Al₂O₃ (<1 wt%) concentration. This phase exhibits significantly higher FeO content (>20 wt%) and corresponds to a large amount of an aegirine component [NaFe³⁺Si₂O₆]. This drastic increase in Fe³⁺ indicates a large increase in oxygen activity in the late-stage of metasomatizing fluids. Such aegirine-bearing clinopyroxene is also present in diamondiferous xenoliths [30].

There are two possible sources for the fluids that induced the partial melting of the eclogites. The difference between these two lies in the timing of the metasomatism. These two hypotheses are: 1) kimberlite metasomatism, with the alteration of captured xenoliths by fluids from the kimberlitic magma; and 2) pre-kimberlite metasomatism, with melting brought about by metasomatism in the mantle before entrapment of the xenoliths by the kimberlite.

Virtually all mantle xenoliths have undergone some form of metasomatism while resident in the mantle, mostly long before their entrainment in the kimberlite. Several observations are applicable here: a) although partial melting occurred in samples of deep-seated xenoliths, little such evidence seems to have been noted from crustal rocks; b) eclogites, which show evidences of extensive melting often bear traces of deformation (cataclasis, mylonitization, etc.), supposedly only formed in the mantle before the kimberlite; c) a spatial connection between the intensity of melting versus the surface of the xenoliths does not seem to appear; d) an inhomogeneous distribution of the degree of partial melting within a given sample is available; e) intersecting veinlets of partial-melt products as well as evidences for two or more types of melting events, perhaps closely related in time are the case; f) there is a rim on the exterior of some eclogites; it is a direct result of interaction with the kimberlite, as opposed to the partial melting which takes place throughout the xenolith, g) differences exist in the intensity of partial melting of similar xenoliths in the same pipe; and h) the degree of partial melting in eclogites varies from pipe to pipe within a given kimberlite field. Based upon the above factors and others [33], a possible scenario would have the first stage of the overall partial-melting process „begin as mantle metasomatism under the influence of fluids that originated in deep mantle, possibly associated with a slight reduction in pressure. This process could have taken place close just preceding kimberlite eruption

The overall effects of metasomatism on mantle xenoliths and their trace-element fingerprints on the chemistry and mineralogy of eclogites were described by Ireland et al. [13]. In addition, there are spatial correlations with the presence of some diamonds and the presence of partial-melt crystallization products. The partial-melting process was most likely connected with the formation of last-stage fibrous diamonds and some microdiamonds [29, 30].

METASOMATISM OF ULTRAMAFIC XENOLITHS

Many of the mantle peridotites from Yakutian kimberlites have been subjected to a different stage of metasomatism in which new visible phases are developed; this stage has been referred to as “patent” or “modal” [6, 12 and references therein]. Separate ultramafic xenoliths with obvious occurrence of phlogopite or other metasomatic minerals are found and described in all well studied pipes of Yakutia [33] but in comparison with the data for kimberlites of South Africa (e.g., 7, 12 and references therein) there is no systematic data on their distribution in different pipes.

“Cryptic” metasomatism is less investigated in the ultramafic xenolith from Yakutian kimberlites. It is possible to find in papers only some evidence about zoning of minerals or more rare data on trace elements distributions that suggest the enrichment of rocks or minerals [e.g., 25, 33]. Here we have systematized the results on xenoliths from main investigated and worldwide known pipes. We tried to make the first attempt to estimate the relative distribution of metasomatized rocks in different pipes, subsequently in different parts of Siberian craton and intensity of metasomatic processes and coupled deformation of rocks.

Petrographic examination and set of data on major chemistry and trace elements distribution suggest that ultramafic xenoliths from the Yakutian kimberlites undergone the metasomatic enrichment and late partial melting in rare cases. The most impressive this is evidenced by widespread flogopitization of the mantle ultramafic xenoliths and kelyphitization of garnet. Phlogopites in xenoliths are highmagnesian with the wide variations of TiO_2 , Al_2O_3 , Cr_2O_3 and FeO . Content of phlogopites varies from separate grains up to 80% of volume of the rock.

Partial melting processes are observed in rare clinopyroxenite xenoliths. Decrystallized and partly the glassy state products of melting are developed between rockforming minerals. Besides they form cutting veins, pockets and blebs up to 10-20 mm in size occupying sometimes about 20% the initial rock volume. To a lesser extent, a partial melting has its signs in xenoliths of the peridotites and in the first place it is expressed in general kelyphitization of the garnet. The ultramafic rocks are subjected to cataclasis and deformation shears. It is confirmed by the presence of porphyritic and porphyroclastic textures, fluidality and partial decrystallization of olivine matrix in xenoliths from all kimberlite pipes.

The cryptic metasomatism is recorded by the presence of the major and trace element zoning in garnets of sheared peridotites from the Udachnaya pipe and in garnets of pyroxenites from the Mir pipe. Some peridotitic xenoliths from the Siberian craton have uniquely extreme Nd and Os isotopic characteristic indicative of ancient incompatible element enrichment [10]. The predominant Archaean ages of mantle xenoliths from kimberlites indicate the longevity of the SCLM under Siberian platform and long term coupling between crust and mantle. Evidence for the cryptic metasomatism is incompatible trace element concentrations in garnets

of fertile harzburgites and garnet peridotites from the Udachnaya pipe that was established by ICPMS-data for minerals more than 10 samples.

Summarizing the results of investigations of metasomatic processes in ultramafic xenoliths from the Yakutian kimberlites it is possible to combine next evidence: i) modal metasomatic minerals or trace-element enrichment occur in the almost all varieties of ultramafic xenoliths; ii) the most prominent features of the modal metasomatism are replacement of early phases by phlogopite with addition of spinel and other ore minerals and development of the kelyphitic rims. Trace elements determination by ICP-MS in garnet and their kelyphitic rims in peridotites from the Udachnaya have suggest a deep origin for the kelyphitization [32]; iii) another evidence for modal metasomatism in peridotite xenoliths are replacement of ortho- and clinopyroxene by hydrous and ore phases and development of partial melting blebs consisting of a new hydrous phases in garnets of coarse grained pyroxenites; iv) the metasomatic processes usually are synchronized or very close to the stage of mantle rock deformation; v) according Re-Os determination of sulfide inclusions in olivines from the Udachnaya pipe the disturbing of Os systematic by igneous and metasomatic events took place after forming SCLM of the Siberian craton from 2.8 till 2.0 Ga [10]. One of the last time of the mantle metasomatism of the Siberian SCLM around 1.8 Ga is confirmed by U-Pb SHRIMP-dating of zircon from metasomatized Gt-pyroxenite from the Udachnaya pipe; vi) the metasomatic and deformation processes are more intensive manifested in xenoliths from the central part (Daldyn-Alakitsky region) of the kimberlite province.

CONCLUSION

According to Re-Os and Sm-Nd dating the SCLM of the Siberian platform was formed in the Archaean. The vertical and lateral heterogeneities of the SCLM are the results of primary differentiations of the mantle substance and late addition of the oceanic crust during subduction in central part of the platform and subsequent development of mantle by the processes of mantle metasomatism and couplet tectonic deformation.

In Yakutian kimberlites and worldwide, the mafic xenoliths display evidences of partial melting processes. Modal and cryptic metasomatism are abundant in ultramafic mantle xenoliths from kimberlites. Often they are couplet with tectonic deformation of mantle rock and in rare cases with the partial melting. These processes took place repeatedly in SCLM of the Siberian craton and were more intensive in the central part of the kimberlite province and are connected with the major tectonic-magmatic events observable in the upper crust.

The SCLM of cratons with the kimberlite-lamproite magmatism worldwide was formed in Archaean and has a resemblance in the distribution of petrographic types of mantle xenoliths and coupled crustal rocks. The evolution of the SCLM of different cratons as well of different regions inside kimberlite provinces could be

different in terms of timing of tectonic-magmatic events as well in intensity of mantle metasomatism, partial melting and tectonic deformation.

REFERENCES

1. Bobrievich A.P., Bondarenko M.N., Gnevushev M.A., Krasov A.M., Smirnov G.I., Yurkevich R.K. The diamond deposits of Yakutia //Gosgeoltekhizdat, Moscow. 1959. 527 p. (in Russian).
2. Bulanova G.P., Griffin W.L. and Ryan C.G. Trace elements in sulfide inclusions from Yakutian diamonds //Contr. Mineral. Petrol. 1996. V. 124. P. 111-125.
3. Bulanova G.P., Griffin W.L., Kaminsky F.V., Davies R., Spetsius Z.V., Ryan C.G., Andrew A. and Zahkarchenko O.D. Diamonds from Zarnitsa and Dalnaya kimberlites (Yakutia), their nature and lithospheric mantle source //Proceedings of 7th Int.Kimberlite Conf., Cape Town, 1999. V. 2. P. 49-56.
4. Bulanova G. P., Shelkov D., Milledge H. J., Haury E. H. and Smith S. B. Nature of eclogitic diamonds from Yakutian kimberlites: Evidence from isotopic composition and chemistry of inclusions //Proceedings of 7th Intern. Kimberlite Conf., Cape Town, South Africa, 1999. V. 1. P. 57-65.
5. Dawson J. B. Kimberlites and their xenoliths. Springer-Verlag, Berlin. 1980. 252p.
6. Dawson J.B. Metasomatized harzburgites in kimberlite and alkaline magmas: enriched restites and "flushed" lherzolites in mantle metasomatism, edited by M.A. Menzies and C.J. Hawkesworth //Academic Press, London. 1987. P. 125-144.
7. Erlank A.J., Water F. G., Hawkesworth C. J., Haggerty S. E., Allsopp H. L., Rickard R. S., and Menzies M. Evidence for mantle metasomatism in peridotite nodules from kimberlite pipes, South Africa, in Mantle metasomatism, edited by M.A. Menzies and C. J. Hawkesworth //Academic Press, London. 1987. P. 221-311.
8. Fadili S. El. and Demaiffe D. Petrology of eclogite and granulite nodules from the Mbuji Mayi Kimberlites (Kasai, Congo): Significance of kyanite-omphacite intergrowths //Proceedings of 7th Intern. Kimberlite Conf., Cape Town, South Africa. 1999 V. 1. P. 205-213.
9. Griffin W.L., Ryan C.G., Kaminsky F.V., O'Reilly S.Y., Natapov L.M., Win T.T., Kinny P.D. and Ilupin I.P. The Siberian lithosphere traverse: Mantle terranes and the assembly of the Siberian craton //Tectonophysics. 1999. V. 310 P. 1-35.
10. Griffin W.L., Spetsius Z.V., Pearson N.J., and O'Reilly S.Y. In-situ Re-Os analysis of sulfide inclusions in kimberlitic olivine: new constraints on depletion events in the Siberian lithospheric mantle //Geochem. Geophys. Geosystems. 2002. subm.
11. Harte B., Hutchison M.T., Lee M. and Harris J.W. Inclusions of (Mg, Fe)O in mantle diamonds/ Ext. Abstract of 7th Int.Kimberlite Conf., Cape Town, South Africa. 1999 P. 308-310.
12. Harte B., Winternburn P.A., and Gurney J.J. Metasomatic and enrichment phenomena in garnet peridotite facies mantle xenoliths from the Matsoku kimberlite pipe, Lesotho, edited by M.A. Menzies and C. J. Hawkesworth //Academic Press, London. 1987. P. 145-220.
13. Ireland T. R., Rudnick R. L and Spetsius Z. V. Trace elements in diamond inclusions from eclogites reveal link to Archean granites //Earth Planet. Sci. Letters. 1994. V. 128. P. 199-213.
14. Meyer H.O.A. Genesis of diamond: a mantle saga //Amer. Mineral. 1985. V. 70. P. 344-355.
15. Pearson D.G. The age of continental roots //Lithos. 1999 V. 48. P. 171-194.
16. Pearson D.G., Kelley S.P., Pokhilenko N.P. and Boyd F.R. Laser $^{40}\text{Ar}/^{39}\text{Ar}$ analyses of phlogopites from southern African and Siberian kimberlites and their xenoliths: constraints on eruption ages, melt degassing and mantle volatile composition //Russian Geology and Geophysics. 1997. V. 38. P. 106-117.
17. Pearson D. G., Shirey S. B., Carlson R. W., Boyd F. R., Pokhilenko N. P. and Shimizu N. Re-Os, Sm-Nd and Rb-Sr isotope evidence for thick Archean lithospheric mantle beneath the Siberia craton modified by multi-stage metasomatism //Geochim. Cosmochim. Acta. 1995. V. 59. P. 959-977.
18. Pearson D.G., Shirey S.B., Harris J.W. and Carlson R.W. Sulphide inclusions in diamonds from the Koffiefontein kimberlite, S. Africa: constraints on diamond ages and mantle Re-Os systematics //Earth Planet. Sci. Lett. 1998. V. 160. P. 311-326.
19. Pearson D.G., Shirey S.B., Bulanova G. P., Carlson R.W. and Milledge H.J. Re-Os isotopic measurements of single sulfide inclusions in a Siberian diamond and its nitrogen aggregation systematic //Geochim. Cosmochim. Acta. 1999. V. 63 P. 703-711.

20. Pearson N. J., Alard O., Griffin W.L., Jackson S. E. and O'Reilly S.Y. In situ measurement of Re-Os isotopes in mantle sulfides by Laser Ablation Multi-Collector Inductively-Coupled Mass Spectrometry: analytical methods and preliminary results // *Geochim. Cosmochim. Acta.* 2002. in press.
21. Rosen O.M., Serenko V.P., Spetsius Z.V., Manakov A.V. and Zinchuk N.N. Yakutian kimberlite province: position in the structure of the Siberian craton and composition of the upper and lower crust // *Geology and Geophysics.* 2002 V. 43. P. 3-26 (in Russian).
22. Shirey S.B., Carlson R.W., Richardson S.H., Menzies A., Gurney J., Pearson. D.G., Harris J.W. and Wiechert U. Archean emplacement of eclogitic components into the lithospheric mantle during formation of the Kaapvaal Craton // *Geophys. Res. Lett.* 2001. V. 28. P. 2509-2512.
23. Shirey S.B. and Walker R.J. The Re-Os isotope system in cosmochemistry and high-temperature geochemistry // *Ann. Rev. Earth Planet. Sci.* 1998. V. 26. P. 423-500.
24. Snyder G.A., Taylor L.A., Crozaz G., Halliday A.N., Beard B.L., Sobolev V.N. and Sobolev N.V. The origin of Yakutian eclogite xenoliths // *Jour. Petrol.* 1997. V. 38. P. 85-113.
25. Snyder G.A., Taylor L.A., Crozaz G., Halliday A.N., Beard B.L., Sobolev V.N. and Sobolev N.V. The diamond-bearing Mir eclogites, Yakutia: Nd and Sr isotopic evidence for the continental crustal input in an Archean oceanic environment / *Ext. Abstract of 7th Int.Kimberlite Conf., Cape Town, South Africa.* 1998. P. 826-828.
26. Sobolev N.V., Yefimova E.S. and Koptil V.I. Mineral inclusions in diamonds in the northeast of the Yakutian diamondiferous province // *Proceedings of 7th Int.Kimberlite Conf., Cape Town.* 199. V. 2. P. 318-322.
27. Sobolev V.N., Taylor L.A., Snyder G.A., Sobolev N.V., Pokhilenko N.P. and Kharkiv A. D. A unique metasomatized peridotite from the Siberian Platform. *Proc. 6th Int. Kimberlite Conf., v. 1: Kimberlites, Related Rocks, and Mantle Xenoliths // Russian Geol. Geophys.* 1997. V. 38. P. 218-228.
28. Spetsius Z.V. Occurrence of diamond in the mantle: a case study from the Siberian Platform // *Journal of Geochemical Exploration.* 1995. V. 53. P. 25-39.
29. Spetsius Z.V. Two generation of diamonds in the eclogite xenoliths // *Proceedings of 7th Int.Kimberlite Conf., Cape Town.* 1999. P. 823-828.
30. Spetsius Z.V. and Griffin B.J. Secondary phases associated with diamonds in eclogites from the Udachnaya kimberlite pipe: Implications for diamond genesis, / *Ext. Abstract of 7th Int.Kimberlite Conf., Cape Town, South Africa.* 1998. P. 850-852.
31. Spetsius Z.V. and Griffin W. L. Trace elements in minerals from eclogites from the Udachnaya kimberlite pipe, Yakutia // *Russian Geology and Geophysics.* 1997. V. 38. P. 240-246.
32. Spetsius Z.V. and Griffin W.L Trace element composition of garnet kelyphites in xenoliths from Udachnaya as evidence of their origin // *Ext. Abstract of 7th Int.Kimberlite Conf., Cape Town, South Africa.* 1998. P. 853-855.
33. Spetsius Z.V., and Serenko V.P. Composition of continental upper mantle and lower crust beneath the Siberian platform. Moscow: Nauka. 1990. 272 p. (in Russian).
34. Spetsius Z.V., Taylor W.R. and Griffin B.J. Major and trace-element partitioning between mineral phases in diamondiferous and non-diamondiferous eclogites from the Udachnaya kimberlite pipe, Yakutia. *Ext /Abstract of 7th Int.Kimberlite Conf., Cape Town, South Africa.* 1998. P. 856-858.
35. Switzer G., and Melson W. G. Partially melted kyanite eclogite from the Roberts Victor mine. South Africa, Smithsonian // *Contrib. Earth Sci.* 1969. V. 1. P. 1-9.

**APPLICATION OF RARE ELEMENT COMPOSITION
OF GARNET AND CLINOPYROXENE FROM PERIDOTITE
XENOLITHS (UDACHNAYA KIMBERLITE PIPE) FOR MODELLING
OF THE PRIMITIVE MANTLE MELTING**

Gornova M.A.¹, Solovjeva L.V.²

1 - Institute of Geochemistry, SB RAS, 664033, Irkutsk, Favorsky str. 1 «a»

2 - Institute of the Earth's crust, SB RAS, 664033, Irkutsk, Lermontov 128

Abundances of trace elements (Nb, Zr, Hf, Ti, La, Ce, Nd, Sm, Eu, Dy, Er, Yb и Y) were determined by the secondary-ion mass-spectrometry method in garnets and clinopyroxenes of coarse-grained low-temperature garnet and spinel peridotites (7 samples) from the Udachnaya kimberlite pipe. The mantle metasomatism has an effect on peridotite minerals. However, this effect is of various intensity. The least metasomatized samples of garnet and clinopyroxene were used for simulation of the melting and reconstruction of rock origin settings. Sp and Gr peridotites from the Udachnaya kimberlite pipe could originate as Ol+Opx residues of variable degrees of the polybaric fractional melting of PM in the 60-27 kbars range. Gr, Sp and Cpx in peridotites result from granule exsolution from the primary orthopyroxene.

INRODUCTEION

Deep xenoliths from kimberlites provide the information on the composition, structure, and origin of the continental mantle as deep as 200 km and more. However, the interpretation of geochemical data for major and trace elements is complicated as after the origin the samples were subjected to metamorphic recrystallization and mantle metasomatism [7, 11, 19].

In terms of structural-petrographic features of rocks, chemical peculiarities of minerals, and PT-characteristics two main groups of peridotite xenoliths in the kimberlites are distinguished. They include coarse-grained low-temperature and deformed high-temperature peridotites [3, 4, 6, 15, 18]. Many investigators consider that the grained spinel, spinel-garnet, and garnet harzburgites and lherzolites form the rigid mantle lithosphere of cratons.

As compared with a primitive mantle (PM) and oceanic lithosphere mantle these rocks are characterized by a significant depletion by such oxides as TiO₂, Al₂O₃, FeO, CaO, Na₂O [4,12]. Two main hypotheses are in competition when explaining this fact. The most widely used viewpoint considers the grained low temperature peridotites as restite remained after the removal of fluid with the komatiitic composition when the primitive mantle is melted [21]. The second model suggests them to be olivine-orthopyroxene cumulates [5, 9,13]. The rock texture and the presence of spinel ± clinopyroxene (in the spinel facies) and garnet

± clinopyroxene (in the garnet facies) are due to the granule exsolution from primary high CaO and Al₂O₃ orthopyroxene.

The present article gives the simulation of restite model based on using concentrations of incompatible elements in the garnet and clinopyroxene from 5 grained garnet lherzolites and 2 grained spinel lherzolites of the Udachnaya kimberlite pipe.

PETROGRAPHY

Studied spinel and garnet lherzolites from the Udachnaya kimberlite pipe are grained peridotites of a common type, forming a major part of the mantle lithosphere under ancient cratons [4, 6, 18].

The rocks possess granoblastic texture and a marked orientation of minerals. A textural pattern of rocks is owing to subhedral olivine grains (2-8 mm, in cases to 10-12 mm) and orthopyroxene (2-5 mm). Small (0.5-2 mm) anhedral garnet and clinopyroxene or spinel and clinopyroxene in spinel lherzolites are found between these subhedral grains. Samples 48/82, 2/84, 343/87 contain rare relict orthopyroxene megacrysts (10-17 mm). Megacrysts are strongly deformed and separated into blocks and domains. The blocks and domains partially preserve a common orientation and include rare tabular orthopyroxene growths and chains of small garnet grains, oriented in orthopyroxene in terms of the cleavage or system of subparallel fissures. The rocks show unclear bedding, which is derived from discontinuous chains, containing Sp±Cpx and Gnt ± Cpx grains, located conformably to the common cleavage. The above indicates a possible recrystallization of Sp, Gnt, and Cpx coming from the primary orthopyroxene exsolution. The modal mineral composition of the rocks is given in Table 1.

Table 1.

Modal mineral composition of spinel and garnet peridotites

Sample	Ol	Opx	Cpx	Sp	Gar
48/82	58,5	38,5	2,5	0,5	-
47/82	80,2	18,9	0,5	0,4	-
43/82	74,7	18,9	3,0	-	3,4
2/84	68	25,0	2,0	-	5,0
325/87	52,4	27,1	1,9	-	18,6
343/87	69,0	20,0	0,3	-	10,7
42/82	62,0	28,5	2,5	-	7,0

Notes. Ol – olivine, Opx – orthopyroxene, Cpx – clinopyroxene, Sp – spinel, Gar- garnet.

All studied samples exhibit prekimberlite metasomatism and secondary transformations of post-pipe stage. Minerals, associated with metasomatism include fine rims on the primary minerals: dark kelyphitic rims on the garnet with micrograins of phlogopite and Al-Cr-spinel in the outer part; fibrous amphibole + secondary clinopyroxene +Ti-spinel and Ti-magnetite on the orthopyroxene;

narrow zones of lightening with Ti-spinel and Ti-magnetite ore on the clinopyroxene; and Ti-magnetite rims on the spinel. Sample 343/87 contains a large (3mm) weakly PhII curved plate, which most likely indicates the premetamorphic metasomatism.

The post-pipe changes. Samples 2/84, 343/87 and 325/87 exhibit serpentine alteration (from 5 to 25%). Samples 48/82 and 43/82 do not have serpentine alteration. All samples include fine calcite selvages ($\leq 0,5\%$) and point impregnations ($\leq 0,1\%$) along the mineral grains. The X-ray analysis shows that the latter involve scarce Al-Cr-spinel, troilite, magnesioferrite, and periclase phases.

GEOCHEMISTRY: RESULTS AND DISCUSSION

Investigations of minerals via microprobe JEOL Superprobe 733 showed the absence of zoning for petrogenic elements within the grain except for very narrow ($\approx 50\ \mu\text{m}$) marginal zones. It can be caused by the influence of pre-kimberlite metasomatism. The concentrations of trace elements (Nb, Zr, Hf, Ti, La, Ce, Nd, Sm, Eu, Dy, Er, Yb и Y) in garnets and clinopyroxenes were measured by the secondary-ion mass-spectrometry following the procedure from [14]. This procedure provided the precision of determinations to be not lower than 10% for trace elements with concentrations of ≥ 0.1 ppm and not lower than 15-20% for contents < 0.1 ppm. Table 2 gives contents of trace elements in minerals. Garnets from various samples show sharp variations both in terms of content and distribution pattern of rare elements (Fig. 1, 2). Garnets from samples 42/82 and 43/82 exhibit low REE concentrations (≈ 0.006 - 0.015 chondrite level for La, Ce and Nd and 1,2-2 chondrite level for Yb). Garnet from sample 2/84 shows the same level of average/and heavy rare earths while La and Ce contents sharply increase (≈ 0.6 - 0.7 chondrite level). The concentrations of heavy rare earths and Ti in garnets from samples 42/82, 43/82 and 2/84 are similar to those in the most depleted purple garnets from low-temperature harzburgites of the Udachnaya pipe [17] - fig.1A. In terms of light and middle REE, Zr and Hf, garnets from samples 42/82, 43/82 are the most depleted ones among the analyzed garnets from garnet peridotites in kimberlites. A specific feature of these garnets is maximal on curves for Zr and Hf.

Garnet from sample 325/87 exhibits REE content similar to that in purple garnets from low-temperature garnet harzburgites with clinopyroxene [17] - fig. 1B. Hf content in garnet 325/87 shows a sharp maximum.

Garnet from sample 343/87 (Fig. 1A) has higher concentrations of all rare elements except for Nb and a characteristic sinusoid-like curve for REE. The curve is plotted in the field of purple garnets from high-temperature garnet lherzolite of the Udachnaya pipe [17]. In terms of the composition it is similar to the central parts of garnet grains from the low-temperature peridotites of the Vesselton pipe, South Africa [7]. Marked minima are found for Zr, Hf and Ti as compared with

Table 2.

Abundances of trace-elements (ppm) in minerals from peridotites of the Udachnaya kimberlite pipe.

	48/82	47/82	43/82		2/84		325/87		343/87		42/82	
	Cpx	Cpx	Cpx	Gar	Cpx	Gar	Cpx	Gar	Cpx	Gar	Cpx	Gar
Nb	0.342	0.011	0.352	0.338	0.376	0.672	1.925	0.232	2.385	0.360	0.349	0.302
La	1.772	0.002	0.046	0.002	14.761	0.140	1.665	0.054	22.214	0.048	0.001	0.004
Ce	5.662	0.005	0.125	0.008	10.070	0.429	4.009	0.06	71.829	0.676	0.004	0.009
Nd	4.443	0.003	0.042	0.005	0.047	0.003	1.597	0.095	50.030	3.195	<0.002	0.003
Zr	5.517	0.166	0.294	0.227	0.315	0.254	3.317	0.298	39.345	21.363	0.263	0.178
Hf	0.078	<0.002	<0.002	0.006	0.115	<0.002	0.093	0.195	1.288	0.391	<0.002	0.012
Sm	1.073	<0.002	0.012	0.006	0.004	0.011	0.224	0.014	4.770	1.178	<0.002	0.003
Eu	0.194	0.001	0.001	0.003		0.003	0.124	0.010	0.909	0.260	<0.0005	<0.0004
Ti	183	16.1	31.8	29.0	13.3	16.7	84.4	115.5	489	601	27.9	19.3
Dy	0.348	0.005	0.003	0.026	0.024	0.01	0.125	0.289	0.693	0.497	0.002	0.04
Y	1.945	0.041	0.018	0.530	0.015	0.160	0.427	4.978	1.219	3.972	0.031	0.701
Er	0.226	0.003	<0.001	0.058	0.047	0.037	0.055	0.806	0.385	0.464	0.007	0.136
Yb	0.290	0.022	0.006	0.229	0.006	0.118	0.034	1.381	0.218	0.624	0.017	0.366

Notes. Abundances of trace-elements were determined by the secondary-ion mass-spectrometry method at the Institute of Microelectronics and Informatics, RAS, in 2001 (analyst – S.G. Simakina)

REE Samples with three types of rare earth element distribution in garnet preserve individual specific features in terms of clinopyroxene geochemistry (Fig. 2 A, B). Clinopyroxenes from garnet lherzolites 42/82 and 43/82 and spinel lherzolite 47/82 (Fig. 2A) contain low concentrations of all rare elements and show a significant increase of concentrations from Dy to Yb. Zr, Hf, Ti maxima are typical of all three samples. Except for high concentrations of La and Ce, clinopyroxene from garnet lherzolite 2/84 is similar to these three samples. Clinopyroxenes from the considered samples contain less rare elements than the clinopyroxene from low temperature garnet harzburgites (100/91), being the most depleted in rare elements [17].

The distribution pattern and concentrations of rare elements in clinopyroxene from garnet lherzolite 325/87 are similar to that for clinopyroxenes from low-temperature garnet harzburgites containing clinopyroxene of the Udachnaya pipe [17] - fig. 2 B. Clinopyroxene 325/87 exhibits the enrichment with light and middle rare earth elements as compared with heavy ones. They are characterized by minimal Zr, Hf and Ti.

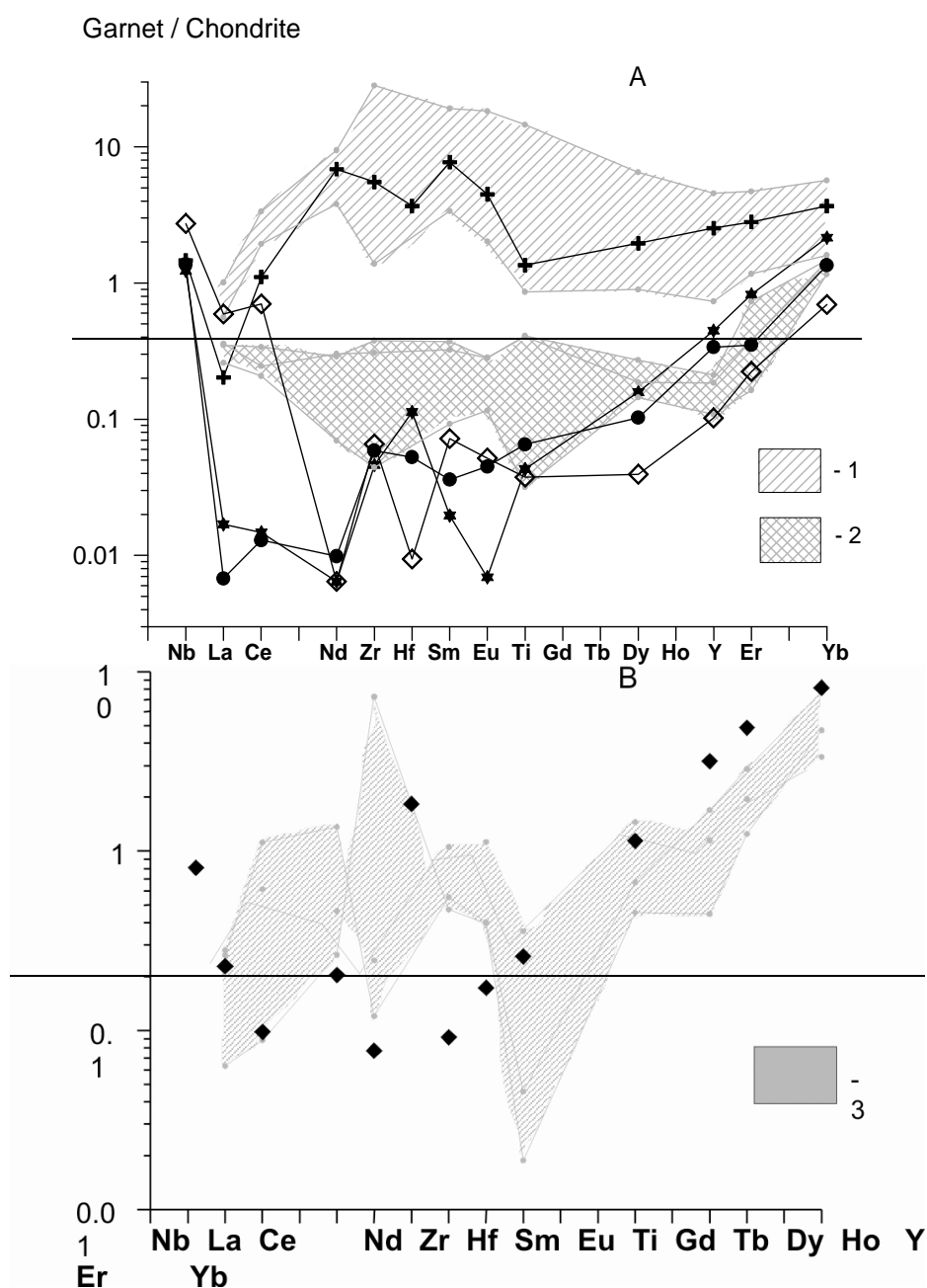


Fig. 1. Chondrite-normalized distributions of rare elements in garnets from coarse-grained low-temperature peridotites of the Udachnaya kimberlite pipe.

Cross – 343/87 sample, star – 42/82 sample, filled circled – 43/82 sample, unfilled rhomb – 2/84 sample, filled rhomb – 325/87 sample.

1 – field of purple garnets from high-temperature peridotites of the Udachnaya pipe [17]; 2 – field of purple garnets from low-temperature coarse-grained harzburgites without clinopyroxene, the Udachnaya pipe [17]; 3 – field of purple garnets from low-temperature coarse-grained harzburgites with clinopyroxene, the Udachnaya pipe [17].

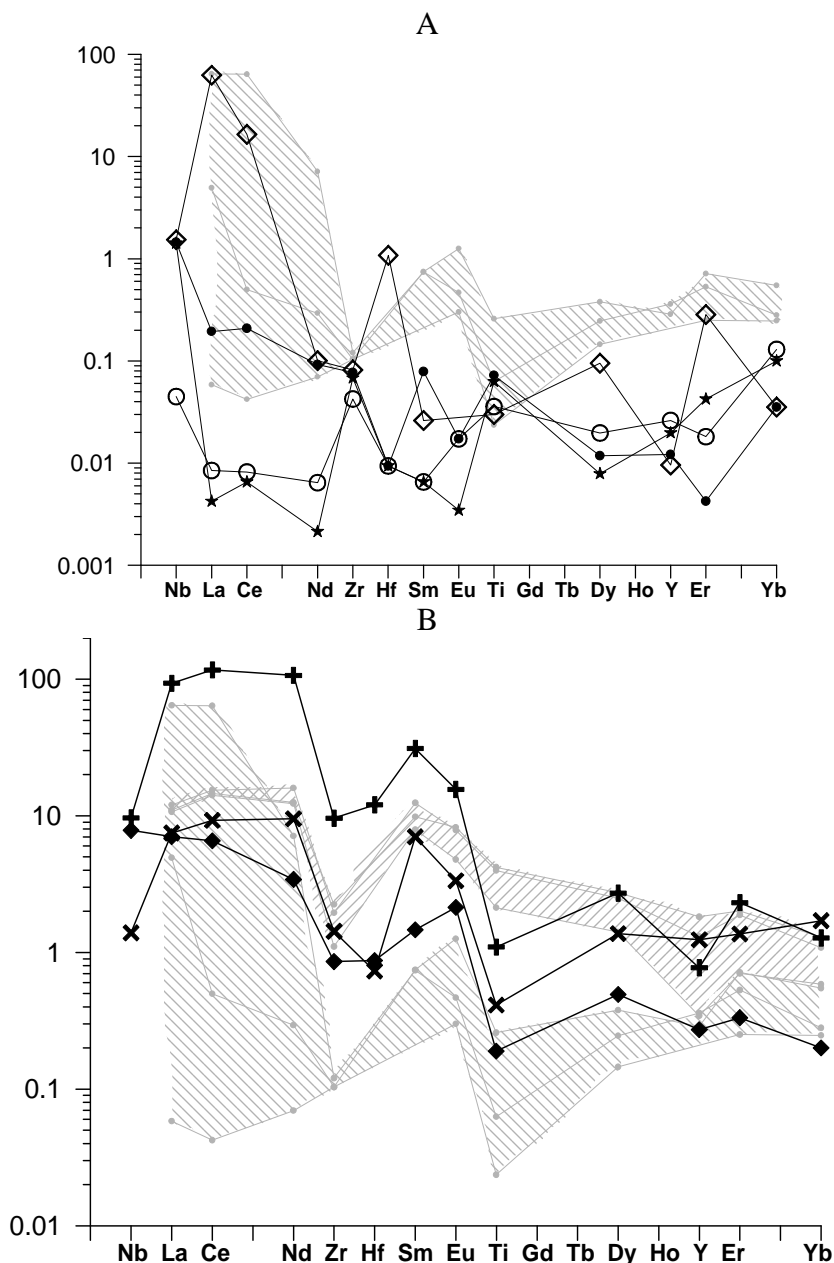


Fig. 2. Chondrite-normalized distributions of rare elements in clinopyroxene from coarse-grained low-temperature peridotites of the Udachnaya kimberlite pipe. Unfilled circle – 47/82 sample; oblique cross – 48/82 sample. Other symbols are similar to those on Fig. 1.

Clinopyroxenes from garnet lherzolite 343/87 and spinel lherzolite 48/83 are marked by higher concentrations of rare elements (Fig. 2 B). Nb, Zr, Hf and Ti are minimal. The concentrations and distribution pattern of rare elements are similar to those for clinopyroxenes from high-temperature garnet lherzolites [17].

The above data indicate that garnets and clinopyroxenes from coarse-grained garnet lherzolites of one and the same type show sharply differentiated contents and distribution of incompatible rare elements. It can result from a possible influence of fluids or melts with high abundance of incompatible elements on rocks generated due to melting [1, 7, 8, 17]. Garnet and spinel lherzolites 343/87

and 48/82 are the most metasomatized rocks in the studied series. It agrees with occurrence of the primary phlogopite plate in sample 343/87.

The distribution of rare elements in garnets and clinopyroxenes from garnet and spinel lherzolites (samples 42/82, 43/82, 47/87) can be regarded as the most similar to the primary ones. According to the model of the mantle metasomatism of peridotites [2, 17], LREE concentrations in the latter can exceed the content in the interacting melt/fluid while the content of heavy REE is not changed.

-Clinopyroxene in sample 325/87 approximates the compositions of the most metasomatized samples while the garnet is less changed. Clinopyroxene from sample 2/84 is more changed as compared with garnet. The disequilibrium of garnet and clinopyroxene representing different metasomatic stages and more rapid reaction of clinopyroxene with the melt were found for low-temperature garnet harzburgites of the Udachnaya pipe [17].

Partition coefficients of rare elements [23] suggest negative Ti anomalies on spider diagrams in primary garnets and clinopyroxenes originated from melting while they provide positive Hf and Ti anomalies in orthopyroxene. The maxima for Zr, Hf and Ti on spider diagrams of incompatible rare elements both for garnets and clinopyroxenes can result from the origin of these minerals through granule exsolution from high-temperature orthopyroxene. In this case the anomalous curve of rare element distribution in garnets and clinopyroxenes is inherited from the primary orthopyroxene [1, 8]. The “primary” inherited from the orthopyroxene and metasomatic distribution of incompatible rare elements is found both in the spinel and garnet zones of the lithosphere mantle under the Udachnaya kimberlite pipe.

MODELLING OF MELTING. DISCUSSION

As opposed to melting in the mid-oceanic ridges, which had formed the oceanic lithosphere, the processes responsible for forming the Precambrian craton lithosphere have been poorly studied. As the dynamics is not clear, models of both isobaric or polybaric batch melting to be expected for sites with buoyant mantle upwelling and polybaric fractional melting typical of settings with a passively upwelling mantle [20] are to be calculated.

The analysis of experimental investigations [21, 22] indicates that MgO content increases relative to the composition of primitive mantle while Al₂O₃, CaO concentrations decrease proportionally to the melting degree. The concentration of ΣFeO is directly correlated with the pressure that's why it is less in restites formed under higher pressures. SiO₂ content in residues shouldn't exceed the composition of the primitive mantle (~ 45 wt.%) and it insignificantly decreases with melting. Abundant interactions of restite peridotites with infiltrating melts and fluids can lead to an additional formation of orthopyroxene, increase of SiO₂ content, and decrease of FeO in a rock that hinders the determination of parameters of the primary melting from the petrochemical composition of the rock.

Considered peridotites from the Udachnaya pipe (Fig. 3) show low ΣFeO concentrations and variations in Al_2O_3 and MgO contents that suggests that these rocks originated under high pressure and variable degrees of melting. The comparison of petrochemical rock composition with residue composition, calculated by Walter [22] using the experimental data, provides the estimation of melting parameters. The rocks could originate as residues from the polybaric fractional melting of the primitive mantle in the 60-20 kbars pressure range or from the equilibrium melting of the primary mantle under 60 kbars and degrees of melting from 20 to 40%.

Rare earth and HFS elements are sensitive indicators of magmatic and metasomatic processes thus they were selected to test possible mechanisms of formation of peridotite from the Udachnaya kimberlite pipe. The partition coefficients of rare elements for high-pressure settings are taken from Xie [23].

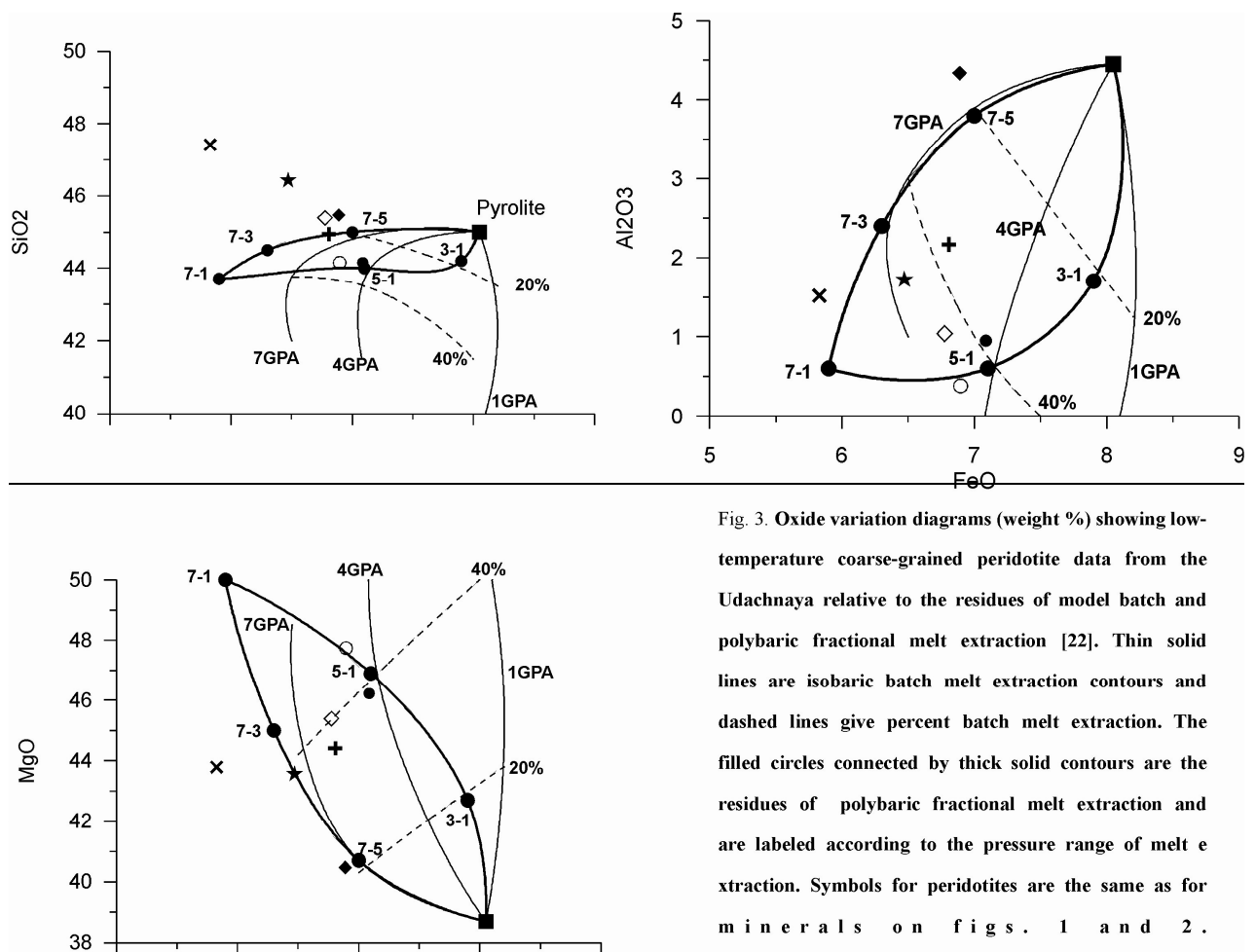


Fig. 3. Oxide variation diagrams (weight %) showing low-temperature coarse-grained peridotite data from the Udachnaya relative to the residues of model batch and polybaric fractional melt extraction [22]. Thin solid lines are isobaric batch melt extraction contours and dashed lines give percent batch melt extraction. The filled circles connected by thick solid contours are the residues of polybaric fractional melt extraction and are labeled according to the pressure range of melt extraction. Symbols for peridotites are the same as for minerals on figs. 1 and 2.

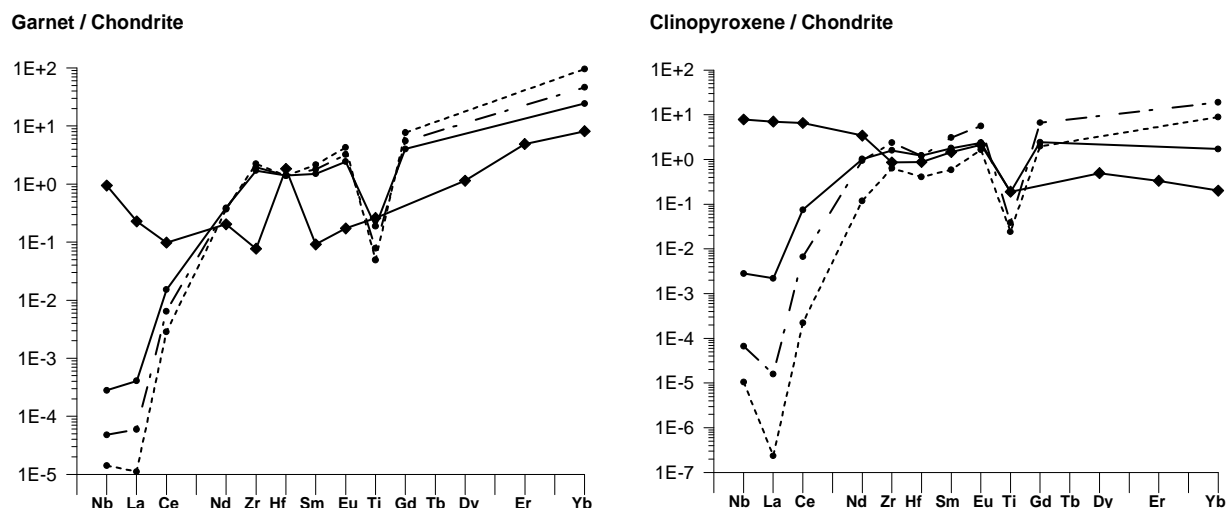


Fig. 4. Chondrite-normalized calculated distributions of rare elements in restite garnets (A) and clinopyroxenes (B) for polybaric fractional melt extraction from PM in the 60-34 kbars interval. A: solid line – 60-44 kbars, point-dashed line – 60-44 kbars, dashed line – 60-38 kbars. B: solid line – 60-44 kbars, point-dashed line – 60-37 kbars, dashed line – 60-34 kbars. Filled rhomb – 325/87 sample.

Table 3.

Parameters used in polybaric fractional melting model (0.1 GPa – 1% melt).

Crystal / Liquid partition coefficients					P, GPa	Modal mineral composition of melting solid (M) and melting reaction (P)	
Nb	Ol	Opx	Cpx	Gr	PM	6 - 4,4	M: 0,54 Ol + 0,31 Cpx + 0,15 Gar P: 0,22 Ol + 0,26 Cpx + 0,52 Gar = 1L
La	0,01	0,01	0,05	0,005	0,713		
Ce	0,005	0,002	0,054	0,01	0,687	4,4 – 3,7	M: 0,6 Ol + 0,32 Cpx + 0,08 Gar P: 0,07 Ol + 4,3 Cpx + 1,14 Gar = 4,51 Opx + 1L
Nd	0,005	0,007	0,21	0,08	1,354		
Zr	0,01	0,01	0,233	0,25	11,2	3,7 – 3,4	M: 0,64 Ol + 0,34 Opx + 0,02 Cpx P: 0,32 Ol + 0,02 Opx + 0,66 Cpx = 1L
Hf	0,005	0,03	0,2	0,23	0,309		
Sm	0,005	0,01	0,26	0,22	0,444	3,4 – 2,0	M: 0,64 Ol + 0,35 Opx P: 0,03 Ol + 0,97 Opx = 1L
Eu	0,007	0,013	0,31	0,32	0,168		
Ti	0,006	0,1	0,1	0,1	1300		
Gd	0,006	0,016	0,3	0,5	0,596		
Yb	0,002	0,049	0,28	4	0,493		

Notes. PM – primitive mantle, L - melt.

Equations for calculating residual bulk compositions taken from Shaw [16]: $C_i^s = [1 - PF/D_i^0]^{1/P} \times C_i^0 / (1-F)$. Equations for calculating the composition of residual minerals taken from and Johnson [10]: $C_i^{min} = [1 - PF/D_i^0]^{1/P} \times [D_i^{min/1} / (D_i^0 - PF)] \times C_i^0$. C_i^s – composition of bulk solid, C_i^0 – composition of melting solid, initial composition is PM, D_i^0 – bulk solid partition coefficient, P – bulk melt coefficient, F – degree of melting, C_i^{min} – composition of mineral, $D_i^{min/1}$ – mineral partition coefficient. C_i^0 , D_i^0 and P are recalculated according to melting reaction.

The quantitative reactions of the polybaric fractional melting of PM were calculated for the 60-20 kbars range using experimental works on the peridotite mantle melting [21] and following the idea that 1% melt is extracted for each 1

kbar in an upwelling “column” of mantle material. The parameters, used in the melting model are given in Table 3.

If the fractional polybaric melting of PM starting from 60 kbars is the case, then garnet doesn't occur among residue minerals beyond 37 kbars and clinopyroxene is not available beyond 34 kbars. Calculated composition of residual garnets and clinopyroxenes in the range from 60 to 34 kbars are given on Fig.4. The corresponding minerals of peridotites from the Udachnaya pipe contain markedly less HREE. Thus, garnet and clinopyroxene couldn't form in such settings and are not primary restite minerals. Beyond 34 kbars the residue contains olivine and orthopyroxene. Petrographic observations and geochemical analysis of concentrations of rare element in garnets and clinopyroxenes in peridotites from the Udachnaya pipe indicate that these minerals could form from exsolution structures in orthopyroxene. Thus, compositions of restite orthopyroxene for the melting in the range from 60 to 25 kbars were calculated first and then compositions of garnet and clinopyroxene were calculated using partition coefficients and real ratio of r , Opx, Cpx in samples. Calculations are given on figure 5. It should be noted that due to abundant mantle metasomatism heavy rare earths are to be considered for the comparison of real compositions of peridotite minerals with the calculated ones.

HREE distribution in garnets (Fig. 5A) from less metasomatized peridotites (sample 2/84, 43/82, 42/82, 325/87) well agrees with the calculated curves for garnets originated from exsolution structures of residual orthopyroxene resulting from fractional polybaric melting of the primitive mantle occurring within 60 to 30 kbars range. A successive decrease of HREE concentrations in garnet is associated with Al_2O_3 decrease in rocks that reflects the increase of melting degree. Zr, Hf, and Ti concentrations are in less agreement with the calculated values, which can be derived from imprecise, selected partition coefficients of these elements and possible metasomatic influence.

Er and Yb concentrations in clinopyroxene (Fig. 5B) also conform to the calculated values. They decrease with the decrease of Al_2O_3 content in the rock. The disturbance of this regularity in the clinopyroxene from the most depleted sample of spinel peridotite (47/82) is apparent. It is due to the exsolution of the most depleted orthopyroxene into spinel and clinopyroxene but not into garnet and clinopyroxene like in other samples.

Thus, Sp and Gr peridotites from the Udachnaya pipe are most likely the residues of melting of variable degrees (from 25 to 33%). Their presence in one and the same pipe can be accounted for polybaric melting of the upwelling “column” of mantle material when small increments of the melt continuously extracted from the residues. Composite melts, complementary to such peridotites are to be komatiitic

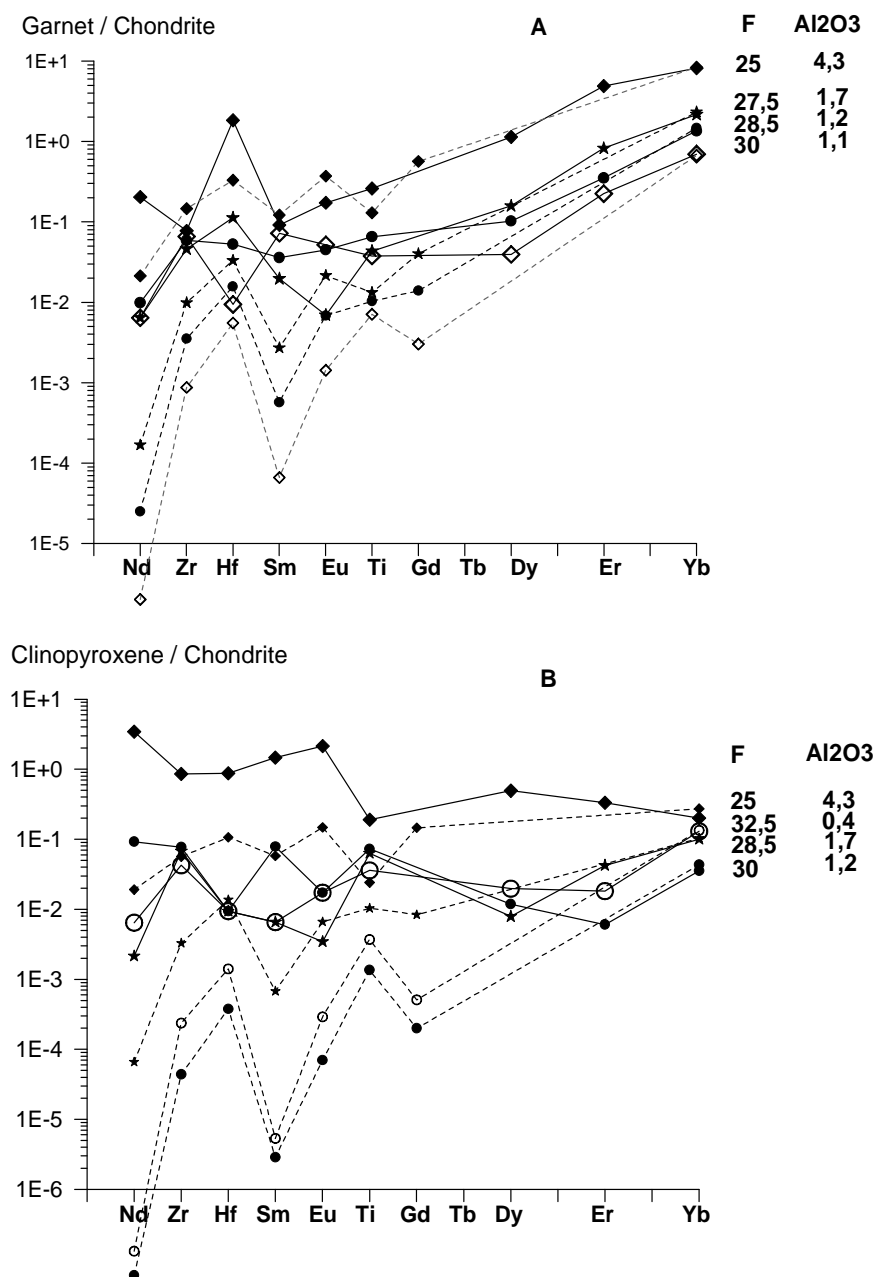


Fig. 5. Chondrite-normalized calculated distributions of rare elements in garnets (A) and clinopyroxene (B), originating from exsolution structures in the restite orthopyroxene for polybaric fractional melt extraction from PM in the 60-27 kbar range. F – melting degree given in %. Al₂O₃ – content in the rock, in weight %. Dotted line – calculated curves, line – compositions of minerals from peridotites in the Udachnaya pipe. Symbols on the curve of the real mineral and compared calculated curve are the same and similar to those on Figs. 1 and 2.

CONCLUSIONS

1. The mantle metasomatism has an effect on peridotite minerals. However, this effect is of various intensity. Thus, the least metasomatized samples of garnet and

clinopyroxene can be used for simulation of the melting from HREE and for reconstructing the setting of rock formation.

2. Sp and Gr peridotites from the Udachnaya kimberlite pipe could originate as Ol+Opx residues from the polybaric fractional melting of PM in the 60-27 kbars range.

3. Gr, Sp, and Cpx in peridotites from the Udachnaya pipe result from the granule exsolution from primary orthopyroxene.

The investigations were supported by RFBR (grant # 02-05-64746).

REFERENCES

1. Abe N., Arai S., Yurimoto H. 1998. Texture-dependent geochemical variations of Sub-Arc peridotite from Japan Island Arcs. 7th intern. Kimb.Conf. Cape Town (Ed. Dawson J. B), 1: 13-22.
2. Bodinier J. L., Vasseur G., Vernieres J., Dupuy C. and Fabries J. 1990. Mechanism of mantle metasomatism: geochemical evidence from the Lherz Orogenic peridotite. *J. Petrol.*, 31(3): 597-628.
3. Boyd F. R., Nixon P. H. 1978. Ultramafic nodules from the Kimberly pipes, South Africa. *Geochim. Cosmochim. Acta*, 42: 1367-1382.
4. Boyd F. R., Pokhilenko N. P., Pearson D. G. et al. 1997. Composition of the Siberian cratonic mantle: evidence from the Udachnaya peridotite xenoliths. *Contrib. Mineral. Petrol.*, 128: 228-246.
5. Davies G. F. 1995. Punctuated tectonic evolution of the earth. *Earth Planet Sci. Lett.*, 136: 363-379.
6. Dawson J. B. 1980. Kimberlites and their xenoliths. Springer-Verlag, Berlin, Heidelberg, New York, 300 pp.
7. Griffin W. L., Shee S. R., Ryan C. Y., Win T. T. 1999. Harzburgite to lherzolite and back again: metasomatic processes in ultramafic xenoliths from the Wesselton kimberlite, Kimberly, South Africa. *Contr. Mineral. Petrol.*, 134: 232-250.
8. Hauri E. H., Hart S. R. 1994. Constraints on melt migration from mantle plumes: a trace elements study of peridotite xenoliths from Savaii, Western Samoa. *J. Geophys. Res.*, 55(B12): 24301-24321.
9. Herzberg C. T. 1993. Lithosphere peridotites of the Kaapvaal craton. *Earth Planet Sci. Lett.*, 120: 13-29.
10. Johnson K. T. M., Dick J. B. H., Shimizu N. 1990. Melting in the oceanic upper mantle: an ion microprobe study of diopsides in abyssal peridotites. *J. Geophys. Res.*, 95 (B3): 2661-2678.
11. Mantle metasomatism. 1987. (Ed.: M. A. Menzies, C. J. Hawkesworth). New York, Academic Press, 472.
12. McDonough W. F. 1990. Constraints on composition of continental lithospheric mantle. *Earth Planet. Sci. Letts.*, 101: 1-18.
13. Nisbet E. G., Walker D. 1982. Komatites and the structure of the Archean mantle. *Earth Planet. Sci. Letts.*, 60: 105-116.
14. Nosova A.A., Sazonova L.V., Narkisova V.V., Simakin S.G. 2002. Trace elements in clinopyroxenes from the Paleozoic volcanics of the Tagil island arc, Middle Ural Mountains. *Geochemistry*, 3: 254-268. (in Russian).
15. Sobolev V., S. 1973. Structure of the upper mantle and ways of magma formation. M.: Nauka, 34pp. (in Russian).
16. Shaw D. M. 1970. Trace element fractionation during anatexis. *Geochim Cosmochim. Acta*, 34: 237-243.

17. Shimizu N., Pokhilenko N. P., Boyd F. R., Pearson D. G. 1997. Geochemical characteristics of mantle xenoliths from the Udachnaya kimberlite pipe. *Russian Geology and Geophysics*, 1/38: 194-205.
18. Solovjeva L.V., Vladimirov V. M., Dneprovskaja L. V. et al. 1994. Kimberlites and kimberlite-like rocks. Upper mantle beneath Siberian craton. Nauka, Novosibirsk, 256 pp. (in Russian).
19. Solovjeva L. V., Egorov K. N., Markova M. E. et al. 1997. Mantle metasomatism and melting in mantle-derived xenoliths from the Udachnaya kimberlite: their possible relationship with diamond and kimberlite formation. *Russian Geology and Geophysics*, 1/38: 182-204.
20. Turcotte D. L., Morgan J. P. 1992. The physics of magma migration and mantle flow beneath a mid-ocean ridge. *Mantle flow and melt generation at mid-ocean ridges*. (Ed.: J. P. Morgan, D. K. Blackman, J. M. Sinton). American Geophysical Union, Geophysical monograph 71: 155-182.
21. Walter M. J. 1998. Melting of garnet peridotite and the origin of komatiite and depleted lithosphere. *J. Petrology*, 39 (1): 29-60.
22. Walter M. J. 1999. Melting residues of fertile peridotite and the origin of cratonic lithosphere. *Mantle petrology: field observations and high-pressure experimentation* (Ed.: Y. Fei, C. M. Bertka, B. O. Mysen). The Geochemical Society, Special publication 6: 225-239.
23. Xie Q., McCuaig T. C., Kerrich R. 1995. Secular trends in the melting depths of mantle plumes: evidence from HFSE/REE systematics of Archean high-Mg lavas and modern oceanic basalts. *Chem. Geology*, 126: 29-42.

GEOCHEMICAL FEATURES OF THE MINERALS FROM THE HEAVY CONCENTRATE FROM KL-1 (KELSEY LAKE) KIMBERLITE PIPE, STATE LINE, COLORADO: PETROLOGIC RECONSTRUCTION.

Ashchepkov I. V.¹, Vladykin N.V.², Mitchell R. H.³, Coopersmith H.⁴, Garanin V. G.⁴, Saprykin A.I.¹, Khmelnikova O. S.¹, Anoshin G.N.¹.

¹*United Institute of Geology Geophysics and Mineralogy, Novosibirsk, garnet@uiggm.nsc.ru*

²*Institute of the Geochemistry, SD RASc, Irkutsk, vlad@igc.irk.ru*

³*Lakehead University, 955 Oliver Rd., Thunder Bay, Ontario, Canada P7B 5E1*

rmitchel@gale.lakeheadu.ca

⁴*Great Western Diamond Company, Front Range, Colorado, USA, diamonds@verinet.com*

Garnets, clinopyroxenes, spinels and ilmenites from the concentrate of KL-1 kimberlite pipe, (Kelsey lake) Front Range, State Line field, were analyzed to reconstruct the mantle section and the processes in the mantle beneath Wyoming craton. Garnets show a trend up to 12% Cr₂O₃ within the Iherzolite field with decreasing frequency for deeper garnets. Several Cr₂O₃ -TiO₂ trends suggest multistage pulses of melt percolation. Their amount coincides with the amount of groups for Cr-diopsides and spinels. Deformed garnets – clinopyroxene intergrowths higher in TiO₂ give more heated TP conditions (to 40-45 mv/m²) than individual grains. Ilmenites showing a long (polybaric) differentiation trend becoming more Cr-rich in Fe-part but spinels increase Ti content in Al-rich (shallow level) varieties. Trace elements for Cr-diopsides suggest participation of subduction-related material with high U content. Increase of HREE and U decrease is in accord with AFC with garnet dissolution. The Ti enrichment took place in the surroundings of the rising evolving pre-eruption kimberlite liquid produced megacrystalline association.

INTRODUCTION

Colorado kimberlites are located at the south boundary of the Wyoming craton. This region concentrate the deep seated volcanism for a long time starting from Late Precambrian to the Cenozoic (Leucite Hill) [7, 9]. State Line district of include several diamondiferous kimberlite groups. Devonian ages reported for the most of State Line diatremes. More ancient 800 to 500 ma were determined for Iron mountain and other kimberlites. Pipes contain a lot of the megacrysts and nearly completely serpentized mantle xenoliths. Pyropes and ilmenites are abundant at and near the pipes and in the placers sometimes together with diamonds. Iron Mountain kimberlites carry abundant and various pyropes [7] belonging mainly to the Iherzolite field according to N.V.Sobolev diagram [15] though the subcalcium harzburgitic garnets from diomondiferrous groups G9-10 were also found.

Kimberlites and deep seated inclusions were studied in detail for many years [7]. In this paper we represent the material from the Colorado KL1 (Kelsey Lake kimberlites, Front range group). The heavy concentrate (fraction +1+-) was analyzed by EPMA and selected minerals by LAM ICP method in UIGGM SD RAS. Studied mineral: pyropes, chromites, Ilmenites, clinopyroxenes were used to

reconstruct the processes taken place at the margin of the lithospheric keel of the Wyoming craton.

RESULTS

GARNETS (fraction +1) from this pipe reveal a long trend on the $\text{Cr}_2\text{O}_3 - \text{CaO}$ diagram (up to 12% Cr_2O_3). (Fig.1) (Table.1). From the beginning to 1% the pyropes with the elevated usually starts from the 4- 5% Cr_2O_3 what refer according

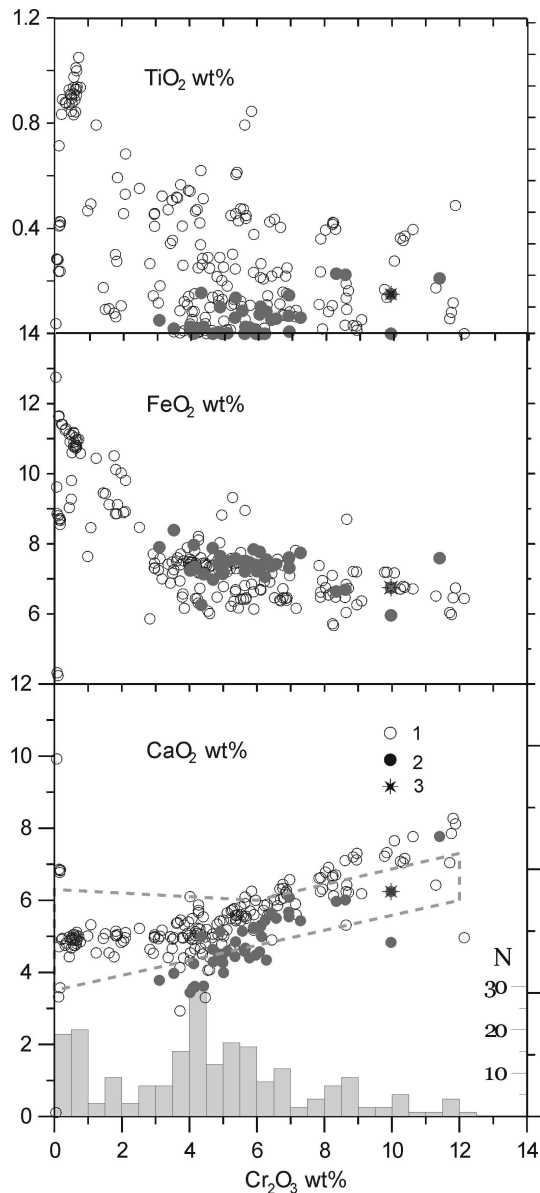


Fig1. Cr_2O_3 -CaO -FeO- TiO_2 (wt%) plots and Cr frequency histograms for the garnets from KL-1 pipe. 1- separate grains; 2. - intergrowths with clinopyroxenes and garnets; 3.garnet from Ilm - serpentine nodules.

to Ryan [13] barometry to the pressures close to diamond stability boundary. The separate $\text{Cr}_2\text{O}_3 - \text{CaO}$ trends usually corresponds to the garnets from different in size fractions and morphology. The Iron Mountain pyropes demonstrate the lower angle inclination of this trend of much higher proportion of subcalcic garnets that were possibly analyzed from a finer fraction. The garnets found in the serpentinized ilmenite harzburgites drop to the herzolite field but lower than the main part of garnets.

Deviation to lower CaO values corresponds to the deformed garnet grains found in intergrowths with the clinopyroxenes and spinels. They are also more ferriferous and their higher Fe# can't be explained by heating (Fig.1).

Proportion of the Cr-less pyroxenites and eclogite garnets in the KL1 pipe is much lower than for Iron Mountain kimberlites [7].

The interesting features of KL -1 pyropes is presence of 4 $\text{Cr}_2\text{O}_3 - \text{TiO}_2$ trends in which Ti values Fe# correspond to gently

Table 1.

Representative analyses of the minerals from the Kl-1 pipe, Colorado
Separate grains

Oxides	5-11	3-47	3-47	3-47	3-39	3-60	3-92	2-27	4-16	2-32	2-44	3-53	3-37
	Pyropes												
SiO2	40.88	40.04	40.92	40.51	41.03	41.29	41.23	41.37	41.63	41.60	42.01	41.3	41.49
TiO2	0.00	0.49	0.40	0.14	0.42	0.09	0.25	0.85	0.51	0.52	0.27	0.793	0.85
Al2O3	14.85	13.31	14.79	15.59	16.50	17.66	17.67	17.88	19.11	19.47	21.16	21.13	21.15
Cr2O3	12.14	11.88	10.62	9.85	8.25	7.16	6.89	5.84	4.41	3.65	2.83	1.24	0.51
FeO	6.44	6.74	6.71	7.19	6.62	6.16	6.46	6.85	7.45	7.60	5.86	10.44	9.80
MnO	0.32		0.00										0.00
MgO	20.76	18.20	18.35	17.97	19.72	20.57	20.82	20.28	20.80	20.72	22.43	19.72	19.24
CaO	4.96	8.12	7.77	7.32	6.68	5.60	6.15	6.25	5.54	5.38	4.64	4.54	4.68
Na2O	0.02	0.06	0.04	0.05	0.05	0.02	0.04	0.07	0.06	0.05	0.06	0.064	0.09
K2O	0.00	0.04	0.00	0.00	0.00	0.02	0.00	0.01	0.01	0.00	0.07	0.007	0.00
NiO		0.02	0.00	0.02	0.014	0.017	0.018	0.03	0.02	0.00	0.01	0.006	0.00
Total	100.37	98.87	99.59	98.62	99.27	98.56	99.51	99.39	99.52	98.99	99.33	99.23	97.82
Fe/(Fe+Mg) %	14.83	17.21	17.04	18.34	15.85	14.39	14.83	15.93	16.74	17.07	12.79	22.90	22.24

Oxides	1KL1	2KL1	5KL1	10KL1	12KL1	7KL1	8KL1	9KL1	22KL1	13KL1	19KL1	20KL1	21KL1	22KL1
	Cr-Diopside													
SiO2	54.74	54.02	54.82	53.95	54.98	54.55	54.40	55.13	55.49	54.73	55.11	55.06	55.07	55.49
TiO2	0.16	0.09	0.21	0.17	0.08	0.18	0.16	0.14	0.09	0.12	0.17	0.15	0.20	0.09
Al2O3	2.61	2.27	2.78	1.21	3.76	1.91	1.97	0.48	0.45	2.15	1.95	0.57	2.36	0.45
Cr2O3	3.26	2.58	3.14	1.77	3.94	2.50	2.86	1.31	1.63	2.77	3.28	3.08	1.35	1.63
FeO	2.39	2.34	2.62	3.46	2.52	2.50	2.52	2.28	2.14	2.15	2.48	2.26	2.28	2.14
MnO	0.10	0.08	0.10	0.10	0.11	0.10	0.10	0.09	0.08	0.09	0.11	0.06	0.09	0.08
MgO	15.12	15.41	14.48	15.74	13.61	16.24	15.10	16.90	17.02	15.25	15.42	16.17	15.85	17.02
CaO	18.88	19.18	18.00	21.29	16.61	19.07	19.72	23.06	22.37	19.42	18.68	20.64	20.48	22.37
Na2O	2.96	2.32	3.49	1.54	4.49	2.15	2.52	1.09	1.32	2.52	3.08	2.14	2.20	1.32
K2O	0.00	0.04	0.00	0.02	0.00	0.00	0.00	0.00	0.00					
NiO														
Total	100.22	98.33	99.64	99.24	100.10	99.20	99.35	100.47	100.59	99.19	100.27	100.13	99.88	100.59
Fe/(Fe+Mg) %	8.15	7.85	9.22	10.98	9.41	7.95	8.56	7.04	6.59	7.33	8.28	7.27	7.47	6.59

Table 1.

Continuation

Oxides	KII-1-16	KII-1-21	KII-1-22	KII-1-23	KII-1-26	KII-1-28	KII-1-29	KII-1-30	KII-1-31	KII-1-32
<i>Cr-Spinels</i>										
TiO ₂	0.24	5.27	1.67	0.47	0.28	0.29	1.63	1.64	2.60	0.78
Al ₂ O ₃	18.79	6.58	6.65	2.11	19.05	26.01	7.00	9.14	6.54	7.22
Cr ₂ O ₃	39.20	44.12	57.22	62.32	42.69	37.11	58.57	53.85	59.20	60.05
FeO	27.76	36.87	22.22	25.11	24.79	22.10	21.24	26.35	20.34	19.68
MgO	13.62	6.91	11.26	10.06	13.43	15.65	12.15	9.80	9.61	12.25
Total	99.61	99.76	99.02	100.0	100.2	101.1	100.5	100.7	98.28	99.97
Fe/(Fe+Mg)%	53.36	74.96	52.54	58.34	50.88	44.21	49.51	60.13	54.30	47.42

KII-5-76	KII-5-79	KII-5-88	KII-5-89	KII-5-90	KII-5-91	KII-5-93	KII-5-39	KII-5-40	KII-5-78
<i>Ilmenites</i>								<i>Rutiles</i>	
58.76	59.59	55.90	58.73	52.22	49.67	50.36	52.01	96.46	95.98
0.96	1.07	1.15	0.96	0.67	0.65	0.66	0.63	0.06	0.17
1.56	2.55	4.98	1.20	0.44	0.80	0.67	0.46	0.66	0.13
27.56	24.25	24.64	27.21	39.18	42.25	42.21	38.34	0.69	2.80
12.93	11.54	13.72	12.16	4.82	7.06	5.43	7.54	0.03	0.34
101.7	99.01	100.3	100.2	97.33	100.44	99.33	98.98	97.91	99.42
8		9	6						
54.47	54.11	50.19	55.65	82.02	77.05	81.35	74.06	91.94	82.37

Ilmenites and Rutiles

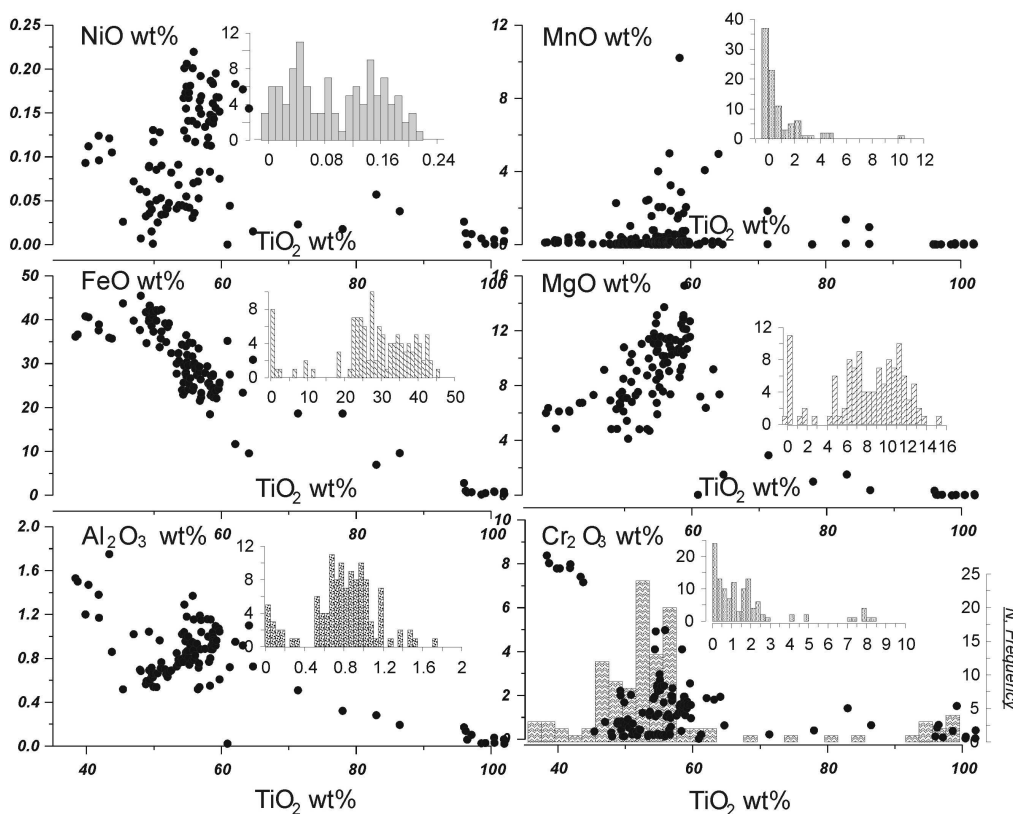


Fig.2. Composition of Ilmenites from KI-1 pipe and the frequency histogram for major components.

(exponentially?) rise with the Cr decrease. They trace through all the interval of Cr₂O₃ values. The garnets were analyzed in three different series and the general features and configuration of the fields was similar.

Clinopyroxenes found in concentrate occurs in two main varieties. Most common are the individual bright grains of Cr-diopsides have relatively low concentration Na₂O, Al₂O₃, Cr₂O₃ and FeO but are much higher in TiO₂ content. Those found in intergrowth with the fractured garnets are evidently enriched in the Fe, Al, and Na (Fig.2)(Tabl.1). On the variation diagram one can find also 4 positive FeO- Na₂O, Al₂O₃, TiO₂ and negative Cr₂O₃ trends.

Ilmenites from this pipe have Ti values which sometimes exceed 1.0 in structural formula (Fig.3)(Tabl.1). Polycrystalline ilmenite fine grained nodules are common. Larger ilmenites contain irregular rutile exsolutions and seems to be cemented by more fine grained material. All these ilmenites came from the desintegrated larger polycrystalline nodules (5-3 mm or more). Polycrystalline equal fine grained aggregates often include rounded rutile grains in intergranularspace between polygonal ilmenites. More rarely these aggregates contain apatite and perovskite. One quartz grain (coesite originally) was found in contact with ilmenites.

In the variation diagrams Ilmenite demonstrate complicated behavior of Ni, Al and Cr contents. Main tendency is common: rise of FeO Al₂O₃ concentrations and decrease of MgO, NiO, Cr₂O₃, TiO₂ but it is evident that this is not a continuous trend but consisting from several branches with the similar tendencies. Very high admixture of MnO (to 12%) in ilmenites and two lines of rapid decrease of this component with the FeO is uncommon feature of this pipe.

Table 2

Representative analyses of the minerals from the K1-1 pipe, Colorado Intergrowths

Oxides	K11-33		K11-37			K11-39		K11-48		K11-45	
	Cpx	Gar	Sp	Cpx	Gar	Ga	CPx	Cpx	Ga	Cpx	Ga
SiO ₂	55.33	42.36	0.05	54.24	41.74	41.71	55.29	54.25	40.78	54.19	41.27
TiO ₂	0.07	0.02	0.93	0.36	0.22	0.01	0.05	0.14	0.08	0.02	0.02
Al ₂ O ₃	5.25	21.00	7.63	2.28	17.11	18.51	3.43	4.39	18.46	3.33	18.94
Cr ₂ O ₃	3.86	3.54	58.08	3.41	8.62	6.96	4.19	3.80	6.28	3.71	5.78
FeO	2.87	8.39	19.41	2.71	6.69	7.31	2.21	2.65	7.55	2.41	7.47
MnO	0.10	0.63	0.63	0.07	0.39	0.50	0.06	0.10	0.55	0.07	0.51
MgO	12.44	20.48	12.95	15.93	20.12	19.43	13.97	13.45	20.32	14.21	20.69
CaO	15.06	3.97	0.00	18.75	6.01	6.08	17.64	15.11	4.34	17.52	4.40
Na ₂ O	5.23	0.06	0.04	2.52	0.04	0.03	3.71	4.29	0.09	3.59	0.06
Total	100.21	100.44	99.72	100.26	100.95	100.53	100.55	98.17	98.46	99.06	99.14
Fe/(Fe+Mg)%	11.46	18.69	45.68	8.71	15.72	17.43	8.15	9.96	17.25	8.69	16.85

Table 2 finished

Oxides	K11-46			K11-88		K11-82		K11-85	
	Cpx	Gar	Sp	Ilm	Ga	Q	Ilm	Ilm	Rut
SiO₂	54.32	41.14	0.78	0.13	41.04	98.25	0.30	0.26	0.85
TiO₂	0.00	0.00	0.02	56.98	0.15	0.02	56.79	55.96	97.19
Al₂O₃	3.28	19.11	9.69	0.83	15.81	0.47	1.10	0.92	0.10
Cr₂O₃	3.42	5.64	55.67	1.80	9.97	0.02	1.72	0.14	0.05
FeO	2.36	7.21	20.07	26.99	6.75	0.07	29.12	31.98	0.41
MnO	0.09	0.45	0.72	0.84	0.43	0.02	1.65	0.39	0.03
MgO	14.42	20.39	11.23	11.87	19.09	0.02	7.92	9.37	0.11
CaO	17.11	4.58	0.04		6.24	0.02			0.27
Na₂O	3.12	0.02	0.05		0.036	0.02			0.14
Total	98.12	98.54	98.26	99.43	99.52	98.92	98.60	99.01	99.14
Fe/(Fe+Mg)%	8.41	16.56	50.08	56.06	16.56	70.95	67.34	65.69	67.39

garnets are located exactly on the mantle array and shows rather restricted compositional range (55-60% Cr₂O₃) that refers here to 5-7% in coexisting garnets.

Ip conditions for mantle peridotites were determined using clinopyroxene thermobarometry [11] and new Jd-Di barometer [3]. Separate grains of Cr-diopsides are located close to 35 mv/m² and between 35-40 mv/m² geotherms within the 30-50 kbar interval, but the clinopyroxenes in intergrowths with garnets produce the more heated branch (or branches) close to 45 mv/m². (Fig.5).

Trace elements determined by LAM ICP MS for four clinopyroxenes demonstrate common REE patterns for lithospheric mantle peridotites patterns with high La/Yb_n ratios and divergent HREE. Trace element spidergram do not show strong minima in HREE except for Ta and smaller for Nb but they reveal evident peak in U, Ba, Sr which is typical for the subduction processes (Fig.6, Table 3).

DISCUSSION

The Cr₂O₃ frequency histogram for the garnets probably reflecting the amount of the deep peridotite material carried by the kimberlite. Presence of separate clots (5 or 8) in this trend probably reflect separate pressure intervals and mantle sections since the Cr- content is variable. The highest peak may correspond to the location of the main intermediate magmatic chamber or it may be explained by the dissolving or loss of the more deeper Cr-rich garnets and rocks during magma upwelling or/and possibly may correspond to the progressive depletion of the lithospheric keel in the depth what is common for well studied pipes like Udachnaya [4] etc. Different inclination of the Cr-Ca trends may be found even at the same kimberlite pipe what is evidently seen in the garnet diagrams from the nearby located Iron Mountain kimberlite [7]. It most likely reflects the TP gradient variations and/or variations in lithology.

The Cr-Fe-Ti relations (Fig.1) for garnets suggests that even in the same pressure interval the lithology of the mantle substrate was not homogeneous and the rocks from the same interval were probably modified by several stages of melt

percolation (Cr-Ti-trends). Relative amount of depleted rocks commonly rises with the depth. Looking on the Cr-Ti trends one can suggest the mixing process supposing the interaction of evolving megacryst forming melts with mantle peri

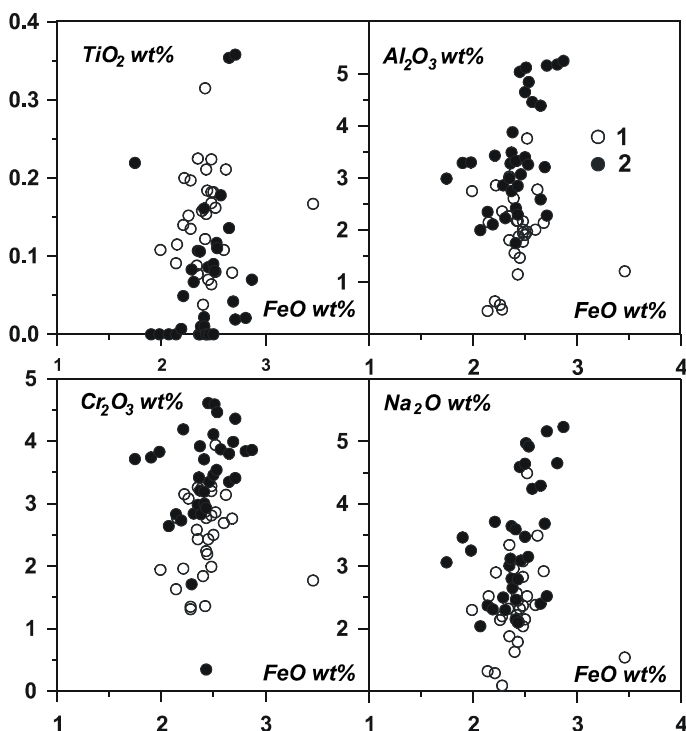


Fig. 4. Variations of the clinopyroxenes from KI-1 pipe. 1-2 the same as for Fig.3.

The lower Ti varieties an opposite are more Cr-rich and slightly lower in FeO. Polycrystalline aggregates containing garnets and essential amount of serpentine have very high Cr_2O_3 concentration in ilmenite (>7%) and garnet (~11%). Two serpentine varieties- with high (56%) and low (~40%) SiO_2 content substitute Opx and Ol respectively (Table 2) (Fig.3).

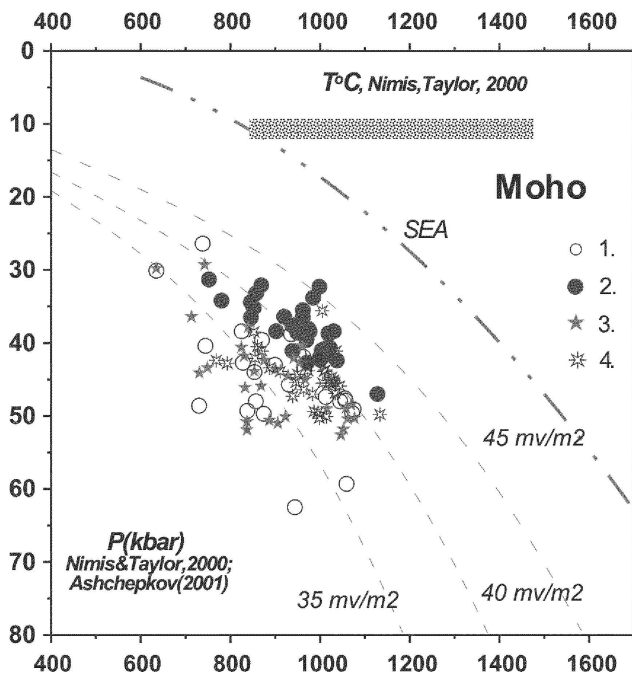


Fig. 5. TP plot for the clinopyroxenes determined by Nimis and Taylor, 2001 method: 1. separate grains; 2 intergrowths; determined by the Jd-Di barometer Ashchepkov, 2001. 3- single grains; 4- intergrowths.

Chromites from concentrate of this pipe reveal two main modes (Fig.4)(Table 1), but a more detailed histogram shows that there are at least 4-5 peaks as well as for the pyroxenes and garnets. The Ti and Al rise together in the chromian spinels in this pipe and other kimberlites also. The chromites found in the intergrowth with

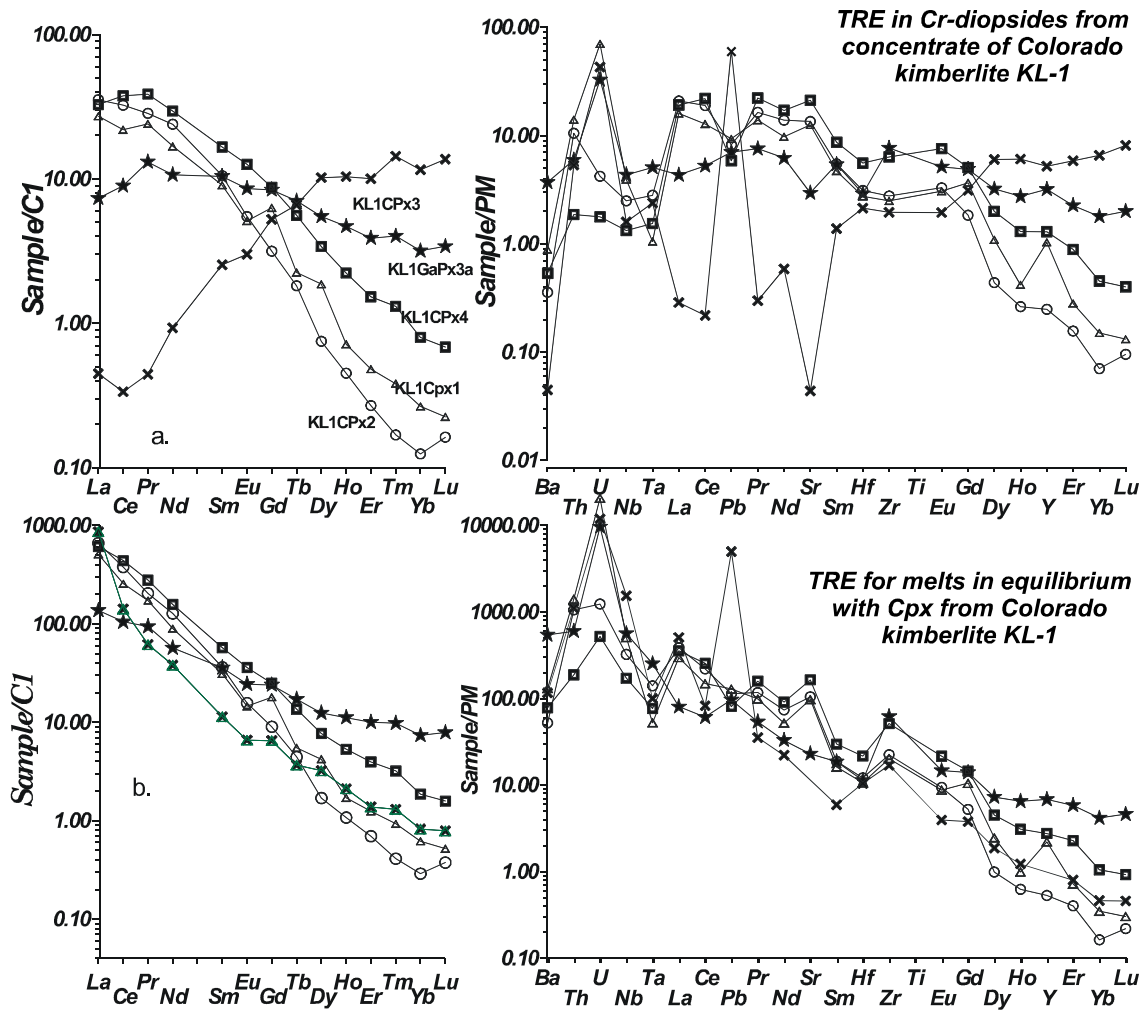


Fig.6 TRE patterns for the clinopyroxenes and some garnets in intergrowth with Cpx and Spinel and TRE patterns for the melts parental for this phases.

grains spinels for Suggestion about the interactions in a short pressure interval is against common Cr- barometry [13]. Cr-rich subcalcic garnet usually refer to depleted harzburgite affinity. In this concentrate these are deformed garnets with intermediate Cr_2O_3 concentration lower in CaO and TiO_2 found in intergrowth with spinels. They show a flat FeO trend on the Cr_2O_3 -FeO diagram and are derived from the heated depleted lherzolites or harzburgites relatively enriched in Fe but low in Ti.

The Cr content in the spinels usually is regulated by the pressure in common mantle peridotites. This feature is proved by good correlations between the calculated pressures and Cr in Udachnaya [4] and other pipes. The highest contents of Cr_2O_3 (65-50%) probably refer to the minerals entrained from the deeper part of the mantle section (50-60 kbar) while 30-50% Cr_2O_3 should come from the rocks from the middle part, which refer to 3-5% Cr_2O_3 in garnets locating in the beginning of the ascending Cr_2O_3 -CaO trend for the pyropes. Ti enrichment in the

spinels most likely has the same nature as for the garnets and means the interaction of the pre-eruptional kimberlite liquid with the wall rock mantle peridotites.

Table 3.

Composition of major and trace elements from the clinopyroxenes and garnet from KL-1

Компонент	12KL1	14KL1	20KL1	48KL1	48KL1	72KL1
	<i>Cpx</i>	<i>Cpx</i>	<i>Cpx</i>	<i>Cpx</i>	<i>Garnet(kel)</i>	<i>Garnet</i>
<i>SiO2</i>	54.98	54.72	55.06	54.25	40.78	40.2
<i>TiO2</i>	0.08	0.22	0.15	0.14	0.08	0.21
<i>Al2O3</i>	3.76	1.78	0.57	4.39	18.46	14.25
<i>Cr2O3</i>	3.94	3.20	3.08	3.80	6.28	11.41
<i>FeO</i>	2.52	2.48	2.26	2.65	7.55	7.59
<i>MnO</i>	0.11	0.11	0.06	0.10	0.55	0.475
<i>MgO</i>	13.61	16.48	16.17	13.45	20.32	17.42
<i>CaO</i>	16.61	18.79	20.64	15.11	4.34	7.77
<i>Na2O</i>	4.49	2.37	2.14	4.29	0.09	0.055
Сумма	100.10	100.15	100.13	98.17	98.46	99.38
<i>Ba</i>	0.55	0.22	2.29	0.61	0.33	0.07
<i>La</i>	1.00	1.30	0.27	0.06	1.20	0.16
<i>Ce</i>	2.10	3.10	0.86	0.23	3.60	0.32
<i>Pr</i>	0.33	0.39	0.18	0.03	0.53	0.06
<i>Nd</i>	1.20	1.70	0.76	0.19	2.10	0.66
<i>Eu</i>	0.04	0.05	0.08	0.05	0.11	0.59
<i>Sm</i>	0.21	0.24	0.24	0.11	0.38	0.26
<i>Gd</i>	0.19	0.10	0.26	0.17	0.27	1.61
<i>Tb</i>	0.01	0.01	0.04	0.03	0.03	0.38
<i>Dy</i>	0.07	0.03	0.21	0.14	0.13	3.90
<i>Ho</i>	0.01	0.00	0.04	0.02	0.02	0.88
<i>Er</i>	0.01	0.01	0.10	0.06	0.04	2.50
<i>Tm</i>	0.00	0.00	0.01	0.01	0.00	0.51
<i>Yb</i>	0.01	0.00	0.08	0.04	0.02	2.87
<i>Lu</i>	0.00	0.00	0.01	0.01	0.00	0.52
<i>Hf</i>	0.08	0.09	0.08	0.02	0.16	0.60
<i>Ta</i>	0.00	0.01	0.02	0.01	0.01	0.07
<i>Pb</i>	1.68	1.48	1.26	0.22	1.05	10.85
<i>Th</i>	1.20	0.90	0.51	0.09	0.16	0.46
<i>U</i>	1.50	0.09	0.70	0.13	0.04	0.92
<i>Sr</i>	202.04	278.50	60.90	2.70	438.00	0.00
<i>Y</i>	0.77	1.13	14.50	7.00	5.89	23.57
<i>Zr</i>	22.65	30.97	85.95	27.95	71.16	21.88
<i>Nb</i>	0.05	1.62	2.82	0.74	0.86	0.91

kimberlite pipe Colorado Separate grains

Note. Major components are determined on CamebaxMicro operator (O.S.Khmelnikova) TRE by LAM ICP MS, analyst Garanin V.G., Analytic Center UIGGM, SD RASc

About the evolution of the melts forming the megacrystalline association in this pipe we can judge only by the ilmenites megacrysts and most ferriferous garnets. Ilmenite chemistry is usually explained by the fraction crystallization [6]. But unlike the rather simple trends found for the Monastery [10] and several other

pipes with the single crystallization lines there in KL-1 pipe it consists from at least three separate lines.

Trends with the different Al_2O_3 concentration suggest the differentiation of the liquid derived varying proportion of garnets. Different Cr_2O_3 -enrichment suggests diverse degree of contamination in wall rock peridotites and possibly varying lithology. The most enriched in Ti varieties with high Cr content are less in Fe and probably means the crystallization of the remaining portion of the melts within the thin veins in peridotites according to the AFC process.

Origin of other Cr-bearing groups suggests several events of the contamination during differentiation. This usually is associated with the migration of the parental magmatic liquid [1]. Intermediate compositions between rutiles and ilmenites are explained by tiny exsolutions.

TP conditions determined with the clinopyroxene thermobarometry suggest at least two heating events which are associated with the percolation and interaction with the melts of different geochemistry. It is likely that nearly all studied mantle column was subjected to the interaction with mantle peridotites and heated. The last stage suppose local and very irregular heating.

The deformed and more ferriferous associations (and parental melts) were enriched in Na_2O but were lower in TiO_2 . This features may correspond to the remelting of the subduction eclogites. The local and very high MnO content in ilmenites also may mean a contamination in the sediments subducted from the ocean floor.

Some fluctuations near Eu in one Cpx and other minerals may also suggest participation of the subducted material in melting and pyroxenite generation. Pyroxene found in intergrowth with garnets reveal lower HREE and lack Sr and other peaks, which suggest the dissolution of garnet possibly by AFC process. The peaks in the U, Ba, Sr also most likely has the subduction nature and were determined for mantle peridotites from Somerset island kimberlite [14].

CONCLUSIONS

Mantle section beneath the pipe Kl-1 was subjected to several (at least two) stages of melt percolation that produced also the heating of mantle column. The earliest one was followed by Ti-enrichment in minerals and should be produced by plume-related evolving melts while the latest was followed by the Na, Al, Cr enrichment in pyroxenes and deformations in garnets. The Ti rich trends are associated with the creation of the megacrystalline associations and took place at the wall rocks of the protokimberlite pre-eruptional very enriched and highly differentiated liquid.

In this section study of coarse grained material do not found the minerals with the signs of the sheared lherzolites typical for the Lesotho [12] or Udachnaya pipe [4]. Mantle section consists from at least 3 or 4 major units but seems to be more layered. It was nearly continuously captured by the host kimberlites but the main

portion of xenoliths was carried from 30-50 kbar interval where the lenses of coarse eclogite – like pyroxenites similar to the mantle beneath Jericho pipe [8], Chompolo field Aldan [2] should exist. Subduction – related material participated in generation of Al-rich Cr- bearing pyroxenites and contaminated the melts that produced the megacrystalline association.

Thus the enrichment and heating of the lithospheric keel of the Wyoming craton and other region was produced by the step by step rising of several portions of the evolving melts with different geochemical and genetic nature. Comparison with the other pipes in this kimberlite group should show lateral scale of is this process.

Acknowledgements. Work was supported by RFBR grants 99-05-65688, 00-05-65288

REFERENCES

1. Ashchepkov I.V., Andre L. Differentiation of the mantle melts: an example of the pyroxenites xenoliths from picrite basalts of Vitim plateau. // *Russian Geology and Geophysics*. 2002. V.43. N4. P. 343-363
2. Ashchepkov I., Vladykin N., Ovchinnikov Yu., Anoshin G., Gerasimov P., Saprykin A. Thermal Gradient, Mantle Layering and Geochemistry beneath Aldan Shield According to the Kimberlitic Deep Seated Disintegrated Inclusions. // *J.Confer. Abstr.* 2000. V.5/2. P.162-163
3. Ashchepkov I.V. An Empirical Clinopyroxene Thermobarometer for Mantle Rocks Based on the Jadeite-Diopside Exchange. *Trans. (Doklady) RAS (ESS)*. 2002. v.382. N1. P.78-82.
4. Boyd, F.R., Pokhilenko, N.P., Pearson, D.G., Mertzman, S.A., Sobolev, N.V., Finger, L.W., 1997. Composition of the Siberian cratonic mantle: evidence from Udachnaya peridotites xenoliths. // *Contrib. Mineral. Petrol.* 1997. V.128. P. 228–246.
5. Burgess R., Harte B. Tracing Lithosphere Evolution through the Analysis of Heterogeneous G9/G10 Garnets in Peridotite xenoliths I. Major Element Chemistry. /*Proceedings of the VII international Kimberlite Conference*. 2001. The P.H. Nixon volume. P.61-80.
6. Griffin W.L., Moore R.O., Ryan C.G., Gurney J.J., and Win T.T. Geochemistry of magnesian ilmenite megacrysts from Southern African kimberlites. // *Russian Geol. Geophys.* 1997. V. 38/2. P.398-419.
7. Hausel W.D. Diamonds and mantle source rocks in the Wyoming Craton, with a discussion of other US occurrences. // *Wyoming State Geological Survey Report of Investigations*. 1998. V.53. P.93.
8. Kopylova M.G., Russell J.K., Cookenboo H. Petrology of peridotite and pyroxenite xenoliths from the Jericho kimberlite: Implications for the thermal state of the mantle beneath the Slave craton, northern Canada. // *J. Petrol.* 1999. V. 40/1. P. 79-104.
9. Lester A., Larson E. New geochronological evidence for the Late Proterozoic emplacement of Colorado-Wyoming kimberlites belt. // *EOS Trans. Am. Geoph. Union*. 1996. V.77. N 41. P. 821.
10. Moor R.O., Griffin W.L. Gurney et al. Trace element geochemistry of ilmenites megacrysts from the Monastery kimberlite, South Africa. // *Lithos*. 1992. V.29. P.1-18.

11. Nimis P., Taylor W. Single clinopyroxene thermobarometry for garnet peridotites. Part I. Calibration and testing of a Cr-in-Cpx barometer and an enstatite-in-Cpx thermometer. // *Contrib. Mineral. Petrol.* 2000. V.139/5, P. 541-554.
12. Nixon, P.H., Boyd, F.R. Petrogenesis of the granular and sheared ultrabasic nodule suite in kimberlite. / Ed. : Nixon, P.H. *Lesotho Kimberlites*. Cape and Transvaal, Cape Town. 1973. P. 48–56.
13. Ryan, C.G., Griffin, W.L., Pearson, N. Garnet Geotherms: a technique for derivation of P–T data from Cr-pyrope garnets. // *J. Geophys. Res.* 1996. v.101. P. 5611–5625.
14. Schmidberger S. S., Francis D. Constraints on the Trace Element Composition of the Archean Mantle Root beneath Somerset Island, Arctic Canada. // *J. Petrology.* 2001. V. 42. P.1095-1117.
15. Sobolev N.V. *Deep-Seated Inclusions in Kimberlites and the Problem of the Composition of the Upper Mantle (in Russian)*. // Nauka Press. Novosibirsk. 1974. 264 p. English Translation. Ed. F.R. Boyd. American Geophysical Union. Washington. DC. 1977. 279 P.

ESSENTIAL TYPES OF MANTLE SUBSTRATE IN THE ZIMNY BEREG REGION IN CONNECTION WITH THE FORMATION OF KIMBERLITE HOSTING ROUNDED AND FLAT-FACED DIAMONDS

Sablukov S.M.¹ , Sablukova L.I.¹ , Verichev E.M.²

¹ *Central Research Institute of Geological Prospecting for Base and Precious Metals, Moscow*

² *ZAO "Arkhangelskgeolrazvedka", Novodvinsk [S. Sablukov@g23.relcom.ru](mailto:S.Sablukov@g23.relcom.ru)*

Two main types of mantle substrate have been identified for the Zimny Bereg kimberlite district. Examination of more than 3500 mantle xenoliths and their host igneous rocks from the study area revealed that some of the xenoliths are related to a homogeneous, dunite-type mantle substrate, while other samples suggest a relationship to a heterogeneous mantle substrate represented by eclogite-peridotite and eclogite-clinopyroxenite-peridotite varieties (subtypes). The two substrate types differ markedly, primarily by the presence of ilmenite ultramafics in the heterogeneous substrate. Based on local kimberlite geochemistry, it is suggested that the central part of the study area is characterized by a heterogeneous mantle substrate, and the homogeneous substrate is characteristic of the marginal zones of the district. The zone of water-alkaline (K-Na) mantle metasomatism covers much of the study area, including the homogeneous dunite substrate and eclogite-peridotite heterogeneous substrate variety (subtype). Kimberlite rocks from this zone are characterized by amphibolization of mantle ultramafic nodules (xenoliths), presence of melilite (more rarely, nepheline), and predominance of rounded, "Uralian-type" diamond crystals, which may be due to the dissolving action of Na-enriched kimberlite melts. Abyssal inclusions from the V.Grib pipe show no evidence of mantle amphibolization, however clinopyroxene-phlogopite metasomatites are abundant there, which suggests that the study area includes a zone of water-limy-alkaline (K-Ca) mantle metasomatism related to the eclogite-clinopyroxenite-peridotite heterogeneous substrate subtype. The specific mantle metasomatism characteristics of this substrate variety, with no supply of highly active, dissolving Na component to kimberlite melt, could have favored the survival of most diamond crystals as flat-faced octahedral.

INTRODUCTION

Arkhangelsk geologists have discovered the Zimny Bereg kimberlite district in the 1970s to 1980s. This district is unique, both in great diversity of igneous rocks and abundant information on the relationship between compositional characteristics of these rocks and compositional peculiarities of their mantle source.

The Zimny Bereg kimberlite district is located in the southeastern White Sea shore area, in the zone of junction of the Russian plate and the Baltic shield. More than 60 eruptive bodies (pipes, dykes and sills) are known in this district [9,13]. Twenty-four of these entities consist of Fe-Ti series kimberlites [8] (analogues to Group 1 of South African kimberlites [5,24]). Another 26 occurrences are composed of Al series kimberlites [8], unique rocks similar to "isotopic transitional type" kimberlites (rocks with isotopic characteristics intermediate between those of Group 1 and Group 2 South African kimberlites [5,23,24]). Lately, another 12

occurrences consist of tholeiitic and subalkaline basalts [9]. The Zimny Bereg kimberlites represent two full rock series, contrastingly different in structure and composition. Showing a broad spectrum of rock varieties, from highly diamondiferous kimberlites to non-diamondiferous melilitites and picrites [8,9,21], these rock series have even more contrasting compositional characteristics as compared with Group 1 and Group 2 of South African kimberlites [24]. Besides, there are sharp distinctions in diamond morphology: most of the kimberlite occurrences of both kimberlite series are characterized by a sharp predominance of "Uralian-type" diamonds (rounded dodecahedroids and tetrahexahedroids) [17], whereas the recently discovered V.Grib pipe shows the predominance of flat-faced octahedral diamonds [12,16]. Peculiarities of mantle nodules from local kimberlite and kimberlite-related rock occurrences with predominating rounded diamonds have been studied previously [11]. Of prime interest for the study are mantle xenoliths from the V.Grib pipe, which would yield the information about the mantle source composition for the new Zimny Bereg diamond deposit type, the upper mantle structural features for the whole Zimny Bereg district, the probable effect of the mantle rock composition on compositional characteristics of kimberlites being formed as a result of these mantle rocks melting, and the role of mantle metasomatism in the formation of diamond deposits with predominantly flat-faced diamonds and those with predominant "Uralian-type" rounded diamond crystals in the Zimny Bereg district.

EXPERIMENTAL STUDIES

We examined a set of mantle nodules collected from more than 30,000 m core (including approximately 5000 m of the core from the V.Grib pipe), of 58, i.e. almost all presently known, igneous rock occurrences in the Zimny Bereg kimberlite district during 1982-2002. The collection consisted of more than 3500 mantle nodules (including more than 500 samples from the V.Grib pipe), excluding numerous xenocrysts. Examination of deep-seated inclusions involved 1300 X-ray spectral microanalyses of minerals, and more than 350 thin and polished sections of abyssal rock samples have been studied. In addition, 42 chemical analysis of nodules and 35 instrumental neutron activation analyses have been made. Concurrently with examination of deep-seated inclusions, we studied the structure and compositional characteristics of all known igneous rock occurrences in the region under study. The results of this research have been published in our previous works [7-10,21].

EVIDENCE OF CONSANGUINITY OF ZIMNY BEREG VOLCANUTES

Although the Zimny Bereg igneous rocks vary in geological structure and composition, they do form a common magmatic family. All the local igneous rock occurrences are located close to each other, with similar shape, size, morphological

characteristics (pipes with craters, sills, dykes) and structure-textural features. Besides, all these rock occurrences are of nearly the same age, and they show similar distribution of geochemical parameters, therewith having similar tectonic controls.

Age. Based on paleofloristic data (*Callixylon* sp., *Arhaeopteris sibirica* Zal., *Xenocladia* cf. *medullosina* Arnold., *Leptophleum* sp.) from diatreme and crater rocks of volcanic pipes, all local volcanites (the two kimberlite series and the basalts) were dated as the Late Devonian, or, with maximal accuracy, 367+/-7 Ma [7,9,18].

Geochemical zoning. The fact the different compositional features of local igneous rocks are characterized by quite regular distribution within the Zimny Bereg district confirms the consanguinity of these rocks [9,10,11]. In particular, Ta distribution in igneous rock autoliths throughout the area under study is regular, with central-type symmetry. Ta is the indicator of ilmenite ultramafics for the deep-seated substrate such as picroilmenite being an essential high-pressure Ta-concentrating mineral in kimberlites [4,8,9]. The Ta concentration contours form a well defined concentric pattern within the Zimny Bereg area, with peak Ta concentrations in the central part of the area and minimal Ta contents in the marginal zones, which agrees well with local volcanite mineralogy features (Fe-Ti series kimberlites occur in the central part of the study area, and the marginal zones are dominated by Al series kimberlites and basaltic rocks [9,10,22], Figure 1A). The Ta concentration contour map has been compiled in 1990. All the pipes discovered during the recent few years well fall into the pattern described above, both petrologically and geochemically. This proves the described zoning to be realistic and may be useful for the mapping of the mantle substrate rocks distribution. In particular, the presumed/proven Ta content (ppm) ratio is 2.0/0.8 for the Vesennyaya pipe (discovered in 1992), 8.5/8.6 for the V.Grib pipe (1996), 1.0/0.89 for the Ozernaya pipe (2001), and 1.0/0.71 for the Letnyaya pipe (2001).

The distribution of compatible elements in the study area shows much different, linear type of symmetry. This is related to the W-E trend of decrease in ultramaficity of local igneous rocks, from the highest-Mg kimberlites of the Zolotiza field through Fe-Ti series kimberlites, kimpicrites and kimmelilitites to typical basalts [9,10]. In this direction, i.e. from west to east, Al₂O₃ content of rocks increases (Figure 1B), while Ni content, Mg index, deep-seated material content and diamond potential of the rocks tend to decrease.

Tectonic controls. The spatial distribution of eruptive bodies in the Zimny Bereg area shows a pronounced symmetry pointing to their common tectonic controls (fracture zones) which inferably formed (or renewed) in response to a common regional tectono-magmatic activity cycle.

Igneous rock occurrences are heterogeneously distributed in the Zimny Bereg area. Some of them are arranged in chains, some clustered in groups, and some occur as isolated bodies. The overall pattern of their distribution is geometrically regular, with well defined symmetry, which calls for explanation. The chains of

eruptive bodies are oriented along the main directions of global jointing (longitudinal, latitudinal, NE and NW), and they follow the tectonically controlled directions of hydrographic outlines of the study area, including the White Sea wave-cut niche, the Dvina Gulf, the Kuloy River course, and the lines symmetric about the outline of the western cape of Zimny Bereg (Figure 2). Basically, the following chains of eruptive bodies are evident:

Two sublongitudinal chains: 1) Mela - Pervomayskaya - Snegurochka - Chidvinskaya - Izhma - Letnyaya, and 2) Anomaly-720 - Anomaly-721.

The sublatitudinal chain: Pomorskaya - Shocha - Oktyabrskaya - Rusalka - Pobeda - Anomaly-796 - Anomaly-711.

The NW chain: Mela - Megorskaya - Anomaly-685 - Anomaly-734 - Anomaly-713.

The NE chain: Vesenniyaya - Aprelskaya - Anomaly-840 - Anomaly-748 - Anomaly-713.

All these chains of eruptive bodies are arranged symmetrically about the sublatitudinal chain (through which the symmetry plane goes), such that even the entities complicating the geometrically regular pattern (the V.Grib pipe and the pipes of the Verkhotinsky cluster on the north and the Klyuchevaya group of pipes on the south) are also located symmetrically about the same sublatitudinal chain. The recently discovered Vesenniyaya, V.Grib, Ozernaya and Letnyaya pipes do not disturb the overall symmetric distribution pattern of eruptive bodies in the region under study.

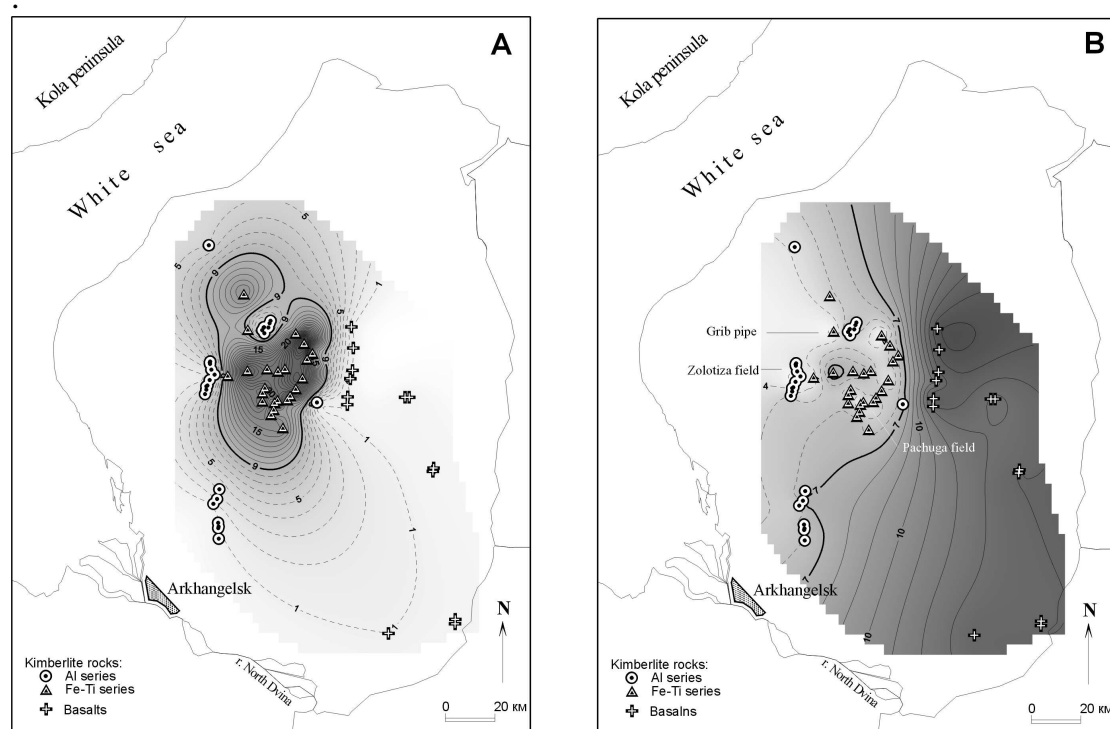


Fig. 1. Isolines (A) of Ta (through 1 ppm) and (B) of Al₂O₃ contents (through 1 wt. %) in the autoliths of the Zimny Bereg volcanic rocks.

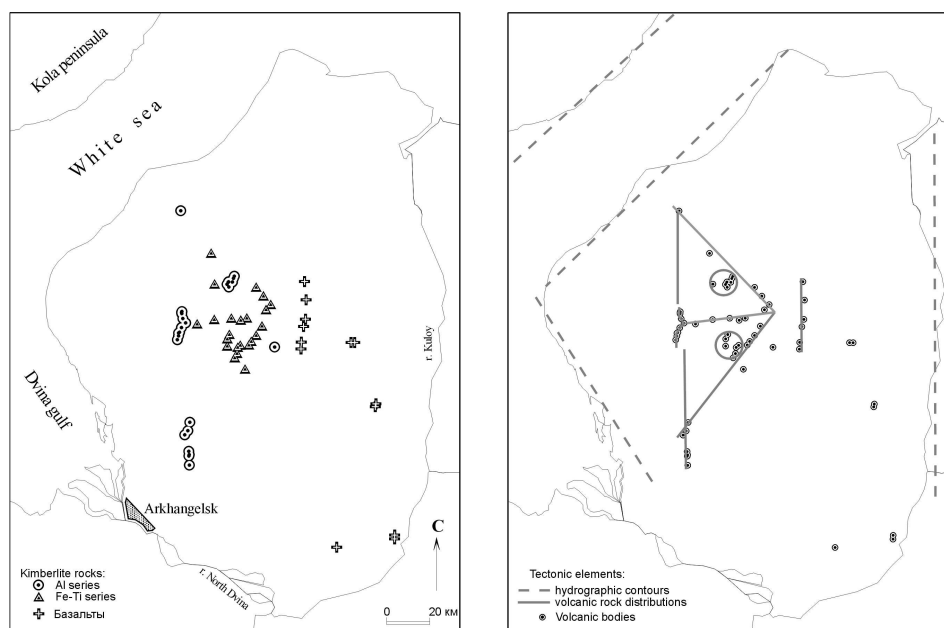


Fig.2. Symmetric elements in the pattern of volcanic bodies distribution in the Zimny Bereg area: A - location of volcanic bodies, B - chains of volcanic bodies and outlines of tectonically controlled hydrographic contours.

The similar situation is proved by detailed analysis of the eruptive bodies distribution. In particular, the pipes involved in the Zolotiza field are also arranged in chains along the main global directions:

Two sublongitudinal chains: 1) Pervomayskaya - Koltsovskaya, and 2) Karpinskogo-1 - Snegurochka.

The *NW chain:* Koltsovskaya - Lomonosovskaya - Pomorskaya.

The *NE chain:* Karpinskogo-2 - Pionerskaya - Pomorskaya.

For these pipes, the arrangement pattern is also symmetric about the regional subaltitudinal chain: Pomorskaya - Anomaly-711.

In general, almost all the pipes known in the area under study well fall into the symmetric pattern, except for the kimberlite pipes Suksoma and Olginskaya and the basaltic pipes in the southeastern part of the district (Anomaly-781, 782, 753, 754, 1040, 1042 and 1026)

The symmetric distribution of eruptive bodies with differing composition in the study area still calls for explanation, but, anyway, it represent an additional argument in favor of consanguinity of these rocks. It is evident that local igneous rocks with widely varying composition are confined to the common structural controls. This suggests that compositional variations of kimberlite rocks are primarily due to different sets and composition of mantle substrate rocks, from which the kimberlites formed during the common regional tectono-magmatic activity cycle.

To summarize, the spatiotemporal relationships and similarity of geological structure of all Early Hercynian volcanites in the region under study suggests their consanguinity. Therefore, it would be quite correct to map the zones with

inferredly differing mantle substrate based on the characteristics of mantle rock fragments found in kimberlite pipes and on compositional peculiarities of the rocks marking up the pipes, themselves because these two components of eruptive bodies reflect the compositional features of mantle rocks as for a *common* "time section".

Mantle rock xenoliths in kimberlites hosting rounded diamonds.

Results of a detailed study of mantle nodules from 26 kimberlite and kimberlite-related bodies of the study district (all eruptive bodies with deep-seated inclusions, except for the V.Grib pipe) are presented in [11,22]. There was revealed and substantiated almost complete agreement between the composition of mantle substrate in the area under study (determined on the basis of deep-seated inclusions analysis) and compositional peculiarities of kimberlite rocks hosting rounded diamonds. Mineral composition features of mantle rock xenoliths were found to specify geochemical characteristics of their host kimberlites. Two types of mantle substrate have been identified for the Zimny Bereg area: homogeneous, dunite-type substrate, and e heterogeneous, eclogite-peridotite substrate, as sources of, respectively, Al series and Fe-Ti series kimberlites [11,22]. It has been shown that ultramafic rocks of local mantle substrate were intensively affected by water-alkaline (K-Na) infiltration-type metasomatism within 20 to 110 km depth interval, which resulted in great abundance of amphibole (pargasite) and phlogopite in these rocks. Partial melting of metasomatized mantle zones enriched the kimberlite melt in Na and K, which in turn could be responsible for the development of melilite and nepheline in the most differentiated kimberlite rock varieties, both of the Al series and of the Fe-Ti series, and also for partial dissolution of diamond crystals, which imparted to them a rounded shape typical of diamonds from the Zimny Bereg kimberlite district (pipes of the Lomonosov deposit and the Pachuga field).

The V.Grib pipe still is the only deposit of *flat-faced* diamonds in the Bereg district. Therefore, deep-seated rock nodules from this pipe are of prime interest for researchers.

Mantle rock xenoliths in kimberlites from the V.Grib pipe.

A tentative study of deep-seated inclusions from kimberlites of the V.Grib pipe revealed the following peculiar features.

Mantle xenoliths are abundant (by Zimny Bereg pipes standards) in the rock of the V./Grib pipe, being very unevenly distributed in different rock varieties. They are most common in diatreme tuffisites, with concentrations as high as up to five xenoliths per meter of core. For comparison, in pipes Anomaly-688 and Arkhangelskaya having the highest deep-seated xenolith concentrations among the Zimny Bereg area pipes, the values of this parameter are, respectively, 0.9 and 0.5 xenoliths per meter of core. Deep-seated inclusions vary in size from 1-2 cm to 15 cm, with a sizeable proportion of 5 to 8 cm nodules, which noticeably differentiate the V.Grib pipe from the rest of the Zimny Bereg pipes (Figure 3).

Varieties of deep-seated inclusions. The deep-seated inclusions in the V.Grib pipe kimberlites represent a broad spectrum of rock varieties.

Among **ultramafics**, the most abundant are *pyrope dunites* and *pyrope lherzolites*. Macroscopically, these rocks are medium crystalline, light green to dark gray, with brightly colored phenocrysts of emerald-green chrome-diopside and violet or purplish-red pyrope. Olivine is commonly replaced by serpentine, however almost unaltered peridotite inclusions do occur at deep horizons. Pyrope concentration varies from single phenocrysts to 15%, and the shape of pyrope segregations varies from oval to irregular, subangular. Pyrope shows a wide variation in composition, primarily in Cr₂O₃ content (Figure 4). Chrome-diopside occurs as single grains in essentially olivine rock varieties, while in lherzolites its concentration varies from 10 to 15%. Xenoliths of monomineralic olivinites also occur. None of the studied pyrope ultramafic xenoliths showed any evidence of metasomatic amphibolization so typical of ultramafic rock xenoliths from pipes of the Zolotiza and Pachuga fields. *Pyrope clinopyroxenites* composed of chrome-diopside (70%), violet pyrope (20%) and olivine (up to 10%) occur more rarely.

Some of large xenoliths have a complex, zoned (banded) structure with discernible pyrope lherzolite and pyrope clinopyroxenite zones, where the color of pyrope gradually changes from purplish-red to orange, and the color of chrome-diopside grades from emerald-green to grass-green.

Ilmenite ultramafic rock xenoliths occur quite rarely (more rarely than in pipe Anomaly-688). They are represented by *ilmenite* and *pyrope-ilmenite peridotite* nodules of moderate size (usually 1-2 cm, up to 3-4 cm, rarely up to 8 cm), composed of serpentized

olivine, irregular picroilmenite segregations, pale green diopside and, occasionally, orange pyrope. Ilmenite ultramafics are characterized by a higher than average proportion of sheared rocks.

Metasomatic rocks xenoliths form a specific and abundant group of deep-seated inclusions, consisting predominantly of medium-crystalline phlogopite aggregate with a varying proportion of clinopyroxene (more rarely, garnet). In addition, there are almost purely phlogopite and olivine-phlogopite rock xenoliths.

Among **mafic rock** xenoliths, the most common are *eclogite-like rocks* and *granulites* composed of orange garnet, pale green clinopyroxene and plagioclase, with varying proportion of biotite, amphibole and opaque minerals (rutile, ilmenite). Xenoliths of these rocks are largest of all (up to 18 cm), not uncommonly with markedly zoned structure, and they vary in mineral composition from nearly bimineralline garnet-pyroxene rocks (with a minor amount plagioclase) to garnet- and pyroxene-bearing, essentially plagioclase rock varieties (granulites). In addition, there are "*black series*" *clinopyroxenites* consisting of microcrystalline, tobacco-green clinopyroxene aggregate with minor amounts of amphibole, magnetite and, occasionally, plagioclase. Many of these inclusions are likely fragments of rocks of crystalline basement and lower crust horizons, unrelated to mantle formations.

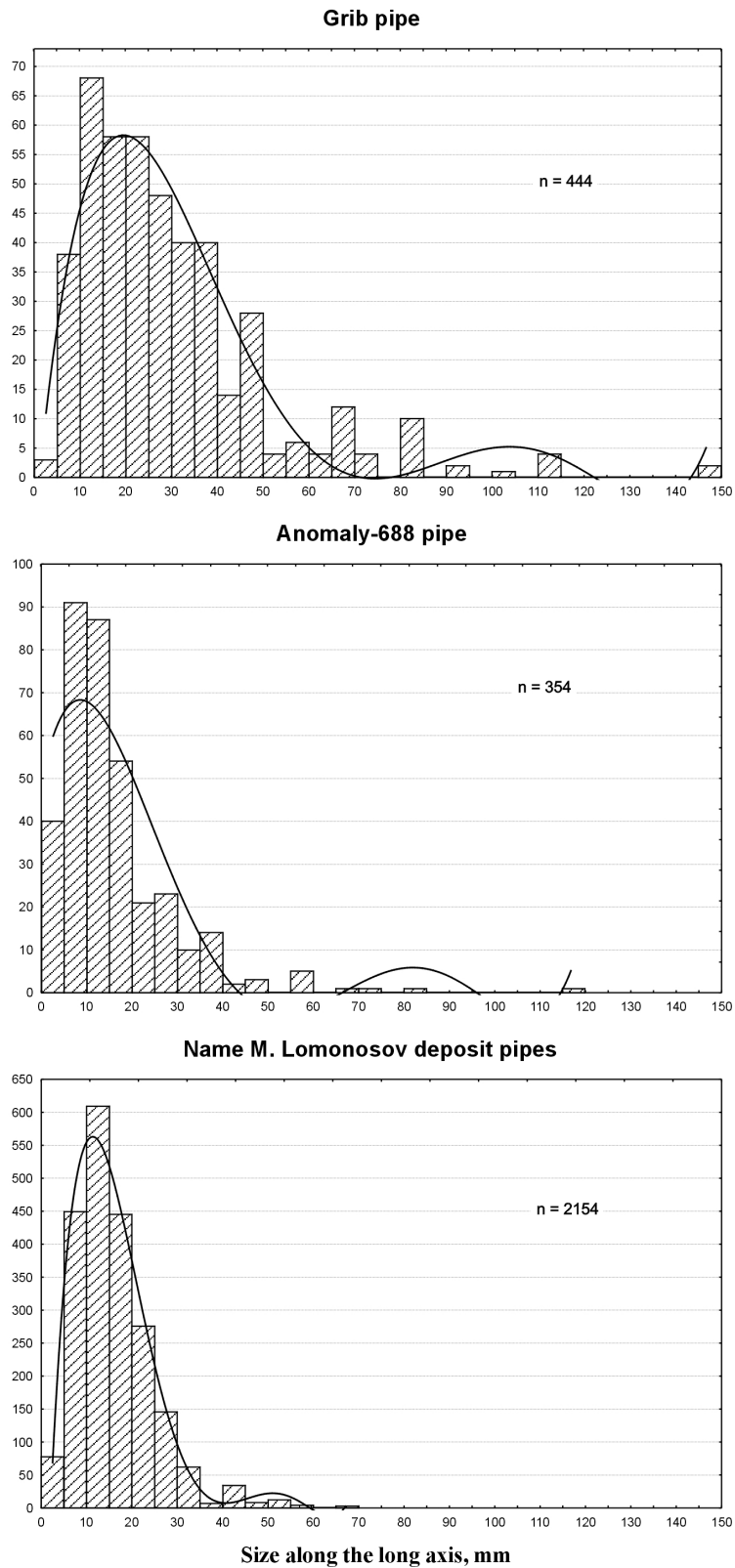


Fig.3. Histogram for the sizes of mantle nodules in the Zimny Bereg kimberlites: A - Grib pipe; B - Anomaly-688 pipe; C - name M. Lomonosov deposit pipes.

Much rarer in occurrence are the typical *bimineral Mg-Fe eclogites* with a coarse- to medium-grained texture, consisting of orange pyrope-almandine and light-green omphacite, occasionally with a varying minor proportion of phlogopite.

Xenocrysts and megacrysts are abundant in rocks of the V. Grib pipe. They occur mostly as oval, subangular, very large grains of violet and purplish-red *pyrope* (2 to 16 mm), orange *Ti-pyrope* (2 to 30 mm), *pyrope-almandine* (2 to 20 mm), *chrome-diopside* (2 to 20 mm), pale green *diopside* (2 to 16 mm), pale yellow *orthopyroxene* (10 to 30), *picroilmenite* (2 to 30 mm), *phlogopite* (2 to 20 mm), and *deformed phlogopite* (4 to 50 mm). Many pyropes have kelyphitic rims; orange garnet grains mostly have "clean" surfaces. Picroilmenite grains have thin, light brown leucoxene rims on their surfaces. There occur picroilmenite inclusions in orange garnet grains and orange garnet inclusions in picroilmenite grains.

The abundance of diverse clinopyroxene, phlogopite-clinopyroxene and phlogopite rocks among the xenoliths may be the evidence of intense mantle water-limy-alkaline (K-Ca) metasomatism in abyssal substrate (source) rocks of kimberlites from the V.Grib pipe.

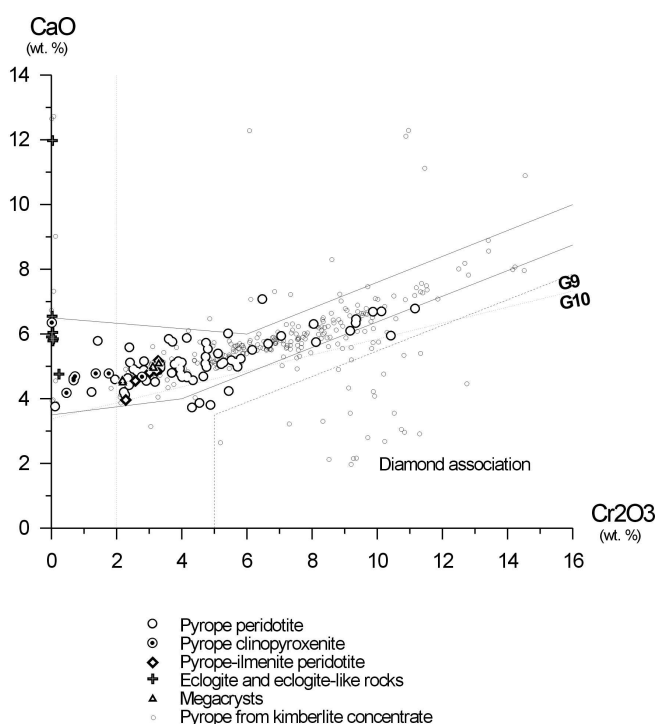


Fig.4. Composition of garnets from the Grib pipe mantle nodules (diagram [00])

The distribution of various deep-seated xenoliths in V.Grib pipe kimberlites is shown in Figure 5. The xenoliths are dominated by eclogite-like rocks and granulite inclusions (mantle origin of which is not indubitable), but undoubtedly mantle rock inclusions are also abundant.

The set of mantle rocks present in the V.Grib pipe drastically differs from those of pipes of the Lomonosov deposit, and is most similar to that of pipe An-

688 (Fe-Ti series kimberlites of Zimny Bereg). The V.Grib pipe differs from pipe An-688 by its higher concentration of nodules, lower proportion of ilmenite peridotite inclusions, and greater abundance of clinopyroxenite, clinopyroxene-phlogopite metasomatic rocks and megacrysts of clinopyroxene and deformed phlogopite.

In general, kimberlites of the V.Grib pipe are similar to diamondiferous kimberlites from the southern Yakutian diamond province as they have the same set of mantle xenolith varieties, and are characterized by large size and high concentration of xenoliths, a sharp predominance of pyrope xenolith varieties and predominance of flat-faced octahedra among the diamonds.

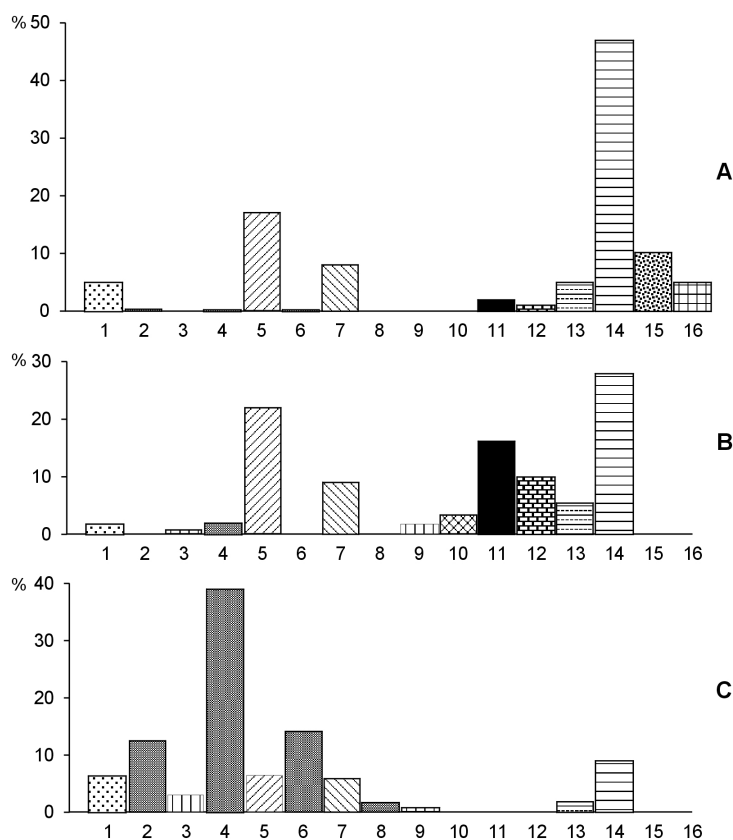


Fig.5. Distribution of various mantle nodules in the kimberlites of the Zimny Bereg area: A - Grib pipe; B - Anomaly-688 pipe; C - name M. Lomonosov deposit pipes.

1 - olivinites, 2-10 - ultrabasites of the Mg-Al-series [00]: 2 - spinel-pyroxene "B" facies, 3 - spinel-pyropic "C1" subfacies, 4,5 - grosspydite "C2" subfacies, 6,7 - coesite "C3" subfacies, 8,9 - diamond-pyrope "D" facies, 10 - garnetized orthopyroxenites (3, 5, 7, 9, 10 - pyropebearing varieties); 11-12 - ultrabasites of the Fe-Ti-series [00]: 11 - ilmenitic rocks, 12 - pyrope-ilmenitic rocks; 13 - eclogites, 14 - eclogite-like rocks and granulites; 15 - clinopyroxene-phlogopite metasomatites; 16 - pyrope clinopyroxenites.

compositional Geochemically, the V.Grig pipe kimberlites are characterized by a very high ultramafic index and a generally lower than average proportion of incoherent elements. In composition they are similar to ultramafic mantle rocks of

melting substrate [16], which is in complete agreement with the high mantle material content of kimberlites. These features make the V.Grib pipe kimberlites similar to Al-series kimberlites of the Zolotitza field of pipes, whereas their higher than average TiO₂, Ta, Co contents, moderate Nb, LREE, K₂O contents and very low Na₂O and Al₂O₃ contents make these kimberlites similar to the kimberlites of the Pachuga pipe cluster of local Fe-Ti series. This geochemical ambiguity of the V.Grib pipe kimberlites is due to the fact that these kimberlites are extremely ultramafic members of the Zimny Bereg Fe-Ti series rock family, very similar in composition to the mantle substrate rocks, such as geochemical distinctions between Al-series and Fe-Ti series kimberlites in this compositional field are minimal [8,16].

ESSENTIAL TYPES OF MANTLE SUBSTRATE IN THE ZIMNY BEREG DISTRICT

Overall examination of the Zimny Bereg kimberlites' composition revealed their petrological, geochemical and mineralogical peculiarities to completely agree with concentration and mineral composition of mantle xenoliths in these kimberlites [8,9,11]. This allowed us to identify the main types to map, although only tentatively, the distribution of these substrate types in the Zimny Bereg area, with compositional characteristics of kimberlites containing only single high-pressure mineral species is also involved.

In general, two essential types of mantle substrate were identified basing on the correlation between compositional characteristics of mantle xenoliths and petrological, geochemical and mineralogical features of local kimberlites. These two substrates, the difference between which is due to intrinsic heterogeneity of mantle rocks and to heterogeneous action of water-alkaline (K-Na) and water-limy-alkaline (K-Ca) metasomatic processes, were identified as follows: 1) *a homogeneous, dunite-type substrate*, and 2) *a heterogeneous, eclogite-peridotite substrate* with the following two subtypes: *2A-essentially eclogite-peridotite substrate*, and *2B-eclogite-clinopyroxenite-peridotite substrate*.

1. ***The homogeneous, dunite substrate.*** The set of mantle rock varieties is very limited. These rocks are mostly almost purely olivinic dunites, with minor or accessory clinopyroxene, orthopyroxene, pyrope and chrome spinel. Lherzolites are rare, and harzburgite and orthopyroxenites occur as single fragments. Ultramafics represent the full set of depth facies, from diamond-pyrope to spinel-pyroxene [3,14]. Chrome spinel rock varieties sharply predominate, with a minor amount of pyrope ultramafics and lacking ilmenite ultramafic rocks. Rocks with typical porphyroclastic texture occur very rarely. Mantle metasomatism (amphibolization and phlogopitization) is intense, however, it is only manifested in grosspydite subfacies and lower-pressure rocks. Mafic rocks are minor, most of them being eclogite-like, with typical eclogites occurring very rarely. The mantle substrate of this type is a source of Al-series kimberlite. Fragments of dunite-type substrate are most fully represented in kimberlite pipes of the Zolotitza field (the

Lomonosov deposit): Lomonosovskaya, Pionerskaya, Karpinskogo-1, Karpinskogo-2, Arkhangelskaya and Snegurochka.

2. **The heterogeneous, eclogite-peridotite substrate type** includes the following two subtypes:

2A. The essentially **eclogite-peridotite substrate**. The spectrum of mantle rock varieties is very rich. The Mg-Al magmatic series ultramafics [6] are dominated by pyrope rock varieties (from diamond-pyrope depth facies to spinel-pyrope subfacies), with single fragments of chrome spinel ultramafics of spinel-pyroxene facies. Pyrope peridotites of grospydite subfacies show intense mantle metasomatism (amphibolization). Shared (cataclastic) rocks are rare, with a minor amount of garnetized breakdown orthopyroxenites. In contrast to dunite substrate, the essentially eclogite-peridotite substrate abounds with ilmenite and pyrope-ilmenite olivinites, peridotites, pyroxenites (not uncommonly phlogopite-bearing), and Fe-Mg and Mg-rich eclogites. Eclogite-like rocks and granulites are also abundant. Substrate of this subtype is a source for Fe-Ti series kimberlites. Its rock fragments are most fully represented in pipes Anomaly-688, 751, 748 and 734 of the Pachuga field.

2B. The **eclogite-clinopyroxenite-peridotite substrate**. The spectrum of mantle rock varieties is very rich. The Mg-Al magmatic series ultramafics are sharply dominated by pyrope rock varieties (from diamond-pyrope depth facies to grospydite subfacies): pyrope dunites, lherzolites and clinopyroxenites. Pyrope-free chrome spinel peridotites and low-pressure spinel peridotites, which are so typical of the dunite-type substrate, occur as single fragments. Ilmenite and, more rarely, pyrope-ilmenite olivinites, peridotites and pyroxenites are abundant. Even more abundant are bimineral Fe-Mg eclogites, eclogite-like rocks and granulites. Shared varieties ultramafics are rare. In contrast to the two substrate types described above, the eclogite-clinopyroxenite-peridotite substrate abounds with diopside, chrome-diopside, orthopyroxene and deformed phlogopite megacrysts and chrome-diopside-phlogopite metasomatic rock fragments, but no evidence of metasomatic amphibolization of peridotites (so typical of mantle substrate types 1 and 2A) has been found here as yet. Mantle substrate of this type is a source for Fe-Ti series kimberlites, and, as of now, fragments of its rocks are most fully represented in the V.Grib pipe only.

The two main types of mantle substrate (homogeneous and heterogeneous) differ drastically. Thus, the heterogeneous substrate abounds with diverse ilmenite ultramafic rock varieties which might represent deep-seated intrusive rocks of Fe-Ti series [6] intruded into different levels of the upper mantle. Pronounced geochemical peculiarities of Fe-Ti series kimberlite, which formed as a result of melting of the heterogeneous mantle substrate (primarily, Ta content of autoliths higher than 8 ppm pointing to the presence of ilmenite ultramafics in melting substrate rocks), allows us to map the heterogeneous mantle substrate in the central Zimny Bereg area and the homogeneous mantle substrate in the marginal zones of the area (Figure 6) [11].

Direct evidence of water-alkaline (K-Na) mantle metasomatism is seen in amphibolization of mantle ultramafic rocks (in pipes of the Zolotiza and Pachuga fields), whereas indirect evidence of this metasomatism can be found in the

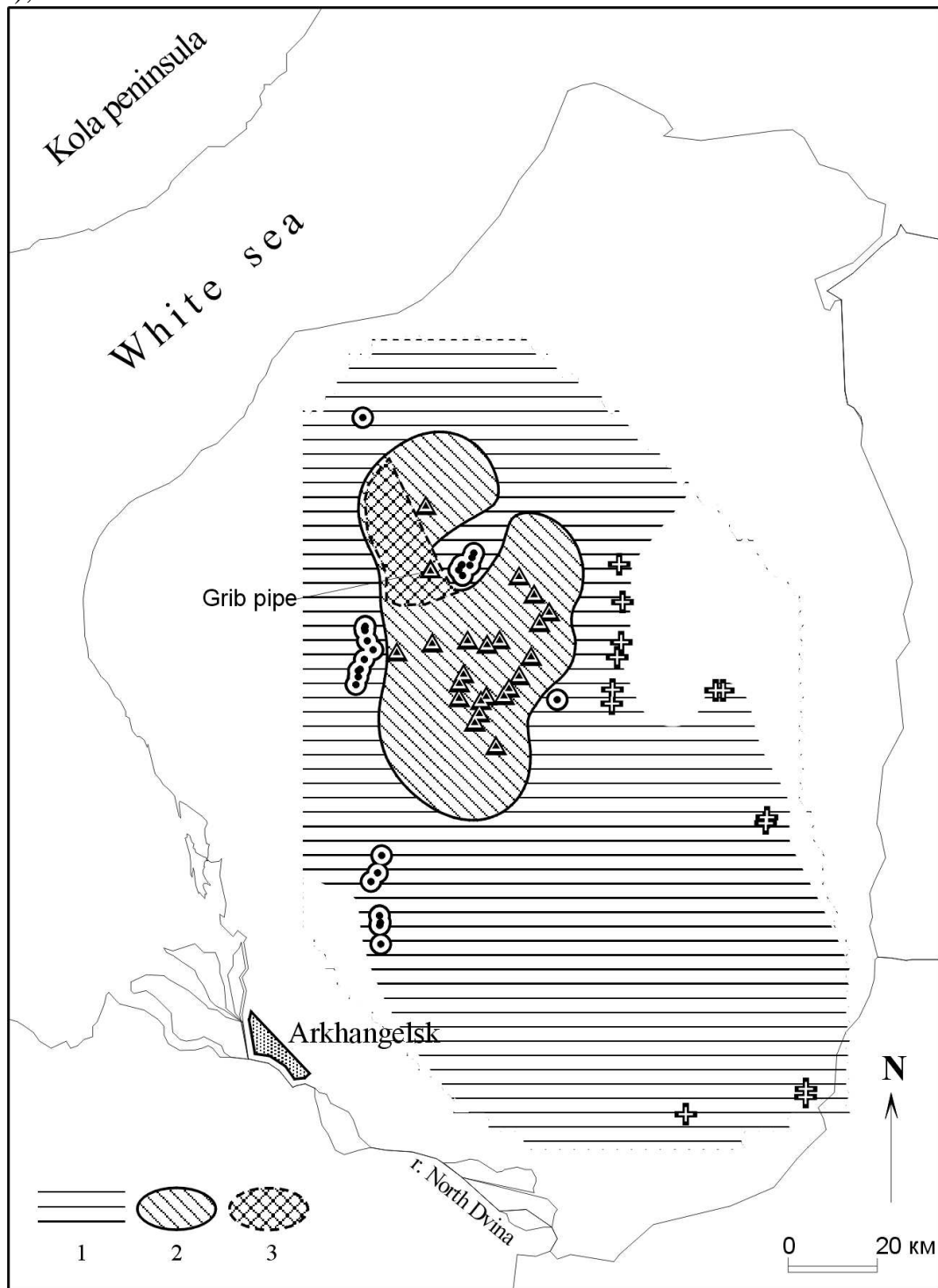


Fig.6. Distribution of various types of mantle sources beneath the Zimny Bereg kimberlite areas.

1, homogeneous «dunite» mantle sources; 2, heterogeneous «eclogite-peridotite» mantle sources; 3, heterogeneous «eclogite-clinopyroxenite-peridotite» mantle sources.

(and more rarely and in minor amounts, nepheline) in Al series kimberlites and in the -majority of Fe presence of Ti series volcanic rocks [11]. This allows us to outline a zone of water-alkaline (K-Na) mantle metasomatism which covers a large portion of the Zimny Bereg area (Figure 6). In this zone, the kimberlites of both series are characterized by predominance of rounded (partially dissolved) "Uralian-type" diamonds, which may be due to dissolving action of Na-enriched kimberlite melts [11]. The only exception in the V.Grib pipe are deep-seated xenoliths, which show no evidence of mantle amphibolization, whereas clinopyroxene-phlogopite metasomatites are abundant.

Basing on these features, we mapped a zone of water-limy-alkaline (K-Ca) mantle metasomatism in the Zimny Bereg area, and identified the eclogite-clinopyroxenite-peridotite subtype of the heterogeneous mantle substrate type for the study area. It is probable, that the substantially peculiar character of mantle metasomatism, in this zone with no supply of highly active dissolving Na component into the kimberlite melt, favored the survival of the majority of diamonds as flat-faced, octahedral crystals.

COMPOSITIONAL FEATURES OF ROCKS OF THE HOMOGENEOUS, DUNITE SUBSTRATE

While the heterogeneous eclogite-peridotite and eclogite-clinopyroxenite-peridotite substrates of the Zimny Bereg kimberlite district generally involve mantle rock varieties that are common to other kimberlite provinces worldwide, the mantle rocks of homogeneous dunite substrate of the Zimny Bereg stand out as being extremely depleted in basaltic components, which shows up in their almost purely olivinic composition with very low pyrope and pyroxene contents as compared to the similar mantle rocks from other regions (Yakutiya, South Africa and some others [2]). The Al series kimberlites, which formed as a result of melting of this dunite-type mantle substrate, are extremely impoverished in incompatible elements as compared to Fe-Ti series kimberlites. The Zimny Bereg homogeneous dunite substrate may thus be considered as the standard or *lithotype*, of "depleted mantle", and its geochemical characteristics, when the calculated as average composition parameters for xenoliths of the most common mantle rocks would be of great petrological importance, together with the average composition parameters of "primitive mantle" [19,20]. Tables 1 and 2 list the results of chemical and INA analyses of ultramafic rock xenoliths from kimberlites of the Zolotiza field pipes and the corresponding average values which could be tentatively considered as average composition parameters for "depleted mantle". Although many of the examined xenoliths are completely serpentinized and some xenoliths are saponitized, at least some of their geochemical parameters may be close to the original.

The great petrological importance of the “depleted mantle” is illustrated in a set of geochemical diagrams plotted for the Zimny Bereg “depleted mantle” volcanic rocks (Figure 7). Compositional trends of all kimberlite varieties, even of the geochemically enriched Fe-Ti series kimberlites, originate in the field of the calculated average composition of “depleted mantle” rather than from the field of average composition of “primitive” (or “fertile”) mantle. This suggests that the main role in the formation of kimberlites with widely varying petrological characteristics was played by the zones of geochemically (but not isotopically) depleted lithospheric mantle, even though isotopic characteristics of some of these kimberlites may point to asthenospheric origin of their magmatic source [5] or suggest that this source is isotopically enriched. The assumption that different kimberlite varieties have a common type of the main mantle source is strengthened by geochemical similarity of the least differentiated, extremely ultramafic kimberlite varieties and lamproites, and, in addition, by the fact that the sets of minerals occurring as inclusions in diamonds are much the same in different kimberlite varieties and in lamproites [15]. The contradiction between the geochemical “depletedness” of kimberlites and their isotopic “enrichedness” (and vice versa) may testify that the last named effect is a result of secondary process.

CONCLUSIONS

The evident spatiotemporal relationships, geological structure similarity and regular changes of geochemical characteristics of rocks throughout the Zimny Bereg district may be the evidence of consanguinity of all Early Hercynian volcanites in the study area. Proceeding from this, the mantle substrate mapping can be based both on characteristics of the mantle rock fragments occurring in kimberlite pipes and on compositional features of the rocks making up the pipes themselves, as these two components of eruptive bodies reflect the compositional peculiarities of the mantle rocks in a common "time section".

Two essential types of mantle substrate have been identified for the Zimny Bereg kimberlite district: homogeneous, dunite-type substrate and heterogeneous, eclogite-peridotite substrate. They differ drastically, primarily in that the various ilmenite ultramafic rock varieties are abundant in heterogeneous substrate. The pronounced geochemical peculiarities of Fe-Ti series kimberlites, which formed as a result of melting of the heterogeneous mantle substrate, allowed us to outline a zone of heterogeneous substrate in the central part of the Zimny Bereg kimberlite district and a zone of homogeneous mantle substrate in the marginal parts of the area. This regularity might reflect the geometry of the intruded mantle diapir.

The zone of water-alkaline (K-Na) mantle metasomatism covers a large portion of the Zimny Bereg area, including the homogeneous, dunite-type substrate and the eclogite-peridotite heterogeneous substrate subtype. In this zone, the kimberlites of both series are characterized by pronounced amphibolization of the mantle ultramafic rock nodules, the presence of melilite (more rarely, nepheline), and predominance of rounded "Uralian-type" diamonds, which may be due to

Table 1
Chemical composition of the mantle nodules from the Zolofiza field kimberlite pipes (wt. %)

No	Sample	SiO ₂	TiO ₂	Al ₂ O ₃	Cr ₂ O ₃	Fe ₂ O ₃	MnO	MgO	CaO	Na ₂ O	K ₂ O	P ₂ O ₅	LOI	Total
1	505/232-4	39.44	0.07	1.58	0.40	7.02	0.25	34.28	0.48	0.30	0.12	0.06	15.86	99.86
2	505/300-320	40.74	0.07	1.18	0.59	7.08	0.28	34.24	0.61	0.21	0.08	0.07	14.90	100.05
3	505/380-8	39.61	0.07	0.89	0.51	6.23	0.26	36.55	0.28	0.39	0.11	0.05	15.36	100.31
4	505/475-490-7	40.01	0.35	2.10	0.41	8.10	0.26	32.22	0.99	0.40	1.19	0.12	13.78	99.93
5	516/281	41.04	0.07	1.20	0.22	7.91	0.40	35.76	0.95	0.30	0.07	0.06	12.18	100.16
6	516/341.91	38.24	0.24	3.88	0.57	8.96	0.28	30.63	1.54	0.49	0.57	0.10	13.56	99.06
7	516/347	39.41	0.07	0.96	0.40	6.50	0.28	35.87	0.37	0.30	0.21	0.07	15.38	99.82
8	516/373	41.89	0.07	0.86	0.02	7.82	0.31	36.03	0.50	0.30	0.12	0.07	12.04	100.03
9	516/434	43.73	0.07	0.97	0.09	8.26	0.30	33.84	0.69	0.30	0.16	0.09	11.16	99.66
10	516/435	43.74	0.07	1.04	0.14	7.51	0.26	34.23	0.61	0.30	0.07	0.05	11.42	99.44
11	516/459.1	39.62	0.07	1.07	0.22	7.39	0.28	33.16	0.91	0.57	0.17	0.10	15.74	99.30
12	516/483-3	42.66	0.12	1.26	0.41	6.02	0.22	35.62	0.48	0.49	0.46	0.09	11.80	99.63
13	516/483-11	43.08	0.10	1.39	0.16	6.49	0.20	34.29	0.67	0.80	0.16	0.08	11.92	99.34
14	516/483-13	41.98	0.07	1.81	0.31	6.69	0.23	35.02	0.63	0.60	0.28	0.06	12.26	99.94
15	516/552	44.12	0.07	2.09	0.37	7.62	0.34	33.33	0.96	0.50	0.16	0.05	10.10	99.71
16	517/421	42.19	0.34	1.74	0.39	7.24	0.33	32.58	2.44	0.28	0.19	0.07	12.16	99.95
17	517/474-4	50.59	0.16	1.46	0.41	5.92	0.28	30.09	0.57	0.35	0.42	0.08	9.55	99.88
18	527/224	49.30	0.07	3.76	0.43	4.97	0.20	27.00	3.35	0.84	0.41	0.13	9.13	99.59
19	527/280	40.77	0.22	2.42	0.40	6.61	0.26	35.08	0.88	0.35	0.13	0.07	12.30	99.49
20	527/402	42.20	0.07	0.86	0.52	8.08	0.33	33.77	0.77	0.39	0.15	0.05	12.74	99.93
21	527/432	45.28	0.07	1.10	0.30	6.78	0.28	32.85	1.01	0.43	0.12	0.05	11.68	99.95
22	527/456.1	48.01	0.07	0.64	0.29	6.19	0.21	33.21	0.46	0.28	0.15	0.05	10.54	100.10
23	527/466.9	42.34	0.07	1.65	0.39	8.00	0.28	32.66	1.24	0.45	0.21	0.07	12.48	99.84
24	530/444	42.28	0.22	1.37	0.36	8.27	0.34	33.76	0.76	0.62	0.18	0.06	11.80	100.02
25	547/420	41.30	0.07	1.00	0.12	7.64	0.26	34.76	0.66	0.34	0.15	0.05	13.90	100.25
26	555/245	49.63	0.07	1.76	0.42	9.25	0.20	27.05	0.92	0.33	0.08	0.23	9.80	99.74
27	568/454*	45.15	0.02	0.80	0.15	4.69	0.30	32.79	1.21	0.42	0.18	0.01	13.80	99.52
28	51/195	44.47	0.20	1.34	0.16	4.99	0.20	34.04	1.08	1.04	0.78	0.42	9.81	98.53
29	1440A/181	44.20	0.07	0.95	0.31	7.40	0.26	29.00	1.86	0.54	0.11	0.02	14.28	99.00
30	1467/310.5	44.63	0.07	0.76	0.23	6.88	0.18	33.96	0.55	0.26	0.12	0.07	12.26	99.97
31	Average	43.06	0.11	1.46	0.32	7.08	0.27	33.26	0.95	0.44	0.24	0.09	12.46	99.73

Note. No 1-27 - nodules from Arkhangelskaya pipe; 28 - nodule from Karpinskogo-1 pipe; 29, 30 - nodules from Pionerskaya pipe. No 4 - mica dunitite, 6, 18 - amphibolised pyrope peridotites, the others analysis - dunitites and chrome spinel dunitites; 31 - the nodule average composition, which corresponds of the «depleted mantle» composition. Chemical analysis, Kurenko E. Ya., TOEI TsNIGRI, 1990

Table 2. Minor element composition of the mantle nodules from the Zolotiza field kimberlite pipes (ppm)

No	Sample	Ni	Cr	Co	Sc	La	Ce	Nd	Sm	Eu	Yb	Lu	Hf	Ta	Th	U
1	505/232-4	3300	-	-	-	-	-	-	-	-	-	-	-	-	-	-
2	505/300-320	3500	3321	102	5.3	4.2	14	2.7	1.6	0.42	2	0.26	0.81	0.7	0.2	0.5
3	505/380-8	2900	2827	96	4.9	2.6	12	3.2	1.9	0.87	1.6	0.2	0.5	1	0.2	0.5
4	505/475-490-7	1500	2067	84	6.4	15	23	7.7	2	0.6	2.5	0.32	0.76	1	0.4	0.74
5	516/281	2700	3300	226	9.8	3.3	7	3	1.8	0.56	3.81	0.1	0.7	0.5	0.7	0.68
6	516/341.91	5000	3750	197	6.3	10	23	18	2.7	1.2	1.2	0.15	0.53	0.7	0.73	0.5
7	516/347	3700	2317	133	5.7	6.2	28	11	3.3	1.2	0.94	0.12	0.5	0.8	0.2	0.5
8	516/373	3300	-	-	-	-	-	-	-	-	-	-	-	-	-	-
9	516/434	2900	-	-	-	-	-	-	-	-	-	-	-	-	-	-
10	516/435	2800	2300	125	2.5	12	30	5	3.8	0.57	0.5	0.1	0.7	0.5	0.7	0.1
11	516/459.1	4100	-	-	-	-	-	-	-	-	-	-	-	-	-	-
12	516/483-3	3700	2528	157	2.5	14	34	7	1.7	0.44	0.5	0.028	0.55	0.34	0.2	0.5
13	516/483-11	3800	947	150	5	15	25	13	1.9	0.59	0.5	0.041	1.32	0.35	0.2	0.5
14	516/483-13	3900	-	-	-	-	-	-	-	-	-	-	-	-	-	-
15	516/552	2600	3100	345	10.4	8	17.6	5	3.5	0.82	1.55	0.19	0.7	0.5	0.7	0.1
16	517/421	2100	2242	298	7.8	20	23	23	2	0.61	3	0.39	1.5	0.7	0.2	0.5
17	517/474-4	2800	2410	115	6.6	8	26	7	1.7	0.57	2	0.26	1.11	0.3	0.33	0.5
18	527/224	1600	2553	68	11	16	19	1	1.2	0.39	0.81	0.087	0.5	0.7	0.2	1.4
19	527/280	2800	2136	97	9	5.2	10	1	0.88	0.1	1.4	0.16	1.1	0.5	0.44	1.6
20	527/402	4200	2542	169	5.8	4.4	12	3	1.8	0.67	1.1	0.15	0.5	0.5	0.2	0.5
21	527/432	4900	1898	151	6.7	3.5	12	3.9	1.6	0.58	0.88	0.09	0.5	0.5	0.2	0.5
22	527/456.1	3500	-	-	-	-	-	-	-	-	-	-	-	-	-	-
23	527/466.9	3700	2574	172	10	5.7	16	6.5	1.9	0.8	0.73	0.1	0.5	0.5	0.2	0.5
24	530/444	3700	2514	172	8.4	5.2	18	14	3.7	1.3	1.5	0.14	0.5	0.5	0.2	0.5
25	547/420	2500	1897	132	3.72	4.6	13.5	9.8	1.57	0.53	0.87	0.12	0.1	0.29	0.12	0.2
26	555/245	1300	-	-	-	-	-	-	-	-	-	-	-	-	-	-
27	568/454*	1900	2336	119.4	4.28	3.9	10.3	5	1.26	0.57	3.75	0.61	0.23	0.08	0.67	0.9
28	51/195	1200	806.3	72.9	2.3	14.6	31	16.4	-	-	1.2	0.21	0.7	0.7	1.86	1.2
29	1440A/181	2300	4130	100	5.42	4.2	10.7	5	0.29	0.14	0.68	0.06	0.25	0.15	0.27	2.1
30	1467/310.5	3000	1276	93	5.7	8	16	6.7	1.4	0.46	1	0.12	0.5	0.5	0.2	0.5
31	Average	3040	2425	147	6.3	8.4	18.7	7.7	1.98	0.64	1.48	0.17	0.65	0.54	0.41	0.67

Note. No 1-31 see table 1 notes. « - » - not determined. Ni - quantitative spectral analysis, Kurenko E.Ya., TOEI TsNIGRI, 1990; the others elements - instrumental neutron activation analysis, Kuligin V.M., Vitozhents G.Ch., TsNIGRI, 1990.

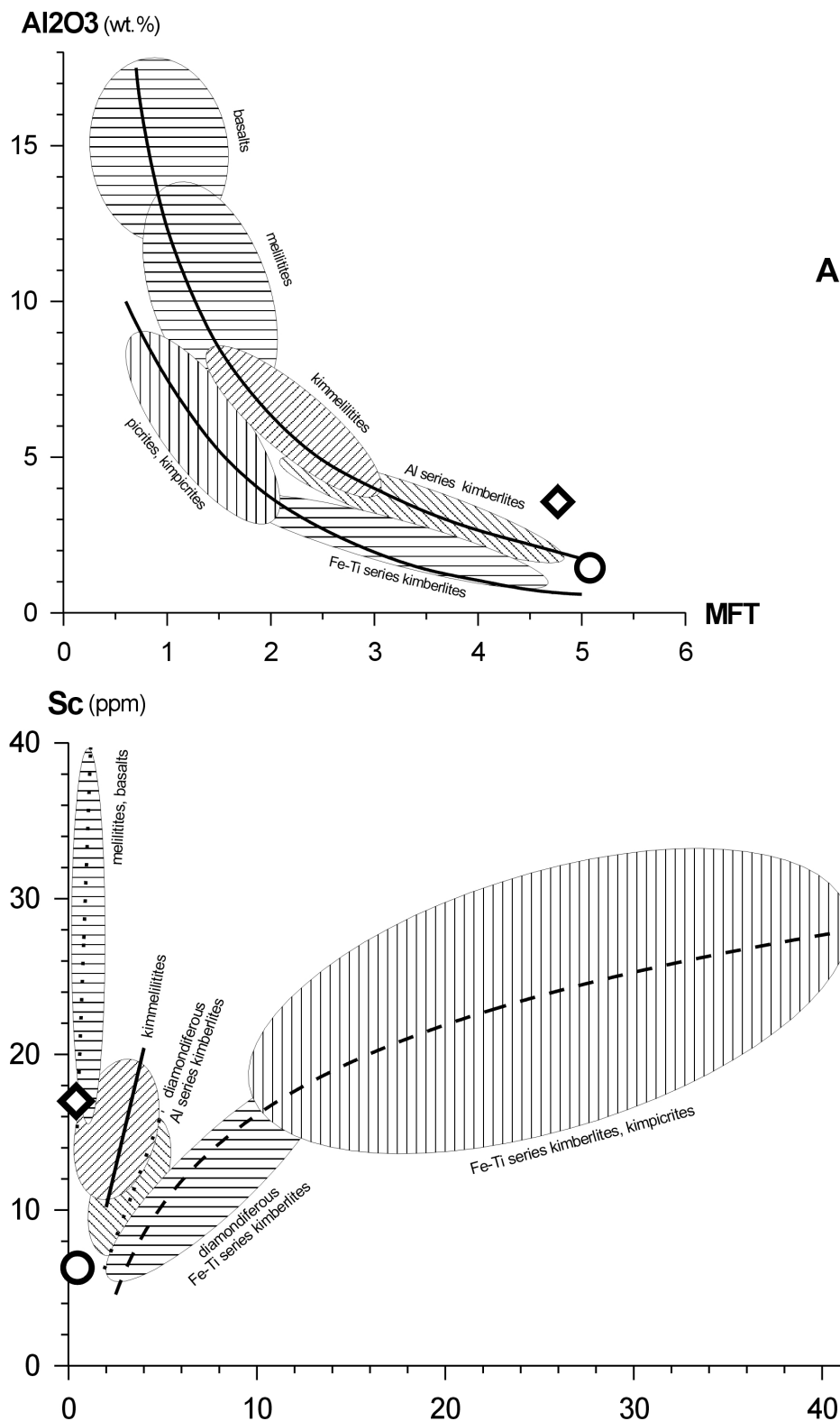


Fig.7. Diagram of (A) MFT ($MgO/FeO_{tot}+TiO_2$)- Al_2O_3 and (B) Ta-Sc for the Zimny Bereg volcanic rocks.

Lines show the Al and Fe-Ti series volcanic rock composition trends. Rhomb shows the «primitive mantle» compositions (Jagoutz et al., 1979); circle shows the «depleted mantle» compositions (table 1 and 2 this articles).

dissolving action of Na-enriched kimberlite melts. No evidence of mantle amphibolization was found in abyssal inclusions of the V.Grib pipe. On the other hand, clinopyroxene-phlogopite metasomatites are abundant among the abyssal inclusions in rocks of this pipe. Basing on these data, we outlined the zone of water-limy-alkaline (K-Ca) mantle metasomatism with the eclogite-clinopyroxenite-peridotite subtype of heterogeneous mantle substrate within the Zimny Bereg area. It is probable that the specific nature of mantle metasomatism in this heterogeneous substrate subtype, which means no supply of highly active dissolving Na component into the kimberlite melt, favored the survival of the majority of diamond crystals as flat-faced octahedral (this habit is typical of diamonds).

The main role in the formation of kimberlites with widely varying petrological characteristics was played by zones of geochemically impoverished, "depleted" lithospheric mantle. The homogeneous, dunite substrate of the Zimny Bereg kimberlite district can be considered a *lithotype* of this depleted mantle, and the geochemical characteristics of this substrate type, when calculated as average composition parameters for xenoliths of the most common mantle rocks, would be of great petrological importance along with the average composition of the "primitive mantle".

This study was supported by the Russian Foundation for Basic Research, grant no. 01-05-64257.

REFERENCES

1. A geologic time scale, *Harland W.B., Cox A.V., Llewellyn P.G. et al.*, Moscow: Mir. 1985. 140 p.
2. *Garanin V.K.* Mineralogical zoning of the kimberlites // *Izvestiya VUZov, Geol. Rasv.* 1991, N 9. P. 38-49.
3. *Dawson, J.*, Kimberlites and their xenoliths. Moscow: Mir. 1983. 300 p.
4. Deep-seated xenoliths and the upper mantle, Eds. Sobolev N.S., *Dobretsov N.L., Sobolev N.V.* Novosibirsk: Nauka. 1975. 272 p.
5. *Ilupin I.P., Kaminsky F.V., Frantsesson E.V.*, Geochemistry of the kimberlites, Moscow: Nedra. 1978. 352 p.
6. *Jagoutz, T., Palme, H., Baddenhausen, H. et al.* The abundance's and trace elements in the earth mantle as derived from primitive ultramafic nodules. // *Proc. X Lunar Planet. Sci. Conf.* 1979. P. 2031-2050.
7. *Makhotkin I.L. and Zhuravlev D.Z.*, Sr and Nd isotope composition of diamondiferous kimberlites and melilitites of the Arkhangelsk region // *Dokl. Ross. Akad. Nauk*, 1993. V. 332, N 4. P.491-495.
8. *Marakushev A.A.*, Peridotite nodules in kimberlites and basalts as indicators of deep lithosphere structure. 1984. *Proc. 27th IGC, Petrol., Sect. S.09, V. 9*, Moscow: Nauka. 1984. P. 153-161.
9. *McDonough W.F., Sun S.* The composition of the Earth // *Chemical Geology*, 1995. V.120. P. 223-253.
10. *Sablukov S.M.* Petrochemical series of kimberlite rocks of Arkhangelsk Province, 6th IKC. Russia, Novosibirsk. Exstented Abstracts. 1995. P. 481-483.
11. *Sablukova L.I.* Mantle nodules in kimberlite rocks of Arkhangelsk, 6th IKC. Russia. Novosibirsk, Exstented Abstracts. 1995. P. 484-486.
12. *Sablukov S.M.* Age of the ultramafic rock pipes // *Tr. TsNIGRI*. 1987. N 218. P. 24-27.
13. *Sablukov S.M.* Petrochemical series of kimberlite rocks // *Dokl. Akad. Nauk SSSR*. 1990. V. 313, N. 4 P. 935-939.
14. *Sablukov S.M.*, Volcanism of the Zimny Bereg and petrological criteria of diamond-bearing potential. Cand. Sc. (Geol.-Min.) dissertation, Moscow: 1995. 24 p.
15. *Sablukov S.M.*, Petrological zoning of the kimberlite region of the Arkhangelsk diamondiferous province. *Proc. Vseross. Conf. Diamonds and the diamond-bearing potential of the Timan-Ural region, Syktyvkar*. 2001. P. 127-129.

16. **Sablukov S.M., Sablukova L.I. and Shavirina M.V.**, Mantle xenoliths in the Zimny Bereg kimberlite deposits of rounded diamonds, Arkhangelsk diamondiferous province, Petrologiya. 2000. V. 8, N 5. P. 466-494.
17. **Sablukova L.I.** Mantle nodules in kimberlite rocks of Arkhangelsk, 6th IKC. Russia. Novosibirsk, Extended Abstracts. 1995. P. 484-486.
18. **Sergeeva O.S.**, Morphological peculiarity of diamonds from V. Grib pipe, in Material on geology and mineral deposits of Arkhangelsk district, Arkhangelsk. 2000. P. 97-102.
19. **Sinitsyn A.V., Dauv Yu.M. and Grib V.P.**, The structure position and productivity of kimberlites of the Arkhangelsk province. //Geol. Geofiz. 1992. N 10. P. 74-83.
20. **Skinner E.M.W., Smith C.B., Viljoen K.S., Clark T.C.** The petrography, tectonic setting and emplacement ages of kimberlites in the south-western border region of the Kaapvaal craton, Prieska area, South Africa //Proceedings of the Fifth IKC, Araxa, Brazil. 1994. V. 1. P. 80-97.
21. **Smith C.B., Gurney J.J., Skinner E.M.W. et al.** Geochemical character of Southern African kimberlites. A new approach based on isotopic contains. //Trans. Geol. Sos. S. Afr. 1985. V. 88. P. 267-280.
22. **Sobolev N.V.**, Deep-seated inclusions in kimberlites and the problem of the upper mantle composition. Novosibirsk: Nauka. 1974. 264 p.
23. **Sobolev N.V., Kharkiv A.D., and Pokhilenko N.P.**, Kimberlites, lamproites and the problem of the upper mantle composition //Geol. Geofiz. 1986. N 7. P. 18-28.
24. **Verichev E.M., Sablukov S.M., Sablukova L.I and Zhuravlev D.Z.** A new type of diamondiferous kimberlites of the Zimny Bereg, Arkhangelsk diamondiferous province //Dokl. Ross. Akad. Nauk 1999. V.368, N 2. P. 226-229.
25. **Zakharchenko O.D., Kharkiv A.D., Botova M.M. et al.** The deep-seated mineral inclusions in the diamond from the kimberlites of the East-European Platform //Mineral. Zhurnal. 1991. V. 13, N 5. P. 42-52.

**LATE VENDIAN AERIAL ALKALINE VOLCANISM OF RIFT TYPE IN
THE ZIMNY BEREG KIMBERLITE AREA
(ARKHANGELSK DIAMONDIFEROUS PROVINCE)**

Shchukin V.S.¹, Sablukov S.M.², Sablukova L.I.², Belousova E.A.³, Griffin W.L.³

¹ ZAO “Arkhangelsk diamonds”, Arkhangelsk

² Central Research Institute of Geological Prospecting for Base and Precious Metals, Moscow

³ ARC National Key Centre GEMOC, Sidney, Australia

Within the Zimny Bereg kimberlite area, where Late Devonian basic and alkaline-ultrabasic volcanites including commercial kimberlites are widely spread, numerous eruptive manifestations of the new type for the northern part of the Russian Platform were discovered: Late Vendian lavas and tuffs of potassic calc-alkaline lamprophyres close to minettes. Volcanites are characterized by large-scale secondary alteration, homogeneous mineral composition (kaolinite, hydromica of montmorillonite mixe-layered formation, hematite, and goetite), by relict porphyric or vitroclastic texture, extremely low concentrations of ultrabasic coherent elements (*Ni*, *Co*, *Cr*), higher concentrations of alkali (*K*, *Rb*, *Cs*, *Li*), *Ba*, and very high concentrations of *Zr*, *Hf*, *Y*, *Th*, *REE*. Petrographic composition and chemical composition of phenocrysts and biotite crystalloclasts, geochemical properties of rocks in general do not contradict the studied rocks proximity to various structural and genetic derivatives of melted magmatic calc-alkaline lamprophyre of minette type. Absolute age of the studied volcanites determined using U-Pb-method in zircon is 570 ± 5 Ma that corresponds to Late Vendian and actually coincides with Proterozoic/Phanerozoic boundary. The discovered volcanites of this new type form a chain of the northeastern trend and are probably correlated with faults extending in transversal direction relatively the Riphean Kola-Dvina paleorift system that could characterize them as «transform» faults and the related alkaline aerial volcanism – as volcanism of the rift type.

INTRODUCTION

The Zimny Bereg kimberlite area is located in the zone of intensive Riphean rift-formation within the Kola-Dvina paleorift system [1, 7] that has become active again in the Early Hercynian. The fact is proved by unique diversity of Late Devonian rocks composed of basic and ultrabasic volcanites, diamondiferous kimberlites of commercial value inclusive [2]. The above situation suggests the earlier, i.e. the Late Proterozoic, specific igneous activity of rift structures. Evidences of Late Vendian igneous activity (Redkin) were earlier found in the Ust' Pinega Upper Vendian deposits within the Zimny Bereg [8] as “interbeds of pelletalitic tuffs of montmorillonitic composition” that are “regional markers” extended for significant distances. One of such layers can be traced near Moscow [8]. These volcanites are not useful for petrological interpretation as their specific occurrence and structure do not allow evaluation, even approximate, of either location or composition of magmas resulting in these volcanic systems.

In February 2000, the Joint Stock Co. ZAO “Arkhangelsk Diamonds” worked in the western Zimny Bereg kimberlite area and in course of the test drilling of local magnetic anomalies numerous volcanic shows were found in Vendian

terrigenous rocks. They were of the type new for the northern Russian Platform and contained the Late Vendian lavas and tuffs of potassium calcareous / alkaline lamprophyres close to minette. They were found within a chain of anomalies extending north-eastward parallel to the White Sea entrance up to 70 km (Fig.1). According to the comments of the geologists from other companies who worked in the Zimny Bereg area in different periods, similar unusual rocks might be widespread.

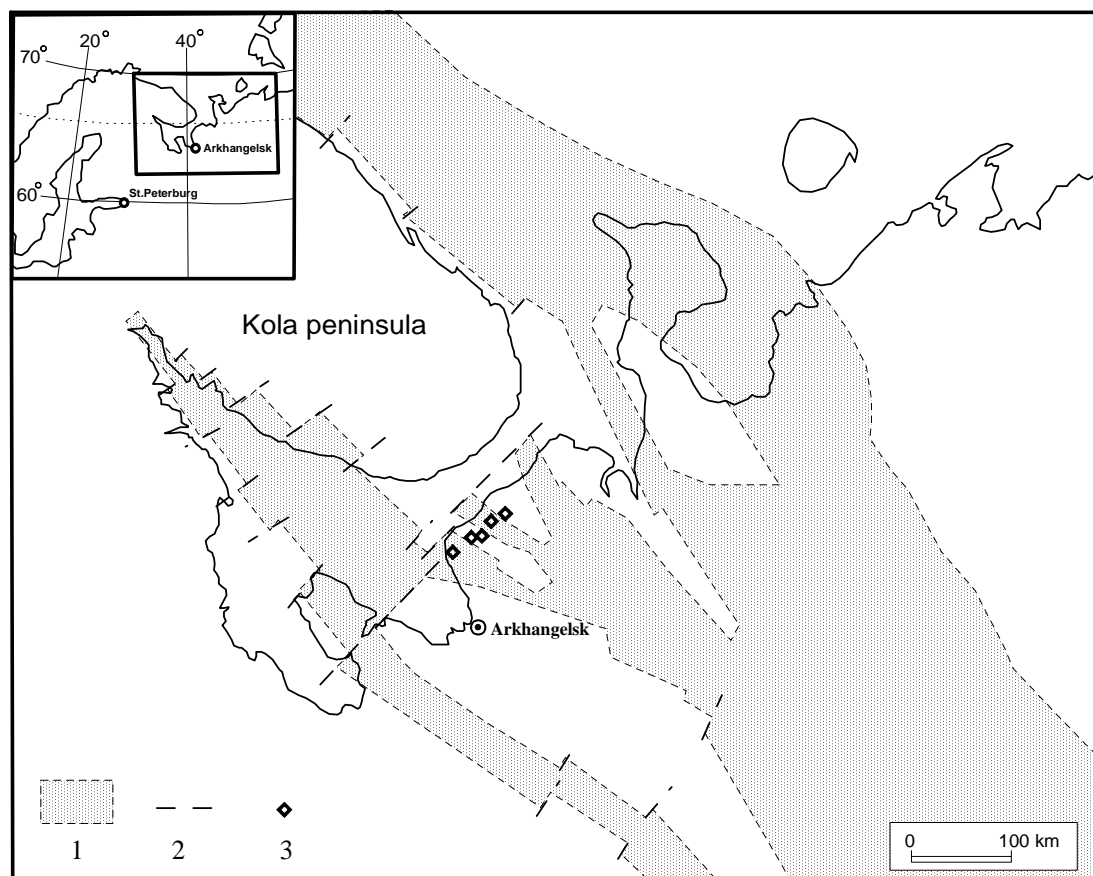


Fig 1. Schem of structure of the Kola-Dvina palerift system [1] and location Late Vendian lamprophyre volcanic rocks.

1 - Riphean poleorift system; 2 - "transform" faults; 3 - Late Vendian lamprophyre volcanic rocks.

ANALYTICAL METHODS AND OBJECTIVES

Our results are based on the examination of 1000 meters of the core sampled in 11 holes drilled on 5 magnetic anomalies (929, LT-32, ZB-11, ZC-14, ZG-46) and composed of volcanic and sedimentary rocks. 129 thin and 30 polished sections were examined, with the following analyses being fulfilled: x-diffractometry (36 runs.), silicate analysis (38 runs.), ICP-MS (42 runs.), mineralogical analysis (8 runs), electron microprobe (67 runs.), LAM-ICPMS of zircon grains by U-Pb (18 runs).

GEOLOGICAL STRUCTURE OF VOLCANIC COMPLEXES

Volcanic bodies of the new type were found as interbeds in terrigenous rocks of the Mezen deposits of Kotlin Regional Stage (Upper Vendian) represented by horizontal interbedding of greenish-gray and reddish-brown thin parallel-laminated mudstones and siltstones with subordinate fine-grained sandstones of the same colouring. X-diffractometry showed that terrigenous rocks of the Mezen sequence were composed mainly of illite, chlorite, quartz, feldspar, sometimes of hydromica/monmorillonite mixed and bedded rocks.

Actually any anomaly contained almost all the main structural and genetic types of volcanic rocks located in different levels of the same cross-section (intersections). They are effusive rocks (lavas, less lava breccia), magmaclasts and sedimentary/ magmaclastic rocks (tuffs and tuffites), volcanic sedimentary rocks (tuff siltstone and tuff mudstone). Volcanic rocks of effusive type form the subhorizontal Vendian flows and the covers 1-18 cm thick (1-4 interbeds in each hole) conformable to the Vendian terrigenous rocks. Occasionally, lavas form intersecting subvertical branching and split the inclusions (veins) of irregular shape and 1-12 mm thick (fragments or offshoots of incurrent canals?). Tuffs and tuffites also occur as subhorizontal covers 0.5-5 cm thick. There also is contamination of lava and tuff layers with terrigenous rocks, and lavas and tuffs upward grading to volcanic and sedimentary rocks (tuff siltstones and tuff mudstones) and to sedimentary rocks without volcanic component. Volcanic rocks alternate with the Vendian sedimentary terrigenous units forming the complex units of volcanic rocks. Terrigenous rocks in such units are characterized by relatively poor grading and irregular lenticular, undulated, and poorly bedded textures. In contrast to the Vendian terrigenous rocks the host volcanic units are characterized by well-sorted, thin, and parallel bedded textures. Just within several first centimetres of the hanging and flat walls of these volcanic units this bedding is of irregular and disturbed type: discontinuous, undulated, and steeply lenticular with microfolds and almost breccia-like textures development.

In general, within the anomalies, volcanic rock thicknesses vary from 0.5 to 4 meters, while the incomplete lateral extension of volcanic complex checked by drilling comes to 150 m. Interbeds of volcanic deposits have local expansion – they are quite quickly pinched out and are mainly represented by subaqueous and exposed eruptions of igneous matter along fractures (in contrast to the regional tuff markers of Vendian deposits of the Redkin sequence) [8]. The changes in terrigenous deposits, both underlying and overlapping the volcanic rocks, indicate that tectonic movements (earthquakes) not only accompanied magma eruptions in the area (that is proved by irregular, disturbed textures of volcanic rocks) but also formed just prior and after eruptions.

PETROGRAPHICAL COMPOSITIONS OF VOLCANIC ROCKS

Macroscopically, the discovered volcanic rocks are poorly consolidated, soft, wax-like, schistose deposits of brownish-gray color, tinged with violet and pink (lavas) or greenish-grey and bluish-grey color (tuffs and tuffites), of heterogeneous small-spotted (due to small inclusions of biotite and leaching) and indistinctly banded (due to subconforming zonules of various shades) coloring. Schistosity is of subhorizontal trend. According to x-diffractometry data, the rocks completely shaly, kaolinite and hematite (rare goethite) dominate, illite, chlorite, and hydromica/montmorillonite occur in less amounts; only in LT-32 rocks hydromica/montmorillonite makes up to 70% of the rock volume.

Despite very high alteration, typical features of volcanic rocks are sufficiently well preserved, their primary mineral composition can be reliably reconstructed. The rocks are characterized by stable paragenesis of primary minerals: *biotite + changed glass +/- apatite +/- zircon +/- feldspathoids +/- ores* in the deposits of lava habit (in tuffs glass is altered by basal cement formed as a result of fine-ashy material destruction).

Rocks of lava habitat (effusive rocks) are characterized by relict porphyric structure caused by the development of idiomorphic and subidiomorphic biotite phenocrysts (packets) differently changed and submerged in apovitreous matrix of plicated and fluidal texture, sometimes with traces of amygdaloidal texture. In general, the rock texture is massive, sometimes fluidal, breccia-like texture of lava breccias also occurs. Crystallization of lavas is rather insignificant; the rocks of aphyric and spodarophytic structure (with traces of glomeroporphyric structure) dominate. In fact, they are represented by volcanic glass, altered by shaly minerals and hematite aggregates, and by the rocks of porphyric and plesiophytic structure. Content of biotite phenocrysts in schistose apovitreous matrix varies from single and occasional grains (occasional grains content = 5% within anomalies 929, LT-32, ZB-11) to 10-35% of rock volume (anomaly ZC-14). **Apatite, zircon, ore mineral (magnetite), and feldspathoids** are contained in rocks in secondary or accessory amounts; they form idiomorphic inclusions of 0,005-0,1 mm size, occasional twins and aggregates with biotite, i.e. **together with biotite they form paragenetic association of primary magmatic minerals.**

Biotite is represented mainly by hexagonal tabular crystals; less amount of crystals (in tuffs) is represented by flakes of irregular shape. Biotite grains are typically of 0,05-0,2 mm in size, occasionally up to 0.8 mm, often the aggregates of 2-5 grains totally being 0,5-1,00 mm in size (up to 1.5 mm) occur. Biotite is of dark greenish-brown to black color, with large crystals. Biotite is mainly fresh, often altered by thin plates of white silica and chlorite along jointing, sometimes up to formation of complete chlorite-quartzine pseudomorphs with typical network structure of alteration. Mica grains are of rather homogeneous composition and of the same type Table 1.

Table 1

Composition of biotite phenocrysts and crystoclasts from lamprophyres of the Zimny Bereg (wt. %)

No	Sample	Rock	SiO ₂	TiO ₂	Al ₂ O ₃	Cr ₂ O ₃	FeO	MnO	MgO	CaO	Na ₂ O	K ₂ O	Total
1	LT-32/3-66.5-6/1	lava	33.07	5.31	12.82	0.00	29.60	0.22	4.31	0.00	0.37	8.86	94.56
2			33.47	5.22	13.05	0.00	29.31	0.25	4.55	0.00	0.37	8.71	94.93
3	ZC-14/2-50	lava	37.54	5.86	13.97	0.00	19.43	0.14	12.27	0.02	0.55	9.82	99.60
4			38.16	6.33	13.48	0.03	19.88	0.16	12.44	0.00	0.66	9.74	100.88
5	ZC-14/3-51.8	lava (vein)	36.69	5.71	13.52	0.01	19.68	0.20	13.28	0.02	0.70	9.41	99.22
6			37.02	5.65	13.17	0.00	19.42	0.13	12.28	0.00	0.57	9.33	97.57
7			36.93	5.32	13.12	0.00	23.32	0.25	9.76	0.00	0.49	9.56	98.75
8	ZC-14/5-86.4-3-2	tuff	35.51	5.48	14.13	0.00	24.96	0.28	5.99	0.00	0.54	7.84	94.73
9			35.30	6.17	12.65	0.00	26.60	0.23	6.83	0.00	0.71	8.97	97.46
10			36.97	5.17	15.96	0.07	24.95	0.08	5.75	0.02	0.34	7.78	97.09
11			35.31	4.85	13.85	0.00	24.35	0.24	6.37	0.00	0.54	7.90	93.41
12	ZC-14/6-95.6	tuff	38.28	4.64	17.42	0.02	15.32	0.05	9.67	0.00	0.60	7.50	93.50
13			36.99	5.41	13.36	0.00	19.76	0.12	11.40	0.00	0.59	9.60	97.23
14			35.72	5.91	13.80	0.00	27.88	0.18	6.62	0.00	0.44	9.27	99.82
15	ZC-46/2-59-1	tuffite	33.69	5.73	12.89	0.00	26.16	0.11	6.26	0.00	0.42	8.69	93.95
16			32.94	5.71	12.99	0.00	26.86	0.17	5.99	0.00	0.28	8.47	93.41
17			32.96	5.88	13.78	0.00	28.00	0.23	6.38	0.00	0.41	7.97	95.61
18			34.20	5.23	13.58	0.00	25.93	0.16	6.27	0.02	0.41	7.88	93.68
19			33.11	5.41	13.23	0.00	26.99	0.17	6.33	0.00	0.32	8.75	94.31
20			33.63	5.66	13.28	0.00	25.92	0.09	6.48	0.01	0.45	8.89	94.41
21			33.34	5.66	13.68	0.00	26.95	0.15	6.42	0.01	0.40	8.41	95.02

Electron microprobe analysis (Micro Beam Camera analyser), IMGRE Laboratory, the analyst I.M.Kulikova, 2000.

as lava phenocrysts and tuff crystoclasts (Table 1); they are characterized by stable high content of TiO₂ (4,64-6,33%) and Al₂O₃ (12,65-17,42%), lack of Cr₂O₃ (0,00-0,07%) with unstable but high content of FeO (15,35-27,88%) and low content of MgO (5,75-13,28%) that allows to define them as Ti-biotite (occasionally as magnesian biotite). The studied grain compositions shown on the Mitchell's graphs [4] partly fall within the field of biotites from minettes, and partly they drift towards the field of higher iron content.

Apatite forms well cut crystals of prismatic, elongated/prismatic, less short-prismatic habit with hexahedral prism, dipyramide, and pinacoid habit development. Crystal size by the long axis varies from 0.15 to 0.4 mm, the short axis is less than 0.05 mm (rarely up to 0.10 mm). Crystals are transparent, colorless, with the finest non-defined dust-like inclusions; the higher content of these inclusions make crystals semitransparent and milk-white. Apatite is

characterized by very simple composition (Table 2) with minimum content of REE; however, with stable Sr-admixture (0,11-0,15% SrO) and moderate admixture of LREE (0,13-0,57% Ce₂O₃).

Table 2.

Composition of apatites from the Vendian lamprophyres of the Zimny Bereg (wt. %)

1	Sample #	Rock	SiO ₂	FeO	MnO	MgO	CaO	Na ₂ O	K ₂ O	P ₂ O ₅	Ce ₂ O ₃	SrO	Total
1	ZC-14/3-51.8	lava	0.63	0.21	0.05	0.07	54.35	0.00	0.02	41.55	0.57	0.15	97.60
2		(vein)	0.35	0.18	0.07	0.10	54.43	0.00	0.00	42.25	0.46	0.15	97.99
3			0.34	0.23	0.05	0.10	54.63	0.02	0.00	42.42	0.52	0.11	98.42
4			0.20	0.16	0.05	0.07	54.77	0.03	0.00	41.75	0.41	0.16	97.60
5			0.22	0.18	0.07	0.06	54.94	0.06	0.00	42.30	0.13	0.12	98.08

Electron microprobe analysis (Micro Beam Camera analyser), IMGRE Laboratory, the analyst I.M.Kulikova, 2000.

Zircon, as well as apatite, is of 0,10 mm in size, occasional grains are of 0,2-0,4 mm along the long axis and the short axis is up to 0.05 mm. Zircon is represented by elongated prismatic (to needle-like), prismatic, rare short-prismatic, well-cut crystals with dipyrmidal ends. Zircon crystals are transparent, almost colorless, slightly tinged with yellow and pink. Some crystals are saturated with various (including melt) inclusions and are characterized by zonal structure underlining their magmatic nature. Elongated prismatic to needle-like, pointed zircon crystals occur usually in magmatic rocks crystallized under conditions of fast cooling that properly conforms the general geological setting and petrographic properties of the studied lamprophyre lavas. U-content in lamprophyric zircon of the sample ZC-14/3-51.8 is of 100-200 g/t that is typical of zircons of non-kimberlite magmatic rocks, in particular, of sienites and carbonatites.

Magnetite was found as individual grains of black, flat octahedral crystals of <0.1mm in size, quite often it is pseudomorphically altered by hematite (martite).

Hematite is represented by very small grains of irregular shape and <0.1mm in size. Lustre is intensive, metallic; hematite is black, brownish-red when in powder.

Feldspathoids occur as small (0.05-0.07 mm in size), close to idiomorphic or irregular grains of potassic feldspar of N<N c.b. and with strike joints, probably, as potassium feldspar grains. Occasional subidiomorphic grains of isotropic potassium (presumably) feldspar (?) of 0/03-0.065 mm size with two orthogonal jointing systems.

In primary light minerals contained in some types of lava occasional grains of quartz 0.2-0.4 mm in size occur. Quartz grains are represented by very well cut crystals of hexagonal dipyrmidal shape and complete absence of prism faces. Crystals are transparent, the largest crystals contain transparent melt (?) inclusions. Crystals of the similar shape are paramorphs of low-temperature α -quartz by high-temperature quartz that forms earlier segregations of liquid magma. Quartz crystals are characterized by significantly pure chemical composition and actually do not contain contaminants (Table 3).

Table 3.
Geochemical properties of lamprophyres and vendian sedimentary races (wt. %)

N	1	2	3	4	5	6	7	8	9	10	11	12	13
Anomaly	929	ZB-11	ZC-14			LT-32				ZG-46			Outcrop
Sample	1-48.0	1-87.6	2-50.0	3-51.8	5-86.4-3	3-66.5-5	3-66.5-4	3-66.5-3	3-66.5-2,6	3-66.5-1/3	2-59.0-1	2-62.0	VZ-25-1
n	1	1	1	1	2	4	4	5	4	1	1	2	1
SiO ₂	-	40.73	42.35	-	44.11	42.59	59.12	61.80	72.56	41.23	55.99	66.60	59.23
TiO ₂	-	1.32	0.67	-	0.64	0.18	0.69	0.76	0.62	0.51	1.25	0.75	1.73
Al ₂ O ₃	-	28.20	27.29	-	29.03	21.27	15.42	14.14	12.10	9.68	22.11	14.23	20.29
Fe ₂ O ₃	-	11.86	11.85	-	2.83	14.27	7.89	6.60	2.58	15.54	5.24	3.13	1.24
FeO	-	0.30	0.27	-	3.55	0.14	0.40	0.32	0.71	0.41	2.07	2.35	1.52
MnO	-	<0.01	0.03	-	0.03	0.05	0.02	0.04	0.04	0.07	0.02	0.02	0.02
MgO	-	1.54	1.25	-	2.38	2.57	1.98	2.28	1.66	1.75	1.35	2.29	2.32
CaO	-	0.57	1.16	-	0.87	0.81	0.70	0.93	0.60	11.06	0.84	0.68	0.59
Na ₂ O	-	0.24	0.07	-	0.28	0.06	0.68	0.74	1.14	0.53	0.55	1.01	1.78
K ₂ O	-	1.31	2.06	-	1.68	4.31	4.33	4.23	3.21	2.88	2.26	3.33	3.26
P ₂ O ₅	-	0.18	0.20	-	0.19	0.03	0.05	0.09	0.08	7.12	0.27	0.10	0.11
LOI	-	13.69	13.22	-	13.92	13.27	8.25	7.69	4.49	8.55	8.35	5.56	7.31
Total	-	99.94	100.42	-	99.49	99.55	99.53	99.63	99.74	99.33	100.30	100.01	99.40
H ₂ O-	-	3.22	4.02	-	3.39	7.28	4.42	4.31	1.78	3.18	1.89	2.09	1.88
H ₂ O+	-	9.93	8.82	-	10.01	5.74	3.56	2.82	2.38	1.87	6.30	3.46	4.83
CO ₂	-	0.54	0.39	-	0.28	0.32	0.26	0.50	0.38	3.32	<0.20	0.15	0.46
So ₆ .	-	<0.05	0.08	-	0.06	<0.05	<0.05	<0.05	<0.05	0.06	<0.05	<0.05	0.11

Note: 1, 2 - aphyric lava (cover); 3 - oligophyric lava (cover); 4 - lestophyric lava (vein); 5 - tuff, lithocryostoclastic, aleuropsammitic; 6 - sporadophyric lava (cover); 7 - reddish-brown silty clay with volcanic material; 8 - dark brown silty clay; 9, 12 Vendian siltstone; 10 - phosphorites nodular, quartzeous, silty; 11 - lithocryostoclastic tuffites; 12 - light greenish-gray Vendian siltstones; 13 - greenish-gray Vendian tuffites of Vayzits deposits of Ust' Pinega suite, (-) - not available. Chemical analysis, Karpushina V.V., Analytical Centre GIN, 2000.

Tuffs and tuffites are of bluish-gray or greenish-gray color, of lithoclastoclastic aleuropsammitic structure and indistinctly undulatory / bedded texture, sometime with elements of gradational texture. Crystoclasts are represented by biotite packets (occasionally by laths) similar to biotite phenocrysts of effusive rocks in size, composition, and alteration type, but of fresher habit, and also by the same accessory minerals (apatite, zircon, feldspathoids, ore mineral) as contained in lavas. Lithoclasts are usually altered by quartzine aggregates. Tuffites of the anomaly ZG-46 are of unusually fresh habit that is indicated by the presence of packets of unaltered biotite in aggregation with apatite and zircon and, that is the main thing, in the presence of lithoclasts and microfragments of scoria and various amygdaloidal lavas, and microdolerites, perfectly preserved and variable in structure.

Volcanic sedimentary rocks (tuff siltstones and tuff mudstones) are usually developed in lava and tuff cover tops – within the zone of gradual transfer of volcanic rocks to sedimentary rocks. They are of reddish-brown color and differ from the usual sedimentary rocks of the area in the presence of occasional fragments of lava material, particularly of typical pseudomorphs of network structure in biotite packets.

In general, in respect of petrographical composition, the studied volcanic rocks are close to different structural-genetic derivatives of magma melts of calcareous/ alkaline lamprophyre of minette type.

The heavy fraction of the studied rocks is composed to a great extent of fine-grained aggregates of clayey minerals saturated with ferric oxides, of less biotite, and occasional zircon. No accessory minerals occur.

GEOCHEMISTRY

All studied volcanic rocks are highly changed under conditions of weathering crust, therefore, their primary chemical composition is significantly distorted. Chemical composition of volcanic rocks is characterized by predominating development of two rock-forming components: SiO_2 and Al_2O_3 (Table 3). SiO_2 content is quite stable, low: 40,73-46,48% in rocks of lava type, ca.44% in tuffs conforming composition of ultrabasic rocks or rocks transitional to basites (picrite-picrobasalt). In this respect, volcanic rocks differ greatly from sedimentary rocks of the region. Very high content of Al_2O_3 (22,97-29,52%) may be likely explained by its accumulation under weathering. Deposits are potassic ($\text{K}_2\text{O}+\text{Na}_2\text{O} >4$), Ti-content is low to moderate (0.16-1.32% of TiO_2). Rocks are characterized by extremely low content of ultrabasic coherent trace elements (Ni, Co, Cr), their content is lower than in country terrigenous rocks by higher content of alkali (K, Rb, Cs, and especially Li), Ba, and very high content of Zr, Hf, Y, Th, REE (Table 4).

In general, macrocomponents and trace elements distribution does not contradict the suggestion that the studied rocks are close to lamprophyres of minette type, and in Zr-Nb relation they are even closer to lamproites. Lavas of

Table 4.
Minor element composition of the lamprophyres and the Vendian sedimentary rocks (ppm)

N	1	2	3	4	5	6	7	8	9	10	11	12	13
Anomaly	929	ZB-11	ZC-14		LT-32					ZG-46		Outcrop	
Sample	1-48.0	1-87.6	2-50.0	3-51.8	5-86.4-3	3-66.5-5	3-66.5-4	3-66.5-3	3-66.5-2,6	3-66.5-1/3	2-59.0-1	2-62.0	VZ-25-1
n	1	1	1	1	2	4	4	5	4	1	1	2	1
Li	199.0	459.3	188.3	122.3	250.85	29.56	28.36	29.76	49.80	27.9	131.1	45.47	54.3
Be	4.71	5.76	3.12	3.05	3.36	3.16	3.33	3.07	1.32	3.00	2.26	1.71	2.46
Sc	11.8	17.6	10.4	19.6	14.0	8.8	14.73	13.68	10.07	10.2	13.2	14.37	23.0
Ti	5275	6872	3652	21068	3641	872	3941	4298	3600	2868	7281	4342	10949
V	62.7	31.3	50.4	170.5	32.21	10.38	64.32	71.10	62.36	70.5	75.2	77.06	178.0
Cr	36.0	6.1	27.1	137.6	6.62	0.12	56.76	72.15	71.07	58.02	41.68	71.39	42.5
Co	5.1	4.6	4.5	15.5	11.64	6.15	10.70	10.47	11.06	7.37	10.68	15.15	7.7
Ni	18.4	22.2	8.4	31.9	31.25	4.70	19.81	17.26	23.49	13.16	20.49	32.25	21.0
Cu	5.2	7.6	11.0	29.9	667.56	8.95	15.02	12.63	12.01	9.52	537.12	31.35	306.9
Zn	46.9	33.4	25.8	92.1	45.8	23.05	61.54	64.68	52.22	42.3	68.4	70.56	56.0
Ga	14.6	25.9	16.2	21.9	18.2	25.48	24.06	22.49	16.96	18.3	20.3	20.25	17.6
Rb	36.7	20.3	24.6	105.4	31.71	38.69	139.30	141.13	101.25	99.6	60.9	118.26	77.4
Sr	73.3	87.4	89.6	95.5	81.43	114.43	111.02	107.61	87.01	240.4	67.2	83.62	89.4
Y	104.0	101.3	53.9	82.4	61.62	26.24	40.41	40.46	37.16	589.7	60.8	38.15	48.9
Zr	822.0	660.1	535.9	1122.1	443.9	220.7	263.5	296.1	311.3	195.3	927.7	365.6	324.3
Nb	38.2	25.4	30.2	76.4	35.2	37.0	23.4	19.2	15.0	12.6	35.0	18.4	20.9
Mo	1.34	1.54	0.82	0.69	0.18	3.37	0.82	0.84	0.22	2.06	0.65	0.21	0.17
Cd	0.27	-	0.25	0.69	-	-	-	-	-	-	-	-	-
Sb	-	-	14.51	8.96	-	-	-	-	-	-	-	-	-
Cs	2.18	1.63	1.54	4.22	1.56	3.35	6.68	5.97	3.52	3.79	1.90	4.03	3.38
Ba	173.7	138.4	338.4	1036.7	307.2	245.8	438.0	402.1	327.6	471.0	497.0	333.2	266.7

different anomalies are rather different in composition.

Differences between the studied volcanic and sedimentary rocks lie in higher content of Zr, Hf, Th, Y, REE, Li and lower content of SiO₂, Rb, Cs, total K in volcanic rocks. The studied volcanic rocks differ from tuffites of the Vayzits deposits in higher content of Li, Th, Zr, Hf, Y, and EER (less contrasting) and lower content of U, Sc, V.

In petrographic properties, especially in the total mineral, macro- and microelement composition the volcanic rocks of lava habit and tuffs are quite close, however, they distinctly differ from sedimentary rocks of the area and from tuffites of the Vendian Ust' Pinega sequence.

ABSOLUTE AGE

Location of volcanic rocks in the section of Vendian sedimentary rocks in the Mezen sequence mostly shows their formation concurrently with country rocks. In some cases volcanic rocks occur as intersecting veins suggesting their younger age. For the purpose of the absolute age determination, a volcanic body representing a vein-like intrusion of 1-12 mm thickness intersecting the Vendian rocks (potentially the youngest body, sample ZC -14/3-51.8) was selected. This body was formed by lamprophyric lava of plesiophytic structure (up to 35% of biotite phenocrysts) with high content of accessory minerals of large sizes (apatite + zircon content = ca.0.1%). With high alteration of rock taken into account, absolute age was determined using U-Pb dating of zircon. Zircon is characterized by small (0.2-0.4 mm length) idiomorphic grains, zonality, presence of numerous melt inclusions, magmatic nature of crystals inclusive.

Determination of absolute age with the use of U-Pb method of zircon dating was carried out in the ARC National Key Center GEMOS, Sidney, Australia. Optimal dating of the studied magmatic rock crystallization is 570 ± 8 Ma that corresponds to the Late Vendian and actually coincides with the Proterozoic/Phanerozoic boundary.

CONCLUSIONS

Discovery of a new type of alkaline magmatism in the southeastern part of the White Sea area is a very significant result of purposeful prospecting works in the western part of the White Sea - Kuloy Plateau.

The studied volcanic rocks are characterized by equitype mineral composition (kaolinite, hydromica- montmorillonite, hematite, goethite), relic porphyric and vitroclastic structure. Petrographical composition (stable paragenesis biotite + changed glass \pm apatite \pm zircon \pm feldspathoids \pm ores), chemical composition of biotite phenocrysts and crystoclasts, geochemical properties of rocks (basic/ultrabasic composition, potassic type with very low content of ultrabasic coherent elements (Ni, Co, Cr), higher content of alkali (K, Rb, Cs, and especially Li), and very high Zr, Hf, Y, Th, EER content in general do not contradict the studied rocks

closeness to various structural and genetic derivatives of magmatic melt of calcareous/alkaline lamprophyre of minette type.

Occasional lava bodies and lamprophyric tuffs of minette type exposed within the anomalies indicate rather wide development of aerial (subaqueous) alkaline volcanism concurrent to sedimentation in the Vendian sea basin within the studied area. Data on absolute age of stratified volcanic rocks verify stratigraphical location of the Mezen deposits and, probably, would require amendments to stratigraphical section of the overlying Vendian Padun sequence.

The discovered volcanic rocks of a new type make a chain of northeastern trend, parallel to the White Sea entrance, along the Zimny Bereg of the White Sea. They possibly correlate with the faults parallel to the fault system of the White Sea entrance graben and transversal to the Kola-Dvina Riphean paleorift system that could characterize them as “transform” faults, and the associated alkaline (specifically potassic) aerial volcanism – as rift-type volcanism.

These are the first magmatic rocks of another petrological type and age different from the well-known Late Devonian explosion pipes and kimberlite sills, picrites, melilithites, and basalts discovered in the Zimny Bereg volcanic area. On the one hand, inaccurate diagnostics of similar volcanic rocks of the new type could result in the wrong trend of Late Devonian kimberlites prospecting; on the other hand, potassic type of these volcanic rocks and presumed relations with the active rift “transform” faults may indicate the mantle nature of their magmatic sources, that in its turn suggests possible occurrence of the Late Vendian mantle melts and other bodies including kimberlites within the Zimny Bereg area.

REFERENCES

1. Erinchek Yu.M., Milshtein E.D. Riphean rift-forming of the central East-European Platform. SPb, VSEGEI. 1995.
2. Geological structure, mineralogical and petrological properties of kimberlites of Arkhangelsk Province/Verichev E.M., Garanin V.K., Grib V.P., Kudryavtseva G.P. // 1991. N 4. P. 88-94.
3. Kaminsky F.V., Sablukov S.M., Sablukova L.I., Shpanov V.E. Diamondiferous minette a new type of diamondiferous rocks. // *Izvestia Earth Sciences Section of Russian Academy of Natural Sciences/ Special Issue. Presented to the 31th session of the International Geological Congress, Brasil. 2000, Iss. 4. P. 85-94.*
4. Mitchell R.H. Compositional variation of mica in kimberlites, orangeites, lamproites, and lamprophyres. Extended Abstr. 6IKC. Novosibirsk: Russia. 1995. P. 390-392.
5. Sablukov S.M. On petrochemical series of kimberlite rocks // *DAS USSR. 1990. V. 313, N 4. P. 935-939.*
6. Sablukov S.M. Petrochemical series of kimberlite rocks of Arkhangelsk Province. Extended Abstr. 6IKC. Novosibirsk: Russia. 1995. P. 481-483.
7. Shirobokov V.N. Some specific features of the Zimny Bereg diamondiferous area structure // *Subsoil Prospecting and Protection. 1997. P. 21-25.*
8. Stankovsky A.F. Vendian rocks of the southeastern White Sea region// *Subsoil Prospecting and Protection. 1997. P. 4-9.*

PETROCHEMISTRY OF MANTLE XENOLITHS FROM SOVGAVAN PLATEAU, FAR EAST RUSSIA.

¹Ashchepkov I.V., ¹Saprykin A.I., ¹Gerasimov P.A., ¹Khmelnikova O.S., ¹Cheremnykh L.V., ¹Safonova I.Yu., ²Rasskazov S.V., ¹Kutolin V.A., ³Vladykin N.V.

¹*United Institute of Geology Geophysics and Mineralogy, SD RASc Novosibirsk,
garnet@uiggm.nsc.ru*

²*Institute of Earth Crust, Irkutsk, SD RASc, rassk@crust.irk.ru*

³*Institute of the Geochemistry, SD RASc, Irkutsk, vlad@igc.irk.ru*

Comparison of data obtained on the mantle xenoliths from SovGavan plateau with those from other localities in Primorie reveal that the last portions of basalts containing large Sp-lherzolites are lower in temperature and more Al-rich (700-900°C) comparing with common close to primitive lherzolites (900-1100°C) and Cr-Di Amph (900-1000°C) bearing websterites. In Shkotov plateau more ancient basalts (13ma) the xenoliths are the hot Fe-lherzolites. Mantle xenoliths from Anui picrite-basalts [4] refer to relatively shallow depleted varieties. Oxygen fugacity for SovGavan xenoliths gently rises from -4 to + 4. In mantle magmatic breccias Fe-Al clinopyroxenite cement several peridotite pieces that reveal at the contacts rapid change in the petrographic and chemical compositions, local associations are equilibrated within 1000-1040°C, 6-12 kbar. Geochemistry of clinopyroxenes reveal the patterns that suggest the equilibration with the relic garnet or mixing with the melts passing from garnet facie. Amph Cr-Di veins reveal more humped patterns then Al rich lherzolites which parental melts are very close to host basalts differing in Sr and HFSE. The REE distributions of all the clinopyroxenes from SovGavan xenoliths sharply differ from highly inclined LREE- rich patterns of clinopyroxenes from Podgelbanochny volcano [8].

INTRODUCTION

Mantle inclusions from the Pacific margin of the Eurasia are studied in detail by many investigators [3, 24 etc and ref. there in] but for the Russian Far East a geochemical data are more restricted [8]. Peridotite xenoliths compositions and variations in Far East [4, 5, 8, 12, 17, 19 etc.] suggest rather heterogeneous mantle substrate [8,12,17,19] studied more detail in Sovgavan Plateau [5]. Xenoliths were mainly investigated in the eastern volcanic branch (fig.1) [13] while geochemistry of xenoliths from western branch is less described in literature. This paper presents some new data on the chemistry of minerals and bulk rocks from SovGavan flood basalt plateau in comparison with those from several other localities of mantle xenoliths in Primorie. (Collected by S.V. Esin, L.V. Cheremnykh., Safonova I.Yu in Sovgavan plateau and by S.V. Rasskazov in Shkotov Plateau.)

BASALT

Miocene -Pliocene basalts of Sovgavan plateau neighboring Nelma and Bikin plateaus and some close regions reveal rather shallow conditions of origin

and fractionation (fig.2). As it were originated in mantle conditions while tholeites seem to be differentiated in shallow magmatic chambers possibly within the crust revealing an increase of the Fe# and silica due to dominating Ol fractionation common the level of the basalt generation (magma derivation) became deeper in time reflecting the decrease of the plume magmatism intensity. Alkali and sub alkaline basaltss

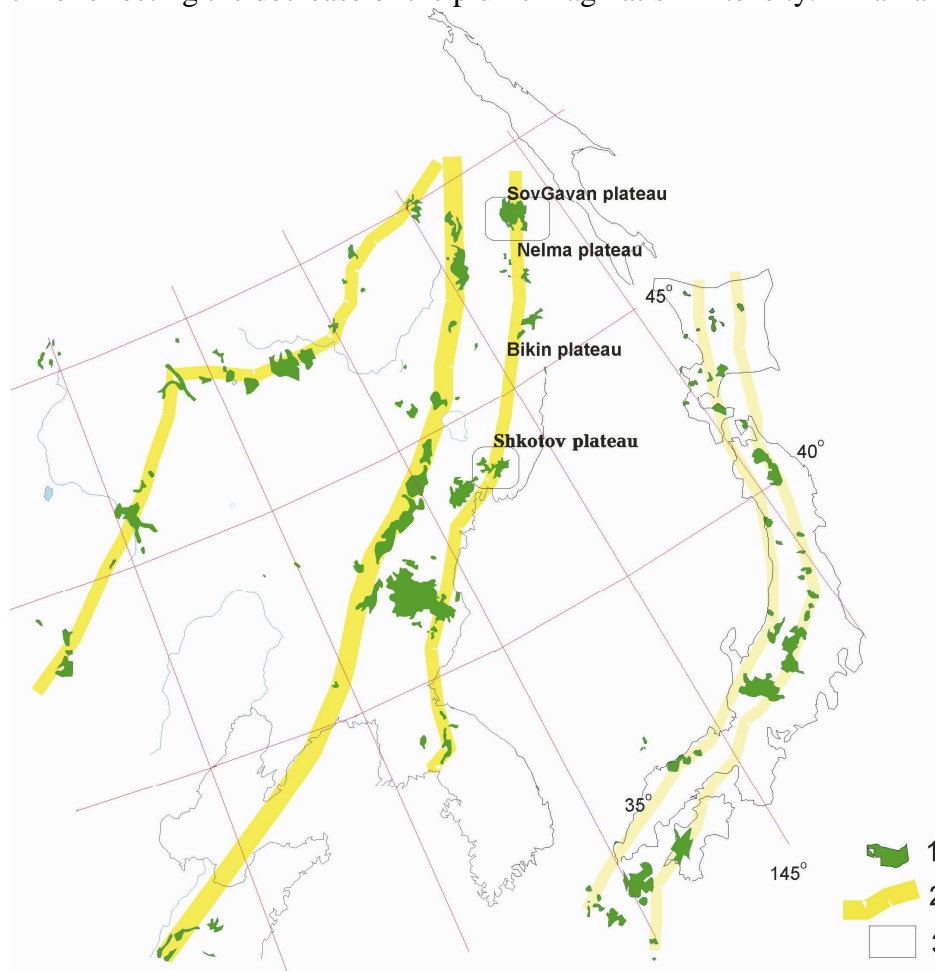


Fig.1. Location of the basaltic plateau in Primorie and nearest regions.

1 - Volcanic rocks. 2. Volcanic belts 3. Plateau studied

PERIDOTITE XENOLITHS

Mantle spinel peridotites were collected from the Kopyy river. Kurgan mountain, Sanky river. They are commonly equal fine- to mean- grained spinel peridotites without the signs of brittle deformation though the signs of plastic motion are common [4]. Commonly, the more light peridotites are more fine grained. Lherzolites contain the glasses in the intergranular space and rarely pink kelyphite-like aggregates similar to kelyphites after garnet. Darker coarse grained websterites contain interstitial amphiboles always partly molten.

Clinopyroxenes from the all localities in Late Miocene basalts of Sovgavan plateau are very similar revealing two main trends. Fertile peridotites as well as

more depleted varieties show the common regularities of Cr decrease and basaltic component increase with the Fe#. These Cr-diopsides are close to the xenoliths from the other localities in Sovgavan plateau being twice lower in Cr₂O₃ content (fig.3). Comparing to Anyui peridotites from Mesozoic picrite basalts [4] the

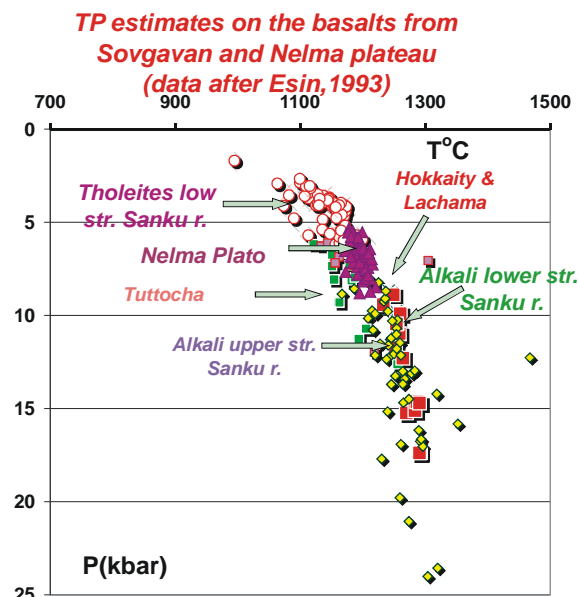


Fig. 2 TP estimates according to (Albarede, 1992) for the basalts of SovGavan Plateau and close located volcanic regions.

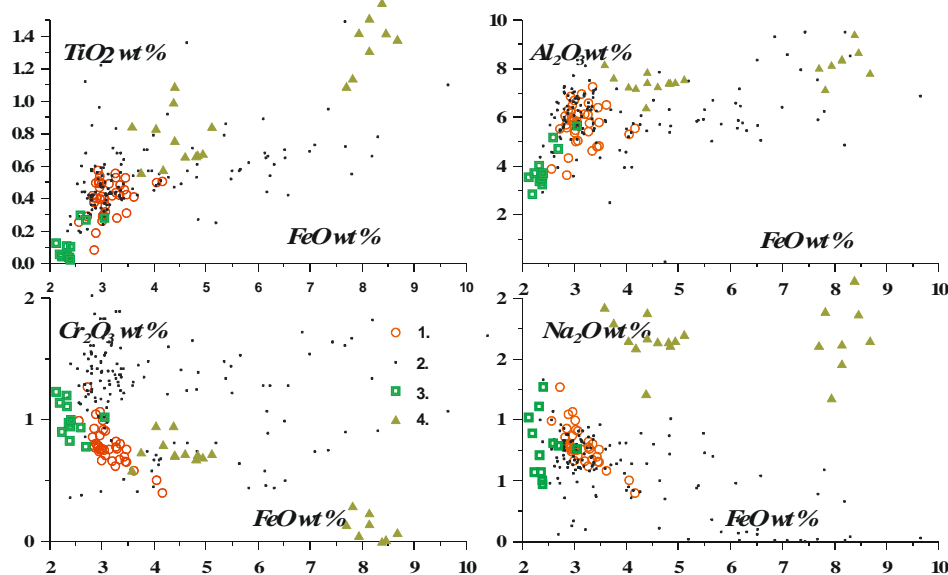


Fig.3 Variation diagram for the clinopyroxenes from Primorie.

1. SovGavan – xenoliths from the latest volcanics. 2. SovGavan all together [5] 3. Anyui [4] 4. Shkotov Plateau

clinopyroxenes in xenoliths from the volcanic lapillus and latest bubbled basalts from Sanky and Kopyy rivers are more ferriferous and enriched in all

basaltic components. But they are slightly more depleted than clinopyroxenes from the massive alkali basalts and rarely display contact relationships with the black and transitional series pyroxenites which are common [5]

Xenoliths from Shkotov plateau are referred to so called Fe-Iherzolite type and are divided into two groups according to Fe and Cr content. The most ferriferous varieties represent direct contacts with the pyroxenites of black series.

Spinels are Al-rich and locate mainly within the mantle array (fig.4). Those from the large xenoliths in bubbled aphyric lavas are more Cr-rich than in common Iherzolite xenoliths [5]. Spinels from Shkotov plateau are enriched in hercynite mineral.

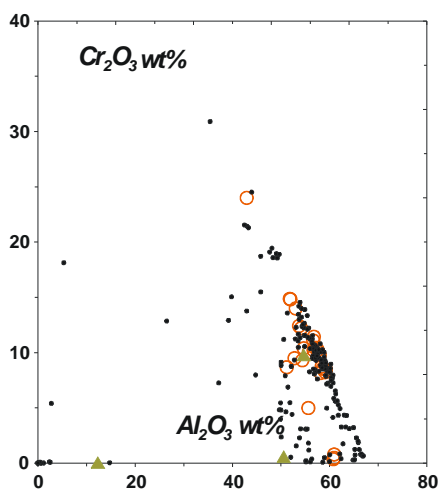


Fig. 4. Composition of the spinels from the mantle xenoliths of Primorie. The signs are the same

PT ESTIMATES FOR PERIDOTITES.

Temperatures and pressures for studied mantle xenoliths were determined using monomineral thermometers and barometers. Clinopyroxene – based [15] estimates correlates with those obtained with the orthopyroxene thermometer [2] but the later give the 100-150° higher temperature. The Cr in Cpx barometer [15] and the Na-Al [1] variant of Cpx barometer used to find the pressure thought these values are not correct because they are calibrated on Ga-peridotites. We also used Opx – based

estimates [16] suggesting the pyroxenes to be in equilibrium with metastable garnets. The CPx -based estimates [1,15] suggests rather low pressures for some peridotites up to 5-6 kbar that should correspond to very thin crust at least beneath the volcanic plateaus. All the methods suggest rather hot mantle geotherms (fig.5) beneath Primorie which coincides with the conclusions for East China [3,24].

Oxygen conditions The oxygen conditions determined using clinopyroxene thermometer [15] and Ol-Sp oxygen barometer [22] reveal rather oxidized conditions for SovGavan mantle peridotites up to +4. The later are referred to Ni-magnetites found in rare xenoliths and Fe-rich spinels. This data support the conclusion about relatively oxidized mantle xenoliths from Primorie [7], possibly influenced by oxidized subducted material. Nearly lineal trend for these peridotites suggest continuous processes of mantle peridotites interaction with the hot (and deep) mater appeared to be mantle melts possibly contaminated by subducted slab material. Small break between the trends seems to be formed due to direct interaction with basaltic related melts. Large xenoliths found as the volcanic

bombs are less oxidized and lower in temperature than those from common basalts (fig.6).

Dependence of the bulk rock compositions from the estimated temperature and pressure. Using the Terra55 program dependence of the peridotite bulk rock compositions from the Opx- and Cpx- based temperatures and pressures was checked for 15 association. Both methods give the same result: SiO₂, MgO, FeO, TiO₂ and less evident (CaO, Na₂O) in general rises with the calculated temperatures (and pressures) while Al₂O₃ decreases. This means decomposition of Al₂O₃ rich phase and migration of alumina to the top of the mantle column and interaction of peridotites with the hot Fe- rich melts from the bottom.

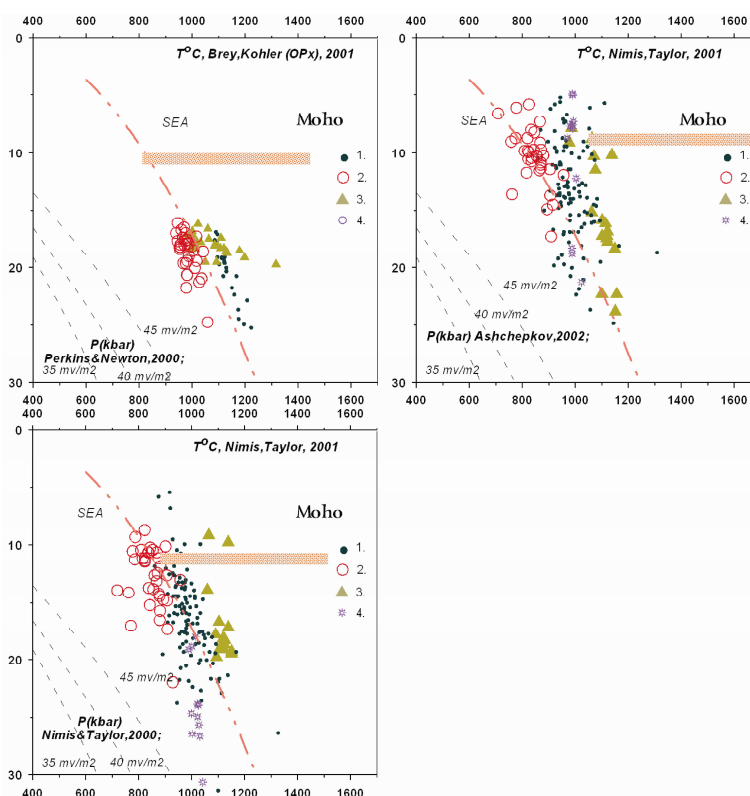


Fig.5. TP estimates for the xenoliths from Primorie

Magmatic breccias. Rare xenoliths represent fragments of magmatic deep seated breccias. Studied xenolith 9/1 contain several pieces of lherzolites cemented by essentially pyroxenite material with rare idiomorphic olivine and alkali feldspar grains incrusting small gaseous cavities. The outer part of peridotites display evident zonation in modal (Ol-Opx-Cpx) and chemical compositions (fig.7). Peridotite fragments referring to Fe lherzolites contain varying in Cr₂O₃ content spinels and varying in Cr, Ti, Al, Fe pyroxenes cemented by the clinopyroxenites formed by basaltic magma containing Ol with Fe# close to that in basalts (19-17% FeO). The TP estimates with the CPx thermometer [15] and CPx barometer [1] give nearly equal values ~6 kbars for different parts of cementing vein pyroxenite

and variations within 6-11 kbars interval for peridotites. Estimated temperatures for peridotite clinopyroxenes in sample 9/1 are ranging within 1000-1040°C.

TRACE ELEMENT GEOCHEMISTRY

Trace elements were determined for 6 clinopyroxenes from mantle xenoliths (Sanky and Kopyy rivers) by LAM ICP method in the Analytic center UIGGM were compared with 4 CPx

compositions

published [8] (fig. 8).

Clinopyroxenes from Kopyy river are divided into three groups. Slightly

depleted Kopyy river demonstrate typical patterns with the depletion in LREE.

They have the depressions in Zr, Hf, Nb, Ta what is common for some

subduction related mantle melts. But this compositions are spinel lherzolites from even relatively higher in REE. Clinopyroxenes from the more dark xenoliths display slightly humped REE patterns corresponding to the rocks with minor garnet. They are more primitive in compositions having very small depletions in Zr but deeper in Ta. Clinopyroxenes from Amph- bearing websteritic are more closer in REE to those from the garnet- bearing lherzolites. Their TRE spidergrams are nearly primitive and even enriched in some HFSE. One of them demonstrate rather strong peak in U and Th. Two clinopyroxenes from xenoliths of Podgelbanochny volcano [8] reveal LREE - enriched distribution close to craton mantle keel being even more enriched, Pb minima suppose sulfide precipitation while high Th, U, Nb, Ta content and small Zr minimum is typical for the enriched or primitive mantle in garnet facie.

The compositions of host plume basaltic lavas determined by LAM ICP are close to published in previous works [8, 12, 13] common compositions of plum basalt corresponding to melting of the primitive mantle source [14], deviating only in Sr (peak) and demonstrating small fluctuations in Zr- Hf.

Reconstructed with clinopyroxene KD [6] compositions of the coexisting magmatic liquids for spinel lherzolites of the Kopyy river basin vary in inclinations (La/Yb_n ratios). They are close to lavas erupted to the surface. The later are slightly lower in LILE content. The compositions of the melts parental for Cr- Di in the xenoliths from Podgelbanochny [8] differ much from the even most enriched

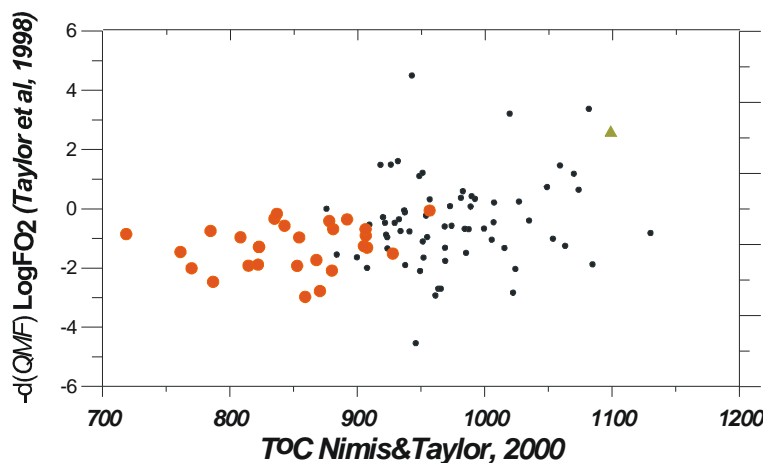


Fig. 6.

Oxygen conditions determined for the mantle xenoliths from Primorie

composition of the lavas from the Western volcanic branch in Sikhote Alin [13] having much more elevated TRE patterns derived from more primitive source in garnet facie.

DISCUSSION

Determined TP conditions for the basalts demonstrate common regularities for the stages of volcanism like in Baikal rift zone that seems to be common also for the oceanic plum basaltic plateaus [23]. Xenoliths from Shkotov plateau demonstrate thermal impact of the plum magmas close in time to the beginning of new plume volcanic circle. Late Miocene -Pliocene volcanics in SovGavan plateau contain xenoliths with Al- rich Cr-Di compositions that are typical for relatively low -temperature intergranular melts crystallization in peridotites usually found in volcanoes from the top of lava plateau and beginning of valley basalts creation.

All general temporal and lateral variations demonstrate strong interaction of mantle substrate beneath Sikhote Alin and Primorie with the plum melts. Nearly continuous trends for clinopyroxenes in variation diagrams showing the enrichment in basaltic components with temperature and increase of the $(La/Yb)_n$ ratios suggest the reactions of the basalt- related melts passing from garnet to spinel facie directly through the lherzolites. This is accompanied by general rise of TRE due to intergranular differentiation resulted from partial melt crystallization. Crossing REE lines for CPx's parental melts suppose not only simple interaction of basalt melts came from Ga-facies percolated through lherzolites but also suggest decomposition of the garnet in the source which relics are found now rarely as kelyphite like masses.

Difference in composition of lavas from Western and Eastern zones in Sikhote Alin [13] is not proved by the trace element diversity due to lack of data for mantle peridotites from the Western zone. The reason of the appearance of two volcanic branches can be recognized in internal continental zones of the Asia are 1) decomposition of amphibole at the depth 120 km in volcanic front [11] and then Phl melting near 400 km [18] producing two peaks of the metasomatism [21] at the distance of ~300 one from another if to suggest the 45° angle of subduction, 2) it may be the decomposition of the serpentine and its varieties in subducted plate giving two peaks of the dehydration being submerging in mantle [9]. An explanation is the superposition of the volatile fluxes derived from the two subducting plates [10], seems to not realistic to this region. Plume interaction with theses hydrated lithosphere regions may regulate the spatial distribution of volcanics in continental margins and also in inner continental zones. Lateral mantle geochemistry variation may be caused by the diversity of the slab- derived metasomatic agencies [11]. It may be also the reaction of two partly molten layer - asthenosphere ~120 km and 420 km boundaries usually accumulating rising plume melts as it seen in tomographic models to the pass of the subducted slab.

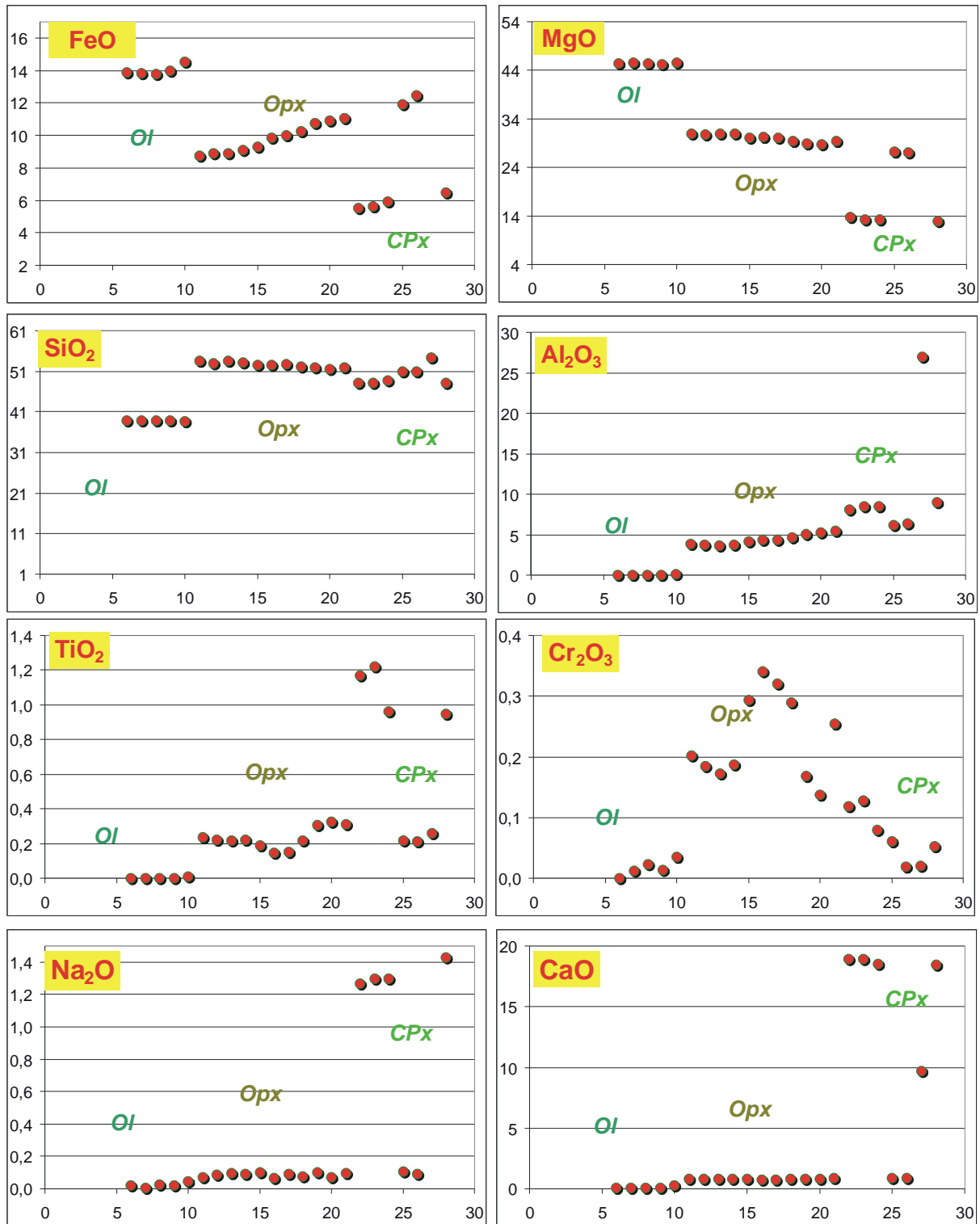


Fig. 7. The profile across the margin of the xenoliths in deep seated magmatic breccia.

Possible reasons of the geochemical difference [13] for the two volcanic branches: 1) initial diversity of lithospheric blocks – when the Western one represent the continental mantle while the Eastern regenerated by melts passed through the subduction wedge; 2) the differentiation and reaction of hydrous melts derived initially from the eclogites in subducted slab.

Two stage process: passage of the subduction related melts and then thermal impact and percolation of the plum melts with the decomposition of early amphiboles is a common probable model for the mantle evolution in the continental margins [21].

CONCLUSIONS

1. The difference in the compositions between the xenoliths from the late stages of volcanic activity and spatial variation in mantle xenoliths compositions was found in Russian Primorie.

2. Trace element and chemical features of peridotite minerals and erupted basalts including the difference between the western and Eastern branch is determined by the vertical and spatial variations of the construction of mantle column.

3. All the regularities found for the mantle xenolith suppose the regeneration of mantle wedge by the slab derived and plum melts came from the depth.

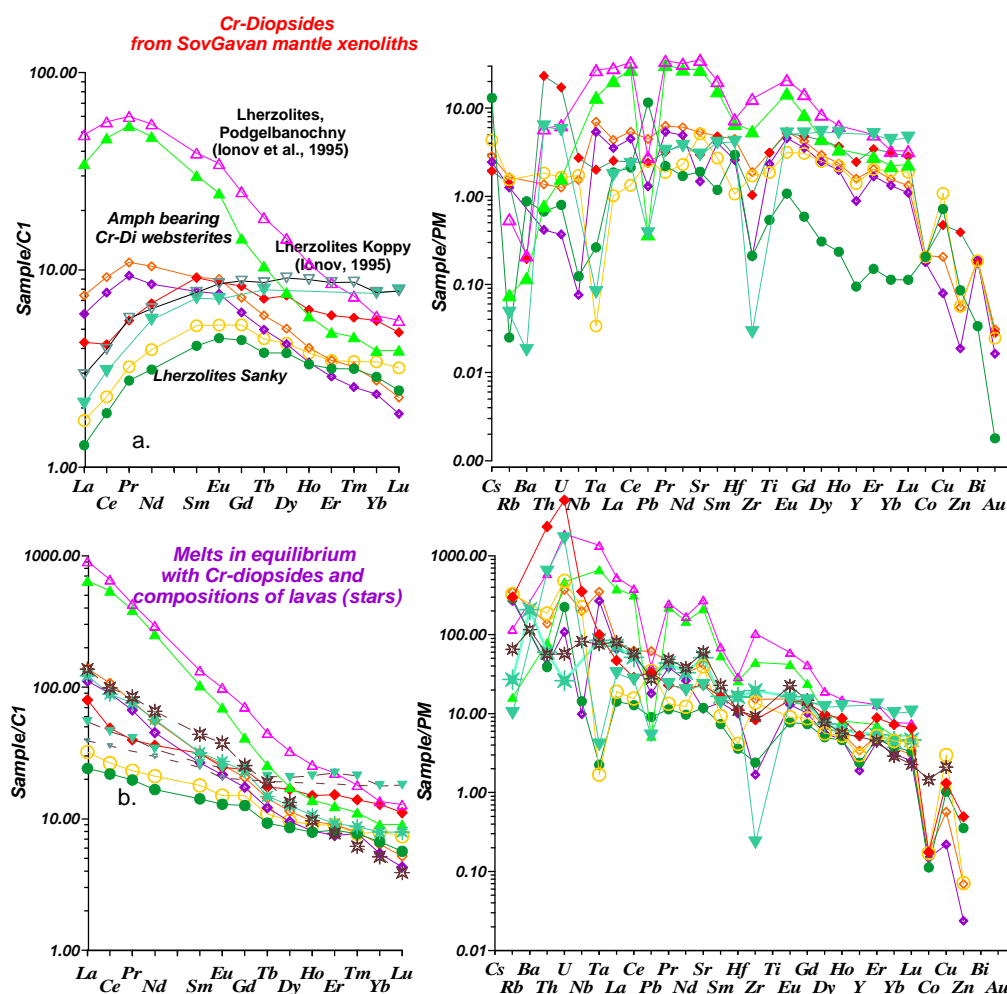


Fig. 8. Trace element patterns for the peridotite xenoliths from SovGavan plateau in comparison with those from Podgelbanochny volcano [8]

Acknowledgements. Many thanks to S.V.Esin and local geologists. Work was supported by grants: 94-17103, 99-05-65688.

REFERENCES

1. Ashchepkov I.V. Empirical clinopyroxene thermobarometer for the mantle rocks based on the jadeite – diopside exchange. // *Trans. RAS (ESS)*. 2002. V. 382. N1. P.78-82.
2. Brey G.P., Kohler T. Geothermobarometry in four phase lherzolites II: new thermo-barometers and practical assessment of using thermobarometers. // *J. Petrol.* 1990. V.31. P.1353-1378.
3. Chen S.H., O'Reilly S.Y., Zhou X.H., Griffin W.L., Zhang G.H., Sun M., Feng J.L., Zhang M. Thermal and petrological structure of the lithosphere beneath Hannuoba, Sino-Korean Craton, China: evidence from xenoliths. // *Lithos*. 2001. V. 56 / 4. P. 267-301.
4. Esin S.V., Ashchepkov I.V. Zircon from the ultramafic nodules in the Mesozoic melaleucites of the Central Sikhote-Alin. // *Trans. RAS (ESS)*. 1997. V.352. N 6. P. 792-794.
5. Esin S.V., Prussevich A.A., Kutolin V. A. Late Cenozoic volcanism and deep seated structure of the Eastern Sikhote Alin. / *Novosibirsk. Nauka*. 1992. 158 P. (in Russian)
6. Hart S.R., Dunn T. Experimental cpx/melt partitioning of 24 trace elements. // *Contrib. Mineral. Petrol.* 1993. V.113. P. 1-8.
7. Ionov D.A., Wood B.J. The oxidation state of subcontinental mantle: oxygen thermobarometry of mantle xenoliths from central Asia. // *Contrib. Miner. Petrol.* 1992. V. 111. N2. P.179-193.
8. Ionov D.A., Prikhod'ko V.S., O'Reilly S.Y. Peridotite xenoliths in alkali basalts from the Sikhote-Alin, southeastern Siberia, Russia: trace-element signatures of mantle beneath a convergent continental margin. // *Chemical Geology*. 1995. V. 120. P. 275-294.
9. Iwamori H. H. Deep subduction of H₂O and detection of volcanic chain towards backarc near triple junction due to lower temperature. // *Earth Planet. Sci. Lett.* 2000. V. 181. P. 41-46.
10. Kaneko T. A. Kinematic subduction model for the genesis of back-arc low-K volcanoes at a two-overlapping subduction zone, central Japan: another volcanic front originated from the Philippine Sea plate subduction. // *J. Volcanol. Geotherm. Res.* 1995. V. 66. N 1- 4. P.9-26.
11. Kenji M., Toshitsugu E., Atsushi Y. Control of the location of the volcanic front in island arcs by aqueous fluid connectivity in the mantle wedge. // *Nature*. 1999. V. 401. N 6750. P. 259-262.
12. Koloskov A.V. Ultramafic inclusions and volcanics as the self regulating geological system. / *Moscow. Scientific World*. 1999. 223 P. (in Russian).
13. Martynov Yu. A., Chashchin A., Rasskazov S. V., Saranina E.V. Late Miocene-Pliocene Basaltic Volcanism in the South of the Russian Far East as an Indicator of the Lithospheric Mantle Heterogeneity in the Continent-Ocean Transition Zone. // *Petrology*. 2002. N2 P.165-184.
14. McDonough, W.F., S.S. and Sun. The Composition of the Earth. // *Chem. Geol.*, 1995, V.120. N3-4 P. 223-253.
15. Nimis P., Taylor W. Single clinopyroxene thermobarometry for garnet peridotites. Part I. Calibration and testing of a Cr-in-Cpx barometer and an enstatite-in-Cpx thermometer. // *Contrib. Mineral. Petrol.* 2000. V. 139. N.5. P. 541-554.
16. Perkins D., Newton R.C. The composition of the coexisting pyroxenes and garnet in the system CaO-MgO-Al₂O₃- SiO₂ at 90-1100°C and high pressures. // *Contrib. Mineral. Petrol.* 1980. V.75. P. 291-300.
17. Prikhod'ko V.S.; Zemlyanouhkin V.N. Composition and structure of upper mantle under Hanka massif // *Pacific Ocean Geol.* 1997. V.16. N4. P. 88-94.
18. Sato K., Katsura T., Ito E. Phase relations of natural phlogopite with and without enstatite up to 8GPa: implication to mantle metasomatism. // *Earth Planet. Sci Lett.* 1997. V. 146. P. 511-526
19. Scheka S.A. Basic and ultrabasic intrusions and inclusions in the effusive rocks of Far East. / *Nauka. Moscow*. 1983. 161 P. (in Russian.)

20. Sen G., Macfarlane A., Srimal N. Significance of rare hydrous melts in Hawaiian xenoliths. // *Contrib. Miner. Petrol.* 1996. V.122. P. 415- 427.
21. Tatsumi Y., Kogiso T. 1997. Trace element transport during dehydration processes in the subducted oceanic crust: 2. Origin of chemical and physical characteristics in arc magmatism. // *Earth. Planet. Sc. Lett.* 1997. V.148. P. 207–221.
22. Taylor W.L., Kamperman M., Hamilton R. New thermometer and oxygen fugacity sensor calibration for ilmenite and Cr-spinel-bearing peridotite assemblage. // 7th IKC Extended abstracts. 1998. P. 891.
23. Touret J.-C. Volcanic geomorphology - an overview. // *Earth Sci. Review.* 1999. V. 47. P. 95-131.
24. Xu X.S., O'Reilly S.Y., Griffin W.L., Zhou X.M. Genesis of young lithospheric mantle in southeastern China: an LAM-ICPMS trace element study. // *J Petrol.*, 2000, V. 41/1 P. 111-148.

MEYMECHITES IN CENTRAL SIKHOTE ALIN

Voinova I.P. and Prikhodko V.S.

Institute of Tectonics and Geophysics, Far Eastern Branch of Russian Academy of Sciences, Khabarovsk, vladimir@itig.as.khb.ru

In Mesozoic accretionary nappe-fold Central Sikhote Alin system two groups of meymechite were recognized. One group is spatially associated with potassic and the second one with sodic intraplate oceanic basalt which correlates well with data on their petrochemistry, geochemistry and mineralogy. Ultramafic volcanics associated with sodic basalt have compositional characteristics almost similar to Siberian platform meymechite. The second group, which is more widespread, is similar to the alkaline series meymechite occurring in fold areas. Geological setting of ultramafic volcanics occurrence, shapes of their bodies (volcanic pipes), sets of xenoliths in them, petrogeochemical peculiarities, regular associations of meymechite with accreted oceanic basalt evidence that those rocks formed at the post-accretionary stage of prism evolution. For the appearance of meymechite, especially that which is similar to platform analogues, thick and "cold" lithosphere had to be formed causing generation of very deep ultramafic melts. Only using detailed isotopic-geochemical and age data it is possible to solve a question about causes of appearance of two types of meymechite, about their place in the accretionary system geodynamic evolution.

INTRODUCTION

In the Central Sikhote Alin there are known [1,3,4,5,6,8,9] the occurrences of ultramafic volcanics (meymechite) spatially confined to the accretionary complexes of the Mesozoic nappe-fold accretionary system. Its geological structure formed as a result of accretion of fragments of paleo-oceanic plate during the subduction process near the eastern margin of Asia and subsequent tectonic transformations among which the left-shift dislocations having replaced oblique subduction played a leading role. First of all, the specific features of meymechite are that having originated from very deep magmatic melts they are atypical of oceanic magmatism. To understand their nature and formation conditions, at what stage of the accretionary prism evolution they formed and what are the basic factors having caused the ultramafic magmatism manifestations geological, petrological and geochemical studies of meymechite are necessary. We studied such rocks in the Anyuisk, Barakhtinsk and Katensk locations of the Samarkinsk and Bikinsk accretionary prisms. Geological information on ultramafic volcanic rocks from the Alchansk [8] and Khutu-Buginsk regions was used.

GEOLOGICAL SETTING

In the Central part of the Sikhote Alin ridge, at the watershed of the Khor and Anuyi rivers upstreams (Anyuisk location), among volcanogenic-cherty deposits recognized within the Dzhaursk suite (T₃-J), there occur subvolcanic sills, dikes and volcanic pipes of meymechite. Volcanogenic-cherty formations make up a lens

within Jurassic-Early Cretaceous terrigenous rocks overlain by its south-western part. We studied magmatic formations outcropping as a band trending north-eastward. Terrigenous rock masses of interlayered siltstone and sandstone tectonically contact them in the north-west and south-east.

In the middle part of the Anyui river (Barakhtinsk location) within a terrigenous-volcanogenic-cherty association there occur ultramafic volcanic rocks having similar habits and petrographic characteristics with the rocks from the Anyui river upstream. According to data by I.P. Boiko, M.V. Martynyuk and B.G. Matveev there was mapped a volcanic structure consisting of sills of diabase, amygdaloidal basalt and hyaloclastite. Dikes and sills of meymechite are widespread near a supposed center of volcanic eruption.

The Katensk location is composed of cherty (T_3 Carnian-Norian and I_1 - I_2), siltstone (I_3 - K_1 Tithonian-Berriasian), mixtite (its groundmass contains Late Jurassic-Early Cretaceous microfauna) and sandstone (I_3 - K_1 Tithonian-Berriasian) formations. Geological setting is characterized by gradual transition from silica accumulation to terrigenous sediment accumulation and a distinct west-eastward alteration from near-continental mixtite (olistostrome) formations and sandstone to hemipelagic and then pelagic facies. Massifs of ultrabasite are confined to a near-subduction zone. Volcanic rocks are mainly associated with cherty deposits and are represented by flows of spilite and hyaloclastite. Stocks and dikes of meymechite occur within the zone of development of massifs of ultrabasite.

In the Barakhtinsk and Katensk locations, as well as in the Alchansk region, the meymechite represented by sills and dikes is associated with potassic intraplate oceanic basalt. In the Anyuisk location, as well as in the Khutu-Buginsk one, ultramafic volcanics are spatially associated with sodic intraplate oceanic basaltoids, and they occur as volcanic pipes.

Therefore, the available geological data suggest the existence within the Central Sikhote Alin, together with two types of oceanic basalt [6,7] of two types of meymechite, respectively: 1) the Anyuisk and Khutu-Buginsk and 2) the Alchansk, Barakhtinsk and Katensk occurrences.

PETROGRAPHY

On the whole, ultramafic volcanic rocks in the regions described have similar petrographic characteristics. Meymechite is dark-green magnophyric amygdaloidal rock of lumpy habit. The structure of rocks is magnophyric, the texture is amygdaloidal. Olivine and chrome-spinellid, sometimes clinopyroxene, refer to the paragenesis of minerals-phenocrysts making up 40-80% of rock. Phenocrysts of olivine are represented by idiomorphic crystals of prism habit 1 cm in size. Often they are completely substituted by serpentine and ore mineral. Chrome-spinellid mineral inclusions in olivine grains. Rare grains of monoclinic pyroxene belonging to the paragenesis of phenocrysts have a habit of short-prism idiomorphic crystals. The groundmass of meymechite is made up by glass, ore

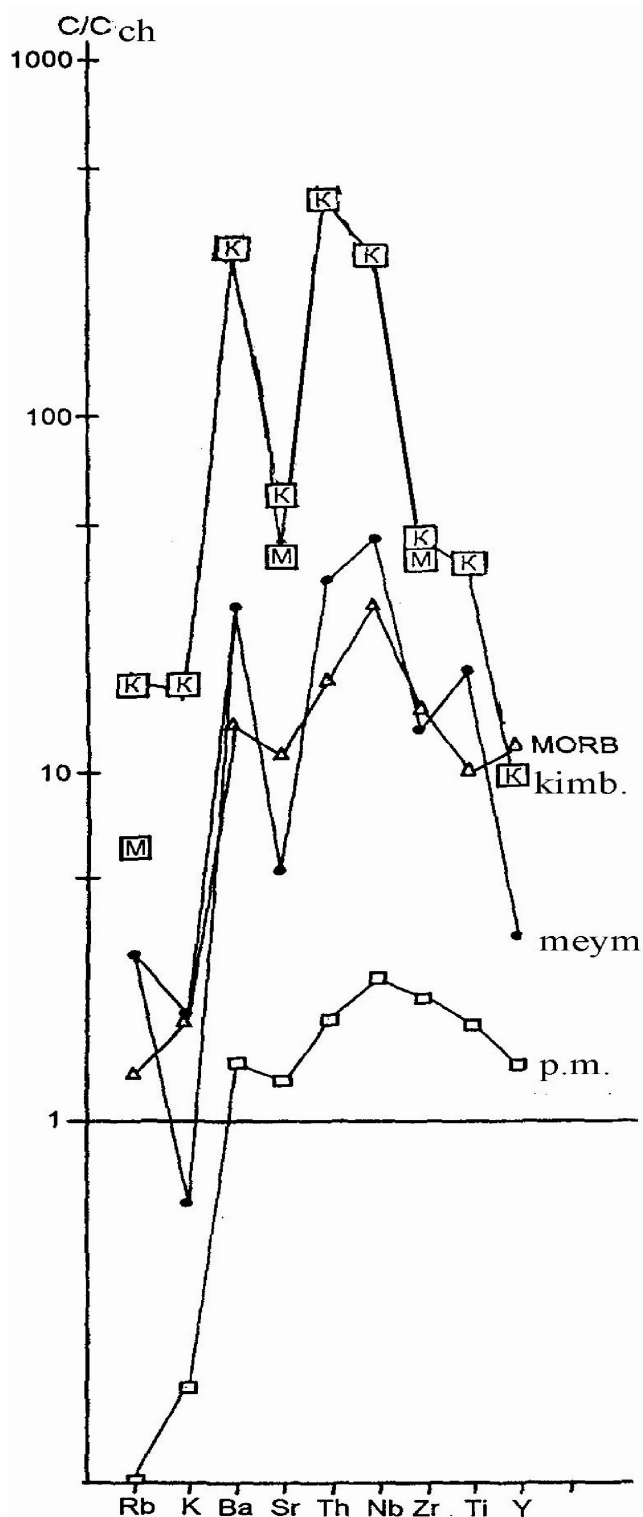


Fig. 1. Spider-diagram of average geochemical compositions normalized to chondrite. Average compositions of meymecheite in Central Sikhote Alin - dots; average "standard" compositions (in squares): M - meymecheite, K - kimberlite.

material (ilmenite and occurs as idiomorphic crystals from 0.1 to 1.0 mm in size, often rimmed by magnetite or as magnetite), microlites of clinopyroxene in various volume proportions due to which the structure of the groundmass varies from vitrophyric (glass is serpentinized) to sideronitic. It has lava or,

sometimes, conchoidal habit. Amygdules are composed of serpentine, chlorite, amphibole (tremolite). Secondary minerals are represented by kersutite, biotite, serpentine, chlorite, sphene, leucoxene and calcite. Serpentine substituting olivine is represented by chrysotile, and the glass in the groundmass by lizardite and serpophite.

Together with magmatic rocks of lava habit there occur eruptive breccias. Clastic material in eruptive breccias of meymecheite is represented by host magmatic (dominating), cherty and terrigenous rocks as well as fragments of isolated crystals. Clasts of magmatic rocks contain: 1) serpentinized high-magnesium volcanic rocks, sometimes clasts of breccias themselves; 2) amygdaloidal augite picrobasalt of various degrees of crystallization and porphyry (similar to lava in flows and dikes from volcanogenic-terrigenous-cherty association). Clasts of rocks are rounded and subrounded, from microscopic to clumpy ones in size, from 15 to 50 cm in diameter. Fragments of picrobasalt are

enriched in carbonate both in amygdules and groundmass, and, probably, in dolomite sometimes making up large crystals (pseudomorphs?). Fragments of crystals in breccias are represented by olivine, clinopyroxene and ore minerals. Groundmass of eruptive breccias is heterogeneous: 1) lava habit; 2) serpentine (lizardite); 3) ore-serpentine; 4) serpentine-carbonate (probably secondary?); 5) sideronite composed of titanium magnetite.

The transition from one type of groundmass to another one takes place at macro- and microscopic levels. The groundmass is characterized by globular or conchoidal structure (globular or ocellar structures). Globules are made up by serpentine, serpentine+calcite, chlorite, chlorite+sericite. Cryptocrystalline glass contains extracts of sphene along which (similar to ore cement) leucoxene develops. Secondary changes of cement are in the development of calcite, serpentine, chlorite, sphene, secondary ore, leucoxene.

PETROGEOCHEMISTRY

Petrochemical characteristics of the ultramafic rocks considered are given in Table. In the meymechite studied, SiO₂ contents range within 37-45% (the

Table

Average concentrations of rock-forming oxides (weight %) and trace elements (ppm) in Central Sikhote Alin meymechite

	Anyuisk location	Barakhtinsk location	Katensk location
SiO ₂	42,57	42.72	41.8
TiO ₂	1,98	1.03	0.96
Al ₂ O ₃	4,16	4.59	3.79
FeO	14,00	12.69	13.73
MnO	0,13	0.34	0.18
MgO	31,58	33.22	34.08
CaO	3,58	4.46	3.39
Na ₂ O	0,15	0.16	0.15
K ₂ O	0,06	0.18	0.05
P ₂ O ₃	0,26	0.11	0.11
n	32	6	3
Rb	<3	14	15
Ba		160	38
Sr	108	43	42
Th	<3	1.4	-
Nb	26	29	8
Zr	130	46	50
Y	7	10	7
n	24	2	3

Note: Sum of rock-forming oxide concentrations is 100 %; FeO = FeO + 0.9 Fe₂O₃. n - number of analyses. Chemical analyses of rock-forming elements were made by method of wet chemistry at the Institute of Tectonics and Geophysics FEB RAS (analyst V.Ye.Zazulina) in 1995. Trace element concentrations were determined by X-Ray spectral method at Central Laboratory of Khabarovsk State Geological Mining Enterprise (analyst V.A.Mishina) in 1995*

varieties with $\text{SiO}_2=41-43\%$ prevail), $\text{MgO} - 27-36\%$, $\Sigma \text{FeO} - 13-17\%$, $\text{TiO}_2 - 1-3\%$, $\text{Al}_2\text{O}_3 - 3-6\%$, $\text{CaO} - 2-9\%$, $\Sigma \text{alkalis} - \text{less than } 1\%$. On the whole, the meymechite studied has similar petrochemical compositions. Still, there were observed different TiO_2 contents in two types of ultramafic volcanics (the Anyuisk meymechite is characterized by enriched titanium contents). Meymechite is characterized by rather low trace element contents compared to standard meymechite, kimberlite, lamproite, and more similar to the MORB contents. On a spider diagram (Fig.1) meymechite has more expressed positive Ba, Th, Nb, Ti, and negative Sr, Y, and K anomalies. At the same time, the nature of trace element distribution in the meymechite studied is similar to that in rocks of a kimberlite-meymechite series. Some variations in Sr, Zr and Rb contents were observed in the meymechite **of both groups (see Table)**.

MINERALOGY

Olivine phenocrysts in meymechite are represented by high-magnesium varieties with $\Sigma \text{FeO} / \Sigma \text{Feo} + \text{MgO}$ within 12-15%. A majority of analyzed grains of olivine are weakly zoned. In the instances when grains of olivine are zoned, the external rim $\Sigma \text{FeO} / \Sigma \text{Feo} + \text{MgO}$ is up to 20%. CaO content is within 0.2-0.3% and NiO within 0.2-0.05%. Chrome-spinellid phenocrysts in the meymechite studied are characterized by wide compositional variations from titanium chrome-picotite to chrome-ulvospinel. They have in common: a) high and relatively stable Cr_2O_3 and Fe_2O_3 contents, b) high contents of TiO_2 (up to 10%), c) a stable negative correlation between Cr_2O_3 and TiO_2 , d) a weak positive correlation between Cr_2O_3 and Al_2O_3 . Chrome-spinellids from volcanic ultramafic rocks in the Anyuisk location are stably depleted in aluminum and enriched in titanium compared with the

Barakhtinsk and Katensk minerals of meymechite. The former are characterized by more intense accumulation of titanium with decreasing chromium content in a mineral (Fig.2).

Compositionally, rare grains of monoclinic pyroxene are close to titanium diopside with small amount of Al_2O_3 and Cr_2O_3 . Minerals are zoned, a direction of the evolution of the compositions is in increasing of ferrosilite mineral, titanium and aluminum. The compositions of the cores of clinopyroxene phenocrysts in the meymechite studied are similar. In clinopyroxene from the Anyuisk meymechite there was observed a more intense accumulation of titanium in the course of the magmatic system evolution (Fig.3).

Clinopyroxene in the meymechite groundmass is compositionally similar to the external rim of the mineral phenocrysts zoned grains. Ilmenite in the groundmass is enriched in MnO (up to 5 weight %).

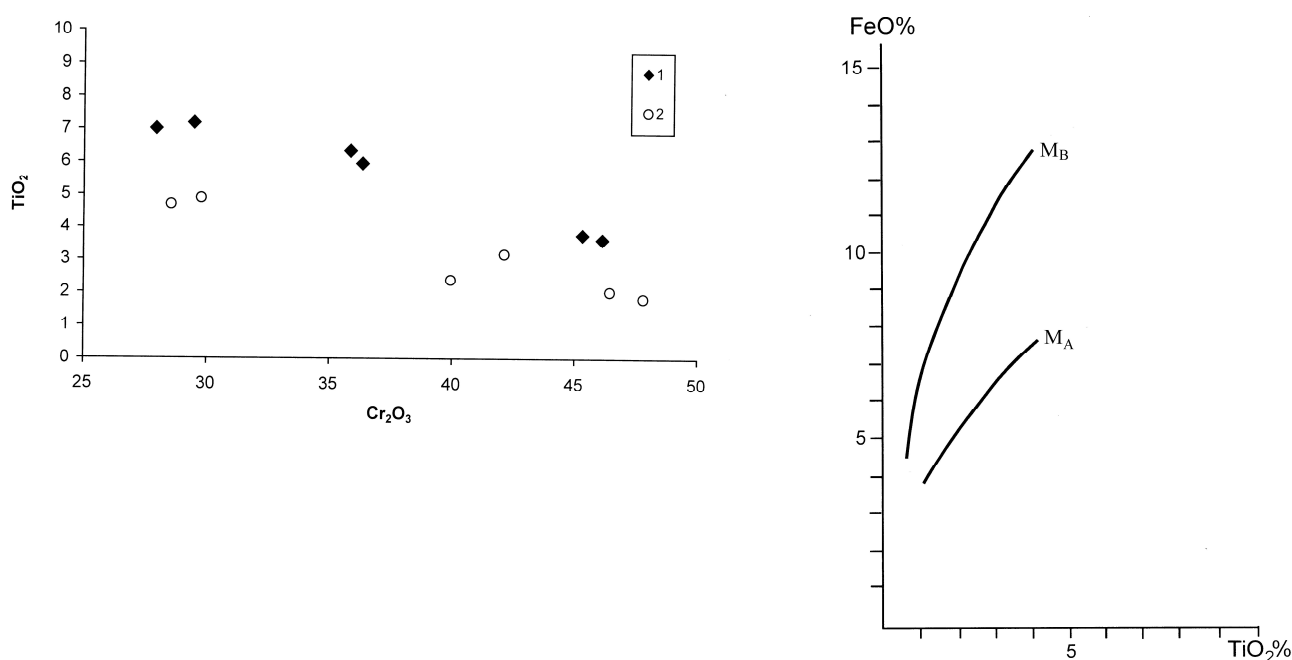


Fig. 3. Monoclinic pyroxene of meymechite in Anyuisk (M_A) and Barakhtinsk (M_B) locations

DISCUSSION OF RESULTS

Recognition of two groups of ultramafic volcanic rocks in the Sikhote Alin nappe-fold system, spatially associating, on the one hand, with potassic and, on the other hand, with sodic oceanic intraplate basalt correlates well with the data on their petrochemistry, geochemistry and mineralogy. On a CaO-TiO₂-A₂O₃ diagram (Fig.4) figurative points of compositions of ultramafic volcanics in the Anyuisk location are situated near the field of compositions of the Siberian platform kimberlite and meymechite [2], and the points of compositions of meymechite in the Barakhtinsk and Katensk locations tend to the field of compositions of Archean komatiite. This similarity is also stressed by their mineralogical characteristics.

Accessory minerals of meymechite are characterized by wide compositional variations caused by varying contents of practically all basic components. Still, chrome-spinellids of ultramafic volcanic rocks in fold and stable areas are characterized by certain typomorphic compositional peculiarities. Thus, accessory minerals in the Siberian platform ultramafic volcanics are characterized by stable high concentrations of TiO₂ and depleted Al₂O₃ opposite to similar minerals of volcanic rocks in fold areas (Kamchatka, Koryakia, Sakhalin, Japan, etc.). Chrome-spinellids of meymechite in the Anyuisk location are compositionally similar to the platform meymechite minerals, and accessory minerals in the

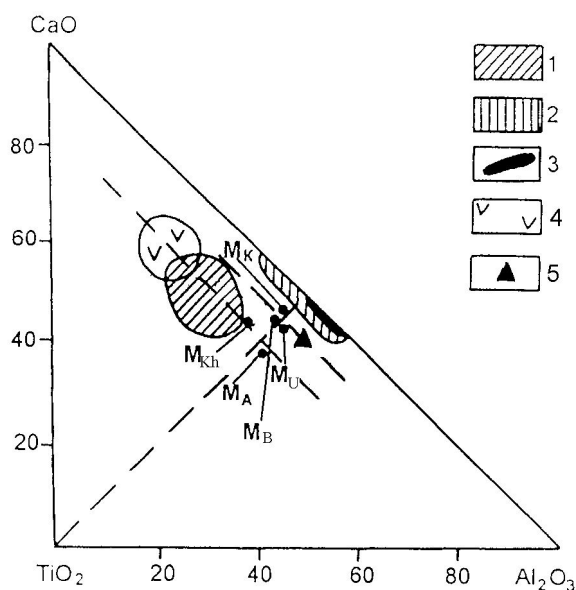


Fig. 4. **CaO - TiO₂ - Al₂O₃ diagram.**

Average compositions of meymechite in Central Sikhote Alin - dots with M symbols. Sub-symbols stand for study areas: A - Anyuisk, B - Barakhtinsk, K - Katensk, Kh - Khutu-Buginsk, U - Alchansk. Fields of compositions: 1 - meymechite in Siberian Platform, 2 - meymechite in Kamchatka, 3 - model lherzolite mantle compositions, 4 - kimberlite. 5 - composition of pyrolith.

Barakhtinsk and Katensk rocks are practically identical with chrome-spinellids of ultramafic volcanic rocks in fold areas [4].

CONCLUSIONS

In the Central Sikhote Alin Mesozoic nappe-fold accretionary system there were found two types of meymechite, one of which is similar to the Siberian platform meymechite by its petrogeochemical and mineralogical characteristics. The second, more widespread, group is similar to the alkali series meymechite from fold areas [4]. Geological setting of the ultramafic volcanics occurrences, shapes of their bodies (volcanic pipes), sets of xenoliths in them, and petrogeochemical characteristics, regular associations of meymechite with accreted oceanic basalt [6,7] evidence that those rocks formed at the post-accretionary stage of the prism evolution. For the appearance of meymechite, thick "cold" lithosphere had to be formed causing the generation of very deep ultramafic melts. Shapes and small sizes of meymechite occurrences testify to a short duration of ultramafic magmatism in that accretionary system. To decide a question about the causes of appearance of two types of meymechite (whether they are the products of the same evolutionary magmatic source or of two different magmatic chambers), about their place in the accretionary system geodynamic evolution is possible only by using detailed isotopic-geochemical and age data.

Work is supported by RFBR grant 01-05-65006.

REFERENCES

1. Prikhodko V.S., Bekhtold A.F. and Berdnikov N.V.// Deep petrology of active continental margins. M., Nauka, 1985, p. 152.
2. Sobolev A.V. Phase composition of meymechite in the north of Siberia and some problems of their genesis.//Problems of the earth crust and upper mantle petrology. Novosibirsk, Nauka, Siberian Branch, 1978, p.330-346.

3. Scheka S.A. Meymechite-picrite complex in Sikhote Alin.// Far Eastern Branch of USSR Academy of Sciences, 1977, V.234, No2, p.444-447.
4. Scheka S.A. and Vrzhosek A.A. Ultramafic volcanism of Pacific belt and problems of meymechite and komatiite systematics.//Volcanology and seismology, 1983, No3, p. 3-15.
5. Voinova I.P., Ziabrev S.V. and Prikhodko V.S. Meymechites of the central Sikhote Alin: a plume underneath an accretionary wedge.//Abstracts 6th Zonenshain conference on plate tectonics. M., 1998, p.40.
6. Voinova I.P. Binary-geodynamic basalt-meymechite associations of accretionary prisms (Central Sikhote Alin)//Petrography at the XXI century eve. Syktyvkar. 2000, p.20-22.
7. Voinova I.P., Prikhodko V.S. Volcanics in accretionary prisms: geodynamic environments of formation (Central Sikhote Alin).//Tectonics, geodynamics and processes of magmatism and metamorphism. M., Geos., 1999, V.I, p.139-141.
8. Vrzhosek A.A. Meymechite-picrite complex in Bikinsk depression.//Geology, magmatism and mineralization in the continent-ocean transition zone. Vladivostok, Far Eastern Branch of USSR Academy of Sciences. 1978, p. 84-86.
9. Zimin S.S., Starkov G.N., Scheka S.A. and Pogorelova M.G. On finding meymechite in Sikhote Alin Main Anticlinorium.//Questions of geology and mineralization in the Far East. Vladivostok, 1965, p. 194-195.

**SOME GENETIC FEATURES OF THE LOVOZERO
RARE-METAL DEPOSITS (NW RUSSIA) AS IT
FOLLOWS FROM NOBLE GAS
(HE, AR) ISOTOPE ABUNDANCES**

Nivin V.A. and Ikorsky S.V

Geological Institute, Kola Sci. Centre RAS, Apatity, nivin@geoksc.apatity.ru

Concentrations and relations of helium and argon isotopes in fluid inclusions, rocks, and minerals as a whole from the Paleozoic Lovozero nepheline-syenite massif and the coupled rare-metal deposits were studied. Great variations in isotope-gas indices have been revealed. They were determined by mixing of the trapped fluid in different proportions, that is in turn a mixture of mantle and atmospheric components, and radiogenic gas isotopes produced in situ. Combined data, on noble gas isotope compositions in particular, confirm or provide the ground to suggest (i) the mantle source of ore (loparite) mineralization, just of the rocks of the whole massif, (ii) the earliest magmatic crystallization of a greater part of loparite relative to associating minerals, (iii) the shorter time interval and smaller temperature gradient between the crystalline matrix and fluid inclusions formation of the ore rocks and minerals, if compared with the non-ore ones, and (iiii) possible partial formation (transformation) of ore ledges or outside zones of some loparite crystals during a relatively low-temperature postmagmatic stage under meteoric water participation.

INTRODUCTION

Rare-metal (loparite) deposits within the Lovozero agpaitic massif of feldspathoid (mainly nepheline) syenites and foidolites are characterized by relatively simple geology. They, like the host pluton, have been investigated to a rather good extent. The research of different geological, petrological, and geochemical features of the massif and, to a less degree, the related ore deposits are described in numerous publications including monographs and recent encompassing papers in popular editions [7,33,6,10,1,13,21,11,4,3,17]. The Devonian age of the pluton (~ 370 Ma) was more exactly defined [18]; the 3-D density model of the massif's deep structure was derived [3,4]; the initial mantle substrate composition was estimated and the models were suggested [18,2,11,3] for the parent melts origin without or with a greatly limited contribution of a crustal source into genesis of the rocks and ores; essential variations in loparite chemical composition including its regular changes through the cross-sections of main complexes of the massif were revealed [21,16,11,17]; the magmatic origin of rare-metal mineralization and the dominant role of crystallization differentiate processes in the formation of both ores and rhythmic layering of the massif as a whole were argued [16,11,17]. Nevertheless, it is also necessary to study some aspects of loparite ore genesis, especially those concerning the fluid regime and possible participation of relatively low-temperature fluids in post-magmatic

transformation of ore mineralization, since certain facts and field observations have not been coordinated yet in between.

Meanwhile, at present, the geochemical tracers of many geological processes such as noble gas isotopes, are recognized by many researchers. Thus, these indicators were successfully used to identify and quantify different source contributions and to determine a degassing pattern of melts, which were parental for the Paleozoic alkaline and carbonatite complexes of the Kola province [19,29,30]. This research revealed that the Devonian alkaline magmatism pulse within the province was initiated by a deep mantle plume. The low-mantle component is determined in the plume for sure. Though the mantle gas-isotope signs have been preserved in the Lovozero rocks and ores to a less extent in comparison with other complexes, joint trends of figurative points of samples from all the examined massifs in different coordinates of the U-Th-He system suggest the common melt sources for these intrusions [23]. There are several papers, which used the noble gas isotope compositions to display the sources and evolution of ore-forming or attendant fluids in some rather young (Mesozoic-Cenozoic) deposits [28,8,5].

In this paper we made an attempt to reveal any features of the Lovozero rare-metal deposits and the host pluton formation on basing on He and Ar isotope distributions in rocks and minerals.

Abbreviations and symbols used in the text and Figures:

ASW - air-saturated (meteoric) water

cal (subscript) - calculated

CM (subscript "m") - crystalline matrix

DC - differentiated complex

DM - depleted mantle

EC - eudialyte complex

FI (subscript "fi") - fluid inclusions

meas (subscript) - measured

WR and WM (subscript "tot") – rock(s) and mineral(s), respectively, as a whole

Superlinear index “ * “ means a radiogenic isotope

BRIEF GEOLOGY, SAMPLES AND METHODS

The Lovozero agpaitic nepheline-syenite massif that ranks the second world's alkaline complex in size, like as the near situated and the larger Khibina pluton, has formed during the peak tectonic-magmatic activation of the eastern part of the Fennoscandian shield. The Archean gneisses and granite-gneisses are the country rocks. On the basis of the data available, one can distinguish three main intrusive phases in the massif formation. The first phase rocks are mainly represented by poikilitic and inequigranular nosean, vishnevite, nepheline and sodalite syenites. They occur as relics of various shape and size (up to 1 km) in the rocks of much later phases and, possibly, predominate in the deepest zones of the

massif. Some poikilitic feldspathoid syenites, their small bodies above all (occur among the second-phase rocks), with their good part being included into the third-phase rocks, seem to belong to the corresponding complexes. The so-called differentiated (layered, loparite-bearing) complex (DC) comprises numerous (to 200) gently dipping, rhythmically alternating layers of lujavrites, foyaite and urtites composing the binary and trimembral packets has formed during the second phase. Some layers range from first centimeters to tens of meters in thickness. Besides the main types of rocks mentioned above, the complex comprises, in subordinate amount, juvites, ijolites, malignites and some other rocks. The main rock-forming minerals are nepheline, alkaline (potassic-sodic) feldspar and clinopyroxene (mainly aegirine). In its greatest part the DC is overlaid by the third intrusive phase rocks that form a funnel-shaped body of the Eudialyte complex (EC). The complex is composed of inequigranular eudialyte lujavrite with some separate foyaite and juvite layers and isolations of poikilitic nepheline-sodalite syenites. Eudialyte is one of the main rock-forming minerals. In the EC and upper DC there occur the massif roof's pendants of the massif composed of the Paleozoic volcanic-sedimentary series. Ore loparite-bearing layers, being, along with the others, the guide horizons, are mainly concentrated within the DC, the largest complex of the massif. Loparite usually forms bed dissemination zones of 0.5 – 2.5 m thick, which are concordant with general (sub-horizontal) stratification of the complex at the low levels of the trimembral layer packets, with its maximal concentration along the contact between urtite and underlying lujavrite layers. A nomenclature is taken for the guide horizons, which includes the number of a series (the accessible for observation DC part consists of 5 series numbered top-down) and the sequence horizon number beginning from the upper series border. In the EC is only one layer (horizon) of loparite juvite with a commercially potential mineralization and local loparite-enriched areas is known.

He and Ar isotope abundances have been studied in 86 samples taken from the massif's host rocks (Table 1), including feldspathoid syenites of, probably, the first phase, the most important rock varieties of phases I and II, the basic commercial loparite ledges of the DC (I-4, II-4, II-7, III-14) and a loparite juvite ledge of the EC. The studied also are the samples taken from the hydrothermal veins associated with rocks of phases II and III, the rocks of the massif's contact zone (nepheline syenites, fenites and fenitized gneisses) and roof pendants (aleurolites and augitic porphyrites).

The helium and argon measurement technique has been repeatedly described earlier [e.g., 19,29,30]. The only thing should be noted that rare gases were extracted from rocks and minerals by two procedures: by melting of samples in high vacuum electrical furnace and by milling them in pumped out glass ampoules. In the former, the total gas is extracted from the whole volume of a rock or mineral sample (WR or WM); in the latter, it is mainly released from fluid micro-inclusions (FI). Subtracting the second from the first, one get the gas content in the sample's crystalline matrix (CM). Below in the text and Figures these types

of gas occurrences are marked by “tot”, “fi” and “m”. The noble gas isotope compositions were analyzed by mass-spectrometer MI-1201 No. 22-78. Comparison of WR and WM abundances of He and Ar isotopes, and the theoretical values with the ones calculated from concentrations of parental (U, Th, Li, K) elements, rock age and the assumptions for closeness of the system, allows to quantify the trapped gas constituent. In FI of many minerals the isotopic ratio of trapped gases may be preserved for a long time, being closer to the initial ratio and with less admixture of a radiogenic component if compared with gases in a crystalline matrix.

To interpret the results obtained, the recent estimates of the isotope ratios in the Earth's reservoirs have been used: $^3\text{He}/^4\text{He}$ (the most informative indicator of deep-seated fluid sources) in the crust $\sim 2 \cdot 10^{-8}$, in the upper mantle $\sim 1.1 \cdot 10^{-5}$, in the lower mantle $\sim 1.1 \cdot 10^{-5}$; $^{40}\text{Ar}/^{36}\text{Ar}$ in the atmosphere – 295.5, in the upper mantle $\sim 40,000$, in the lower mantle $\sim 5.000-6.000$ [31].

RESULTS AND DISCUSSION. BULK NOBLE GAS ISOTOPE ABUNDANCES

Concentrations and ratios of He and Ar isotopes in WR and WM are given in Table 2. The greatest variations (up to 5 orders of magnitude) are characteristic of ^4He whose abundances are mainly determined by the radioactive U and Th concentrations in samples. The maximum amount of ^4He is measured therefore in loparite and loparite ores. The highest $^3\text{He}/^4\text{He}$ ratio has been found in villiaumite from the DC foyaite. The increased ratios are found in phase I feldspathoid syenites, in some (mainly from the deep part of the DC) juvites and foyaites, EC-lujavrite, ussingite and quartz from hydrothermal veins, in augitic porphyrite and fenite. All other samples, primarily the ore ones, are characterized by typically crustal radiogenic values of He isotope ratio. Comparison between the measured (meas) and calculated (cal) He isotope concentrations (Table 3) shows that the majority of the Lovozero rocks have lost the most part (up to 99 %) of radiogenic ^4He ($^4\text{He}^*$). Hydrothermolites, relatively late villiaumite from the DC-foyaite, the rocks of the EC and the massif endocontact zone turned out to be the most degassed. Only in some samples (juvite and foyaite from the DC lowest

Table 1.

Brief characterization of samples			
Tabular number	Author's code	Rock, mineral	Geological position
1	4223-4	Nosean syenite poikilitic	I phase ?
2	709-12	Nepheline syenite poikilitic	I phase ?
3	903-1131	Nepheline syenite uneven-grained	I phase ?
4	II-2a	Juvite-urtite sodalite-and villiomite-bearing	DC, I-1
5	UG-19	Loparite urtite	DC, I-4
6	UG-41	Juvite-urtite with sodalite	DC, I-4
6a	UG-41P	Clinopyroxene from juvite-urtite	DC, I-4
6b	UG-41FS	K-Na feldspar from juvite-urtite	DC, I-4
6c	UG-41N	Nepheline from juvite-urtite	DC, I-4
6d	UG-41S	Sodalite from juvite-urtite	DC, I-4
7	L-136	Juvite	DC, series I
8	MGTS-4	Urtite sodalite-bearing, zeolitized	DC, II-4
9	MGTS-1	Loparite malignite	DC, II-4
9a	MGTS-1L	Loparite from malignite	DC, II-4
9b	MGTS-1WL	Separate without loparite	DC, II-4
10	S-447-48	Urtite zeolitized	DC, II-5
11a	L-10-2L	Loparite from urtite	DC, II-7
11b	L-10-2P	Clinopyroxene from urtite	DC, II-7
11c	L-10-2A	Apatite from urtite	DC, II-7
12	904-1480	Ijolite-urtite	DC, series V
13	S-904-2	Juvite trachtyoid	DC, series V
14	S-904-3	Juvite with eudialyte	DC, series V
15	S-904-3d	Juvite	DC, series V
16	IL-4	Foyaite villiomite-bearing	DC, above I-2
17	IL-11	Foyaite zeolitized	DC, above I-2
18	447-17	Foyaite	DC, II-1
19	IL-5	Foyaite with villiomite and eudialyte	DC, II-3
20	MGZ-7	Foyaite analcite-bearing	DC, II-4
21	MGZ-5	Juvite-foyaite albitized	DC, II-4
22	80-2	Foyaite zeolitized	DC, below II-4
23	TSSH-8-2	Foyaite	DC, below II-4
24	TSSH-18-2	Foyaite with sodalite and cancrinite	DC, below II-4
24a	TSSH-18-2V	Villiomite from foyaite	DC, below II-4
25	S-447-1	Foyaite eudialyte-bearing	DC, above II-5
26	S-447-2	Foyaite eudialyte-bearing	DC, above II-5
27	S-447-19	Foyaite eudialyte-bearing	DC, above II-5
28	S-215-31	Foyaite apatite-and eudialyte-bearing	DC, above III-1
29	S-215-31d	Foyaite with eudialyte	DC, above III-1
30	709-10	Juvite-foyaite villiomite-bearing	DC, III-14
31	724-18	Foyaite villiomite-bearing	DC, III-14
32	S-215-159	Foyaite eudialyte-bearing	DC, below III-16
33	215-159d	Foyaite eudialyte-bearing	DC, below III-16
34	447-1249	Foyaite	DC, below IV-5
35	904-1496	Foyaite	DC, series V
36	UG-18	Lujavrite zeolitized	DC, I-4

Table 1. (End)

37	UG-20	Loparite lujavrite zeolitized	DC, I-4
38	L-18-12	Lujavrite	DC, series II
39	L-10-12	Lujavrite with amphibole	DC, II-7
40	49-11	Amphibole lujavrite	DC, series II
41	724-7	Lujavrite	DC, III-14
42	706-2	Lujavrite	DC, III-14
43	702-1	Loparite lujavrite with villiomite	DC, III-14
44	724-8	Loparite juvite-lujavrite	DC, III-14
44a	724-8L	Loparite from juvite-lujavrite	DC, III-14
44b	724-8P	Clinopyroxene from juvite-lujavrite	DC, III-14
44c	724-8NFS	Nepheline+feldspar from juvite-lujavrite	DC, III-14
45	L-15-13	Nepheline syenite uneven-grained	DC, endocontact zone
46	L-15-12	Nepheline syenite uneven-grained	DC, endocontact zone
47	L-15-11	Nepheline syenite uneven-grained	DC, endocontact zone
48	L-15-1	Nepheline syenite pegmatoidal	DC, endocontact zone
49	L-13-6	Eudialyte juvite with loparite	Eudialyte complex
50	L-16-19	Loparite-eudialyte juvite sodalite-bearing	Eudialyte complex
51	179-249	Eudialyte foyaite	Eudialyte complex
52	L-16-11	Eudialyte lujavrite	Eudialyte complex
53	L-16-26	Eudialyte lujavrite	Eudialyte complex
54	179-185	Eudialyte lujavrite	Eudialyte complex
55	L-16-6	Murmanite-eudialyte lujavrite porphyritic	Eudialyte complex
56	657-B-2	Sodalite syenite poikilitic	Eudialyte complex
57	L-16-16	Albitite	Eudialyte complex
58	731-1a	Ussingite hydrothermolite	Hydrothermal vein
59a	LA-1v	Zeolites from hydrothermolite	Hydrothermal vein
59b	LA-1ab	Quartz from hydrothermolite	Hydrothermal vein
60	L-17-14	Aleurolite	Roof pendant
61	L-17-15	Aleurolite	Roof pendant
62	L-19-11	Tuff of augitic porphyrite	Roof pendant
63	L-19-13	Augitic porphyrite	Roof pendant
64	L-19-15	Augitic porphyrite	Roof pendant
65	L-15-2	Pyroxene-feldspar fenite	Exocontact zone
66	L-15-3	Pyroxene-feldspar fenite	Exocontact zone
67	L-18-6	Amphibole-pyroxene-feldspar fenite	Exocontact zone
68	L-18-1	Gneiss fenitized	Exocontact zone
69	L-15-4	Gneiss fenitized	Exocontact zone
70	L-15-5	Gneiss fenitized	Exocontact zone
71	L-15-6	Gneiss fenitized	Exocontact zone
72	L-15-9	Biotite gneiss	Country rock

Notes. DC – Differentiated Complex; I-1 ÷ III-16 are series number – sequence number of the reference layer within series.

Table 2. Bulk noble gas isotope abundances

Sample	Rock/mineral	⁴ He μcm ³ /g	³ He/ ⁴ He 10 ⁻⁸	⁴⁰ Ar μcm ³ /g	⁴⁰ Ar/ ³⁶ Ar
1	Nosean syenite	74	22.9	33.6	3743
2	Nepheline syenite	185	9.4	80.7	7326
5	Loparite urtite	9800	1	52	4930
6	Juvite-urtite	374	6	150	601
6a	Pyroxene	715	7.4	22.7	2991
6b	Feldspar	269	7.8	89.7	6720
6c	Nepheline	469	6.7	78.2	6751
6d	Sodalite	528	7.4	21.3	1270
8	Urtite	382	2	122	7830
9	Loparite malignite	28000	1	17	4085
9a	Loparite	40200	1	9.8	360
9b	Minus loparite fraction	1910	1	49	7550
11a	Loparite	17860	0.2	2	504
11b	Pyroxene	570	4.7	6.5	953
11c	Apatite	1013	0.3	1	393
12	Ijolite-urtite	199	12.3	69.6	8315
13	Juvite	372	9.1	46	7823
15	Juvite	777	15	48.5	18110
17	Foyaite	73	4	75.3	6341
20	Foyaite	127	9.2	98	11000
21	Juvite-foyaite	367	2.5	109	8800
22	Foyaite	1980	0.5	44	6830
24	Foyaite	115	7	59	7171
24a	Villiomite	44	56.3	1.3	437.7
28	Foyaite	148	3.6	82	6116
29	Foyaite	110	6.4	103	5473
32	Foyaite	254	7.4	71	11700
33	Foyaite	99	14	59	14100
36	Lujavrite	195	4	76	6100
37	Loparite lujavrite	1060	1	49	2136
44	Loparite juvite-lujavrite	1600	0.3	75	11514
44a	Loparite	24560	0.2	5.8	316
44b	Pyroxene	1092	1.9	9.2	436
45	Nepheline syenite	58	4.5	43.5	14726
47	Nepheline syenite	233	3.2	39	3432
49	Eudialyte juvite	39	4.3	54.3	12921
50	Loparite-eudialyte juvite	2142	0.3	76.1	3234
51	Eudialyte foyaite	55	4.2	55.1	6527
52	Eudialyte lujavrite	73	9.2	66.4	8986
53	Eudialyte lujavrite	825	1.7	36.7	4768
55	Eudialyte lujavrite	278	1.1	57.1	11470
57	Albitite	225	6	82	3513
58	Hydrothermolite	108	16.8	14	1072
59a	Zeolites	1.4	4.3	2.2	410
59b	Quartz	0.4	27	2.9	310
64	Augitic porphyrite	313	7.7	12.1	3600
66	Fenite	23.2	10.2	26.9	6432

Note. The mass-spectrometer measurements have been mostly performed by Dr. I.L. Kamensky

Table 3.

A comparison between bulk measured and calculated He and Ar concentrations

Sample	Rock/mineral	Measured			Calculated		
		⁴ He μcm ³ /g	³ He pcm ³ /g	⁴⁰ Ar* μcm ³ /g	⁴ He* μcm ³ /g	³ He* pcm ³ /g	⁴⁰ Ar* μcm ³ /g
1	Nosean syenite	74	16.9	30.9	480	3.2	56.4
2	Nepheline syenite	185	17.4	77.4	483	3.4	77.7
5	Loparite urtite	9800	98.0	48.9	10906	249	52.1
6	Juvite-urtite	374	22.4	76.2	1302	27.2	70.4
8	Urtite	382	7.6	117	1356	10.8	39.0
9	Loparite malignite	28000	280	15.8	14020	54.0	19.8
11a	Loparite	17860	35.7	0.8	54666	0.13	0.7
12	Ijolite-urtite	199	24.5	67.1	220	2.0	44.5
13	Juvite	372	33.9	44.3	352	4.6	72.0
15	Juvite	777	117	47.7	760	2.1	54.0
20	Foyaite	127	11.7	95.4	1359	14.8	93.3
21	Juvite-foyaite	367	9.2	105	1174	9.1	84.5
22	Foyaite	1980	9.9	42.1	954	7.0	46.8
24	Foyaite	115	8.1	56.6	1448	11.4	84.7
24a	Villiomite	44.3	24.9	0.4	1448	101	1.2
28	Foyaite	148	5.3	78.0	1203	17.4	92.4
29	Foyaite	110	7.0	97.1	890	10.6	96.8
32	Foyaite	254	18.8	69.2	894	8.1	66.5
33	Foyaite	99	13.9	57.8	1103	10.6	66.5
36	Lujavrite	195	7.8	72.0	1245	15.9	92.4
37	Loparite lujavrite	1060	10.6	42.2	1583	21.4	52.1
44	Juvite-lujavrite	1600	4.8	73.1	12134	39.8	64.5
44a	Loparite	24560	49.1	0.4	37333	0.16	0.5
44b	Pyroxene	1092	20.7	3.0	569	2.4	2.6
45	Nepheline syenite	58	2.6	42.6	834	9.0	85.8
47	Nepheline syenite	233	7.5	35.6	286	4.0	78.0
49	Eudialyte juvite	38.8	1.7	53.1	925	1.7	0.5
50	Loparite-eudialyte juvite	2142	7.3	69.1	7088	19.5	51.7
51	Eudialyte foyaite	54.8	2.3	52.6	2932	58.4	85.4
52	Eudialyte lujavrite	73	6.7	64.2	2213	16.7	82.0
53	Eudialyte lujavrite	825	14.0	34.4	1712	32.6	52.2
55	Eudialyte lujavrite	278	3.1	55.6	1747	16.2	71.0
57	Albitite	225	13.5	75.1	2840	55.0	83.4
58	Hydrothermolite	108	18.1	10.1	8007	658	3.8
64	Augitic porphyrite	313	24.1	11.1	224	1.4	8.9
66	Fenite	23.2	2.4	25.7	164	0.7	32.2

Note. * - a radiogenic isotope.

and middle parts, pyroxene from juvite-lujavrite and augitic porphyrite) the ${}^4\text{He}_{\text{meas}}/{}^4\text{He}_{\text{cal}}$ is 1-2, which does not exceed the maximal possible calculation error and does not allow us to confidently speak about the essential amounts of ${}^4\text{He}^*$ trapped. As for ${}^3\text{He}$, its loss is much less in all samples and rather high (5–297) $\text{He}_{\text{meas}}/{}^3\text{He}_{\text{cal}}$ ratios in many samples imply significant amount of the

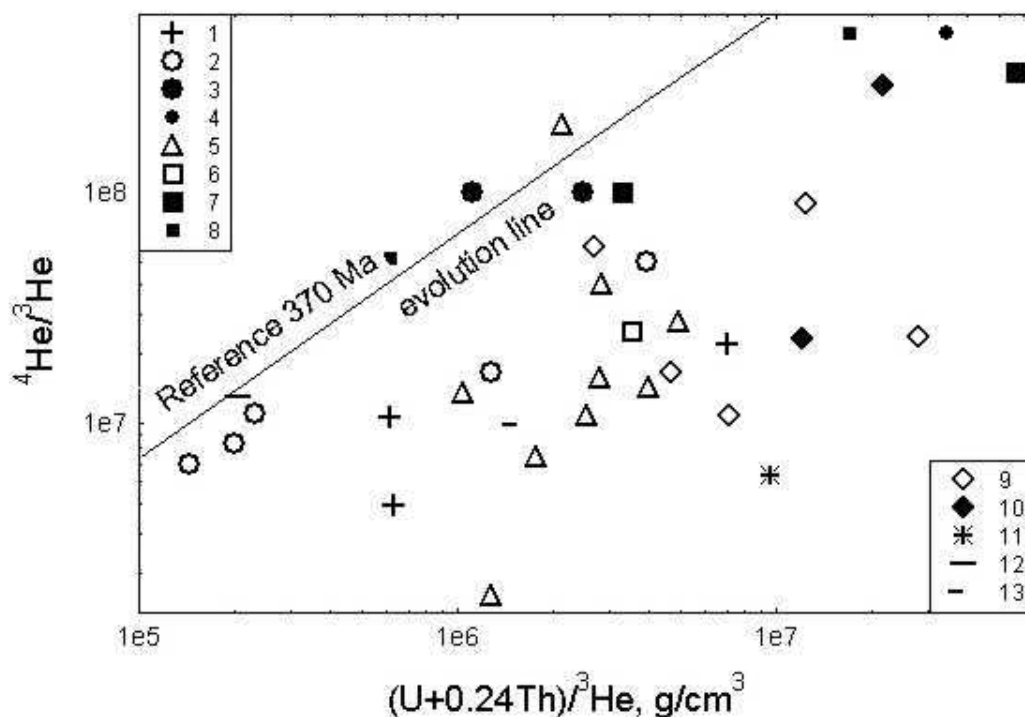


Fig. 1. Interrelation between the whole-rock (mineral) abundances of parent and daughter species in the U-Th-He system.

Samples: poikilitic feldspathoid syenite and endocontact zone nepheline syenite (1); urtite and juvite (2), loparite urtite and malignite (3), mineral separates from loparite-bearing urtite and malignite (4), foyaite (5), lujavrite (6), loparite lujavrite (7) and mineral separates from loparite lujavrite (8) of the Differentiated complex; non-metalliferous (9) and ore (10) rocks of the Eudialyte complex; hydrothermolite (11); rocks from the massif roof's pendants (12); fenites and gneisses of massif exocontact zone (13).

mantle fluid enriched in the light helium isotope. The maximal portion of trapped ${}^3\text{He}$ has been preserved in loparite. Moreover, ${}^3\text{He}$ was apparently trapped by foyaite and, especially, juvites of the DC lowest part, by ore malignite, feldspathoid syenites (Phase I), pyroxene from ore and by augitic porphyrite.

Helium loss from rocks and significant contribution of radiogenic isotope into its balance are testified by the fact that most samples are located lower than the evolution line calculated over the age of 370 Ma at the plot showing the relations between parental U and Th and helium isotopes (Fig. 1). The figurative points of rocks, the closest to the evolution line and with the lowest ${}^4\text{He}/{}^3\text{He}$ ratios, which have been plotted in the same co-ordinates but in a linear scale (Fig. 2), allowed us to determine the possible range of ${}^3\text{He}/{}^4\text{He}$ ratio for the trapped fluid, being equal to $(7-25) \cdot 10^{-8}$. These values, being by a factor of $10^2 - 10^3$ lower than the initial

ratio alkaline-ultrabasic complexes of the province, appear to be underestimated for the Lovozero rocks. Changes in $^3\text{He}/^4\text{He}$ ratio in the trapped fluid could have taken place due to both the postmagmatic loss of He isotopes and due to the permanent addition of radiogenic ^4He whose concentrations, to a greater extent than those of ^3He , here condition $(^3\text{He}/^4\text{He})_{\text{tot}}$ ratio [23], which also can be concluded from the negative correlation between ^4He and $^3\text{He}/^4\text{He}$ and from the absence of any correlation between ^3He and $^3\text{He}/^4\text{He}$. determined earlier [29,30] for

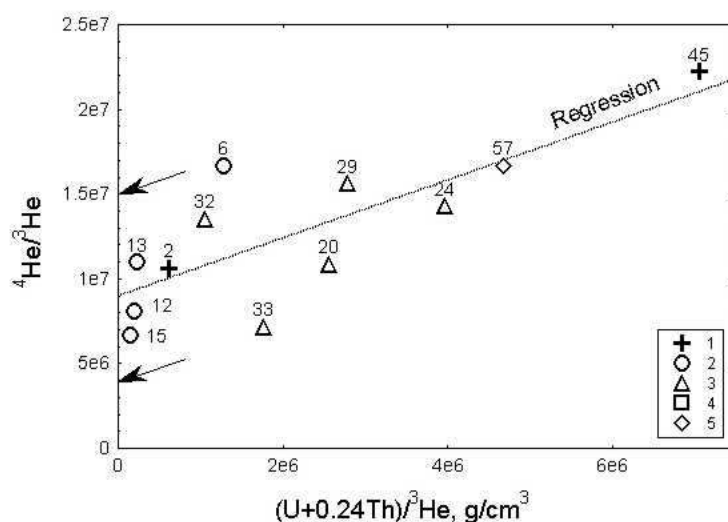


Fig.2. Relationship between the whole-rock abundances of parent and daughter species in the U-Th-He system (linear scales).

Rocks: 1 – nepheline syenites; 2, 3, and 4 – juvite-urtites, foyaites and lujavrites, respectively, of the Differentiated complex; 5 – albitite from the Eudialyte complex. Sample numbers correspond to tabular numbers in Tables 1 and 2.

^{40}Ar concentrations in the studied rocks and minerals range from 1 to 150 $\mu\text{cm}^3/\text{g}$ and $^{40}\text{Ar}/^{36}\text{Ar}$ ratios vary from 310 (close to that in the air) to 18110 (Table 2). The minimal ratios are characteristic of loparite, pyroxene from ore ledges and hydrothermolites. A collation between the measured and calculated concentrations of $^{40}\text{Ar}^*$ (Table 3) shows that in most samples a less Ar amount has been lost if compared with that of He. The increased $^{40}\text{Ar}_{\text{meas}}/^{40}\text{Ar}_{\text{cal}}$ ratios being equal 3 and 2.6, for urtite II-4 and ussingite hydrothermolite, respectively, suggest that some amount of this isotope has been trapped. In the evolution diagram of K-Ar systematics (Fig. 3) most samples are near the isochrone appropriate to age of 370 Ma. This Figure also confirms possibility of Ar trapping by some samples, with the isotope ratio being higher than that in the air. The degree of the Ar loss is the highest in nepheline syenite of the contact zone and loparite-bearing juvite from the EC.

Dominating loss in $^4\text{He}^*$, if compared with that of $^{40}\text{Ar}^*$, and the addition of radiogenic isotopes generated in situ are also testified by the position of the samples in the diagram showing the relations between the parental elemental (U, Th, K) and daughter isotope ($^4\text{He}/^{40}\text{Ar}^*$) ratios (Fig. 4).

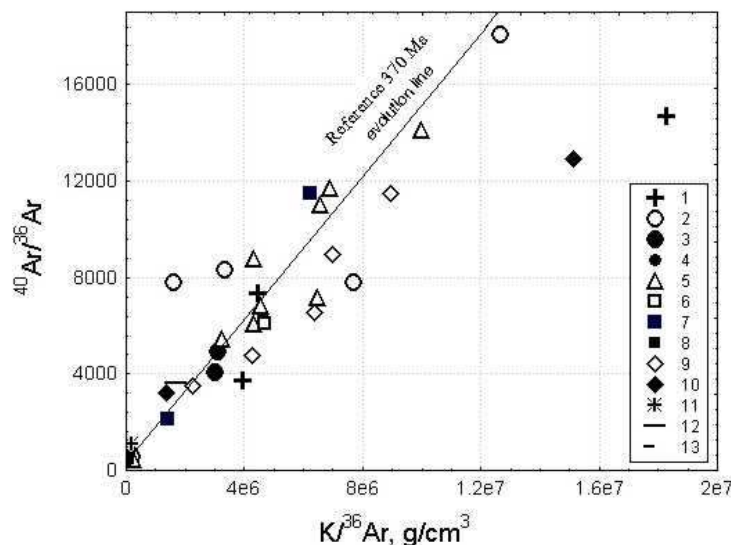


Fig. 3. K-Ar evolution diagram.

Conventional signs are the same as in Fig. 1.

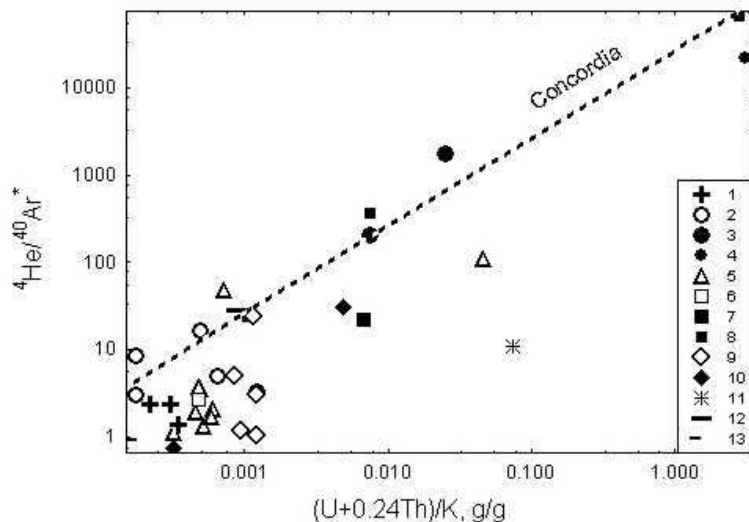


Fig. 4. Relationship between the parent element (U, Th, K) and daughter isotope (^4He , $^{40}\text{Ar}^*$) ratios.

Conventional signs are the same as in Fig. 1.

Most samples are located below concordia. In the $^{36}\text{Ar}/^3\text{He} - ^4\text{He}/^3\text{He}$ diagram (Fig. 5) non-ore rocks form a trend suggesting the mantle (DM) and crustal end members mixing influenced somehow by meteoric water saturated with dissolved air (ASW). Due to addition of $^4\text{He}^*$, loparite ores are shifted up-left in this diagram. An appreciable contribution of air ^{36}Ar into non-metalliferous rocks in particular is also evidenced by a positive correlation being outlined between $^{40}\text{Ar}/^{36}\text{Ar}$ and $1/^{36}\text{Ar}$ ratios (Fig. 6). No similar dependence between ore rocks and minerals from ores has been observed.

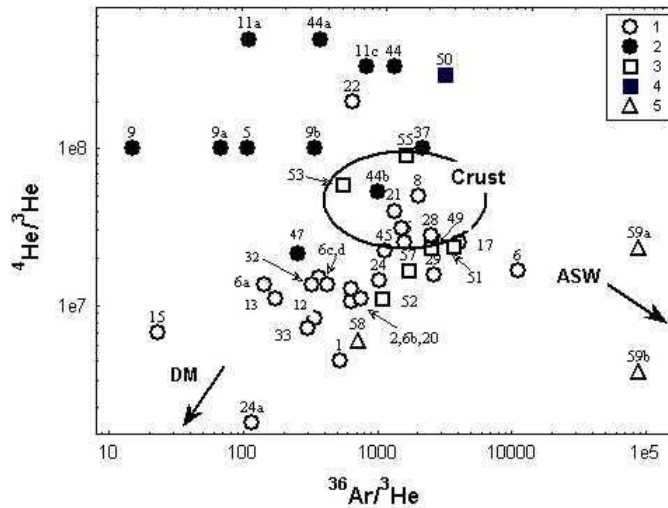


Fig. 5. $^{36}\text{Ar}/^3\text{He}$ vs. $^4\text{He}/^3\text{He}$ for non-metallic (1 and 3) and ore (2 and 4) rocks of the DC and EC respectively, and hydrothermolites (5).

Sample numbers correspond to tabular numbers in Tables 1 and 2.

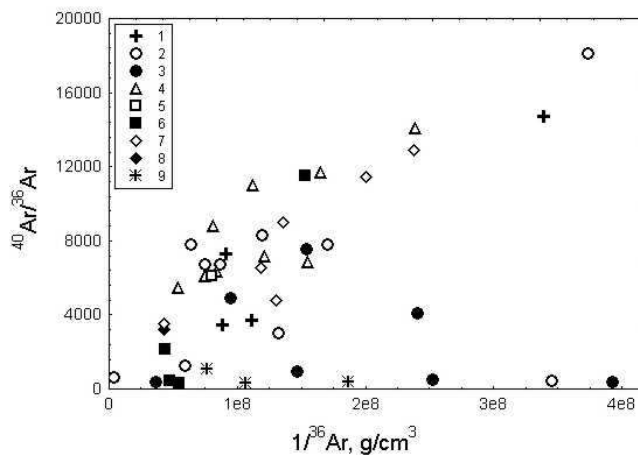


Fig. 6. $^{40}\text{Ar}/^{36}\text{Ar}$ vs. $1/^{36}\text{Ar}$ for rocks and minerals as a whole.

Samples: poikilitic feldspathoid syenite and nepheline syenite of the endocontact zone (1); non-metallic (2) and ore (3) urtites, juvites and malignite and mineral separates of DC; DC foyaites (4); non-metallic (5) and ore (6) lujavrites of DC; EC non-metallic (7) and ore (8) rocks; hydrothermolites (9).

HE AND AR ISOTOPES IN FLUID INCLUSIONS.

Fluid inclusions (FI) observed in the minerals of the Lovozero rocks are predominantly gaseous – hydrocarbonaceous in essence and secondary in origin [15,14,22,9,26]. Most ^3He amount and significant part of ^4He , extracted from samples by milling, are supposed to be in the same inclusions like hydrocarbon components [9,24]. The ^4He concentrations and Ar isotope

Table 4.

He and Ar isotope abundances in fluid inclusions

Sample	Rock/mineral	⁴ He μcm ³ /g	³ He/ ⁴ He 10 ⁻⁸	⁴⁰ Ar μcm ³ /g	⁴⁰ Ar/ ³⁶ Ar
1	Nosean syenite	1.2	110	2.2	491
2	Nepheline syenite	27	27	n.d.	n.d.
3	Nepheline syenite	0.5	12.7	n.d.	n.d.
4	Juvite-urtite	2.1	4.2	n.d.	n.d.
5	Loparite urtite	190	1	n.d.	n.d.
6	Juvite-urtite	260	7.2	n.d.	n.d.
7	Juvite	2.3	2.2	0.8	590
8	Urtite	47	3	n.d.	n.d.
9	Loparite malignite	632	1	n.d.	n.d.
9a	Loparite	960	0.7	n.d.	n.d.
10	Urtite	2.4	4	n.d.	n.d.
11a	Loparite	693	0.5	0.13	343
11b	Pyroxene	8.2	17.9	0.3	357
11c	Apatite	15.2	2.9	0.08	311
12	Ijolite-urtite	64.8	19.2	13.9	3602
13	Juvite	63.7	15.8	n.d.	n.d.
14	Juvite	329	16	n.d.	n.d.
15	Juvite	295	20	2.2	491
16	Foyaite	3.2	4.9	n.d.	n.d.
17	Foyaite	1.2	4.9	3.5	394
18	Foyaite	1.6	4.1	1.4	461
19	Foyaite	4.9	3.8	n.d.	n.d.
20	Foyaite	37	4.5	n.d.	n.d.
21	Juvite-foyaite	25	2.3	n.d.	n.d.
22	Foyaite	47	1.2	n.d.	n.d.
23	Foyaite	2.2	4.3	n.d.	n.d.
24	Foyaite	21.9	5.2	n.d.	n.d.
25	Foyaite	1.1	6.5	n.d.	n.d.
26	Foyaite	1.4	3.7	n.d.	n.d.
27	Foyaite	0.8	8.6	n.d.	n.d.
28	Foyaite	6	24	n.d.	n.d.
29	Foyaite	7.7	26.8	n.d.	n.d.
30	Juvite-foyaite	29.5	25.3	5.9	1672
31	Foyaite	6.8	25.2	2.7	792
32	Foyaite	32	25	n.d.	n.d.
33	Foyaite	24	30.2	n.d.	n.d.
34	Foyaite	26.7	27.4	8.8	1432
35	Foyaite	149	12.2	21.8	4634
36	Lujavrite	4.4	1.6	n.d.	n.d.
37	Loparite lujavrite	145	0.5	n.d.	n.d.
38	Lujavrite	2.15	5.5	n.d.	n.d.
39	Lujavrite	6.3	3.2	n.d.	n.d.
40	Lujavrite	14.4	2.1	n.d.	n.d.
41	Lujavrite	7.6	10.9	6.6	1579

Table 4 (End)

42	Lujavrite	13	15	6.1	1123
43	Loparite lujavrite	49.5	1.6	5	1572
44	Loparite juvite- lujavrite	70	1	3.9	1731
44a	Loparite	515	0.5	0.08	347
44b	Pyroxene	17.7	11.2	0.5	338
44c	Nepheline+feldspar	4	13	1.6	811
45	Nepheline syenite	1.47	4.8	n.d.	n.d.
46	Nepheline syenite	6	4.8	n.d.	n.d.
47	Nepheline syenite	0.84	4.4	n.d.	n.d.
48	Nepheline syenite	1.01	3.7	n.d.	n.d.
49	Eudialyte juvite	0.9	12	2.5	524
50	Loparite-eudialyte juvite	41.3	0.4	n.d.	n.d.
51	Eudialyte foyaite	0.8	10.2	3.4	378
52	Eudialyte lujavrite	0.6	17.5	3.3	603
53	Eudialyte lujavrite	2.4	6.4	n.d.	n.d.
54	Eudialyte lujavrite	3.3	5.8	1.5	496
55	Eudialyte lujavrite	1.8	5.5	n.d.	n.d.
56	Sodalite syenite	31.4	5.6	n.d.	n.d.
57	Albitite	4.4	10.2	5.9	368
60	Aleurolite	2.6	20.1	n.d.	n.d.
61	Aleurolite	1.3	17	2.3	2059
62	Tuff of augitic porphyrite	20.8	1.4	n.d.	n.d.
63	Augitic porphyrite	2	176	1.8	890
64	Augitic porphyrite	5.9	118	n.d.	n.d.
65	Fenite	0.5	85	n.d.	n.d.
66	Fenite	0.5	111	n.d.	n.d.
67	Fenite	1.7	3.3	n.d.	n.d.
68	Gneiss	1.4	7.8	n.d.	n.d.
69	Gneiss	0.8	78	n.d.	n.d.
70	Gneiss	7	93	n.d.	n.d.
71	Gneiss	0.7	54	n.d.	n.d.
72	Gneiss	0.7	17.4	n.d.	n.d.

Notes. Isotopic analyses were mostly performed by Dr. I.L. Kamensky under participating of authors; n.d. – not determined.

composition in FI are in a smaller range, the $^3\text{He}/^4\text{He}$ ratio, on the contrary, is notable for its wide range, if compared with those in rocks and minerals as a whole (Table 4). The maximum possible mixing of values of the $^3\text{He}/^4\text{He}$ ratio exceeding 10^{-6} have been measured in nosean syenites (Phase I), in fenite of the massif exocontact and in augitic porphyrites. These values exceed as well those evaluated above for the massif as a whole, verifying thus higher $^3\text{He}/^4\text{He}$ ratios in the magmatic and high-temperature postmagmatic fluid. Taking into consideration that the most probable temperature for syenite fenite formation is as high as 800-600° C [27], the present-day He isotope composition in most rocks under study has

originated under the lower temperature. **There is a tendency for $^3\text{He}/^4\text{He}$ ratio in rocks of the same type to increase with depth (Fig. 7). Ore rocks characterized by low radiogenic values of the same ratio not only in WR and WM but in FI as well, however, do not follow this tendency.**

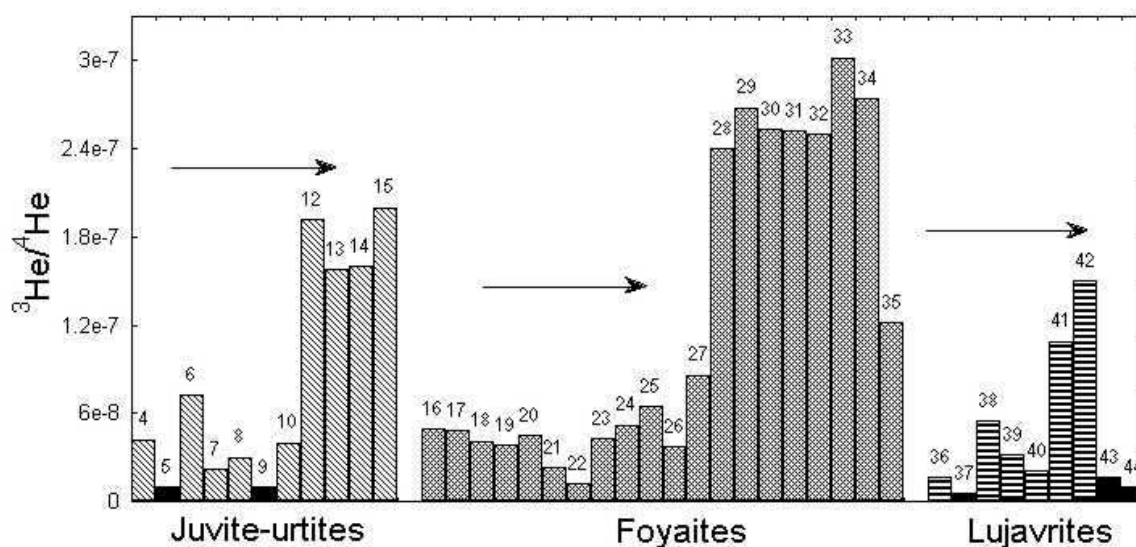


Fig. 7. Systematic variations in $^3\text{He}/^4\text{He}$ ratios for fluid inclusions of the DC rocks.

The increase of sampling depth is shown by arrows. Sample numbers correspond to tabular numbers in Tables 1 and 4. Solid (black) bars are ore (loparite) rocks.

$^{40}\text{Ar}/^{36}\text{Ar}$ ratio in FI (Tables 4, 1) also tends to increase with depth. A much weaker, than in the case with WR, but appreciable positive correlation of $(\text{U}+0.24\text{Th})/^3\text{He}$ and $^4\text{He}/^3\text{He}$ ratios (the Figure is not supplied) is indicative of some contribution of in situ produced $^4\text{He}^*$ to the helium inventory in FI as well. The positive, in general, correlation between ^4He and ^3He (Fig. 8) and between ^{40}Ar and ^{36}Ar (Fig. 9) in FI suggests that the role of additional radiogenic isotope amounts resulted from the parental elements decay after consolidation of the rocks, is not determinative. A direct interrelationship between $^3\text{He}/^{36}\text{Ar}$ and $^{40}\text{Ar}/^{36}\text{Ar}$ ratios (Fig. 10) implies two end members in a trapped fluid: i.e. atmospheric and mantle constituents with low and high values of these ratios, respectively. The mineral separates from loparite rocks characterized by rather high $^3\text{He}/^{36}\text{Ar}$ ratio and by nearly atmospheric ratios of Ar isotopes, are out of the trend again. ASW exerts a stronger effect on the noble gas isotope compositions in FI than on those in rocks as a whole (Fig. 11, cf. Fig. 4). According to the above said, ^3He in FI is predominantly mantle and ^{36}Ar is mainly atmogenic, $^3\text{He}/^{36}\text{Ar}$ ratio can be an informative index characterizing the mixture of these end members and can reflect the fluid evolution both in time and in space. Indeed, there outlined are the tendencies in decreasing the given ratio in common rocks from much deeper parts of the pluton o the surface and from the earliest co-existing minerals to the later ones (Fig. 12). In the latter case the lower $^3\text{He}/^{36}\text{Ar}$ ratio in feldspar-nepheline

fraction, if compared with clinopyroxene, whose formation under agpaitic order of crystallization should occur later than that of other main rock-forming minerals, does not seem to follow the regularity mentioned. In fact, however, it is determined perhaps by the later completion of postmagmatic nepheline and feldspar transformation, if compared with that of pyroxene. The maximal values (the intermediate between crustal and mantle ones) of $^3\text{He}/^{36}\text{Ar}$ ratio, being the closest to those in the mantle, are characteristic of loparite, pyroxene, foyaite of Series IV, augitic porphyrite, and the minimal values (intermediate between typically crustal and ASW) are characteristic of foyaite from the upper part of DC and the EC-rocks.

COMPARISON OF HE AND AR ISOTOPE COMPOSITIONS IN FLUID INCLUSIONS AND CRYSTAL MATRIXES.

Juxtaposition of He and Ar isotopes in FI and CM (Table 5) shows that (1) ^4He and ^{40}Ar concentrations in FI are, as a rule, less by a few tens than those in CM, being in average of 16 and 8 %, respectively, of the latter; (2) the portion of ^3He in FI is much higher (on the average 36 % of CM), and the $^{36}\text{Ar}_{\text{fi}}/^{36}\text{Ar}_{\text{m}}$ ratio changes within the widest range (from 0.01 to 3); (3) the $^3\text{He}/^4\text{He}$

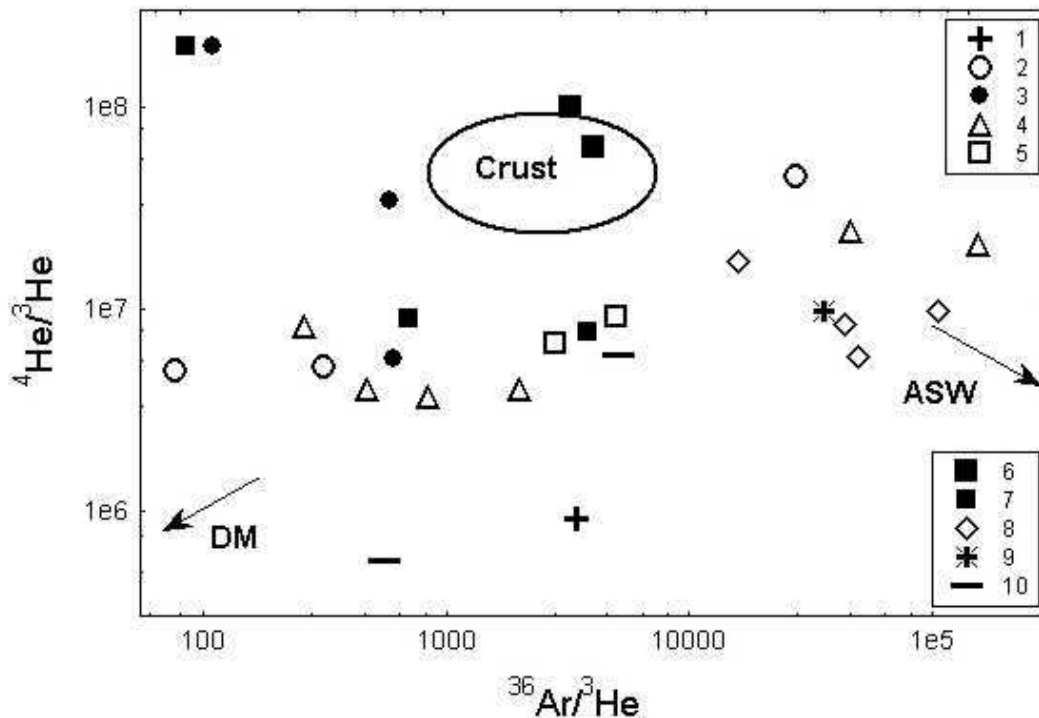


Fig. 8. Interrelation. Conventional signs are the same as in Fig. 1

ratio is greater in between helium isotopes in fluid inclusions most cases, sometimes by far, in FI than in the matrix, and the $^{40}\text{Ar}/^{36}\text{Ar}$ ratio is almost always lower. In so doing, ores and loparite in particular, are characterized more often by a relatively small amount of He isotopes in FI if compared with that in CM, and by

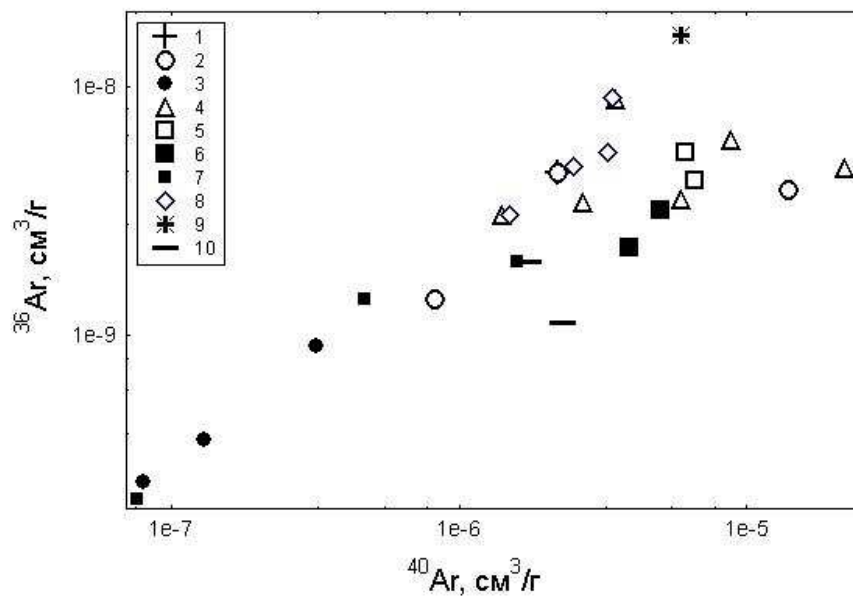


Fig. 9. Relationship between argon isotopes in fluid inclusions.

Samples: nosean syenite (1); juvite-urtites (2), mineral separates from ore juvite-urtites (3), foyaites (4), lujavrites (5), ore lujavrites (6) and mineral separates from ore lujavrite (7) of the Differentiated complex; EC non-metallic rocks (8); hydrothermolite (9); rocks from the massif roof's pendant (10).

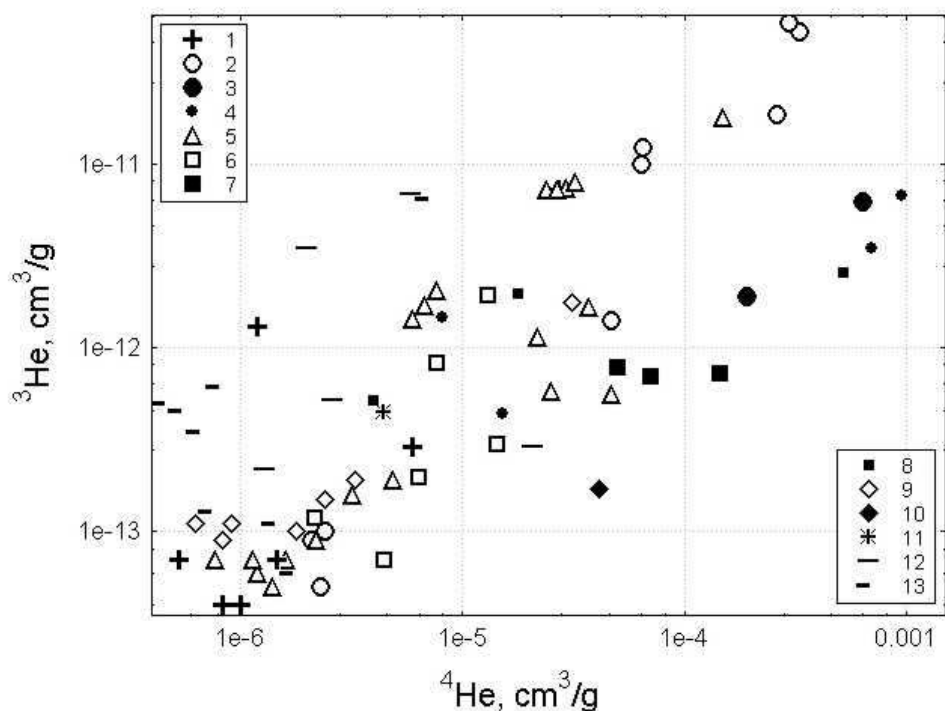


Fig. 10. $^{40}\text{Ar}/^{36}\text{Ar}$ vs. $^3\text{He}/^{36}\text{Ar}$ in fluid inclusions.

Conventional signs are the same as in Fig. 9.

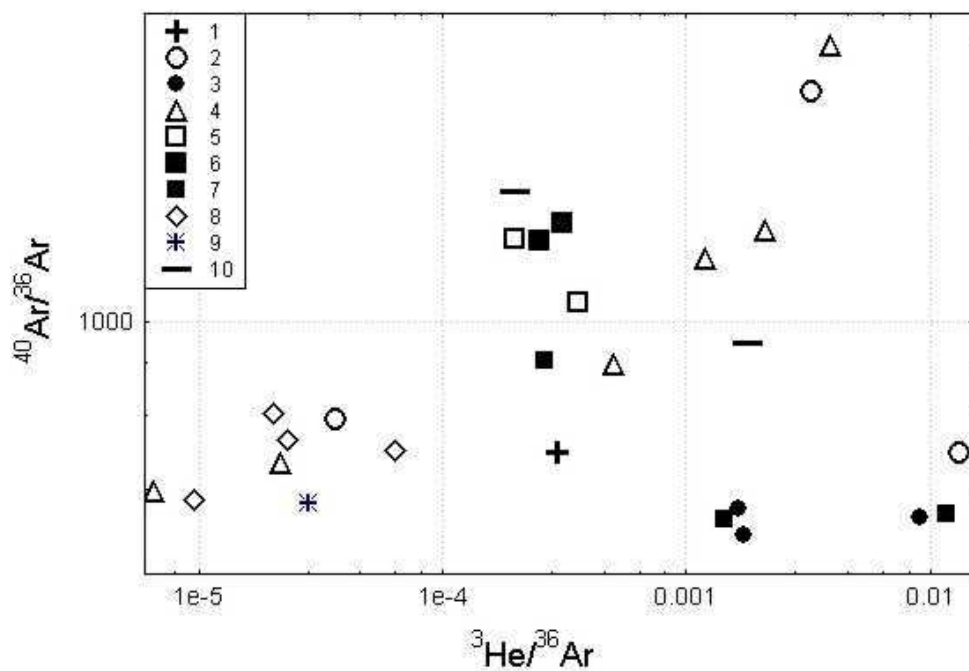
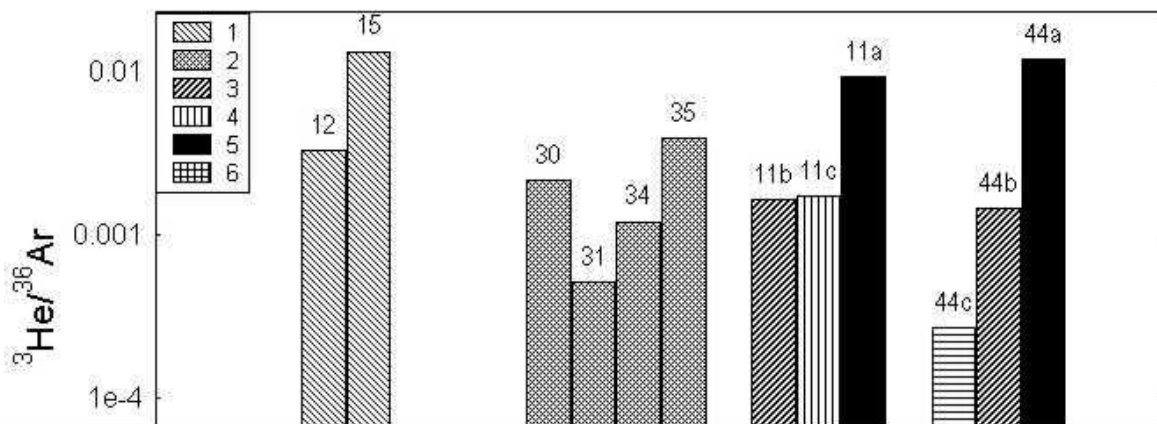


Fig. 11. $^4\text{He}/^3\text{He}$ vs. $^{36}\text{Ar}/^3\text{He}$ in fluid inclusions.
Conventional signs are the same as in Fig. 9.

Bar/Column Plot (Hor336.STA 18v*5c)



ERROR: ioerror
OFFENDING COMMAND: image

STACK: